THE JOURNAL OF
PHYSICAL CHEMISTRY

VOLUME 70, NUMBER 10 OCTOBER 14, 1966

Surface Viscosity of Polydimethylsiloxane Monolayers

by N. L. Jarvis

Surface Chemistry Branch, Chemistry Division, U. S. Naval Research Laboratory, Washington, D. C. 20390 *(Received May 23, 1966)*

The surface viscosities of a series of polydimethylsiloxanes were studied using a canal viscometer as well as a torsional surface viscometer. The siloxane monolayers investigated had molecular weights ranging from 520 to approximately 105,000 and included both the ethoxy and trimethyl end-blocked polymers. The surface viscosity of even the highest molecular weight polydimethylsiloxane monolayer was extremely low, below the limit of sensitivity of the canal viscometer, which is of the order of 10^{-5} surface poise. This surface viscosity is remarkably low when compared with monolayers of other polymeric materials that have been studied at the water–air interface. Many of these polymers such as poly-e-capramide (6-nylon), the proteins, and synthetic polypeptides, gave highly viscous or viscoelastic non-Newtonian films even at film pressures of only a few dynes per centimeter. The low surface viscosity of the siloxanes reflects the relatively low intermolecular cohesion that exists between adjacent siloxane chains in a monolayer. This low surface viscosity may in part explain the defoaming and antifoaming ability of the polydimethylsiloxane fluids.

Introduction

Monomolecular films of many polymeric materials adsorbed at the water–air interface are known to have high surface viscosities, even at film pressures as low as 1 or 2 dynes/cm.[1-3] This is particularly true for protein monolayers, which often become plastic or viscoelastic as the film pressure increases.[4-8] The high surface viscosity or viscoelasticity of these films has been attributed to the strong intermolecular cohesive forces, such as hydrogen bonding, that occur between adjacent molecules in the film. The rheological properties reported for films of a variety of synthetic polypeptides were similar to those of the natural proteins, the surface viscosities being high and generally non-Newtonian as the films were compressed.[9-12] Studies have also been made of the viscoelastic properties of other synthetic polymer monolayers such as the various

---

(1) I. Langmuir and V. J. Schaefer, *Chem. Rev.*, **24**, 181 (1939).

(2) L. Fourt, *J. Phys. Chem.*, **43**, 887 (1939).

(3) M. Joly, *Biochim. Biophys. Acta*, **2**, 624 (1948).

(4). J. Llopis and A. Albert, *Anales Real Soc. Espan. Fis. Quim., Ser. B*, **55B**, 109 (1959).

(5). K. Motomura, *J. Phys. Chem.*, **68**, 2826 (1964).

(6) B. Biswas and D. A. Haydon, *Proc. Roy. Soc.* (London), **A271**, 296, 317 (1963).

(7) K. Inokuchi, *Bull. Chem. Soc. Japan*, **26**, 500 (1953); **27**, 203 (1954).

(8) N. W. Tschoegl and A. E. Alexander, *J. Colloid Sci.*, **15**, 168 (1960).

nylons, polyvinylacetate (PVAc), polymethylacrylate (PMA), and poly(methyl methacrylate) (PMMA).[13-15] The nylon monolayers were found to be highly viscous or viscoelastic at close packing, indicating a high degree of intermolecular cohesion. Motomura and Matuura[14] reported the surface viscosities of the following polymers to be in the order PMMA > PMA > PVAc, the same order as the relative cohesive energies between monomers of the polymers, with the PVAc perhaps being slightly soluble.

Unlike the above polymer films, polyorganosiloxanes should exhibit low intermolecular cohesion, and one would predict their surface viscosities to be extremely low. Monomolecular films of the siloxanes (or "silicones") have been spread at the water-air interface, and their film pressure *vs.* area per molecle (*F vs. A*) and surface potential *vs.* area per molecule (ΔV *vs.* *A*) properties have been discussed,[16-19] but little has been reported regarding their rheological behavior. The viscosity of siloxane monolayers is of particular interest in view of their known proficiency as defoaming and antifoaming agents;[18] however, the mechanism by which the silicone monolayers act as defoaming agents is still not known. The role of surface viscosity in determining the ability of many surface-active agents to stabilize foams is also not completely understood, although with foams stabilized by proteins the high surface viscosity appears to be a dominant stabilizing factor.[20,21] On the other hand, many of the common defoaming agents such as 2-ethylhexanol or methylisobutylcarbinal will have very low surface viscosities. In addition to the viscosity effect, Ellison and Zisman[22] proposed that the defoaming ability of the siloxanes in both aqueous and nonaqueous systems is due to (a) the ability of silicone monolayers to adsorb at the liquid-gas interface and displace the previously adsorbed foam stabilizing materials, and (b) the inability of the silicone monolayers to increase the viscosity of the water-air or organic liquid-air interfaces.

In this study, the rheological properties of a number of siloxane monolayers were investigated. Where applicable, the surface viscosities were determined with a canal viscometer, which is capable of greater sensitivity and accuracy than those methods based on the torsional behavior of a ring or disk suspended in the interface.[23,24]

The canal viscometer is satisfactory at film pressures below the characteristic "plateaus" in the force-area curves of siloxane monolayers. At higher film pressures, extending into the plateau region, the adsorbed molecules on each side of the canal will have quite different orientations and compressibilities, and it is difficult to assign an average viscosity to the film in the canal. Another disadvantage of the canal technique is that it is difficult to correlate the surface viscosities with the various inflection points of the *F vs. A* curves of the siloxanes, particularly in the plateau. For these reasons, it was decided to use a torsional viscometer as well as the canal viscometer, especially at the higher film pressures.

Experimental Section

Materials. Two series of well-defined polydimethylsiloxanes, kindly supplied by the Dow Corning Co., were available for this investigation, the ethoxy end-blocked compounds with the general formula C_2H_5O-$[Si(CH_3)_2O]_nC_2H_5$ and the trimethyl end-blocked series $(CH_3)_3Si[OSi(CH_3)_2]_nOSi(CH_3)_3$. Of these compounds the ethoxy end-blocked siloxanes having $n = 4$, 6, 8, 10, 14.5, and 67, and the trimethyl end-blocked compounds having $n = 6$, 10, 15, and 43 were studied. A phenylated siloxane from Dow Corning DC 510, also was used in this study. Two samples of this phenylated compound, containing one phenyl group for every 20 methyl groups, were investigated, the 50-cstoke and the 100-cstoke fluids. Compared with many polymers, the molecular weights of these compounds are all rather low, the molecular weight of the $n = 67$ ethoxy end-blocked siloxane being only about 5000. In order to study the surface viscosity of higher molecular weight silicones, it was necessary to go to the less well-defined higher bulk viscosity compounds. Dow Corning DC 210 (30,000 cstokes at 25°) and Viscasil 100,000 (100,000 cstokes at 25°) from the General Electric Co. were

---

(9) S. Ikeda and T. Isemura, *Bull. Chem. Soc. Japan*, **32**, 659 (1959); **33**, 137 (1960).

(10) T. Isemura, K. Hamaguchi, and S. Ikeda, *J. Polymer Sci.*, **23**, 651 (1957).

(11) T. Isemura and K. Hamaguchi, *Bull. Chem. Soc. Japan*, **27**, 125, 339 (1954).

(12) T. Yamashita and T. Isemura, *ibid.*, **38**, 420, 426 (1965).

(13) K. Inokuchi, *ibid.*, **28**, 453 (1955).

(14) K. Motomura and R. Matuura, *J. Colloid Sci.*, **18**, 295 (1963).

(15) T. Yamashita, *Bull. Chem. Soc. Japan*, **38**, 426 (1965).

(16) H. W. Fox, P. W. Taylor, and W. A. Zisman, *Ind. Eng. Chem.*, **39**, 1401 (1947).

(17) H. W. Fox, E. M. Solomon, and W. A. Zisman, *J. Phys. Colloid Chem.*, **54**, 723 (1950).

(18) R. L. Bass, *Chem. Ind.* (London), 912 (1959).

(19) W. Noll, J. Steinbach, and C. Sucker, *Ber. Bunsenges. Physik. Chem.*, **67**, 407 (1963).

(20) W. E. Ewers and K. L. Sutherland, *Australian J. Sci. Res., Ser. A*, **5**, 697 (1952).

(21) J. A. Kitchener and C. F. Cooper, *Quart. Rev.* (London), **13**, 71 (1959).

(22) A. E. Ellison and W. A. Zisman, *J. Phys. Chem.*, **60**, 416 (1956).

(23) G. C. Nutting and W. D. Harkins, *J. Am. Chem. Soc.*, **62**, 3155 (1940).

(24) G. E. Boyd and F. Vaslow, *J. Colloid Sci.*, **13**, 275 (1958).

selected as the higher molecular weight siloxanes, the average molecular weight of Viscasil 100,000 being estimated at about 105,000.

To remove surface-active impurities, the lower viscosity siloxane fluids were put through adsorption columns containing activated Florisil. Those silicones too viscous to flow readily through adsorption columns were used as received. Spreading solutions of the siloxanes were prepared by dissolving known amounts of each compound in CP petroleum ether (bp 41–55°). The petroleum ether was also percolated through activated Florisil. The spreading solutions were delivered to the water surface from Misco micropipets. In each case the substrate was triply distilled water, the final two distillations from an all-quartz apparatus.

Canal Viscometer. The canal surface viscometer used in this study was described in detail in a previous report.[25] Briefly, it employed a narrow, deep canal as suggested by Harkins and Nutting.[23] The canal was formed from two glass microscope slides 7.5 cm long, 0.1 cm thick, and 1.6 cm wide. The slides were placed in a film balance trough so that the upper edges were exactly level with the free water surface. Only the upper edges of the slides were coated with paraffin; those portions of the slides remaining in contact with water were left hydrophilic to prevent slipping between the substrate water and the sides of the canal. The viscometer was constructed in such a manner that the canal width and alignment could be carefully controlled. The canal assembly was mounted in a Cenco hydrophil balance. A Cenco-type torsion head was used to measure the drop in film pressure across the ends of the canal. A Wilhelmy-type tensiometer continuously monitored the film pressure on one side of the canal. All film balance surfaces that came in contact with the substrate were made hydrophobic by coating with a thin layer of paraffin.

The procedure used to determine surface viscosity with the canal viscometer essentially involved measuring the amount of film passing through the canal in unit time with a given pressure difference across the canal. A monolayer was initially spread on both sides of the canal and then compressed with the barriers until the film on one side registered a pressure F_1 and the film on the other side a pressure F_2. The pressure differential across the canal was then $\Delta F = F_1 - F_2$, and the average film pressure in the canal was assumed to be $(F_1 + F_2)/2$. During the present investigation a pressure difference of 2 dynes/cm was routinely maintained across the canal.

For a canal of this design, Harkins and Kirkwood[26] proposed that the rate of flow of film material through the canal is related to the absolute viscosity η of the monolayer by the equation

$$\eta = \frac{(F_1 - F_2)a^3}{12lQ} - \frac{a\eta_0}{\pi} \tag{1}$$

in which a is the width of the canal in centimeters, Q is the area in square centimeters of film flowing through the canal in 1 sec, l is the length of the canal in centimeters, and η_0 is the bulk viscosity of the aqueous substrate. These measurements were all carried out at 20 ± 0.2°.

Torsional Surface Viscometer. The torsional viscometer was similar to many that have been reported in the literature.[24,27,28] It consisted of a sharp-edged brass cylinder 1.750 cm in diameter, and was suspended from a torsion wire 41.8 cm long and 0.010 cm in diameter. The sides of the cylinder were coated with a fluorocarbon polymer[29] to prevent erratic wetting of the cylinder by the substrate. In practice, the cylinder height was adjusted so that it just touched the water surface. The moment of inertia of the cylinder was 44.92 g cm², but could be increased to more than 150 g cm² by adding circular disks of known moment of inertia. The outer wall of the cylinder was calibrated in degrees, and its periodic motion was determined using a cathetometer telescope. The torsional viscometer was mounted in a Langmuir–Adam type film balance equipped with a Cenco du Nuoy torsion head. The film balance consisted of a Pyrex glass trough 12 cm wide, 74 cm long, and 0.5 cm deep, with the rim lightly coated with paraffin. The torsion head was sensitive to changes in film pressure of 0.05 dyne/cm. The viscometer cylinder was located approximately 6 cm from the paraffin-coated mica float and about 5 cm from each side of the trough. This film balance was also used to determine the *F vs. A* curves of the siloxane monolayers prior to the viscosity determinations.

Surface viscosity was determined by measuring the logarithmic decrement of the torsional oscillation of the ring at a clean water surface and comparing it with a similar measurement for the monolayer-covered surfaces. The surface viscosity η was calculated using the equation[30]

---

(25) N. L. Jarvis, *J. Phys. Chem.*, **69**, 1789 (1965).

(26) W. D. Harkins and J. G. Kirkwood, *J. Chem. Phys.*, **6**, 53, 298 (1938).

(27) R. J. Myers and W. D. Harkins, *ibid.*, **5**, 601 (1937).

(28) L. Fourt and W. D. Harkins, *J. Phys. Chem.*, **42**, 897 (1938).

(29) M. K. Bernett and W. A. Zisman, *ibid.*, **66**, 1207 (1962); "Prevention of Liquid Spreading or Creeping," Advances in Chemistry Series, No. 43, American Chemical Society, Washington, D. C., 1964, p 332.

(30) N. W. Tschoegl, *Kolloid-Z.*, **181**, 19 (1961).

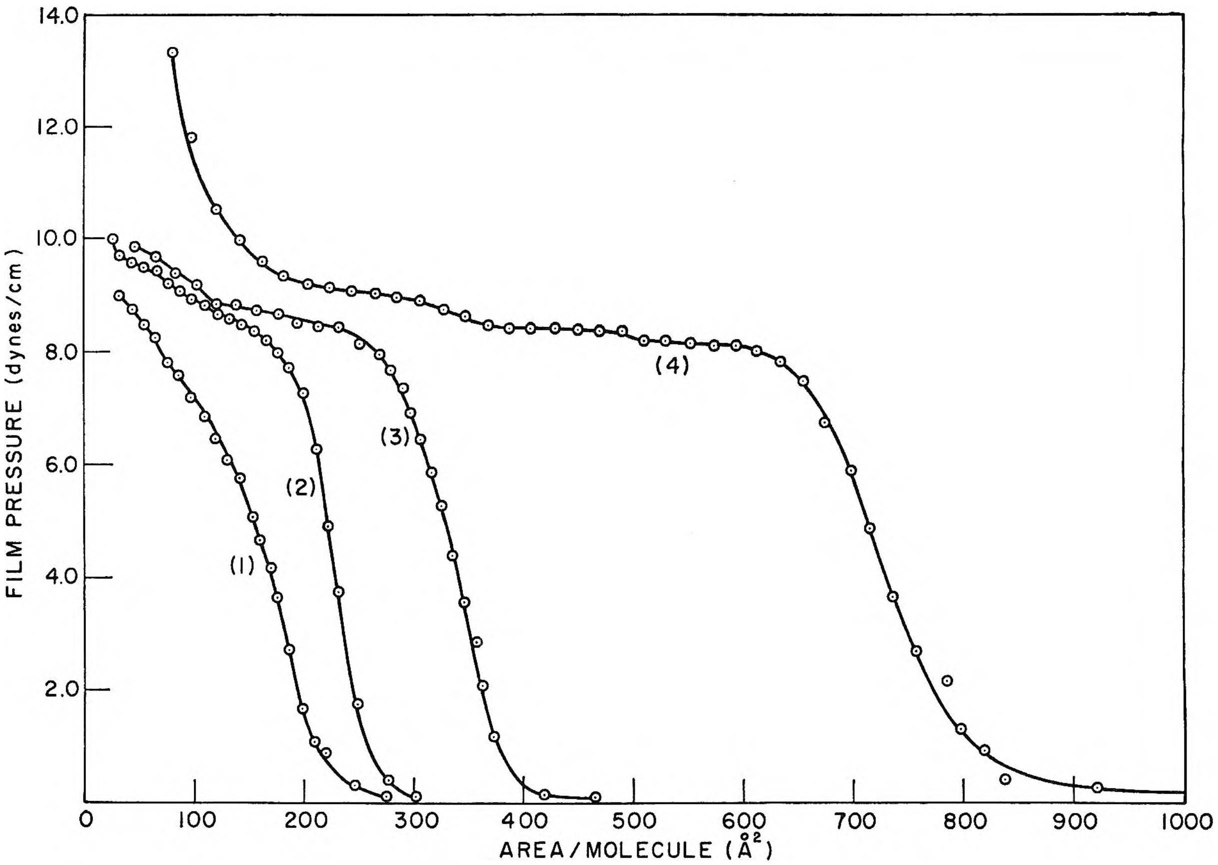

Figure 1. Film pressure *vs.* area per molecule curves for polydimethylsiloxanes of the type $(CH_3)_3Si[OSi(CH_3)_2]_nOSi(CH_3)_3$ on distilled water: (1) $n = 6$; (2) $n = 10$; (3) $n = 15$; and (4) $n = 43$.

$$\eta = 2H_sI_r\left[\frac{\lambda}{T} - \frac{\lambda_0}{T_0}\right] \tag{2}$$

where T is the period of oscillation (subscript 0 refers to the clean water surface), λ is the natural logarithmic decrement of the damped oscillations, I_r is the moment of inertia of the oscillating assembly, and H_s is an apparatus constant dependent upon the geometry of the equipment. During most of the experiments, I_r was 114.47 g cm^2 and T was 16.8 sec. The period of oscillation was the same for both clean and monolayer-covered surfaces. The apparatus constant H_s is given by the equation

$$H_s = \frac{1}{4\pi}\left[\frac{1}{r_1^2} - \frac{1}{r_2^2}\right] \tag{3}$$

where r_1 is the radius of the ring and r_2 is the effective radius of the film balance. In the present experiments, H_s is equal to 0.0237 cm^{-2}; λ is determined by plotting the natural logarithm of the peak amplitudes of the oscillations against the number of oscillations, the slope of the line being the logarithmic decrement. In this study at least ten periodic oscillations were plotted for each λ determination. As required by theory, the logarithmic decrement was found to be independent of the amplitude of the oscillations. All measurements with this apparatus were carried out in a constant temperature room at 25 ± 0.5°. The apparatus was further enclosed in a glass and aluminum box with exterior controls.

Results

Film Pressure vs. Area per Molecule Isotherms. F *vs.* A isotherms were determined on triply distilled water for each of the siloxane monolayers studied. The data shown in Figure 1 are for a series of trimethyl end-blocked polydimethylsiloxanes, but are typical of the results obtained with each of the siloxanes. Each F *vs.* A curve was repeated at least three times, the variation between the separate runs being less than ±0.2 dyne/cm at any area per molecule. These curves are also in agreement with those previously reported in the literature for similar siloxanes.[16–19] Monolayers of the low molecular weight siloxanes ($\eta < 6$) were not stable with time, and appeared to be either slightly soluble or volatile. Also, they did not show the plateau

Table I: Combined Canal Viscometer Data for All Polydimethylsiloxanes at All Average Film Pressures Studied (Data Given for Five Canal Widths)

(1) Canal width, cm	(2) Film flow rate, Q, cm^2/sec	(3) Std dev of film flow rate	(4) Uncor surface viscosity, surface poise	(5) Std dev of uncor surface viscosity	(6) Correction factor from eq 1	(7) Corrected surface viscosity [(4) − (6)], surface poise
0.092	0.0565	0.0020	0.000295	0.000015	0.000293	0.000002
0.117	0.0946	0.0039	0.000370	0.000015	0.000373	−0.000003
0.141	0.140	0.006	0.000446	0.000019	0.000449	−0.000003
0.166	0.190	0.008	0.000526	0.000021	0.000529	−0.000003
0.190	0.248	0.011	0.000625	0.000028	0.000605	0.000020

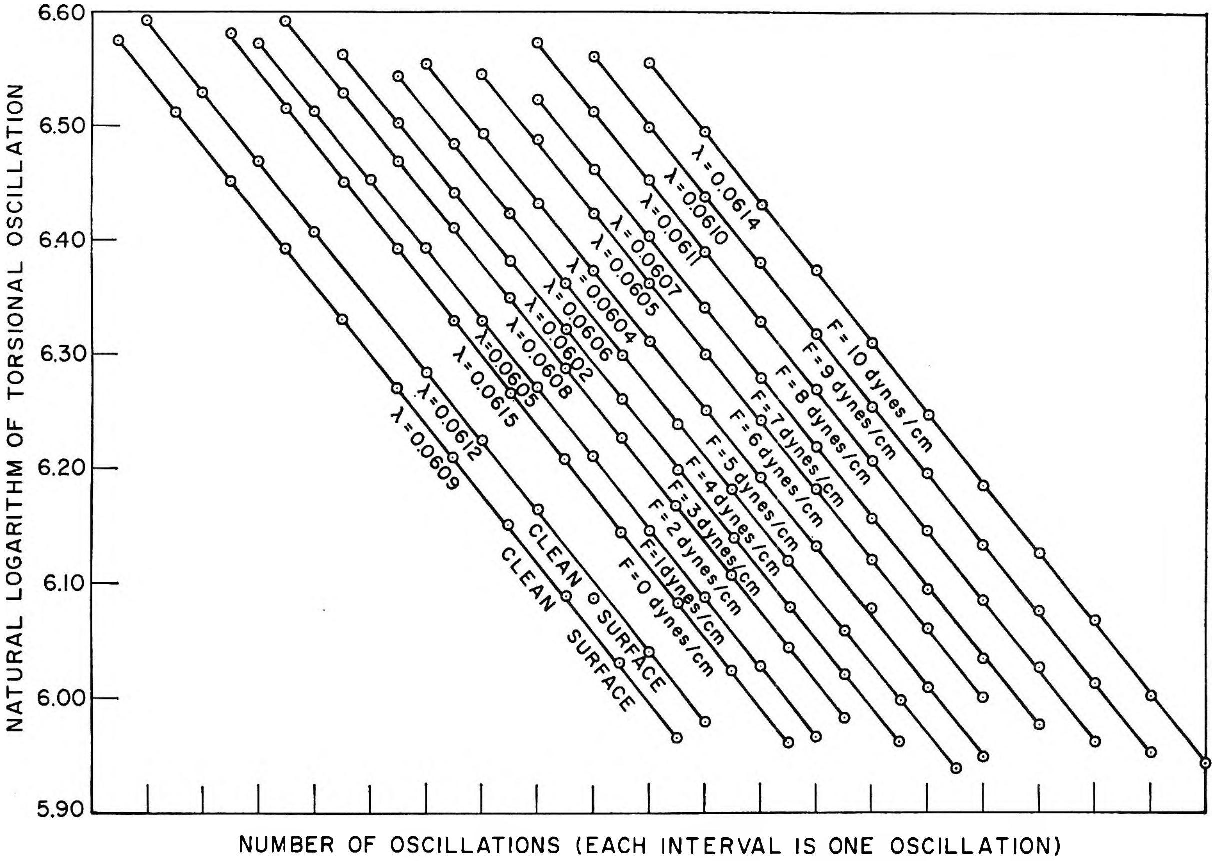

Figure 2. A plot of the natural logarithm of the peak amplitudes of the torsional oscillations *vs.* the number of oscillations for monolayers of a polydimethylsiloxane (30,000 cstokes at 25°). The slope of the plot gives λ, the logarithmic decrement of the torsional oscillation.

in the F *vs.* A curve, or the inflection points that are characteristic of the higher molecular weight siloxanes.

Surface Viscosity by Canal Viscometer. Use of the canal viscometer was limited to siloxane monolayers having an average film pressure in the canal of 1 to 7 dynes/cm. Due to instability of monolayers of the low molecular weight siloxanes, the method was also limited to those siloxanes where $n \geq 8$. Surface viscosities were determined at several canal widths up to 0.190 cm as an independent check on the technique. With the narrower canals, less than about 0.092 cm, there was a significant scatter in the results, perhaps due to frequent blocking of the narrow canal by dust particles and other small obstructions.

For every compound studied, at a given canal width and film pressure, at least three independent determinations of the film flow rate were made, and every determination was the average of at least five consecutive measurements. It was found that at a given canal width the film flow rate Q was independent of the molecular weight of the polydimethylsiloxane (with $n \geq 8$) and independent of film pressure, at least up to 7 dynes/cm. The combined film flow rate data for all siloxanes at all film pressures studied gave more than 100 independent determinations of Q at each canal width. The average film flow rates and the standard deviations at each canal width are listed in Table I. In column 4 of Table I are given the average uncorrected surface viscosities of the siloxane monolayers as calculated from the first term in eq 1, followed by their standard deviations in column 5. In column 6 the correction factors are given as calculated from the second term of eq 1. It is apparent that the surface viscosities of the polydimethylsiloxanes are determined as the difference between the two relatively large numbers. The differences between columns 4 and 6, or the corrected surface viscosities, are seen to be extremely small, of the order of 10^{-5} surface poise or less. In each case, the corrected surface viscosities are less than the standard deviations in column 5. It is apparent then that the true surface viscosities of polydimethylsiloxane monolayers will be extremely small, probably less than 10^{-5} surface poise. The surface viscosities of those slightly phenylated siloxanes studied were not significantly different from the polydimethylsiloxanes. Surface viscosities were not reported for the more highly phenylated siloxanes as well-defined samples of these materials were not available.

Surface Viscosity by Torsional Viscometer. The torsional viscometer was used primarily to determine whether the siloxane monolayers developed an appreciable viscosity at high film pressures, and further to see if any of the inflection points in the F *vs.* A curve gave corresponding changes in surface viscosity. Fewer of the siloxanes were studied by this technique than by the canal viscometer, the experiments being limited primarily to those compounds having higher molecular weights. For each compound studied, a plot of the natural logarithm of the peak amplitude of each oscillation *vs.* the number of oscillations was constructed, as shown in Figure 2 for the 30,000-cstoke polydimethylsiloxane. The slope of this plot gives λ, the logarithmic decrement of the torsional oscillation. In Figure 2, λ varied from 0.0602 to 0.0615, with no obvious trend being observed in going from a clean water surface to a film pressure of 10 dynes/cm. The difference of 0.0013 between the extreme values of λ is typical of the data for the other siloxanes, the maximum difference being less than 0.0020 in all cases. This can be seen in Figure 3, where the natural logarithmic decrements for several of the siloxanes are plotted against the film pressure of the monolayers. The solid lines correspond to the value of λ_0 for a clean water surface, and the points to the logarithmic decrements determined in the presence of the monolayers. As the values of λ_0 are within the extremes of λ for the monolayers, it is apparent that the logarithmic damping of the oscillating cylinder on clean water is not significantly different from that on a monolayer-covered surface. Therefore, the surface viscosities of polydimethylsiloxane monolayers are certainly below the sensitivity limit of this torsional viscometer, even at film pressures corresponding to the collapse pressure of the monolayers. A difference of 0.020 in the logarithmic decrement corresponds to a surface viscosity difference of 0.00065 surface poise, which may be taken as the sensitivity limit of this torsional viscometer. The surface viscosities of the siloxane monolayers are certainly well below this value.

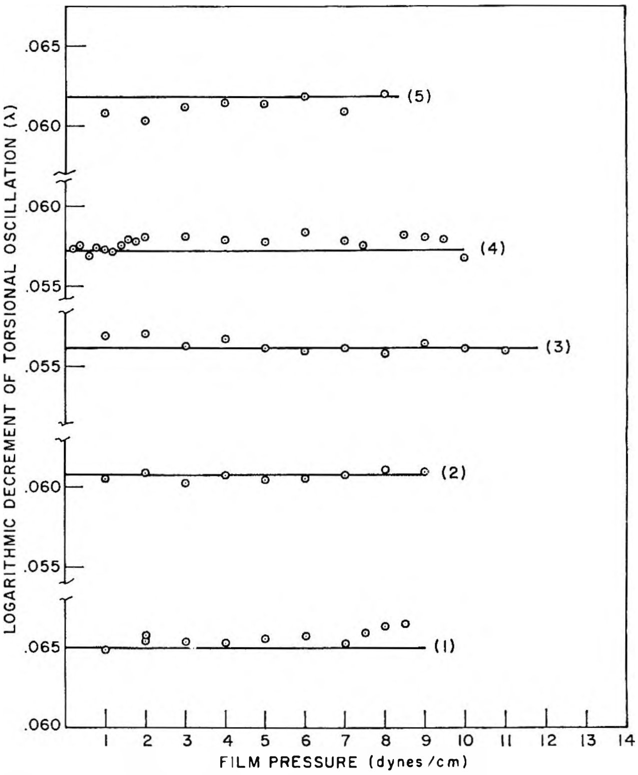

Figure 3. The logarithmic decrements of torsional oscillation (λ) of several polydimethylsiloxanes as a function of the film pressure of the monolayer. The solid line corresponds to λ_0, the logarithmic decrement for clean water: (1) $(CH_3)_3[Si(CH_3)_2O]_{43}Si(CH_3)_3$; (2) 30,000-cstoke polydimethylsiloxane; (3) $C_2H_6O[Si(CH_3)_2O]_{67}\,C_2H_5$; (4) $C_2H_6O\,[Si(CH_3)_2O]_{14.5}C_2H_5$; (5) 100,000-cstoke polydimethylsiloxane.

Discussion

The results of this study show that the surface viscosities of the polydimethylsiloxanes are certainly below the limit of detectability of the surface viscometers used and are exceptionally low for polymers adsorbed at the water–air interface. Based on the results of the canal viscometer, their viscosities are probably below 10^{-5} surface poise. Even when the monolayers are highly compressed and begin to show visible evidence of film collapse, there is no measurable surface viscosity. A surface viscosity of this low order of magnitude seems quite remarkable for a long-chain polymeric material, particularly one having a molecular weight as high as about 105,000. This must reflect the low intermolecular cohesion that is present in siloxane films, compared with monolayers of proteins and certain linear synthetic organic polymers.[14] Therefore, it can be concluded that the ability of siloxane polymers to act as defoaming and antifoaming agents is undoubtedly related to their unusually low surface viscosities and their ability to displace the less strongly adsorbed foam-stabilizing materials.

Garrett and Zisman[31] have reported another remarkable and interesting property of the linear polydimethylsiloxane films, namely, the effect of the films on the so-called capillary waves on water. They reported that these films can be very effective in damping the capillary waves, but only at certain states of compression of the monolayer. These siloxanes gave large "damping coefficient" peaks at areas per molecule corresponding to (1) the initial rapid increase in film pressure with decreasing area, (2) the beginning of the plateau region of the F *vs.* A curve, (3) the inflection point on the plateau, and (4) at the approach to closest packing of the adsorbed molecules. Between these peaks the monolayers had only a small effect on the amplitude of the capillary waves. It is interesting that surface viscosity shows no such correlation with structure of the monolayer, or that such a remarkable damping of capillary waves can occur at all in the absence of a measurable surface viscosity.

---

[31] W. D. Garrett and W. A. Zisman, "Damping of Capillary Waves by Monomolecular Layers of Linear Polyorganosiloxanes," presented at the 150th National Meeting of the American Chemical Society, Colloid and Surface Chemistry Division, Atlantic City, N. J., Sept 16, 1965.

Zinc Oxide Sensitized Photochemical Reduction and Oxidation[1,2]

by Gerald Oster and Masahide Yamamoto

Department of Chemistry, Polytechnic Institute of Brooklyn, Brooklyn, New York *(Received August 2, 1965)*

Ultraviolet radiation below 380 mμ causes zinc oxide to reduce many organic compounds. Rate studies were carried out with indophenol. Diphenylpicrylhydrazyl in organic solvents is reduced to the hydrazine if water is present. In the presence of oxygen the excited zinc oxide causes oxidation. This is ascribed to an autoxidation of a transient species produced in the light-excited solid.

Introduction

It has long been appreciated that zinc oxide when illuminated by ultraviolet light causes chemical oxidations and reductions. For example, Eibner in 1911[3] found that the reduction of Prussian blue (in the presence of sugars) takes place when zinc oxide is illuminated. Baur and Neuweiler in 1927[4] showed that ultraviolet-irradiated zinc oxide produces hydrogen peroxide from oxygen and water. The literature on the photocatalytic properties of zinc oxide is quite extensive (see, for example, ref 5 and 6) but is usually

---

[1] Work supported by the U. S. Atomic Energy Commission under Contract AT (30-1)-2206. Presented at the International Conference on Photosensitization in Solids, Chicago, Ill., June 23, 1964.

of a descriptive nature. Furthermore, no conclusive experiments regarding the mechanism of the reaction have been presented.

The purpose of the present work is to carry out some quantitative rate studies of indophenol reduction with a single sample of zinc oxide whose chemical content and luminescence properties[7] are known, where the atmosphere is controlled, and the products of the reaction are characterized.

Zinc oxide is an important industrial material (*e.g.*, as a filler in rubbers) and is known to cause photocatalytic destruction.[5] It also serves as a photocatalyst for the initiation of vinyl polymerization,[8] the detailed mechanism of which is treated elsewhere.[9] Excitation of zinc oxide by X-rays is similar in its effects to ultraviolet excitation,[7] and in the present work some comparisons of the chemical effects produced by these two types of radiation are considered.

Experimental Procedures and Results

A. Materials and Radiation Sources. Throughout we have used a highly pure zinc oxide (Type SP-500) obtained from the New Jersey Zinc Co. This material which is produced by the French process has as its greatest impurity calcium in 10 ppm (iron in 1 ppm). All other materials were obtained from Fisher Scientific Co. or from Eastman Chemical Co. and were, when possible, purified by repeated crystallization.

The principal ultraviolet source used was a GE 100-w AH4 mercury lamp in conjunction with a Wood's glass filter to isolate the 365-mμ lines to give an intensity incident on the sample of 4×10^{-10} einstein/cm^2 sec, as measured on a calibrated thermopile (Eppley Laboratories). For wavelength-dependence studies this lamp and a 100-w intermediate pressure mercury lamp (Hanovia SH) were used (without a filter) with a Bausch and Lomb grating monochrometer. The X-ray source employed was a tungsten target Machlett tube operated at 50 kw and 10 ma to give an intensity at the surface of the sample of 8000 rads/hr.

B. Reduction of Indophenol. In order to examine the photoreducing property of zinc oxide, sodium 2,6-dichlorobenzenone was employed as the indicator. This indophenol absorbs maximally at 600 mμ above pH 6 with a molar extinction coefficient of 1.80×10^4. At pH 7 its oxidation reduction potential is 0.217 v.[10] On reduction it becomes colorless (note: the colored and the colorless species have molar extinction coefficients at 365 mμ of 3.7×10^3 and 2.1×10^3, respectively). The dye alone is photochemically inactive and the reduced species can be completely reoxidized by air to the colored species.

The zinc oxide powder (average particle diameter 0.3 μ) was added to an aqueous indophenol solution and was flushed with purified nitrogen 20 min prior to and during the irradiation accompanied by magnetic stirring. At various times an aliquot sample was withdrawn and centrifuged in a chemical centrifuge. The absorption at 600 mμ of the clear supernatant was then determined. No appreciable amount of dye was adsorbed to the zinc oxide powder.

In Figure 1A is shown the quantum yield of photoreduction of indophenol as a function of wavelength of exciting light. For the calculation of quantum yield, we have assumed that all of the incident light is totally absorbed by the zinc oxide and the small light filtering effect of the dye in the ultraviolet range is also corrected. It is of interest to compare this result with the reflectance spectrum (Figure 1B) of the zinc oxide sample, as determined on a Perkin-Elmer spectrophotometer.

The rate of photoreduction of indophenol as function of amount of zinc oxide added is given in Figure 2. The rate was found to be independent of the indophenol concentration within the concentration range 10^{-4} *M* and to be proportional to the first power of the intensity (varied by the introduction of fine-mesh wire screens). When the exciting light is removed, the reaction stops immediately (the time scale is on the order of minutes), *i.e.*, there is no posteffect, and it commences immediately when the light is turned on. From a study of the temperature dependence of the rate, it was found that the reaction has an over-all activation energy of 1.2 kcal/mole.

Phosphate ions but not phthalate ions stop the photoreduction. It was noticed that an aqueous suspension of zinc oxide which normally is at pH 7.4 becomes acidic (down to pH 6.8) on illumination.

C. Reduction of Diphenylpicrylhydrazyl. A zinc oxide suspension in organic solvents (benzene, carbon tetrachloride, and chloroform) will on irradiation with

---

(2) Taken in part from the dissertation of M. Yamamoto submitted to the faculty of the Polytechnic Institute of Brooklyn in partial fulfillment of the requirements for the degree of Doctor of Philosophy, June, 1966.

(3) A. Eibner, *Chem. Z.*, **35**, 786 (1911).

(4) E. Baur and C. Neuweiler, *Helv. Chim. Acta*, **10**, 901 (1927).

(5) C. Ellis, A. A. Wells, and F. F. Heyroth, "The Chemical Action of Ultraviolet Rays," Reinhold Publishing Corp., New York, N. Y., 1941.

(6) H. E. Brown, "Zinc Oxide Rediscovered," New Jersey Zinc Co., New York, N. Y., 1957.

(7) G. Oster and M. Yamamoto, *J. Appl. Phys.*, **37**, 823 (1966).

(8) M. C. Markham and K. J. Laidler, *J. Phys. Chem.*, **57**, 363 (1953).

(9) M. Yamamoto and G. Oster, *J. Polymer Sci.*, **A-14**, 1683 (1966).

(10) W. M. Clark, "Oxidation-Reduction Potentials of Organic Systems," The Williams & Wilkins Co., Baltimore, Md., 1960, p 130.

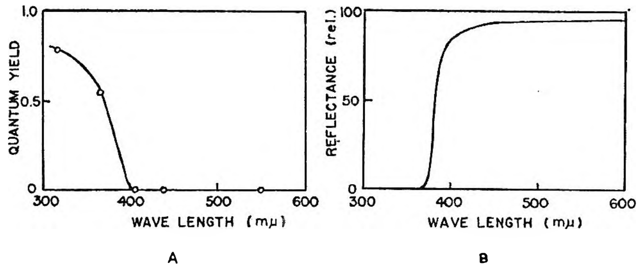

Figure 1. (A) Spectral dependence of the quantum yield of zinc oxide sensitized indophenol photoreduction. Indophenol concentration 7.6 × 10^{-5} M; zinc oxide concentration 1.5 g/l.; temperature 30°. (B) Diffuse reflectance spectrum of zinc oxide. Reflectance standard: MgO.

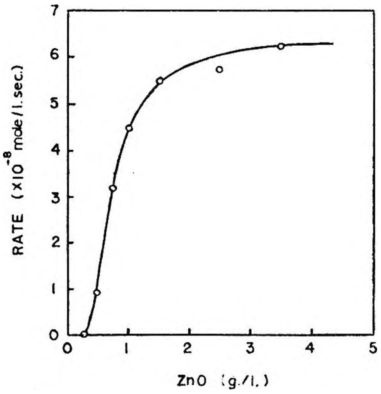

Figure 2. Rate of indophenol photoreduction *vs.* amount of zinc oxide added. Indophenol concentration 7.6 × 10^{-5} M; temperature 30°.

ultraviolet light cause 2,2-diphenyl-β-picrylhydrazyl (DPPH) to become discolored. More specifically, the maximum at 520 mμ (molar extinction coefficient of 1.3 × 10^4) is decreased and a yellow product is obtained. Water is essential for this reaction. Thus the reaction will not proceed for carefully dried (sodium-treated) benzene. On addition of small amounts of water, the rate increases proportionally to the water content. In these studies oxygen was rigorously excluded from the solution. Prior heating at 300° of the zinc oxide *in vacuo* had no effect on the rate of reduction of DPPH.

The products of the reduction of DPPH in various solvents were examined. Chromatographic separation (on paper using a pentane and carbon disulfide mixture, 1:1) revealed that only one product was produced (R_f 0.988 for DPPH and R_f 0.970 for the product, which corresponds to diphenylpicrylhydrazine). This product absorbs maximally at 320 mμ in ethanol or in benzene. The infrared absorption spectrum of the product in KBr pellets shows a strong peak at 3.04 μ regardless of the solvents in which the DPPH was photoreduced, which can be assigned to the NH group in diphenylpicrylhydrazine. On treatment of the product with PbO_2 one easily obtains DPPH.

Although X-rays will cause the decoloration of DPPH in carbon tetrachloride, the reaction proceeds much more rapidly in the presence of zinc oxide. Here again the process is accelerated with trace amounts of water and the product obtained was diphenylpicrylhydrazine.

D. Reduction of Metal Ions. Silver ion (in the form of the nitrate) in aqueous solution is rapidly reduced in the presence of zinc oxide under ultraviolet irradiation,[11] and we found that the reaction proceeds at an increased rate even when red light is used, although silver metal deposits gradually at very slow rate in the dark. The product is colloidal metallic silver. With ionizing radiation the product is discernible with dosages as low as 100 rads.

Mercuric ion (in the form of mercuric chloride) in aqueous solution is likewise photoreduced with zinc oxide to give grayish colloidal mercury,[11] but in the presence of oxygen one obtains a brownish product which is probably mercuric oxide, and on further irradiation colloidal mercury is obtained.

E. Oxidations. Chemically reduced crystal violet (reduced by sodium hydrosulfite) in aqueous solution is readily oxidized to give the colored dye on illumination of zinc oxide. This reaction proceeds only in the presence of oxygen. The oxidation is visible with X-rays of dosages as low as 100 rads. Zinc oxide in aqueous solution also serves as a photocatalyst for the rapid oxidation of *p*-toluenediamine (to give a brownish product) if oxygen is present.

These oxidations can be ascribed to the formation of hydrogen peroxide. This reaction requires the presence of both oxygen and water. Even prior heating at 300° *in vacuo* of zinc oxide does not sufficiently remove oxygen to stop the reaction.[7] However, zinc oxide treated in this manner becomes a better photocatalyst for the production of hydrogen peroxide (as shown by iodometric titration) if oxygen is added to the aqueous suspension.

Discussion

Many of our results can be interpreted in terms of the photochemical transformation of zinc oxide to zinc (photolysis of zinc oxide). For example, metallic zinc (first treated with HCl to remove the passive layer) will reduce in the absence of oxygen all of the compounds described in this work. In the presence of oxygen metallic zinc with moisture will produce hy-

---

[11] E. Baur and A. Perret, *J. Chim. Phys.*, **23**, 97 (1926); G. A. Korsunovskii, *Zh. Fiz. Khim.*, **39**, 2136 (1965).

drogen peroxide. This autoxidation of zinc as well as the decomposition of hydrogen peroxide with metallic zinc has been known for many years.[12] In this case zinc cannot be in the metallic state but rather exists as zinc atoms, since prolonged irradiation of zinc oxide does not produce colloidal coloration as is the case with, for example, silver salts.

A more favorable scheme is the formation of zinc ion on zinc oxide surface under ultraviolet irradiation. The concentration of zinc ions in solution is increased when an aqueous zinc oxide suspension is illuminated.[13] Since our work does not show postirradiation effects, produced zinc ion is very unstable and may not accumulate. The decrease in pH observed with illumination of zinc oxide suspensions is compatible with this result. The inhibitory effect of phosphate ion may be a complexation of photochemically produced zinc ion. In terms of the electronic theory of photoconductivity of zinc oxide,[14] this can be interpreted that ultraviolet excitation produces electrons and holes, the latter having very low mobility (*i.e.*, n-type conductivity), and the electrons in the conduction band can transfer to other molecules at the surface of the solid. Hence, the excited zinc oxide solid serves as an electron donor. Ultraviolet light causes a desorption of oxygen from the surface of zinc oxide.[13] This would allow direct exposure of the surface to the solvent and hence allow the reaction of zinc ions of the solid with, for example, water or oxygen to take place. It is of interest to note that oxygen quenches the photoconductivity as well as the luminescence of zinc oxide. The quenching effect is considerably greater if water vapor is added to the oxygen.[7] Apparently, the formation of hydrogen peroxide removes electrons which would normally recombine with holes.

The rate of the photochemical reduction as a function of exciting wavelength (Figure 1A) follows the absorption spectrum of zinc oxide as seen from the reflection spectrum (Figure 1B). The absorption edge of 380 mμ is not infinitely sharp and has a tail into the visible range. This is seen from the silver reduction experiments where extremely small amounts of reduced silver are detectible by eye. In this connection, we have found that red light will quench the low-temperature phosphorescence (as well as thermoluminescence) of zinc oxide[7] indicating appreciable absorption in the long-wavelength region.

The form of the rate curve as a function of zinc oxide concentration (Figure 2) arises from photometric considerations. For low concentrations of the solid much of the incident light is lost by scattering. For the higher concentrations employed, the suspension is so dense the reaction is confined to the front surface and hence the rate is practically independent of the solid content. The fact that the quantum yield is independent of intensity in the range employed shows that the reaction on zinc oxide surface is very rapid and not diffusion limited. The independence of the rate on indophenol concentration indicates merely that the concentration of the indicator is much higher than the concentration of active sites produced on the zinc oxide surface at any moment. The small activation energy observed may be associated with energy of electron transfer.

---

(12) M. Traube, *Ber.*, **26**, 1471 (1893).

(13) G. V. Elmore and H. A. Tanner, *J. Phys. Chem.*, **60**, 1328 (1956); B. Beranek, E. Barton, K. Smrceck, and I. Sekerka, *Collection Czech. Chem. Commun.*, **25**, 369 (1960).

(14) See, for example, J. T. Law in "Semiconductors," N. B. Hanney, Ed., Reinhold Publishing Corp., New York, N. Y., 1959.

Surface Tension of Liquid Uranium and Thorium Tetrafluorides and a Discussion on the Relationship between the Surface Tension and Critical Temperature of Salts[1]

by **A. D. Kirshenbaum and J. A. Cahill**

Research Institute of Temple University, Philadelphia, Pennsylvania 19144 *(Received August 16, 1965)*

The surface tension of liquid uranium and thorium tetrafluorides was measured by the maximum bubble pressure method. The salts were contained in molybdenum crucibles and pressure measurements made with capillary-tipped molybdenum tubes. The surface tension of water and liquid sodium chloride was satisfactorily measured prior to measuring the fluorides. The probable error of the values obtained is ±5 dynes/cm. Approximately 25 surface tension measurements were made on each salt and the least-mean-square equations fitting the data are σ_{UF_4} (dynes/cm) = $447 - 19.2 \times 10^{-2}T$ (°K) and σ_{ThF_4} (dynes/cm) = $461 - 16.12 \times 10^{-2}T$ (°K). The surface tension–temperature functions of salts, metals, and homopolar substances are discussed in relation to their behavior near the critical temperature.

Introduction

The purpose of this study was to adapt the conventional maximum bubble pressure method, which has been used to measure surface tensions reliably at moderately high temperature (≃1000°K) for use in determining surface tensions to 2000°K and above. A critical discussion of the theory of the maximum bubble pressure method has been outlined by Harkins.[2] Jaeger[3] developed a technique with this method which made possible the precision measurement of the surface tensions of salts to 1600°. Since Jaeger's contribution, interest in surface tension measurements of liquid salts has generally been confined to temperatures below 1000°K.

Usually platinum, rhodium, or their alloys are used as bubble tips; however, they could not be used for these studies owing to their low melting point. Tube materials that could be used above 2000°K are tantalum, tungsten, and molybdenum, melting at 3270, 3650, and 2890°K, respectively. Molybdenum was chosen because of its relative ease of fabrication and availability. It was also desirable from a chemical standpoint since it was successfully used to determine the densities of several salts including UF_4 and ThF_4.[4] Since the latter salts boil at 1723 and 1953°K, respectively, and no surface tension data on them were available, we selected them for initial surface tension measurements in the range of 2000°K.

Apparatus and Procedure. The apparatus shown in Figure 1 was described in detail recently in connection with the surface tension of liquid uranium.[5] In these studies, molybdenum tubes and crucibles were substituted for their refractory oxides counterparts. A molybdenum capillary tip 1.5-mm o.d. × 0.8 mm i.d. × 1 cm long was machined on a plug which was welded to a molybdenum tube 0.94 cm o.d. × 1 mm wall, 45 cm long. The diameter of the capillary tip was measured with a calibrated microscope with an accuracy of ±6 μ.

---

[1] This work was supported by the U. S. Atomic Energy Commission under Contract AT(30-1)-2082.

[2] W. D. Harkins, "Physical Methods of Organic Chemistry," Part I, 2nd ed, A. Weissberger, Ed., Interscience Publishers, New York, N. Y., 1949, pp 355–425.

[3] F. M. Jaeger, "Optical Activity and High Temperature Measurements," McGraw-Hill Book Co., Inc., New York, N. Y., 1930, pp 252–277.

[4] A. D. Kirshenbaum and J. A. Cahill, *J. Inorg. Nucl. Chem.*, **19**, 65 (1961).

[5] J. A. Cahill and A. D. Kirshenbaum, *ibid.*, **27**, 73 (1965).

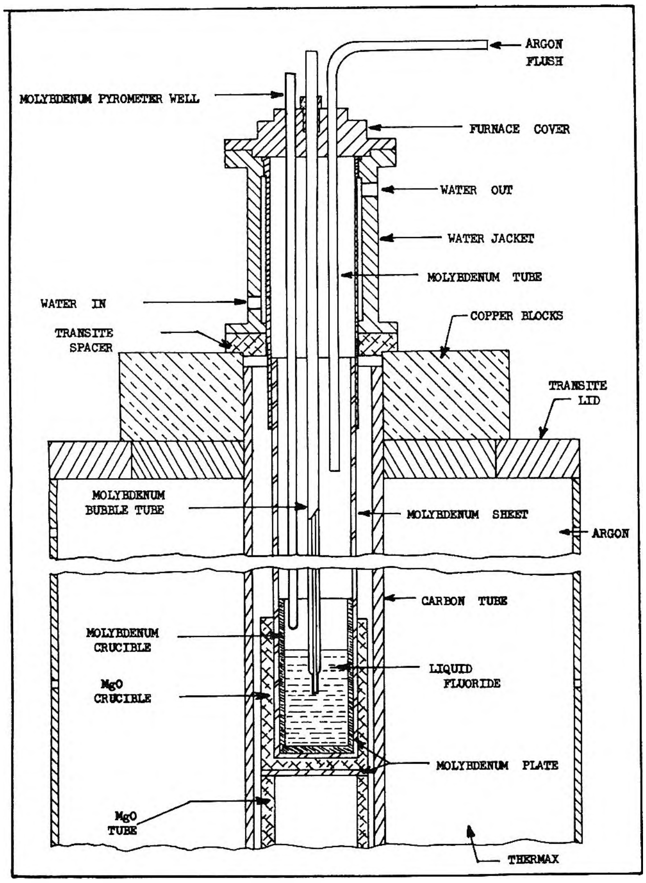

Figure 1. Surface tension apparatus.

The procedure consisted of bringing the melt to temperature in the apparatus shown in Figure 1 under a few centimeters of argon pressure. Trace amounts of N, O, and H_2O were removed from the argon by passing it through titanium flakes maintained at 400°. The molybdenum capillary tip was then lowered into the furnace just above the melt while argon was flushed through it at a rate of 60 bubbles/min. The capillary tip was placed $\simeq$1.5 cm below the surface of the melt along with the pyrometer well. The relative heights of the capillary tube and an adjustable $^1/_{16}$-in. diameter molybdenum rod (not shown in Figure 1) were measured with a cathetometer when the rod completed a 6-v circuit upon contacting the melt. In this way, the exact depth of immersion of the capillary tip could be measured from the relative height difference and their actual length difference measured at room temperature.

The temperature was measured under black-body conditions in the molybdenum pyrometer well with a previously calibrated optical pyrometer.[6] The argon flow to the capillary was reduced to 10 bubbles/min, while the maximum bubble pressure was read on a water manometer. The measured maximum pressure was converted to centimeters of UF_4 or ThF_4 using previously determined[4] density values described by the following equations.

$$D_{UF_4} = 7.784 - 9.920 \times 10^{-4}T\ (°K)$$

$$D_{ThF_4} = 7.108 - 7.590 \times 10^{-4}T\ (°K)$$

Yound and his associates[7,8] found that if a bubble is allowed to form slowly, its shape corresponds to a static bubble and an accurate measurement of the maximum pressure is possible. From these measurements and by employing the equation of Schroedinger,[9] one can calculate the surface tension

$$\sigma\ (\text{dynes/cm}) = \frac{a^2 d_t g}{2}$$

where d_t = density of the melt at operating temperature in g/cc, $g = 980$ cm/sec^2, $a^2 = rh_0[1 - {}^2/_3 r/h_0 - {}^1/_6 (r/h_0)^2 + \cdots]$, r = radius of tip = i.d./2, $h_0 = (H - L)$, where L is the length of the capillary tip immersed and $H = (P_{max})(D_{H_2O})/d_t$ (P_{max} = maximum bubble pressure read on manometer and D_{H_2O} = density H_2O at ambient temperature in g/cc).

The apparatus was first tested using water and NaCl, and satisfactory agreement with the values of Jaeger[3] was obtained. The capillary tips were inspected after each run and redrilled, reground, and polished with crocus cloth prior to use. A smooth round hole centered in the unscratched face of the capillary tip was visible under 60× magnification. All precautions necessary for precision measurement of surface tensions recently outlined by White[10] were adhered to in these measurements.

Materials Used. Nuclear purity anhydrous uranium and thorium tetrafluorides containing 99.5 to 99.9% fluoride were used. The chief impurities were UO_2F_2 and ThO_2, respectively. Analysis of the UF_4 melts after the runs indicated the presence of 0.5 to 1 wt % UO_2F_2, whereas a check analysis of the starting material showed 0.21 wt % UO_2F_2. Surface tension data obtained from the melts which contained 0.5 and $\simeq$1 wt % UO_2F_2 indicate that the effect of this impurity in concentrations up to 1 wt % is within the accuracy of the measurements, *i.e.*, ±3%. Similar concentrations of ThO_2 in the ThF_4 melts are to be expected. X-Ray powder diffraction patterns of the ThF_4 melt did

---

(6) A. D. Kirshenbaum and J. A. Cahill, *J. Inorg. Nucl. Chem.*, **25**, 232 (1963).

(7) M. Hoffman, M.S. Thesis, University of Chicago, 1926.

(8) H. P. Tripp, Ph.D. Thesis, University of Chicago, 1934.

(9) E. Schroedinger, *Ann. Phys.*, **46**, 413 (1915).

(10) D. W. G. White, *Am. Soc. Metals, Trans. Quart.*, **55**, 757 (1962).

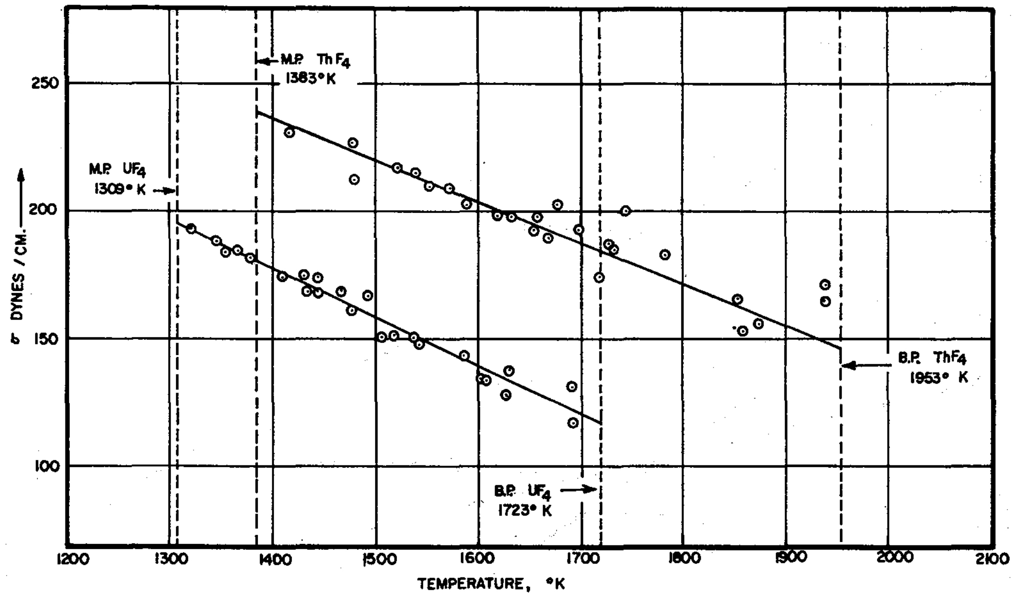

Figure 2. Surface tension of ThF_4 and UF_4 *vs.* temperature.

not reveal any lines of ThO_2 that were not also given by anhydrous ThF_4, and eight of the principal lines of ThO_2 did not appear. The concentration of ThO_2, then, must have been 1% or less, the detection limit for powder diffraction patterns. Microscopic examination of the molybdenum crucible and the molybdenum melt interface indicated no reaction took place here with molybdenum and either UF_4 or ThF_4. No molybdenum, in any form, was found in either salt by chemical analysis, and the wall thickness of the molybdenum crucibles did not decrease after being in contact with the liquid fluorides for even a few hours.

Results

Twenty-five values were determined for each salt between their melting and boiling points. A least-mean-square treatment of the respective data gave the following equations.

$$\sigma_{UF_4}\ (\text{dynes/cm}) = 447 - 19.20 \times 10^{-2}T\ (^\circ\text{K})$$

$$\sigma_{ThF_4}\ (\text{dynes/cm}) = 461 - 16.12 \times 10^{-2}T\ (^\circ\text{K})$$

The probable error of these measurements is ±5 dynes/cm. The experimental results are plotted in Figure 2 and the smoothed data calculated from the equations are shown in Table I. These values are the only ones now available for the surface tension of UF_4 and ThF_4.

Discussion

Critical temperatures of 3150 and 3525°K were estimated for UF_4 and ThF_4, respectively, by the method previously outlined,[11] *i.e.*, from our liquid density data,[4] the ideal vapor density, and the law of rectilinear diameter, and hence represent an upper limit for T_c. The critical temperature, T_c, of organic and inorganic substances which obey the law of corresponding states can be related to the surface tension by the well-known empirical equation

$$\sigma = \sigma_0(1 - T_r)^N \qquad (1)$$

where σ_0 is the extrapolated surface tension at 0°K, $N = {}^{11}/_9$, and T_r is the reduced temperature (T/T_c). The above equation or its linear form ($N = 1$) also applies to most liquid metals;[12] however, neither of those forms applies to salts.

The surface tension of homopolar liquids can be

Table I: Smoothed Surface Tension Data for UF_4 and ThF_4

UF_4		ThF_4	
Temp, °K	σ, dynes/cm	Temp, °K	σ, dynes/cm
1309 (mp)	195	1383 (mp)	238
1400	178	1500	219
1500	159	1600	203
1600	140	1700	187
1723 (bp)	116	1800	171
		1900	155
		1953 (bp)	146

---

[11] A. V. Grosse, *J. Inorg. Nucl. Chem.*, **22**, 23 (1961).

[12] A. V. Grosse, *ibid.*, **24**, 147 (1962).

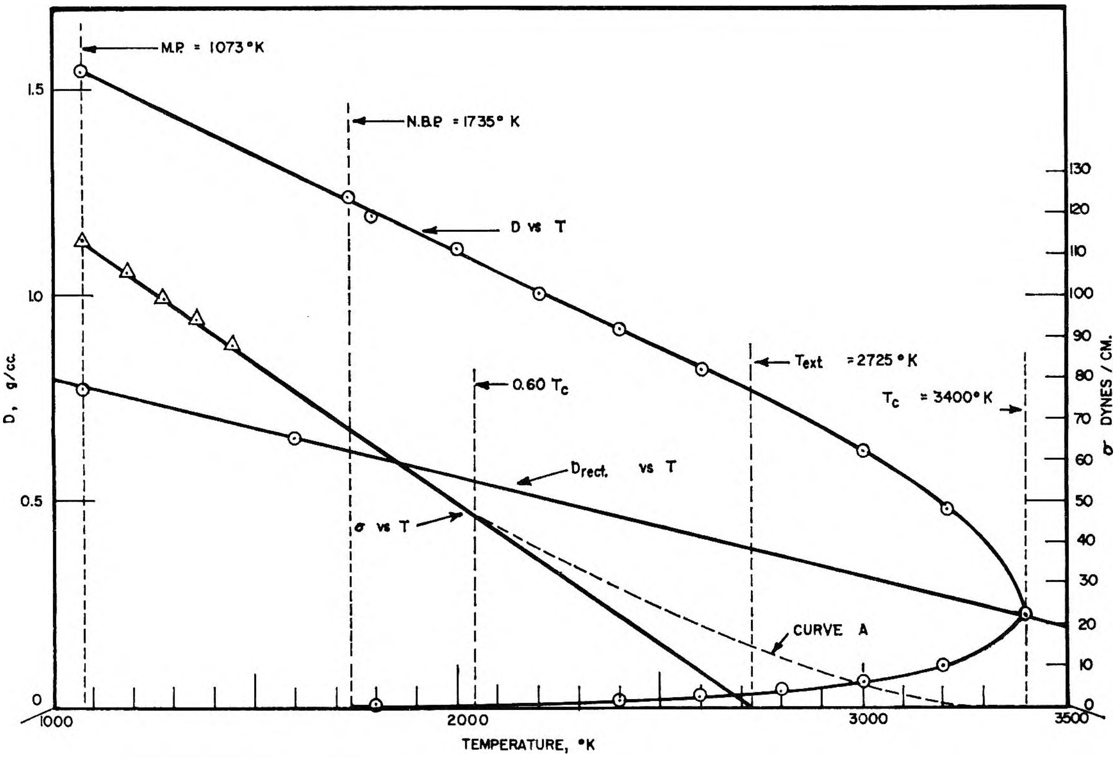

Figure 3. Comparison of T_c and T_{ext} for NaCl.

related to their critical temperature by Eotvos' law, expressed by

$$\sigma_T = K\frac{(T_c - T)}{(V_m)^{2/3}} \quad (2)$$

where $K = 2.12$ ergs/(mole$^{2/3}$ °K), σ_T = the surface tension in dynes/cm, and V_m = molar volume in cc/mole at T°K. Recently Grosse[12] has shown that the Eotvos law can be applied to many liquid metals if the constant, $K = 2.12$ ergs/(mole$^{2/3}$ °K), is replaced by $C = 0.64$ erg/(mole$^{2/3}$ °K), and σ and V_m replaced by their respective values extrapolated to 0°K, *i.e.*, σ° and V_m°. The Eotvos relation then becomes

$$\sigma^\circ = C\frac{T_c}{(V_m^\circ)^{2/3}} \quad (3)$$

No correlation can be made between σ and T_c for salts with either eq 2 or 3. However, the quantity C or $\sigma^\circ(V_m^\circ)^{2/3}/T_c$ in erg/(mole$^{2/3}$ °K) from eq 3 gives a series of values for the salts listed in Table II that are consistent with their relative ionic strength. Also shown is the ratio of T_c/T_{bp}.

The most ionic salt, LiF, gives a value of C lower than was found for liquid metals, that is, $C = 0.64$ erg/(mole$^{2/3}$ °K), while $BiCl_3$ has a C value much closer to what could be expected for a molecular substance. When the surface tensions of many organic and inorganic liquids as well as liquid metals are extrapolated linearly to 0 dynes/cm, the temperatures reached closely approach T_c. Hereafter the temperature arrived at by such an extrapolation will be designated T_{ext}. Values of T_{ext} for ThF_4 and UF_4 were 655 and 880°K, or 20 and 25% lower than their respective critical temperatures estimated from density data. Similar differences were noted between T_{ext} and T_c for the alkali halides using Jaeger's surface tension data[3] and previously estimated values for T_c.[13] A comparison of T_c and T_{ext} for the above salts and also for $BiCl_3$, whose critical temperature was recently directly observed,[14] is shown in Table III. T_{ext} was obtained from the surface tension data of Bradhurst and Buchanan.[15] In view of the large differences

Table II

	LiF	NaF	NaCl	KCl	ThF_4	UF_4	$BiCl_3$
C	0.465	0.493	0.505	0.603	1.61	1.66	1.90
T_c/T_{bp}	2.12	2.16	1.96	1.91	1.83	1.82	1.65

---

(13) A. D. Kirshenbaum, J. A. Cahill, P. J. McGonigal, and A. V. Grosse, *J. Inorg Nucl. Chem.*, **24**, 1287 (1962).

(14) J. W. Johnson and D. Cobicciotti, *J. Phys. Chem.*, **68**, 2235 (1964).

Table III

Salt	LiF	NaF	NaCl	KCl	ThF_4	UF_4	$BiCl_3$
T_c	4140	4270	3400	3200	3525	3150	1178
T_{ext}	3220	3150	2725	2400	2860	2380	1005
T_{ext}/T_c	0.78	0.74	0.79	0.75	0.81	0.74	0.85

between T_c and T_{ext} and the fact that σ must be 0 at T_c, the surface tension–temperature function of salts may curve at much lower reduced temperatures than do the σ *vs.* T functions of homopolar liquids or liquid metals, which are linear practically all the way to T_c. Figure 3 illustrates the marked difference between T_c and T_{ext} for the particular case of NaCl. Recent measurements[16] on the electrical conductivity of $BiCl_3$ show that the conductivity reaches a maximum at about $0.6T_c$ and then decreases with increasing temperature. This behavior, which is attributed to the formation of molecules in the liquid phase at and above $0.6T_c$ for $BiCl_3$, can be expected for salts generally. As the critical temperature of salts is approached and the number of molecules increases, salts will behave more like molecular liquids. Since a transition from ionic to van der Waals type bonding occurs, the surface tension, a property which depends on the forces of attraction present, is also likely to be affected. An actual measurement of the surface tension between the normal boiling point and the critical temperature of a typical salt like NaCl to determine this effect would be a demanding task. A possible shape for the σ *vs.* T function for salts in this latter temperature range is shown in Figure 3 by curve A which could also curve off the σ *vs.* T line at reduced temperatures greater than $0.6T_c$. The orthobaric and mean densities of NaCl shown in Figure 3 have been previously presented.[13]

Methods for either directly or indirectly measuring or calculating the surface tension at these high temperatures are under consideration.

Acknowledgment. The authors thank Dr. A. V. Grosse for his helpful comments and suggestions throughout the course of this work.

---

(15) D. A. Bradhurst and A. S. Buchanan, *Australian J. Chem.*, **14**, 409 (1961).

(16) F. Grantham and S. J. Yosim, *J. Phys. Chem.*, **67**, 2506 (1963)

Thermodynamics of Binary Alloys. II. The Lithium–Tin System[1]

by Melvin S. Foster, Carl E. Crouthamel, and Scott E. Wood

Chemical Engineering Division, Argonne National Laboratory, Argonne, Illinois *(Received January 10, 1966)*

Electromotive force measurements have been made on cells which may be represented as Li|LiCl–LiF|Li in Sn (l, X_{Li} = atom fraction of Li). The alloy compositions varied from $X_{\mathrm{Li}} = 0.1$ to Sn saturated with solid Li_5Sn_2. The temperature range was 800 to 1050°K. A secondary reference electrode which consisted of liquid Bi saturated with solid Li_3Bi was used in many of the measurements. An equation relating the excess chemical potential of Li in binary Li–Sn alloys as a function of temperature and composition for the region studied was derived by a least-squares treatment. The standard free energy of formation of solid Li_5Sn_2 has also been calculated.

Introduction

Concentration cells without transference consisting of a lithium anode and a lithium–tin alloy cathode may be applicable either in a regenerative galvanic cell system or as a primary or secondary battery.

The merits of lithium as the most active component of the binary system have been discussed in an earlier work.[2] The ability of lithium to form relatively stable intermetallic compounds with many of the more noble elements is one of its chief advantages. The stability of these compounds produces cell voltages in concentration cells without transference which are substantially larger than those predicted from ideal solution theory.

One of the elements which forms stable stoichiometric intermetallic compounds with lithium is tin. The phase diagram of the lithium–tin systems as given by Hansen and Anderko[3] shows that six stoichiometric compounds are formed. The compound Li_7Sn_2 is reported to have the highest melting point, 783°.

The potentials of cells without transference have been measured, using cathode compositions between pure tin and 0.30 atom fraction tin in lithium and in the temperature range between 502 and 720°. In this region, the cathode consisted of either a one-phase liquid alloy or a liquid alloy of tin saturated with pure solid Li_5Sn_2.

Experimental Section

Materials. The electrolyte used in these studies was the same as described in ref 2. The eutectic composition of 70 mole % LiCl–30 mole % LiF was made by weighing reagent grade and relatively anhydrous salts in air and further purified by chlorine treatment of the melt, flushed with pure helium, and then evacuated, sealed, and transferred in a Pyrex container to an inert-atmosphere box. The helium atmosphere in the box was continuously recirculated and repurified during the course of the experiments as previously described.[2]

Lithium metal was obtained from the Foote Mineral Co., Philadelphia, Pa., in the form of 1-lb ingots sealed in cans under an argon atmosphere. The impurity analysis supplied by the Foote Mineral Co. was 0.003% Na, 0.0028% K, 0.003% Cl, and 0.0031% N_2. From the J. T. Baker Chemical Co., Phillipsburg, N. J., tin metal was obtained in shot form. The impurity analysis supplied by Baker was As, 0.2 ppm; Cu, 5 ppm; Fe, 30 ppm; Pb, 30 ppm; and Zn, 5 ppm.

Apparatus and Procedures. The cells used in this investigation were the same as those described in ref 2. A porous beryllia crucible was used to contain the anode or cathode and to minimize the effect of lithium and intermetallic compound solubility in the electrolyte. All electrode alloys used were prepared by combining appropriate weighed quantities of the elements in the inert-atmosphere box.

Because of the previously observed experimental

---

[1] This work was performed under the auspices of the U. S. Atomic Energy Commission.

[2] M. S. Foster, S. E. Wood, and C. E. Crouthamel, *Inorg. Chem.*, 3, 1428 (1964).

[3] M. Hansen and K. Anderko, "Constitution of Binary Alloys," McGraw-Hill Book Co., Inc., New York, N. Y., 1958, p 904.

fact that lithium metal transferred from an anode of pure liquid lithium to a liquid alloy cathode at rates sufficient to preclude stable, reproducible cell potential measurement, the original intent was to use as a reference electrode a tin alloy saturated with solid Li_5Sn_2 (over-all composition of 0.30 atom fraction of tin). This is analogous to the reference electrode of a bismuth alloy saturated with Li_3Bi (over-all composition of 0.40 atom fraction of bismuth) that had been used in studies of the Li–Bi system.[2] When cells consisting of a lithium anode and a saturated cathode alloy (over-all composition of 0.30 atom fraction of tin) were operated, the voltages observed appeared to be stable at constant temperature, but the reversible cell voltage was difficult to ascertain because of the slow response of cell voltage with change of temperature. Many points required 10 hr to achieve equilibrium. Before doing further experimental work in this system, it was decided to check the electrode consisting of liquid tin saturated with solid Li_5Sn_2 against the electrode of liquid bismuth saturated with Li_3Bi and, if possible, to apply the latter as the reference electrode in further studies. This check was accomplished without any difficulty other than the slow approach to equilibrium mentioned above. The voltages obtained, combined with the reference electrode potentials established,[2] yielded identical results, within experimental error, when compared with those obtained with a pure lithium anode. Thus, the reference electrode used in these studies consisted of an alloy of bismuth saturated with Li_3Bi. In this cell, a species of Li_3Bi is the most soluble entity in the electrolyte (approximately one order of magnitude greater than any Li–Sn species). Lithium metal solubility in the electrolyte, however, was negligible in the absence of the pure liquid lithium anode. The stability of the cell potential with time and with temperature cycling indicated that changes of electrode potential by any irreversible transfer of these species was negligible.

Results

The cell potential–temperature–composition data for single-phase liquid lithium–tin alloys were obtained from two types of cell: (1) Bi(l) saturated with $Li_3Bi(s)|LiCl–LiF|Li$ in Sn(l, X_{Li}), where X_{Li} = (atom fraction of Li in Sn) = 0.10, 0.20, 0.30, 0.40, 0.50, 0.60 and 0.65; and (2) Li(l)|LiCl–LiF|Bi(l) saturated with $Li_3Bi(s)$. Adding the potentials of type 1 and type 2 cells at a given temperature yields the potential of a third type of cell: (3) Li(l)|LiCl–LiF|Li in Sn(l, X_{Li}).

The potentials of cells of type 3 are shown in Figure 1 as a function of temperature at several cathode compositions (the experimental points are in circles).

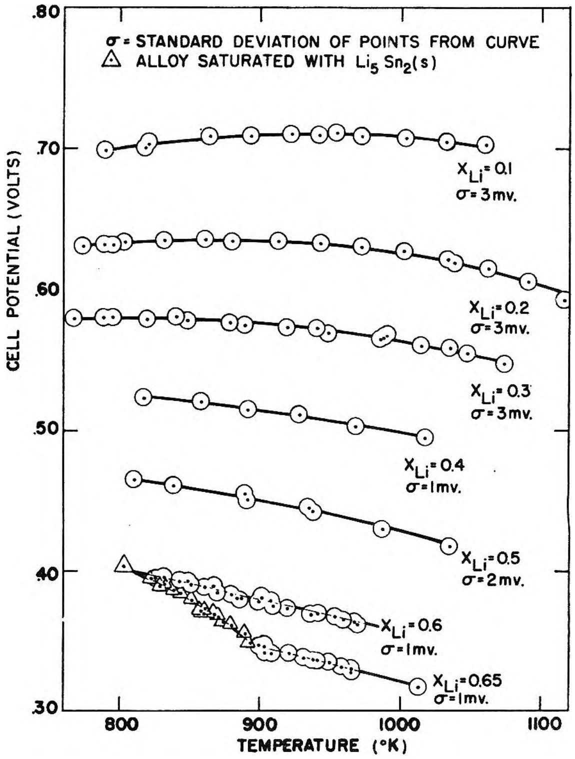

Figure 1. Voltage–temperature–composition data for the cell Li(l)|LiCl–LiF|Li in Sn(l, X_{Li}) (X_{Li} = atom fraction of Li).

Also shown in the figure (the experimental points are in triangles) is the potential of type 4 cell: (4) Li(l)|LiCl–LiF|Sn saturated with $Li_5Sn_2(s)$.

The smooth curve for each composition represents the cell potential as a linear or quadratic function of temperature. This function was derived by a least-squares treatment of the data. The standard deviation, σ, of the individual experimental points from the smooth curve is indicated.

The cell reaction for type 3 cells may be written as the transfer of lithium from pure lithium (saturated with electrolyte) to the alloy, for which the change in the Gibbs free energy is

$$\Delta G = -FE = RT \ln a_{Li} \tag{1}$$

where F is the value of the Faraday, E is the cell potential, R is the gas constant, T is the absolute temperature, and a_{Li} is the activity of lithium in liquid tin alloy. The standard state of lithium is taken to be the pure liquid metal in the cell environment, *i.e.*, saturated with electrolyte, at the temperature of interest. The excess chemical potential of lithium in the liquid alloy is then given by the relationship

$$\Delta\mu_{Li}^{E} = -FE - RT \ln X_{Li} \tag{2}$$

The values so calculated were fitted by a least-squares method to the equation

$$\Delta\mu_{\mathrm{Li}}{}^{\mathrm{E}} = \sum_{i=1}^{3}(a_i + b_iT + c_iT^2)X_{\mathrm{Li}}{}^{i-1} \qquad (3)$$

where the data for each composition were weighted equally according to the number of experimental values for that composition. The values of the constants are shown in Table I. The standard deviation of the observed cell potentials from the values indicated by this equation was 0.5 mv.

Table I: Coefficients Used in Evaluating Eq 3

	$i = 1$	$i = 2$	$i = 3$
a_i	2018.75	−38,187.4	33,403.92
b_i	−35.5044	84.9183	−53.6456
c_i	0.021445	−0.044818	0.030409

The curves shown in Figure 2 represent the calculated values for $\Delta\mu_{\mathrm{Li}}{}^{\mathrm{E}}$ from eq 3 as a function of composition at temperatures of 800 and 950°K. The experimental points shown were calculated from the smooth curves in Figure 1. Also shown for comparison in Figure 2 are the values for $\Delta\mu_{\mathrm{Li}}{}^{\mathrm{E}}$, calculated from the composition of the liquid phase indicated by the published phase diagram[3] and the cell potential obtained from a type 4 cell (cathode saturated with solid $\mathrm{Li_5Sn_2}$). It must be emphasized that the region of the applicability of eq 3 extends only over that portion of the phase diagram in which tin-rich, unsaturated alloys exist, and only for temperatures between 800 and 1050°K.

Discussion

The solubility of $\mathrm{Li_5Sn_2}$ in liquid tin has been calculated at chosen temperatures. Equations 3 and 2 were equated at a given temperature. The corresponding potential of a type 4 cell (cathode saturated with solid $\mathrm{Li_5Sn_2}$) was used in the calculation of X_{Li} at the saturation point. The results are shown in Figure 3 and are compared with the phase diagram given by Hansen and Anderko.[3]

Several attempts were made to fit the data to a function of the form $\Delta\mu_{\mathrm{Li}}{}^{\mathrm{E}} = X_{\mathrm{Sn}}{}^2\mathrm{f}(T,X_{\mathrm{Li}})$ where $\mathrm{f}(T,X_{\mathrm{Li}})$ is a function of the temperature and composition. These attempts failed in that the calculated values deviated widely from the observed values at the lower values of the concentration of tin in the alloy. Apparently, this behavior is forced in the particular way in which the function attempts to reach zero point of the curve (at a composition of pure Li).

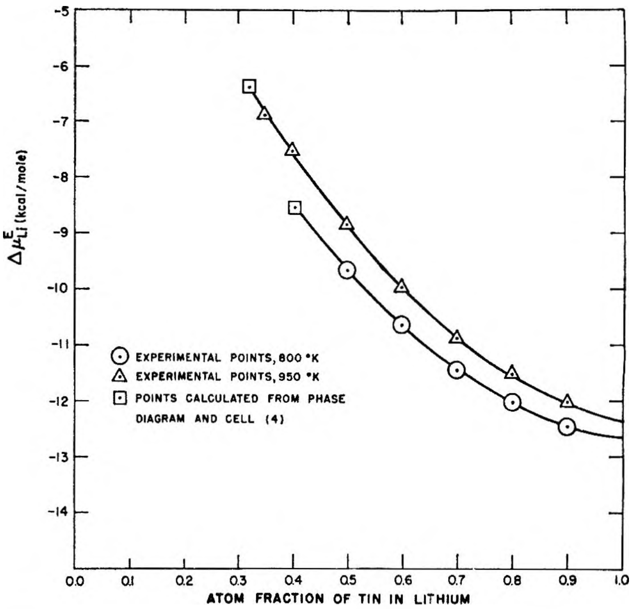

Figure 2. Excess chemical potential of lithium in tin.

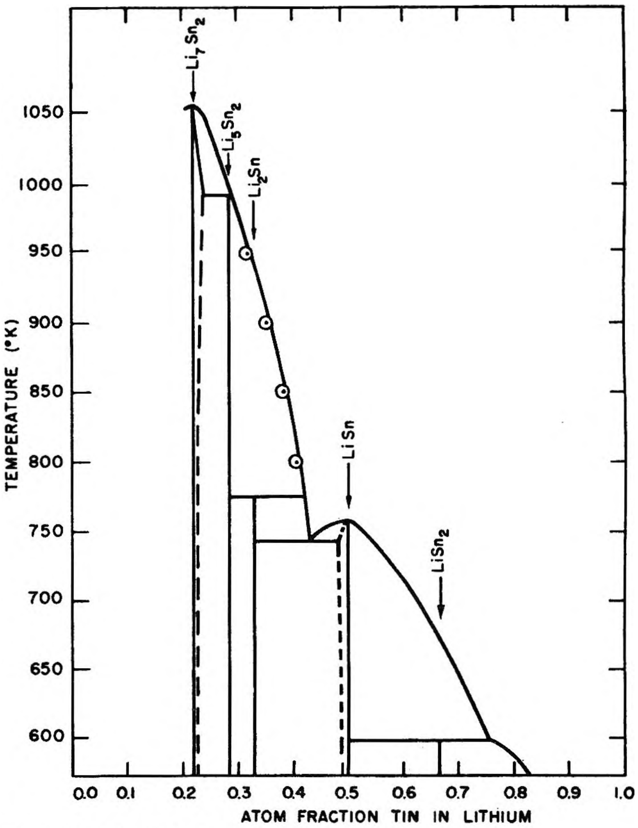

Figure 3. Partial phase diagram of the Li–Sn system showing calculated solubility points.

In reality, for an equilibrium system the curve representing the excess chemical potential of lithium in the binary liquid at constant temperature as a function of the mole fraction of the liquid phase must be discontinuous through the composition range where solid Li_5Sn_2 is present in equilibrium with a liquid alloy, since no liquid of these compositions exists. Because of these difficulties and the experimental difficulties noted, it was decided to use the simpler, but empirical, function given in eq 3.

If the cell reaction for a type 4 cell may be written as

$$Li(l) + {}^2/_5Sn(l)\ (\text{satd with } Li_5Sn_2) \longrightarrow {}^1/_5Li_5Sn_2(s) \quad (4)$$

then one may represent the Gibbs free energy change for the cell reaction as

$$\Delta G = -FE = {}^1/_5\Delta G_f{}^\circ - {}^2/_5RT \ln a_{Sn} \quad (5)$$

where E is the voltage of the cell of type 4, $\Delta G_f{}^\circ$ is the standard Gibbs free energy of formation of $Li_5Sn_2(s)$ from the elements, and a_{Sn} is the activity of tin in the saturated alloy. Li(l) and $Li_5Sn_2(s)$ are said to exist in their standard state in the cell environment. The activity of tin was calculated by applying the Gibbs–Duhem relationship and eq 3. Values of $\Delta G_f{}^\circ$ for the formation per mole of Li_5Sn_2 at various temperatures are given in Table II. The estimated error of these values is 1.0 kcal/mole.

Table II: Standard Free Energy of Formation of $Li_5Sn_2(s)$

Temp, °K	$\Delta G_f{}^\circ$, kcal/mole
800	−61.4
850	−59.8
900	−57.9
950	−55.3
1000	−52.4

Acknowledgments. The aid of Mr. Richard E. Eppley and Mrs. Gene H. McCloud in obtaining the experimental data is gratefully acknowledged.

Fluoranil-Pyridine Charge-Transfer Complexes

by W. R. Carper[1]

Department of Chemistry, California State College at Los Angeles, Los Angeles, California

and R. M. Hedges

Department of Chemistry, Texas A & M University, College Station, Texas

(Received January 24, 1966)

Pyridine and nine of its methyl derivatives are complexed with fluoranil in carbon tetrachloride and other solvents at 25°. The spectra may be interpreted as charge-transfer complexes and ion pairs ("inner complexes in the Mulliken sense").

Introduction

Charge-transfer complexes between pyridine and various acceptors have been studied extensively by various investigators[2-9] by means of both ultraviolet and infrared spectroscopy. Kosower and co-workers[10] have investigated various pyridinium iodide complexes and looked at solvent effects while the solid-state structures of the pyridine and 4-picoline-iodine complexes have been reported by Hassel.[11]

In a previous study[12] aniline-chloranil complexes were investigated and a successful test of the molecular orbital[13] approach was made. As an extension of this type of investigation, pyridine and nine methyl derivatives thereof were complexed with fluoranil in carbon tetrachloride, chloroform, and water at 25°.

Experimental Section

Fluoranil (mp 171.5–172.5°) was obtained from the Pierce Chemical Co. and used without further purification. Spectral grade solvents were used throughout the investigation. The pyridines were generously donated by the Reilly Tar and Chemical Corp. and were quadruply distilled shortly before their use. Boiling points corresponded to those found in the literature and chemical handbooks. Solutions were made up in the manner described previously,[12] and measurements were made at 25 ± 0.01° with a Beckman DK-1 spectrophotometer.

Results

Two new absorption bands appear when fluoranil is added to various methyl derivatives of pyridine in carbon tetrachloride at 25°. These new absorption bands are listed in Table I. These same absorption bands (both visible and ultraviolet) are seen to increase in intensity with decreasing temperature. This phenomena is reversible and is a consequence of the exothermic charge-transfer complexation.

As an electron donor, pyridine offers both the nitrogen lone-pair and the π electrons in the ring. With this in mind, the following questions arise: (1) Are the new transitions n → π^*, $\pi \rightarrow \pi^*$, or both? (2) Are the new bands representative of separate complex species, or are they associated with the same complex?

In an attempt to answer the first question, molecular

---

(1) To whom correspondence may be addressed.

(2) (a) D. L. Glusker and H. W. Thompson, *J. Chem. Soc.*, **471** (1955); (b) V. G. Krishna and M. Chowdhury, *J. Phys. Chem.*, **67**, 1067 (1963).

(3) R. E. Merrifeld and W. D. Phillips, *J. Am. Chem. Soc.*, **80**, 2778 (1958).

(4) J. Nag-Chaudhuri and S. Basu, *Trans. Faraday Soc.*, **55**, 898 (1959).

(5) E. K. Plyler and R. S. Mulliken, *J. Am. Chem. Soc.*, **81**, 823 (1959).

(6) A. I. Popov and R. T. Pflaum, *ibid.*, **79**, 570 (1957).

(7) A. I. Popov and R. H. Rygg, *ibid.*, **79**, 4622 (1957).

(8) C. Reid and R. S. Mulliken, *ibid.*, **76**, 3869 (1954).

(9) R. A. Zingaro and W. B. Witmer, *J. Phys. Chem.*, **64**, 1705 (1960).

(10) E. M. Kosower, *J. Am. Chem. Soc.*, **77**, 3883 (1955); **78**, 5838 (1956); **80**, 3253 (1958); **82**, 2195 (1960); **83**, 2013, 3142, 3147 (1961).

(11) O. Hassel and H. Hope, *Acta Chem. Scand.*, **15**, 407 (1961); 967 (1961).

(12) W. R. Carper, R. M. Hedges, and H. N. Simpson, *J. Phys. Chem.*, **69**, 1707 (1965).

(13) R. E. Miller and W. F. K. Wynne-Jones, *J. Chem. Soc.*, 2375 (1959).

Table I: Fluoranil–Pyridine Complexes in Carbon Tetrachloride at 25°

Donor[a]		New transitions,[b] mμ	
Pyridine	(1)	396 (1)	455 (3)
2-Picoline	(2)	385 (1)	455 (2)
3-Picoline	(3)	393 (1)	455 (2)
4-Picoline	(4)	382 (2)	455 (2)
2,4-Lutidine	(5)	375 (1)	455 (2)
2,5-Lutidine	(6)	355 (1)	455 (1)
2,6-Lutidine	(7)	355 (1)	455 (1)
3,4-Lutidine	(8)	377 (1)	455 (2)
3,5-Lutidine	(9)	390 (2)	455 (3)
2,4,6-Collidine	(10)	369 (1)	No additional band

[a] Numbers in parentheses correspond to data points in Figure 2. [b] Numbers in parentheses are standard deviations.

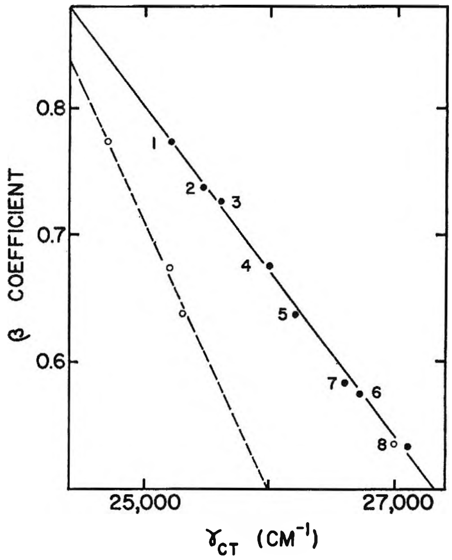

Figure 1. β coefficient *vs.* γ_{ct} (cm^{-1}): (1) pyridine, (2) 3-picoline, (3) 3,5-lutidine, (4) 2-picoline, (5) 4-picoline, (6) 2,4-lutidine, (7) 3,4-lutidine, (8) 2,4,6-collidine.

orbital calculations were obtained (see Computations section) on pyridine and its derivatives, and the results are given in Table II. The coefficient of the highest filled donor orbital (in β units) was plotted *vs.* γ_{ct} (cm^{-1}) of the highest energy band. The result of this plot is contained in Figure 1. The work of Nag-Chaudhuri and Basu[4] on iodine complexes is also included.

Table II: Results of Hückel Molecular Orbital Calculations

Compound	No. of electron centers	β coeff of lowest AO	β coeff of highest BO	β coeff of 2nd highest BO	π-Electron density on nitrogen
Pyridine	6	0.9265	0.7744	1.0000	0.9043
2-Picoline	6	0.9411	0.6762	0.9176	0.9973
3-Picoline	6	0.9365	0.7374	0.8943	0.8998
4-Picoline	6	1.0000	0.6410	1.0000	0.9720
2,4-Lutidine	6	1.0370	0.5754	0.8977	1.0650
2,5-Lutidine	6	0.9415	0.5904	0.8665	0.9936
2,6-Lutidine	6	1.0133	0.6399	0.7808	1.0962
3,4-Lutidine	6	1.0552	0.5849	0.8916	0.9683
3,5-Lutidine	6	0.9799	0.7298	0.7808	0.8951
2,4,6-Collidine	6	1.1912	0.5380	0.7808	1.1637

The linearity of the Figure 1 plot indicates that the two transitions which appear for each of the new complexes are (a) n → π* (450-mμ band) and (b) π → π* (as indicated by Figure 1).

If the identification of the transition energies is correct, then there is the question concerning the possibility of isomeric complexes. That is to say, are the transition energies associated with the same species, or are there two distinctly different complexes present in the same solution?

The next step was to consider the effect of other solvents (chloroform and water) on the same complexes. The spectra of a sample pyridine–fluoranil complex in carbon tetrachloride, chloroform, and water is contained in Figures 2 and 3. Each spectrum is broken up into the two separate bands (n → π* and π → π*) so as to indicate the relative intensities of the two transitions. A summary of the data given in Figures 2 and 3 is contained in Table III.

Table III: Analysis of Spectral Data Contained in Figures 2 and 3

	ϵ_α for the transition[a]	
Solvent	n → π*	π → π*
CCl_4	86 (∼450 mμ)	600 (∼396 mμ)
$CHCl_3$	3,800 (∼450 mμ)	2400 (∼396 mμ)
H_2O	10,600 (∼370 mμ)	6000 (∼335 mμ)

[a] ϵ_α = apparent molar extinction coefficient = absorbance of pyridine–fluoranil charge-transfer band/[fluoranil].

Before considering this table, it should be pointed out that the observed spectra in chloroform and water were seen to be temperature independent, thus indicating the presence of a new species which cannot be the same type as that observed earlier in carbon tetrachloride. Examination of Table III reveals a blue shift of the two bands as one proceeds to a sol-

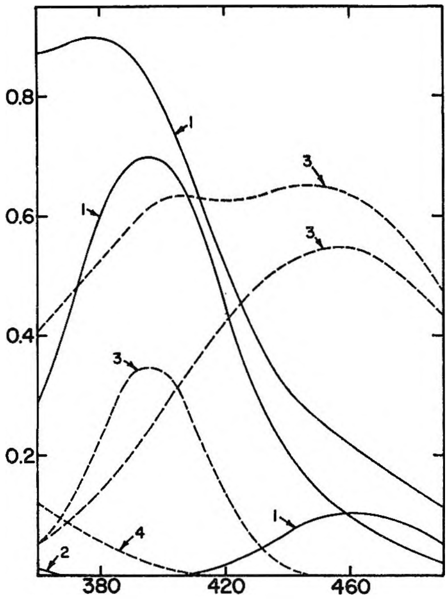

Figure 2. Spectra of pyridine–fluoranil solutions in CCl_4 and $CHCl_3$; absorbance *vs.* wavelength (mμ): (1) fluoranil, 1.167×10^{-3} *M* in CCl_4; pyridine, 0.505 *M;* (2) fluoranil, 1.167×10^{-3} *M* in CCl_4; (3) fluoranil, 1.44×10^{-4} *M* in $CHCl_3$; pyridine, 0.505 *M;* (4) fluoranil, 1.44×10^{-4} *M* in $CHCl_3$.

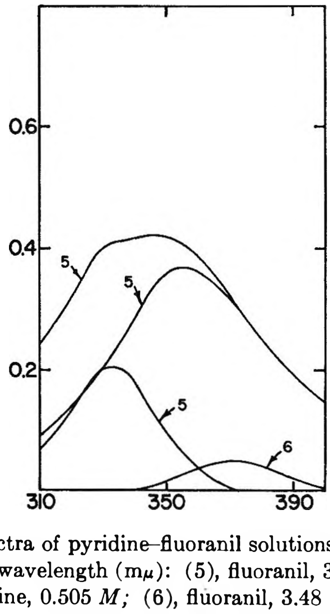

Figure 3. Spectra of pyridine–fluoranil solutions in H_2O; absorbance *vs.* wavelength (mμ): (5), fluoranil, 3.48×10^{-5} *M;* pyridine, 0.505 *M;* (6), fluoranil, 3.48×10^{-5} *M.*

vent of higher dielectric constant. Furthermore, the relative intensities (see Table III) have reversed themselves (the n → π* transition is more dominant in the solvent of higher dielectric constant) and also have been compressed (there is a separation of 2.5 ev in water as compared with a separation of 4.0 ev) in carbon tetrachloride.

All of the above can be represented by the mechanism

$$D + A \rightleftharpoons C_1 \text{ (outer complex)} \longrightarrow C_2 \text{ (inner complex, } D^+A^-)$$

Such a mechanism was first postulated by Mulliken and Reid[8] for pyridine–iodine complexes. More recently, Miller and Wynne-Jones[13,14] have used this model for a variety of trinitrobenzene–amine complexes.

The relative intensities are explained by assuming that the geometry of the complex varies from solvent to solvent. That is to say, the inner complex (favored in the more polar solvent of high dielectric constant) exists in a form such that most of the transfer occurs through the nitrogen atom. Consequently, the n → π* transition becomes enhanced as one proceeds to the more polar solvent.

As a final point, one would expect that if two separate types of complexes existed simultaneously in solution and if these types were (a) π → π* and (b) n → π*, that the spectrum of (a) would be only mildly perturbed (if at all) by the various changes in solvent. The fact that both transitions are affected simultaneously, coupled with the results in Figure 1, leads the investigators to conclude that the new transition energies are indeed all representative of the same species of complex.

Computations

In order to apply the Dewar approach[15] it was necessary to obtain molecular orbital calculations on all of the donor molecules. These were calculated by the Hückel method using a modified version of Wiberg's program[16] and an IBM 7094 digital computer. The results of the calculations are given in Table II.

A six-electron model was used to calculate the energy levels in the usual form

$$\alpha_c - x\beta_{cc} = \text{AO (antibonding orbital)}$$
$$\alpha_c + x\beta_{cc} = \text{BO (bonding orbital)}$$

The heteroparameter used for nitrogen was −0.19 in accordance with Brown's work[17] while the methyl inductive parameter used was −0.50.[18]

---

(14) R. E. Miller and W. F. K. Wynne-Jones, *J. Am. Chem. Soc.*, 4886 (1961).

(15) M. J. S. Dewar and A. R. Lepley, *J. Am. Chem. Soc.*, **83**, 4560 (1961).

(16) K. B. Wiberg, "Physical Organic Chemistry," John Wiley and Sons, Inc., New York, N. Y., 1964.

(17) R. D. Brown and M. L. Heffernan, *Australian J. Chem.*, **12**, 554 (1959).

(18) A. Streitwieser, "Molecular Orbital Theory for Organic Chemists," John Wiley and Sons, Inc., New York, N. Y., 1961.

Acknowledgment. This work was supported by Robert A. Welch Foundation Grant A-106. Computer facilities were provided by the Texas A & M Data Processing Center.

The Choice of Reference Frame in the Treatment of Membrane Transport by Nonequilibrium Thermodynamics

by D. C. Mikulecky and S. R. Caplan[1]

Weizmann Institute of Science, Rehovoth, Israel *(Received January 25, 1966)*

It is shown quite generally for isotropic membranes, and with some restrictions for anisotropic membranes, that in describing transport under stationary-state conditions, the membrane may be chosen legitimately as the frame of reference for a local dissipation function. This is true even when there is no mechanical equilibrium, in other words when viscous flow occurs, provided that the mean density of the membrane over a lateral plane is constant in the direction of flow. The forces conjugate to the membrane-centered flows are the gradients of chemical or electrochemical potential of the permeating species. However, the local dissipation function must be *averaged* over a cross section at any depth within the membrane, and hence the flows likewise must represent averages, which measured values usually do. The local phenomenological relations corresponding to the average local dissipation function are then symmetrical. The assumption that this is so is implicit in the Kedem–Katchalsky treatment of membrane processes.[2] As an example, an important limiting case, that of a set of charged pores having a diameter very large compared to the thickness of the electrical double layer, is examined in detail. In a recent treatment of this model, Kobatake and Fujita obtained unsymmetrical phenomenological relations for the average flows.[3,4] This result is not correct. It turns out that their approach indeed leads to symmetrical relations if the local forces and flows are chosen so as to form a set of conjugate pairs.

Introduction

In the study of transport processes in free solution, using the nonequilibrium thermodynamics of continuous systems, the local center of mass is the usual frame of reference for diffusional flows.[5] Other frames of reference available are the local center of volume or any of the individual components of the system, in particular the solvent. In membrane transport, the most convenient component to choose as a frame of reference, both experimentally and theoretically, is clearly the membrane itself. Some cases of membrane transport may be approached from the point of view of solution theory. This is possible when the membrane is essentially a system of rather large pores (compared to

---

[1] Biophysical Laboratory, Harvard Medical School, Boston 15, Mass.

[2] O. Kedem and A. Katchalsky, *J. Gen. Physiol.*, **45**, 143 (1961).

[3] Y. Kobatake and H. Fujita, *J. Chem. Phys.*, **40**, 2212, 2219 (1964).

[4] Y. Kobatake and H. Fujita, *Kolloid-Z.*, **196**, 58 (1964).

[5] S. R. de Groot and P. Mazur, "Non-Equilibrium Thermodynamics," North-Holland Publishing Co., Amsterdam, 1962.

the mean free path of the permeating molecules) which may or may not carry wall charges. In such treatments, it is always found advantageous to transform the frame of reference from the local center of mass to the pore walls. When the transport process is described by nonequilibrium thermodynamics, then whatever the structure of the membrane, it is necessary to ascertain whether or not such changes of reference frame preserve Onsager symmetry in the local phenomenological equations. The treatment of Kedem and Katchalsky assumes implicitly that this is the case.[2] de Groot and Mazur have shown by considering a discontinuous (three-compartment) system that the over-all or integral phenomenological coefficients, characteristic of the membrane as a whole, obey Onsager symmetry when the gradients across the membrane are all linear.[5] However, this treatment throws no light on the local coefficients. Kirkwood and co-workers, in dealing with the problem in free solution, found that in certain circumstances transforming the reference frame to the walls of the container does not result in symmetrical coefficients.[6] Snell and Stein recently treated the symmetry of the over-all coefficients in a complex membrane, basing their considerations on symmetrical local coefficients with the membrane as a frame of reference.[7]

Attention was first drawn to this question by Schlögl,[8] who was able to show that the transformation can be symmetry-preserving when the pores are small enough to satisfy the following criteria: (a) the fluid is homogeneous over the pore cross section; and (b) the electrical space charge per unit volume of fluid is constant over the pore cross section. Kobatake and Fujita have recently considered the opposite situation, that of an array of cylindrical pores having a diameter very large with respect to the thickness of the electrical double layer.[3,4] Here the argument developed by Schlögl cannot be applied. Indeed, it turns out that the local phenomenological equations relating to a streamline within a pore are not symmetrical when referred to the membrane. Kobatake and Fujita arrived at mean local flows which also are not described by symmetrical equations. It will be shown below that a correct averaging procedure restores the symmetry.

For systems in mechanical equilibrium, which here implies that not only acceleration but also velocity gradients have vanished, Prigogine's theorem states that the barycentric velocity in the definition of local flows may simply be replaced by any other velocity without changing the entropy production.[5] However, in many cases of interest in membrane transport, mechanical equilibrium does not exist in this sense even in the stationary state, since radial velocity gradients are present in the pores owing to the occurrence of viscous flow. However, it is worth pointing out that the flows normally measured are *average* flows over the plane of the membrane. Since average flows are independent of position in the stationary state, one might suppose that they offer a means of avoiding the problem of velocity gradients. The correctness of this supposition is demonstrated below.

The Local Dissipation Function

For simplicity, we restrict ourselves to isothermal systems. If we disregard the possibility of chemical reactions for the moment, the local entropy production σ at any point within the membrane is given, in the notation of de Groot and Mazur, by

$$T\sigma = -\sum_{k=1}^{n-1} \mathbf{J}_k \cdot [\{\text{grad } (\mu_k - \mu_n)\}_T - \mathbf{F}_k + \mathbf{F}_n] - \tilde{\Pi}: \text{ grad } \mathbf{v} + 2\mathbf{P}^a \cdot \boldsymbol{\omega} \quad (1)$$

where n represents the number of components present, *including* the membrane. The $\mathbf{J}_k$ are diffusional flows relative to the local center of mass, $\mathbf{v}$ is the barycentric velocity, and μ_k and $\mathbf{F}_k$ are, respectively, the chemical potential of the kth component and the external force acting on it. The transposed viscous pressure tensor $\tilde{\Pi}$ arises by splitting the total pressure tensor P into two parts, one of which is the scalar hydrostatic (equilibrium) pressure p multiplied by the unit tensor U

$$\mathsf{P} = p\mathsf{U} + \Pi \quad (2)$$

The assumption that a scalar hydrostatic pressure can be separated out in this way limits the discussion to inelastic media. For our purposes, this is an unimportant limitation, since we deal only with stationary states. It does not exclude changes in specific volume; *i.e.*, the flow need not be incompressible, but such changes will generally be negligible in the condensed systems we are considering. The final term on the right-hand side of eq 1 only arises if the system exhibits rotational viscosity, in which case P and hence Π will not be symmetric. The axial vector $\mathbf{P}^a$ then represents the antisymmetric part of P, while $\boldsymbol{\omega}$ is the mean angular velocity of the constituent particles. The inertial terms in the driving forces for diffusional flows above have been omitted, since these are generally negligible,[5,9] and the conservative external forces acting on

---

(6) J. G. Kirkwood, R. L. Baldwin, P. J. Dunlop, L. G. Gosting, and G. Kegeles, *J. Chem. Phys.*, **33**, 1505 (1960).

(7) F. M. Snell and B. Stein, *J. Theoret. Biol.*, **10**, 177 (1966).

(8) R. Schlögl, *Discussions Faraday Soc.*, **21**, 46 (1956).

(9) D. D. Fitts, "Nonequilibrium Thermodynamics," McGraw-Hill Book Co., Inc., New York, N. Y., 1962.

the particles are presumed not to give rise to intrinsic angular momentum.

Equation 1 refers to local volumes in a continuous phase, sufficiently "macroscopic" to make the concept of entropy production meaningful. The intensive properties of the membrane are therefore required to be continuous functions of the space coordinates. It should be borne in mind, however, that in a nonequilibrium system, the local intensive properties are averages over microscopically large, although macroscopically small, regions of space and time.[9] In short we are dealing with what de Groot and Mazur call "coarse-grained" variables. We shall consider two cases.

(a) The membrane pores are smaller than, of the same order of magnitude as, or not very much larger than the mean free path of the permeating molecules. Such a membrane represents a continuous phase.

(b) The membrane pores are very much larger than the mean free path of the permeating molecules. This type of membrane will be regarded as a two-phase system in which entropy production occurs only in the "internal" fluid phase, *i.e.*, not within the actual membrane fabric. Equation 1 may then be restricted to local volumes in the internal phase, the local density of the membrane component being everywhere zero.

The situations envisaged in case a are those in which the membrane component is interspersed, essentially at a molecular level, among the components of the permeating fluid, and therefore partakes intimately (by frictional and other interactions) in the processes occurring. In case b, the membrane component is considered to be a separate phase segregated from the permeating fluid, which is stationary at the interface between the phases; consequently, the membrane partakes only marginally in the processes. Biological cell membranes having both lipid and aqueous regions of permeability may, from an over-all phenomenological point of view, be included in case a. Both cases are covered in the following analysis.

If chemical reactions take place in the membrane, the entropy production contains an additional term, a summation over the products of the affinities and velocities of the reactions. In an isotropic system, the first term on the right-hand side of eq 1 is separately positive definite. The second term breaks into three parts: (i) a term referring to the scalar process involving bulk viscosity (negligible when changes in specific volume are negligible), which should be grouped with the chemical reaction term since this process can couple only to chemical processes in an isotropic system; (ii) a term containing the symmetric parts of each tensor (with zero trace); and (iii) a further term referring to rotational processes, which may be combined readily with the third term in eq 1 since it also involves the axial vector $\mathbf{P}^{\mathrm{a}}$. The three contributions to the entropy production just described are each separately positive definite in isotropic systems. The total entropy production in such systems thus gives rise to four independent sets of phenomenological relations. In an anisotropic system this is no longer true; the properties of the complete array of phenomenological coefficients depend on the symmetries of the system. However, the cross-coefficients must obey Onsager's reciprocal relations in their most general form.[5,9] For the most part, anisotropic membranes are not excluded from consideration here, but in case a we do exclude any variation, in the direction normal to the membrane surface, of the total density averaged over a cross section. In case b we exclude any such variation of the density of the *internal* phase, averaged over the *entire* area of a cross section. It will be noted that the internal phase in case b is usually isotropic, so that rotational processes (and chemical reactions) do not couple to the flows, but since rotational viscosity is only significant in solutions of macromolecules, it is virtually confined to case b.

We now identify the membrane with component n, and define the quantities

$$(\text{grad } \tilde{\mu}_k)_T = (\text{grad } \mu_k)_T - \mathbf{F}_k \tag{3}$$

$$\mathbf{J}_k{}^{\mathrm{m}} = \mathbf{J}_k + \rho_k \mathbf{v} \tag{4}$$

where ρ_k denotes the mass per unit volume of component k. Thus the $\mathbf{J}_k{}^{\mathrm{m}}$ are flows relative to the membrane. Introducing into eq 1 eq 3, 4, and the Gibbs–Duhem relation

$$\sum_{k=1}^{n} \rho_k \,(\text{grad } \mu_k)_T = \text{grad } p$$

and remembering that the membrane does not move and that $\rho_n = 0$ in case b, we obtain directly

$$T\sigma = -\sum_{k=1}^{n-1} \mathbf{J}_k{}^{\mathrm{m}} \cdot (\text{grad } \tilde{\mu}_k)_T + \mathbf{v} \cdot \text{grad } p - \sum_{k=1}^{n} \rho_k \mathbf{F}_k \cdot \mathbf{v} - \tilde{\Pi} : \text{ grad } \mathbf{v} + 2\mathbf{P}^{\mathrm{a}} \cdot \boldsymbol{\omega} \tag{5}$$

In mechanical equilibrium, only the first term on the right-hand side remains and eq 5 reduces to a particular case of Prigogine's theorem. (Π and hence $\mathbf{P}^{\mathrm{a}}$ may be neglected and the second and third terms together give zero.) The corresponding phenomenological equations are then symmetrical, since the new flows and forces result from linear transformations of the original flows and forces, respectively.

We are interested in the more general situation in which mechanical equilibrium does not hold, but we do assume stationarity. Then from the local kinetic and intrinsic rotational energy balances,[5] writing θ for the average moment of inertia per unit mass of the constituent particles and ρ for the total density, eq 5 is transformed to

$$\begin{aligned} T\sigma = {} & -\sum_{k=1}^{n-1}\mathbf{J}_k{}^{\mathrm{m}}\cdot(\mathrm{grad}\ \tilde{\mu}_k)_T + \mathbf{v}\cdot\mathrm{grad}\ p - \\ & \mathrm{div}\ (\mathsf{P}\cdot\mathbf{v}) + \tilde{\ }: \mathrm{grad}\ \mathbf{v} - \tilde{\Pi}: \mathrm{grad}\ \mathbf{v} - \\ & \mathrm{div}\ ([{}^1/_2]\rho\mathbf{v}^2\mathbf{v}) - \mathrm{div}\ ([{}^1/_2]\rho\theta\boldsymbol{\omega}^2\mathbf{v}) = \\ & -\sum_{k=1}^{n-1}\mathbf{J}_k{}^{\mathrm{m}}\cdot(\mathrm{grad}\ \tilde{\mu}_k)_T + \mathbf{v}\cdot\mathrm{grad}\ p - \\ & \mathrm{div}\ (\mathsf{P}\cdot\mathbf{v}) + p\ \mathrm{div}\ \mathbf{v} - \\ & \mathrm{div}\ ([{}^1/_2]\rho\mathbf{v}^2\mathbf{v}) - \mathrm{div}\ ([{}^1/_2]\rho\theta\boldsymbol{\omega}^2\mathbf{v}) \end{aligned}$$

since U: grad $\mathbf{v}$ = div $\mathbf{v}$. This may be condensed to give

$$\begin{aligned} \phi = {} & -\sum_{k=1}^{n-1}\mathbf{J}_k{}^{\mathrm{m}}\cdot(\mathrm{grad}\ \tilde{\mu}_k)_T - \mathrm{div}\ (\Pi\cdot\mathbf{v}) - \\ & \mathrm{div}\ ([{}^1/_2]\rho\mathbf{v}^2\mathbf{v}) - \mathrm{div}\ ([{}^1/_2]\rho\theta\boldsymbol{\omega}^2\mathbf{v}) \end{aligned} \tag{6}$$

where $\phi = T\sigma$ is the local dissipation function per unit volume. Since this quantity is dependent on position within the membrane, we denote it $\phi_{x,y,z}$, where x is the direction perpendicular to the plane of the membrane. We now wish to derive a related function, the *average* local dissipation function at a depth x within the membrane, $\bar{\phi}_x$. This is the local dissipation function involved implicitly in the work of Kedem and Katchalsky,[2] since they obtain the total dissipation function for the membrane, per unit area, by integrating in the x direction only.

Consider the volume V of an infinitesimally thin cross-sectional slab of membrane of thickness δx at x. Then

$$\bar{\phi}_x = (1/V)\int_V \phi_{x,y,z}\mathrm{d}\tau \tag{7}$$

where $\mathrm{d}\tau$ is an element of volume in the slab. If A is the cross-sectional area of the membrane, then from (6) and (7)

$$\begin{aligned} A\,\delta x\bar{\phi}_x = {} & -\int_V\left\{\sum_{k=1}^{n-1}\mathbf{J}_k{}^{\mathrm{m}}\cdot(\mathrm{grad}\ \tilde{\mu}_k)_T\right\}\mathrm{d}\tau - \\ & \int_\Omega \Pi\cdot\mathbf{v}\cdot\mathrm{d}\Omega - \int_\Omega [{}^1/_2]\rho\mathbf{v}^2\mathbf{v}\cdot\mathrm{d}\Omega - \int_\Omega [{}^1/_2]\rho\theta\boldsymbol{\omega}^2\mathbf{v}\cdot\mathrm{d}\Omega \end{aligned} \tag{8}$$

where $\mathrm{d}\Omega$ is an outwardly directed vectorial area element, and the last three integrals extend over the whole surface of the slab. These surface integrals (together with their signs) represent net inward fluxes normal to the slab faces of, respectively, viscous mechanical energy, kinetic energy, and intrinsic rotational energy. Since we have considered a stationary state, each inward flux would represent, if positive, an expenditure within the slab of the form of energy concerned—either by total dissipation or by partial conversion to another form (which may appear in the volume integral). If an inward flux is negative, *i.e.*, actually an outward flux, it evidently represents the output of an energy conversion. In isotropic systems, including most examples of case b, the final integral in eq 8 may be omitted from further consideration. This follows not only from the symmetry properties of the system, but also from the observation that in isotropic systems $\mathbf{P}^{\mathrm{a}}$ usually has a short relaxation time and vanishes in the stationary state.[5]

It can be seen now why it was necessary to exclude membranes which exhibit average density variations, as discussed, in the x direction. Under steady conditions, the average momentum density $\overline{\rho\mathbf{v}}$, which is equal to the average mass flux, is constant for all slabs. Consequently, any variation in the mean total density $\bar{\rho}$ must be accompanied by a corresponding variation in the mean barycentric velocity $\bar{\mathbf{v}}$. In determining $\bar{\rho}$ in case b, ρ_n is counted as zero as before, since we are only concerned with the average concentration of the fluid phase over the whole cross section. If $\bar{\mathbf{v}}$ does not change, the average flow of momentum in the slab is independent of the position x. The flow of kinetic energy is therefore constant in the x direction. The flows of intrinsic angular momentum and rotational energy, and of viscous mechanical energy (which anyway appears as a second-order term among the energy flows in the treatment of de Groot and Mazur[5]), will in general also be constant or nearly so in the x direction. Thus the surface integrals in eq 8 are all zero or vanishingly small. In the presence of anisotropy of the kind described, however, an energy dissipation or conversion occurs which causes these integrals to take on finite positive or negative values.

The averaging is completed by writing

$$\mathrm{d}\tau = \delta x\mathrm{d}A \tag{9}$$

We assume that $\tilde{\mu}_k$ is constant everywhere over the slab of thickness δx,[10] which of course does not imply that ρ_k is similarly constant. This is nothing other than an extension of the usual hypothesis of local equilibrium in nonequilibrium thermodynamics. It is ensured if no absolute barriers exist to diffusion of the permeating species from one local volume to another in the plane of the slab. We may define the average flow

---

(10) R. L. Cleland, J. K. Brinck, and R. K. Shaw, *J. Phys. Chem.*, **68**, 2779 (1964); R. L. Cleland, *Trans. Faraday Soc.*, **62**, 336 (1966).

$\bar{\mathbf{J}}_k^{\mathrm{m}}$ of the kth component relative to the membrane by the expression

$$\bar{\mathbf{J}}_k^{\mathrm{m}} = (1/A)\int_A \mathbf{J}_k^{\mathrm{m}}\mathrm{d}A \qquad (10)$$

where A is either the cross-sectional area of the whole membrane as before or of a subsection of it over which the local equilibrium hypothesis, as set out above, holds good for all x. Then from (8), (9), and (10)

$$\bar{\phi}_x = -\sum_{k=1}^{n-1}\bar{\mathbf{J}}_k^{\mathrm{m}}\cdot(\mathrm{grad}\ \tilde{\mu}_k)_T \qquad (11)$$

Equation 11 is the local dissipation function used by Kedem and Katchalsky.[2] It is seen, by comparison of eq 11 and 5, that the averaging procedure has in effect reduced the problem to one of mechanical equilibrium after all. If the local dissipation function refers to a *cross section* of the membrane over which there is local equilibrium, the conditions of Prigogine's theorem are automatically fulfilled. It follows that the corresponding phenomenological equations are symmetrical. The occurrence of chemical reactions would contribute further averaged terms to $\bar{\phi}_x$, without contributing to the surface integrals of eq 8 unless significant changes in specific volume or viscosity were brought about. It should be emphasized that viscous dissipation, within the membrane, of hydrostatic mechanical energy or of potential energy in general is *not* excluded.

The Phenomenological Relations in a Wide-Pore Model

Our object now is to describe the flow of a single salt and water through a membrane consisting of uniform right-circular cylindrical pores. We are concerned only with pores having a radius a much greater than the thickness of the electrical double layer. The latter results from a surface charge on the cylinder walls of density σ_e.

We consider steady-state ion flows, viscous forces being a negligible contribution to the total driving forces for the diffusional ion flows, but the major contribution for solvent flow. Bearman and Kirkwood[11] have shown that whenever viscosity terms can be neglected in the driving forces for diffusional flows and steady-state conditions exist, the individual equations of motion are equivalent to linear phenomenological relations. We assume for simplicity that the solution is dilute; consequently, the contribution of water diffusion relative to the local center of mass is negligible and the equations of motion of the solution and of the water are identical.[11,12] Flows through the membrane will be analyzed in terms of flows through a single capillary, and the membrane will not be included as a species.

Along any streamline, the diffusional flows of the ions (relative to the local center of mass) are given by

$$\mathbf{J}_k = -\sum_{i=1}^{2}L_{ki}(\partial\tilde{\mu}_i/\partial x) = \\ -\sum_{i=1}^{2}L_{ki}[e_i\partial\psi/\partial x + v_i\partial p/\partial x + \partial\mu_i^{\mathrm{c}}/\partial x] \qquad (12)$$

where k and i represent either cation or anion (1 or 2, respectively) and the remaining symbols are either defined above or as follows: $\partial\psi/\partial x$, potential gradient at any point; e_i, specific charge of species i; μ_i^{c}, concentration-dependent part of the electrochemical potential $\tilde{\mu}_i$, where $\tilde{\mu}_i$ is the partial *specific* Gibbs free energy of species i; v_i, partial specific volume of species i. Diffusion relative to the center of mass due to pressure gradients is generally vanishingly small and the terms $v_i\partial p/\partial x$ in eq 12 may be neglected.[3,4]

It is desirable to express the electrochemical potential gradients of the ions in terms of the chemical potential gradient of the neutral salt. To do so, it must be assumed that electroneutrality holds for each local volume element of the solution, neglecting the effect of the wall charge

$$e_1\rho_1 + e_2\rho_2 = 0 \qquad (13)$$

This is an approximation only near the wall, and an accurate description elsewhere. It has been shown that the terms introduced by not making this assumption are negligible.[4] The use of eq 13 at this point allows us to express the ion flows in terms of current and salt flow and their conjugate forces.

The salt concentration is defined by

$$\rho_1 + \rho_2 = \rho_{\mathrm{s}} \qquad (14)$$

The gradient of the concentration-dependent part of the chemical potential can be written

$$\partial\mu_i^{\mathrm{c}}/\partial x = \sum_{j=1}^{2}(\partial\mu_i^{\mathrm{c}}/\partial\rho_j)(\partial\rho_j/\partial x) \qquad (15)$$

which reduces to the following form when the activity coefficients γ_i are taken into consideration (M_i represents molar weight)

$$\partial\mu_i^{\mathrm{c}}/\partial x = (RT/M_i)[(1/\rho_i)(\partial\rho_i/\partial x) + \\ (1/\gamma_i)(\partial\gamma_i/\partial x)] \qquad (16)$$

In dilute solution, we have $\gamma_1 \approx \gamma_2 \approx \gamma_{\mathrm{S}}$ (the mean ionic activity coefficient of the salt), and using (13)

---

[11] R. J. Bearman and J. G. Kirkwood, *J. Chem. Phys.*, **28**, 136 (1958).

[12] R. H. Aranow, *Proc. Natl. Acad. Sci. U. S.*, **50**, 1066 (1963).

and (14) to express the ion concentrations in terms of the salt concentration and the specific charges, the following simplification results

$$M_1\partial\mu_1{}^{c}/\partial x = M_2\partial\mu_2{}^{c}/\partial x = (M_s/\nu)\partial\mu_s{}^{c}/\partial x \quad (17)$$

where $\nu = \nu_1 + \nu_2$, the stoichiometric coefficients of the salt. Combining (16) and (17), eq 12 becomes

$$\mathbf{J}_k = -\sum_{i=1}^{2} L_{ki}[e_i\partial\psi/\partial x + (M_s/\nu M_i)\partial\mu_s{}^{c}/\partial x] \quad (18)$$

The ion flows are transformed to flows of salt and current by

$$\mathbf{J}_s = (M_s/\nu)(\mathbf{J}_1/M_1 + \mathbf{J}_2/M_2) \quad (19)$$

$$\mathbf{I} = e_1\mathbf{J}_1 + e_2\mathbf{J}_2 \quad (20)$$

The result of this transformation is

$$\mathbf{J}_s = (M_s/\nu)^2[L_{11}/M_1{}^2 + 2L_{12}/M_1M_2 + L_{22}/M_2{}^2] \times \partial\mu_s{}^{c}/\partial x - (M_s/\nu)[(e_1/M_1)L_{11} + (e_2/M_1 + e_1/M_2)L_{12} + (e_2/M_2)L_{22}]\partial\psi/\partial x \quad (21)$$

$$\mathbf{I} = -(M_s/\nu)[(e_1/M_1)L_{11} + (e_1/M_2 + e_2/M_1)L_{12} + (e_2/M_2)L_{22}]\partial\mu_s{}^{c}/\partial x - [e_1{}^2L_{11} + 2e_1e_2L_{12} + e_2{}^2L_{22}]\partial\psi/\partial x \quad (22)$$

Using the same argument (eq 13–17) and similarly neglecting the pressure contribution to diffusion relative to the center of mass, the transformation from ion flows to salt and current flows may be performed on the dissipation function and a symmetrical matrix of coefficients written directly. In order for the transformation to leave the rate of entropy production invariant the salt flow *must* be defined as in eq 19. Kobatake and Fujita[4] defined salt flow by the relation

$$\mathbf{J}_s = \mathbf{J}_1 + \mathbf{J}_2 \quad (23)$$

This flow is not conjugate to the driving force $\partial\mu_s{}^{c}/\partial x$. For convenience, we now define a new set of coefficients

$$\mathcal{L}_{11} = (M_s/\nu)^2[L_{11}/M_1{}^2 + L_{12}/M_1M_2 + L_{22}/M_2{}^2] \quad (24)$$

$$\mathcal{L}_{12} = \mathcal{L}_{21} = (M_s/\nu)[(e_1/M_1)L_{11} + (e_2/M_1 + e_1/M_2)L_{12} + (e_2/M_2)L_{22}] \quad (25)$$

$$\mathcal{L}_{22} = [e_1{}^2L_{11} + e_1e_2L_{12} + e_2{}^2L_{22}] \quad (26)$$

The reference frame for the flows in eq 21 and 22 is transformed to the capillary wall by use of the relations

$$\mathbf{I}^{m} = \mathbf{I} + (e_1\rho_1 + e_2\rho_2)\mathbf{v} \quad (27)$$

$$\mathbf{J}_s{}^{m} = \mathbf{J}_s + \rho_s\mathbf{v} \quad (28)$$

where $\mathbf{v}$, the barycentric velocity, is given by the following solution to the Navier–Stokes equation[3]

$$\mathbf{v} = -\alpha\partial p/\partial x - \beta\partial\psi/\partial x \quad (29)$$

Here α and β are defined by

$$\alpha = (a^2 - r^2)/4\eta$$

$$\beta = (\epsilon/4\pi\eta)(\Phi - \Phi_0)$$

and the remaining symbols are ϵ, dielectric constant of the medium; Φ, electrostatic potential due to the wall charge; Φ_0, electrostatic potential at the wall ($r = a$); r, variable distance in the radial direction; and a, capillary radius. The second term on the right-hand side of eq 27 accounts now for the influence of wall charge on the current, and will be discussed presently. The transformed flows, related to the membrane as frame of reference, are

$$\mathbf{J}_s{}^{m} = -\mathcal{L}_{11}\partial\mu_s{}^{c}/\partial x - \mathcal{L}_{12}\partial\psi/\partial x + \rho_s\mathbf{v} \quad (30)$$

$$\mathbf{I}^{m} = -\mathcal{L}_{21}\partial\mu_s{}^{c}/\partial x - \mathcal{L}_{22}\partial\psi/\partial x + (e_1\rho_1 - e_2\rho_2)\mathbf{v} \quad (31)$$

Using eq 29 and rearranging, these equations can be rewritten in terms of the forces conjugate to the flows. Together with eq 29, they constitute the phenomenological description of local membrane-fixed flows along a particular streamline

$$\mathbf{J}_s{}^{m} = -[\mathcal{L}_{11} + \alpha\rho_s{}^2]\partial\mu_s{}^{c}/\partial x - [\mathcal{L}_{12} + \beta\rho_s]\partial\psi/\partial x - [\alpha\rho_s]\partial(p - \nu RT\rho_s/M_s)/\partial x \quad (32)$$

$$\mathbf{I}^{m} = -[\mathcal{L}_{21} + \alpha\rho_s(e_1\rho_1 + e_2\rho_2)]\partial\mu_s{}^{c}/\partial x - [\mathcal{L}_{22} + \beta(e_1\rho_1 + e_2\rho_2)]\partial\psi/\partial x - [\alpha(e_1\rho_1 + e_2\rho_2)]\partial(p - \nu RT\rho_s/M_s)/\partial x \quad (33)$$

$$\mathbf{v} = -[\alpha\rho_s]\partial\mu_s{}^{c}/\partial x - [\beta]\partial\psi/\partial x - [\alpha]\partial(p - \nu RT\rho_s/M_s)/\partial x \quad (34)$$

In writing these equations we have assumed for simplicity that at all points $(1/\gamma_s)(\partial\gamma_s/\partial x) \ll (1/\rho_s)\cdot(\partial\rho_s/\partial x)$. Clearly, the matrix of coefficients is not symmetric. We now show that averaging the flows results in symmetry. For ease in calculation, eq 29, 30, and 31 are used. The flows are averaged over the capillary cross section by means of the relations

$$\bar{\mathbf{J}}_i{}^{m} = \int_0^a \mathbf{J}_i{}^{m}2\pi r\mathrm{d}r \Big/ \int_0^a 2\pi r\mathrm{d}r \quad (35)$$

where $\mathbf{J}_i{}^{m}$ represents a flow along a streamline, and $\bar{\mathbf{J}}_i{}^{m}$ its averaged value. The contribution of the wall charge is taken into consideration in this averaging process and eq 13 is replaced by a more accurate expression of the electroneutrality condition

$$e_1\rho_1 + e_2\rho_2 = -(\epsilon/4\pi)(1/r)(\partial/\partial r)(r\partial\Phi/\partial r) \quad (36)$$

Neglecting the wall charge at this point would be equivalent to neglecting the streaming current and the effect of transmembrane potential on barycentric velocity.

The integration over the capillary cross section is self-evident except for the last term in eq 31. This integration is performed by twice integrating by parts (see ref 5, pp 423–426) using the boundary conditions

(i) $\partial\Phi/\partial r = 0$ at $r = 0$

(ii) $\mathbf{v} = 0;\ \partial\Phi/\partial r = 4\pi\sigma_e/\epsilon;\ \Phi = \Phi_0$ at $r = a$ (37)

For simplicity in notation, let

$$\mathcal{I} = \int_0^a (1/r)(\partial/\partial r)(r\partial\Phi/\partial r)\mathbf{v}r\mathrm{d}r = \int_0^a [\nabla^2\Phi]\mathbf{v}r\mathrm{d}r \quad (38)$$

Performing the integration by parts twice, and applying the conditions (37)

$$\mathcal{I} = \int_0^a (\Phi - \Phi_0)(\nabla^2\mathbf{v})r\mathrm{d}r \quad (39)$$

Substituting from the Navier–Stokes equation[3] for $\nabla^2\mathbf{v}$

$$\mathcal{I} = \left[\int_0^a \{(\Phi - \Phi_0)/\eta\}r\mathrm{d}r\right]\partial p/\partial x - (\epsilon/4\pi)\left[\int_0^a \{(\Phi - \Phi_0)/\eta\}(\nabla^2\Phi)r\mathrm{d}r\right]\partial\psi/\partial x \quad (40a)$$

We shall abbreviate this equation as

$$\mathcal{I} = \mathcal{G}\partial p/\partial x - (\epsilon/4\pi)\mathcal{H}\partial\psi/\partial x \quad (40b)$$

The flow equations averaged across the cross section can now be written in terms of the integrals $\mathcal{G}$, $\mathcal{H}$, and $\mathcal{I}$ defined by eq 40

$$\bar{\mathbf{J}}_s^m = -\bar{\mathfrak{L}}_{11}\partial\mu_s^c/\partial x - \bar{\mathfrak{L}}_{12}\partial\psi/\partial x + \rho_s\bar{\mathbf{v}} \quad (41)$$

$$\bar{\mathbf{I}}^m = -\bar{\mathfrak{L}}_{21}\partial\mu_s^c/\partial x - \bar{\mathfrak{L}}_{22}\partial\psi/\partial x - (\epsilon/2\pi a^2)\mathcal{I} \quad (42)$$

$$\bar{\mathbf{v}} = -(a^2/8\eta)\partial p/\partial x - (\epsilon\mathcal{G}/2\pi a^2)\partial\psi/\partial x \quad (43)$$

where all barred symbols represent averages in the sense of eq 35, and as a consequence of eq 25

$$\bar{\mathfrak{L}}_{12} = \bar{\mathfrak{L}}_{21}$$

The variation of ρ_s in the vicinity of the walls is considered negligible here. These equations can be transformed into the following symmetrical set

$$\bar{\mathbf{J}}_s^m = -[\bar{\mathfrak{L}}_{11} + a^2\rho_s^2/8\eta]\partial\mu_s^c/\partial x - [\bar{\mathfrak{L}}_{12} + (\epsilon\mathcal{G}\rho_s/2\pi a^2)]\partial\psi/\partial x - [a^2\rho_s/8\eta]\partial(p - \nu RT\rho_s/M_s)/\partial x \quad (44)$$

$$\bar{\mathbf{I}}^m = -[\bar{\mathfrak{L}}_{21} + (\epsilon\mathcal{G}\rho_s/2\pi a^2)]\partial\mu_s^c/\partial x - [\bar{\mathfrak{L}}_{22} - (\epsilon/2\pi a)^2(\mathcal{H}/2)]\partial\psi/\partial x - [\epsilon\mathcal{G}/2\pi a^2]\partial(p - \nu RT\rho_s/M_s)/\partial x \quad (45)$$

$$\bar{\mathbf{v}} = -[a^2\rho_s/8\eta]\partial\mu_s^c/\partial x - [\epsilon\mathcal{G}/2\pi a^2]\partial\psi/\partial x - [a^2/8\eta]\partial(p - \nu RT\rho_s/M_s)/\partial x \quad (46)$$

Although this completes our demonstration, it is worthwhile proceeding further with the calculation. The integrals $\mathcal{G}$ and $\mathcal{H}$ are evaluated in the Appendix and are related to the concentration-dependent electroosmotic coefficient $B/\rho_s^{1/2}$ of Kobatake and Fujita in the following manner

$$\epsilon\mathcal{G}/2\pi x^2 = (\epsilon/2\pi a)^2(\mathcal{H}/2)(a/\sigma_e) = B/\rho_s^{1/2} \quad (47)$$

where

$$B = -(\sigma_e/\eta)(\epsilon kT/4\pi|e_1||e_2|)^{1/2} \quad (48)$$

The result above differs from that of Kobatake and Fujita[4,13] for two reasons. Firstly, by defining a salt flow which is not conjugate to its driving force, the gradient of chemical potential, they removed symmetry from their coefficient matrix. Secondly, the term $[B/\rho_s^{1/2}]\partial p/\partial x$ was omitted in the integration.

To compare this work with that of Kobatake and Fujita in more detail, three of the coefficients derived in eq 21 and 22 can be identified with similar coefficients in their phenomenological equations as

$$\Lambda' M_s\rho_s/\nu RT = \mathfrak{L}_{21} = \mathfrak{L}_{12} \quad (49)$$

$$\Lambda\rho_s = \mathfrak{L}_{22} \quad (50)$$

Two others which depend on their definition of salt flow can also be expressed in terms of the phenomenological coefficients in eq 12. The coefficient analogous to $\mathfrak{L}_{11}$ is

$$D\rho_s/RT = [L_{11}/M_1 + L_{12}(M_1 + M_2)/M_1M_2 + L_{22}/M_2] \quad (51)$$

while a further coefficient analogous to $\mathfrak{L}_{12}$ is

$$D'\rho_s = [L_{11}e_1 + L_{12}(e_1 + e_2) + L_{22}e_2] \quad (52)$$

The final step in the derivation of equations useful for describing flows through the membrane is to invert the matrix of coefficients (eq 44–46). The transformed phenomenological equations can then be integrated across the thickness of the membrane under steady-state conditions. Although the concentration dependence of the coefficients above prevents one from

---

(13) S. R. Caplan and D. C. Mikulecky in "Ion Exchange," Vol. I, J. A. Marinsky, Ed., Marcel Dekker Publishing Co., New York, N. Y., in press

expressing the over-all coefficients in explicit terms (they appear as integrals), the over-all matrix remains symmetrical.

Acknowledgment. This work was supported in part by Public Health Service Research Grant GM-09432-03 and Public Health Service Postdoctoral Fellowship 1-F2-GM-11,608-02 from the National Institute of General Medical Sciences, Public Health Service.

Appendix

The integrals $\mathcal{G}$ and $\mathcal{H}$ are evaluated by expressing the potential Φ in terms of modified Bessel functions of zeroth and first order[4]

$$\Phi = \Phi_0 I_0(\kappa r)/I_1(\kappa a) \qquad (53)$$

where κ is the Debye–Hückel reciprocal double-layer thickness, defined by

$$\kappa^2 = 4\pi|e_1||e_2|\rho_s/\epsilon kT \qquad (54)$$

and Φ_0, the potential at $r = a$, is given by

$$\Phi_0 = 4\pi\sigma_e/\kappa\epsilon \qquad (55)$$

The integral $\mathcal{G}$ can now be obtained by utilizing the properties of the modified Bessel functions. From (40) and (53)

$$\mathcal{G} = \int_0^a \{(\Phi - \Phi_0)/\eta\} r\mathrm{d}r = (\Phi_0/2\eta)\left[(2/I_1(\kappa a))\int_0^a I_0(\kappa r) r\mathrm{d}r - a^2\right] \qquad (56)$$

The integral in eq 56 is evaluated by use of the relations

$$\int_0^a I_0(\kappa r) r\mathrm{d}r = (a/\kappa)I_0'(\kappa a) \qquad (57)$$

(see ref 14, p 43) and

$$I_0'(\kappa a) = I_1(\kappa a) \qquad (58)$$

(see ref 15, p 201). From (56), (57), and (58)

$$\mathcal{G} = (\Phi_0/2\eta)[2a/\kappa - a^2] \qquad (59)$$

and when $\kappa a \gg 1$, this reduces to

$$\mathcal{G} = -\Phi_0 a^2/2\eta \qquad (60)$$

The more complicated integral $\mathcal{H}$ can be simplified, using integration by parts

$$\mathcal{H} = \int_0^a [(\Phi - \Phi_0)/\eta](\nabla^2\Phi) r\mathrm{d}r = -(1/\eta)\int_0^a [\mathrm{d}(\Phi - \Phi_0)/\mathrm{d}r]^2 r\mathrm{d}r \qquad (61)$$

Using eq 53 and 58, this becomes

$$\mathcal{H} = -[\Phi_0^2/\eta I_1^2(\kappa a)]\int_0^a [I_1(\kappa r)]^2(\kappa r)\mathrm{d}(\kappa r) \qquad (62)$$

Performing the integration

$$\int_0^a [I_1(\kappa r)]^2(\kappa r)\mathrm{d}(\kappa r) = -[{}^1/_2]\kappa^2 a^2[\{I_1'(\kappa a)\}^2 - (1 + 1/a^2\kappa^2)I_1^2(\kappa a)] \qquad (63)$$

(see ref 15, p 203) and using the relation

$$I_1'(\kappa a) = I_0(\kappa a) - I_1(\kappa a)/\kappa a \qquad (64)$$

(ref 15, p 201), eq 62 becomes

$$\mathcal{H} = (\Phi_0^2\kappa^2 a^2/2\eta)\{[(I_0(\kappa a)/I_1(\kappa a)) - 1/\kappa a]^2 - 1 - 1/\kappa^2 a^2\} \qquad (65)$$

For $\kappa a \gg 1$, the ratio of Bessel functions in (65) can be expanded as follows (see ref 14, p 49)

$$I_0(\kappa a)/I_1(\kappa a) = 1 + 1/2\kappa a + 3/(8\kappa^2 a^2) + \ldots \qquad (66)$$

This leads to the result

$$\mathcal{H} = -\Phi_0^2\kappa a/2\eta = 4\pi\sigma_e\mathcal{G}/a\epsilon \qquad (67)$$

---

(14) F. Bowman, "Introduction to Bessel Functions," Dover Publications, Inc., New York, N. Y., 1958.

(15) N. W. McLachlan, "Bessel Functions for Engineers," Oxford University Press, London, 1955.

On the Temperature Coefficient of Unperturbed Dimensions of Atactic Polystyrene

by Umberto Bianchi, Eligio Patrone, and Enrico Pedemonte

Istituto di Chimica Industriale, Sez. V Centro Nazionale di Chimica delle Macromolecole, Università di Genova, Genova, Italy *(Received February 15, 1966)*

Conflicting results concerned with the temperature coefficient of unperturbed dimensions in atactic polystyrene are discussed, taking into account the method by which they have been derived. By measuring the specific solvent effect present in various Θ-solvent series, it is shown that positive values of the temperature coefficient (around room temperature) cannot be attributed to polystyrene on safe grounds, whereas evidence is increasing supporting the opposite tendency of the polystyrene chain to decrease its dimension on increasing the temperature.

Introduction

The experimental study of the temperature variation of unperturbed mean-square end-to-end distance $\langle r_0^2 \rangle$ in atactic polystyrene started with the pioneering work of Flory and Fox.[1]

These authors found, from the values of $K_\Theta = \Phi \cdot [\langle r_0^2 \rangle / M]^{3/2}$ at two temperatures (34 and 70°), a value of $\mathrm{d} \ln \langle r_0^2 \rangle / \mathrm{d}T = -1.8 \times 10^{-3}$ deg^{-1}, which has been subsequently confirmed.[2]

Very recently, Orofino and Ciferri[3] reported a positive value of the temperature coefficient $\mathrm{d} \ln \langle r_0^2 \rangle / \mathrm{d}T = 0.4 \times 10^{-3}$ deg^{-1} derived both from solution and bulk studies, which has been used[4] in discussing the conformational properties of vinyl polymers.

In an attempt to clarify the situation, we shall discuss the kind of evidence on which negative and positive values of $\mathrm{d} \ln \langle r_0^2 \rangle / \mathrm{d}T$ are based.

Specific Solvent Effects in Solution

As we have already pointed out,[5,6] the use of unrelated Θ solvents can easily arrive at misleading results, as in this case the experimental $\mathrm{d} \ln \langle r_0^2 \rangle / \mathrm{d}T$ involves not only the temperature variation of $\langle r_0^2 \rangle$ but also the change in conformational properties due to short-range solvent effects.[7-12] In light of this observation, values of $\mathrm{d} \ln \langle r_0^2 \rangle / \mathrm{d}T$ given in ref 1 and 13 are to be considered with caution.

It is obvious that, to obtain a significant value of $\mathrm{d} \ln \langle r_0^2 \rangle / \mathrm{d}T$ (attributable at least to the couple polymer + solvent), it is sufficient that solvent effects, if present, will not change sensibly in going from one Θ solvent to the other. This is the reason why Bianchi and Magnasco[2] and Orofino and Ciferri[3] have used a set of related Θ solvents: in the first case, three toluene–methanol mixtures with a methanol concentration slightly increasing from low (25°) to high (45°) Θ temperatures, and in the second case, three structurally similar Θ solvents, 1-chlorodecane (Θ = 6.6°), 1-chloroundecane (Θ = 32.8°), and 1-chlorododecane (Θ = 58.6°) (referred to in the following as Cl10, Cl11, and Cl12).

---

(1) T. G Fox and P. J. Flory, *J. Am. Chem. Soc.*, **73**, 1915 (1951).

(2) U. Bianchi and V. Magnasco, *J. Polymer Sci.*, **41**, 177 (1959).

(3) T. A. Orofino and A. Ciferri, *J. Phys. Chem.*, **68**, 3136 (1964).

(4) J. E. Mark and P. J. Flory, *J. Am. Chem. Soc.*, **87**, 1423 (1965).

(5) U. Bianchi, *J. Polymer Sci.*, **A2**, 3083 (1964); A. Ciferri, *ibid.*, **A2**, 3088 (1964).

(6) U. Bianchi, E. Patrone, and M. DalPiaz, *Makromol. Chem.*, **84**, 230 (1965).

(7) A. R. Schultz and P. J. Flory, *J. Polymer Sci.*, **15**, 231 (1955).

(8) U. Bianchi, V. Magnasco, and C. Rossi, *Chim. Ind.* (Milan), **40**, 263 (1958).

(9) K. J. Ivin, H. A. Ende, and G. Meyerhoff, *Polymer*, **3**, 129 (1962).

(10) H. G. Elias and O. Etter, *Makromol. Chem.*, **65**, 56 (1963).

(11) T. A. Orofino and J. W. Mickey, Jr., *J. Chem. Phys.*, **38**, 2512 (1963).

(12) V. Crescenzi and P. J. Flory, *J. Am. Chem. Soc.*, **86**, 141 (1964).

(13) G. V. Schulz and H. Baumann, *Makromol. Chem.*, **60**, 120 (1963).

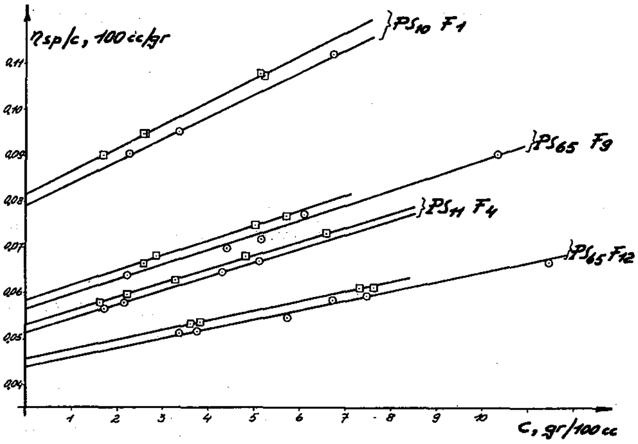

Figure 1. Plot of $\eta_{sp/c}$ *vs.* c for some polystyrene (PS) fractions in 1-chlorodecane (open circles) and 1-chlorododecane (squares) at 35°.

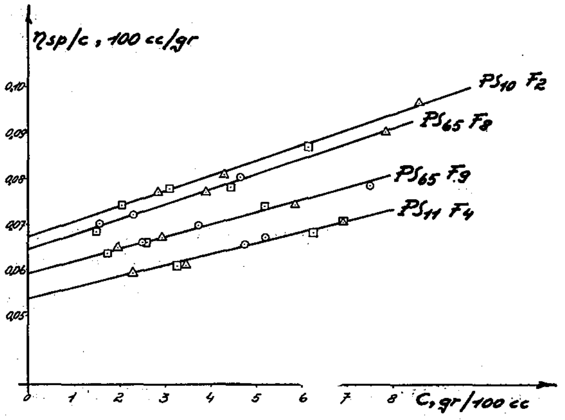

Figure 2. Plot of $\eta_{sp/c}$ *vs.* c for some polystyrene fractions in θ_1 (squares), θ_2 (open circles), and θ_3 (triangles). θ_1, θ_2, and θ_3 have the same meaning as in Table I.

Even so, our result ($d \ln \langle r_0^2 \rangle / dT = -1.8\ (\pm 0.4) \times 10^{-3}$) is in striking disagreement with that of Orofino and Ciferri (0.4×10^{-3}). This is a surprising result, as it is by no means clear why one set of Θ solvents should be considered more structurally related than the other.

A possible explanation of the disagreement between the two values of $d \ln \langle r_0^2 \rangle / dT$, both obtained in at least apparently related Θ solvents, is the existence of a varying specific effect within one or both the Θ-solvent series.

We have already shown[14,15] how it is possible to discover the existence of solvent effects by measuring the constant K_0 in the equation

$$[\eta] = K_0 M^{1/2} \qquad (1)$$

which has been found to be valid in sufficiently low molecular weight ranges for many polymers[14-20] in normal (non-Θ) solvents. It has been shown that K_0 is very near K_Θ provided specific solvent effects are absent or very small.

Previous works[14,19] have shown that the range in which eq 1 is applicable goes from $M = 5 \times 10^2$ to about 10^4 for atactic polystyrene in good solvents (benzene, toluene, etc.) and extends to higher molecular weights in poorer solvents[20] (methyl ethyl ketone).

By measuring, at the same temperature, $[\eta]$ ($= K_0 \cdot M^{1/2}$) for some polystyrene fractions (with molecular weight comprised in this range) in the various Θ solvents, it should then be possible to discover the existence of a varying solvent effect.

Experimental Section

Polystyrene fractions, with $\bar{M}_n$ ranging from 2.7×10^3 to 9.5×10^3, calculated from the equation

$$\log [\eta] = -3.05 + 0.5 \log M \qquad (2)$$

have been obtained from previously described fractionations.[14]

The range of temperature covered by the two sets of Θ solvents being 25–45° in our case[2] and 6–58° in ref 3, we have chosen 35° as the temperature at which to measure $[\eta]$ ($= K_0 M^{1/2}$). Polydispersity, if present, would not matter, as we are comparing $[\eta]$ in different solvents but all measured on the same fractions.

Figures 1 and 2 show some of the $\eta_{sp/c}$ *vs.* c plots and Table I collects the experimental values of $[\eta]$.

Discussion

Viscosity measurements in Table I show that, for all of the polystyrene fractions examined, $[\eta]$ values at 35° in Cl12 are consistently higher than values in Cl10 or Cl11. Even supposing the expansion coefficient α not to be strictly equal to 1 for such low molecular weights, one would expect $[\eta]$ in Cl12 to be less than in Cl10 or Cl11, as polystyrene in Cl12 at 35° *is below* Θ conditions (Cl12 is Θ at 58.6°) and *above* Θ conditions in Cl10 (Θ = 6.6°) and Cl11 (Θ = 32.8°).

The opposite result thus strongly points toward the presence of a specific solvent effect, which alters the polystyrene conformational properties to a different

---

(14) C. Rossi, U. Bianchi, and E. Bianchi, *Makromol. Chem.*, **41**, 31 (1960).

(15) U. Bianchi, M. Dal Piaz, and E. Patrone, *ibid.*, **80**, 112 (1964).

(16) E. Patrone and U. Bianchi, *ibid.*, **94**, 52 (1966).

(17) C. Rossi and C. Cuniberti, *J. Polymer Sci.*, **B2**, 681 (1964).

(18) T. G Fox, J. B. Kinsinger, H. F. Mason, and E. M. Schuele, *Polymer*, **3**, 71 (1962).

(19) T. Altares, D. P. Wyman, and V. R. Allen, *J. Polymer Sci.*, **A2**, 4533 (1964).

(20) R. Okada, Y. Toyoshima, and H. Fujita, *Makromol. Chem.*, **59**, 137 (1963).

Table I: Intrinsic Viscosities (dl/g) of Various Polystyrene (PS) Fractions in Cl10, Cl11, and Cl12 in Θ_1, Θ_2, and Θ_3 at 35°[a]

Fraction	$\bar{M}_n \times 10^{-3}$	$[\eta]$, 100 cc/g Cl10	Cl11	Cl12	$[\eta]_{\Theta_1(=\Theta_2=\Theta_3)}$ 100 cc/g
$PS_{10}F1$	9.5	0.079	...	0.081_5	...
$PS_{10}F2$	5.6	...	0.067	0.067	0.067_5
6PSF6	5.5	0.060_5	0.063_5	0.065_5	...
$PS_{65}F8$	5.2	...	...	0.064_5	0.064_5
$PS_{65}F9$	4.4	0.056_5	...	0.058_5	0.059
$PS_{11}F4$	3.6	0.051_5	...	0.053	0.054
$PS_{65}F12$	2.7	0.044	...	0.046	...

[a] Θ_1, Θ_2, and Θ_3 are toluene–methanol mixtures with 23.1, 24.8, and 27.2% methanol (in volume), respectively. Only $[\eta]$ in Θ_1 is given, $[\eta]_{\Theta_2}$ and $[\eta]_{\Theta_3}$ being identical.

extent in going from Cl10 to Cl12. Moreover, $[\eta]$ values measured in our three Θ-solvent mixtures are coincident within experimental error. Consequently, the value $\mathrm{d}\ln\langle r_0^2\rangle/\mathrm{d}T = -1.8(\pm 0.4) \times 10^{-3}$ deg^{-1} should be attributed to the temperature effect *per se*, whereas the experimental value of ref 3, $\mathrm{d}\ln\langle r_0^2\rangle/\mathrm{d}T = 0.4 \times 10^{-3}$ deg^{-1}, contains a *positive* contribution from specific solvent effects.

It seems appropriate at this point to discuss the positive value of $\mathrm{d}\ln\langle r_0^2\rangle/\mathrm{d}T$ found for atactic polystyrene PS by thermoelasticity measurements.[3] We shall simply make two observations. One is connected with the large difference in the average temperatures at which $\mathrm{d}\ln\langle r_0^2\rangle/\mathrm{d}T$ has been measured, $\bar{T} = 40°$ in the case of viscosity and $\bar{T} = 150°$ in thermoelasticity measurements. As stated by Orofino and Ciferri themselves, there are already indications[21–23] that the quantity $\mathrm{d}\ln\langle r_0^2\rangle/\mathrm{d}T$ could not remain constant over wide temperature intervals. Consequently, agreement between the two values is not necessarily expected and cannot in general be used as a proof of internal consistency.

The second observation is a more fundamental one and is concerned with the fact that a noncoincidence between $\mathrm{d}\ln\langle r_0^2\rangle/\mathrm{d}T$ values derived from solution and bulk properties could originate from the difference in environmental properties existing in the two systems; as stated in previous papers,[3,5,6] it seems important to refer $\mathrm{d}\ln\langle r_0^2\rangle/\mathrm{d}T$ values obtained from solution studies to the complex structure polymer + solvent *and not* to the isolated, unperturbed polymer chain.

As a last comment, we refer to the temperature range (120–170°) covered in ref 3 by stress–temperature measurements, where cross-linked atactic polystyrene has been assumed to behave like a rubber. It is known,[24,25] however, that the glass transition temperature of a cross-linked, stretched sample is higher than that of the uncross-linked polymer ($T_g = 100°$ for polystyrene) for at least two reasons. (A) Cross linking increases T_g (in the case of Orofino and Ciferri, the increase ΔT_g due to a divinylbenzene mole fraction $= 0.52 \times 10^{-2}$ is about 5°[26]). (B) Stretching increases T_g (according to Gee[27] and DiMarzio,[28] the effect should amount to only 1–2°).

Moreover, it is well known that T_g is time-dependent,[25,29] and in the present case depends on the rate of heating (or cooling) applied during the stress–temperature analysis. We have measured[30] the glass transition temperature of a polystyrene sample of identical preparation as that used in ref 3, applying two different rates of heating (and cooling): 25°/hr (the rate used in ref 3) and 1°/day. ΔT_g was found to be 5°. Summing up all these contributions, we can conclude that the "apparent" glass transition temperature of the polystyrene sample during the thermoelasticity measurements was around 111–112°.

Taking into account that the glass transition always occurs over a range of temperature, it is possible that the tension–temperature study of ref 3 has been performed over too low a temperature range, at the beginning of which the sample was not completely in the rubbery "state."

It is easy to see[31] that this effect would make the apparent $\mathrm{d}\ln\langle r_0^2\rangle/\mathrm{d}T$ more positive than it should be.

Conclusions

We conclude that so far a positive value of $\mathrm{d}\ln\langle r_0^2\rangle/\mathrm{d}T$ for atactic polystyrene has not received sufficiently safe grounds.

It has been shown that the related Θ solvents Cl10, Cl11, and Cl12 still present a varying specific effect which results in an apparently positive temperature coefficient. On the opposite side, our present results give support to early solution studies[1,2] indicating a tendency of polystyrene unperturbed dimension to decrease with increasing temperature.

---

(21) C. Reiss and H. Benoit, *Compt. Rend.*, **253**, 268 (1961).

(22) I. Sakurada, A. Nakajima, O. Yoshizaki, and K. Nakamae, *Kolloid-Z.*, **186**, 41 (1962).

(23) U. Bianchi, C. Cuniberti, and G. Dellepiane, *Ric. Sci.*, **A2**, 506 (1962).

(24) T. G Fox and P. J. Flory, *J. Polymer Sci.*, **14**, 315 (1954).

(25) F. Bueche, "Physical Properties of Polymers," Interscience Publishers, Inc., New York, N. Y., 1962.

(26) K. Ueberreiter and G. Kanig, *J. Chem. Phys.*, **18**, 399 (1950).

(27) G. Gee, P. N. Hartley, J. B. M. Herbertand, and H. A. Lanceley, *Polymer* **1**, 365 (1960).

(28) E. A. DiMarzio, *J. Res. Natl. Bur. Std.*, **68A**, 611 (1964).

(29) A. J. Kovacs, *Fortschr. Hochpolymer. Forsch.*, **3**, 394 (1963).

(30) U. Bianchi and E. Pedemonte, to be published.

(31) L. R. G. Treloar, "The Physics of Rubber Elasticity," Oxford Press, London, 1958.

Additional evidence can be found in our work[32] on the $[\eta]/T$ behavior for low molecular weight polystyrene fractions in various solvents; as shown previously,[6,33] for sufficiently low molecular weights where the expansion factor α is very near unity, we have $d \ln [\eta]/dT \simeq {}^2/_3\, d \ln \langle r_0^2 \rangle/dT$.

Our measurements give the following values: for polystyrene ($M \simeq 3 \times 10^3$) in toluene at $T = 40°$, $d \ln [\eta]/dT = -1.9 \times 10^{-3}$; for polystyrene in cyclohexane at $T = 40°$, $d \ln (\eta)/dT = -1.5 \times 10^{-3}$. This last value is particularly illuminating, as in cyclohexane the thermodynamic contribution to α, if acting alone, would certainly make α and therefore $[\eta]$ increase with temperature.

Acknowledgments. This work has originated from the stimulating discussions we had with Dr. A. Ciferri and Dr. T. A. Orofino during their visit to the Genoa University. We wish also to thank Dr. Orofino for having given all of the details about the preparation of polystyrene–divinylbenzene networks. Our thanks are also due to Professor C. Rossi for his constant interest in this work.

---

(32) E. Patrone and U. Bianchi, to be published.

(33) E. Patrone and U. Bianchi, *Ric. Sci.*, **1**, 17 (1966).

An Electron Spin Resonance Study of Intermediates Formed during Photosensitized Oxidation of Alcohols[1]

by Peter J. Baugh,[2] Glyn O. Phillips,[3] and Jett C. Arthur, Jr.

Southern Regional Research Laboratory,[4] New Orleans, Louisiana *(Received February 18, 1966)*

Electron spin resonance spectroscopy was used to identify and to examine the role and kinetics of semiquinone radicals and radical ions in the photosensitized oxidation of aqueous solutions of D-sorbitol, cellobiose, D-glucose, glycerol, and methyl, ethyl, isopropyl, and *n*-propyl alcohols. Sodium anthraquinone-1- and -2-sulfonates and -2,6- and -1,5-disulfonates were used as sensitizers. When aqueous solutions of sodium anthraquinone-2,6-disulfonate and -2-sulfonate were photolyzed, a singlet was observed which could be associated with the formation of the semiquinone radical. Photolysis of the sensitizers in the presence of carbohydrates and alcohols caused the singlet which formed on photolysis to decay with first-order dependence on concentration of alcohol and anthraquinonesulfonate salt. Second-order rate constants were calculated, and relative values compared with those of previous workers obtained by other methods. In alkaline solution of anthraquinone salts containing carbohydrates, anthrasemiquinone radical ions were formed and were the same whether produced by photolysis and/or thermolysis. From the observed spectra the hyperfine splitting constants were calculated and possible assignments proposed in relation to the structure of the anthrasemiquinone radical ions. Attempts have been made to identify the precursor of the semiquinone radicals formed during photolysis of aqueous solutions of sodium anthraquinone-2-sulfonate and -2,6-disulfonate, containing carbohydrates or alcohols. It is possible that the precursor of the radicals may be the triplet state.

Introduction

The commonly accepted mechanism of the photosensitized oxidation of ethanol is that proposed initially by Bolland and Cooper,[5] and extended by Wells.[6] The initial reactions proposed in neutral oxygenated solutions were

$$A + h\nu \longrightarrow A^* \qquad (1)$$

$$A^* + CH_3CH_2OH \xrightarrow{k_1} AH\cdot + CH_3\dot{C}HOH \qquad (2)$$

A represents the sensitizer; A*, the excited state of the sensitizer; and AH·, the semiquinone radical. A series of additional reactions were proposed to account for the participation of oxygen, perhydroxyl radicals, and sensitizer.

In a series of kinetic investigations based on oxygen absorption, Wells[7] proposed that the deactivation of the sensitizer proceeds in two ways only, as shown in reactions 2 and

$$A^* \xrightarrow{k_0} A \qquad (3)$$

Oxygen absorption obeyed the expression

$$-\frac{dt}{d[O_2]} = \frac{1}{I} + \frac{1}{I}\frac{1}{[RH]}\frac{k_0}{k_1}$$

---

[1] Presented in part at the 151st National Meeting of the American Chemical Society, Pittsburgh, Pa., March 22-31, 1966.

[2] Resident Postdoctoral Research Associate.

[3] University College, Cardiff, Wales.

[4] One of the laboratories of the Southern Utilization Research and Development Division, Agricultural Research Service, U. S. Department of Agriculture.

[5] J. L. Bolland and H. R. Cooper, *Proc. Roy. Soc.* (London), **A225**, 405 (1954).

[6] C. F. Wells, *Trans. Faraday Soc.*, **57**, 1703 (1961).

[7] C. F. Wells, *ibid.*, **57**, 1719 (1961); *Discussions Faraday Soc.*, **29**, 219 (1960); *J. Chem. Soc.*, 3100 (1962).

where [RH] is the concentration of alcohol and I the rate of activation proportional to the intensity of light. Using this relationship k_1/k_0 can be calculated. The values of k_1/k_0 for a series of alcohols using the same quinone give the related reactivities of these alcohols to hydrogen transfer promoted by the *excited* sensitizer. Based on actual product estimations, Phillips, Barber, and Rickards[8] found that the effective kinetics for D-sorbitol (RCH_2OH) degradation sensitized by sodium anthraquinone-2-sulfonate or -2,6-disulfonate could be represented by

$$-\frac{dt}{d[RCH_2OH]} = \frac{1}{I} + \frac{1}{I}\,\frac{1}{[RCH_2OH]}\,\frac{k_0}{k_1}$$

We have been interested in this reaction because of its close relation to the photodegradation of cotton cellulose sensitized by anthraquinonoid vat dyes. To devise protective methods it is particularly important to elucidate the role of the semiquinone radical ($AH\cdot$) relative to the excited sensitizer (A^*). Electron spin resonance was used to identify and to examine the role of semiquinone radicals and radical ions in the photodegradation of D-sorbitol sensitized sodium anthraquinones. We have found that the reaction

$$RCH_2OH + AH\cdot{}^* \xrightarrow{k_2} R\dot{C}HOH + AH_2 \qquad (4)$$

is of particular significance in the photodegradation process where $AH\cdot{}^*$ may be the semiquinone in its ground or excited state.

Experimental Section

Materials. The anthraquinones used were obtained from commercial chemical sources and were recrystallized from C_6H_6, C_2H_5OH, or distilled H_2O before use. Alcohols and sugars used were reagent grade and were used without further purification.

Apparatus and Procedure. The electron spin resonance spectra of the intermediates formed during the photosensitized oxidation of alcohols in solution were determined in a Varian 4502-15 epr spectrometer system.[9] The system was equipped with a variable temperature accessory allowing operation from about −185 to 300°, a dual sample cavity having a slotted opening in one side of one cavity, and an aqueous solution sample cell accessory. A PEK 110 Hg short-arc, point-source, high-pressure lamp[9] was used to irradiate the solutions directly in the sample cell within the resonant cavity. The light from the lamp was focused to about 1 cm^2 on the slotted opening in the cavity and had a rated luminous intensity of 140,000 candles/cm^2. The lamp was placed at a distance from the sample so that the light from the lamp did not sensibly heat the sample. The spectral distribution of the radiant energy output of the lamp contained characteristic high-pressure Hg vapor lines. Except where indicated, the solutions were irradiated at 25°. Absolute splitting constants were obtained by calibrating the system with p-benzoquinone (a = 2.37 gauss).[10]

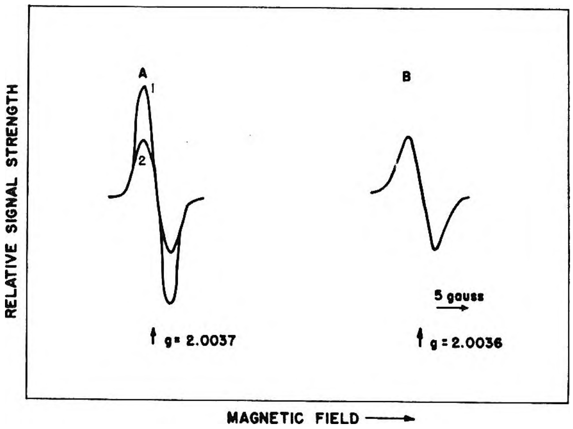

Figure 1. Esr spectra of photolyzed aqueous solutions (0.037 M) of sodium anthraquinone-2,6-disulfonate (A-1, 370 sec; A-2, 150 sec) and sodium anthraquinone-2-sulfonate (B, 150 sec).

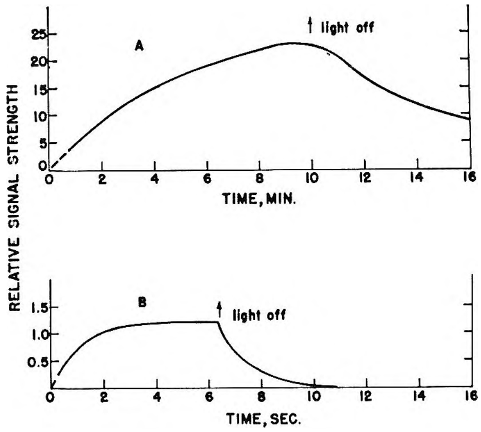

Figure 2. Rate of change of esr signal strength of photolyzed aqueous solutions of sodium anthraquinone-2,6-disulfonate: (A) 0.037 M, (B) 0.0037 M.

Results

Sodium Anthraquinone-2,6-disulfonate. A narrow singlet (line width about 5 gauss with g = 2.0036) was observed when an aqueous neutral solution of sodium anthraquinone-2,6-disulfonate (3.7×10^{-2} M) was

---

(8) G. O. Phillips, P. Barber, and T. Rickards, *J. Chem. Soc.*, 3443 (1964).

(9) Trade names are given as part of the exact experimental conditions and not as an endorsement of the products over those of other manufacturers.

(10) B. Venkataraman, B. G. Segal, and G. K. Fraenkel, *J. Chem. Phys.*, **30**, 1006 (1959); *J. Am. Chem. Soc.*, **77**, 2707 (1955).

photolyzed with ultraviolet light (see Figure 1). The rates of formation of the radical species during photolysis of this solution and of a less concentrated solution (3.7×10^{-3} *M*) are shown in Figure 2. For the lower concentration of the 2,6-disulfonate on photolysis the esr signal increased to a maximum value in a few seconds. The rate of decay of the radical species when the light was extinguished was much lower in the more concentrated solution.

Effects of Sugars. When an aqueous neutral solution of sodium anthraquinone-2,6-disulfonate (3.7×10^{-3} *M*) and D-sorbitol (0.55 *M*) was photolyzed (preoxygenated or *in vacuo*), an esr signal was observed (same as in Figure 1A). This species appeared almost immediately (within 5 sec of initiation of irradiation) and decayed rapidly as the photolysis continued (see Figure 3). The maximum free-radical concentration, obtained after about 5 sec of photolysis, varied with sensitizer concentration, as shown in Figure 4, the carbohydrate concentration being kept constant. Point C in Figure 4 shows that for a given sensitizer concentration the maximum concentration of free radical is independent of the sugar used.

The rate of disappearance of the radical during continuous photolysis was dependent on the concentration of D-sorbitol (see Figure 5). For these data the plot of 1/[radical concentration] *vs.* time was linear and could therefore be used to calculate initial rates for the radical decay. The plots of log $(\text{rate})_{t=0}$ *vs.* log $[\text{solute}]_{t=0}$ are linear (see Figure 6). From the slopes of the lines it can be calculated that the rate was proportional to $[\text{D-sorbitol}]^{0.96}$, $[\text{cellobiose}]^{1.06}$, and $[\text{D-glucose}]^{1.02}$. It has been similarly shown that the reaction rate was proportional to the first power of the sensitizer concentration. We therefore calculated second-order rate constants using the expression: $[\text{rate of decay of radical}]_{t=0} = k_2[\text{sensitizer}][\text{solute}]$. For D-sorbitol k_2 was 2×10^{-2} l. mole^{-1} sec^{-1}; for cellobiose, 4×10^{-2} l. mole^{-1} sec^{-1}; and for D-glucose, 3×10^{-2} l. mole^{-1} sec^{-1}.

In alkaline solution (0.2 *M* NaOH) of sensitizer (3.7×10^{-3} *M*) and sugars (0.1–0.5 *M*), the esr signal (similar to that for neutral solution) was stronger by several orders of magnitude than that for neutral solution. The strength of the esr signal, which formed within a few seconds after the light was turned on, varied linearly with sensitizer concentration (see Figure 4A). The decay rate showed some dependence on solute concentration during continuous photolysis (see Figure 7).

Sodium Anthraquinone-2-sulfonate. When aqueous solutions of sodium anthraquinone-2-sulfonate were irradiated, an esr signal was observed (see Figure 1B)

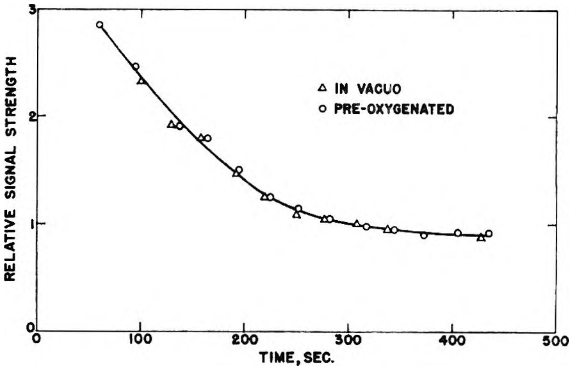

Figure 3. Rate of decay of radical species formed by continuous photolysis of aqueous solutions of D-sorbitol (0.55 *M*) containing sodium anthraquinone-2,6-disulfonate (0.0037 *M*).

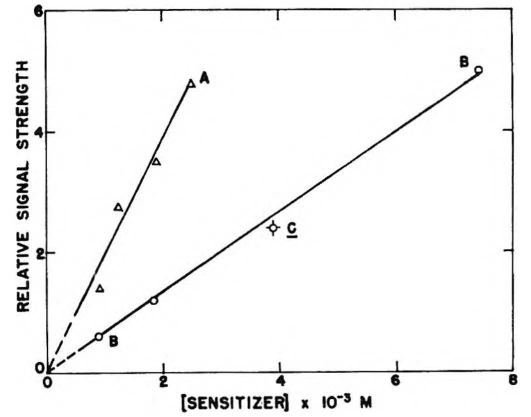

Figure 4. Effect of concentration of sodium anthraquinone-2,6-disulfonate on the initial esr signal strength in photolyzed aqueous solutions of D-sorbitol (0.4 *M*) and NaOH (0.2 *M*) (A), of D-sorbitol (0.275 *M*) (B), and of D-sorbitol, cellobiose, and D-glucose (0.1375 *M*) (C).

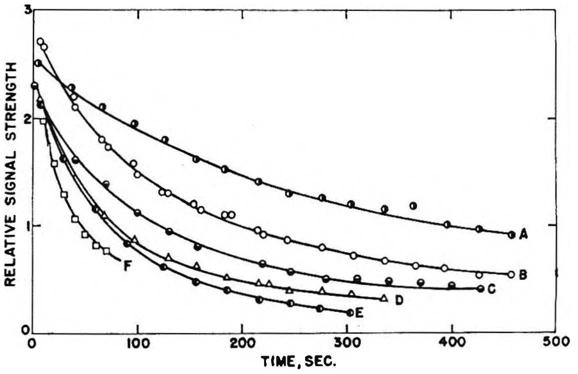

Figure 5. Effect of varying the concentration of D-sorbitol, in the presence of sodium anthraquinone-2,6-disulfonate (0.0037 *M*), on rate of decay of radical species formed by continuous photolysis: (A) 0.05 *M*, (B) 0.1 *M*, (C) 0.2 *M*, (D) 0.4 *M*, (E) 0.55 *M*, (F) 0.75 *M*.

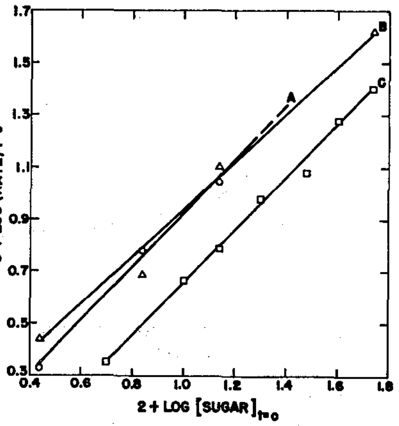

Figure 6. Order of reaction for decay of radical species formed by continuous photolysis of aqueous solutions of cellobiose (A), D-glucose (B), and D-sorbitol (C) containing sodium anthraquinone-2,6-disulfonate (0.0037 M)

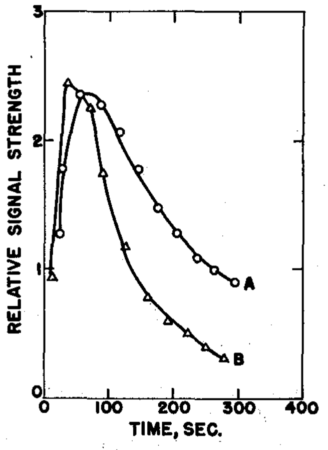

Figure 7. Dependence of rate of decay of radical species formed by photolysis on concentration of D-sorbitol (A, 0.3 M; B, 0.1 M) in alkaline solutions (NaOH, 0.2 M) containing sodium anthraquinone-2,6-disulfonate (0.0037 M).

which decayed with a rate dependent on sensitizer and solute concentration. A kinetic expression was found for this sensitizer similar to that for the 2,6-disulfonate. The reaction was first order in D-sorbitol and sensitizer. For D-sorbitol k_2, calculated as above, was 1×10^{-3} l. mole^{-1} sec^{-1}.

Sodium Anthraquinone-1-sulfonate and -1,5-disulfonate. When the 1-sulfonate and 1,5-disulfonate were irradiated in neutral solutions under conditions identical with those described above for the 2-sulfonate and 2,6-disulfonate, no esr signal was observed. In alkaline solution under similar conditions an esr signal was observed, probably due to the formation of the semiquinone radical ions.

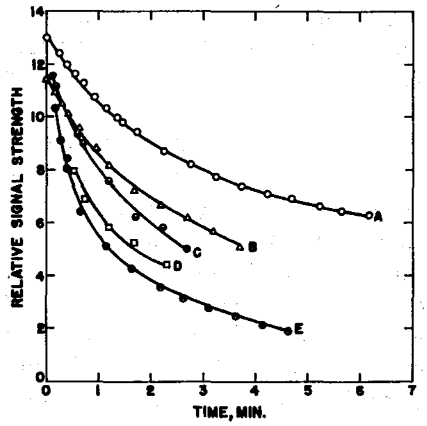

Figure 8. Rate of decay of radical species formed during photolysis of aqueous solutions of alcohols (0.5 M) containing sodium anthraquinone-2,6-disulfonate (0.0037 M) (light on): (A) methanol, (B) glycerol, (C) ethanol, (D) 1-propanol, (E) 2-propanol.

Aliphatic Alcohols. When sodium anthraquinone-2,6-disulfonate was irradiated in aqueous alcoholic solution at pH 7, there was a pronounced difference in decay rate of the radical depending on the alcohol. Typical results for glycerol, methanol, 1-propanol, 2-propanol, and ethanol are shown in Figure 8. The initial rates for the reaction were calculated at varying alcohol and sensitizer concentrations, and from the data the second-order rate constants, shown in Table I, were calculated.

Table I: Rate Constants for Reaction of Semiquinone Radicals with Aliphatic Alcohols

	Alcohol				
	Methyl	Ethyl	Iso-propyl	n-Propyl	Glycerol
$k_2 \times 10^{-2}$ l. mole^{-1} sec^{-1}	1.4	3.4	6.4	5.1	2.5
k_2(ROH)/k_2(EtOH)	0.4	1	1.9	1.5	0.7

Esr Spectra of Semiquinone Ions. The esr spectra of the semiquinone ions are not obtained instantly when aqueous alkaline solutions of sodium anthraquinonesulfonates are irradiated. This behavior for the 1-sulfonate (3.7×10^{-3} M) in the presence of D-sorbitol (0.4 M) and NaOH (0.2 M) is shown in Figure 9. The final spectra of the irradiated solutions of the sulfonate are shown in Figure 10. Less hyperfine splitting was found at the lower temperatures. The esr spectrum of the semiquinone radical ion from sodium anthraquinone-2,6-disulfonate at −76° is shown in Figure 11.

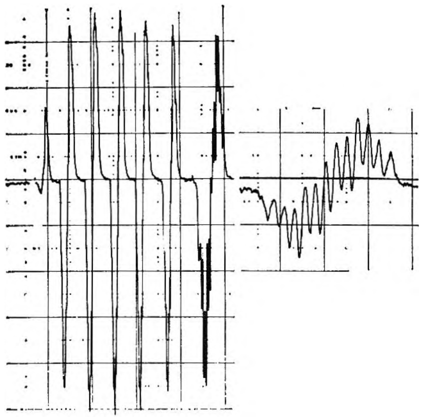

Figure 9. Rate of formation of semiquinone radical ion by photolysis of aqueous alkaline solution (NaOH, 0.2 *M*) of sodium anthraquinone-1-sulfonate (0.0037 *M*) containing D-sorbitol (0.4 *M*): first six sweeps, 10 gauss, 30 sec; seventh sweep, 10 gauss, 1 min; eighth sweep, 10 gauss, 5 min.

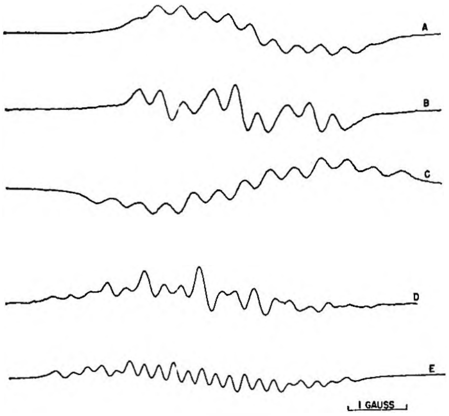

Figure 10. Esr spectra of semiquinone radical ions formed by thermolysis of photolysis of aqueous solutions or sodium anthraquinonesulfonates (0.0037 *M*) containing D-sorbitol (0.4 *M*): (A) sodium anthrasemiquinone-2,6-disulfonate, heat or light; (B) sodium anthrasemiquinone-1,5-disulfonate, heat or light; (C) sodium anthrasemiquinone-1-sulfonate, after 5-min photolysis, heat or light; (D) sodium anthrasemiquinone-1-sulfonate, after 15-min photolysis, light only or light after heat; (E) sodium anthrasemiquinone-2-sulfonate, light only (compare Table II).

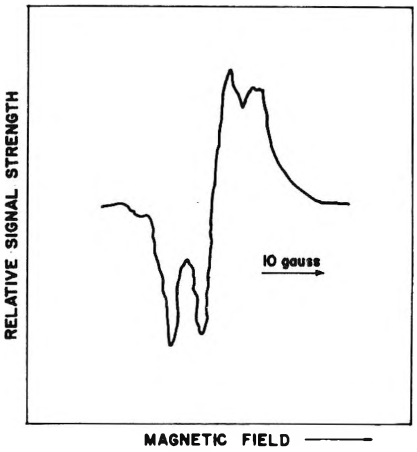

Figure 11. Esr spectrum of radical formed by photolysis at −76° of an aqueous alkaline solution (NaOH, 0.2 *M*) of D-sorbitol (0.4 *M*) containing sodium anthraquinone-2,6-disulfonate (0.0037 *M*).

The sodium anthraquinone-2,6- and -1,5-disulfonates and -1-sulfonate (3.7×10^{-3} *M*) in alkaline D-sorbitol solutions (0.4 *M*) on heating to about 80° for 10 min gave a wine-red coloration. The esr spectra of these solutions were identical with those shown in Figure 10A, B, and C, respectively. On being irradiated the radical ion from the 1-sulfonate was transformed from a 12-line to a 19-line spectra. This effect was similar to that produced by light alone. The 2-sulfonate under the same conditions of heating gave an ill-defined spectrum. The effect on the spectrum by irradiation after heating was similar to that due to irradiation alone; that is, a 21-line spectrum was obtained. The hyperfine spacings and *g* values for the anthrasemiquinone radical ions are given in Table II.

Table II: Hyperfine Spacings of the Anthrasemiquinone Radicals Produced by Light and/or Heat in Alkaline Solutions of Sodium Anthraquinonesulfonates (0.0037 *M*) Containing D-Sorbitol (0.4 *M*)

Sodium anthraquinone-	*g* value[a]	Conditions	No. of lines	Over-all hyperfine splitting, gauss	ΔH, gauss
2,6-Disulfonate	2.0036	Heat or light	11	3.93	0.39
1,5-Disulfonate	2.0038	Heat or light	9	3.286	0.38 0.51
1-Sulfonate	2.0039	Heat or light	12	4.99	0.45
1-Sulfonate	. . .	Light only	19	6.28	. . .
2-Sulfonate	. . .	Heat	Not resolved		
2-Sulfonate	2.0037	Light	21	4.96	0.25

[a] Based on peroxylamine disulfonate, $g = 2.00550$: "EPR at Work, No. 28," Varian Associates, Palo Alto, Calif.

The semiquinone ion derived from the 2,6-disulfonate has a spectrum consisting of 11 lines. This number of lines could result from the coupling of four α protons and two β protons with some of the lines falling so close that overlapping essentially occurs. The correct number of lines would arise if the splitting constant of the α protons was double that of the β protons, which was found to be 0.39 gauss. If $a_\alpha = 2a_\beta + \delta$ where $\delta < a_\beta$, the hyperfine spacings taken from the central component would be $\pm a_\beta + \delta$, $\pm 2a_\beta + \delta$, $\pm 3a_\beta + 2\delta$, $\pm 4a_\beta + 2\delta$, $\pm 5a_\beta + 2\delta$. From the spectrum δ has a maximum value of 0.07 gauss, setting an upper limit of 0.85 for a_α.

The ion derived from sodium anthrasemiquinone-1,5-disulfonate has a spectrum consisting of nine lines due to coupling with two α protons and four β protons, but with some overlapping lines. The observed splitting constants are $a_\beta = 0.37$ gauss, $a_\alpha = 0.89$ gauss with the hyperfine spacings taken from the central component equal to $\pm a_\beta$, $\pm 2a_\beta + \delta$, $\pm 3a_\beta + \delta$, $\pm 4a_\beta + \delta$.

Sodium anthrasemiquinone-1-sulfonate has a spectrum consisting of 12 equally spaced lines which could arise from the interaction of four β protons and three α protons. If the splitting constant of the β proton was approximately double that of the α proton, 12 equally spaced lines would be observed. The splitting constant (a_α) for the α proton was found to be 0.45 gauss. This sets an upper limit of 0.97 gauss for a_β. The 12-line spectrum changes on continued irradiation to 19 lines. Resolution of this spectrum was not obtained.

The ion derived from the sodium salt of the 2-sulfonate gave an equally spaced 21-line spectrum, ΔH = 0.25 gauss.

Energy Transfer. In neutral and alkaline solutions the addition of naphthalene or anthracene (*ca.* 10^{-2} *M*) inhibited the production of anthrasemiquinone radical during irradiation of anthraquinone (2.75×10^{-2} *M*) in degassed 2-propanol–benzene (1:4). For the light filter saturated solution of anthracene or naphthalene in C_6H_6 used, two radical species were observed. The radical species, which could be observed at 25 and −50° in neutral solution, occurred at a higher magnetic field than the other species which could be stabilized only by freezing the solution at −50°. An estimate of the protection afforded by the addition of aromatic hydrocarbons was obtained at −50°. The effect of naphthalene and biphenyl, when added to a solution of anthraquinone (2.75×10^{-2} *M*) in 2-propanol–benzene (1:4) and then irradiated *in vacuo* through the appropriate filter, is shown in Figure 12.

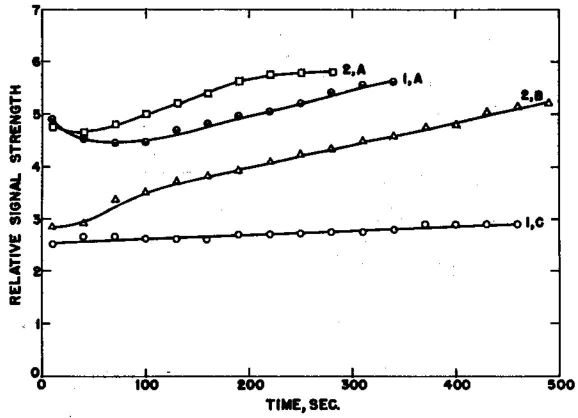

Figure 12. Rate of formation of semiquinone radicals by photolysis at −50° of anthraquinone (0.0275 *M*) in 2-propanol–benzene (1:4) as related to energy transfer. Solutions: (A) anthraquinone (0.0275 *M*); (B) biphenyl (0.01 *M*) and anthraquinone (0.0275 *M*); (C) naphthalene (0.01 *M*) and anthraquinone (0.0275 *M*). Filters: (1) saturated naphthalene in benzene, (2) saturated biphenyl in benzene.

Discussion

There has been considerable discussion of the mechanism of the photooxidation of alcohols by sodium anthraquinonesulfonates.[5–8,11] Although the intermediates active in this process have not previously been directly observed, radicals have been noted during the photoreduction of alkaline solutions of sodium anthraquinone-2-sulfonate[12] and anthraquinonesulfonic acids.[13] Elschner, *et al.*, observed semiquinone radical ions during photoreduction in both the anthraquinone-2-sulfonic and 2,6-disulfonic acids but not in the cases of the 1-sulfonic and 1,5-disulfonic acids.[13] Spectra consisting of at least 30 lines have been observed in hydroxyanthraquinonesulfonates when photoreduced.[14]

It is common practice[15–18] to prepare the substituted anthrasemiquinone radical ions from alkaline organic solutions of the corresponding anthraquinones by use of heat and/or light. Attention has been directed, almost exclusively, to the conditions where ionization of the semiquinone to the radical ion occurs.

---

(11) F. Wilkinson, *J. Phys. Chem.*, **66**, 2569 (1962).

(12) B. Mooney and H. I. Stonehill, *Chem. Ind.* (London), 1309 (1961).

(13) B. Elschner, R. Neubert, H. Berg, and D. Tresselt, *Z. Chem.*, **1**, 361 (1961).

(14) A. D. Broadbent and H. Zollinger, *Helv. Chim. Acta*, **47**, 2140 (1964).

(15) R. W. Brandon and E. A. Lucken, *J. Chem. Soc.*, 4273 (1961).

(16) R. W. Elofson, K. F. Schulz, B. E. Galbraith, and R. Newton, *Can. J. Chem.*, **43**, 1553 (1965).

(17) G. Vincow and G. K. Fraenkel, *J. Chem. Phys.*, **34**, 1333 (1961).

(18) M. Adams, M. S. Blois, and R. H. Sands, *ibid.*, **28**, 774 (1958).

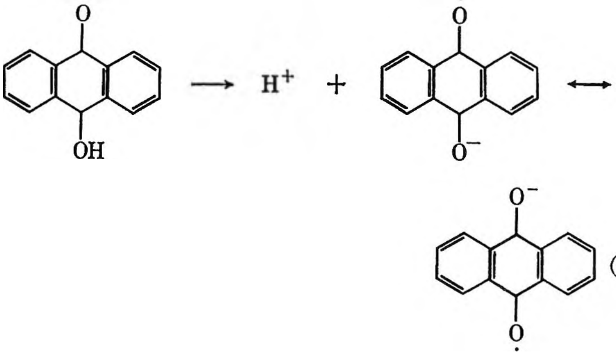

(5)

Mechanistic studies, on the other hand, have been carried out in neutral solution where the reactive intermediate (AH·) could not be detected.[19]

Our initial efforts were, therefore, directed toward identifying and observing the behavior of the radical species which we readily observed in neutral and alkaline aqueous solutions of sodium anthraquinonesulfonates, on irradiation with heat or light, in the presence and absence of alcohols and carbohydrates.

In alkaline solution there can be little doubt that we are observing the esr spectra of the semiquinone radical ions. However, with the evidence available, it is not possible to identify unequivocally the individual proton splitting constants. For the semiquinones derived from the 2,6- and 1,5-disulfonates at least two possibilities exist, and these are indicated in relation to those of substituted anthraquinones which have been studied in Table III. For the 2,6-disulfonate the esr spectrum accords better with the splitting constants a_2 = 0.39 gauss (4), a_1 = 1.21 gauss (2). Furthermore, the splitting constants designated a_1 and a_2 are more consistent with those observed generally in the anthraquinone series (Table III), and would indicate that a_1 protons may be identified with β protons and a_2 protons with α protons. Comparable values (a_2 = 0.37 gauss, a_1 = 1.27 gauss) are consistent with the nine-line spectrum from the 1,5-disulfonate on the basis of two hydroxyl groups having been introduced symmetrically into the molecule. Hydroxylation during this operation is a distinct possibility and was initially proposed by Mooney and Stonehill[12] to account for the colored products arising from the 2,6-disulfonate in aqueous alkali with light. This side reaction is also observed in photooxidation reactions sensitized by the 2,6-disulfonate at low alcohol concentrations.[6-8] It has been suggested that OH radicals can be produced by sensitized photolysis of water and would initiate the hydroxylation process.[12,20] Alternatively, OH ions may lead to hydroxylation as observed during esr examination of substituted mono- and dihydric phenols.[21,22]

Spin densities may be calculated using the expression[23] $a^{H}_{i} = Q^{H}_{CH}\rho^{\pi}_{i}$ where a^{H}_{i} is the proton coupling constant for the proton at position i, ρ^{π}_{i} is the electron spin density at carbon atom i, and Q^{H}_{CH} is a constant. A value of Q close to −22.5 satisfied Vincow and Fraenkel's[17] calculation of unpaired electron density in semiquinones by calculation and experiment and is used here. On this basis the unpaired electron density or more precisely the spin density[24] in the 2,6-disulfonate semiquinone is $\rho^{\pi}_{\alpha} = 0.38$, $\rho^{\pi}_{\beta} = 0.017$ or $\rho^{\pi}_{1} = 0.054$, $\rho^{\pi}_{2} = 0.017$. In each case only about 20% of the spin density is associated with the carbon atoms of the ring. A closely similar low proportion is also associated with the carbon atoms in the 1,5-disulfonate semiquinones. For alkylated phenoxy radicals the major proportion (80%) of the spin density resides in the carbon atoms of the ring not directly attached to the phenolic oxygen. On the other hand, *o*- and *p*-benzosemiquinones have about 65 and 60%, respectively, of the spin density associated with the two oxygen atoms and more nearly resembles our observations with the anthraquinonesulfonates.[21,22]

No detailed consideration is given here to the spectra of the species produced from sodium anthraquinone-1- and -2-sulfonates. The changes in the spectrum, particularly for the 2-sulfonate to give 21 equally spaced lines, could be due to secondary photoreduction of the initial species. Broadbent and Zollinger[14] have reported 30 lines observable by esr during photoreduction of hydroxyanthraquinone-2,7-disulfonic acid. The tentative assignments [a_{α} = 0.45 gauss (3); a_{β} = 0.97 gauss (4)] for the 12-line spectrum from the 1-sulfonate is, at least, consistent with our other observations (see Table III).

In alkaline conditions the semiquinone radical ion is the species which is probably formed by irradiation of the aqueous solution containing sodium anthraquinonesulfonates and D-sorbitol. The species in which no hyperfine splitting was detectably observed in neutral solution is most probably the unionized semiquinone radical, since all other conditions are comparable. Previously, Mooney and Stonehill[12] suggested that a semiquinone could be produced by photodecomposition of a molecule of hydration water

---

(19) J. H. Sharp, T. Kuwana, A. Osborne, and J. N. Pitts, *Chem. Ind.* (London), 508 (1962).

(20) G. K. Oster and N. Wotherspoon, *J. Am. Chem. Soc.*, **79**, 4837 (1957).

(21) F. R. Hengill, T. J. Stone, and W. A. Waters, *J. Chem. Soc.*, 408 (1964).

(22) T. J. Stone and W. A. Waters, *ibid.*, 213 (1964).

(23) H. M. McConnell, *J. Chem. Phys.*, **24**, 632 (1956).

(24) E. de Boer and S. I. Weissman, *J. Am. Chem. Soc.*, **80**, 4549 (1958).

Table III: Hyperfine Splitting Constants (gauss) of 9,10-Anthrasemiquinone Ion and Its Derivatives

Derivative	a_α	a_2	a_β	a_1
Unsubstituted[16]	0.41 (4)[a]		0.83 (4)	
2,6-Disulfonate	0.85 (4)	0.39 (4)	0.39 (2)	1.21 (2)
1,5-Disulfonate	0.89 (2)	0.37 (2)	0.37 (4)	1.29 (2)
1-Sulfonate	0.45 (3)		0.97 (4)	
2-Sulfonate	... (4)		... (3)	
2,6-Dimethyl[16]	0.47 (4)		0.71 (2)	
1,4-Dimethyl[16]	0.33 (2)		0.68 (2)	
			0.64 (2)	

[a] Number in parentheses indicates number of protons.

hydrogen-bonded to the carbonyl oxygen atom of the 2-sulfonate, a process which was strongly pH dependent leading to colored products. When an alcohol is present, on energetic grounds, reaction 2 is the most probable route to the semiquinone AH·. Our results, however, point to further reaction between AH·* or AH· and the alcohol, and it is our suggestion that reaction 2, which is fast, is followed by a slower process reaction 4 or

$$RCH_2OH + AH\cdot \xrightarrow{k_2} R\dot{C}HOH + AH_2 \qquad (6)$$

Reaction 4 is energetically more probable with subsequent aldehyde formation by disproportionation

$$2R\dot{C}HOH \longrightarrow RCH_2OH + RCHO \qquad (7)$$

Evidence from the radiation chemistry of aqueous solutions of alcohols supports reaction 7. The evidence in support of reaction 4 or 6 is, as follows. The rate of disappearance of AH· is first order in AH· and RCH_2OH. Thus the process

$$2AH\cdot \longrightarrow AH_2 + A \qquad (8)$$

for removal of AH· cannot be significant. The concentration of AH· is proportional to the light absorbed as required by reactions 1 and 2, and the over-all stoichiometry observed in oxygen[6-8] is satisfied. More sensitizer can be regenerated by the reaction

$$AH_2 + O_2 \longrightarrow A + H_2O_2 \qquad (9)$$

and similarly the quantum yield of production of AH_2 would be 1.0 in the absence of oxygen. On this basis second-order rate constants for reaction 6 have been calculated (see Table I). It is significant that the ratio of the reactivities closely parallel those calculated by Wells[6,7] based on oxygen absorption measurements and attributed by him to the relative reactivities of the alcohols to A*. The ratio of k_2(ROH)/k_2(EtOH) for AH· + ROH → is in good agreement with the relative reactivities of alcohols to photoexcited dichromate solutions, as shown in Table IV. Here Bowen[25] suggests that the first reaction on photochemical oxidation of the dichromate ion is H-atom abstraction from the alcohol. Reaction 6 would therefore appear to be the rate-controlling reaction which determines the absorption of oxygen. The reactivity of carbohydrates, based on oxygen absorption,[26] is similar also to the reactivity of D-sorbitol, D-glucose, and cellobiose with AH·. When studying the photochemical oxidation of alcohols by *p*-benzoquinone in CCl_4 at 25°, Atkinson and Di[27] found it necessary to propose a reaction such as (6) to account for the dependence of quantum efficiency on alcohol concentration.

Table IV: Reactivities of Alcohols to Transient Species Produced by Photoexcitation

k_2(ROH)/ k_2(EtOH)	Alcohol Methyl	Ethyl	Iso-propyl	*n*-Propyl	Glycerol
This report	0.4	1	1.9	1.5	0.7
Bowen[25]	0.3	1.0	2.0	1.5	0.5
Wells[6,7]	0.12	1.00	2.14	1.53	0.28

To obtain some estimate of the relative values of the rate constants for reactions 6 and 2 and information also about the nature of the photoreactive A* which is the precursor of AH·, we have utilized triplet energy transfer. The principles have been described by Wilkinson.[11] The triplet energy levels (cm^{-1}) of anthraquinone, anthracene, naphthalene, and biphenyl are, respectively, 22,000,[28] 14,700,[29] 21,300,[29] and 22,800.[29] These hydrocarbons have lower triplet levels but higher singlet levels than anthraquinone. Thus, when a suitable filter is introduced to prevent direct population of the singlet level in the hydrocarbons, only the anthraquinone is excited directly. If the triplet state of anthraquinone is produced as an intermediate in the photoinduced reaction, conditions are suitable for energy transfer to the lower lying triplet state of the hydrocarbon. These reactions may be represented

$$A \longrightarrow A^* \text{ (singlet)}$$

$$A^* \longrightarrow A^* \text{ (triplet)}$$

---

(25) E. J. Bowen, *Nature*, **177**, 889 (1956); E. J. Bowen and C. W. Bunn, *J. Chem. Soc.*, 2353 (1927); E. J. Bowen and E. T. Yarnold, *ibid.*, 1648 (1929).

(26) G. O. Phillips and T. W. Rickards, unpublished data.

(27) B. Atkinson and M. Di, *Trans. Faraday Soc.*, **54**, 1331 (1958).

(28) M. Kasha, *Radiation Res. Suppl.*, **2**, 243 (1960).

(29) G. N. Lewis and M. Kasha, *J. Am. Chem. Soc.*, **66**, 2100 (1944).

Triplet–triplet energy transfer may therefore occur in competition with reaction 2. As the triplet energy levels of the donor and acceptor become comparable, the transfer efficiency decreases.[30] Our observations are that the rate of formation of and final equilibrium concentration of AH· during irradiation of a solution of anthraquinone in 2-propanol–benzene (1:4) are reduced by the addition of 10^{-2} M naphthalene in neutral and alkaline solution. It is possible, therefore, that the triplet state is the precursor of AH·. The presence of biphenyl (10^{-2} M) does not change the final concentration of AH·, which would be anticipated because of its higher lying triplet state and hence making energy transfer energetically impossible.

It would appear, therefore, that the ability of AH· to abstract a hydrogen atom from the alcohol or carbohydrate, in addition to its formation by reaction 2, will determine its ability to act as a sensitizer in photooxidation reactions. The 2-sulfonate is well known to be less reactive than the 2,6-disulfonate,[6–8] and this is confirmed by the lower k_2 for the 2-sulfonate in reaction 6. The 1-sulfonate and 1,5-disulfonate are poor sensitizers with quantum yields for the production of AH_2 in evacuated systems <0.1. Correspondingly, we have been unable to observe any reactivity of the semiquinone of these sulfonates with alcohols or carbohydrates.

The significance of these observations, when considering the sensitized photodegradation of cotton cellulose by vat dyes, will be considered elsewhere. It may be observed here, however, that semiquinones have been observed in dyed cotton yarns and would appear to control the photodegradation processes.

---

[30] G. Porter and F. Wilkinson, *Trans. Faraday Soc.*, **56**, 1635 (1960).

A Comparative Study of Adsorption by Ellipsometric and Radiotracer Methods

by J. R. Miller and J. E. Berger

Shell Oil Company, Research Laboratory, Wood River, Illinois *(Received February 18, 1966)*

Ellipsometric and radiochemical techniques correlate well in comparative measurements involving adsorption of polar organic compounds on polished metal surfaces. The linear thickness found ellipsometrically is a direct function of the surface concentration determined radiochemically to levels well below that of a tightly packed monolayer. Deposition of capric and benzoic acid vapor onto various metals at 25° was monitored simultaneously by both methods. Under these conditions, chromium and gold exhibit a slow film formation limited to one tightly packed monolayer. On the other hand, steel and nickel build films equivalent to at least three monolayers overnight. In contrast to the acids, octylamine vapor quickly adsorbs beyond a monolayer on all metals tested in air. In the case of the amine, the simultaneous adsorption of atmospheric constituents is strongly indicated. The two techniques further correlate in studies of deposition of stearic and benzoic acids from isooctane or nitromethane solutions.

Introduction

This work was undertaken primarily as a comparative study of ellipsometry and radiotracer techniques in measuring the adsorption of vapors of certain polar organic compounds on metals. Radioisotopes have found wide application in solution adsorption studies,[1-4] and recently ellipsometry has been employed to study adsorption on metals.[5-8] However, to our knowledge only two reports comparing the techniques have appeared.[5,9] The careful work of Bartell and Betts[5] shows a direct proportionality between the optical readings and radiochemical measurements and illustrates the need for further studies. In addition to supplying good corroborating evidence and establishing limitations of the methods, such a comparison can add to the understanding of surfaces and adsorbed films. In the present work, the techniques are applied in a study of the adsorption of the vapor of polar organic compounds on metals, hopefully to contribute to our understanding of vapor phase corrosion inhibition processes.

Experimental Section

Materials. Isooctane (Phillips reagent grade) and nitromethane (Matheson Coleman and Bell) were percolated through a column of silica gel, and benzene and acetone (Mallinckrodt AR grade) were used as received. Stearic acid (Eastman White Label) was recrystallized twice and dried under vacuum, benzoic acid (Mallinckrodt primary standard) was sublimed, but capric acid (Applied Science Laboratories, 99.8+%) and octylamine (Matheson Coleman and Bell) were used as received.

Four tagged compounds were used. Labeled capric acid was prepared by treating $CH_3(CH_2)_8C^{14}OONa$ (New England Nuclear Corp., 4.0 mcuries/mmole) with dilute aqueous sulfuric acid. The resulting organic acid was extracted with benzene and dried with Na_2SO_4. Benzoic acid, labeled in the carboxyl group (5.0 mcuries/mmole), was used as received from New England Nuclear Corp. Stearic acid also was labeled

---

(1) H. Sobotka, Ed., "Monomolecular Layers," American Association for the Advancement of Science, Washington, D. C., 1954.

(2) E. H. Loerer, R. C. Wiquist, and S. B. Twiss, Preprint 70, Nuclear Engineering and Science Conference, Chicago, Ill., March 17-22, 1958.

(3) H. A. Smith and R. L. Bennett, Paper No. 60-LUB-14, ASME-ASLE Lubrication Conference, Boston, Mass., Oct 17-19, 1960.

(4) D. C. Walker and H. E. Ries, Jr., *J. Colloid Sci.*, **17**, 789 (1962).

(5) L. S. Bartell and J. F. Betts, *J. Phys. Chem.*, **64**, 1075 (1960).

(6) F. L. McCrakin, E. Passaglia, R. R. Stromberg, and H. L. Steinberg, *J. Res. Natl. Bur. Std.*, **67A**, 363 (1963).

(7) R. R. Stromberg, E. Passaglia, and D. J. Tulas, *ibid.*, **67A**, 431 (1963).

(8) W. T. Pimbley and H. R. MacQueen, *J. Phys. Chem.*, **68**, 1101 (1964).

(9) R. R. Stromberg, W. G. Grant, and E. Passaglia, *J. Res. Natl. Bur. Std.*, **68A**, 391 (1964).

the carboxyl group with C^{14} (21.6 mcuries/mmole) and was used as received from Nuclear-Chicago Corp. The *n*-octylamine hydrochloride-1-C^{14} (Nichem, 0.4 mcuries/mmole) was converted to free amine by treatment with aqueous NaOH. Benzene was used to extract the amine, and the solution was dried with Na_2SO_4 and stored in a nitrogen atmosphere.

Apparatus. Ellipsometry measurements were performed with a Rudolph Model 437/200E photoelectric device; use of instruments of this type has been described in detail previously.[6,10] Step wedges of barium stearate served to calibrate the instrument which always was operated using the mercury 5461-A line. Thicknesses of unknown films were determined by comparing the changes in characteristics of reflected polarized light with the changes obtained using step wedges. Langmuir–Blodgett step wedges of barium stearate were constructed on evaporated films of chromium, nickel, and aluminum and on polished Type 304 stainless steel. Although these substrate metals exhibit different optical constants, calibrations were the same and could be transferred from one metal to another. Errors introduced because of variations in refractive index for different films are believed to be negligible with stearic and capric acids. Barium stearate standards may introduce an error in measuring benzoic acid films due to differences in refractive index between unknown and standard.

Radiotracer counting procedures involved exposing a selected specimen area to a thin-window Geiger tube (TGC-2) which was equipped with an aluminum mask having a 1-cm^2 circular aperture. To allow easy decontamination of the counter, a very thin, easily replaceable plastic film (Pliofilm <25 $\mu g/cm^2$) was positioned over the tube face. This physical arrangement resulted in about 10% counting efficiency for thin deposits of C^{14} tagged materials. In most instances, specimens were counted for a sufficiently long interval to limit counting errors to less than about 5% (standard deviation/total count).

Procedures. For many of the experiments, the same metal specimen was examined by both ellipsometry and by radiotracer methods. Ellipsometry demands a reflective surface; for this reason, disks (4 cm in diameter, 0.8 cm thick) of chromium, copper, nickel, 1018 steel, and 304 stainless steel were polished by usual metallurgical procedures immediately before they were needed. Levigated alumina abrasives having nominal particle diameters of 0.3 and 0.1 μ were used with Buehler red felt and microcloth polishing laps, reselectively. Polishing on clean microcloth under flowing distilled water removed residual alumina from the polished surface. The mirrorlike hydrophilic surfaces were dried in an air current and immersed immediately in the appropriate environment.

Chromium-plated ferrotype plates used by photographers also make convenient substrates and sections of ferrotype were cleaned by a procedure similar to that described previously.[7] Fine gold foil (A. D. Mackay, Inc., 0.01 in. thick) was cleaned in a mixture of three parts of H_2SO_4 and one part of HNO_3, rinsed in distilled water, in acetone, and in benzene. Gold specimens were flamed gently and cooled in a nitrogen atmosphere just prior to use.

Vapor phase adsorption experiments were conducted by exposing a metal specimen to vapors of capric acid, benzoic acid, or octylamine in a closed vessel. Frequently, a closed optical cell was used to allow direct, continuous measurement by ellipsometry. Radiotracer experiments required that metal specimens be removed from the adsorption cell for counting; this was done quickly. Loss of adsorbed acid prior to and during counting was reduced by exposing the metal specimens briefly to an atmosphere of ethylenediamine vapor immediately after removal from the adsorption cell. A residence time of about 1 min in the amine vapor temporarily "fixed" the volatile acids. To fix amines, specimens were exposed to vapors of a 10% aqueous HCl solution for about 5 sec.

Experiments involving adsorption from dilute solutions were conducted by immersing a freshly cleaned or a freshly polished metal specimen in the appropriate solution. After some of these experiments, it was necessary to rinse away the film of liquid which was withdrawn with the metal. Rinsing was accomplished by dipping the metals five times in fresh solvent. Since metals emerged dry from nitromethane solutions of stearic or capric acid, rinsing with this solvent was unnecessary. Optical constants of bare substrates used in adsorption experiments or for the preparation of step-wedges were measured in air with clean, dry metal specimens.

Results and Discussion

The work described here attempts to answer the question: "Is ellipsometry a reliable method for studying monolayer adsorption of polar molecules on metal surfaces?" To help answer this question, ellipsometric data were compared with those obtained by radiotracer techniques. The general agreement between these two experimental methods is good, but some discrepancies were noted. These discrepancies, usually minor ones, appear to have rational explanations and they will be considered following a discussion

---

(10) A. Rothen, *Rev. Sci. Instr.*, **28**, 283 (1957).

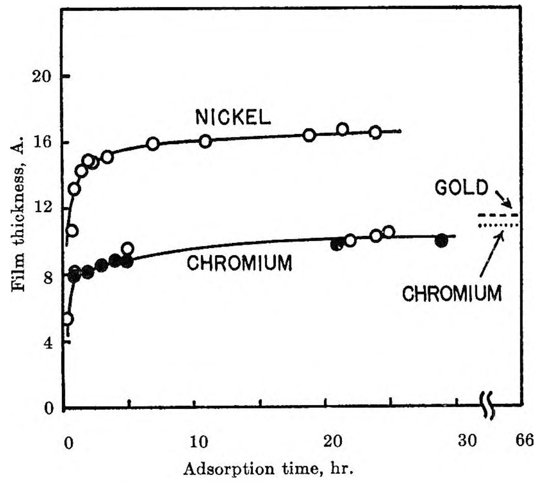

Figure 1. Adsorption at 25° of untagged capric acid vapor on several metals by ellipsometry. (Broken lines represent 66-hr values, and solid and open circles are data from different experiments.)

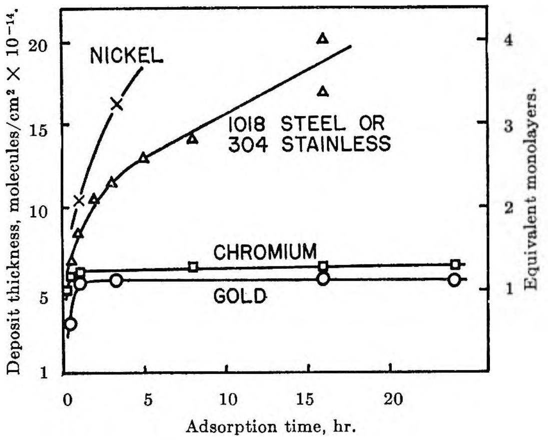

Figure 2. Adsorption of C^{14} tagged capric acid vapor on several metals by radiotracer method. (The equivalent monolayer values are given assuming a smooth surface and a molecular area of 20 A^2.)

of the areas of agreement between ellipsometry and the radiotracer method.

Deposition of capric and benzoic acids on various metals from vapor in air at 25° was monitored by both methods for long time intervals. Ellipsometric data obtained with untagged capric acid are shown in Figure 1 and radiotracer data are presented in Figure 2. Metal substrates can be divided into two classes: the first class (gold and chromium) adsorbs a monolayer of acid, and the second class (nickel or stainless steel) accepts considerably more than a monomolecular layer. On gold and chromium, both methods indicate that an equilibrium surface deposit is reached in 1 hr; further changes in film thickness are negligible. Evidently, a monolayer is formed since the thickness measured by ellipsometry for capric acid films (10–11 A) is close to that expected for vertical, well-aligned molecules. Radiotracer experiments demonstrate that packing is tight since a molecular area of 20 A^2 can be calculated if a roughness factor of 1.2 is assumed. (Independent experiments indicate that chrome ferrotype is only slightly rougher than freshly cleaved mica. This work will be described in a subsequent publication.)

Experiments in which the adsorption of tagged capric acid vapor on ferrotype was studied simultaneously by both methods are summarized in Table I. Films appeared uniform and constant in thickness and the agreement between the two experimental methods is excellent.

Table I: Adsorption of Tagged Capric Acid Vapor by Chromium Plate (Ferrotype)

Absorption time, min	Film thickness, A: Radio-tracer[a]	Film thickness, A: Ellip-sometry
30	4.1	4.4
45	...	7.8
60	9.0	9.2
135	9.8	10.0
3900	11.2	10.9

[a] Calculated from an independent observation that an equilibrium capric acid film on ferrotype produces 860 cpm (surface roughness factor of 1.2). The assumption is made that a "perfect" monolayer is 11 A thick.

Both techniques show that reactive metals (1018 steel, 304 stainless steel, and nickel) permit a gradual buildup of capric acid to yield films much thicker than a monolayer. A direct comparison of the two methods again reveals a good correlation (see Table II). A comparison of data in Table II (tagged capric acid on nickel) with the results shown in Figure 1 (untagged capric acid on nickel) reveals a difference in adsorption level which will be discussed later.

Table II: Adsorption of Tagged Capric Acid Vapor by Nickel at 25°

Exposure time	Film thickness, A: Radio-tracer[a]	Film thickness, A: Ellip-sometry
7 min	3.6	4.2
80 min	11.0	11.8
18 hr	32.1	33.0

[a] Assuming that a tightly packed capric acid monolayer is 11 A thick, and that the roughness factor for polished nickel remains constant at 1.3.

Results obtained with benzoic acid were much the same as those obtained with capric acid. Both experimental methods agree that adsorption of benzoic acid at room temperature is limited to monolayer formation on chromium and gold. Equilibrium adsorption is reached within 30 min from vapor which is in equilibrium with benzoic acid crystals. The ellipsometer measures the formation of a film about 6.0 A thick which is significantly less than the expected molecular length of 9 A. This difference may be due to imperfect packing or to errors arising because of refractive index differences between bulk and film. Radiotracer data indicate a relatively loose packing (about 40 A^2 per molecule) and suggest that adsorbed molecules are free to spin. Rigid phenyl groups have a limiting molecular area of about 20 A^2, but if phenyl groups are free to spin, they sweep out an area of about 40 A^2.

Radiotracer and ellipsometric methods show that the adsorption of octylamine vapor results in deposits which are much thicker than a monolayer on most metals. With stainless steel, the equivalent of four monolayers is measured after 20 hr. As shown in Figure 3, reactivity of octylamine toward metals varies considerably and is greatest in the case of copper. Both methods show that an octylamine monolayer forms on steel almost immediately. However, initial deposition rates do not give any clues about the extent of adsorption which occurs in long-term experiments. This is illustrated in Figure 4, which is an enlargement of the early portion of Figure 3. Rapid deposition of octylamine on copper continues unabated but on gold and steel, reasonably constant films of about 1 monolayer are present during the first 20 min. The relatively high vapor pressure of octylamine apparently allows very rapid monolayer formation.

Measurements were also compared for films adsorbed from dilute solutions. Nitromethane and isooctane were chosen as solvents since it is unlikely that these materials participate in adsorption to give mixed films.[11] Nitromethane is particularly convenient since rinsing is unnecessary: specimens can be removed dry from many nitromethane solutions. Table III contains data comparing radiotracer and ellipsometric methods for measuring adsorption of stearic acid from nitromethane. The two sets of data correlate well. Both methods lead to the conclusion that a tightly packed monolayer is formed within 50 min on 304 stainless steel but only a sparse film is formed on ferrotype after 1.5 hr. Some desorption of stearic acid due to solvent rinsing is apparent in this set of experiments.

Adsorption of benzoic acid from isooctane yields a monolayer on chromium within 1 hr, and this film remains constant in thickness for at least 4 hr. The film thickness for benzoic acid on chromium (6–7 A) is about the same as that observed previously in vapor-phase adsorption. Molecular areas, too, are the same in vapor-phase and solution adsorption experiments: radiotracer experiments yield a value of 40 A^2.

Several minor discrepancies have been passed over in the preceding discussion. For example, Figures 1 and 3 show that radiotracer measurements find a 10% higher surface concentration of capric acid on chromium than on gold. In contrast, ellipsometry indicates

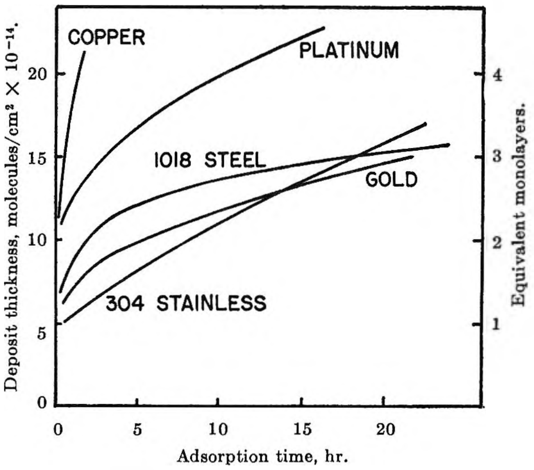

Figure 3. Adsorption at 25° of C^{14} tagged octylamine vapor on several metals by tradiotracer method. (The equivalent monolayer values are given assuming a smooth surface and a molecular area of 20 A^2.,

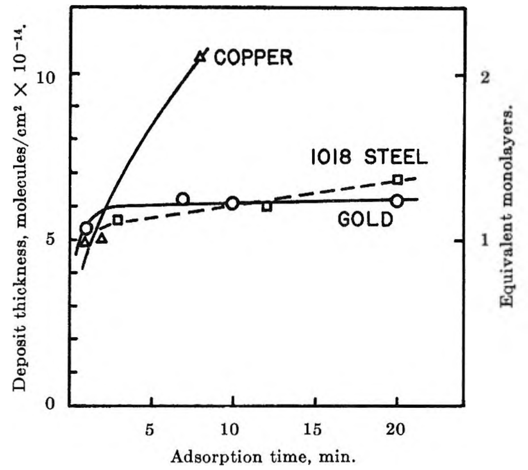

Figure 4. Adsorption at 25° of C^{14} tagged octylamine vapor on several metals by the radiotracer method. (The equivalent monolayer values are given assuming a smooth surface and a molecular area of 20 A^2.)

---

[11] O. Levine and W. A. Zisman, *J. Phys. Chem.*, 61, 1188 (1957).

Table III: Adsorption of Labeled Stearic Acid on Chromium and Steel (Solute Concentration 140 mg/l. of Nitromethane)

Adsorption time, min	Rinse	Metal	Film thickness, A Ellipsometry	Radiotracer[a]
5	CH_3NO_2	304 Stainless	3.5	5.1
5	None	304 Stainless	13.1	14.6
50	None	304 Stainless	21.4	21.4
90	None	Ferrotype plate	6.0	6.2
90	CH_3NO_2	Ferrotype plate	5.0	3.5

[a] A roughness factor of 1.2 is assumed which corresponds, for this system, to 225 cpm for a film 21.4 A thick.

that films of capric acid are about 5% thicker on gold than on ferrotype. This difference lies close to the limit of precision for both techniques and might be due to roughness differences. If the chromium is slightly rougher than gold, the tracer method would show higher apparent surface concentration on chromium, and the ellipsometer possibly would reveal a thinner film because of a somewhat reduced optical accessibility.

Previous discussion has demonstrated that radiotracer methods and ellipsometry agree in conclusions about adsorption of capric acid on active and passive metals, provided that care is taken to avoid contamination. If contamination is not avoided, ellipsometric and radiotracer data diverge, especially when reactive metals and lengthy exposures are employed. In contaminated systems, ellipsometry indicates a thicker film than that measured by the radiotracer method. For example, when direct comparison of the two methods is made by measuring tagged capric acid adsorption on nickel surfaces in an optical cell having epoxy-cemented joints, large discrepancies are noted. Table IV shows the extent of divergence when the amount of tagged capric acid is small (~0.7 mg) in a 150-ml cell with eight cemented joints. Codeposition of amine catalyst with the acid and a reduction in acid vapor pressure presumably has occurred. If the cell was cleaned carefully and heated in a stream of nitrogen for a few hours, then good correlation resulted initially, although eventually it became poor again.

Certain other discrepancies suggest strongly that tagged acid might stimulate vapor deposition on reactive metal surfaces. Although ellipsometry shows that deposition of acid on nonreactive metals is the same regardless of whether capric acid is tagged or not, it detects a difference in the response of nickel to tagged *vs.* untagged acid. From a comparison of data in Figure 1 and Table I, it can be seen that tagging capric acid has no influence on adsorption of this vapor on chromium. On the other hand, if nickel is the adsorbent, tagged capric acid produces thicker films than does inactive acid; this is revealed in a comparison of data from Figures 1 and 2 and from Table II. For example, Figure 1 shows that untagged capric acid produces films 16 A thick, but Figure 2 reveals that tagged capric acid deposits films >16 A thick. Tagged acid also was used in simultaneous measurements by both methods (see Table II), and these experiments verified that tagged acid forms thick layers on nickel. Although these observations and measurements were repeated and verified several times, further very meticulous work is required to establish beyond reasonable doubt the nature of this apparent enhanced adsorption. Perhaps the corrosivity of the atmosphere in the small reaction chambers is slightly intensified by the β radiation. One problem common to radiotracer experiments, the presence of spurious tagged compounds, probably is not involved here. Gas chromatographic analyses substantiated the manufacturer's thin-layer chromatographic analyses of the acids and showed very good radiochemical purity with regard to volatile, tagged contaminants. While the presence of a minor quantity of a tagged material of very much lower volatility but of unknown activity has been demonstrated by gas chromatography of one preparation, it seems improbable that this material can account for the observed effect. In addition, further radiotracer experiments revealed that the use of larger quantities of radioactivity in the reaction chamber (the same quantity of material but from a different source and of higher specific activity) resulted in even greater deposits on the nickel surfaces while showing simple monolayer adsorption on gold.

Table IV: Adsorption of Capric Acid Vapor on Nickel at 25° in the Presence of Epoxy Cement

Exposure time	Film thickness, A Radiotracer	Ellipsometry
25 min	3.4	11.3
17 hr	23	32
45 hr	23	35

Work on amines disclosed another discrepancy between the radiotracer and ellipsometric methods. Ellipsometric data sometimes show thicker amine films than does the radiotracer method. This probably is due to coadsorption of other materials which increase film thickness but not the radioactivity. Atmospheric CO_2, the concentration of which was reduced but not eliminated in our experiments, may be involved here.

Acknowledgment. The authors thank their colleagues in the analytical department in the Shell Development Company Laboratories at Emeryville, California, for a helpful radiochemical analysis.

Aberrations Peculiar to the Use of Rayleigh Optics with the Ultracentrifuge. Magnitude in Sedimentation Equilibrium

by P. A. Charlwood and M. V. Mussett

National Institute for Medical Research, London, N.W.7, England *(Received February 23, 1966)*

The surfaces of equal solute concentration in an ultracentrifuge cell are cylindrical, whereas the slits of a Rayleigh diaphragm are set parallel with a radius. In general, therefore, there is a gradient of concentration in any plane perpendicular to the slits. The effect of this gradient on the positions of interference fringe minima has been calculated. Even when the additional complications of partial illumination of one (or both) Rayleigh slit(s) during the revolution of the rotor were taken into account, the aberrations proved to be, in the least favorable experimentally attainable situations, only about the same magnitude as the random errors of measuring fringe positions.

Introduction

It has been recognized since Rayleigh optics were first adopted for ultracentrifuge work[1] that the record is complicated by (a) the surfaces of equal solute concentration not being flat and perpendicular to the aperture slits, and (b) light reaching the photographic plate when the cell is not in the correct position for interference. The effect of (a) is equivalent to a gradient of concentration "across" the slit apertures, whereas the feature of primary interest is the gradient parallel to the slits. As a preliminary to developing methods of making differential measurements of molecular weights from equilibrium patterns, it seemed desirable to investigate the magnitudes of the aberrations arising from the above factors.

The components of the optical system and their relative dispositions are shown schematically in section in Figure 1. The mirror which normally reflects the light through a right angle is omitted as being nonessential, merely an experimental convenience. The rotor revolves in a plane which is perpendicular to the optical axis, the distance between this axis and the axis of rotation being about 7 cm in most machines. The light source slit and the slits of the Rayleigh diaphragm lie parallel with the plane of rotation and perpendicular to the section shown in Figure 1. The cell sectors and associated cell slit diaphragm move relative to the rest of the optical system so that only once in each revolution do the slits of the cell diaphragm become parallel with the slits of the Rayleigh diaphragm. The contributions produced at all other orientations are included in the following treatment.

Theory

The symbols used will in most cases be defined as they occur in the mathematical development, but a complete

---

[1] E. G. Richards and H. K. Schachman, *J. Am. Chem. Soc.*, 79, 5324 (1957).

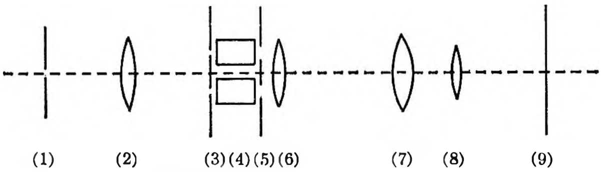

Figure 1. Rayleigh interference optical system: (1) slit source, (2) collimating lens, (3) cell twin-slit diaphragm, (4) double-sector cell center, (5) Rayleigh double-slit diaphragm, (6) condensing lens, (7) camera lens, (8) cylindrical lens, (9) photographic plate. The optical axis is represented by the dashed line. Cell windows are not shown.

list is given for easy reference at the end of this section. All distances, unless it is stated to the contrary, are in centimeters.

1. Relation of Solute Concentration and Position at Equilibrium. It is assumed that equilibrium has been attained in an ideal, two-component system and that n, the difference between refractive index of solution and solvent, is proportional to solute concentration, so that d ln $n/\mathrm{d}(r^2) = k$. Here r is the distance from the axis of rotation and $k = M\omega^2(1 - \bar{v}\rho)/2RT$, the symbols in this expression having their usual significance.

Consider the plane of rotation CYZ (Figure 2) which cuts the axis of rotation at C. Let Y be a point in the cell and YZC a right angle, the optical axis intersecting the plane of rotation at a point on CZ not very far from Z. If H is another point in the cell such that CZ = CH = h, then

$$\ln (n_\mathrm{Y}/n_\mathrm{H}) = k\{(\mathrm{CY})^2 - (\mathrm{CH})^2\} = k\{(y^2 + h^2) - h^2\} = ky^2$$

and

$$n_\mathrm{Y} = n_\mathrm{H}e^{ky^2} = n_\mathrm{H}(1 + ky^2 + \cdots) \qquad (1)$$

As the maximum value of ky^2 is about 0.1 under usable equilibrium conditions, higher terms inside the bracket will be neglected.

2. Interference Optical Theory. A number of the usual assumptions and approximations are made in the following. In the dimension primarily involved, the combined effect of the camera and cylindrical lenses (Figure 1) is merely to produce at the photographic plate a magnified image of the interference fringes which are formed in the focal plane of the condensing lens, so that what happens to the right of this focal plane need not be considered. (In the second dimension the combined effect of all three lenses is to focus between cell and photographic plate, thereby giving a true representation of radial distances.) Here the condensing lens (focal length g), cell diaphragm, and Rayleigh diaphragm are regarded as being very close

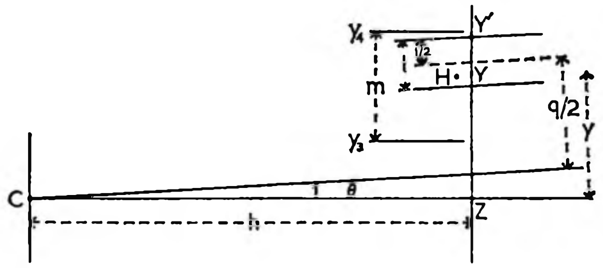

Figure 2. Instantaneous position of one cell slit (width l) relative to one of the Rayleigh slits (width m, edges, respectively, y_3 and y_4 from the optical axis). Rotation occurs in the plane YZC. Optical axis, which is perpendicular to YZC, passes through a point on CZ near Z.

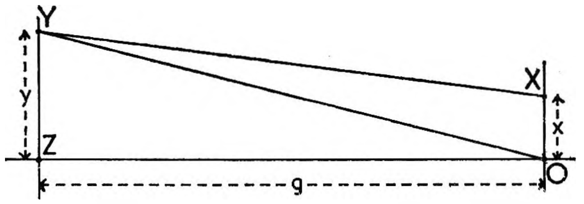

Figure 3. Effect of condensing lens (not shown) on image formation. The plane YZO is perpendicular to the plane of rotation YZC (Figure 2), but parallel to the optical axis.

to the plane CYZ (Figure 2). The focal plane of the condensing lens, which passes through OX (Figure 3) is parallel with the plane of rotation CYZ, and therefore perpendicular to OZ. Light from a point Y in the cell makes a contribution to the light intensity at any point X of the line OX. If OX = x, compared with ideal focusing at O, the path difference is seen from Figure 3 to be

$$\begin{aligned}(\mathrm{YX} - \mathrm{YO}) &= \sqrt{[g^2 + (y - x)^2]} - \sqrt{[g^2 + y^2]} \\ &= g\{\sqrt{[1 + (y - x)^2/g^2]} - \sqrt{[1 + y^2/g^2]}\} \\ &= g\{[1 + (y - x)^2/2g^2 \cdots] - [1 + y^2/2g^2 \cdots]\}\end{aligned}$$

To the usual degree of approximation, as $g >> x, y$

$$(\mathrm{YX} - \mathrm{YO}) = [(y - x)^2 - y^2]/2g = x^2/2g - xy/g \qquad (2)$$

The first term, being independent of y, does not contribute to the interference, but merely determines the phase of the resultant light. It enters into K (see below), but K is eliminated when the product $\psi(x)\psi^*(x)$ is taken in the single-slit arrangement. In a twin-slit arrangement its effect again disappears when $\psi(x)\psi^*(x)$ is taken because the term independent of y which it gives rise to enters equally into K_1 and K_2

(see eq 5 below). In working out the phase-difference function we must add the contribution arising from the solute refractive index increment (see section 1). The phase-difference function

$$\phi = (2\pi/\lambda)[pn_{\mathrm{H}}(1 + ky^2) - xy/g] \qquad (3)$$

taking the refractive index of air as unity and making the approximations stated above. Here p is the optical path length in the cell and λ is the wavelength of the light. (Note: the term unity within the inner bracket gives rise to $2\pi pn_{\mathrm{H}}/\lambda$ on expansion. Although this is independent of y across one sector, it is retained because it enters into the theory of the twin-slit arrangement which is necessary when both cell sectors are involved.)

The amplitude $\psi(x)$ at X is proportional to $\int e^{-i\phi(y)}\mathrm{d}y$ between appropriate limits.[2] For simplicity we take the proportionality constant as unity so that $\psi(x) = \int e^{-i\phi(y)}\mathrm{d}y$.

(*i*) *Single-Slit Aperture* (*Diffraction Pattern*). If we have a slit with edges distant y_1 and y_2 from the axis of the optical system

$$\psi(x) = \int_{y_1}^{y_2} e^{-2\pi i[pn\mathrm{H}(1 + ky^2) - xy/g]/\lambda}\mathrm{d}y$$

$$= \int_{y_1}^{y_2} \exp[-i(Ay^2 + By + A/k)]\mathrm{d}y$$

where $A = 2\pi n_{\mathrm{H}}pk/\lambda$ and $B = -2\pi x/g\lambda$. Putting $u = \sqrt{A}(y + B/2A)$ and $K = (A/k - B^2/4A)$, $\mathrm{d}y = \mathrm{d}u/\sqrt{A}$ and

$$\psi(x) = \frac{1}{\sqrt{A}}\int_{u_1}^{u_2} \exp(-iu^2)\exp(-iK)\mathrm{d}u$$

Intensity is proportional to $\psi(x)\psi^*(x)$ where $\psi^*(x)$ is the conjugate of $\psi(x)$. Again taking the constant of proportionality as unity we have

$$\psi(x)\psi^*(x) = \frac{\exp(-iK)}{\sqrt{A}}\,\frac{\exp(iK)}{\sqrt{A}} \times \left[\int_{u_1}^{u_2}\exp(-iu^2)\mathrm{d}u\right]\left[\int_{u_1}^{u_2}\exp(iu^2)\mathrm{d}u\right] = \frac{1}{A}\left[\int_{u_1}^{u_2}(\cos u^2 - i\sin u^2)\mathrm{d}u\right] \times \left[\int_{u_1}^{u_2}(\cos u^2 + i\sin u^2)\mathrm{d}u\right]$$

Putting $\int_{u_1}^{u_2}\cos u^2\mathrm{d}u = P$ and $\int_{u_1}^{u_2}\sin u^2\mathrm{d}u = Q$

$$\psi(x)\psi^*(x) = (P - iQ)(P + iQ)/A = (P^2 + Q^2)/A = \xi(x) \qquad (4)$$

(*ii*) *Twin-Slit Aperture* (*Interference Pattern*). The effect is similar to the above except that the integrals now extend over two intervals. It is important to ensure correct representation of the refractive index at the center of each slit, corresponding to the separate cell channels. With an extension of the above notation

$$\psi(x) = \frac{1}{\sqrt{A_1}}\int_{u_1}^{u_2}\exp(-iu^2)\exp(-iK_1)\mathrm{d}u + \frac{1}{\sqrt{A_2}}\int_{u_3}^{u_4}\exp(-iu^2)\exp(-iK_2)\mathrm{d}u$$

Putting $\int_{u_1}^{u_2}\cos u^2\,\mathrm{d}u = P_1$, $\int_{u_1}^{u_2}\sin u^2\mathrm{d}u = Q_1$, $\int_{u_3}^{u_4}\cos u^2\mathrm{d}u = P_2$, and $\int_{u_3}^{u_4}\sin u^2\,\mathrm{d}u = Q_2$

$$\psi(x) = \frac{(P_1 - iQ_1)}{\sqrt{A_1}}\exp(-iK_1) + \frac{(P_2 - iQ_2)}{\sqrt{A_2}}\exp(-iK_2)$$

Hence

$$\psi(x)\psi^*(x) = (P_1^2 + Q_1^2)/A_1 + (P_2^2 + Q_2^2)/A_2 + 2[(P_1P_2 + Q_1Q_2)\cos L - (P_1Q_2 - P_2Q_1)\sin L]/\sqrt{A_1A_2} = \xi(x) \qquad (5)$$

where $L = (K_2 - K_1)$. This and the preceding section deal with a static situation. In practice the extent of slit illumination is a function of time, as rotation alters the cell orientation and position relative to the Rayleigh diaphragm.

3. Effects of Cell Motion on Aperture Sizes as a Function of Time. Let the distances of the edges of the Rayleigh slits from the optic axis be y_1, y_2, y_3, and y_4 as exemplified in Figure 2. Of course, $(y_4 - y_3) = (y_2 - y_1) = m$, the width of each slit, and the distance between slit centers, q, is $[(y_4 + y_3) - (y_2 + y_1)]/2$. We also define $\bar{y} = (y_4 + y_3 + y_2 + y_1)/4$, which is zero if the diaphragm is in the symmetrical position.

When the cell has rotated through an angle θ (from a position symmetrical with respect to the optical axis) until one cell slit is in the orientation shown in Figure 2, the position of the point Y′ which lies on one edge of it is given by $\mathrm{ZY}' = h\tan\theta + 0.5(q + l)\sec\theta$. Here l is the width of a cell slit and q the distance between centers of cell slits, the same as that between centers of Rayleigh slits (see above). In the optical systems used, θ is always quite small when light passes. If $|y_4| > |y_1|$, the maximum value of $|\theta|$ is obtained by

---

(2) G. Joos, "Theoretical Physics," Blackie and Son Ltd., London, 1934.

Table I: Integration Limits for the Calculation of Terms of Eq 7

Subscript of P or Q	Upper limit	Lower limit
1a	$\sqrt{A_1}[B/2A_1 + y_3 + h\theta + (m + l)/2]$	$\sqrt{A_1}(B/2A_1 + y_3)$
2a	$\sqrt{A_2}[B/2A_2 + y_1 + h\theta + (m + l)/2]$	$\sqrt{A_2}(B/2A_2 + y_1)$
4a	$\sqrt{A_2}[B/2A_2 + y_3 + h\theta + (m + l)/2]$	$\sqrt{A_2}(B/2A_2 + y_3)$
5a	$\sqrt{A_1}[B/2A_1 + y_1 + h\theta + (m + l)/2]$	$\sqrt{A_1}(B/2A_1 + y_1)$
1b	As for 1a	$\sqrt{A_1}[B/2A_1 + y_3 + h\theta + (m - l)/2]$
2b	As for 2a	$\sqrt{A_2}[B/2A_2 + y_1 + h\theta + (m - l)/2]$
4b	As for 4a	$\sqrt{A_2}[B/2A_2 + y_3 + h\theta + (m - l)/2]$
5b	As for 5a	$\sqrt{A_1}[B/2A_1 + y_1 + h\theta + (m - l)/2]$
1c	$\sqrt{A_1}(B/2A_1 + y_4)$	As for 1b
2c	$\sqrt{A_2}(B/2A_2 + y_2)$	As for 2b
4c	$\sqrt{A_2}(B/2A_2 + y_4)$	As for 4b
5c	$\sqrt{A_1}(B/2A_1 + y_2)$	As for 5b

considering the position of the edge of the cell slit furthest from y_4 when the cell is symmetrically situated relative to the optical axis. This distance is $[0.5\cdot(q + l) + |y_4|]$, so that $|\theta| \doteq \tan|\theta| \doteq [|y_4| + 0.5\cdot(q + l)]/h$. The relations above show that this is equivalent to $[|\bar{y}| + q + 0.5(l + m)]/h$. This expression, which is arrived at by a similar process if $|y_1| > |y_4|$, has a maximum value of 0.1 radian when calculated from the fourth column of figures in Table II. Thus, to a sufficient degree of accuracy

$$\mathrm{ZY}' = h\theta + 0.5(q + l) \qquad (6)$$

In other words, since $\theta = \omega t$ (where ω is the constant angular velocity), the rotational movement can be regarded, for a given value of h, as practically equivalent to a uniform translational displacement of the cell and its associated diaphragm across the stationary Rayleigh double slit.

Table II: Parameters Expressing Effects of Solvent in Both Channels[a]

l	0.054	0.054	0.054	0.054	0.100	0.100
m	0.075	0.150	0.075	0.150	0.025	0.025
$\bar{y}$	0.0	0.0	−0.2	−0.2	0.0	−0.2

[a] In all these cases $A_1 = A_2 = 0.001$ and $k_1 = k_2 = 1 \times 10^{-6}$.

In all that follows, attention is confined to a fixed value of h, *i.e.*, in Figure 2 to a section through ZY parallel with the axis of rotation. When the cell rotation corresponds with Figure 2, the instantaneous contribution to the light intensity at any point X (Figure 3) is given by eq 5 with the limits for the integrals defined by the y coordinates of the cell slits (such as ZY′). However, if ZY′ exceeds y_4, then u_4 is fixed by y_4 and not by ZY′. Thus at any moment during this part of the rotation there are four points formed by the intersections of ZY with the edges of the cell slits, or with one edge of each cell slit and one edge of each Rayleigh slit.

The y coordinates of these four points, which are plotted in Figure 4(ii) at the appropriate t $(=\theta/\omega)$, determine the limits u_1, u_2, u_3, and u_4 applicable at that instant for the terms of eq 5. When only one Rayleigh slit is illuminated by reason of the cell position, the situation can be represented by Figure 4(i) or (iii). Then eq 4 is used, the integration limits again being fixed by erection of an ordinate at the correct value of t. The correspondence between Figure 4 and the physical situation can be visualized as follows. No light passes until, at the beginning of Figure 4(i)a, one edge of a cell slit reaches y_1. The portion of the width of the Rayleigh slit illuminated then increases

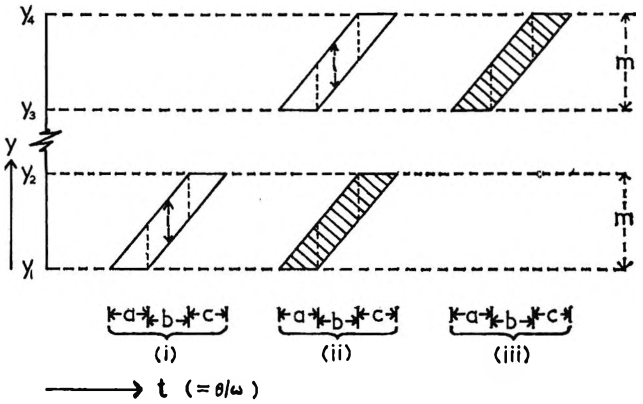

Figure 4. Extent of Rayleigh slit aperture effective at $r = h$ during cell rotation. Shaded and plain areas correspond, respectively, to the two cell channels. The intervals a, b, c are common to the three situations within the limits of accuracy of approximations used. Situations (i) and (iii) produce the fogging effects, and (ii) the interference fringes of interest.

until at the end of the interval 4(i)a it covers the range y_1 to $(y_1 + l)$ at which stage the second edge of the same cell slit has reached y_1. In 4(i)b the region transmitting light is defined by the edges of the cell slit, which are distance l apart but moving relative to y_1 and y_2. The interval (i)c is rather similar to 4(i)a in reverse. During 4(ii) the first cell slit passes across the other Rayleigh slit while the second cell slit scans the first Rayleigh slit. Finally, during 4(iii) the second cell slit traverses the second Rayleigh slit.

4. Light Intensity at Any Point, Integrated over a Complete Scan. As the relative intensity, I(x), at the point X is given by $\xi(x)$ (eq 4 or 5) at any instant, the total effect is obtained by taking $\int \xi(x)\mathrm{d}t$ over the requisite time interval. Since, as explained above, the limits of the integrals used to evaluate $\xi(x)$ are themselves functions of time, a double integration is involved. Because θ varies directly with t, the resultant intensity may be taken as $\int \xi(x,\theta)\mathrm{d}\theta$.

As an example of what is involved, we consider the time interval (i)a (Figure 4), throughout which eq 4 applies with the lower limits of P and Q constant at $\sqrt{A_1}(y_1 + B/2A_1)$. As the upper limits increase from $\sqrt{A_1}(y_1 + B/2A_1)$ to $\sqrt{A_1}(y_1 + l + B/2A_1)$ during this time, in terms of the previous convention for the origin of θ they would be written as $\sqrt{A_1}[h\theta + 0.5(q + l) + B/2A_1]$ with θ increasing from $[y_1 - 0.5(q + l)]/h$ to $[y_1 - 0.5(q - l)]/h$. It is permissible and more convenient for subsequent collection of like terms to change the origin of θ by the constant $\{y_1 + 0.5(m - q)\}/h$ so that the upper limits become $\sqrt{A_1}[h\theta + 0.5(m + l) + B/2A_1 + y_1]$ with θ now increasing from $-(m + l)/2h$ to $-(m - l)/2h$ during 4(i)a. If we denote $\xi(x,\theta)$ thus obtained as $\xi_{5\mathrm{a}}$, the contribution to the total light reaching x is

$$I_{5\mathrm{a}}(x) = \int_{-(m+l)/2h}^{-(m-l)/2h} \xi_{5\mathrm{a}}(x,\theta)\mathrm{d}\theta$$

In a similar manner we get $\xi_{4\mathrm{a}}$ and $I_{4\mathrm{a}}(x)$ from 4(iii)a. It is necessary to apply eq 5 to the interval 4(ii)a, thereby obtaining $\xi_{1\mathrm{a}} = (P_{1\mathrm{a}}{}^2 + Q_{1\mathrm{a}}{}^2)/A_1$, $\xi_{2\mathrm{a}} = (P_{2\mathrm{a}}{}^2 + Q_{2\mathrm{a}}{}^2)/A_2$, $\xi_{3\mathrm{a}} = 2[(P_{1\mathrm{a}}P_{2\mathrm{a}} + Q_{1\mathrm{a}}Q_{2\mathrm{a}}) \cos L - (P_{1\mathrm{a}}Q_{2\mathrm{a}} - P_{2\mathrm{a}}Q_{1\mathrm{a}}) \sin L]/\sqrt{A_1A_2}$ and corresponding contributions to $I(x)$. For brevity

$$I_{\mathrm{a}}(x) = \int_{-(m+l)/2h}^{-(m-l)/2h} \xi_{\mathrm{a}}(x,\theta)\mathrm{d}\theta$$

where $\xi_{\mathrm{a}}(x,\theta) = \sum_{s=1}^{5} \xi_{s,\mathrm{a}}$. By similar reasoning $I_{\mathrm{b}}(x)$ and $I_{\mathrm{c}}(x)$ can be defined so that in summary

$$I(x) = \int_{-(m+l)/2h}^{-(m-l)/2h} \xi_{\mathrm{a}}(x,\theta)\mathrm{d}\theta + \int_{-(m-l)/2h}^{(m-l)/2h} \xi_{\mathrm{b}}(x,\theta)\mathrm{d}\theta + \int_{(m-l)/2h}^{(m+l)/2h} \xi_{\mathrm{c}}(x,\theta)\mathrm{d}\theta \quad (7)$$

The integration limits for all the P's and Q's are given in Table I.

The "fogging" contribution, which is given by ξ terms with subscripts containing 4 and 5, can be calculated separately if it is desired. For $l > m$ separate sets of equations might be written, but the accuracy of computer calculations makes it possible to use the same set by employing a subterfuge (see below).

Notation

a, b, c	particular time intervals during cell rotation
A	$= 2\pi n_{\mathrm{H}}pk/\lambda$
B	$= -2\pi x/\lambda g$
g	focal length of condensing lens
h	fixed distance from axis of rotation to plane of interest in cell
I	integrated light intensity
k	$= M\omega^2(1 - \bar{v}\rho)/2RT$
K	$= (A/k - B^2/4A)$
l	width of slit in cell window holder
L	$= (K_2 - K_1)$
M	molecular weight of solute
m	width of slit in Rayleigh diaphragm
n	difference between refractive index of solution and solvent (corresponding to any value of r)
p	optical path length in cell
P, Q	Fresnel-type integrals $\int \cos u^2\mathrm{d}u$ and $\int \sin u^2\mathrm{d}u$, respectively
q	distance between centers of a pair of slits
r	distance from axis of rotation (general)
R	gas constant
t	time
T	absolute temperature
u	$= \sqrt{A}(y + B/2A)$
$\bar{v}$	partial specific volume of solute
x	coordinate in image plane ("across" fringes)
y	coordinate in Rayleigh diaphragm plane (perpendicular to slits)
Δ	distance between consecutive fringe minima
Δ^*	displacement of fringe system
θ	angle of rotation
λ	wavelength of light in air
ξ	instantaneous contribution to intensity
ρ	density of solution
ϕ	phase-difference function
ψ	amplitude function
ω	angular velocity

Computer Programs and Calculations

The computer was programmed in EMA (extended mercury autocode) to calculate the integrals of eq 7 by Gaussian quadrature for specified values of the constants and a series of values of x. This involves values of P and Q corresponding to particular values of θ. The P and Q terms were themselves computed by Gaussian quadrature. Comparison of typical calculations using six- and eight-point quadrature showed that the six-point was sufficiently accurate.

The main restrictions in the basic derivation are that $l \leqslant m$ and the separations (q) between centers of slits are identical in the two pairs. The case $l > m$ was dealt with as follows. If we calculate $I(x)$ for l' almost identical with m, say $l' = m[1 - (l - m) \times 10^{-5}/2m]$, then $I_b(x)$ is very small, corresponding to a change in θ of $(l - m) \times 10^{-5}/2h$. If the computer is instructed to sum $I_a(x)$, $I_c(x)$, and $10^5 I_b(x)$, we get $I(x)$ for $l > m$ with adequate accuracy.

To obtain the effect of uniform solvent in one sector we can make one of the k's extremely small, but the corresponding A should be reduced so that $A_1/k_1 = A_2/k_2$. This saves working out different types of integrals which are required when $k = 0$ exactly. To compare fringe patterns with those obtained with uniform solvent in both channels a similar procedure can be used.

The program makes possible the calculation of $I(x)$ for symmetrical ($\bar{y} = 0$), asymmetrical ($\bar{y} = -0.2$), or intermediate positions of the Rayleigh diaphragm, for different slit widths, and as just mentioned, for solvent *vs.* solvent, solution *vs.* solvent, or one solution *vs.* another.

Positions of interference minima, located in computer results, were compared with what would be obtained for a static situation if there were opposite each cell slit uniform solution having the refractive index obtaining at the center of the actual slit. The interval (in x) between consecutive minima is given by the usual expression for a double slit

$$\Delta = \lambda g/q \tag{8}$$

The displacement of the band system from the symmetrical position is given by

$$\Delta^* = \lambda g[A_1/k_1 - A_2/k_2 + A_1(y_2 + y_1)^2/4 - A_2(y_4 + y_3)^2/4]/2\pi q \tag{9}$$

In all this work parameters typical of the optical system of the Beckman-Spinco ultracentrifuge were used, q, h, and g being taken as 0.4, 7.0, and 62.5 cm, respectively, and λ as 546 mμ. Then $\Delta = 0.008536$ cm. (In practice the plate image is magnified in this direction by about 3.4 because of the cylindrical lens, but this is unimportant from the point of view of the present investigation, as previously mentioned.)

It is not at present possible experimentally to measure the positions of intensity minima to better than about 0.02 of a fringe. It should, therefore, be sufficient to calculate $I(x)$ in the neighborhood of the anticipated minima at intervals of x of 0.0002 cm in general. This enables the minima to be located within ±0.0001 cm. The typical portions of central bands of fringes which are shown in Figures 5 and 6 were, however, computed mainly at rather wider intervals (0.0005 cm in x).

The size of A is governed by the magnitude of the refractive index gradient "across" the Rayleigh diaphragm. For a given optical system, with light of fixed wavelength, A is proportional to pn_Hk. When interference optics are used it is not possible to exceed a certain value of A without completely losing resolution of the fringes. In the calculations a maximum permissible value of A of 66 was usually taken, which is not far from the limit found when using the steep gradients of the method of Yphantis.[3] More frequently in equilibrium work $A \sim 10$. The stipulation made earlier that $A_1/k_1 = A_2/k_2$ need not hold in practice, but saves modifying the program to take account of the rather arbitrary difference of refractive index between the centers of channels.

The values taken for other parameters are given in Tables II–IV. The speed of the ultracentrifuge in equilibrium experiments is usually selected to give k values of the magnitudes shown. The usual cell slits have $l = 0.054$ cm, and the Rayleigh diaphragms $m = 0.075$ or 0.15 cm. Of course, the number of minima in the central band of fringes is determined by the smaller of l and m (in conjunction with q). Calculations have generally been confined to the eight minima nearest the center of the main band, the ones which would be used in practice for measurement.

Table III: Parameters Corresponding to Occupation of One Channel by Solution, Other by Solvent[a]

l	0.054	0.054	0.054	0.100	0.100	0.100
m	0.075	0.075	0.150	0.025	0.025	0.025
$\bar{y}$	0.0	−0.2	−0.2	0.0	−0.1	−0.2

[a] In all these cases $A_1 = 60$, $A_2 = 6 \times 10^{-4}$, $k_1 = 0.3$, and $k_2 = 3 \times 10^{-6}$.

Results and Discussion

In most cases the computer results gave the positions of minima within ±0.0001 cm in x of the values calculated from the simple eq 8 and 9. The exceptions are shown in Table V. Even these departures are only about the same size as experimental errors involved in measuring positions of fringe minima. In practice the Rayleigh diaphragm is not in the same plane as the

---

[3] D. A. Yphantis, *Biochemistry*, **3**, 297 (1964).

Table IV: Parameters Used for Calculating Differential Effects[a]

	(i)							(ii)		
A_1	60	60	66	10	10	11	l	0.054	0.054	0.100
A_2	60	60	60	10	10	10	m	0.075	0.054	0.025
k_1	0.3	0.3	0.33	0.1	0.1	0.11				
k_2	0.33	0.3	0.3	0.11	0.1	0.1				

[a] Each column of set (i) was combined in turn with each column of set (ii), giving a total of 18 combinations, all also having $\bar{y} = 0$. One other combination was used, obtained by taking the first column of each set with $\bar{y} = 0.1$.

Table V: Comparison of Positions of Intensity Minima Obtained by Computer and from Simple Formulas[a]

A_1	0.001	60	60	60	60	66
A_2	0.001	6×10^{-4}	60	60	60	60
k_1	1×10^{-6}	0.3	0.3	0.3	0.3	0.33
k_2	1×10^{-6}	3×10^{-8}	0.33	0.33	0.33	0.3
l	0.100	0.054	0.054	0.054	0.054	0.054
m	0.025	0.150	0.054	0.075	0.075	0.075
$\bar{y}$	−0.2	−0.2	0.0	0.0	0.1	0.0
x	±0.0213	−0.0043	0.0460	0.0375	−0.0328	0.0302
x^*	±0.0215	−0.0041	0.0462	0.0377	−0.0331	0.0304
x	±0.0299	0.0128	0.0546			
x^*	±0.0301	0.0130	0.0548			
x		0.0213				
x^*		0.0215				

[a] x and x^* are respectively the positions of minima as given by eq 8 and 9 and by computer.

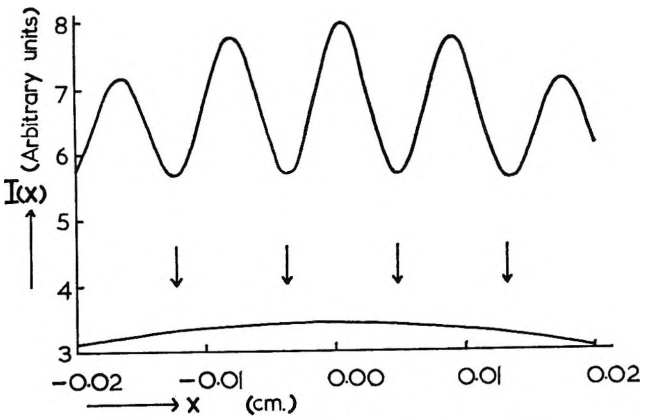

Figure 5. Intensity variation, $I(x)$, as a function of x for $A_1 = 110$, $A_2 = 100$, $k_1 = 0.66$, $k_2 = 0.6$, $l = 0.054$, $m = 0.075$, and $\bar{y} = 0$. Arrows indicate positions of intensity minima calculated by means of eq 8 and 9. Lower curve indicates fogging contribution.

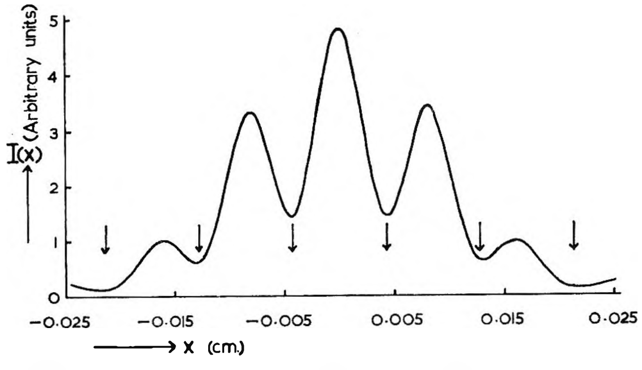

Figure 6. Intensity variation, $I(x)$, as a function of x for $A_1 = A_2 = 0.001$, $k_1 = k_2 = 1 \times 10^{-6}$, $l = 0.195$, $m = 0.15$, and $\bar{y} = -0.2$. Arrows indicate positions of intensity minima expected from eq 8.

cell slits, but the effects of this, and of other approximations made in the theory, could hardly alter the general findings.

It must be concluded that, with existing equipment, the "fogging" effects and aberrations considered here, which are of a different type from those discussed by Yphantis,[3] have a negligible influence on results. In experiments carried out with wedge-centerpiece cells and interference optics, there is an additional term, linear in y, entering into the expressions which form the basis for the calculations (section 2i). Although no computations for this type of case have been carried out, it seems obvious from the results of the present work that these effects also must be negligible. Similarly, our original intention to investigate the consequences of errors in slit-width fabrication was deemed superfluous. The results of cell misalignment can be calculated in the normal, elementary way because of the relatively small magnitude of the aberrations established in this work.

Acknowledgments. We are much indebted to Mr. F. Hussein and also to Dr. L. J. Gosting for helpful criticisms of the manuscript. We also thank Mr. S. Gresswell for assisting in some preliminary calculations.

The Production of Perfluorocyclopropane in the Reaction of Oxygen Atoms with Tetrafluoroethylene

by Norman Cohen and Julian Heicklen

Aerospace Corporation, El Segundo, California *(Received February 28, 1966)*

The reaction of $O(^3P)$ with C_2F_4 proceeds by the reaction scheme

$$O + C_2F_4 \xrightarrow{k_{11}} CF_2O + CF_2$$

$$O + C_2F_4 \xrightarrow{k_5} C_2F_4O^*$$

$$2CF_2 \xrightarrow{k_2} C_2F_4$$

$$CF_2 + C_2F_4 \xrightarrow{k_3} \text{cyclo-}C_3F_6$$

$$C_2F_4O^* + C_2F_4 \xrightarrow{k_6} CF_2O + \text{cyclo-}C_3F_6$$

$$C_2F_4O^* \xrightarrow{k_7} CF_2O + CF_2$$

where $C_2F_4O^*$ is an excited intermediate. The ratio $k_5/(k_{11} + k_5)$ is 0.15 at 22° and drops slightly as the temperature is raised. The CF_2 radicals produced give the same values for $k_3/k_2^{1/2}$ as do singlet CF_2 radicals produced in another system.

Introduction

In recent reports from this laboratory,[1,2] it has been shown that the reaction of triplet oxygen atoms with C_2F_4 yields CF_2O as the sole oxygen-containing product independent of conditions for temperatures from 23 to 125°. However, at room temperature the cyclo-C_3F_6 formed was about 0.15 that of the CF_2O for C_2F_4 pressures up to 30 mm. This invariance with pressure is contrary to that expected from the sequence of reactions

$$O + C_2F_4 \longrightarrow CF_2O + CF_2 \text{ (singlet)} \qquad (1)$$

$$2CF_2 \longrightarrow C_2F_4 \qquad (2)$$

$$CF_2 + C_2F_4 \longrightarrow \text{cyclo-}C_3F_6 \qquad (3)$$

Therefore, two possible alternatives were suggested[1,3]

$$O + C_2F_4 \longrightarrow CF_2O + CF_2 \text{ (triplet)} \qquad (4)$$

$$O + C_2F_4 \longrightarrow C_2F_4O^* \qquad (5)$$

---

(1) D. Saunders and J. Heicklen, *J. Am. Chem. Soc.*, **87**, 2088 (1965).

(2) D. Saunders and J. Heicklen, *J. Phys. Chem.*, **70**, 1950 (1966).

(3) J. Heicklen, N. Cohen, and D. Saunders, *ibid.*, **69**, 1774 (1965).

where the triplet CF_2 from reaction 4 would disappear by (2) or (3) but with different rate constants from the singlet reactions. The product of reaction 5 is an excited C_2F_4O molecule which never becomes stabilized (neither tetrafluoroethylene oxide nor CF_3CFO is a product of the reaction) but may react *via*

$$C_2F_4O^* + C_2F_4 \longrightarrow CF_2O + \text{cyclo-}C_3F_6 \qquad (6)$$

$$C_2F_4O^* \longrightarrow CF_2O + CF_2 \qquad (7)$$

The results[1] in the presence of molecular oxygen favored reaction 4, but reaction 5 could not be eliminated as a possibility. Therefore, we studied the cyclo-C_3F_6 yield over a wide range of conditions to see if we could decide among the possibilities. The results of that study are reported here.

Experimental Section

The experimental procedure was identical with that of an earlier study,[4] except that an excess of N_2O (Matheson, degassed), usually 500 mm, was present in all runs, and the C_2F_4 was prepared by reacting Zn with 1,2-$C_2F_4Br_2$.[2] The amount of nitrogen produced was computed from the residual pressure of the gas noncondensable at −196°.

Results

The quantum yield of cyclo-C_3F_6 formation from mercury-sensitized photolyses of mixtures of 500 mm N_2O with smaller amounts of C_2F_4 is shown in Tables I–III and Figures 1–3. The quantum yields Φ(cyclo-C_3F_6) are computed as the amount of cyclo-C_3F_6 produced divided by the N_2 produced.

At 22°, Φ(cyclo-C_3F_6) rises proportionately (slope = 1.0 on log–log plot of Figure 1) with C_2F_4 pressure for C_2F_4 pressures up to 0.6 mm. For C_2F_4 pressures between 0.6 and 30 mm, Φ(cyclo-C_3F_6) is constant at about 0.15, but at higher pressures Φ(cyclo-C_3F_6) rises. The data for ref 1 are included in Figure 1; they lie on the same curve as the data from this study. A variation of the absorbed intensity by a factor of 50 had no effect for C_2F_4 pressures below 30 mm. Possible trends at higher pressures are obscured by the scatter in the data, but the low-intensity points lie above those at the higher intensities.

At 95° and C_2F_4 pressures between 1 and 4 mm, Φ(cyclo-C_3F_6) is about 0.11 irrespective of intensity, as shown in Figure 2. At higher C_2F_4 pressures, Φ(cyclo-C_3F_6) rises toward unity with increasing pressure; the steeper the rise, the lower the intensity.

At 150°, there is no intensity-independent, pressure-independent region. Φ(cyclo-C_3F_6) is increased by raising the C_2F_4 pressure or lowering the intensity. The limiting high-pressure, low-intensity limit for

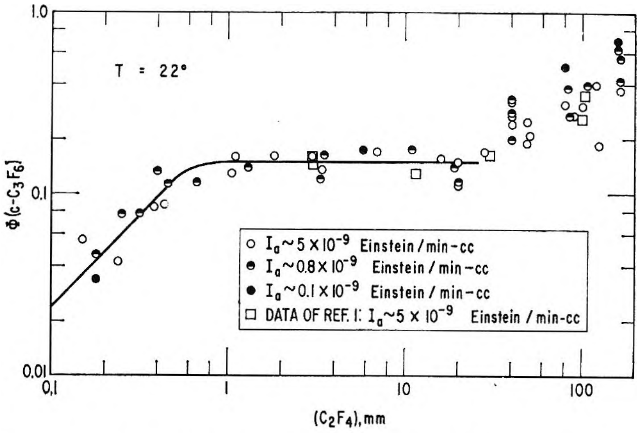

Figure 1. Plot of Φ(cyclo-C_3F_6) *vs.* (C_2F_4) at 22°.

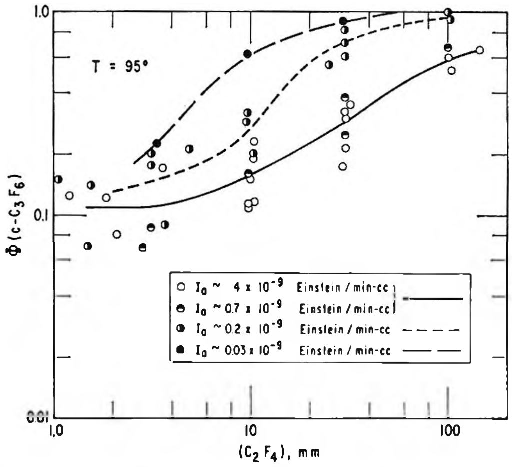

Figure 2. Plot of Φ(cyclo-C_2F_6) *vs.* (C_2F_4) at 95°.

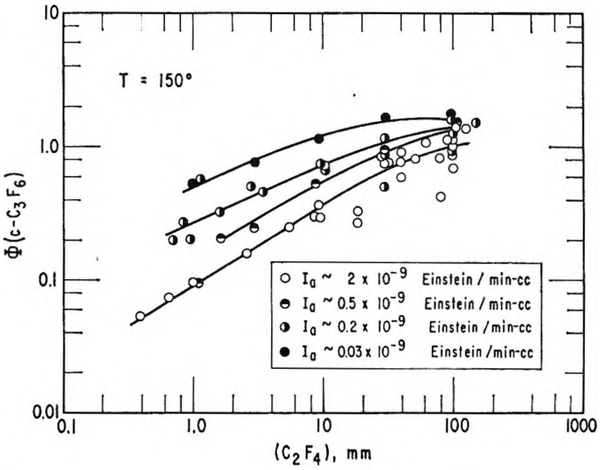

Figure 3. Plot of Φ(cyclo-C_3F_6) *vs.* (C_2F_4) at 150°.

---

[4] N. Cohen and J. Heicklen, *J. Chem. Phys.*, **43**, 871 (1965).

1.3585, 3703 cm^{-1}, 2728 cm^{-1}, 1.3589. This closely approximates the theoretical value of the isomer shift expected for identical OH and OD structures and, with the observation that the growth of a band in the OD region was accompanied by the decline of a corresponding band in the OH region, indicates that the four absorptions were brought about by surface OH groups, the deuteration involving the exchange of the hydrogen atom of an OH group by a deuterium atom.

The bands of the residual OH groups declined at different rates on heating *in vacuo*, shown, for example, by the sequence A, B, C, D of Figure 2. The exchange reactions similarly occur at different rates. For example, the ratio of peak heights of the sharp OD bands at 2760 and 2728 cm^{-1} changed from about 0.6 after 2.5 hr at 500° to about 1.1 after 10 min at 600°, and to about 1.7 after 75 min at 600°. These differences indicate that a distinct surface OH species is responsible for each of the sharp bands.

The deuteration was accompanied by a frequency shift of the unexchanged silanol groups, except at very high stages of degassing. For the data of Figure 4, for example, the free OH band moved from an initial value of 3743 cm^{-1} on the deuterium-free surface to a final value of 3748 cm^{-1} for the residual OH groups. A similar small shift was observed for small and high OD surface concentrations.

Identical results could be produced by treating porous glass with D_2O, although deuteration of the surface occurred at lower temperatures than with D_2. For example, a sample was exposed to D_2O vapor at 2 cm pressure at 100° for 4 hr and was then degassed at 400° for 4 hr. Upon repetition of this cycle for five or six times about 90% of the surface OH species could be converted to the corresponding OD species.

HF Treatment. A porous glass specimen was degassed at 750° for 16 hr, was then exposed to HF at 1 cm pressure for 1 hr, and then was degassed at 500° for 4 hr. This successive HF treatment and degassing was repeated twice. The results are shown in Figure 5, the spectra showing that all bands could be removed completely by the HF treatment, thus indicating the sharp 3748- and 3703-cm^{-1} bands to be caused by surface species. A slight shift to higher frequency in the Si–OH vibration can be seen as the removal of hydroxyls proceeds. The two sharp hydroxyl bands could be restored by adsorbing water on a fluoridated sample at room temperature and degassing at temperatures varying from 30 to 300°. Such experiments, which will be reported in detail elsewhere, indicate that the removal of surface boron through the formation of volatile BF_3 could not have occurred to an appreciable extent.

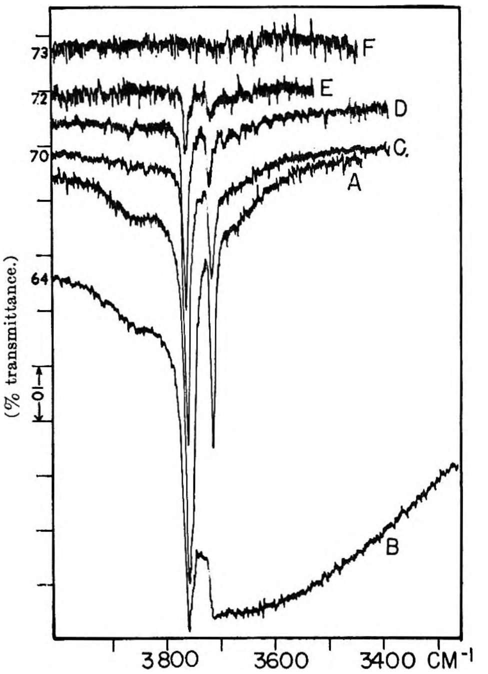

Figure 5. HF treatment: A, after 20 hr degassing at 750°; B, after 1 hr contact with 1 cm of HF at room temperature; C, after 0.5 hr degassing at 500°; D, after 4 hr degassing at 500°; E, after HF treatment as in B followed by 3 hr degassing at 500°.

HNO_3 Leaching. A porous glass specimen was leached with nitric acid following the procedure of Little, Klauser, and Amberg.[19] They had shown the boron content of the glass to be unaffected by this treatment, but the aluminum and zirconium content as R_2O_3 changed from 0.89 to 0.36%. The spectra of the leached and unleached specimens, after identical degassing, were similar in the OH region and also in the 2700-cm^{-1} region where bands attributed to the boric oxide in the glass occur. As the leaching did not affect the ratio of intensities of the sharp bands, this excludes the possibility that the 3703-cm^{-1} band was caused by an OH associated with R_2O_3.

Boric Acid Impregnation. Cab-O-Sil[20] silica was impregnated with boric acid to result in a SiO_2–2% B_2O_3 sample approximating the chemical composition of the porous Vycor.

A slurry made from Cab-O-Sil and the required amount of an aqueous boric acid solution was air-dried at 135° for 2 hr. Self-supporting 1-in. diameter wafers of about 0.1 g of the pure and the impregnated Cab-O-Sil were prepared by pressing at 30 tons/in.^{2}. Spectra were recorded at different stages of degassing,

---

[19] L. H. Little, H. E. Klauser, and C. H. Amberg, *Can. J. Chem.*, 39, 42 (1961).

[20] Cabot Co., Boston, Mass.

Table III: Mercury-Sensitized Photolysis of N_2O-C_2F_4 Mixtures at 150°; $N_2O \sim 500$ mm

(C_2F_4), mm	$R(N_2) \times 10^9$, moles/min cc	Φ(cyclo-C_3F_6)
$I_a \sim 2 \times 10^{-9}$ einstein/min cc		
0.39	1.44	0.053
0.66	1.6	0.073
1.0	2.6	0.095
2.53	1.73	0.16
5.5	1.92	0.25
8.7	1.7	0.30
9.2	1.92	0.37
9.5	1.76	0.29
10.5	5.8	0.72
18.5	1.8	0.27
18.5	2.1	0.33
28	1.12	0.85
30	2.9	0.77
33	2.4	0.87
40	4.2	0.59
40	3.8	0.77
40	...	0.93
52	1.12	0.81
61	1.0	1.08
80	3.2	0.82
80	3.2	0.42
90	1.2	1.15
100	4.0	0.87
100	4.8	0.69
100	2.3	1.15
100	3.2	1.0
104	1.68	1.4
125	1.87	1.35
$I_a \sim 0.5 \times 10^{-9}$ einstein/min cc		
1.1	0.65	0.093
1.65	0.38	0.21
2.9	0.80	0.25
8.6	0.73	0.53
31	0.75	0.94
101	0.68	1.5
$I_a \sim 0.2 \times 10^{-9}$ einstein/min cc		
0.71	0.21	0.20
0.84	0.139	0.27
0.95	0.21	0.20
1.18	0.175	0.58
1.6	0.22	0.34
2.85	0.160	0.50
3.5	0.23	0.46
9.8	0.147	0.75
10.3	0.25	0.67
30	0.28	1.18
30	0.172	0.50
31	0.150	0.88
98	0.21	1.6
100	0.174	1.27
100	0.096	1.15
100	0.067	0.96
150	0.22	1.5
$I_a \sim 0.03 \times 10^{-9}$ einstein/min cc		
1.0	0.027	0.53
3.0	0.037	0.77
9.35	0.036	1.15
31	0.033	1.66
99	0.035	1.8

Discussion

In this system, the initial photolytic act is excitation of the mercury vapor

$$Hg + h\nu \longrightarrow Hg^* \qquad (8)$$

The excited mercury atom might react with either N_2O or C_2F_4

$$Hg^* + N_2O \longrightarrow Hg + N_2 + O(^3P) \qquad (9)$$

$$Hg^* + C_2F_4 \longrightarrow Hg + 2CF_2 \text{ (singlet)} \qquad (10)$$

Reaction 9 is a well-known method for producing oxygen atoms and is the only reaction by which N_2O quenches Hg^*.[5] Reaction 10 is almost the only result of quenching Hg^* by C_2F_4.[6,7] A small fraction of the quenching leads to excited C_2F_4 molecules which can deactivate. However, in this work this process is negligible under all conditions and can be ignored. The relative rate constants k_9/k_{10} have been measured to be about 3.0 at room temperature.[1,8] We measured this ratio at elevated temperatures and found it to be insensitive to temperature.[9] In the experiments reported in this paper, the ratio $(N_2O)/(C_2F_4)$ was always greater than 3.0. Thus at least 90% of the quenching of the mercury was by reaction 9.

The oxygen atom produced then reacts exclusively with C_2F_4 to yield ultimately one molecule of CF_2O for every oxygen atom consumed. The possible reactions are (1), (4), and (5). At present we are unable to distinguish between (1) and (4), so we combine them into a composite reaction (11).

---

(5) R. J. Cvetanović, *Advan. Photochem.*, **1**, 115 (1963).

(6) B. Atkinson, *J. Chem. Soc.*, 2684 (1952).

(7) J. Heicklen, V. Knight, and S. A. Greene, *J. Chem. Phys.*, **42**, 221 (1965).

(8) A. J. Yarwood, O. P. Strausz, and H. E. Gunning, *ibid.*, **41**, 1705 (1964).

(9) Unpublished work of this laboratory.

$$O + C_2F_4 \longrightarrow CF_2O + CF_2 \qquad (11)$$

where the multiplicity of the CF_2 is unspecified.

If CF_2 radicals were the only precursors to cyclo-C_3F_6 formation (*i.e.*, reaction 5 is unimportant) and the only reactions of CF_2 are (2) and (3), then application of a stationary-state treatment to O atoms and to CF_2 radicals as determined by reactions 9, 2, 3, and 11 gives two limiting expressions for Φ(cyclo-C_3F_6), depending on the relative rates of reactions 2 and 3

$$\Phi(\text{cyclo-}C_3F_6) = 1 \qquad (R_2 < R_3) \qquad (12)$$

$$\Phi(\text{cyclo-}C_3F_6) = k_3\left(\frac{I_a}{2k_2}\right)^{1/2}(C_2F_4) \qquad (R_3 < R_2) \qquad (13)$$

Thus, Φ(cyclo-C_3F_6) would depend on the intensity and the C_2F_4 pressure ($R_2 > R_3$) or it would be independent of both variables ($R_3 > R_2$); it could not depend on one variable and be independent of the other. The data at 22° and C_2F_4 pressures less than 0.6 mm show that Φ(cyclo-C_3F_6) increases with C_2F_4 pressure but is unaffected by variations in the intensity. Thus another reaction must be playing a role; we presume it is reaction 5. Conversely, if reaction 5 were the only result of oxygen atom–C_2F_4 encounters, then

$$\Phi(\text{cyclo-}C_3F_6) = 1 \qquad (R_2 < R_3) \qquad (14)$$

$$\Phi(\text{cyclo-}C_3F_6) = k_3(C_2F_4)\left\{\frac{k_7}{2I_ak_2[k_6(C_2F_4) + k_7]}\right\}^{1/2} + \frac{k_6(C_2F_4)}{k_6(C_2F_4) + k_7} \qquad (R_3 < R_2) \qquad (15)$$

but at all pressures of C_2F_4 greater than 1 mm, $k_6(C_2F_4) > k_7$ as will be shown. Therefore, the last equation reduces to

$$\Phi(\text{cyclo-}C_3F_6) \cong 1 \qquad (16)$$

That is, Φ(cyclo-C_3F_6) would be unity under all conditions except at the very lowest C_2F_4 pressures. The results indicate that this is not the case. Thus, reaction 11 must participate. Henceforth, discussion is based on the mechanism consisting of reactions 2, 3, 5–9, and 11.

If we apply the steady-state approximation to (CF_2), (O), and ($C_2F_4O^*$), recognizing that reaction 7 is an unimportant source of CF_2 radicals, we obtain

$$\Phi(\text{cyclo-}C_3F_6) = 1.0 \qquad (R_2 < R_3) \qquad (17)$$

$$\Phi(\text{cyclo-}C_3F_6) = \frac{k_3(C_2F_4)}{I_a^{1/2}}\left[\frac{k_{11}}{2k_2(k_{11} + k_5)}\right]^{1/2} + \frac{k_5k_6(C_2F_4)}{(k_{11} + k_5)[k_6(C_2F_4) + k_7]} \qquad (R_3 < R_2) \qquad (18)$$

An important prediction of the mechanism is that in the high C_2F_4 pressure, low-intensity limit, Φ(cyclo-C_3F_6) = 1.0 as long as reaction 10 is negligible. Since we have defined Φ(cyclo-C_3F_6) as (cyclo-C_3F_6)/(N_2), then the actual limit for Φ(cyclo-C_3F_6) called Φ_∞(cyclo-C_3F_6), is

$$\Phi_\infty(\text{cyclo-}C_3F_6) = 1.0 + 2\,\frac{k_{10}}{k_9}\,\frac{(C_2F_4)}{(N_2O)} \qquad (19)$$

Under our experimental conditions, the last term on the right side of (19) can approach 0.20. At 22 and 95°, Φ_∞(cyclo-C_3F_6) is about unity, whereas at 150° it is about 1.5 compared to the theoretical limit of 1.2. Presumably this discrepancy reflects errors in our analytical procedure.

Equation 18 will hold reasonably well for Φ(cyclo-C_3F_6) $\leq$ 0.5 and will become more and more exact as Φ(cyclo-C_3F_6) decreases.

Let us first examine the results at 22°. For C_2F_4 pressures less than 30 mm, Φ(cyclo-C_3F_6) is independent of intensity. Consequently, the first term on the right side of (18) must be unimportant. At very low pressures, $k_7 \gg k_6(C_2F_4)$ and (18) reduces to

$$\Phi(\text{cyclo-}C_3F_6) \approx \frac{k_5k_6(C_2F_4)}{k_7(k_{11} + k_5)} \qquad (20)$$

In accordance with (20), Figure 1 shows that Φ(cyclo-C_3F_6) is proportional to (C_2F_4) at low C_2F_4 pressures and is independent of I_a. From the intercept of the log–log plot, $k_5k_6/k_7(k_{11} + k_5)$ is estimated to be 0.24 mm^{-1}. As the C_2F_4 pressure is raised, $k_6(C_2F_4) \gg k_7$, and (18) becomes

$$\Phi(\text{cyclo-}C_3F_6) \approx \frac{k_5}{k_{11} + k_5} \qquad (21)$$

Again, Figure 1 shows a large region where Φ(cyclo-C_3F_6) is independent of (C_2F_4) and I_a. The ratio $k_5/(k_{11} + k_5)$ is 0.15. Finally, at higher pressures eq 18 can be rearranged to yield

$$I_a^{1/2}\left[\Phi(\text{cyclo-}C_3F_6) - \frac{k_5}{k_{11} + k_5}\right] = k_3(C_2F_4)\left[\frac{k_{11}}{2k_2(k_{11} + k_5)}\right]^{1/2} \qquad (22)$$

Using the value of 0.15 for $k_5/(k_{11} + k_5)$, we can compute the left side of (22) [$I_a = R(N_2)$], and in Figure 4 it is plotted *vs.* (C_2F_4). The data are limited (only values for Φ(cyclo-C_3F_6) between 0.2 and 0.5 are used) and are scattered. Nevertheless, we force the best straight line of slope unity through the points and from the intercept estimate $k_3/k_2^{1/2}$ to be 1.0 × 10^{-2} (l./mole

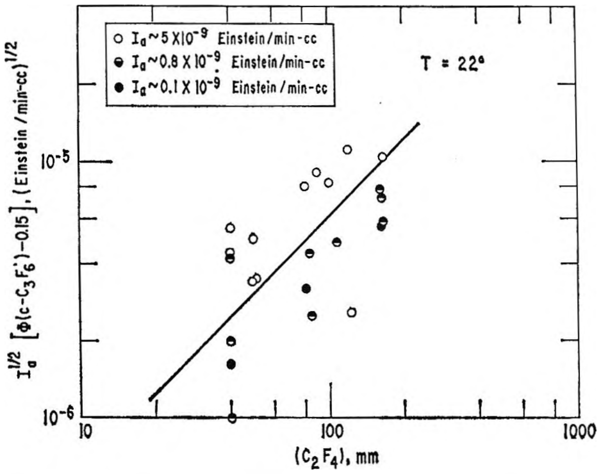

Figure 4. Plot of $I_a^{1/2}[\Phi(\text{cyclo-C}_3F_6) - 0.15]$ *vs.* (C_2F_4) at 22° for values of $\Phi(\text{cyclo-C}_3F_6) < 0.5$.

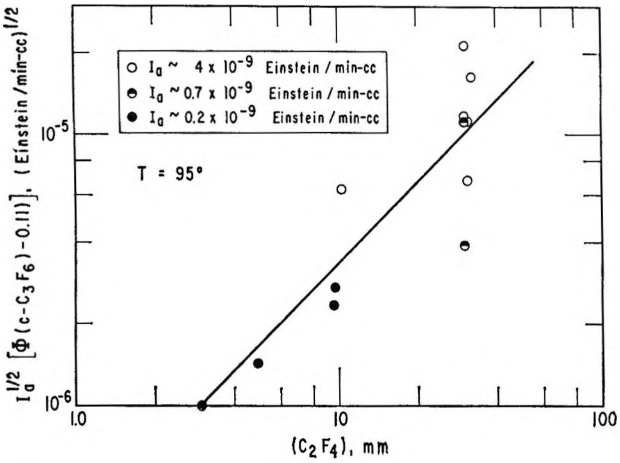

Figure 5. Plot of $I_a^{1/2}[\Phi(\text{cyclo-C}_3F_6) - 0.11]$ *vs.* (C_2F_4) at 95° for values of $\Phi(\text{cyclo-C}_3F_6) < 0.5$.

sec)$^{1/2}$. This estimate is probably good to about a factor of 2.

At 95° the same analysis can be made as at 22°. The very low-pressure region was not reached, and $k_5k_6/k_7(k_{11} + k_5)$ cannot be estimated. The flat region in Figure 2 is below 4 mm and yields a value of about 0.11 for $k_5/(k_{11} + k_5)$. The left side of (22) is plotted *vs.* (C_2F_4) in Figure 5, and again the best straight line of unit slope if forced through the badly scattered data. The estimate of $k_3/k_2^{1/2}$ at 95° is 3.1 × 10^{-2} (l./mole sec)$^{1/2}$.

At 150°, Figure 3 shows that there is no intensity-independent region. Consequently, the first term on the right side of (18) must always be important. However, there is no region where $\Phi(\text{cyclo-C}_3F_6)$ is proportional to (C_2F_4), so the second term on the right side of (18) must also play a role. In fact, $k_5/(k_{11} + k_5)$ must be about 0.10. If it were much smaller, then there would be a linear region for $\Phi(\text{cyclo-C}_3F_6) \sim 0.3$; but if it were much larger, then there would be a linear region for $\Phi(\text{cyclo-C}_3F_6) < 0.10$. If we use a value of about 0.10 for $k_5/(k_{11} + k_5)$, then $k_5k_6/k_7(k_{11} + k_5)$ must be similar to that at room temperature and $k_3/k_2^{1/2}$ can be estimated from the appropriate plot, Figure 6, based on eq 22. The estimate is 0.13 (l./mole sec)$^{1/2}$.

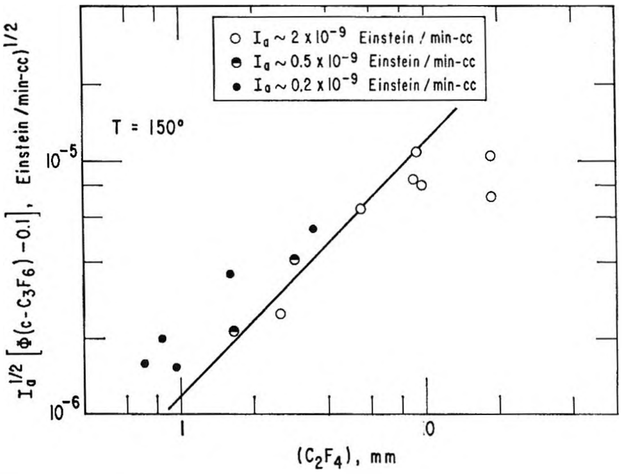

Figure 6. Plot of $I_a^{1/2}[\Phi(\text{cyclo-C}_3F_6) - 0.10]$ *vs.* (C_2F_4) at 150° for values of $\Phi(\text{cyclo-C}_3F_6) < 0.5$.

Table IV summarizes the rate constant data. Reactions 5 and 11 are the competing reactions for the highly exothermic O + C_2F_4 reaction. The chemical energy greatly exceeds any thermal energy, and the activation energy is only about 0.6 kcal/mole;[2] thus temperature variations should have little effect on the rates. However, if there is any effect it should be such that reaction 11 is favored with increasing temperature, as the $C_2F_4O^*$ would be more unstable. Our results agree with expectation. Reactions 6 and 7 are highly exothermic, and no temperature effect would be expected for them. Again our crude results agree with this hypothesis. The ratio k_6/k_7 is about 2.0 mm^{-1}, so reaction 7 is unimportant for C_2F_4 pressures in excess of 1 mm. Reaction 3 might well have an activation energy, and thus $k_3/k_2^{1/2}$ could be markedly enhanced at elevated temperatures. In fact, this occurs, and Table IV shows a comparison of the ratio obtained with that obtained in another study for singlet CF_2 radicals. Within experimental error, the results are identical.

We may now address ourselves to the question of what is the nature of the excited species designated $C_2F_4O^*$. Thermochemical considerations indicate that $C_2F_4O^*$ has at least 70 kcal/mole excess energy over the ground state. If all this energy appeared as vi-

Table IV: Rate Constant Data

Temp, °C	$k_5/(k_{11} + k_5)$	$k_8k_5/[k_7(k_{11} + k_5)]$, mm^{-1}	$10^3 \times k_8/k_2^{1/2}$ (l./mole sec)$^{1/2}$ This work	Ref 4
22	0.15	0.24	10.0	4.3
95	~0.11	...	31	40
150	~0.10	*a*	130	130

[a] Similar to value at 22°.

brational energy, $C_2F_4O^*$ would never be stabilized under our conditions and would always dissociate. Consequently, $C_2F_4O^*$ must be an excited electronic level, presumably a triplet in accordance with the spin conservation rules.

Finally we return to the problem of the multiplicity of the CF_2 radicals formed in reaction 11. Originally, the suggestion that the CF_2 radicals in this system were triplets was based on their excessive reactivity with C_2F_4 and O_2. However, the results of this study have shown that their reactivity toward C_2F_4 is identical with that for singlet CF_2 radicals. Thus if they are triplets, the evidence must rest on the reactivity with O_2. The appropriate experiments are being conducted in the Aerospace Laboratories, and will be the subject of a future report.

Acknowledgment. This research was supported by the U. S. Air Force under Contract No. AF 04(695)-669. The authors wish to thank Mr. Richard Frey for performing many of the analyses and experiments and Mrs. Zanette Kohlmeyer for assistance with the manuscript.

Photolysis of Methyl Iodide in the Presence of Nitric Oxide

by Timothy Johnston and Julian Heicklen

Aerospace Corporation, El Segundo, California *(Received March 7, 1966)*

Methyl iodide was photolyzed in the presence of NO at room temperature. Iodine is both a primary and secondary product. Nitrosomethane is a primary product, while $(CH_3NO)_2$, NO_2, CH_3ONO, N_2, and N_2O are secondary products, and CH_3ONO_2, CH_2O, and HNO_2 are tertiary products. The complete reaction sequence is given. Methyl iodide enters the chain step to give CH_3O radicals. The important steps in removing CH_3NO are $2CH_3NO \rightarrow (CH_3NO)_2$ and $CH_3NO + NO \rightarrow CH_3O + N_2O$. The rate constants for both reactions were obtained and are tabulated with several other rate constants. Where comparisons could be made with existing results, agreement was good.

I. Introduction

The methyl radical addition to nitric oxide has been studied extensively, and the rate constant is reasonably well known.[1-6] The adduct has been observed by the use of infrared analysis[7] as well as mass spectral analysis.[8]

Nitrosomethane can be removed in a number of reactions. If the NO pressure is sufficiently low that all methyl radicals are not scavenged by NO, then two methyl radicals can react with CH_3NO. Such a reaction was proposed by Hoare[6] to account for the fact

---

(1) R. W. Durham and E. W. R. Steacie, *J. Chem. Phys.*, **20**, 582 (1952).

(2) F. P. Lossing, K. V. Ingold, and A. W. Tickner, *Discussions Faraday Soc.*, **14**, 34 (1953).

(3) W. A. Bryce and K. V. Ingold, *J. Chem. Phys.*, **23**, 1968 (1955).

(4) M. I. Christie, *Proc. Roy. Soc.* (London), **A249**, 248 (1958).

(5) W. C. Sleppy and J. G. Calvert, *J. Am. Chem. Soc.*, **81**, 769 (1959).

that up to three methyl radicals can be removed per nitric oxide molecule in the gas phase. The reaction was confirmed by the experiment of Maschke, Shapiro, and Lampe,[8] who actually observed CD_3NO and $(CD_3)_2NOCD_3$ in a mass spectrometer.

If the NO pressure is sufficiently great that the methyl radical is completely scavenged, then CH_3NO must be removed by different routes. At temperatures above 200°, CH_3NO can isomerize, and the isomer can decompose both homogeneously and heterogeneously.[9,10] However, both the isomerization reaction and the subsequent decomposition have been reported to occur with an activation energy of about 40 kcal/mole.[11,12] Consequently, they cannot be important at lower temperatures. At room temperature, nitrosoalkanes are quite stable,[7,12,13] but can disappear slowly by polymerization. Thompson and Linnett[14] found a white, solid deposit when mercury dimethyl was photolyzed in the presence of nitric oxide, probably the polymer of CH_3NO. Calvert, Thomas, and Hanst[7] measured the dimerization rate constant for CH_3NO to be 87 l./mole sec at room temperature. Christie, Frost, and Voisey[15] report the dimerization constant to be $0.63 \times 10^5 \exp(-4600/RT)$ l./mole sec, which gives 25 l./mole sec at room temperature in approximate agreement with the Calvert, Thomas, and Hanst value.

In the presence of a great excess of NO, Brown[16] found that alkyl radicals catalyze the conversion of NO to N_2 and NO_2. He proposed the reaction sequence

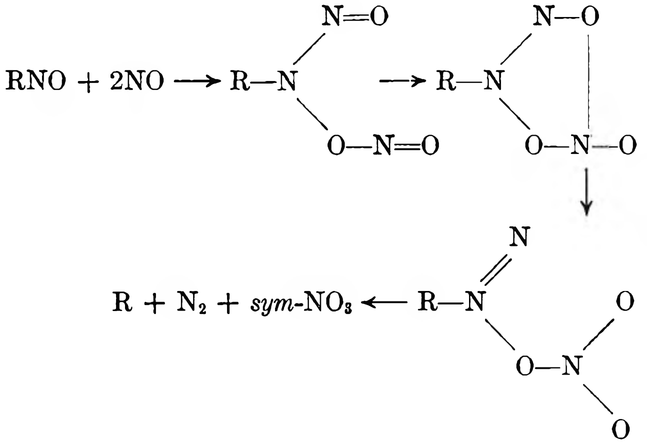

The alkyl radicals then react with nitric oxide to regenerate the nitrosoalkane, and the NO_3 reacts with NO to produce NO_2. A number of recent reports show that N_2 and NO_2 can be formed in very great yields.[12,15,17-20] Christie and her co-workers[12,15,19] show that the above reaction is first order in RNO and second order in NO. In ref 15, the rate constant is reported to be $2.6 \exp(+1800/RT)$ l.²/mole² sec. With CF_3NO, the same reaction occurs; it too is found to be first order in CF_3NO and second order in NO.[21]

However, Christie[12] and Christie, Gilbert, and Voisey[19] found that when a great excess of NO (100–600 mm) was added to CH_3NO, the amount of NO_2 produced was proportional to the *first power* of NO, even though all of the CH_3NO was consumed. Furthermore, Christie, Frost, and Voisey[15] found that CH_3NO can be consumed in a reaction *first order* in CH_3NO. They report a rate constant of $2.45 \exp(-7700/RT)$ sec^{-1} and attribute this reaction to isomerization on the walls. This explanation is inconsistent with the activation energy for the isomerization reaction and with the fact that the isomer definitely is not a product of the reaction at room temperature.[18] Finally, in studies in this laboratory,[20] N_2O was found to be an important product at low intensities. The results could only be interpreted if all the CH_3NO was consumed by the reaction

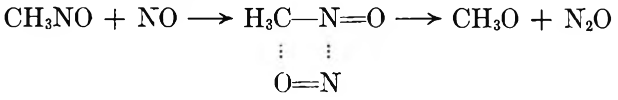

$$CH_3NO + NO \longrightarrow \underset{\substack{\vdots \quad \vdots \\ O{=}N}}{H_3C{-}N{=}O} \longrightarrow CH_3O + N_2O$$

It is also clear that the results of Christie and coworkers imply such a reaction. Consequently, we initiated a study to establish this reaction and to measure its rate constant.

II. Experimental Section

A. Materials. Matheson Co. research grade N_2, O_2, NO, and N_2O were used, the N_2 and O_2 without further purification. Both the NO and N_2O were

---

(6) D. E. Hoare, *Can. J. Chem.*, **40**, 2012 (1962).

(7) J. G. Calvert, S. J. Thomas, and P. L. Hanst, *J. Am. Chem. Soc.*, **82**, 1 (1960).

(8) A. Maschke, B. S. Shapiro, and F. W. Lampe, *ibid.*, **85**, 1876 (1963).

(9) G. L. Pratt and J. H. Purnell, *Trans. Faraday Soc.*, **60**, 371 (1964).

(10) L. Batt and B. G. Gowenlock, *ibid.*, **56**, 682 (1960).

(11) B. G. Gowenlock, L. Batt, and J. Trotman, Special Publication No. 10, The Chemical Society, London, 1957, p 75.

(12) M. I. Christie, *Proc. Roy. Soc.* (London), **A249**, 258 (1958).

(13) F. W. Dalby, *Can. J. Phys.*, **36**, 1336 (1958).

(14) H. W. Thompson and J. W. Linnett, *Trans. Faraday Soc.*, **33**, 874 (1937).

(15) M. I. Christie, J. S. Frost, and M. A. Voisey, *ibid.*, **61**, 674 (1965).

(16) J. F. Brown Jr., *J. Am. Chem. Soc.*, **79**, 2480 (1957).

(17) E. G. Burrell, Jr., *J. Phys. Chem.*, **66**, 401 (1962).

(18) O. P. Strausz and H. E. Gunning, *Can. J. Chem.*, **41**, 1207 (1963).

(19) M. I. Christie, C. Gilbert, and M. A. Voisey, *J. Chem. Soc.*, 3147 (1964).

(20) J. Heicklen, Aerospace Corp., Report No. TDR-469(5250-40)-9 (March 15, 1965).

(21) J. Heicklen, *J. Phys. Chem.*, **70**, 112 (1966).

degassed at −196° before use. In addition, the NO was distilled previously from a bath at −186° to remove any NO_2 and N_2O impurities. Eastman Organic Chemical CH_3I and Peninsular ChemResearch Co. CF_3I were used after degassing at −196°.

B. Procedure. CH_3I and NO were mixed in a Pyrex T-shaped cell. The cross of the T was 5 cm in diameter and 10 cm long, had NaCl windows at each end, and was situated in the sample beam of a Beckman IR-4 infrared spectrometer. The stem of the T was also 5 cm in diameter and 10 cm long. At the end was a quartz window through which the ultraviolet radiation entered the cell. The incident radiation came from a Hanovia U-shaped, Type SH, medium-pressure mercury lamp and passed through a Corning 0-53 filter (to remove radiation below 2800 A) and appropriate screens (to reduce the intensity) before entering the cell.

During exposure, the infrared product bands were monitored continually. After exposure, the bands were monitored until reaction was complete. Then the reacted mixture was expanded through a trap at −212° into a calibrated volume, and the pressure was measured after equilibrium was attained. At −212°, the only noncondensible gas is N_2; thus, this measurement permitted calculation of the nitrogen yield. The N_2 and NO then were removed at −186°, the products were warmed to −160°, and the N_2O was collected for chromatographic analysis.

C. Actinometry. To determine the incident intensity, mixtures of 300 mm of CF_3I and 300 mm of O_2 were photolyzed, and the CF_2O was monitored by infrared analysis. Under these conditions, all radiation between 2800 and 3200 A entering the cell is absorbed, and the quantum yield of CF_2O formation is unity.[21] The absorbed intensity for any CH_3I-NO run, then, was computed from the absorption coefficients of CH_3I at various wavelengths, the transmission characteristics of the Corning 0-53 filter, and the relative lamp intensities at the various mercury lines. The absorption coefficients were found directly on a Cary Model 15 ultraviolet spectrophotometer; the transmission characteristics of the Corning filters are well known, and the relative lamp intensities had been found previously.[22]

D. Calibrations. For N_2 and N_2O we made direct calibrations. For NO_2, measured amounts of O_2 were mixed with CH_3I and NO to correspond to actual runs. The O_2 completely converted to NO_2. Detailed calibration curves for the 6.16-μ band were made for every condition because of the complexity of the NO_2 system. In the first place, NO_2 dimerizes to form a system in equilibrium with N_2O_4; secondly, NO_2 reacts with NO to form a system in equilibrium with N_2O_3; and thirdly, the NO_2-N_2O_4 equilibrium is nonideal. The extinction coefficient depends on the total pressure of the system, even if an inert gas (argon) is used. However, once the calibrations were made, NO_2 could be monitored reliably. Our reported values for NO_2 correspond to total NO_2, *i.e.*, $(NO_2) + 2(N_2O_4) + (N_2O_3)$. For CH_3ONO and CH_3ONO_2, we did not make calibrations. The extinction coefficients used were extracted, respectively, from Tarte[23] and from Brand and Cawthon.[24] The infrared peaks used for the product identification and analysis of NO_2, CH_3ONO, CH_3ONO_2, CH_2O, and HNO_2 were, respectively, at 6.16, 5.88,[23] 9.85,[24] 5.75,[25] and 12.65 μ.[26]

III. Results

The infrared product bands were found for NO_2 (including N_2O_4 and N_2O_3), CH_3ONO, CH_3ONO_2, CH_2O, and HNO_2. The infrared band reported for CH_3NO[7] lies under the large NO_2 band at 6.16 μ; thus no analysis could be made for CH_3NO. The dimer of CH_3NO goes to the wall and polymerizes,[7] so none of its infrared bands would be detected. Iodine and nitrogen have no infrared spectra, and that for N_2O is extremely weak. No analysis was made for iodine, but N_2 and N_2O were measured after the reaction was completed. It is possible that HNO_3 was also formed as a minor product, but its infrared spectrum is similar to that for HNO_2, and analysis would be difficult.

We carefully looked for the CH_3NO_2 bands at 6.35 and 7.2 μ,[27] but did not see them. Consequently, if CH_3NO_2 is formed, it cannot be an important product. The important products of the reaction that can be followed spectrometrically are NO_2, CH_3ONO, and CH_3ONO_2. For a typical run, the results are plotted in Figure 1. It should be understood that NO_2 refers to total NO_2 including N_2O_4 and N_2O_3.

The CH_2O and HNO_2 bands were quite small. In many cases no values could be obtained; in other cases only final values were found; in a few cases CH_2O could be monitored throughout the run.

The curves in Figure 1 show that the NO_2, CH_3ONO, and CH_3ONO_2 all have induction periods; those for CH_3ONO and NO_2 are similar, but the one for CH_3-

---

[22] D. Dutton and J. P. Heicklen, unpublished work at the University of Rochester, 1956.

[23] P. Tarte, *J. Chem. Phys.*, 20, 1570 (1952).

[24] J. C. D. Brand and T. M. Cawthon, *J. Am. Chem. Soc.*, 77, 319 (1955).

[25] R. H. Pierson, E. N. Fletcher, and E. St. C. Gantz, *Anal. Chem.*, 28, 1218 (1956).

[26] L. H. Jones, R. M. Badger, and G. E. Moore, *J. Chem. Phys.*, 19, 1599 (1951).

[27] D. C. Smith, C. Pan, and J. R. Nielsen, *ibid.*, 18, 706 (1950).

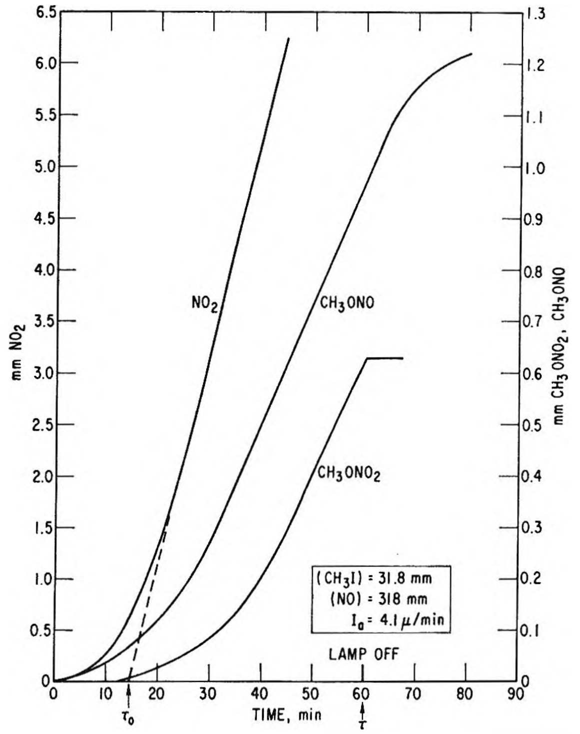

Figure 1. Plot of product formation *vs.* time for $(CH_3I) = 31.8$ mm, $(NO) = 318$ mm, and $I_a = 4.1\ \mu$/min.

ONO_2 is considerably longer. These effects were noticed in all runs where data were obtained. After the induction period, the products rise linearly with time. The linear portion of the NO_2 curve has been extrapolated to zero and an induction time τ_0 has been found. After the lamp was turned off, at time τ, the product curves usually continued to grow for some time before leveling off, after which the products were stable in the dark.

The induction period and the leveling-off period arise from two causes. First, there is a lag due to diffusional mixing in our system. The products form in the stem of the T-shaped cell, but are not analyzed until they diffuse to the cross of the T. Separate experiments in our laboratory have shown the diffusional mixing time to be approximately 1 sec/mm of gas. Thus, at high total pressures, most of the lag time is due to diffusional mixing. Second, one of the primary products of the reaction CH_3NO is unstable and slowly reacts to produce the secondary and tertiary products that we monitor. At low total pressures, this effect accounts for most of the delay.

Based upon our time-history data and information previously obtained by others, the products can be classified as primary, secondary, or tertiary. The classification for each product is listed in Table I. It is well established that the primary products are I_2 and CH_3NO. That I_2 is also formed as a secondary product has not been proposed previously. However, our results require that CH_3I be decomposed in a chain step, and thus part of the I_2 formed would be secondary. Our results clearly show that NO_2 and CH_3ONO are secondary products. Since the N_2 formation is associated with NO_2 production, it too must be secondary. The dimer of CH_3NO is, of course, secondary. For the reasons stated in the Introduction, we believe N_2O to be secondary. For the runs in which CH_2O was monitored, its curves of growth had induction periods similar to CH_3ONO_2; thus, both CH_3ONO_2 and CH_2O are tertiary products. Nitrous acid can be formed only from NO_2, so it too must be a tertiary product.

Table I: Products of the Reaction

Product	Classification	Comments
I_2	Primary and secondary	Not monitored
CH_3NO	Primary	Not monitored
$(CH_3NO)_2$	Secondary	Not monitored
NO_2	Secondary	Monitored continually during exposure
CH_3ONO	Secondary	Monitored continually during exposure
N_2	Secondary	Final amount measured
N_2O	Secondary	Final amount measured
CH_3ONO_2	Tertiary	Monitored continually during exposure
CH_2O	Tertiary	Monitored continually during exposure
HNO_2	Tertiary	Final amount measured

The detailed results of the photolyses are listed in Table II. For those runs in which the induction period is not caused mainly by diffusional mixing, the NO_2 concentration was plotted *vs.* exposure time on a log-log plot, and the data points lay on straight lines of slope 2. From the intercepts of the plots, values of $(NO_2)/t^2$ were found, and they are listed in Table II; they rise with the absorbed intensity and the NO pressure.

Quantum yields of NO_2 and CH_3ONO formation were found from the linear portion of the product *vs.* time curves. The values for CH_3ONO could be obtained for only a few runs because of the interference of an N_2O_3 band at the 5.88-μ band of CH_3ONO. We have reported only $\Phi(CH_3ONO)$ for those cases where the N_2O_3 correction based on its band at 7.65 μ was less than about 30%. Both $\Phi(NO_2)$ and $\Phi(CH_3ONO)$ rise with $(NO)/I_a^{1/2}$ to maximum values far water agree closely with our experimental data (see Figure 2).

For 3 *N* HCl and 1 *N* LiCl, the viscosity of the solutions ("International Critical Tables," Vol. III) is such that their use instead of pure water viscosity in Stokes' equation does not appreciably influence the calculated transport numbers.[20]

If we apply Stokes' equation to concentrated solutions, however, some questions arise. The Fuoss–Onsager theory of conductance of electrolyte solutions underlying Stokes' equation is known to fail even at moderate concentrations. This failure may be due mainly to the treatment of the relaxation effect, which does not appear in the theoretical expression for the transport number. However, it is hard to see how the electrophoretic effect can be described up to saturation by a theory that regards the medium in which the ions move as a continuum with properties independent of the electrolyte concentration.

Regarding the influence of the viscosity of the solution on the calculated transport numbers, it does not seem justifiable to use this viscosity in the electrophoretic retardation terms and still use the limiting equivalent conductivities at infinite dilution. In the theory of electrolyte conductance, the velocity of an ion is regarded as composed of two elements: (a) the velocity of the unhindered ion and (b) the velocity of the ionic atmosphere surrounding the ion (electrophoretic retardation). Both constituent velocities are affected by variations in the viscosity of the surroundings. If these velocities are both affected to the same extent as a result of varying concentration, all terms on the right-hand side of eq 9 will vary by the same factor (*cf.* ref 18). This may be the reason why a close fit is obtained when the viscosity of pure water is used in B_2, the limiting equivalent conductivities (λ_+^0 and Λ^0) being determined at infinite dilution.

At the higher concentrations, the question becomes important whether the transport numbers calculated with Stokes' equation are in fact Hittorf transport numbers, *i.e.*, whether the velocities of the ions are taken with respect to the solvent. In the theory of electrolyte conductance, the velocities of the ions and of the ionic atmospheres are considered with respect to their "surroundings" and it is not certain that water is not moving in this coordinate system. This question is irrelevant, of course, when conductivities of electrolyte solutions are calculated from the ionic mobilities.

Recently, Fuoss and Onsager[21] published a revised treatment of the electrophoretic retardation in solutions of symmetrical electrolytes. With the aid of their eq 61, we modified Stokes' equation for the transport number of 1:1 electrolytes accordingly.

$$t_+ = \frac{\lambda_+^0 - {}^1/_2 S}{\Lambda^0 - S} \qquad (10)$$

where $S = B_2\sqrt{c}\{1 - (\varkappa a b/4)\ F(b)\}$ in which $b = e^2/a\epsilon kT$, e is the protonic charge, and ϵ is the dielectric constant. S is the term describing the electrophoretic retardation of the ions.

It turned out, however, that cation transport numbers calculated with eq 10 for NaCl solutions at 25° showed very large deviations from the observed values at concentrations higher than 0.11 *m* (Table III). Beyond this concentration, the calculated transport numbers start to increase very sharply.

Table III: Comparison of Calculated and Observed Transport Numbers of NaCl Solutions at 25°

c, moles/l.	m, moles/kg of H_2O	$\varkappa a$	S, mho cm²/equiv	t_+ Eq 10	Obsd[a]	Eq 9
0.01	0.01	0.171	5.14	0.3918	0.3918	0.3918
0.1095	0.110	0.566	10	0.387	0.385	0.385
0.434	0.440	1.13	0	0.396	0.378	0.378
1.00	1.02	1.71	−31	0.417	0.375	0.374
5.416	6.144	3.98	−354	0.473	0.363	0.366

[a] For m = 0.01, ref 9; above 0.01 *m*, this work (eq 3).

For these calculations we used the viscosity and dielectric constant of pure water and the same mean ionic diameter (a = 5.2 A) as before.[22] However, when other reasonable values of these constants are used, the general behavior of the transport numbers calculated with eq 10 is not changed.

Table III shows that at concentrations above 0.11 *m* the electrophoretic retardation as represented by S decreases with concentration and even goes through zero at 0.440 *m*. Since the latter represents a physical impossibility, eq 10 does not apply at concentrations above 0.440 *m*. This is because Fuoss and Onsager considered only cases with $\varkappa a$ negligible compared with unity. In particular, in their approximation of the Debye–Hückel expression for the electrical potential, a factor $e^{\varkappa a}/(1 + \varkappa a)$ was omitted. This renders their final

---

[20] KCl was omitted from this comparison. The agreement between observed and calculated transport numbers in KCl solutions cannot provide evidence for the correctness of the electrophoretic retardation term. This is because λ^0_{K} is about equal to ${}^1/_2\Lambda^0_{\mathrm{KCl}}$ and, as can be seen in eq 9, t_{K} is then about 0.5, practically independent of concentration and of the magnitude of the electrophoretic retardation.

[21] R. M. Fuoss and L. Onsager, *J. Phys. Chem.*, **67**, 628 (1963).

[22] For these values b = 1.38; the corresponding value of $F(b)$ is 2.57. This value was obtained by graphical extrapolation over a very short range of Table I of ref 21.

results applicable to very dilute solutions only. In Table III it can be seen that at NaCl concentration of 0.11 *m*, where $\varkappa\alpha = 0.566$, the comparison between observed transport numbers and those calculated with eq 10 is already less satisfactory.

In the two other cases where Stokes' original eq 9 has been verified at high concentrations (3 *N* HCl and 1 *N* LiCl), *S* is negative and eq 10 again does not apply.

It thus appears that the older Fuoss–Onsager theory underlying eq 9 describes the electrophoretic retardation effect in aqueous solutions much better than the recent revised treatment. The refinements in this revised treatment of electrolyte conductance will show up to full advantage if the restriction $\varkappa\alpha \ll 1$ can be removed.

Acknowledgments. The authors wish to thank C. Koole, who took a great part in developing the preparation technique of the electrodes and performed the measurements. The authors are also grateful to Shell Research N.V. for permission to publish this paper.

Coupling Constant and Chemical Shift of Tetrafluoroborate Ion in Mixed Solvents[1]

by R. Haque and L. W. Reeves

Department of Chemistry, University of British Columbia, Vancouver 8, British Columbia, Canada

(Received November 30, 1965)

The coupling constant J_{B-F} and the chemical shift δ_F of the BF_4^- ion have been measured as a function of concentration and solvent composition in water–acetone, water–dioxane, and water–DMSO mixtures. The coupling constant and chemical shift at infinite dilution depends on the solvent mixture as does the variation with concentration. We interpret the results in water, dioxane–water, and acetone–water mixtures in terms of changes in the hydrogen bonding of water to the BF_4^- anion. No inner-sphere ion-pair complex is indicated. In DMSO–water mixtures the behavior of the coupling constant and chemical shift changes are unique. A preferential solvation of the BF_4^- ion by the protolysis product of DMSO in water is suggested. The chemical-shift changes except at the highest concentrations are proportional to the coupling-constant changes, suggesting that variations have a common origin.

Introduction

The ^{11}B–^{19}F coupling constant in sodium tetrafluoroborate was first reported by Reeves and co-workers[2] to be 4.8 cps. Later studies showed that this coupling constant is strongly dependent on the concentration and the cation.[3] The value of the coupling constant *J* is low compared to the isoelectronic species of the series BeF_4^{2-}[4] and CF_4,[5] and it does not follow the correlation suggested by Reeves.[6] Kuhlmann and Grant[3] interpreted these changes in *J* in terms of ion-pair formation between Na^+ and BF_4^- ions and con-

---

[1] This research was supported by the National Research Council of Canada and the Petroleum Research Fund of the American Chemical Society.

[2] R. D. Chambers, H. C. Clark, L. W. Reeves, and C. J. Willis, *Can. J. Chem.*, **39**, 258 (1961).

[3] K. Kuhlmann and D. M. Grant, *J. Phys. Chem.*, **68**, 3208 (1964).

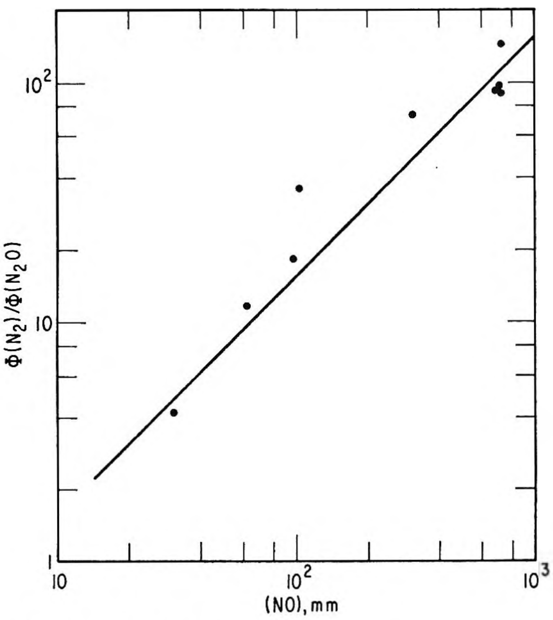

Figure 3. Log–log plot of $\Phi(N_2)/\Phi(N_2O)$ *vs.* (NO).

Frost, and Voisey[15] for the rate constant for the first-order appearance of CH_3NO, because they did not report NO pressure. However, if we use their figures for activation energy, we find $k_d = 8300 \exp(-7700/RT)$ l./mole sec.

Our mechanism also predicts that when reaction e is much more important than f, then $\Phi(CH_3ONO)$ will be unimportant, in agreement with our findings. On the other hand, when reaction e is negligible compared to f, then we find

$$\Phi(N_2) + \Phi(N_2O) = \Phi(CH_3ONO) \tag{4}$$

For the few runs where we have data, the ratio $[\Phi(N_2) + \Phi(N_2O)]/\Phi(CH_3ONO)$ is tabulated in Table II. This ratio is constant, but it is considerably greater than unity. We do not understand this discrepancy. Perhaps it reflects an error in the extinction coefficient for CH_3ONO. The extinction coefficient is crude and was taken from data[23] where yielding extinction coefficients was not the intent.

A number of other predictions can be made from the mechanism. If $R(g) \gg R(h)$, we find

$$\Phi(N_2O) = \frac{k_h}{(2k_g)^{1/2}} \frac{(NO)}{I_a^{1/2}} \tag{5}$$

$$\frac{\Phi(N_2)}{(NO)} = \frac{k_d}{(2k_g)^{1/2}} \frac{(NO)}{I_a^{1/2}} \tag{6}$$

If $R(g) \ll R(h)$, we find

$$\Phi(N_2O) = 1.0 \tag{7}$$

$$\frac{\Phi(N_2)}{(NO)} = \frac{k_d}{k_h} \tag{8}$$

where $R(g)$ and $R(h)$ are the rates of reactions g and h, respectively. The values of $\Phi(N_2O)$ and $\Phi(N_2)/(NO)$ are plotted *vs.* $(NO)/I_a^{1/2}$ on log–log plots in Figure 4. Both plots are linear with a slope of 1 for low values of $(NO)/I_a^{1/2}$, *i.e.*, $R(g) \gg R(h)$, and constant for large values of $(NO)/I_a^{1/2}$, *i.e.*, $R(g) \ll R(h)$. From the intercepts of the linear portions, $k_h/k_g^{1/2}$ and $k_d/k_g^{1/2}$ were found to be, respectively, 4.6×10^{-3} l.$^{1/2}$/mole$^{1/2}$ sec$^{1/2}$ and 5.5 l.$^{3/2}$/mole$^{3/2}$ sec$^{1/2}$. The ratio of these two values yields the same value for k_d/k_h as found from Figure 3. The high value limit for $\Phi(N_2O)$ is 1.0, in agreement with eq 7, whereas the high value limit for $\Phi(N_2)/(NO)$ gives a value of k_d/k_h in agreement with that from Figure 3. From the values of k_d and $k_d/k_g^{1/2}$, our results give $k_g = 71$ l./mole sec, in good agreement with the value of 87 l./mole sec found by Calvert, Thomas, and Hanst,[7] but somewhat higher than the value of 25 l./mole sec found by Christie, Frost, and Voisey.[15]

As the NO_2 builds up, tertiary reactions become important. Nitrogen dioxide is extremely reactive and might compete with NO for either CH_3 or CH_3O. Gray[30] showed that there are three possible reactions of NO_2 with methyl radicals

$$CH_3 + NO_2 \longrightarrow CH_3NO_2$$

$$CH_3 + NO_2 \longrightarrow CH_3ONO$$

$$CH_3 + NO_2 \longrightarrow CH_3O + NO$$

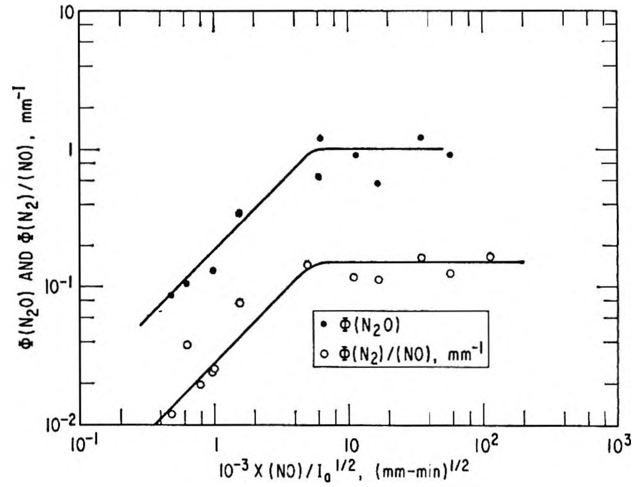

Figure 4. Log–log plots of $\Phi(N_2O)$ and $\Phi(N_2)/(NO)$ *vs.* $(NO)/I_a^{1/2}$.

---

(30) P. Gray, *Trans. Faraday Soc.*, **51**, 1367 (1955).

Table III: Rate Constants at 25°

Rate constant	Value	Units	Source	Comments
k_f/k_e	~10	None	Eq 1, Table II	
k_d	8.2×10^{-6}	$mm^{-2}\ min^{-1}$	Eq 2, Figure 2	
	47	$l.^2/mole^2\ sec$	Eq 2, Figure 2	
	55	$l.^2/mole^2\ sec$	Ref 15	$k_d = 2.6 \exp(+1800/RT) M^{-2}\ sec^{-1}$
k_d/k_h	0.15	mm^{-1}	Eq 3, Figure 3; eq 5 and 6; Figure 4; eq 8, Figure 4	
	2800	l./mole		
k_h	5.5×10^{-5}	$mm^{-1}\ min^{-1}$	k_d and k_d/k_h	$k_h = 8.3 \times 10^3 \exp(-7700/RT)$ $M^{-1}\ sec^{-1}$ using E_a of ref 15
	0.017	l./mole sec		
$k_h/k_g^{1/2}$	2.6×10^{-4}	$mm^{-1/2}\ min^{-1/2}$	Eq 5, Figure 4	
	4.6×10^{-3}	$l.^{1/2}/mole^{1/2}\ sec^{1/2}$	Eq 5, Figure 4	
$k_d/k_g^{1/2}$	1.7×10^{-5}	$mm^{-3/2}\ min^{-1/2}$	Eq 6, Figure 4	
	5.5	$l.^{3/2}/mole^{3/2}\ sec^{1/2}$	Eq 6, Figure 4	
k_g	0.23	$mm^{-1}\ min^{-1}$	k_d and $k_d/k_g^{1/2}$	
	71	l./mole sec	k_d and $k_d/k_g^{1/2}$	
	87	l./mole sec	Ref 7	
	25	l./mole sec	Ref 15	$k_g = 0.63 \times 10^6 \exp(-4600/RT)$ $M^{-1}\ sec^{-1}$
k_j/k_i	~0.7	None	Eq 11, Figure 5	
	0.55	None	Ref 31	

Any of these reactions would terminate the chain step, inhibit NO_2 formation, and reduce the quantum yields. Christie, Gilbert, and Voisey[19] measured the competition between NO and NO_2 for CH_3 radicals. They concluded that NO_2 is less than 12 times as effective as NO. At 90°, Phillips and Shaw[31] found that the rate constant for CH_3NO_2 formation was 1.7 times k_i, that the rate constant for the formation of $CH_3O + NO$ was 3.3 times k_i, and that CH_3ONO formation was unimportant. The oxygen-atom transfer step might have an activation energy. If so, it would be slower at room temperature. We believe the CH_3–NO_2 reaction to be unimportant in our system. We monitored NO_2 formation continually during every run. While there was some drop in NO_2 production, it was not large; we believe it can be explained by reactions of NO_2 with CH_3O. Under our conditions, even at the end of a run, the $(NO)/(NO_2)$ ratio always exceeded 20. However, the chain lengths often reached 50 or 100. Thus our results suggest that NO_2 is less than three times as effective as NO in removing CH_3 radicals.

On the other hand, the products of the reaction of NO_2 with CH_3O were observed. The indicated reactions are

$$CH_3O + NO_2 \longrightarrow CH_3ONO_2 \qquad (j)$$

$$CH_3O + NO_2 \longrightarrow CH_2O + HNO_2 \qquad (k)$$

We only observed CH_3ONO_2 when $R(e) \ll R(f)$. For experiments, under these conditions, it was also true that $R(h) \ll R(g)$. Then the mechanism predicts that for times sufficiently large

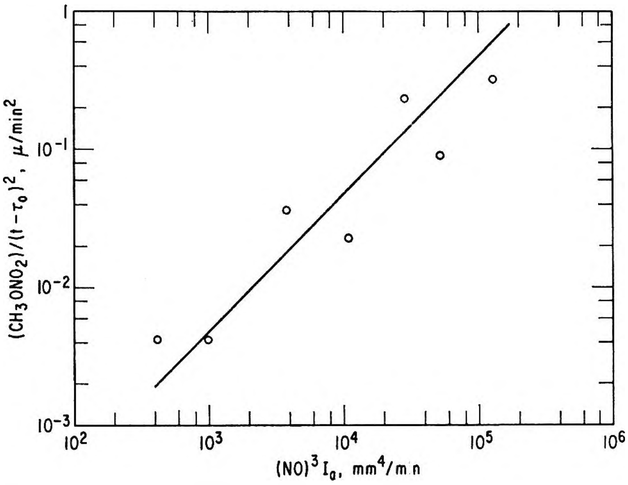

Figure 5. Log–log plot of $(CH_3ONO_2)/(t - \tau_0)^2$ *vs.* $(NO)^3 I_a$.

$$(NO_2) = k_d(NO)^2\left(\frac{I_a}{2k_g}\right)^{1/2}(t - \tau_0) \qquad (9)$$

$$R(CH_3ONO_2) = k_j(NO_2)\frac{k_d}{k_i}(NO)\left(\frac{I_a}{2k_g}\right)^{1/2} \qquad (10)$$

Substituting (9) into (10) and integrating gives

---

[31] L. Phillips and R. Shaw, Tenth Symposium (International) on Combustion, Cambridge, England, Aug 1964, p 453.

$$\frac{(\mathrm{CH_3ONO_2})}{(t - \tau_0)^2} = \frac{k_\mathrm{j}}{4k_\mathrm{i}} \frac{{k_\mathrm{d}}^2}{k_\mathrm{g}} (\mathrm{NO})^3 I_\mathrm{a} \qquad (11)$$

Figure 5 is a log–log plot of $(\mathrm{CH_3ONO_2})/(t - \tau_0)^2$ *vs.* $(\mathrm{NO})^3 I_\mathrm{a}$. The data are scattered, but a trend is clear. The best straight line of slope 1 has been drawn through the data points. From the intercept, an approximate value of about 0.7 is obtained for $k_\mathrm{j}/k_\mathrm{i}$ in good agreement with the value of 0.55 reported by Phillips and Shaw.[31]

Reaction k is the only step producing $\mathrm{HNO_2}$ and $\mathrm{CH_2O}$. Thus, they should be equal. We have no calibration factors for either molecule, but the few results in Table II indicate that their ratio is constant to within the large uncertainty involved in obtaining their values.

V. Summary

A rather complete and consistent mechanism for the $\mathrm{CH_3I}$–NO system is given by reactions a to k. Rate constants have been found, and they are tabulated in Table III. Where comparisons with other work could be made, agreement was good.

Acknowledgment. This work was supported by the U. S. Air Force under Contract No. AF 04(695)-669. The authors wish to thank Mrs. Barbara Peer for assistance with the manuscript.

The Gas Phase Reaction of Sodium with Ethyl, *n*-Propyl, and Isopropyl Alcohols

by E. M. Nemeth[1] and J. F. Reed

Department of Chemistry, Loyola University, Chicago, Illinois

(Received February 28, 1966)

The reactions of sodium vapor with ethyl, propyl, and isopropyl alcohol vapors have been studied by the diffusion flame technique at temperatures near 570°K. Specific rate constants were obtained which along with analysis of the products form the basis of a mechanism deduced. The primary process is a displacement of hydrogen atoms having activation energies of 4.2, 7.0, and 5.3 kcal/mole for ethyl, propyl, and isopropyl alcohols, respectively, calculated assuming unit steric factors. Alcohols also undergo chain reaction with hydrogen atoms similar to their pyrolyses. Some lower limits are adduced for carbon–oxygen and sodium–oxygen bond strengths in sodium alcoholates.

Introduction

The great reactivity of sodium toward a large number of reaction partners has made it a widely used reactant in the "diffusion flame" technique, first reported by v. Hartel and Polanyi.[2] In 1937, Heller[3] made a critical investigation of the method, examining in detail the effect of the experimental parameters and the validity of the assumptions involved in deriving an expression for the specific rate constant. One of the approximations he retained, that of a constant pressure of the reaction partner through the flame, was treated by Cvetanovic and LeRoy[4] and Smith.[5] They obtained solutions to differential equations of mass continuity taking into account the fact that the reaction partner also diffuses and is consumed in the reaction. Reed and Rabinovitch[6] made a critical analysis of the diffusion

---

[1] Abstracted in part from the Ph.D. Dissertation of E. M. Nemeth, Loyola University, Chicago, Ill.

[2] H. v. Hartel and M. Polanyi, *Z. Physik. Chem.*, **B11**, 97 (1930).

[3] W. Heller, *Trans. Faraday Soc.*, **33**, 1556 (1937).

[4] R. J. Cvetanovic and D. J. LeRoy, *Can. J. Chem.*, **29**, 597 (1951); R. J. Cvetanovic, *ibid.*, **34**, 54 (1956).

[5] F. T. Smith, *J. Chem. Phys.*, **22**, 1605 (1954).

[6] J. F. Reed and B. S. Rabinovitch, *J. Phys. Chem.*, **59**, 261 (1955).

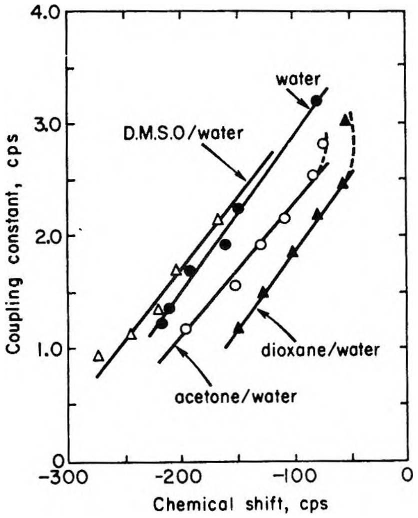

Figure 3. Graph showing dependence of ^{19}F chemical shift and $^{11}B-^{19}F$ coupling constants of $NaBF_4$ in different solvents.

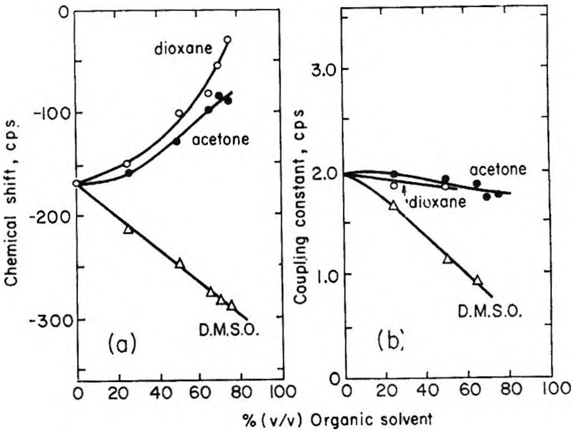

Figure 4. (a) Dependence of $^{11}B-^{19}F$ coupling constant in $NaBF_4$ on solvent composition. (b) Dependence of ^{19}F chemical shift in $NaBF_4$ on solvent composition.

The lack of variation which has been observed for couplings of central atom to fluorine in PF_6^-, SiF_6^{2-}, and AsF_6^- ions (although a detailed study has not yet been made for couplings in SiF_6^{2-} and AsF_6^- ion) may be associated with a very much weaker hydrogen bond [X–F···H–O] when X is electronegative. The strongest hydrogen bond occurs when the X–F bond is completely ionic, *i.e.*, the F^- ion.

For a good portion of the concentration range studied in dioxane–water and acetone–water mixtures the chemical shift change is linearly dependent on the coupling constant. This last statement is true for the whole range of concentrations available in aqueous solution and DMSO–water mixtures (Figure 3).

The chemical shift is a sensitive function of solvent and cation; it is difficult to use it as a reliable measure of any single interaction. In fact, the infinite dilution chemical shift is not the same for the BF_4^- ion in water or any of the solvent mixtures. The second solvent component plays some role, therefore, in the environment of the BF_4^- ion. This effect does not seem to be simply a reduction in the mean distance of the nearest cation, since we would then expect the order of the infinite dilution shift to depend on the dielectric constant of the medium. The order of δ_∞ is dioxane–H_2O > H_2O $\sim$ acetone–H_2O > DMSO–H_2O from high field to low field.

The effect of the organic solvent component is more clearly seen in Figure 4. We have maintained the concentration of BF_4^- ion in moles/1000 g of solvent constant but varied the ratio of water–organic solvent. As the organic solvent component increases in concentration, widely divergent chemical shift changes are observed. DMSO causes a large low-field shift and J_{B-F} also decreases on adding DMSO. The behavior in DMSO–water mixture is unique and cannot be explained on the basis of hydrogen-bonded interactions at the BF_4^- ion. We suggest as before the specific solvation of the protolysis product of DMSO[27-30] at the BF_4^- ion.

Acknowledgments. We thank Professor D. M. Grant for sending us the relevant parts of the Ph.D. Thesis of Dr. K. F. Kuhlmann.

and a calcium sulfate drying tube. The gases were stored in a 2-l. bulb.

Apparatus and Procedure. The kinetic data were obtained in a flow system modeled after that of Reed and Rabinovitch.[7] Hydrogen or nitrogen carrier gas flowed over the molten sodium carrying it through a nozzle of 0.87-mm radius into the reaction zone. The reaction zone was illuminated with a sodium vapor lamp and the flame diameter was measured with a sighting device fixed rigidly to the apparatus. The flow rates of carrier gas were calculated from the Poiseuille equation using coefficients of viscosity from the "International Critical Tables"[16] for nitrogen and from Landolt-Bornstein[17] for hydrogen. Alcohol vapor, flowing from a ballast volume of about 7 l., passed through a calibrated capillary into the reaction zone. The coefficients of viscosity for the alcohols were determined and are reported elsewhere.[18]

The products were trapped in two successive liquid nitrogen traps. Since hydrogen, noncondensible at liquid nitrogen temperature, was formed in the reactions, a manostat was inserted into the system to hold it at constant pressure.

The sodium vapor pressure data were taken from Sittig.[19] The coefficient of diffusion of sodium into the reaction mixture was taken to be that of sodium into pure carrier gas. The values used were 3.14 cm^2/sec for hydrogen[11] and 0.91 cm^2/sec for nitrogen[11,20] at 1 atm and 655°K and were extrapolated to experimental conditions by assuming an inverse dependence on the total pressure and half-power dependence on the absolute temperature.

The alcohol was admitted to the reaction zone and its pressure adjusted to give a flame with a radius in the range of 1 to 1.5 cm. A flame was considered to have reached a steady state only if its radius stayed constant for a period of more than 20 min. During the run, the room was completely darkened and the operator stayed in the dark to increase the visual acuity.

In an effort to obtain large amounts of products as well as to examine other effects, the kinetic data were supplemented by carrying out the reactions in a cylindrical Pyrex vessel about 25 cm long and 3.5 cm in diameter. A removable furnace was used to attain temperatures comparable to the flow reactor. A cold finger and mercury manometer were attached in the dead space just outside the furnace. A small glass boat containing sodium was placed approximately in the center of the reactor and the evacuated reactor was then heated. Sodium vapor flooded the reactor and the alcohol was then admitted. To prevent possible pyrolysis of any of the products by prolonged heating, the furnace was removed immediately.

Analysis of Product. Special product runs in the flow reactor of 15 to 20 hr duration were made to obtain sufficient volatile products for analysis. The carrier gas was pumped off, the products warmed to room temperature and roughly fractionated into three portions, and infrared and mass spectra obtained for each fraction. The infrared spectra were run on a Perkin-Elmer Model 21 infrared spectrophotometer. Mass spectra were obtained on a Consolidated Model 21-103c through the courtesy of Mr. Seymour Meyerson of American Oil Co., Whiting, Ind., and on a Consolidated Model 21-130 through the courtesy of Mr. R. M. Sherril of Northwestern University.

To clarify the situation, several runs of ethanol-*d* were made both in the kinetic and static reactors. The infrared and mass spectra of the gaseous products were compared with published spectra. The number of different species found in the products which were similar in nature, all being small carbon, oxygen, hydrogen (deuterium) compounds, made quantitative analysis of the spectra inaccurate. We may summarize the gaseous products from the reaction of sodium with ethanol-*d* as follows. Hydrogen is by far in the greatest amount. From the H/D ratios, little of the deuterium ended up in HD, and even less in D_2. Ethylene is found as the major volatile carbon-bearing compound with some monodeuterated species being found. Some acetaldehyde, also with monodeuterated species and little more than trace amounts of ethane, carbon monoxide, and methane, possibly with a small fraction of monodeuterated methane, were detected.

It is pertinent to point out some compounds that were not found. No butane was ever found in any analysis. Furthermore, except for the small amounts of acetaldehyde, mentioned above, no other ketones or aldehydes were found, nor were any ethers or peroxides found.

The products of the propyl alcohol reactions were not examined in the same detail. However, the major products found were hydrogen and propylene.

Analysis of the nonvolatile solid product collected under the flame on a Pyrex dish for sodium, carbon, and hydrogen gave a proportion of Na:C:H of 3.06:1.00:1.12 which, if the remainder is oxygen, could be a mixture of NaOH, Na_2CO_3, and $NaHCO_3$.

---

(16) "International Critical Tables," Vol. V, McGraw-Hill Book Co., Inc., New York, N. Y., 1929, p 2.

(17) Landolt-Bornstein, "Zahlenwerts and Funktionen," Band I, Springer-Verlag, Berlin, 1950, p 369.

(18) E. M. Nemeth and J. F. Reed, *J. Chem. Eng. Data*, **9**, 501 (1964).

(19) M. Sittig, "Sodium, Its Manufacture, Properties and Uses," Reinhold Publishing Corp., New York, N. Y., 1965.

(20) R. J. Cvetanovic and D. J. LeRoy, *J. Chem. Phys.*, **20**, 1016 (1952).

Results

Calculation of the Specific Rate Constants. Hartel and Polanyi[2] found the solution to the differential equation of mass continuity for diffusion and bimolecular reaction of sodium to be

$$p = A/r \exp(-Cr) \tag{1}$$

where p is the sodium pressure at r, the radial distance from the nozzle, and C is defined by

$$C^2 = kp'/D \tag{2}$$

where p' is the partial pressure of alcohol in the reaction zone (assumed constant), D is the diffusion coefficient of sodium into the reaction mixture, and k is the bimolecular specific rate constant.

By applying the boundary conditions that the pressure of sodium in the carburetor, p^*, is the pressure of sodium at a distance r_0, equal to the nozzle radius, and the pressure at the flame edge, R, is p_1, the lowest pressure for visibly detectable fluorescence, the Polanyi rate constant can be calculated from

$$C = \ln (p^* r_0/p_1 R)/(R - r_0) \tag{3}$$

A newly applied boundary condition of the "integrated intensity model" was discussed by Reed and Rabinovitch[7] and used by them to calculate a rate constant designated $k^{(3)}$. Since this treatment was extended as part of the present work, the model will be reexamined.

What the eye sees as a flame edge at the limit of visible sodium fluorescence is not due to a point source but rather to the integration of the (fluorescing) sodium concentration along the line of sight. The integrated intensity over the line of sight is proportional to L defined by

$$L = \int_S (p/RT)\mathrm{d}s \tag{4}$$

L is an experimentally determinable parameter which will be constant for a given observer and reactor and can be obtained by observing the limit of visible fluorescence for the case of no reaction. Solving the equation of continuity when no reaction is occurring and substituting the expression for p thus obtained into eq 4 yields

$$L = 2\mathrm{A}'(1 + \ln R_0/r_0) \tag{5}$$

where R_0 is the radius of the reaction and A' is determined from the lower boundary condition for the case of no reaction. From the data used to determine the limiting visible pressure of sodium, values of L were 12.89×10^{-14} and, with improved background conditions, 5.98×10^{-14} and 6.48×10^{-14} mole/cm^2, numerically in close agreement with values obtained previously.[7,14]

In order to obtain the rate constant, p of eq 1 must be substituted into eq 4. The radial coordinate, r, and the line of sight, $2s$, are related by $r^2 = R^2 + s^2$, where R is the flame radius. The equation for L then becomes

$$L = 2A\int_R^{R_0} \frac{\exp(-Cr)}{(r^2 - R^2)^{1/2}}\mathrm{d}r \equiv 2AI \tag{6}$$

Equation 6 is not analytically integrable. Reed and Rabinovitch[7] integrated (6) graphically and plotted the value of the integral, I, *vs.* C for a family of curves of constant R. Their graph is limited to their apparatus geometry and is not completely general.

Introducing a reduced variable, $x = r/R$ and defining $\beta = R_0/R$, the integral becomes

$$I = \int_1^{\beta} \frac{\exp(-CRx)}{(x^2 - 1)^{1/2}}\mathrm{d}x \tag{7}$$

For the case of a large reactor,[21] R_0 is very large and $\beta \rightarrow \infty$. Equation 7 then has the solution

$$\bar{I} = K_0(CR) = \pi/2iH_0^{(1)}(iCR) \tag{8}$$

where $K_0(CR)$ is a zero-order Bessel function of the third type with tabulated values by Watson,[22] and $iH_0^{(1)}(iCR)$ is a Hankel function.[23]

In the present work, it was felt that the approximation of $\beta = \infty$ was not a good one and a better approximation was sought. Equation 7 may be written

$$I = \int_1^{\infty} \frac{\exp(-CRx)}{(x^2 - 1)^{1/2}}\mathrm{d}x - \int_{R_0}^{\infty} \frac{\exp(-Cr)}{(r^2 - R^2)^{1/2}}\mathrm{d}r \tag{9}$$

The first term on the right-hand side of (9) has the solution (8). For the second term, we let $(r^2 - R^2)^{1/2} = r \sin \theta$ and the following inequalities hold, since the maximum value of $\sin \theta = 1$

$$\int_{CR\beta}^{\infty} \frac{\exp(-Cr)}{Cr}\mathrm{d}(Cr) < \int_{CR\beta}^{\infty} \frac{\exp(-Cr)}{Cr \sin \theta}\mathrm{d}(Cr) = \int_{CR(\beta^2-1)^{1/2}}^{\infty} \frac{\exp(-Cs) \sin \theta}{Cs}\mathrm{d}(Cs) < \int_{CR(\beta^2-1)^{1/2}}^{\infty} \frac{\exp(-Cs)}{Cs}\mathrm{d}(Cs) \tag{10}$$

The extreme terms of (10) are exponential integrals with values tabulated in Jahnke and Emde, hence

---

(21) D. Garvin, P. P. Gwynn, and J. W. Moskowitz, *Can. J. Chem.*, 38, 1795 (1960).

(22) G. N. Watson, "A Treatise on the Theory of Bessel Functions," 2nd ed, The MacMillan Co., New York, N. Y., 1944.

(23) E. Jahnke and F. Emde, "Tables of Functions with Formulae and Curves," 4th ed, Dover Publications, Inc., New York, N. Y., 1945.

Table I: Calculated Rate Constants and Activation Energies

Reactant	No. of runs	T, °K	$k \times 10^{11}$, cm^3/mole sec	z	k/Z	E_{act}, kcal/mole
Ethyl alcohol	9	572	60.4 ± 13.5	2464	1/40.8	4.2 ± 0.3
n-Propyl alcohol	9	576	6.2 ± 1.0	2796	1/450.2	7.0 ± 0.2
Isopropyl alcohol	9	568	25.0 ± 9.0	2843	1/113.8	5.3 ± 0.5

$$-Ei(-CR\beta) < \int_{R_0}^{\infty} \frac{\exp(-Cr)}{(r^2 - R^2)^{1/2}}dr < -Ei[-CR(\beta^2 - 1)^{1/2}] \quad (11)$$

The true value of the integral from R_0 to infinity is bracketed by integration along the radial coordinate as a lower limit and by integration along the line of sight as an upper limit. Since $s = r$ when $s \gg R_0$, this approximation is felt to be reasonable and the results bear out this treatment.

A is given by[6]

$$A = \frac{p^* v_0 r_0^2 \exp(Cr_0)}{4RTD(1 + Cr)_0} \quad (12)$$

A very good approximation is $\exp(Cr_0)/(1 + Cr_0) = 1$. For $C = 4$ cm^{-1}, larger than any value applicable to this work, and with $r_0 = 0.08$ cm, $\exp(Cr_0)/(1 + Cr_0) = 1.004$. With this approximation, we define

$$A' = \frac{p^* v_0 r_0^2}{4RTD}$$

which is a calculable quantity. Thus, two cases exist.

$$L/A' < iH_0^{(1)}(iCR) + (2/\pi)Ei(-CR\beta) \quad (13a)$$

$$L/A' > iH_0^{(1)}(iCR) + (2/\pi)Ei(-CR(\beta^2 - 1)^{1/2}) \quad (13b)$$

The right-hand sides of (13a) and (13b) are graphed *vs.* CR for constant values of β and using the values of C thus obtained, k_{max} and k_{min} were calculated. The value of k used was the average of the two.[24]

Values of k with greater than twice the average deviation were not used. In Table I, the average value of k is given with the average deviation and the reaction temperature. Z, the collision number was calculated from kinetic theory. The collision diameter was taken as 2.50 A for sodium, taken from Landolt-Bornstein[16] for ethanol, and calculated from viscosity data of Nemeth and Reed[18] for the propanols. Table I also gives k/Z, the collision yield, and the calculated activation energy, E_{act}, assuming a steric factor of unity.

The integrated intensity model does not account for the depletion of atmosphere reactant in the flame and it would be difficult to incorporate the correction integrally into the model. The empirical correction of Heller[3] as modified by Reed and Rabinovitch[6] would increase k by less than 9%, which is less than the uncertainty in k. The correction, due to Cvetanovic and LeRoy,[4] based on a two-point boundary model may be considered as an overcorrection and would increase the rate constant by almost 30% for the systems studied in this work, with a consequent lowering of the activation energies of about 0.2 kcal/mole for the ethanol and 0.3 kcal/mole for the propanols.

Discussion

The gaseous products of the reaction of sodium and ethanol are hydrogen in relatively large abundance, acetaldehyde, methane, and ethylene. There are minor amounts of other products whose identity is difficult to establish uniquely from the mass spectra. We first state a mechanism consistent with the product analysis and with thermochemistry.

The primary reaction of sodium with ethanol is the displacement of hydrogen atom

$$Na + C_2H_5OH \longrightarrow C_2H_5ONa + H \quad (a)$$

Other conceivable primary reactions might include the abstraction of OH-forming ethyl radical or the abstraction of hydrogen atom forming sodium hydride and ethoxy radical. For those processes, we estimate endothermicities of 44 to 53 kcal, respectively, and therefore consider them unlikely. Further, to establish that ethyl radicals are not produced, we studied the products of the reaction of sodium with ethyl bromide, a process known to produce ethyl radical.[25] We found only the expected products ethylene and ethane in ratio 2:3 and butane, the latter two being absent from the products of the reaction of sodium and ethanol.

A primary reaction of sodium dimers with alcohol, although energetically favorable, was considered unlikely. Dimers are a small fraction of the sodium

---

[24] A later computer result programmed for the IBM 7090 showed that *CR* calculated as the mean of the upper and lower bounds deviated by less than 2% from the value obtained from a graph made from the computer calculations.

[25] A. O. Allen and C. E. H. Bawn, *Trans. Faraday Soc.*, **34**, 463 (1938).

vapor. Observation of the finite fluorescence flame is due to disappearance of monomer and if the primary process involves dimers, the dimers must diminish the monomer concentration by dimerization. To sustain the rate, the process would essentially become third order, and we considered this unlikely at these low pressures.

At the temperature at which these studies were conducted, the sodium ethylate should decompose. We studied this process separately and identified the products as common to those of the reaction of sodium with ethanol, notably hydrogen and ethylene, and in agreement with the results reported by Hurd.[26]

Barnard and Hughes[27] studied the pyrolysis of ethanol and concluded the chain-carrying process was the abstraction of hydrogen by hydrogen atom leaving hydroxy ethyl radical which further decomposed into acetaldehyde and hydrogen atom or a polymeric substance. Barnard[28] found that in the pyrolyses of the propanols, hydrogen atom abstraction of an alkyl hydrogen from the alcohol was the chain-carrying step. Hydrogen atom from the primary process (a) would therefore be expected to react further by abstracting hydrogen from ethanol starting a chain.

$$H + C_2H_5OH \longrightarrow C_2H_4OH + H_2 \qquad (b)$$

$$C_2H_4OH \longrightarrow C_2H_3OH + H \qquad (c)$$

$$C_2H_3OH \longrightarrow CH_3CHO \longrightarrow CH_4 + CO \qquad (d)$$

$$2H + M \longrightarrow H_2 + M \qquad (e)$$

The postulated mechanism is in accord with the nature of the products found. Further, that the hydroxyl hydrogen remains essentially intact in the radical C_2H_4OH is borne out by our study of the reaction of sodium with C_2H_5OD, the products of which indicate that the deuterium is found not in elementary hydrogen but rather in the acetaldehyde and methane.

The radical designated C_2H_4OH might be either $\cdot CH_2CH_2OH$ or $CH_3\underset{\cdot}{C}HOH$, the latter having a heat of formation of -16 kcal/mole.[29] If indeed this is the radical produced, as seems likely from other properties,[30] the thermochemistry of all these radical reactions can be evaluated from known heats of formation.[31]

$$H + C_2H_5OH \longrightarrow CH_3\underset{\cdot}{C}HOH + H_2 + 12\ \text{kcal} \qquad (b')$$

$$CH_3CHOH\cdot \longrightarrow CH_3CHO + H - 28.5\ \text{kcal} \qquad (c')$$

$$CH_3CHO \longrightarrow CH_4 + CO + 4.6\ \text{kcal} \qquad (d')$$

$$2H + M \longrightarrow H_2 + M + 104\ \text{kcal} \qquad (e')$$

The heats of these reactions are consistent with radical reactions establishing a chain process. The chain length cannot be very long since the ratio of alcohol to sodium flow rates was not very great and a significant amount of alcohol is found unreacted with the products. This might indicate that the chain termination occurs between H· and $CH_3\underset{\cdot}{C}HOH$. Although some of the acetaldehyde formed from the decomposition of the hydroxy ethyl radical in step d would be swept out of the reactor, explaining its presence in the products found in the cold trap, an appreciable fraction of it would be expected to undergo decomposition itself. The decomposition of acetaldehyde has been studied both by itself and in the presence of hydrogen[32] and hydrogen atoms,[33] and the final products of its unimolecular decomposition and of its reaction with hydrogen atoms are methane, carbon monoxide, and small amounts of hydrogen, also in accord with our products.

The calculated specific rate constants might be in error due to depletion of alcohol from a value assumed constant in the flame. Correcting the rate constant by the method of Cvetanovic and LeRoy,[7] using an integrated intensity for a boundary condition, was not practical. Making the correction using two-point boundary conditions indicates the rate constant should be increased by about 30% with a consequent lowering of the activation energy by 0.3 kcal/mole.

For the reaction of sodium with propanols, analysis of the products was not as thorough, but from their nature, we assume a similar mechanism and calculate an activation energy in the same way as for ethanol.

It can be seen from Table I that the reactivity toward sodium is greatest for ethanol and that of isopropyl alcohol is greater than that of *n*-propyl alcohol, paralleling the values of D(R–OH). The activation energies are approximately 5% of the dissociation energy of the bond broken as one might expect from Hirschfelder's rule.[34] These reactions are not abstraction processes as are the bulk of sodium diffusion flame reactions; rather they are displacement reactions.

By setting the activation energy of the primary reac-

---

[26] C. D. Hurd, "Pyrolysis of Carbon Compounds," Chemical Catalog Co., Inc., New York, N. Y., 1929, p 192.

[27] J. A. Barnard and H. W. D. Hughes, *Trans. Faraday Soc.*, **56**, 55 (1960).

[28] J. A. Barnard and H. W. D. Hughes, *ibid.*, **56**, 64 (1960); J. A. Barnard, *ibid.*, **56**, 72 (1960).

[29] F. H. Field and J. L. Franklin, "Electron Impact Phenomena," Academic Press, Inc., New York, N. Y., 1957, p 137.

[30] W. H. Urry, F. W. Stacey, E. S. Huyser, and O. O. Juveland, *J. Am. Chem. Soc.*, **76**, 450 (1954).

[31] R. R. Bernecker and F. A. Long, *J. Phys. Chem.*, **65**, 1565 (1961).

[32] C. J. M. Fletcher and C. N. Hinshelwood, *Trans. Faraday Soc.*, **30**, 614 (1934).

[33] W. B. Trest, B. deB. Darwent, and E. W. R. Steacie, *J. Chem. Phys.*, **16**, 353 (1948).

[34] J. Hirschfelder, *ibid.*, **9**, 645 (1941).

Table II: Thermochemical Data, Kcal/Mole

	R				
	H	Na	C_2H_5	$CH_3CH_2CH_2$	$(CH_3)_2CH$
ΔH_f(R)	52.0	26.0	25.4	22.1	16.8
ΔH_f(RO)	9.0	13	−8.5	−12.9	−18.0
ΔH_f(ROH)	−57.8	−55.4	−56.2	−62.3	−65.6
ΔH_f(RONa)	−55.4	(−51)	$\leqslant -78.0^a$	$\leqslant -81.3^a$	$\leqslant -86.3^a$
D(RO–H)	119	120	99.7	101.4	99.6
D(RO–OH)	119	90	90.6	93.4	91.4
D(RO–Na)	90	(90)	$\geqslant 95.5^a$	$\geqslant 94.4^a$	$\geqslant 94.3^a$
D(R–ONa)	120	(90)	$\geqslant 116.4^a$	$\geqslant 116.3^a$	$\geqslant 116.1^a$
D(OR)	102	(72)	92.9	94.0	93.8

[a] This work.

tion equal to the heat of reaction as an upper limit, we may estimate some thermochemical data for gaseous sodium compounds which are otherwise scarce and difficult to obtain. Comparable data for hydrogen and sodium analogs are also given in Table II. Unless otherwise noted, data are taken from the compilation of Bernecker and Long[31] or Rossini.[35]

That the value of the bond dissociation energy D(RO–Na) is likely close to the value in the table, which is a lower limit, may be inferred from the corresponding value of D(HO–Na) for which two different arguments are available. Using $\Delta H_f°$(NaOH,c) = 102.0 kcal/mole,[35] and the value of the heat of sublimation to the monomer, 46.8 ± 3 kcal/mole,[36] gives $\Delta H_f°$(NaOH,g) = −55.4 ± 3 kcal/mole and consequently, with $\Delta H_f°$(Na) = 26.0 kcal/mole and $\Delta H_f°$(OH) = 9.0 kcal/mole, D(HO–Na) = 90 ± 3 kcal/mole. Bawn and Evans[12] argued to a lower limit of D(Na–O) = 72 kcal/mole from the assumed thermoneutrality of the reaction Na + NO_2 − NaO + NO which would make $\Delta H_f°$(NaO) = 13 kcal/mole and hence, D(NaO–H) = 120 kcal/mole. Conversely, if D(NaO–H) is the same as D(HO–H), and D(OH) = 102, then D(Na–OH) = 89 in agreement with the stronger experimental results of Schoonmaker and Porter.

It is to be noted that D(RO–H) appears to be the same whether R is Na or H. If this is also true for D(RO–Na), then $\Delta H_f°(Na_2O,g)$ = −51 kcal/mole. An essentially equivalent assumption is that the second bond in Na_2O is weaker than the first by the same amount as it is in H_2O.

A surprising result is the value of D(R–ONa), where R is alkyl, both with regard to its constancy and magnitude, which is also a lower limit. However, we note that D(R–ONa) is consistently greater than D(R–O) by about 20 kcal whether R is alkyl, H, or Na.

We also attempted the study of the reaction of sodium vapor with methanol and the butanols. In the case of the former, reactivity was such that the partial pressure of the alcohol needed was too large for application of a simple equation of continuity. We estimate an activation energy in excess of 11 kcal/mole. In the case of the butanols, reactivity was low, flames unsteady due to insufficient partial pressures under our experimental conditions.

---

(35) F. D. Rossini, *et al.*, National Bureau of Standards Circular 500, U. S. Government Printing Office, Washington, D. C., 1952.

(36) R. C. Schoonmaker and R. F. Porter, *J. Chem. Phys.*, **28**, 454 (1958).

The Potential of the Ruthenium(II)-Ruthenium(III) Couple[1]

by R. R. Buckley[2] and E. E. Mercer

Department of Chemistry, University of South Carolina, Columbia, South Carolina 29208

(Received March 4, 1966)

The potential of the Ru(II)–Ru(III) couple has been determined by direct measurement using a glass electrode as a reference. The potential of the cell was measured at several temperatures and at several ionic strengths at 25°. From these data $E° = -0.2487$ v, $\Delta G° = 5.74$ kcal/mole, $\Delta H° = -10.1$ kcal/mole, and $\Delta S° = 53$ eu at 25° for the cell reaction, $Ru^{2+} + H^+ = Ru^{3+} + {}^1/_2H_2$. Approximate values for the Ru(II)–Ru(III) couple involving the chloride complexes are also presented.

The chemistry of ruthenium in aqueous solution is very complicated because of the large number of oxidation states, complexes, and polymeric species. A lack of knowledge of the thermodynamics of reactions has resulted from this complexity. With the isolation of the monomeric aquo complex of ruthenium(II),[3] the possibility of measuring the Ru(II)–Ru(III) potential was available in a solution where the species of both oxidation states of the metal were well characterized. A number of values for this couple can be found or calculated from data presented in the literature. However, in all of these cases the actual species present in solution were not known with certainty or the measurements were of very low precision, and involved a number of approximations.

Backhouse and Dwyer[4] measured the potential of the Ru(II)–Ru(III) couple in 1.5 to 6.8 *M* hydrochloric acid. No attempt to maintain constant ionic strength was made, nor were the complexes present known with any certainty. The $E°$ which they calculated was 0.084 v.[5] From polarographic studies of the reduction of Ru(IV) made by Atwood[6] an approximate value for the Ru(II)–Ru(III) couple can be calculated to be 0.06 v in perchloric acid medium. Here also the species present in solution were unknown, but there was a hydrogen ion dependence of the potential which indicated that hydrolytic ions were involved in the electrode reaction. Endicott and Taube[7] have recently reported values of the potential for the couple $Ru(NH_3)_6{}^{2+}$–$Ru(NH_3)_6{}^{3+}$ as −0.24 v. This measurement did involve the estimation of rather large junction potentials. Since there is a great deal of uncertainty in the potential of this couple, we have undertaken its measurement in *p*-toluenesulfonic acid solutions. Most other noncomplexing anions have been found to react with the uncomplexed ruthenium(II). All measurements were made using a glass electrode as a reference to eliminate the need of correcting for liquid junction potentials.

Experimental Section

Solutions. The solutions used in the measurements were prepared from *p*-toluenesulfonic acid which had been recrystallized from anhydrous ether. The ruthenium(II) solutions were prepared as reported previously.[3] The ruthenium(III) solutions were made either by air oxidation of the ruthenium(II) solutions or by electrolytic oxidation of the same solutions at a controlled potential of 0.10 v *vs.* a saturated calomel electrode. All solutions were made using normal distilled water except in the dilution studies, where it was necessary to use deionized water. All solutions

---

(1) Presented in preliminary form at the Southeast–Southwest Regional Meeting of the American Chemical Society, Memphis, Tenn., Dec 1965.

(2) Presented in partial fulfillment of the requirements of the Ph.D. degree, University of South Carolina, 1965. Recipient of the Dupont Teaching Fellowship for the year 1963–1964.

(3) E. E. Mercer and R. R. Buckley, *Inorg. Chem.*, **4**, 1692 (1965).

(4) J. R. Backhouse and F. P. Dwyer, *Proc. Roy. Soc.*, *N. S. W.*, **83**, 138, 146 (1949).

(5) All potentials reported here follow the conventions given in "Oxidation Potentials," by W. M. Latimer, Prentice-Hall, Inc., Englewood Cliffs, N. J., 1952. All half-reactions are written as oxidations, and couples with reducing agents stronger than hydrogen have a positive sign.

(6) D. K. Atwood, Ph.D. Thesis, Purdue University, Lafayette, Ind., 1960.

(7) J. F. Endicott and H. Taube, *Inorg. Chem.*, **4**, 437 (1965).

were freed from dissolved oxygen by purging them with purified nitrogen which had been saturated with water vapor by bubbling it through a solution of *p*-toluenesulfonic acid. Ruthenium analyses were performed as reported previously.[3]

Apparatus. The controlled-potential coulometer used in all experiments was designed by Propst.[8] The operation of the coulometer required the use of three electrodes, a working electrode, a reference electrode, and an isolated electrode. An electrode made from a piece of 0.05-cm gold foil 1 cm square was used as the working electrode. Both the isolated and reference electrodes were connected to the solution through silicic acid bridges, which were made by addition of concentrated sulfuric acid to a saturated solution of sodium silicate, followed by washing with distilled water to remove free electrolyte. A saturated calomel electrode served as the reference, and the isolated electrode was a spiral of platinum wire immersed in 0.01 *F* *p*-toluenesulfonic acid. During an electrolysis, current flowed only between the isolated and working electrodes.

For the measurement of the cell potential, the gold foil electrode was used as the indicating electrode, and a Beckman GP Type 41252 glass electrode served as a reference. The silver–silver chloride electrodes used to determine the standard potential of the glass electrode were prepared by a modification of the method of Shedlovsky and MacInnes.[9] Spirals of 22-gauge platinum wire sealed into the end of 6-mm glass tubing were silver-plated from a cyanide bath at a current of 2 ma for 15 hr. The electrodes were rinsed with distilled water, then anodized in 0.1 *F* hydrochloric acid for 1 to 2 hr at a current of 1 ma. Several such electrodes were connected together after preparation and allowed to stand in 0.1 *F* hydrochloric acid for 1 week. Electrodes prepared in this manner were reproducible to better than 0.2 mv.

Cell potentials were measured to 0.1 mv using a Beckman Research Model pH Meter. Solutions were contained in a jacketed 2.5 × 8-cm cylindrical Pyrex container with a Teflon cap. Five openings in the cap supported the gold, isolated, calomel, and glass electrodes, and a gas inlet tube. The temperature of this vessel was controlled by circulation of water thermostated to ±0.01° through the outer jacket. Nitrogen was bubbled through the solution continuously during all experiments. It was verified that there was no detectable difference in potential recorded in the presence or absence of the gas purge. All polarograms were recorded on a Sargent Model XV Polarograph.

Procedure. The standard potential of the glass electrode was determined in either 0.1 or 0.01 *m* hydrochloric acid by measuring the potential of the cell

$$\text{Ag, AgCl}|\text{HCl}(m)|\text{glass} \qquad (1)$$

From the Nernst equation, then

$$E^\circ_{\text{glass}} = -E_{\text{cell}} + E^\circ_{\text{Ag/AgCl}} - \frac{2RT}{F}\ln a_{\text{HCl}} \qquad (2)$$

Values for $E^\circ_{\text{Ag/AgCl}}$ and a_{HCl} were taken from the report by Zielen.[10] The standard potentials of the silver–silver chloride electrode at other temperatures were calculated from the data presented by Harned and Owen.[11] In each experiment the standard potential of the glass electrode was determined before and after the measurements of the cell potentials. In all cases these two readings agreed within 0.1 mv.

The experiments in which the ratio of Ru(III) to Ru(II) was varied were conducted in the following manner. Ten milliliters of 0.1 *F* *p*-toluenesulfonic acid was placed in the cell, and all of the electrodes and the gas bubbler were inserted. The solution was purged for 30 min with inert gas and was prereduced at −0.5 v *vs.* sce. Five hundred μl of the stock ruthenium(II) solution in *p*-toluenesulfonic acid was added with a pipet. The solution was again reduced electrolytically at −0.4 v *vs.* sce to the limiting current. The polarity of the electrolysis was then reversed, and measured fractions of the ruthenium were oxidized to the +3 oxidation state at a potential of 0.1 v. The electrolysis was interrupted at intervals of 10% of the total ruthenium present to obtain potential measurements. Stable readings of the cell potential were obtained within 3 to 5 min after discontinuation of the electrolysis.

In the dilution experiments, 200 μl of a stock ruthenium(II) solution was added to 2 ml of deaerated, prereduced 0.1 *F* *p*-toluenesulfonic acid. The Ru(III) to Ru(II) ratio was adjusted to unity by electrolytic oxidation. The sample was diluted in increments by addition of 2 ml of deaerated, deionized distilled water, or 0.1 *F* sodium *p*-toluenesulfonate. The potential of the cell was determined after each dilution.

Results

Zielen[10] has shown that a glass electrode may be used as a reference electrode in most solutions if a correction

---

[8] R. E. Propst, U. S. AEC Report, DP-798 (1963).

[9] T. Shedlovsky and D. A. MacInnes, *J. Am. Chem. Soc.*, **58**, 1970 (1936).

[10] A. J. Zielen, *J. Phys. Chem.*, **67**, 1474 (1963).

[11] H. S. Harned and B. B. Owen, "The Physical Chemistry of Electrolyte Solutions," 2nd ed, Reinhold Publishing Corp., New York, N. Y., 1950.

is made for a slow drift of the potential with time. In most cases this drift is very small, and was below the limit of detection in our experiments in *p*-toluenesulfonic acid. The duration of most of these experiments did not exceed 3 hr. The glass electrode offers a convenient means of eliminating liquid junction potentials in the determination of the emf of cells. Since the glass electrode responds in a manner identical with a hydrogen electrode, the potential of the cell

$$\mathrm{Au}|\mathrm{Ru}^{2+}(m_1),\ \mathrm{Ru}^{3+}(m_2),\ \mathrm{H}^+(m_3)|\mathrm{glass} \quad (3)$$

is given by the equation

$$E_{\mathrm{cell}} = E^\circ_{\mathrm{Ru}} - E^\circ_{\mathrm{glass}} - \frac{RT}{F}\ln\left[a_{\mathrm{Ru(III)}}/a_{\mathrm{Ru(II)}}a_{\mathrm{H}}\right] \quad (4)$$

The concentration dependence of the cell potential was tested at constant ionic strength for changes in [Ru(III)], [Ru(II)], and [H$^+$]. Some typical data are presented in Table I. The slopes of the plots of $E_{\mathrm{cell}} + E^\circ_{\mathrm{glass}}$ *vs.* log [Ru^{3+}]/[Ru^{2+}][H$^+$] at all temperatures used were in agreement with that given by the Nernst equation within experimental error. The formal potentials obtained at an ionic strength of approximately 0.1 are summarized as a function of temperature in Table II.

Table I: Some Cell Potentials Measured at $\mu = 0.103 \pm 0.002$, $T = 25.40°$

[Ru^{3+}] × 10^3	[Ru^{2+}] × 10^3	[H$^+$] × 10^2	$-(E_{\mathrm{cell}} + E^\circ_{\mathrm{glass}})$, v	$-E^\circ_{\mathrm{f}}$, v
0.245	0.981	9.56	0.2584	0.2337
0.490	0.736	9.53	0.2818	0.2318
0.736	0.490	9.51	0.3047	0.2338
0.981	0.245	9.48	0.3308	0.2346
3.07	3.07	4.81	0.3129	0.2349
2.08	2.08	3.26	0.3217	0.2337
1.26	1.26	1.98	0.3349	0.2341
0.80	0.80	1.25	0.3489	0.2360

Table II: The Formal Potential for the Half-Reaction, Ru^{2+} = Ru^{3+} + e$^-$, at Constant Ionic Strength, $\mu = 0.103 \pm 0.002$

T, °C	No. of measurements	$-E^\circ_{\mathrm{f}}$, v
25.40	15	0.2342 ± 0.0008[a]
25.00	7	0.2341 ± 0.0005
19.40	7	0.2464 ± 0.0005
15.00	7	0.2578 ± 0.0007

[a] The limits of the uncertainty are 95% confidence level.

Large activity coefficient effects were expected to occur in this cell since the reaction involved highly charged ions. In an attempt to obtain a value of $E°$ at infinite dilution, the cell potential was determined at several different ionic strengths, at 25°, and a fixed ratio of ruthenium(III) to ruthenium(II) of unity. In all of these measurements, however, the concentration of the acid was greater than 10^{-2} M to avoid the necessity of corrections for the hydrolysis of the metal cations. The formal potentials at each ionic strength were calculated from the experimental data, and are related to the standard oxidation potential by the expression

$$E^\circ_{\mathrm{f}} = E^\circ_{\mathrm{Ru}} - 0.05916\log\left\{\gamma_{\mathrm{Ru(III)}}/\gamma_{\mathrm{Ru(II)}}\gamma_{\mathrm{H}}\right\} \quad (5)$$

The values of the γ's were calculated from the equation

$$\log\gamma = \frac{-0.5085z^2\sqrt{\mu}}{1 + 0.3281a^\circ\sqrt{\mu}} \quad (6)$$

where z is the charge of the ion, $a°$ is the effective diameter of the hydrated ion in angstroms, and μ is the ionic strength. The values of $a°$ used for each ion were estimated from similar ions given by Kielland.[12] For Ru^{3+} and H$^+$ $a°$ was assumed to be 9, while a value of 5 was used for Ru^{2+}. The standard oxidation potential of the electrode at each ionic strength is shown in Figure 1, and is independent of ionic strength well within experimental error. The extrapolated value of E°_{Ru} was −0.2487 v.

From the potential and the thermal coefficient of the cell, the following values for the reaction

$$\mathrm{Ru}^{2+} + \mathrm{H}^+ = \mathrm{Ru}^{3+} + {}^1/{}_2\mathrm{H}_2 \quad (7)$$

have been calculated at 25°: $\Delta G^\circ = 5.74 \pm 0.03$ kcal/

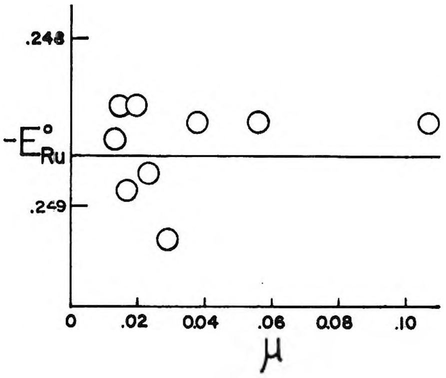

Figure 1. The standard oxidation potential as a function of ionic strength at 25°. E°_{Ru} was calculated using eq 5 and 6 in the text.

---

[12] J. Kielland, *J. Am. Chem. Soc.*, **59**, 1675 (1937).

Table II: Torsion–Langmuir Sublimation Pressure for Barium Fluoride[a]

T, °K	P, atm	$-\left(\frac{\Delta F°_T - \Delta H°_{298}}{T}\right)$, cal/deg	$\Delta H°_{298}$, kcal/mole
1445	1.11×10^{-5}	40.05	90.61
1470	1.79×10^{-5}	39.90	90.59
1492	2.67×10^{-5}	39.75	90.52
1318	9.72×10^{-7}	40.63	89.90
1394	3.65×10^{-6}	40.31	90.88
1425	7.16×10^{-6}	40.16	90.78
1395	4.11×10^{-6}	40.31	90.61
1390	3.33×10^{-6}	40.34	90.91
1331	1.28×10^{-6}	40.59	89.85
1347	1.48×10^{-6}	40.53	90.52
1365	2.09×10^{-6}	40.45	90.68
1417	6.09×10^{-6}	40.20	90.71
1365	2.00×10^{-6}	40.45	90.74
1408	5.06×10^{-6}	40.24	90.78
1377	2.53×10^{-6}	40.40	90.89
1430	9.05×10^{-6}	40.12	90.37
1402	4.93×10^{-6}	40.28	90.45
1331	9.00×10^{-7}	40.59	90.85
1328	8.43×10^{-7}	40.60	90.83
1315	6.27×10^{-7}	40.65	90.77
1345	1.13×10^{-6}	40.53	91.11
1323	7.20×10^{-7}	40.62	90.92
1340	1.32×10^{-6}	40.55	90.38
1361	2.06×10^{-6}	40.48	90.49
1350	1.56×10^{-6}	40.52	90.56
			Av = 90.62 ± 0.30

[a] First 18 points with orifice set 4; last 7 points with orifice set 5.

$\pm$ 1.8)/4.576] × $(10^3/T)$ + 7.22 ± 0.29 between 1315 and 1492°K for the Langmuir experiment. The errors are the standard deviations from least-squares fits.

The heats of sublimation of barium fluoride at 298°K for the Knudsen and Langmuir data were calculated by both the second-law and third-law methods. In all calculations, BaF_2 was considered to be the major vapor species[2] because thermodynamic calculations indicate that the pressures produced by the reactions $BaF_2(s) + C(s) = BaF(g) + CF(g)$, $BaF_2(s) + C(s) = Ba(g) + CF_2(g)$, and $BaF_2(s) + {}^1/_2C(s) = BaF(g) + {}^1/_2CF_2(g)$, would be several orders of magnitude below the observed pressures.

The same heat capacity equations and free-energy functions for solid barium fluoride[20] and the same estimated heat capacity and free-energy functions for barium fluoride gas[21] were used in calculating heats of sublimation as were used by Green, *et al.*,[2] and by Bautista and Margrave.[4] The free-energy functions used are expected to be as reliable as can presently be estimated[21] whether or not the $BaF_2(g)$ molecule is linear or bent as suggested by recent electric dipole studies.[19] The second-law treatment yielded $\Delta H°_{298} = 88.78 \pm 1.26$ kcal/mole from the Knudsen experiments and $\Delta H°_{298} = 90.29 \pm 1.81$ kcal/mole from the Langmuir experiments. The third-law calculations for the 46 Knudsen measurements for which $\lambda/d > 1.0$ yielded $\Delta H°_{298} = 90.25 \pm 0.28$ kcal/mole and for the 25 Langmuir measurements yielded $\Delta H°_{298} = 90.62 \pm 0.30$. The indicated errors are the standard deviations. The free-energy functions could be in error by enough to contribute a 4 kcal error to the calculated heats at 298°K; however, the heat of sublimation calculated by the third-law method is probably correct to within ±3 kcal/mole. Assuming a +5° error at the high end of measurements and a −5° error at the lower end (correspondingly ±10% errors in pressures) yields an estimated maximum error of 2.8 kcal for the second-law calculation.

Brewer, *et al.*[21] concluded from the early work of Ruff and LeBoucher[1] that the heat of sublimation of barium fluoride is about 88 kcal/mole at 298°K. Green, *et al.*,[2] in the mass spectrometer study found $\Delta H°_{298} = 92.3$ kcal/mole by the third-law method and $\Delta H°_{298} = 93.8$ kcal/mole by the second-law method. Torsion–effusion studies of Hildenbrand, *et al.*,[3] yield $\Delta H°_{298} = 88.6$ kcal when recalculated with the same free-energy functions used by the other investigators. The Langmuir measurements of Bautista and Margrave[4] yield $\Delta H°_{298} = 92.3$ kcal/mole from third-law analysis and $\Delta H°_{298} = 94.7$ kcal/mole by second-law analysis.

Hildenbrand and co-workers[3] believe their experimental results indicate that barium fluoride is bent. We will not comment further on this point because the work of Hildenbrand, *et al.*, is not yet published except in company reports. The second- and third-law measurements of the present work agree well when Brewer's[21] free-energy functions are used. The second-law Knudsen measurements should be given greatest weight until supporting thermochemical data for third-law calculations are better established.

Since the same free-energy functions were used by Green, *et al.*,[2] by Bautista and Margrave,[4] and by us and since the measurements were made in approximately the same temperature ranges, the differences in calculated heats of sublimation at 298°K reflect the systematic differences of approximately a factor of 2 in measured pressures and not possible errors in the free-energy functions. Mass spectrometer pressure measure-

---

[20] K. K. Kelley, U. S. Bureau of Mines Bulletin, 584, U. S. Government Printing Office, Washington, D. C., 1960, p 23.

[21] L. Brewer, G. Somayajulu, and E. Bracket, *Chem. Rev.*, **63**, 111 (1963).

ments are usually expected to be uncertain by a factor of 2 or more. Presumably, it was in recognition of the inherent uncertainty in mass spectrometer measurements that Bautista and Margrave did not draw the conclusion from the excellent agreement of their Langmuir results for barium fluoride with mass spectrometer measurements in their laboratory that $\alpha = 1$.

Instead, they concluded from comparison of the Langmuir data with effusion measurements of other investigators that evaporation coefficients for alkaline earth halides probably generally lie in the range 0.1 to 0.3. For barium fluoride specifically, comparison of Bautista's results to our effusion results would lead to the conclusion that the value of α is about 0.5.

A recent paper of Loehman, Kent, and Margrave[22] does describe both Knudsen measurements (above the melting point) and Langmuir measurements (below the melting point) for strontium chloride. The Langmuir experiments were performed on single crystals suspended in the furnace. Extrapolation of Knudsen data into the range below the melting point clearly indicates an evaporation coefficient of 0.3 for the solid.

Comparison of our own free-surface and effusion data for barium fluoride yields $\alpha = 0.9 \pm 0.1$. The *relative* error in our measurements of free surface and effusion data probably should not exceed 10% because most sources of systematic error are common to the free-surface and effusion measurements. The most probable source of serious error in determination of α is a discrepancy between measured temperature and true temperature of the evaporating surface of a Langmuir sample. In this research the Langmuir specimens were mounted in the same position as the orifices of the effusion cells in a chamber of demonstrated uniform temperature. If the true value of α were 0.5, our free-surface temperatures would have to be approximately 35° higher than the temperature inside an effusion cell placed in the same positions in order to account for the results presented in this paper. An actual temperature difference of more than 5° is very unlikely.

The 111 faces of the barium fluoride surfaces remained smooth when examined at 240 magnifications; surface roughening did not, therefore, significantly inincrease the effective rate of evaporation. The evaporation coefficient for this face of a barium fluoride crystal is near unity within a small probable experimental error, and the evaporation coefficients for other alkaline earth fluorides are probably also near unity.

Acknowledgments. We extend our thanks to Dr. Reuben Hammer and Professor Joseph Pask, who designed and constructed the apparatus used in this research. This work was done under the auspices of the U. S. Atomic Energy Commission.

---

(22) R. E. Loehman, R. A. Kent, and J. L. Margrave, *J. Chem. Eng. Data*, **10**, 296 (1965).

The Study of Annelation Series of Benzenoid Hydrocarbons. I. The Influence of Annelation on the Changes of the Excitation Energy of the p Band

by Jaroslav Koutecký,[1] Petr Hochmann, and Miloš Titz

Institute of Physical Chemistry, Czechoslovak Academy of Sciences, Prague, Czechoslovakia

(Received January 10, 1966)

For the group of 86 catacondensed and pericondensed benzenoid hydrocarbons, the theoretical estimates of the excitation energy of the p band, calculated by the Hückel method and by the semiempirical method of the limited configuration interaction, as well as the experimental values of the same quantity, are plotted against the number of atoms of the respective molecules. In the plots thus obtained, the influence of the topology and size of the molecules on the changes of the theoretical and experimental values of the p-band excitation energy may be traced. A surprising similarity of plots for the three quantities mentioned has been found, and the importance of the molecular topology as the molecule characteristics is shown. Approximate rules based on the distribution of the "nodal points" in the highest occupied molecular orbital of the parent hydrocarbon have been derived, predicting the direction of the p-band shift with benzene ring annelation.

Introduction

When comparing the differences in energy of the lowest unoccupied and the highest occupied molecular orbital in Hückel approximations ($E(\mathrm{N} \rightarrow \mathrm{V_1})$) with the experimental value of the excitation energy corresponding to the p band according to Clar's classification[2] (ϵ_{exptl}), a statistically significant correlation is found for benzenoid hydrocarbons[3] as well as for other types of hydrocarbons.[4] However, the dependence of ϵ_{exptl} on $E(\mathrm{N} \rightarrow \mathrm{V_1})$ shows a considerable scattering. This scattering is connected with the decomposition of the dependence in question into partial dependences for narrower structural types. *E.g.*, the benzenoid hydrocarbons arising from 1,2-benzopyrene or 3,4-benzopyrene by a linear annelation, *i.e.*, hydrocarbons of the Pa[0,*n*] or Pb[0,*n*] type, respectively (see Table I), show systematic deviations from the regression line of dependence ϵ_{exptl} on $E(\mathrm{N} \rightarrow \mathrm{V_1})$ (*cf.* Table II). If, however, the decomposition of the dependence in still finer subclasses is considered, the amount of information contained in every dependence is lowered, which results in a reduced predictability.

This is the reason why this work has not been limited to the study of the dependence ϵ_{exptl} on $E(\mathrm{N} \rightarrow \mathrm{V_1})$ as a superposition of partial dependences. The endeavor has been made to differentiate the influence of the size of the conjugated system from the influence of its topology. For hydrocarbons where the use of the conventional Hückel method does not depend on the choice of parameters, the matrix of the effective Hamiltonian is identical with the topological matrix which represents in a unique way the structural formula belonging to the carbon skeleton of the molecule considered as an unweighted graph.[5,6] The connection of the Hückel eigenproblem with the diagonalization of the topological matrix is very well known.[7-9] It was

---

(1) Department of Chemistry, The John Hopkins University, Baltimore, Md. 21218.

(2) E. Clar, "Polycyclic Hydrocarbons," Academic Press Inc., New York, N. Y., 1964.

(3) (a) A. Streitweiser, Jr., "Molecular Orbital Theory for Organic Chemists," John Wiley and Sons, Inc., New York, N. Y., 1961; (b) J. Koutecký, J. Paldus, and R. Zahradník, *J. Chem. Phys.*, **36**, 3129 (1962).

(4) D. Meuche, K. Strauss, and E. Heilbronner, *Helv. Chim. Acta*, **41**, 57, 414 (1958).

(5) C. Berge, "Théorie des Graphes et ses Applications," Dunod, Paris, 1958.

(6) J. Sedláček, "Kombinatorika v theorii a praxi," Nakladatelství ČSAV, Praha, 1964.

(7) M. M. Günthardt and H. Primas, *Helv. Chim. Acta*, **39**, 1645 (1956).

(8) K. Ruedenberg, *J. Chem. Phys.*, **22**, 1828 (1954).

used also to establish important relationships between the Hückel and the one-dimensional free electron theory on one hand[10] and between the Hückel and valence-bond method on the other hand.[11] The resonance energies of the π-electron systems were discussed recently in terms of topological concepts.[12]

Even if the importance of the topology is generally understood, the quantitative aspects of the influence of the topology seem to be not fully exhausted. Therefore, the dependence of the quantity $E = 2e$, where e designates the lowest eigenvalue in the absolute sense (*e.g.*, regardless the sign) of the topological matrix, on the number of carbon atoms (N) of the relevant hydrocarbon is studied. The first quantity, being a characteristic of the topological matrix, is in relation with the graph representing the π-electronic system, *i.e.*, with the structural formula of the molecule. This quantity represents the estimate of the lowest excitation energy for alternant hydrocarbons in Hückel's scheme (*i.e.*, $E(\mathrm{N} \rightarrow \mathrm{V}_1) = E$). On the other hand, the number of carbon atoms may be considered as one of the possible size measures of the conjugated system. Another possible measure would be the number of benzene rings contained in the hydrocarbon. This quantity, however, makes the comparison of catacondensed and pericondensed hydrocarbons difficult.

In the E–N plots mentioned above, individual points corresponding to the given annelation series are connected with straight lines so that the influence of the size of the conjugated system on the quantity E in a series of topologically similar skeletons may be easily followed. A similar method has, in principle, been applied by Clar to the study of dependence of the individual bands in the ultraviolet spectrum of benzenoid hydrocarbons on the structure of the respective molecules.[2] Such a presentation is a generalization of the graphs in which spectroscopic properties, either in a series of linear polyacenes or in the series of the hydrocarbons with constant number of benzene rings, are plotted.[13,14]

On the other hand, the E–N graphs enable us to study the influence of the carbon skeleton topology on the quantity E for the fixed size of the molecule.

In the selection of the annelation series of topologically similar carbon skeletons, the following three modes of benzene ring attachment have been considered.

(1) The ring to be annexed has one bond in common with the original system (catacondensation). The most important partial case is the elongation of the existing straight chain of benzene rings following the direction of this chain: in a word, the linear annelation. The transition from naphthalene to anthracene or from phenanthrene to tetraphene may serve as an example.

(2) The new system arises from the original one through elongation of the linear chain of benzene rings by the addition of one benzene ring; the linear chain in question connects two characteristic and constant groups of benzene rings. This case is illustrated by the transition from the skeleton Ha[0] to Ha[1].

(3) The annexed benzene ring has three neighboring bonds in common with the parent system (pericondensation). The transition from phenanthrene to pyrene serves as an example.

The individual points in the E–N plots belonging to different annelation series in the above-defined sense are connected as mentioned above. These plots are then compared with similar plots in which the experimental value $\epsilon_{\mathrm{exptl}}$ or the theoretical value of the p-transition excitation energy (ϵ_{p}), calculated by the method of the limited configuration interaction (LCI), is given as the function of N.

The Hydrocarbons Studied and the Method Used

Besides the plots mentioned in which the quantity E has been plotted against N (Figures 1a–5a), the values of the excitation energy corresponding to the p band found experimentally ($\epsilon_{\mathrm{exptl}}$) (Figures 1c–5c) and calculated by means of the LCI (ϵ_{p}) method (Figures 1b–5b) have also been plotted against the number of atom N. The values E, ϵ_{p}, and $\epsilon_{\mathrm{exptl}}$ are given in electron volts. The value of the resonance integral β, both in Hückel and LCI methods, is -2.318 ev. Table II presents the parameters of the linear regression dependence $\epsilon_{\mathrm{exptl}}$ upon E for different groups of studied molecules for which the experimental data were attainable.

The survey of molecules studied is given in Table I. For the sake of a simple designation of hydrocarbons studied which form the series in the above-mentioned sense, the symbols defined in Table I differ from the conventional chemical nomenclature. To simplify the description of the plots, molecules are numbered as shown in Table I.

The numerical values based on the energy of molecular orbitals in the Hückel approximation have been

---

[9] K. Ruedenberg, *J. Chem. Phys.*, **34**, 1861, 1884 (1961).

[10] J. R. Platt, "Free Electron Theory of Conjugated Molecules," John Wiley and Sons, Inc., New York, N. Y., 1964.

[11] E. Heilbronner, *Helv. Chim. Acta*, **45**, 1722 (1962).

[12] R. A. Marcus, *J. Chem. Phys.*, **43**, 2643 (1965).

[13] *Cf.* W. Moffit, *ibid.*, **22**, 320 (1954).

[14] *Cf.* N. S. Ham and K. Ruedenberg, *ibid.*, **25**, 13 (1956).

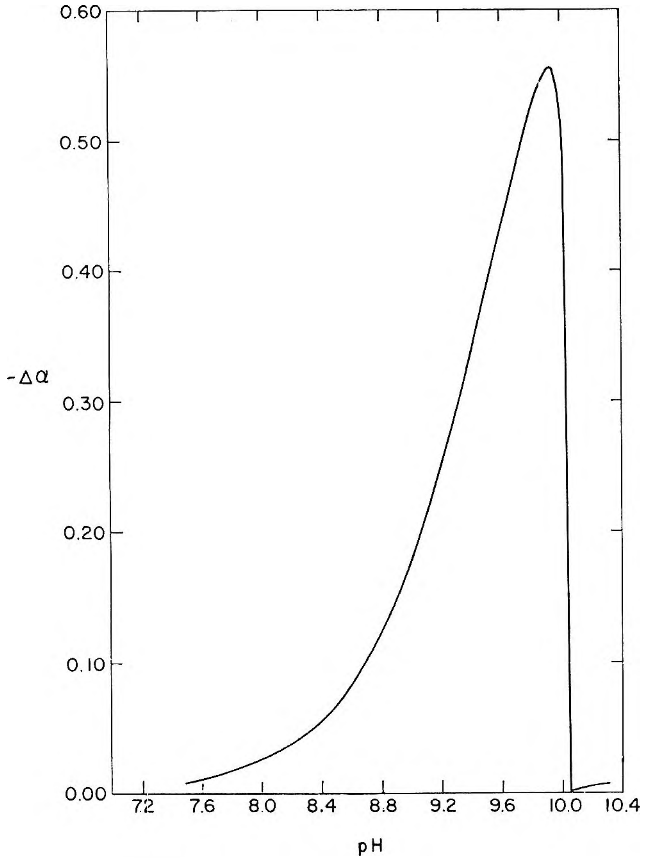

Figure 3. Curve calculated from curves in Figures 1 and 2, according to identity 9.

was determined by a total hydrolysis method:[17] an aliquot was diluted about tenfold with 0.3 M NaOH, left overnight at 40°, and diluted to a known volume with 1 M phosphate buffer of pH 7.0. The nucleotide concentration in the resulting solution was obtained by dividing its O.D.$_{260}$ − O.D.$_{290}$, measured in 1-cm cells, by $\epsilon_{260} - \epsilon_{290} = 0.976 \times 10^4$ l. mole^{-1} cm^{-1}. The concentration of the poly A solution was first determined by the above method (taking $\epsilon_{260} - \epsilon_{290} = 1.51 \times 10^4$ l. mole^{-1} cm^{-1}) and then made equal to that of the poly U solution (0.0085 monomole/l.) by dilution with 0.2 M KCl. These solutions were stored in a deep freezer.

Apparatus. The TTA31 titration assembly, G202B glass electrode, K4112 saturated calomel electrode, and the pH meter 4 were all Radiometer equipment. To ensure exact delivery of the polymer solutions, the pipets were first silicone coated and calibrated. Alkali and acid were added by means of Agla micrometer syringes.

Procedure. All experiments were carried out at a temperature of 30.0 ± 0.1° and under an atmosphere of purified nitrogen. Calibrations were made against Beckman buffer solutions of pH 7 and 10 and Radiometer buffer of pH 6.5. Differences in readings before and after the titration were found to be within ±0.015 pH unit. Titrations with 0.07 M NaOH and 0.04 M HCl were carried out on separate solutions of poly A and poly U at initial concentrations of 0.00425 and 0.00080 monomolar, and also on mixtures with the same initial concentrations in each of the polymers. Each solution underwent a "forward" titration with alkali, from about pH 7 to 11.2, followed by a "back" titration with acid. A blank solution, 0.2 M KCl in water, was carried through three similar titration cycles in succession.

Method of Calculating Degrees of Ionization. The titrations which any solution has undergone are numbered consecutively in the order: first forward-, first back-, second forward-titration, and so on. The following notation is subsequently used: $V^{\mathrm{B(or\ P)}}_{i,\mathrm{NaOH(or\ HCl)}}$, volume of titrant which had been added to the solution (blank, or polymer solution, according to the superscript used) when a certain pH value was reached in the course of the ith titration; V_0, initial volume of the blank solution (it is practically equal to the initial volume of the polymer solutions); M_{HCl}, M'_{NaOH}, molarities of the titrants; the alkali contains traces of carbonate which cause its effective molarity to depend on pH; and $n^{\mathrm{P}}_{1,\mathrm{H}^+}$, $n^{\mathrm{P}}_{2,\mathrm{H}^+}$, numbers of moles H$^+$ dissociated from the polymer when a certain pH has been reached in the course of the forward and back titration, respectively. (If the polymer ionizes reversibly, then the two quantities are equal to each other.)

All of the solutions and titrants were 0.2 M in KCl and the polymer concentrations were lower by a factor of about 40. It therefore seems plausible to assume that for any given pH value, the molarity of OH$^-$, C_{OH^-}, has the same value in each solution[15] and is given by

$$C_{\mathrm{OH}^-} = (V^{\mathrm{B}}_{i,\mathrm{NaOH}}M'_{\mathrm{NaOH}} - V^{\mathrm{B}}_{i,\mathrm{HCl}}M_{\mathrm{HCl}})/(V_0 + V^{\mathrm{B}}_{i,\mathrm{NaOH}} + V^{\mathrm{B}}_{i,\mathrm{HCl}})$$
$$= (V^{\mathrm{P}}_{1,\mathrm{NaOH}}M'_{\mathrm{NaOH}} - n^{\mathrm{P}}_{1,\mathrm{H}^+})/(V_0 + V^{\mathrm{P}}_{1,\mathrm{NaOH}})$$
$$= (V^{\mathrm{P}}_{2,\mathrm{NaOH}}M'_{\mathrm{NaOH}} - V^{\mathrm{P}}_{2,\mathrm{HCl}}M_{\mathrm{HCl}} - n^{\mathrm{P}}_{2,\mathrm{H}^+})/(V_0 + V^{\mathrm{P}}_{2,\mathrm{NaOH}} + V^{\mathrm{P}}_{2,\mathrm{HCl}}) \quad (11)$$

(The various expressions in eq 11 yield, in fact, the value of $C_{\mathrm{OH}^-} - C_{\mathrm{H}^+}$, and in all subsequent equations C_{OH^-} can be replaced accordingly. In the alkaline pH range, C_{H^+} will indeed be negligible compared to C_{OH^-}.) Using the fact that if $a/b = c/d$ then $(a - c)/$

---

[17] D. Elson, T. Gustafson, and E. Chargaff, *J. Biol. Chem.*, **209**, 285 (1954).

$(b - d) = a/b$, and rearranging properly, we deduce the following equalities from eq 11 for any $i \neq j$

$$(V^{B}_{i,HCl} - V^{B}_{j,HCl})/(V^{B}_{i,NaOH} - V^{B}_{j,NaOH}) = (M'_{NaOH} - C_{OH^-})/(M_{HCl} + C_{OH^-}) \equiv Q(\text{pH}) \tag{12}$$

$$n^{P}_{1,H^+} = (V^{P}_{1,NaOH} - V^{B}_{1,NaOH})(M'_{NaOH} - C_{OH^-}) \tag{13}$$

and

$$n^{P}_{2,H^+} = (V^{P}_{2,NaOH} - V^{B}_{1,NaOH})(M'_{NaOH} - C_{OH^-}) - V^{P}_{2,HCl}(M_{HCl} + C_{OH^-}) \tag{14}$$

The quantity Q(pH) is derived from the blank titrations (see eq 12) and M_{HCl} is known. Hence, if $(M'_{NaOH} - C_{OH^-})$ in eq 13 and 14 is replaced by $(M_{HCl} + C_{OH^-})\cdot Q(\text{pH})$, C_{OH^-} remains the only quantity (on the right-hand side of these equations) which is not directly measurable; it usually constitutes a small increment to M_{HCl} and is calculated in the following way. The first quotient in eq 11 is written for $i = 1$ ($V^{B}_{1,HCl} = 0$)

$$C_{OH^-} = V^{B}_{1,NaOH}M'_{NaOH}/(V_0 + V^{B}_{1,NaOH}) \tag{15}$$

Combining eq 12 and 15, we obtain

$$C_{OH^-} = M_{HCl}Q(\text{pH})V^{B}_{1,NaOH}/(V_0 - Q(\text{pH})V^{B}_{1,NaOH}) \tag{16}$$

A comparison of experimental values of $V^{P}_{2,HCl}/(V^{P}_{2,NaOH} - V^{P}_{1,NaOH})$ with those obtained for Q(pH) at the same pH values yields a check on the reversibility of the polymer ionization; the corresponding values are equal to each other if the ionization is reversible, *i.e.*, if $n^{P}_{1,H^+} = n^{P}_{2,H^+}$ (*cf.* eq 12, 13, and 14).

Division of n^{P}_{1,H^+} and n^{P}_{2,H^+} by the total number of moles A or U residues yields the corresponding degrees of ionization (for which α is used as a general denotation).

The above method for calculating degrees of ionization takes into account volume changes and carbonate traces in the alkali. The method requires that the concentration of neutral salt be constant throughout the titration and high as compared to polymer and titrant concentrations.

Treatment of Experimental Data. The data obtained from any titration consist of volumes of titrants added and corresponding pH values. For the blank, these data were plotted and the "best" smooth lines were drawn through the experimental points. These graphs served to calculate Q(pH) (estimated error ±0.3%) and to read off $V^{B}_{1,NaOH}$ at pH values that correspond to experimental points in the polymer titration, *cf.* eq 13 and 14. There are two main errors in $V^{B}_{1,NaOH}$, the one due to the uncertainty in drawing the aforementioned "best" line, and the other due to a possible difference of ±0.01 between two pH values considered equal, the one measured in a polymer solution and the other in the blank solution. For the polymer titration, each experimental point is converted into the corresponding α, pH pair of values. These pairs are plotted and the "best" smooth line is drawn (see Figures 1 and 2). From three such curves, corresponding to poly A, poly U, and poly(A + U), respectively, a curve of $\Delta\alpha$ *vs.* pH is constructed; *cf.* identity 9 and Figure 3. The integral in eq 10 is then evaluated graphically. In calculating the error in $\Delta\alpha$, care should be taken not to overcount the errors in Q(pH), in polymer concentration (±2%), and in M_{HCl}(± 0.6%), which appear several times in the course of the above calculations. Uncertainties in pH measurements contribute to the error in the ultimate result, $\Delta\mu_{exp}$, in two ways (in addition to the error in $V^{B}_{1,NaOH}$ mentioned previously).

(1) An estimated difference of ±0.015 pH unit may exist between two pH values considered equal, the one measured in a poly U solution and the other in a poly(A + U) solution. This means a possible shift, along the pH axis, of the α_U curve, Figure 1, relative to the α_{A+U} curve, Figure 2. It is easy to assess the effect of this error on the value of the integral of eq 10.

(2) The upper limit of the above integral is that pH for which $\Delta\mu_{exp}$ is ultimately given, and an error of ±0.015 pH unit causes a corresponding error in the value of this integral, *i.e.* in $\Delta\mu_{exp}$. Since all the errors are assigned to $\Delta\mu_{exp}$, the pH values for which $\Delta\mu_{exp}$ is finally given are to be considered correct.

Results and Discussion

The titration curves of poly A, poly U, and of their 1:1 mixture are given in Figures 1 and 2. The curve in Figure 3 is constructed from the former curves according to identity 9. Figure 4 gives $\Delta\mu_{exp}$ as a function of pH; it is obtained by integrating the curve of Figure 3 according to eq 10, taking pH* = 10.05. Calculations of degrees of ionization and of errors in $\Delta\mu_{exp}$ are described in the Experimental Section.

The significance of $\Delta\mu_{exp}$ is now investigated, assuming at first that poly A and poly U are monodisperse, of the same degree of polymerization, ν, and that every poly(A + U) molecule contains just one poly A and one poly U chain. These assumptions are expressed by rewriting reaction 1 as

$$A_\nu + U_\nu \rightleftharpoons (A + U)_\nu \tag{17}$$

In a monodisperse system, it is natural to define quantities in terms of polymeric molecules rather than in terms of monomeric residues. Hence, the chemical

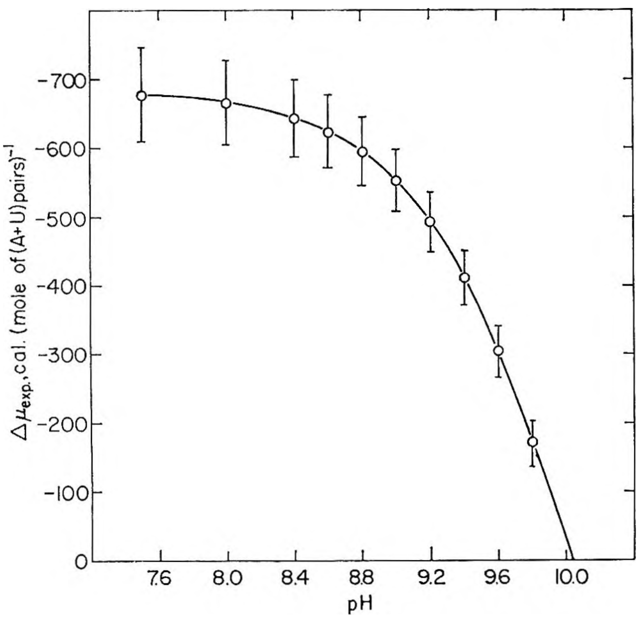

Figure 4. Free energy change for the reaction between poly A and poly U in 0.2 M KCl and 30° as a function of pH. Vertical lines represent experimental errors.

potential is now defined as the partial derivative of the free energy with respect to the number of moles of *polymeric* molecules, and is related to μ_X of eq 2 by

$$\mu(X_\nu) = \nu\mu_X \qquad (18)$$

Similarly, the concentration of X is expressed in moles of X per unit volume and denoted by C.

The chemical potential $\mu(X_\nu)$ can be written as

$$\mu(X_\nu) = \mu^0(X_\nu) + RT \ln C + RT \ln \gamma \qquad (19)$$

The standard chemical potential $\mu^0(X_\nu)$ depends on the chemical potentials of the solvent components (including the counterions of X_ν) and when these are held constant, γ tends to unity as C tends to zero. Anticipating that under appropriate conditions $RT \ln \gamma$ can be omitted from eq 19, we write

$$\mu_X = \nu^{-1}[\mu^0(X_\nu) + RT \ln C] \qquad (20)$$

for X equal to either A, U, or A + U. By eq 3 and 20

$$\Delta\mu(\text{pH}) = \Delta\mu^{(\nu)} \equiv \nu^{-1}\{\mu^0[(A + U)_\nu] - \mu^0(A_\nu) - \mu^0(U_\nu) - RT \ln C\} \qquad (21)$$

When ν is sufficiently large and C not too low, the quantity $\Delta\mu^{(\nu)}$ is expected to become practically equal to a limiting value, $\Delta\mu^{(\infty)}$, which is independent of both ν and C, and which plays a central role in the statistical thermodynamic treatments of the poly(A + U) molecule (*cf.* Appendix).[18] In this case, eq 4 and 21 yield

$$\Delta\mu_{exp} \cong \Delta\mu(\text{pH}) \cong \Delta\mu^{(\infty)} \qquad (22)$$

This relation is expected to hold also for a polydisperse system, provided all its molecules are of sufficiently high degrees of polymerization.

The omission of the $RT \ln \gamma$ term from eq 19 implies the neglect of nonspecific interactions between different macromolecules, *i.e.*, of all interactions other than those involved in reaction 17. The value of $\ln \gamma$ can be obtained from light scattering measurements which, in view of the definitions of $\mu^0(X_\nu)$ and γ in eq 19, should be carried out at constant chemical potentials of all the solvent components.[19] The second virial coefficient $\mathfrak{A}_2$ obtained from such measurements can be related to $\ln \gamma$ by using the Gibbs–Duhem relation (eq 6 in ref 19) and neglecting higher virial coefficients

$$\ln \gamma = 2\nu\mathfrak{A}_2 c \qquad (23)$$

where c is the monomolar polymer concentration. For the helical poly(A + U), $\ln \gamma$ was estimated as $1.5 \times 10^{-4}\ \nu$, by taking $\mathfrak{A}_2 = 1.5 \times 10^{-2}$ l. (mole of nucleotide pairs)$^{-1}$—the value obtained[20] for sonicated DNA of about 700 nucleotide pairs per molecule, in 0.2 M NaCl—and $c = 5 \times 10^{-3}$ (mole (A + U) pairs) l.$^{-1}$. By eq 19, 18, 3, and 4, $\Delta\mu_{exp}$ will contain several $\nu^{-1}RT \ln \gamma$ terms. A rough estimation of their contribution to $\Delta\mu_{exp}$, using the value of $\ln \gamma$ just obtained, yields $\sim 5 \times 10^{-4}RT$ which is more than two orders of magnitude smaller than the experimental errors indicated in Figure 4.

To sum up, appropriate conditions for neglecting the $RT \ln \gamma$ term in eq 19 seem to have been realized in the present study, and the $\Delta\mu_{exp}$ values obtained are therefore expected to have the meaning attributed to them by eq 22, provided that practically all of the molecules were of sufficiently high degrees of polymerization.

The quantity $\Delta\mu^{(\infty)} \cong \Delta\mu_{exp}$ has a simple meaning when the poly(A + U) is completely helical. Reaction 17 can then be represented by the following ν consecutive steps. The first step involves the linking together of the two single strands by hydrogen bonds between their first nucleotides. Each of the remaining $\nu - 1$ steps adds another bonded pair "on top" of the preceding bonded pairs. It is usually assumed[21] that,

---

[18] Speaking loosely, the free energy of interaction between A_ν and U_ν involves a large number (proportional to ν) of internal degrees of freedom and is therefore expected to be negligibly affected by the few degrees of freedom corresponding to translation (and rotation) of the whole macromolecules.

[19] H. Eisenberg, *J. Chem. Phys.*, **36**, 1837 (1962).

[20] G. Cohen and H. Eisenberg, *Biopolymers*, **4**, 429 (1966). The author is thankful to G. Cohen for having kindly communicated to him the results prior to publication.

[21] B. H. Zimm, *J. Chem. Phys.*, **33**, 1349 (1960).

apart from the first step, every step has the same equilibrium constant s. Denoting the equilibrium constant of the first step by us, the equilibrium constant of the over-all reaction 17 can be written as us^{ν}. The quantity $\Delta\mu^{(\nu)}$, defined by identity 21, can then be written as

$$\Delta\mu^{(\nu)}_{\text{helix}} = -\nu^{-1}RT \ln (us^{\nu}C) \tag{24}$$

When ν is sufficiently large, we expect[18,22]

$$\Delta\mu^{(\nu)}_{\text{helix}} \cong \Delta\mu^{(\infty)}_{\text{helix}} = -RT \ln s \tag{25}$$

From eq 25 and 22 we conclude that when poly(A + U) is completely helical, $\Delta\mu_{\text{exp}} \cong -RT \ln s$ (with the recurring proviso, that the polymers used in measuring $\Delta\mu_{\text{exp}}$ are of sufficiently high degrees of polymerization).

At neutral pH and room temperature, poly(A + U) seems to be completely helical,[23] and it seems to remain so up to about pH 9.5.[13] In this pH range, the uracils in poly(A + U) hardly ionize at all (the low values of $\alpha_{\text{A+U}}$ in Figure 2 are practically equal to those of α_{A} in Figure 1) while the ionization of the free poly U may be appreciable. The dependence of s on the activity of H+ is then given by $s = s_0(1 + K_{\text{U}}a_{\text{H}^+}{}^{-1})^{-1}$, where K_{U} is the ionization constant of poly U,[14] and s_0 is the value which s would have obtained, had the poly U been un-ionized. In general, the value of s depends on all the factors which influence the stability of the helical poly(A + U), namely hydrogen bonds, interactions between successive bonded A, U pairs (the so-called "stacking" interactions), and other electrostatic and solvent effects. Determinations of $RT \ln s$ at different temperatures and solvent compositions may help in separating the contributions of the factors listed.

At pH 7.5, where the poly(A + U) seems to be completely helical,[23] the value of $\Delta\mu_{\text{exp}} \cong -RT \ln s$ is of the order of $-RT$ (see Figure 4). A similar result has been obtained before[8] by a different method. This relatively low value supports the mechanism suggested by Felsenfeld[23] for perfect pairing of all A and U nucleotides, and also clearly indicates the cooperative nature of the pairing process.[8]

When the poly(A + U) is partly "melted," $\Delta\mu_{\text{exp}}$ is no longer equal to $-RT \ln s$. The value of $-RT \ln s$ can then, however, be derived in the following way.[4,7] The $\alpha_{\text{A+U}}$ curve (Figure 2) is extrapolated from the lower pH values, where the poly(A + U) is practically completely helical, to higher values (dashed line in Figure 2), thus providing a titration curve for the hypothetical case of a permanently helical poly(A + U). The corresponding $\Delta\alpha$ *vs.* pH curve is constructed (see identity 9) and integrated from a low pH, where $-RT \ln s \cong \Delta\mu_{\text{exp}}$, and up to the pH at which $-RT \ln s$ is to be evaluated. The value of $-RT \ln s$ at the upper pH is then given by the sum of its value at the lower pH and the product of the integral by $-2.30RT$ (*cf.* eq 8 after replacing $\Delta\mu$ by $-RT \ln s$). The error in $-RT \ln s$ thus calculated will of course be affected by the uncertainty in the extrapolation of $\alpha_{\text{A+U}}$.

The statistical thermodynamic treatments of a molecule like poly(A + U) usually yield a relation between $\exp(-\Delta\mu^{(\infty)}/RT)$ (*cf.* eq A7), s, and other parameters characterizing the interaction between the two strands. Such a relation is provided, for example, by eq 12b and 9 of ref 24, where α^{-2} stands for[25] $\exp(-\Delta\mu^{(\infty)}/RT)$, s is the equilibrium constant defined above, and ρ_i with $i = 1, 2, 3 \ldots$ are the "other parameters" just mentioned.[26] Experimental values of $\Delta\mu^{(\infty)}$ and s should, in principle, enable us to derive the values of the ρ_i parameters. At the present time, however, such an evaluation is impractical due to the large number of these parameters. A simplifying assumption reduces the number of unknown parameters to one—the so-called "stacking" parameter, τ (*cf.* eq 7 in ref 24). Just for the sake of illustration, the order of magnitude of τ was determined at pH 9.9, taking $\Delta\mu^{(\infty)}(\cong\Delta\mu_{\text{exp}})$ from Figure 4 and calculating s by the extrapolation method explained in the previous paragraph. The result is $\tau = O(5 \times 10^2)$ which, according to ref 24, corresponds to about -4 kcal of stacking free energy.

In the present work, the partial enthalpy change

$$\Delta\bar{H} = -T^2[\partial(\Delta\mu_{\text{exp}}/T)/\partial T]_p \tag{26}$$

is only estimated, at pH 7.5, in the following way. Figure 4 indicates that, at pH 7.5 and 30°, $\Delta\mu_{\text{exp}}/T = 2.25$ cal deg^{-1}; at the same pH, the "melting" temperature is about 65°[8,27,28] and, in the vicinity of this temperature, $\Delta\mu_{\text{exp}}$ will be zero. Since $\Delta\bar{H}/T^2$ seems not to change much in the temperature interval considered,[10] eq 26 is rewritten as

$$\Delta\bar{H}/T^2 \approx -[(\Delta\mu_{\text{exp}}/T)_{65^\circ} - (\Delta\mu_{\text{exp}}/T)_{30^\circ}]/(65 - 30) = 6.4 \times 10^{-2} \text{ cal (mole of (A + U)pairs)}^{-1} \text{ deg}^{-2} \tag{27}$$

At 40°, for example, we obtain $\Delta\bar{H} \approx 6.3$ kcal (mole of

---

[22] Equation 25 follows directly from eq A7 in the Appendix because, when poly(A + U) is completely helical, $\ln Z^{(\nu)} \cong \nu \ln s$.

[23] G. Felsenfeld, *Biochim. Biophys. Acta*, **29**, 133 (1958).

[24] D. M. Crothers and B. H. Zimm, *J. Mol. Biol.*, **9**, 1 (1964).

[25] A. Litan and S. Lifson, *J. Chem. Phys.*, **42**, 2528 (1965).

[26] When poly(A + U) is completely helical, the relation reduces to $\alpha^{-2} = s$.

[27] This value refers to pH 7.0, but in this pH range the "melting" temperature, is almost constant.[28]

[28] R. A. Cox, *Biochim. Biophys. Acta*, **68**, 401 (1963).

(A + U) pairs)$^{-1}$, which agrees with the value obtained[9,10] calorimetrically.

The main issue of the foregoing discussion is that the important quantity $\Delta\mu^{(\infty)}$ (*cf.* eq 25 and A7) can be derived by the potentiometric method described before. The reliability with which $\Delta\mu^{(\infty)}$ is obtained depends first on the validity of the identification of $\Delta\mu^{(\infty)}$ with $\Delta\mu_{\mathrm{exp}}$ and, secondly, on the reliability with which $\Delta\mu_{\mathrm{exp}}$ itself is obtained. The first point involves three assumptions: (a) that the degrees of polymerization of the polymers studied are sufficiently large to make $\Delta\mu_{\mathrm{exp}}$ independent of them; this assumption can be checked by comparing $\Delta\mu_{\mathrm{exp}}$ values obtained with polymers of different degrees of polymerization; (b) that activity coefficients of the polymeric molecules can be disregarded, an assumption based on a rough estimation presented above; when their neglect is uncertain, they can be measured by light scattering; (c) that the quantity $\Delta\mu(\mathrm{pH}^*)$ is negligibly small (*cf.* eq 4 and the paragraph preceding it). This assumption will be verified if the two strands of the poly-(A + U) are found to separate altogether at pH $\geq$ pH*; in a similar polynucleotide system, such a separation was clearly demonstrated.[29]

The reliability with which $\Delta\mu_{\mathrm{exp}}$ was here obtained can be improved if, instead of pH measurements in a *continuous* titration of a polymer solution, HCl activity is measured in *batches* of polymer solution. This procedure enables a direct application of the thermodynamically rigorous eq 6 and also minimizes various experimental errors.

The method discussed in the present article is based on a simple thermodynamic relation (eq 5), and it can, in principle, be used to determine the partial free energy changes accompanying the formation of various complexes from their component molecules. The required titrations of the separate components (reactants) and of their mixture can be carried out with any substance the activity of which is readily measurable, and the addition or removal of which can reversibly reduce the stability of the complex up to a complete dissociation into the component molecules. It may be an advantage that the nature of the interactions between the titrant and the titrated substances is immaterial for the purpose of calculating the partial free energy change, provided these interactions are reversible. It is noteworthy that in each of the previous applications of the method,[3–7] the reaction studied involved just one reactant and one product, *e.g.*, the coil-to-helix transformation of polyglutamic acid. In this case, the analog of titration curves of separated reactants is a titration curve of a hypothetical polyglutamic acid which remains in the coiled form throughout the titration. This curve can only be estimated by extrapolating the experimental titration curve from high pH values, where the polyglutamic acid is indeed expected to be entirely in the coiled form.

Acknowledgments. The author is deeply indebted to Dr. A. Shatkay for valuable suggestions and for putting at his disposal every facility in his laboratory. The discussions with Dr. Z. Alexandrowicz, and the comments of Professor S. Lifson were of enormous help. The author is also grateful to Mrs. S. Rogozinsky for the magnesium analyses.

Appendix

The Relation between $\Delta\mu^{(\nu)}$ (Cf. Identity 21) and the Partition Function of an $(A + U)_\nu$ Molecule.[30] In the statistical thermodynamic treatments,[31] a *microscopic state* of an $(\mathrm{A + U})_\nu$ molecule is usually specified by stating which A nucleotides from one strand are hydrogen bonded to which U nucleotides of the other strand. One of the microscopic states, which we shall denote by S_{std}, is chosen as the *standard state* and is arbitrarily assigned a *statistical weight* equal to unity. Any other state, S, is assigned a statistical weight K_S, which is in fact the equilibrium constant for the reaction

$$\mathrm{S_{std}} \rightleftharpoons \mathrm{S} \tag{A1}$$

Interactions between different $(\mathrm{A + U})_\nu$ molecules are neglected, K_S can be therefore expressed in terms of concentrations

$$K_S = [\mathrm{S}]/[\mathrm{S_{std}}] \tag{A2}$$

and is seen to be proportional to the occurrence probability of state S. The value of K_S will depend on the type and chemical potentials of the various solvent components.

The sum of statistical weights of all possible microscopic states of the molecule $(\mathrm{A + U})_\nu$ defines the *partition function*, $Z^{(\nu)}$. It can be shown that

$$-RT \ln Z^{(\nu)} = \mu^0[(\mathrm{A + U})_\nu] - \mu^0(\mathrm{S_{std}}) \tag{A3}$$

where $\mu^0[(\mathrm{A + U})_\nu]$ is the standard chemical potential (*cf.* eq 19) of the $(\mathrm{A + U})_\nu$ molecule which is free to assume any of its microscopic states, and $\mu^0(\mathrm{S_{std}})$ refers to the standard state.

From eq A3 and identity 21 we obtain

$$\Delta\mu^{(\nu)} + \nu^{-1} RT \ln Z^{(\nu)} = \nu^{-1}\{\mu^0(\mathrm{S_{std}}) - \mu^0(\mathrm{A}_\nu) - \mu^0(\mathrm{U}_\nu) - RT \ln C\} \tag{A4}$$

---

[29] R. B. Inman, *J. Mol. Biol.*, 9, 624 (1964).

[30] *Cf.* reaction 17 and paragraph preceding it.

[31] *Cf.* ref 25 and references cited therein.

where C denotes the total concentration of A_ν and also of U_ν in the solution in which the $(A + U)_\nu$ molecule is considered to be present. Had the reaction

$$A_\nu + U_\nu \rightleftharpoons S_{std} \qquad (A5)$$

been the only one to occur, the fraction Θ_{std} of A_ν or U_ν strands in the form of S_{std} would obey the relation

$$-RT \ln [\Theta_{std}/(1 - \Theta_{std})^2] = \mu^0(S_{std}) - \mu^0(A_\nu) - \mu^0(U_\nu) - RT \ln C \qquad (A6)$$

Let the standard state S_{std} be chosen as that microscopic state where the first $\nu_0(1 \leq \nu_0 \ll \nu)$ nucleotide pairs are bonded and all the rest non-bonded.[32] For given values of ν_0 and C, Θ_{std} is expected to have some finite value, almost independent of ν. (A rough estimate of the values of Θ_{std} corresponding to different values of ν_0 and C should be obtainable from experiments with A_{ν_0} and U_{ν_0} oligomers.) Hence, for sufficiently large values of ν, the right-hand side of eq A4 becomes negligibly small, and in the limit of $\nu \rightarrow \infty$

$$\Delta\mu^{(\infty)} = -RT \lim_{\nu \rightarrow \infty} \nu^{-1} \ln Z^{(\nu)} \qquad (A7)$$

This limiting value [or rather $\exp(-\Delta\mu^{(\infty)}/RT)$] is evaluated by the statistical thermodynamic treatments for a *model* molecule where only a certain type of microscopic states is assumed to exist and where simplifying, though plausible assumptions are made about the mathematical structure of the statistical weights.[25]

---

[32] With this choice, the degree of ionization of the standard state will be practically equal to the sum of degrees of ionization of the separated strands.

Hydrogen Sorption by Alumina at Low Pressures

by M. J. D. Low and E. S. Argano

School of Chemistry, Rutgers, The State University, New Brunswick, New Jersey *(Received March 8, 1966)*

The sorption of hydrogen by γ-alumina powder was measured from −193 to 663° at pressures from about 10^{-4} to 10^{-8} torr. A flow system was used. Hydrogen sorption increased with increasing degassing temperature until, after a 950° pumping, the reproducibility was about 5%. Some dissociative chemisorption occurs over the entire temperature range studied. Physical adsorption predominates below 200°. The maximum chemisorption occurs near 300°. The mechanism is discussed.

The high surface area forms of alumina have found extensive use of heterogeneous catalysis, and a voluminous literature on alumina and alumina-containing catalysts has developed. To this have been added, in recent years, the results of many investigations designed to clarify the catalytic process by studying the structure and properties of pure alumina surfaces by a variety of instrumental techniques. Yet, one of the simplest reactions, the sorption of hydrogen by alumina surfaces, seems to have been neglected. The hydrogen–deuterium exchange catalyzed by alumina has been studied,[1-6] as have the reaction of surface hydroxyls on alumina with gaseous deuterium[7,8] and the ortho–

---

(1) K. C. F. Holm and R. W. Blue, *Ind. Eng. Chem.*, **43**, 1506 (1951); **44**, 107 (1952).

(2) S. W. Weller and S. G. Hindin, *J. Phys. Chem.*, **60**, 1506 (1956).

(3) H. W. Kohn and E. H. Taylor, *ibid.*, **63**, 500 (1959).

(4) H. Pines and J. Ravoire, *ibid.*, **65**, 1859 (1961).

(5) W. K. Hall and F. E. Lutinski, *J. Catalysis*, **2**, 518 (1963).

(6) G. J. K. Acres, D. D. Eley, and J. M. Trillo, *ibid.*, **4**, 12 (1965).

(7) M. J. D. Low, J. Courtois, and N. Ramasubramanian, unpublished results.

parahydrogen conversion.[6] Some indirect knowledge of the hydrogen–alumina interaction is thus available. However, direct studies of hydrogen adsorption by alumina appear to be few in number and limited in extent.[9-13] As such information should aid our understanding of alumina surfaces, we have measured the hydrogen sorption on γ-alumina from −193 to 663°. Highly degassed surfaces were used and, as previous work had been done at pressures above about 1 torr, hydrogen sorption was measured at pressures ranging from about 10^{-4} to about 10^{-8} torr, using a flow system.

Experimental Section

The dynamic flow method and apparatus of Wagener,[14] as modified for work on W and Ba films,[15-17] was used. The adsorption system was constructed of Pyrex glass with the exception of the sample chamber, which was of Vycor. The sorption system itself was enclosed in a movable oven, shown in Figure 1 by the area enclosed by dotted lines. The Vycor sample chamber could be heated with an auxiliary furnace. The sorption system consisted of a pair of inverted Bayard–Alpert ionization gauges used to monitor pressures, a capillary with a fixed conductance of 22.4 cm^{-3} sec^{-1}, the Vycor sample chamber, and a Granville–Phillips ultrahigh vacuum valve, P. Hydrogen from a storage bulb (or, deuterium) was purified by diffusion through the walls of a palladium thimble and entered the system through an adjustable needle valve E (Edwards High Vacuum Ltd.), passing through two liquid nitrogen-cooled traps. The pressure was reduced by means of a three-stage oil diffusion pump using Corning 704 fluid, backed by a high-volume mechanical vacuum pump. The ionization gauges had iridium filaments and, in order to avoid spurious pumping effects, the low filament temperature of 950° was used, below the temperature of about 1200° at which the dissociation of hydrogen molecules to atoms proceeds. The ionization current used was kept low at 1 ma. The adsorbent used was 0.2 g of Alon-C γ-alumina[18] having an initial nitrogen BET surface area of 102 m^2/g.

The measuring procedure was as follows. After baking the system at 450° and outgassing the ionization gauges, using normal ultrahigh vacuum procedures, pressures below 10^{-9} torr were reached when liquid nitrogen was added to the upper trap. After closing valve P, hydrogen was introduced through valve E until the desired pressure P_s on the sample was reached. The speed of uptake V was then calculated from the pressure drop using the relation

$$V = (P_m - P_s)F$$

where V is in units of cm^3 torr sec^{-1} (1 cm^3 torr = 0.00132 ml STP), P_m is the pressure in the manifold in torr, P_s is the pressure in the sample space in torr, and F is the capillary conductance in cm^3 sec^{-1}. After recording the initial speed of adsorption, the pressure P_s in the sample vessel was maintained constant by decreasing the hydrogen flow through the valve E so that P_m decreased until, at the end of the experiment, $P_m = P_s$. The amount of hydrogen taken up was calculated by the graphical integration of velocity–time plots. As the hydrogen sorption was estimated to be seven orders of magnitude larger than hydrogen diffusion through the walls of the Vycor sample chamber, errors due to this diffusion were negligible. When measurements were done at different temperatures, the P_s value was corrected in order to keep collision frequency at the adsorbent surface constant, by using the relation $(P_1/P_2) = (T_2/T_1)^{1/2}$, derived from the kinetic theory of gases.

Experiments and Results

Some difficulty was initially experienced in obtaining reproducible results. As it is impossible to free an alumina surface of residual OH groups completely even at 1000°,[19] this was not unexpected. Some results of the effects of degassing temperature on the hydrogen sorption are shown in Figure 2. The amount of hydrogen taken up by the alumina at room temperature at 7×10^{-7} torr increased with increasing outgassing temperatures. The higher the temperature, however, the relatively smaller the effect became. The results became more reproducible with increasing outgassing temperature, shown, for example, by the results of Figure 3. Hydrogen sorption was measured at 27° at a pressure P_s of 7.2×10^{-7} torr for each experiment. Prior to each experiment the system was outgassed for 21 hr at 450° and the adsorbent for 18 hr at 850° and for 3 hr at 950° to a residual pressure below 1 ×

---

(8) J. L. Carter, P. J. Lucchesi, P. Corneil, D. J. C. Yates, and J. H. Sinfelt, *J. Phys. Chem.*, **69**, 3070 (1965).

(9) H. S. Taylor, *Z. Physik. Chem.* (Bodenstein Festband), 475 (1931).

(10) Th. Schoon and H. Klette, *Naturwissenschaften*, **29**, 653 (1941).

(11) A. S. Russell and J. J. Stokes, *J. Am. Chem. Soc.*, **69**, 1316 (1947).

(12) K. V. Topchieva and I. F. Moskovskaya, *Vestn. Mosk. Univ., Ser. II, Khim.*, **15** (2), 22 (1960).

(13) D. B. Rosenblatt and G. J. Dienes, *J. Catalysis*, **4**, 271 (1965).

(14) S. Wagener, *Brit. J. Appl. Phys.*, **1**, 225 (1950); **2**, 132 (1951); *J. Phys. Chem.*, **60**, 507 (1956); **61**, 267 (1957).

(15) A. G. Nasini, F. Ricca, and G. Saini, *Vacuum*, **10**, 68 (1960).

(16) P. della Porte and E. Argano, *ibid.*, **10**, 190, 198 (1960).

(17) F. Ricca and P. della Porte, *ibid.*, **10**, 215 (1960).

(18) G. Cabot Corp., Boston, Mass.

(19) J. B. Peri, *J. Phys. Chem.*, **69**, 711 (1965).

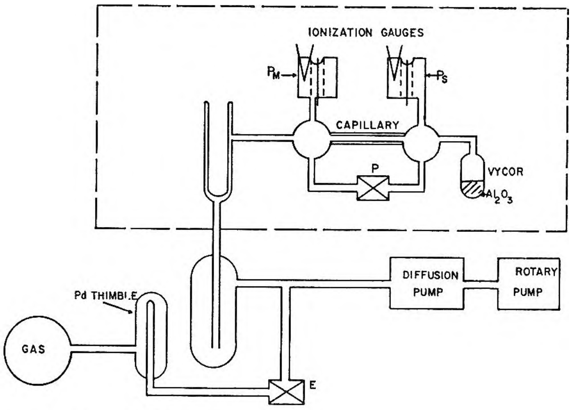

Figure 1. Ultrahigh vacuum system.

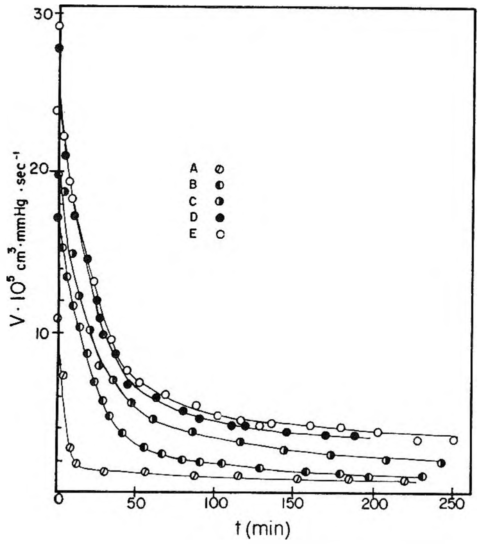

Figure 2. Effect of outgassing temperature (hydrogen sorption at 27° at constant pressure of 7.2×10^{-7} torr): (A) 650° for 20 hr, residual pressure 6×10^{-7} torr with system hot, 1×10^{-9} torr after cooling; (B) 750° for 18 hr, residual pressure 4×10^{-8} torr with system hot, 1×10^{-9} torr after cooling; (C) 850° for 18 hr, residual pressure 2×10^{-7} torr with system hot, 1×10^{-9} torr after cooling; (D) 850° for 50 hr, residual pressure 1.5×10^{-7} torr with system hot, 1×10^{-9} torr after cooling; (E) 850° for 18 hr and 950° for 3 hr, residual pressure $<10^{-7}$ torr with system hot, $<10^{-9}$ torr after cooling.

10^{-7} torr with the system hot. The pressure fell to below 1×10^{-9} torr when the system was cooled. The data agree within about 5% for the first three consecutive experiments and within about 10% for all five experiments shown. A small change in the activity of the alumina surface occurred. This may be connected with the sintering of the alumina to some extent. At the end of the experiments the surface area of the alumina had decreased by 25%. This sintering, although causing a not negligible diminution of the surface, appears to be of minor importance to the hydrogen sorption because only small changes in rates and amounts of hydrogen taken up were observed. The degassing of the adsorbent for 18 hr at 850° plus 3 hr at 950° was used prior to all other experiments.

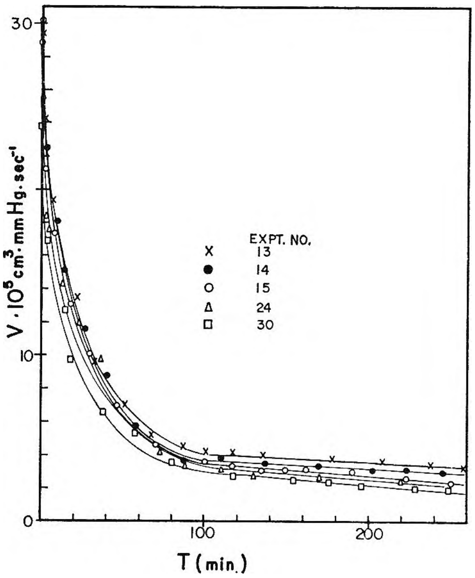

Figure 3. Sorption reproducibility (hydrogen sorption at 27°, $P_s = 7.2 \times 10^{-7}$ torr): outgassing, 18 hr at 850° plus 3 hr at 950°; residual pressure of $<10^{-9}$ torr in the cool system.

The results of a series of experiments performed at 27° but at different pressures are shown in Figure 4. A slope of $0.54 \approx 0.5$ was found for a plot of the logarithm of the initial hydrogen adsorption rate V_0 *vs.* the logarithm of P_s for the range 1.8×10^{-8} to 7.5×10^{-5} torr. The initial part of the uptake thus obeys the relation

$$V_0 = kP^{1/2}$$

The total amount of hydrogen adsorbed, q_T, at pressures from 3×10^{-7} to 5×10^{-5} torr at 27° is shown in Figure 5. The Freundlich relation

$$q_T = AP^k$$

holds with the parameter k having the value 0.09. Russell and Stokes[11] found the value $k = 0.25$ at much higher pressures.

The results of various experiments at different temperatures at $P_s = 7 \times 10^{-7}$ torr are shown in Figures 6–8. Figure 6 shows the change in the sorption velocity V with the total amount sorbed, q, at different temperatures. The decrease in q with increasing temperature is similar to the effect reported by others working at higher pressures.[11,12] The curves at the

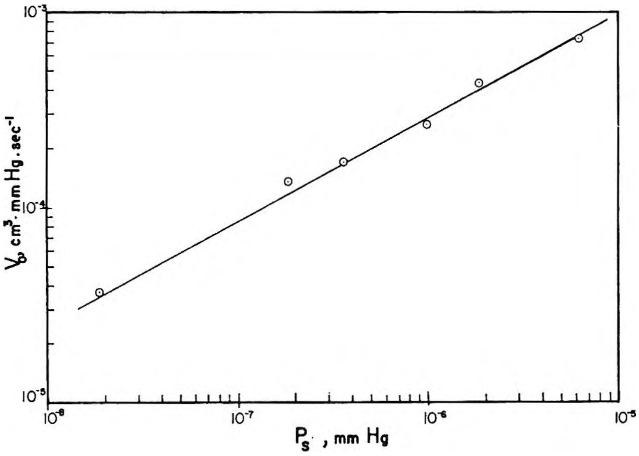

Figure 4. Pressure effect: pressure dependence of the initial rate of hydrogen sorption, V_0, at 27°.

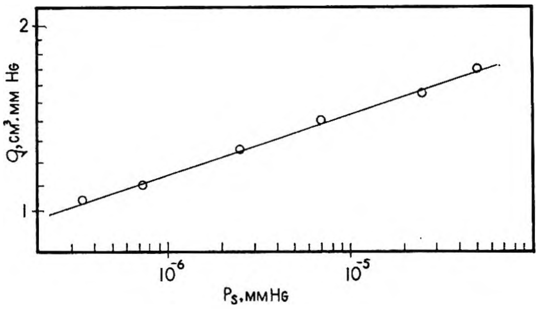

Figure 5. Pressure effect: pressure dependence of the total amount of hydrogen adsorbed, q_T, at 27°.

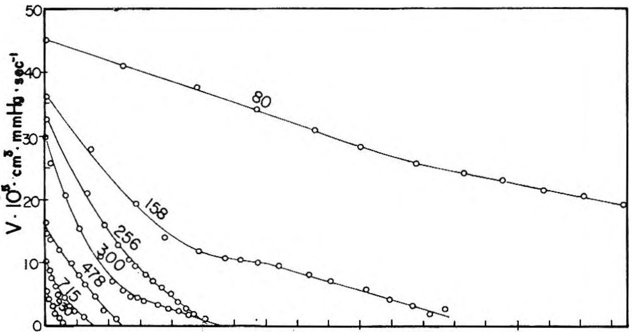

Figure 6. Effect of temperature ($P_s = 7 \times 10^{-7}$ torr). The number next to each plot is the temperature in °K.

higher temperatures show a rapid decline in velocity with increasing amounts of sorption. At the lowest temperature the velocity decrease is nearly constant during the sorption. Some of these results are replotted in Figure 7. The plot of the total amounts sorbed, shown as open circles, *vs.* the temperature

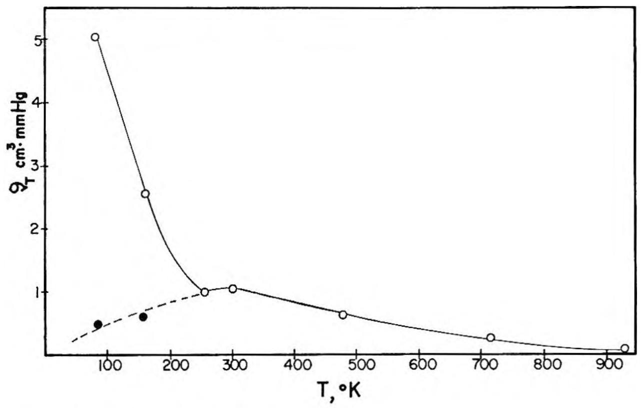

Figure 7. Sorption isobar.

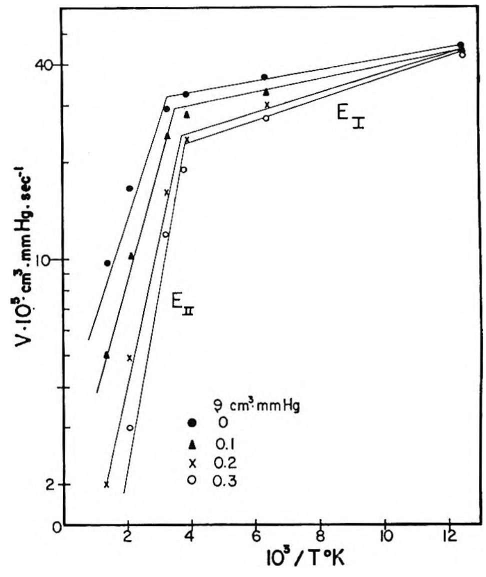

Figure 8. Activation energy.

constitutes an isobar. It indicates that two over-all processes are involved in the hydrogen sorption over the temperature range investigated. The voluminous sorption below about −70° is attributed predominantly to the physical adsorption of molecular hydrogen.

At the end of the sorption of each of the two experiments at the lowest temperatures, the valve P of Figure 1 was opened so that the system could be pumped out readily and valve E was closed. The sample was then degassed for 4 hr at the temperature at which the sorption occurred. The sample was then warmed to 27°, and the amount of hydrogen that was desorbed was measured. Those amounts are shown as filled circles in Figure 7. As physically adsorbed hydrogen is weakly bound, it can reasonably be assumed that all or, at least, most of the physically adsorbed hydrogen was removed by the low-temperature pumping. The residual gas desorbed at 27° was more tightly bound to the surface, and can be ascribed to chemisorption. The region in Figure 7 indicated by the broken line thus can be ascribed to chemisorption. This indicates that chemisorption occurs over the entire temperature range. The existence of one maximum in the vicinity of 27° indicates that only one type of chemisorption is involved.

From the absolute reaction rate theory, the sorption speed can be expressed by

$$N = Qf(\Theta) \exp[E(\Theta)/RT]$$

where N is the number of molecules taken up per unit time, Q is a frequency factor, $f(\Theta)$ is a fraction of the number of sites available for sorption, and $\exp[E(\Theta)/RT]$ is a temperature factor. That expression can be approximated by the relation

$$V = K \exp[E(\Theta)/RT]$$

where V is the speed of sorption in cm^3 mm sec^{-1}, and K is a constant. The values of E calculated for various q values using the plots of Figure 8 are given in Table I. The existence of two processes in two separate temperature regions is indicated. The low-temperature process with negligible E is again ascribed to the physical adsorption of molecular hydrogen. The high-temperature process with an E value varying from 1.25 to 4.27 kcal/mole is ascribed to chemisorption. As there is a chemisorption contribution to the low-temperature sorption at temperatures below the maximum near 27° shown in Figure 7, this may contribute to the small variation of E of the over-all low-temperature sorption.

Table I: E as a Function of Coverage[a]

q, cm^3 mm	0	0.1	0.2	0.3
E_{I}, cal mole^{-1}	80	118	150	200
E_{II}, cal mole^{-1}	1250	1850	2540	4270

[a] The segments E_{I} or E_{II} of the plots of Figure 8 were used to derive values of the energies E_{I} or E_{II}.

The kinetics of the sorption process was unusual in that the widely used Elovich equation[20] was not applicable. It was not possible to fit the kinetic data to an expression of the type

$$q = k_1 \log (t + t_0) + k_2$$

by choosing a suitable value of t_0 in order to linearize the plot, sigmoidal curves being obtained. This suggests that it is not likely that any of the mechanisms proposed to account for Elovichian kinetics would make a significant contribution to the sorption mechanism. It was, however, possible to express the data by an equation

$$q_t = q_{\text{T}}[1 - \exp(ct^n)]$$

where q_t and q_{T} are the amounts adsorbed at time t and at the end of the adsorption. Figure 9 shows that, for data in the temperature region where chemisorption occurs, the fit according to this last equation is good. The fit is poor for the data at the lowest two temperatures, where physical adsorption predominates. The values for the parameters n and c are given in Table II. For chemisorption, the n values can be taken to be constant with an average value of 0.80, differing by about 3%. The c values for chemisorption are taken constant at 0.44. Different values can be calculated for the linear portions of the two low-temperature plots.

Table II: Hydrogen Sorption Kinetics

Temp, °K	n	c
80	1.01	0.43
158	0.96	0.43
256	0.81	0.440
277	0.827	0.438
478	0.77	0.443
715	0.787	0.442

Information on the rate-determining step in a process may frequently be obtained by experiments involving the use of different isotopes. Consequently, some sorption experiments were made with deuterium at −193, 207, and 442° under conditions identical with those made with hydrogen. It was found that the differences between sorption speeds and amounts sorbed for corresponding hydrogen and deuterium experiments fell within the limits of the error encountered with reproducibility, *i.e.*, there was some scatter between corresponding hydrogen and deuterium values, without any specific pattern. Or, the sorptions of hydrogen and deuterium were identical within experimental error, so that either the isotope effect is entirely absent, or it is smaller than about 5%. The complete absence of an isotope effect cannot be claimed, but the effect, if present, is at least an order of magnitude smaller than the predicted value of $2^{1/2}$.

Values of the sticking probability (St.P.), the ratio

---

[20] M. J. D. Low, *Chem. Rev.*, **60**, 262 (1960).

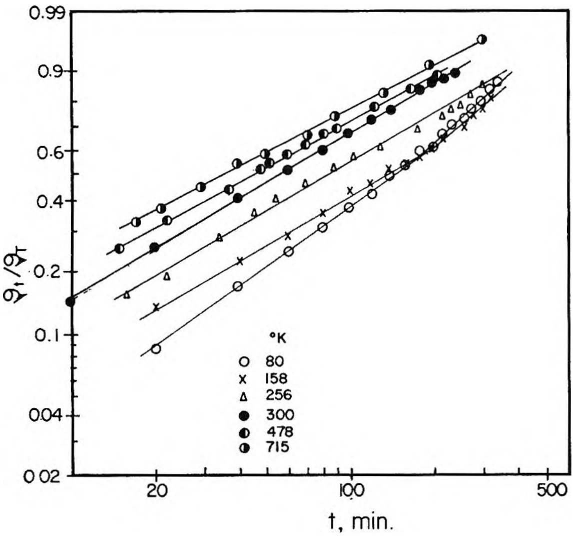

Figure 9. Lateral spreading kinetics. Rate data used to obtain the curves of Figure 6 were recalculated using the lateral spreading equation and are shown as Weibull probability plots.[46]

between the number of molecules taken up and the number striking the surface, can be calculated from[17]

$$\text{St.P.} = \frac{V(MT)^{1/2}(3.74 \times 10^{16})}{P_A(3.51 \times 10^{22})S}$$

where V is the sorption velocity in cm^3 torr sec^{-1}, M is the mass of the hydrogen molecule, P_A is the pressure on the surface, T is in °K, and S is the surface area in cm^2. The calculated sticking probabilities for V_0 vary from 2×10^{-12} to 7×10^{-12} over the temperature range from 427 to $-193°$. These values are considerably smaller than those found with metals; *e.g.*, for nitrogen sorption on tungsten the sticking probabilities varied from 0.55 to 0.1.[21,22] Such low values indicate that collisions with the surface are extremely inefficient in causing sorption, and that most of the surface is inactive for sorption. This is also shown by estimates of the extent to which the surface is covered by adsorbed hydrogen. For 0.2 g of Al_2O_3 having a surface area of 77 m^2/g, using the values of the total amount adsorbed at the various temperatures, the summary shown in Table III results. The number of sites occupied per 1000 A^2 and the fraction of the total surface covered, Θ, were computed on the basis of close packing of one hydrogen atom bound to each available surface O^{2-} ion. A value of 8 A^2 was taken for the area of such an adsorption site.[19] The extent to which the surface is covered is quite small.

Table III: Surface Coverage

Temp, °K	q_T (27°), cm^3 mm	No. of occupied sites/ 1000 A^2	$10^2\Theta$
80	5.04	0.85	1.69
158	2.28	0.38	3.6
256	1	0.17	0.32
300	1.1	0.185	0.37
478	0.5	0.0845	0.14
715	0.244	0.0412	0.11
936	0.11	0.0185	0.05

Discussion

During the course of this work the kinetic data were obtained after very low residual pressures had been reached. This was done in order to obtain "clean" and stable surfaces and also to reduce as much as possible any uncertainty caused by the adsorption of H_2O and CO_2 always present in any low-pressure system as residual gases. In the case of oxides, however, the problem of surface cleaning is not as simple as that found with metals, where rigorously clean surface conditions can be established by the generation of a clean surface by evaporation, the flashing of a ribbon, and the like. In the case of alumina, where a complex and heterogeneous surface exists, problems arise in terms of high-temperature stability, sintering, and particularly of residual surface hydroxyl groups. The latter are probably involved in an equilibrium, $H_2O + O^{-2} \rightleftarrows 2OH^-$, with residual gaseous H_2O, this accounting predominantly for the temperature dependence of the residual pressures observed during outgassing experiments such as those of Figure 2. The amount of residual gases taken up by the surface on cooling to room temperature after high-temperature degassing was small, being of the order of 0.1% of the total amount of hydrogen sorbed at $-193°$. Variations in gettering of this type may be responsible for some of the scatter observed, as in Figure 3, if the reproducibility depends on the establishment of identical equilibrium pressures. The extent of poisoning effects by this means cannot be assessed. The hydrogen sorption became more voluminous with increasing severity of degassing conditions, but the enhancing effect became smaller the higher the degassing temperature. In similar fashion, the dehydroxylation of alumina becomes more complete, but at a declining rate, with increasing severity of degassing.[19] This indicates that the removal of surface hydroxyl groups makes sites available for hydrogen chemisorption. It was found,[7] during a study of the surface of Alon-C aluminum by infrared spectroscopic techniques, that small increases

---

[21] R. E. Schlier, *J. Chem. Phys.*, 29, 1169 (1957).

[22] J. Eisinger, *ibid.*, 28, 169 (1957); 30, 412 (1957).

in the intensities of hydroxyl and deuteroxyl bands occurred on exposure of the alumina to hydrogen and deuterium. Evidence for a net formation of deuteroxyl groups over and above that due to exchange was also reported in a similar study of the exchange of deuterium with the hydroxyl groups of a different alumina.[8] Dissociative chemisorption is thus tied to the formation of surface hydroxyls, at least to some extent. However, the sticking probabilities were decreased and E values increased by very small amounts of adsorbate, so that the chemisorption was "self-poisoning." Also, the degree of surface coverage was low, the number of sites occupied being much smaller than the number of available surface oxide ions, assuming that every adsorbed hydrogen atom formed one hydroxyl group. Random reaction of hydrogen with surface oxide groups to form hydroxyls, replacing those destroyed during degassing, can then be ruled out, and sites of a special nature become necessary.

Dehydrated alumina surfaces have been considered to be strained,[23,24] active sites being identified with strained oxide linkages,[25,26] cation vacancies,[27,28] anion vacancies and exposed aluminum ions,[29] cation vacancies that have captured protons,[30] and anion-cation vacancy pairs.[31] The very complicated nature of the surface has been discussed in detail by Peri.[19,32,33] Pines and Ravoire[4] proposed the heterolytic dissociation of hydrogen or deuterium for the exchange reaction, so that hydride or deuteride adsorbed on an incompletely coordinated aluminum ion while protons and deuterons adsorbed preferentially on surface oxide ions. Acres, Eley, and Trillo[6] similarly suggested that groups of at least two adjacent free valencies are necessary for chemical dissociation of the hydrogen molecule, and Peri suggested paired sites for ammonia adsorption.[33] A variety of mechanisms is thus available. However, it is pertinent to note that the similarity of hydrogen and deuterium chemisorptions indicates that the rate-determining step in the chemisorption is not affected by the mass of the adsorbate.

Previously, the absence of the expected isotope effect with $ZnO \cdot Cr_2O_3$, Ni-kieselguhr, and Cr_2O_3 led Pace and Taylor to suggest that the activation energy of the adsorption process is required by the solid adsorbent.[34] This idea was further developed by Boudart and Taylor[35] and, on the basis of more sensitive measurements with ZnO, by Parravano, Friedrick, and Boudart:[36] the absence of an isotope effect eliminates chemical bombardment-dissociation and also surface diffusion mechanisms for the ZnO case, the slow step being one not involving hydrogen as a molecule or adsorbed fragment but the generation of an active site. Alternately, Kesavulu and Taylor[37] pointed out that these and other effects with ZnO could be explained in terms of a surface step involving an electron transfer and hence not requiring an isotope effect. A similar electronic step may be invoked for the case of alumina. The mechanism, however, is complicated by the nature of the chemisorption kinetics.

A double-logarithmic representation of chemisorption kinetics seems to have been first used by Maxted and Moon[38] to describe the adsorption of hydrogen and of deuterium by platinum, but has been generally neglected. The equation used above has been proposed for the lateral spreading of oxide films on metals,[39-42] the mechanism involving the diffusion of adsorbate away from surface adsorption sites. This model leads to a value of 2 for n for a surface having a fixed number of sites, and to a value of 3 for n for the case of site creation during adsorption.[41,42] Experimental values of n are smaller than unity, as shown in Table III and elsewhere,[38,43-46] indicating that the model is either entirely wrong or that modifications are needed.

In either case, the nature of the adsorption site is speculative. If the lateral spreading mechanism is rejected, then an electronic step is required. A possible

---

(23) W. A. Weyl, *Trans. N. Y. Acad. Sci.*, [2] 12, 245 (1950).

(24) G. A. Mills and S. G. Hindin, *J. Am. Chem. Soc.*, 72, 5549 (1950).

(25) S. G. Hindin and S. W. Weller, *J. Phys. Chem.*, 60, 1501 (1956).

(26) E. B. Cornelius, T. H. Milliken, G. A. Mills, and A. G. Oblad, *ibid.*, 59, 809 (1955).

(27) E. J. W. Verwey, *J. Chem. Phys.*, 3, 592 (1956).

(28) A. Eucken, *Discussions Faraday Soc.*, 8, 128 (1950).

(29) J. B. Peri, *Actes Congr. Intern. Catalyse, 2e, Paris*, 1, 1333 (1961).

(30) D. A. Dowden, *J. Chem. Soc.*, 242 (1950).

(31) S. E. Tung and E. McIninch, *J. Catalysis*, 3, 229 (1964).

(32) J. B. Peri, *J. Phys. Chem.*, 69, 220 (1965).

(33) J. B. Peri, *ibid.*, 69, 231 (1965).

(34) J. Pace and H. S. Taylor, *J. Chem. Phys.*, 2, 578 (1934).

(35) M. Boudart and H. S. Taylor, "L. Farkes Memorial Volume," A. Farkes and E. P. Wigner, Ed., Research Council of Israel, Special Publication No. 1 Jerusalem, 1952, p 223 ff.

(36) G. Parravano, H. G. Friedrick, and M. Boudart, *J. Phys. Chem.*, 63, 1144 (1959).

(37) V. Kesavulu and H. A. Taylor, *ibid.*, 63, 1317 (1959); 66, 54 (1962).

(38) E. B. Maxted and C. H. Moon, *J. Chem. Soc.*, 1542 (1936).

(39) W. A. Johnson and R. F. Mehl, *Trans. AIME*, 134, 416 (1939).

(40) M. Avrami, *J. Chem. Phys.*, 7, 1103 (1939); 8, 212 (1940); 9, 177 (1941).

(41) U. R. Evans, *Trans. Faraday Soc.*, 41, 365 (1945).

(42) U. R. Evans, "The Corrosion and Oxidation of Metals," Edward Arnold Ltd., London, 1960, pp 838 ff, 939 ff.

(43) E. B. Maxted and C. H. Moon, *J. Chem. Soc.*, 1228 (1938).

(44) E. B. Maxted and N. J. Hassid, *Trans. Faraday Soc.*, 29, 698 (1933).

(45) L. J. Hillenbrand, *J. Chem. Phys.*, 42, 4318 (1965).

(46) M. J. D. Low and H. Brown, unpublished results.

Rice[5] showed that for a number of important types of reaction mechanisms the assumption is valid when the above condition is met. A general proof of the conditions under which the steady-state hypothesis is valid has never been given. Such a proof is difficult because the mathematical relations depend on the mechanism of the reaction system. To make the demonstration general, mechanisms must be considered which contain several radicals. Then several expressions of the form of eq 3′ will exist, and their simultaneous solutions may not be possible in an explicit way. A numerical solution is still possible, and in the process of solution the terms involving ϵ are negligibly small.

Therefore, the hypothesis is valid when the results of the rate integrations show that the radical concentrations remain small compared with molecular quantities. During some induction period ϵ in eq 3′ may not be small. For this reason the computer program uses standard integration to explore the induction period and switches to the steady-state method only after it gives acceptable agreement with the direct integration method.

C. Numerical Calculation of Radical Concentrations. According to the steady-state assumption, the right side of eq 3 is set equal to zero for each radical, and the equations are solved for the radical concentrations. In general, this cannot be done explicitly, so Newton's method is used.

Newton's method for solving two simultaneous equations implicit in two variables by iteration is described by Willers.[6a] The method can be generalized to n variables.

The Newton procedure makes use of derivatives of the rate of production of each material with respect to changes in the concentration of each other material. For a specific mechanism expressions for these derivatives could be written down, but for a general numerical procedure they are determined by recalculating each rate from eq 3 for an arbitrary incremental change in each concentration. Another possible approach would be to let the program derive such expressions from the stoichiometric matrix.

The Newton determination of radical concentrations must be carried out at each step in the integration. In addition to the radical concentrations, eq 3 involves the molecular concentrations. These remain constant during the Newton iteration at each point in time. After values for the radical concentrations have been obtained, eq 3 can be evaluated to give the rate of formation of each compound.

Newton's method did not converge unless it was given starting values near the steady-state radical concentrations. This difficulty was overcome by adding a weighting factor to the Newton correction. A weighting formula was obtained by generalizing a formula given by Forsythe[6b] to speed convergence when finding roots of a particular function. That generalized formula is

$$W = 1 - \frac{\Delta x}{|\Delta x| + x} \tag{5}$$

where Δx is the correction computed from Newton's formula. Note that when $0 < x <$ positive root, the weighting function times the computed correction is always less than x, and the procedure cannot diverge. If $x >$ positive root, the weighting function is >1 and the process becomes more unstable although it still converges rapidly when the starting value is close to the root. Fortunately, the induction period calculation always gives starting values for the radicals that are smaller than the steady-state values; therefore, the formula works.

Both the Runga–Kutta and Milne[7] four-point predictor–corrector integration methods were tried. The rate of calculation with both methods is limited by a tendency toward instability, and the calculation was too slow. A marked improvement in calculation rate was obtained by taking advantage of the tendency of the concentrations to become steady. For the radicals, the predictor equation was replaced by a modified Newton interpolation formula containing the mean of the last two computed derivatives. This technique speeded the calculations about 100-fold, while the predicted and calculated radical concentrations agreed to one part per thousand.

Difficulties were traced also to the use of Milne's three-point formula for interpolating concentrations and derivatives when the interval is halved. This formula was replaced by a Newton backward-difference formula based on the first difference and the mean of the two previous second differences

$$C_0 = [C_1 + C_2 + 1.5\Delta t(\dot{C}_1 + \dot{C}_2)]/2 \tag{6}$$

where C is the concentration, $\dot{C}$ is the time derivative of concentration, t is the time increment, subscript 0 refers to the present time, subscript 1 refers to a preceding instant of time, and subscript 2 refers to an instant of time preceding subscript 1. Formula 6

---

(5) O. K. Rice, *J. Phys. Chem.*, **64**, 1851 (1960).

(6) (a) F. A. Willers, "Practical Analysis," Dover Publications, New York, N. Y., 1948, pp 223–225; (b) G. E. Forsythe, *Am. Math. Monthly*, **65**, 229 (1958).

(7) W. E. Milne, "Numerical Solution of Differential Equations," John Wiley and Sons, Inc., New York, N. Y., 1953.

strongly damps out oscillations but still follows any persistent trend in the values.

Every 500 Milne steps a Newton steady-state calculation is tried for the last radical in the list of components. If the concentration of this radical agrees within a given factor with the value from the Milne integration, this radical is assumed to have reached a steady state. If more than one radical is present, the test is applied to each until one that is not steady is found. Then the Milne procedure is continued by using the steady method for these steady radicals. At each 500th step the test is repeated to determine whether other radicals have become steady, until all are steady.

D. Regression of Rate Constants. The program can be used to fit values of rate constants to experimental product distributions. If too many of the constants have to be determined by fitting product distributions, there may be too many unknowns for the number of quantitative restrictions imposed by the data. Therefore, the program is of greatest use when all but a few rate constants are already known. The program includes a regression procedure to fit values for rate constants. A general procedure is derived as follows.

Suppose that a product distribution is computed from assumed rate constants, k_n, and that the results are compared with the experimental points in Figure 2. The problem is to find a set of values for the uncertain rate constants such that the calculated product distribution best fits the experimental points.

Let Δ_i represent the deviation of a product from an experimental point i. These points can be numbered in any arbitrary way, and involve all the important products and reactants. In order to calculate the best fitting values of each k_n, it is necessary to determine the change in product distribution that will result from a change in k_n, $\partial\Delta_i/\partial k_n$. This product distribution change can be determined exactly only by repeating the whole product distribution calculation with a changed value of k_n. This repetition must be done for each rate constant to be fitted, but it would be too costly in computer time.

The computer program does calculate the *rate* of production for each product at successive time intervals. Calculation of the change in these rates resulting from a change in each of the rate constants is a simple matter. The change in product distribution then can be estimated by assuming that the deviation is linear. The production of a product, therefore, is that given by the product distribution calculation plus a difference. This is equal to the mean change in production rate at two instants of time, multiplied by the elapsed time, plus the accumulated difference at the first of these instants of time. The resulting new product distribution curves will give new deviations, Δ_i', from the available experimental points.

If only one k_n at a time is changed, partial derivatives can be computed from

$$\frac{\partial \Delta_i}{\partial k_n} = \frac{\Delta_i' - \Delta_i}{\Delta k_n} \tag{7}$$

The other rate constants are changed, one by one, to compute the other derivatives.

If n rate constants are changed at once, the deviations are

$$\Delta_i' = \Delta_i + \sum_n \frac{\partial \Delta_i}{\partial k_n}\Delta k_n \tag{8}$$

We wish to determine changes Δk in the rate constants to minimize the sum of the squares of the deviations, Δ_i'. The sum of the deviations is

$$\text{sum} = \sum_i (\Delta_i')^2 = \sum_i \left[\Delta_i + \sum_n \frac{\partial \Delta_i}{\partial k_n}\partial k_n\right]^2 \tag{9}$$

To find the minimum, we differentiate with respect to each Δk and set the derivatives equal to zero.

$$\frac{\partial(\text{sum})}{\partial \Lambda k_{\mathrm{e}}} = \sum_i \left[\left(\Delta_i - \sum_n \frac{\partial \Delta_i}{\partial k_n}\Delta k_n\right)\frac{\partial \Delta_i}{\partial k_{\mathrm{e}}}\right] = 0 \tag{10}$$

$$\sum_i \left[\frac{\partial \Delta_i}{\partial k_{\mathrm{e}}}\Delta_i + \frac{\partial \Delta_i}{\partial k_{\mathrm{e}}}\sum_n \frac{\partial \Delta_i}{\partial k_n}\Delta k_n\right] = 0 \tag{11}$$

Here is a system of equations, one for each Δk, designated by subscript e. Each equation involves all of the other Δk's, designated by subscript n. This system can be solved by matrix methods to determine the correction, Δk_{e}, to apply to the rate constants. A new calculation for the product distribution can then be carried out with the corrected rate constants to check the fit with experimental data.

E. Sample Calculations. A trial calculation was made on the simplest type of free-radical reaction mechanism: reactions I, II, and III. This mechanism was discussed by Benson,[8] who derived equations giving the products and free radical concentrations. These results can be compared with the results computed numerically by the program.

The following rate constants were assumed for a temperature of 1000°K.

	Rate constants	
Reaction	Forward	Reverse
I	1.6×10^{-2}	7×10^{-3}
II	6.52×10^{9}	0
III	6.52×10^{9}	0

---

(8) S. W. Benson, "The Foundations of Chemical Kinetics," McGraw-Hill Book Co., Inc., New York, N. Y. 1960, pp 50–54.

data available to him showed two relaxation frequencies (at most) for the 2:2 sulfate solutions instead of the required three. However, Smithson and Litovitz[26] had reported a "middle" relaxation in aqueous $MnSO_4$ solutions at about 30 Mc in addition to the 3- and 200-Mc relaxations reported by Tamm. This was then verified in this laboratory.[22] The existence of all three relaxation frequencies has also been demonstrated[27,28] for aqueous $CoSO_4$. It was then decided to reexamine the classic case of aqueous $MgSO_4$ solutions in an attempt to find a third relaxation peak in addition to the two used by Eigen. In addition, the $MgSO_4$ equilibrium is inherently interesting because of its responsibility for the large excess absorption at ultrasound in sea water. Aqueous $MgSO_4$ solutions have been examined acoustically by several workers in the past 20 years. The pioneering work of Leonard[29] and Liebermann[30] was followed by the more systematic measurements of Bies,[31] Wilson,[32] and Tamm.[33] A very well-defined peak was found with a maximum in the region of 0.15 Mc. In the region above 1 Mc some relatively inaccurate measurements were reported by Beyer, *et al.*, over the range 3–43 Mc.[34] Then Kurtze and Tamm[35] published a second paper showing a second maximum at approximately 200 Mc for a 0.1 *M* solution at about 20°.

In this paper measurements are reported in 0.10, 0.15, and 0.20 *M* solutions at 25° over the frequency range 3–255 Mc.

Experimental Section

Apparatus. The transmitted pulse technique[36] was used for all measurements. For the frequency range 1–60 Mc the apparatus used has been previously described.[37] In the range 40–200 Mc, the apparatus used consisted of a 1-in. path length interferometer cell, a Chesapeake U-100 pulser, an RDO receiver, and a Tektronix 531A oscilloscope. The calibrated comparison signal was obtained from a Hewlett-Packard 608D signal generator pulse modulated by a Dumont 256 AR scope. For the range 100–255 Mc, the Chesapeake pulser-RDO receiver combination was replaced by a Madison PR 201 transmitter-receiver.

The technique consists of displaying the received pulse train on the oscilloscope together with the standard pulse. Initially, the first received pulse and the standard pulse are adjusted to the same amplitude. The standard pulse is then decreased by a given number of decibels and the path length increased until the two signals are again equal. Usually two or three received echos can be used so as to give replicate measurements. A plot of attenuation (decibels) *vs.* distance (centimeters) gives a straight line with the absorption coefficient as the slope.

All measurements were made at 25° with the temperature controlled to ±0.05°. The 1-in. cell used a 0.5-in. diameter X-cut quartz crystal fronted by a 1-in. length quartz delay line as a sender, and a 1-in. diameter X-cut crystal as the receiver. Crystals with fundamentals of 3, 4, 5, 7, 10, 15, and 20 Mc were used. It should be pointed out that in water at 25°, 1 db attentuation requires 20 cm path length at 5 Mc but only 0.077 cm at 255 Mc. This explains the necessity for the specific cell instrumentation for the different frequency ranges.

Materials. The $MgSO_4$ was AR grade dried to its anhydrous form at 200° for 36–48 hr. Analysis of the solutions by ion-exchange techniques confirmed the weighed concentrations within 0.2%. The solvent used was conductance water obtained by passing distilled water through a double ion-exchange column.

Results and Calculations

Measurements of the absorption coefficient were repeated at least twice at each frequency with a fresh solution. The results reported are the averages of the replicate runs. The basic information desired is the excess absorption coefficient per wavelength

$$\mu = (\alpha\lambda - \alpha_s\lambda_s) \qquad (1)$$

where α = absorption coefficient in solution, λ = wavelength in solution, α_s = absorption coefficient in solvent, and λ_s = wavelength in solvent. Since the velocity dispersion is quite small, we let $\lambda = \lambda_s$ and used the data of Greenspan and Tschiegg[38] for the velocity of sound in pure water. For α_s we used the average value determined in this laboratory with the three pulse

---

(26) J. R. Smithson and T. A. Litovitz, *J. Acoust. Soc. Am.*, **28**, 462 (1956).

(27) H. Siegert, *Acustica*, **13**, 48 (1963).

(28) G. Atkinson and S. K. Kor, Physical Chemistry Symposium "Fast Reactions in Solution," Buffalo, N. Y., 1965, to be published.

(29) R. Leonard, P. Combs, and L. Stridmore, *J. Acoust. Soc. Am.*, **21**, 63A (1949).

(30) L. Liebermann, *ibid.*, **20**, 868 (1948).

(31) D. Bies, *J. Chem. Phys.*, **23**, 428 (1955).

(32) O. Wilson and R. Leonard, *J. Acoust. Soc. Am.*, **26**, 223 (1954).

(33) G. Kurtze and K. Tamm, *Acustica*, **3**, 33 (1953).

(34) W. C. Smith, R. E. Barrett, and R. T. Beyer, *J. Acoust. Soc. Am.*, **23**, 71 (1951).

(35) K. Tamm, G. Kurtze, and R. Kaiser, *Acustica*, **4**, 380 (1954).

(36) J. M. M. Pinkerton, *Proc. Phys. Soc.* (London), **B62**, 129, 286, (1949).

(37) G. Atkinson, S. K. Kor, and R. L. Jones, *Rev. Sci. Instr.*, **35**, 1270 (1964).

(38) M. Greenspan and C. E. Tschiegg, *J. Res. Natl. Bur. Std.*, **59**, 249 (1957).

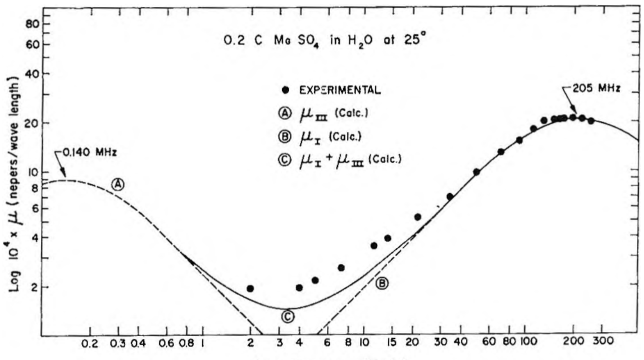

Figure 1.

apparatuses available over the range 1–290 Mc at 25°.

$$\alpha_s/f^2 = \text{constant} = 23.1 \times 10^{-17}\ \text{cm}^{-1}\ \text{sec}^2 \tag{2}$$

The frequencies were determined by a beat method using a standard frequency meter (Gertsch FM-3). Figure 1 shows the relaxation spectra at the highest concentration measured. The high-frequency peak is assigned to μ_{I} and the low-frequency peak to μ_{III}. Using a tentative value for f_{I} and the literature value for f_{III}, we can calculate

$$\mu_{\mathrm{I,III}} = 2\mu_{\mathrm{MI}}\left(\frac{\omega\tau_{\mathrm{I}}}{1+\omega^2\tau_{\mathrm{I}}^2}\right) + 2\mu_{\mathrm{MIII}}\left(\frac{\omega\tau_{\mathrm{III}}}{1+\omega^2\tau_{\mathrm{III}}^2}\right) \tag{3}$$

This curve falls distinctly below the experimental curve in the frequency region 2–35 Mc. It is then possible to fit the curve

$$(\mu_{\mathrm{exptl}} - \mu_{\mathrm{I,III}}) = 2\mu_{\mathrm{MII}}\left(\frac{\omega\tau_{\mathrm{II}}}{1+\omega^2\tau_{\mathrm{II}}^2}\right)$$

This "middle" relaxation is shown in Figure 2.

Using (f_{II}, μ_{MII}) it is now possible to refine the μ_{I} peak. The relaxation frequencies were derived from the measured (μ, f) data by two techniques. The first technique is due to Mikhailov.[39] Here

$$\frac{1}{2v^3}\,\frac{\omega^2}{(\alpha - \alpha_s)} = \frac{\tau\omega^2}{(v_\infty^2 - v_0^2)} + \frac{1}{(v_\infty^2 - v_0^2)\tau} \tag{4}$$

where v = real velocity, v_∞ = "infinite frequency" velocity, and v_0 = "zero frequency" velocity. A plot of $(1/2v^3)\omega^2/[(\alpha - \alpha_s)]$ *vs.* ω^2 gives a straight line. The ratio of the slope to the intercept is τ^2. The second technique simply consists of fitting the (μ, f) data to eq 3 with arbitrary $\mu_{\max}$, $\mu'_{\max}$, τ, and τ' to give the best fit. Table I gives the results of these calculations as well as the results previously obtained for the lowest relaxation by Wilson and Leonard[40] and Kurtze and Tamm.[41] The latter results were obtained by examining both sets of data as a function of concentration and statistically deriving the f_{III} values at the concentrations of interest to us.

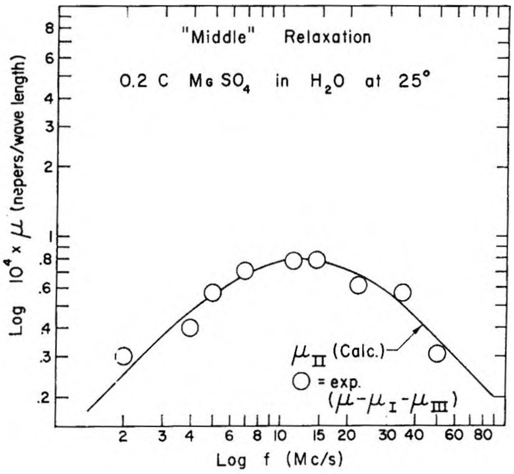

Figure 2.

Two methods of calculating the kinetic parameters from the relaxation data were employed. The first is essentially the method of Atkinson and Kor.[22] The second depends on the concentration dependence of f_{I}.

A. Atkinson and Kor. A three-step association model is assumed. It is then assumed that an equilibrium constant can be calculated for step I by the Bjerrum equation. In step I the ions are assumed to have reached a center-to-center distance of 9.8 A ($r_{\mathrm{Mg^{+2}}} + r_{\mathrm{SO_4^{-2}}} + 4r_{\mathrm{H_2O}}$). This corresponds to the simplest model assumed by Eigen and the above authors and gives a K_{12} (dissociation constant) of 0.0192 l./mole.

As Eigen has shown,[42] the equations relating the

Table I: Relaxation Parameters in Aqueous $MgSO_4$ at 25°

	C, *M*		
	0.09889	0.1493	0.1965
f_{I}[a]	170	192	205
$10^4\mu_{\mathrm{MI}}$[b]	7.2	17.5	21.3
f_{II}[a]	11.3	12.0	12.4
$10^4\mu_{\mathrm{MII}}$[b]	0.5	0.5	0.8
f_{III}[a]	0.133	0.137	0.140
$10^4\mu_{\mathrm{MIII}}$[b]	4.5	6.8	9.0

[a] In Mc/sec. [b] In nepers/wavelength.

---

(39) I. G. Mikhailov, *Dokl. Akad. Nauk USSR*, **89**, 991 (1953).

(40) O. Wilson and R. Leonard, Technical Report 4, ONR Contract N6 onr, UCLA 27507.

(41) G. Kurtze and K. Tamm, *Acustica*, **3**, 33 (1953).

(42) M. Eigen and L. De Maeyer in "Techniques of Organic Chemistry," Vol. VIII, Part 2, A. Weissberger, Ed., John Wiley and Sons, Inc., New York, N. Y., 1963, p 895 ff.

relaxation times to the rate constants for the three-step process are

$$2\pi f_{\mathrm{I}} = k_{21} + k_{12}^{0}\theta(C) \qquad (5)$$

$$\theta(C) = \sigma C \gamma_{\pm}^{2}\left[2 + \frac{\partial \ln \gamma_{\pm}^{2}}{\partial \ln \sigma}\right] \qquad (6)$$

where σ = degree of dissociation, $\gamma_{\pm}$ = mean ionic activity coefficient, C = electrolyte concentration.

$$2\pi f_{\mathrm{II}} = k_{32} + k_{23}\left[\frac{\theta(C)}{K_{12} + \theta(C)}\right] \qquad (7)$$

$$= k_{32} + k_{23}\Phi(C)$$

$$2\pi f_{\mathrm{III}} = k_{43} + k_{34}\left[\frac{\Phi(C)k_{23}}{k_{32} + \Phi(C)k_{23}}\right] \qquad (8)$$

We now assume that the $\gamma_{\pm}$ are given by an extended form of the Debye–Hückel theory. Since Brubaker has shown this to be quite good for an unassociated 2:2 salt,[43] this seems like a reasonable assumption for the free ions. Using the assumed K_{12} and Debye–Hückel expression, $\theta(C)$ is calculated by a series of successive approximations using a small computer program. Equations 5, 7, and 8 can then be used to calculate the six rate constants for the three steps.

B. Refined Method. The refined technique merely consists of taking the k_{12}^{0} and k_{21} values derived above and calculated K_{12} from

$$K_{12} = \frac{k_{21}}{k_{12}^{0}} \qquad (9)$$

This K_{12} is then fed back into procedure A. The cycling is continued until output K_{12} equals input K_{12}. The procedure converges quite rapidly so that even if the original assumed K_{12} were off by an order of magnitude, convergence is obtained in three cycles or less.

We can define the equilibrium constants for the stepwise process by

$$K_{12} = \frac{k_{21}}{k_{12}} \qquad (10)$$

$$K_{23} = \frac{k_{32}}{k_{23}} \qquad (11)$$

$$K_{43} = \frac{k_{43}}{k_{34}} \qquad (12)$$

and

$$K_{\Sigma}^{-1} = \frac{1 + K_{34} + K_{23}K_{34}}{K_{12}K_{23}K_{34}} = K_{\mathrm{A}} \qquad (13)$$

Table II contrasts the results of this work with those of Eigen. Since Eigen only had the f_{I} and f_{III} relaxations to work with, he had to assume a superposition of f_{I} and f_{II}.

Table II: Kinetic Parameters for $MgSO_4$ Association in H_2O at 25°

	Eigen–Tamm	This work
k_{12}^{0}, M^{-1} sec^{-1}	4.6×10^{10}	2.8×10^{10}
k_{21}, sec^{-1}	8×10^{8}	5.6×10^{8}
K_{12}, M^{-1}	0.017	0.020
k_{23}, sec^{-1}	1×10^{9}	7.2×10^{7}
k_{32}, sec^{-1}	5×10^{8}	3.7×10^{7}
K_{23}	0.5	0.51
k_{34}, sec^{-1}	1×10^{5}	1.4×10^{6}
k_{43}, sec^{-1}	8×10^{5}	8.0×10^{5}
K_{34}	7.5	5.8
K_{Σ}^{-1}	197	165
K_{A} (conductance)	169	169

Discussion

The first step of the association process (step I) has been attributed to a diffusion-controlled reaction. The rate constants for such a reaction have been calculated by Debye[44] and Eigen[45] as

$$k_{12}^{0} = \frac{4\pi N_{\mathrm{A}} Z_1 Z_2 \epsilon^2}{DkT} \frac{(\mathfrak{D}_1 + \mathfrak{D}_2)}{\left[\exp\left(\frac{Z_1 Z_2 \epsilon^2}{aDkT}\right) - 1\right]} \quad \text{mole}^{-1}\ \text{cm}^3\ \text{sec}^{-1} \qquad (14)$$

and

$$k_{21} = \frac{3Z_1 Z_2 \epsilon^2}{DkTa^3} \frac{(\mathfrak{D}_1 + \mathfrak{D}_2)}{\left[1 - \exp\left(-\frac{Z_1 Z_2 \epsilon^2}{aDkT}\right)\right]} \ \text{sec}^{-1} \qquad (15)$$

where Z_1 and Z_2 are the charges on the ions, $\mathfrak{D}_1$ and $\mathfrak{D}_2$ are the diffusion coefficients, and N_{A} is Avogadro's number. a is the distance to which the two ions approach one another in the diffusion-controlled step.

On examining Table II it is clear that our experimental value of k_{12}^{0} is very close to that calculated by Eigen from the known diffusion coefficients of $MgSO_4$. The equilibrium constant K_{12} found experimentally was 0.020 corresponding to a Bjerrum distance of 10.4 A. This is quite close to the 9.8 A assumed by Kor and Atkinson in their $MnSO_4$ work and lends credence

---

(43) C. H. Brubaker and P. G. Rasmussen, *J. Phys. Chem.*, **67**, 330 (1963).

(44) P. Debye, *Trans. Electrochem. Soc.*, **82**, 265 (1942).

(45) M. Eigen, *Z. Physik. Chem.* (Frankfurt), **1**, 176 (1964).

to the model that the product of step I is a solvent-separated ion pair with a separation equal to that given by two water molecules. It seems obvious that there are more complex arrangements of water molecules that would give the same distance.

Table III contrasts the kinetic parameters for steps II and III in the cases of $MnSO_4$ and $MgSO_4$. Step II presents the greatest contrast between Eigen's results and our results. This is due completely to our measurement of the "middle" relaxation. Since step III is substantially lower in frequency than step II, the two calculations agree very nicely here.

Table III: Comparison of $MgSO_4$ and $MnSO_4$

	$MgSO_4$ (this work)	$MnSO_4$[22]
k_{23}, sec^{-1}	7.2×10^7	6.9×10^7
k_{32}, sec^{-1}	3.7×10^7	18.5×10^7
K_{23}	0.51	2.7
k_{34}, sec^{-1}	1.4×10^5	4.8×10^7
k_{43}, sec^{-1}	8.0×10^5	13.5×10^6
K_{34}	5.8	0.28

An examination of Table III shows that k_{23} is essentially the same for the two salts.[46] This step (step II) seems primarily dependent on the anion and the insensitivity of k_{23} to cation implies an SN1-type mechanism for this forward rate. If step II is anion dehydration, step III is cation dehydration. Internal evidence was available to support this in the case of Mn^{+2} where k_{34} is virtually identical with the rate of water exchange on Mn^{+2} as measured by O^{17} nmr.[47] This again implies an SN1-type mechanism. This internal check is not available for Mg^{+2} but consistency insists that the k_{34} of 1.4×10^5 sec^{-1} gives us a very good idea of the water exchange rate on Mg^{+2}.

It should now be pointed out that the back rates (k_{32} and k_{43}) and, so, the equilibrium constants (K_{23} and K_{34}), reflect the individual character of the cation involved.

We now summarize our present view of association in aqueous $MgSO_4$ and $MnSO_4$. The process takes place in three steps: step I, the diffusion-controlled approach of the M^{+2} and SO_4^{-2} ions to form a solvent separated ion pair; step II, an ion-pair desolvation step whose forward rate depends on the rate of solvent exchange on the anion; step III, an ion-pair desolvation step leading to a contact ion pair. The forward rate of this step depends on the rate of solvent exchange on the cation.

It should be noted that the above scheme is only applicable in the case where the rates of the ($k_{12} \gg k_{23} \gg k_{34}$) three steps are substantially different. Both the data treatment process and the interpretation must be altered in the more complex case where the rate constants for two (or more) steps differ by less than a factor of 10. The work of Eigen and Tamm and preliminary work in this laboratory show this to be the case in aqueous $CuSO_4$ and $ZnSO_4$.

As a final check on the approach presented here we can compare the over-all association constant calculated from the ultrasonic data with that calculated from conductance data[48] using the Fuoss–Onsager theory for data treatment. Here we find that K_{Σ}^{-1} (ultrasonics) = 165 and K_A (conductance) = 169. The agreement is really much better than the precision of the ultrasonic results would lead one to expect. However, the agreement is good and indicates that the conductance measurements find that none of the three types of ion pairs contribute to the conductance of the solution.

The authors feel that even though the detailed results to date are on a limited number and restricted type of electrolyte solution, they indicate an exceptionally valuable approach to the resolution of many electrolyte problems. It seems obvious that the relaxation approach so brilliantly developed by Eigen and his co-workers can yield the type of information needed to go beyond the confines of the continuum solvent model. The continuum model gives very useful results as long as we are considering ions separated by distinct layers of solvent molecules. However, once the ions approach the point where their primary solvation shells touch, we must acknowledge the inadequacy of the continuum solvent model. The cases where the continuum model gives unambiguous results are most fruitfully looked upon as degenerate cases where the rates of solvent exchange on the ions are of the same order as the rate of diffusion-controlled approach. The most generally significant parameter that emerges from the relaxation method approach is the rate of exchange of solvent molecules in the primary solvation sphere of the ion. Unfortunately, it is, in general, an extremely difficult parameter to obtain by direct measurement.

We are now applying the ultrasonic absorption technique to 1:1 salts in solvent mixtures in an attempt

---

[46] This has also proved to be true for aqueous $CoSO_4$; to be published.

[47] R. F. Cornick, "Advances in the Chemistry of Coordination Compounds," S. Kirschner, Ed., The Macmillan Co., New York, N. Y., 1961, p 15.

[48] C. W. Davies, *J. Chem. Soc.*, 2093 (1938).

These include the opportunity to establish the formation of gaseous desorption products and the amounts of such products formed, to relate these amounts to metal surface area, and further to study the kinetics of their formation. In the present case, a small bakeable mass spectrometer was used to identify the desorption products.

Experimental Section

The reaction cell was of conventional design (Figure 1), *i.e.*, a 250-ml flask with four outlets, the omegatron, ion gauge, gas supply, and diffusion pump. The cell and vacuum gauges could be isolated from pumps and gas source by a ground-glass valve and a variable leak, respectively. Two ion gauges were used in this work. One was a conventional Bayard-Alpert (BA) gauge[6] with a tungsten filament; the other was a BA gauge with a lanthanum boride coated tungsten filament.[7] The partial pressure analyzer was a Leybold omegatron[8,9] mass spectrometer tube. The ion gauge and the omegatron were connected to the reaction cell through 25-mm tubulation. The ion current from the BA ion gauge was amplified and recorded on a Model 3S Moseley x–y recorder, and the ion current from the omegatron was measured with a vibrating-reed electrometer and recorded. The response time of the omegatron–electrometer system is too long to be suitable for kinetic studies with the flash filament technique, although it is quite suitable for the identification of desorption products of mass less than 30 amu. When iridium was dosed with acetylene or ethylene at 100°K and flashed, the rate of desorption of physically adsorbed gas was so great that the omegatron and associated circuitry could not respond sufficiently rapidly to follow it; these experiments were repeated in a similar apparatus in which the omegatron was replaced by a General Electric Model 514 partial pressure analyzer mass spectrometer. The gauge constants for both gauges, 5 mm^{-1} for the tungsten filament gauge and 3.6 mm^{-1} for the lanthanum boride coated filament, are in good agreement with Hickmott's[7] value of 4.4 mm^{-1}. The top part of the reaction cell was a reentrant-type dewar which could be filled with the proper coolant to maintain the filament at a given temperature during adsorption. Liquids used for this purpose were liquid nitrogen (~100°K) and water (300°K).

The temperature of the filament was determined by using the filament as a resistance thermometer. The temperature dependence of resistance of the sample filament was determined by measuring the resistance of the filament when it was immersed in various constant-temperature baths covering the temperature range 77 to 640°K. In a desorption experiment, the filament was heated by a constant current, and the voltage drop across the filament, for a given current, was a direct measure of the resistance and, hence, the temperature of the filament.

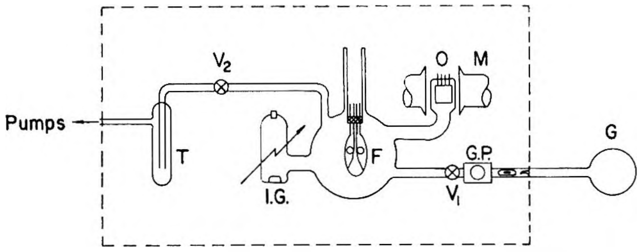

Figure 1. Flash filament desorption spectrometer. Dotted line surrounds bakeable portion. V_1 and V_2, magnetically controlled ball joint valves; F, 5-mil iridium filament; T, liquid nitrogen trap; I.G., Bayard–Alpert ion gauge; M, magnet, 3250 gauss; O, omegatron; G, gas supply; G.P., Granville–Phillips valve.

The hydrogen used was Reagent Research grade obtained from the Matheson Co. in 1-l. flasks with break-off tips. Ethylene (Matheson chemically pure, reported by the manufacturer to be 99.8% pure) and acetylene (Matheson) were passed through a Dry Ice–acetone trap, then further purified by repeated freezings and evacuations at 77°K. Gases were then sealed in ampoules equipped with break-off tips, and the ampoules were sealed onto the vacuum system.

When the filament had been annealed and the pressure in the cell had been reduced to 10^{-10} mm, the break-off tip was broken and the gas was admitted to the system through a Granville–Phillips valve until the pressure was about 10^{-8} mm. The filament was again flashed to 2200°K and then held either at 77 or at 300°K for varying periods of time (results presented are for 8-min dose times unless otherwise specified).

Following the adsorption interval, the reaction cell (including the BA ion gauge and the omegatron) was isolated from the pumps by closing the magnetically operated ground-glass valve, the filament was then flashed at the desired heating rate, and the change in the ion current (pressure) was recorded as a function of time. (Constant current flashing resulted in a temperature–time dependence approximately of the form

---

(3) (a) R. W. Roberts, *J. Phys. Chem.*, **67**, 2035 (1963); (b) *ibid.*, **68**, 2718 (1964).

(4) G. Ehrlich, *J. Appl. Phys.*, **32**, 4 (1961).

(5) G. Ehrlich, *Advan. Catalysis*, **14**, 255 (1963).

(6) R. T. Bayard and D. Alpert, *Rev. Sci. Instr.*, **21**, 571 (1950).

(7) T. W. Hickmott, *J. Chem. Phys.*, **32**, 810 (1960).

(8) H. Sommer, H. A. Thomas, and J. A. Hipple, *Phys. Rev.*, **82**, 697 (1957).

(9) D. Alpert and R. S. Buritz, *J. Appl. Phys.*, **25**, 202 (1954).

$1/T = a + bt$. For a given flash, therefore, dT/dt is not constant. Relatively slow flash rates were used in systems giving multiple peaks to improve their resolution.)

It was found that hydrogen was rapidly pumped during a flash desorption experiment when the pressure increase was monitored with the tungsten filament ion gauge. Separate experiments showed that this pumping rate could not occur through the ground-glass valve. Hydrogen pumping was, therefore, attributed to the hot tungsten filament in the ion gauge; this behavior is to be expected according to the observations of Hickmott.[7,10]

Mass spectra were obtained with the conventional BA ion gauge operated at 0.4-ma emission current and with this ion gauge off. No appreciable difference was found in the cracking patterns indicating that there is no change in the gas phase composition. Very likely, some cracking occurred on the hot filaments, with the hydrogen produced being rapidly pumped by the filament.

The tungsten filaments in the ion gauge were operated at 2500° for 24 hr in an ambient of 10^{-6} mm of oxygen to remove the carbon in the ion gauge filaments. This treatment was necessary to reduce the formation of CO formed by a complex sequence of reactions[11] involving carbon dissolved in the tungsten filament, hydrogen, and oxygen from the glass in the cell walls.

The desorption spectra of hydrogen were analyzed by the method described by Ehrlich,[4] and the heats of desorption for the various species in the desorption spectra of ethylene and acetylene were obtained by using Redhead's[12] treatment.

Results

When hydrogen dosed on iridium at 100°K was flash desorbed with fast pumping for maximum resolution, two desorption peaks were observed (low-temperature α and high-temperature β) as shown in Figure 2. This indicates that hydrogen adsorbed on iridium at 100°K exists in at least two states. Only a single peak, presumably corresponding to the β state, is observed in the flash desorption spectrum from a filament dosed at 300°K. Detailed kinetic and exchange experiments to be reported elsewhere indicate that hydrogen is adsorbed atomically in both states and that the activation energy for desorption from the β state varies from 24 to 18 kcal mole as coverage varies from 40×10^{12} to 230×10^{12} molecules/cm^2.

Typical flash desorption curves for iridium dosed with ethylene for 8 min at 5×10^{-8} mm are shown in Figures 3 and 4. Figure 3 shows that a desorption process occurs from iridium dosed with ethylene at

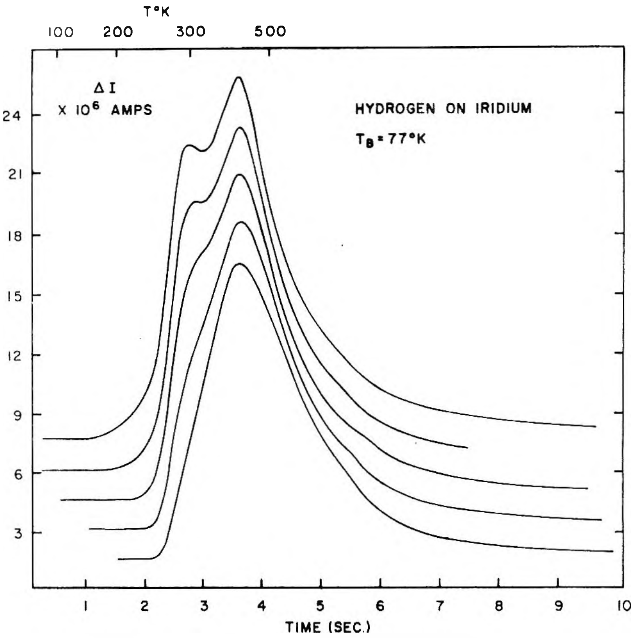

Figure 2. Flash desorption of hydrogen dosed on iridium at 77°K at 5×10^{-8} torr for various dosing times. Curves are translated vertically to avoid overlap. Dosing times, increasing from bottom curve to top curve, are 2, 3, 4, 5, and 6 min.

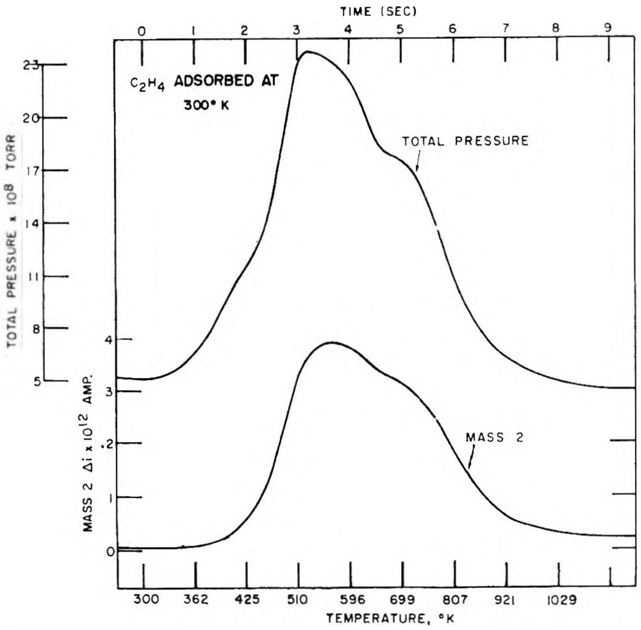

Figure 3. Flash decomposition of C_2H_4 dosed on iridium at 300°K. Total pressure and mass 2 bursts.

---

(10) T. W. Hickmott, *J. Appl. Phys.*, **31**, 128 (1960).

(11) J. A. Becker, E. J. Becker, and R. G. Brandes, *ibid.*, **32**, 411 (1961).

(12) P. A. Redhead, *Vacuum*, **12**, 203 (1962).

served a similar triplet in irradiated KNO_3 with a nearly isotropic g factor and hyperfine splittings (g_{av} = 2.005, A_{iso} = 41 gauss) which has been attributed by Symons[12] to NO_3^{2-}.

If the concentration of nitrate is reduced to 10^{-2} M, then the blue color and esr spectrum associated with trapped electrons are observed in both the photochemical and radiation chemical systems. Subsequent bleaching with visible light results in an increase in the signal attributed to NO_3^{2-} in both systems. Further illumination with 2537-A light causes the change to NO_2 described above. Warming experiments show that the O^- peak disappears below 150°K, whereas both of the species responsible for the rest of the spectrum are stable up to the softening point of the glass.

Neutral Ice Containing NO_3^-. The γ-irradiated neutral ice containing 0.5 M $NaNO_3$ yields an esr spectrum which has contributions from OH, NO_3^{2-}, NO_2, and possibly NO_3. The last species is revealed when the sample is warmed above 110°K. Its spectrum is a singlet of about 10-gauss width situated at g = 2.015 and has been previously observed by Ershov, *et al.*,[13] and by Kevan.[7] Spectra attributed to NO_3 have been observed in γ-irradiated lead nitrate,[14] potassium nitrate,[15] and urea nitrate[16] single crystals. Quoted values for g_{av} are 2.019, 2.017, and 2.013, respectively, with considerable anisotropy. The nitrogen hyperfine splittings vary from 2 to 10 gauss. Our spectrum is compatible with these values assuming considerable rotational freedom for NO_3 at 110°K. The only indication of g-anisotropy is the considerable broadening of this spectrum when the annealed sample is reexamined at 77°K. Unlike Kevan, we also observed the presence of NO_3^{2-} in this system and our spectrum corresponds more closely to that published by Ershov, *et al.*

When a similar neutral ice sample containing nitrate and ferrocyanide is irradiated for several hours, the only spectrum observed is that of NO_2. A similar spectrum is obtained when 10^{-2} M NNN'N'-tetramethyl-p-phenylenediamine (TMPD) is irradiated with ultraviolet light in a methanol glass containing 0.5 M $LiNO_3$.

Acid Glasses Containing NO_3^-. The formation of NO_2 is observed in γ- or ultraviolet-irradiated sulfuric acid glasses containing NO_3^- ions (and Fe_{aq}^{2+} in the case of ultraviolet irradiation). It is not possible to be certain whether NO_3 is present because of overlap from the spectrum of the acid residue, attributed to SO_4^- or to $-SO_2-O$.[4] However, Ershov, *et al.*, have observed NO_3 in γ-irradiated 1 N nitric acid at 77°K and it is very likely that it is present to a smaller extent in our system. No NO_3^{2-} is observed in acid glasses. Hydrogen atoms are observed but are depleted in the presence of nitrate when compared with a sample without additive.

Alkaline Glasses or Neutral Ice Containing NO_2^-. Similar experiments were conducted in alkaline and neutral aqueous media by replacing nitrate with nitrite. The results, together with those from nitrate, are listed in Table I. In γ-irradiated alkaline glasses, a central line at g = 2.005 ± 0.002 is observed which increases in size when e_t^- is photobleached. We assign this peak tentatively to NO_2^{2-} although the esr spectrum of this species is not well established. The observed g factor is in reasonable agreement with that of a species observed in irradiated KNO_3 (g_1 = 2.008, g_2 = 2.010, g_3 = 2.005; g_{av} = 2.008). This was attributed originally[11b] to NO but reinterpreted as NO_2^{2-} by Atkins and Symons.[10] The line width of our spectrum is also compatible with the average hyperfine splitting of 13 gauss for the species observed in KNO_3. In the corresponding ultraviolet-irradiated system, a poor spectrum is obtained with a broad high-field component and is mostly uninterpretable. However, it is possible to identify NO_2 by the presence of the extreme high-field peak of NO_2. In neutral ice containing nitrite, only NO_2 and OH are distinguishable in the γ-irradiated sample, and only NO_2 in the photochemical system. In all the systems involving ultraviolet irradiation, spectra were obtained only in the presence of a reducing solute (Fe^{2+}, $Fe(CN)_6^{4-}$, or TMPD).

Discussion

The observations on neutral and alkaline glasses containing nitrate ions suggest that in these media the initial reaction of a thermal electron with nitrate ions is given by (1). This suggestion is supported by the

$$e^- + NO_3^- \longrightarrow NO_3^{2-} \qquad (1)$$

following evidence: (1) the blue color and the esr spectrum of trapped electrons may be suppressed by a sufficiently high concentration of nitrate ions; (2) in the presence of a smaller concentration of nitrate, the trapped electrons may be remobilized by photolysis with visible light, this process being accompanied by an increase in the esr spectrum of NO_3^{2-}. Furthermore, the change from NO_3^{2-} to NO_2 during ultraviolet irradiation of the γ-irradiated glasses explains the absence of NO_3^{2-} from the spectrum observed

---

(12) P. W. Atkins and M. C. R. Symons, *J. Chem. Soc.*, 4794 (1962).

(13) B. G. Ershov, A. K. Pikaev, P. Ya. Glazunov, and V. I. Spitsyn, *Dokl. Akad. Nauk SSSR*, **154**, 899 (1964).

(14) M. Golding and M. J. Henchman, *J. Chem. Phys.*, **40**, 1554 (1964).

(15) H. Zeldes and R. Livingston, *J. Chem. Phys.*, **37**, 3017 (1962).

(16) G. W. Chantry, A. Horsfield, J. R. Morton, and D. H. Whiffen, *Mol. Phys.*, **5**, 589 (1962).

Table I: Species Identified by Esr Spectra in Irradiated Aqueous Systems Containing NO_3^- or NO_2^- at 77°K

Matrix	Solute	Type of irradiation	Species trapped
8 M NaOH	10^{-2} M $NaNO_3$	γ	e^-, O^-, NO_2, NO_3^{2-} [a,b]
	10^{-2} M $NaNO_3$ 10^{-2} M $K_4Fe(CN)_6$	Ultraviolet	e^-, O^-, NO_2[a,b]
H_2O	0.5 M $NaNO_3$	γ	OH, NO_2, NO_3, NO_3^{2-}
	0.5 M $NaNO_3$ 10^{-2} M $K_4Fe(CN)_6$	Ultraviolet	NO_2
6 M H_2SO_4	10^{-2} M $NaNO_3$	γ	H, SO_4^-, NO_2, NO_3(?)
	10^{-2} M $NaNO_3$ 10^{-2} M $FeSO_4$	Ultraviolet	H, SO_4^-, NO_2, NO_3(?)
8 M NaOH	$<10^{-1}$ $NaNO_2$	γ	e^-, O^-, NO_2, NO_2^{2-}(?)[c]
	0.5 M $NaNO_2$ 10^{-2} M $K_4Fe(CN)_6$	Ultraviolet	O^-, NO_2, NO_2^{2-}(?)
H_2O	0.5 M $NaNO_2$	γ	NO_2, OH
	0.5 M $NaNO_2$ 10^{-2} M $K_4Fe(CN)_6$	Ultraviolet	NO_2

[a] Postirradiation with visible light causes decrease in e^- and increase in NO_3^{2-}. [b] Postirradiation with ultraviolet light causes decrease in NO_3^{2-} and increase in NO_2. [c] Postirradiation with visible light causes decrease in e^- and increase in NO_2^{2-}. Postirradiation with visible or ultraviolet light has no effect on other systems.

when electrons are generated by the ultraviolet irradiation of glasses containing $Fe(CN)_6^{4-}(aq)$ or tetramethyl-*p*-phenylenediamine. Both solutes are photoionized, but in these systems reaction 1 is followed immediately by

$$NO_3^{2-} \xrightarrow{\text{ultraviolet}} NO_2 + O_{aq}^{2-}\ (\longrightarrow 2OH^-) \quad (2)$$

Reaction 2 may also occur during γ irradiation; *i.e.*, "radiation bleaching" may occur to some extent and could be responsible for the production of some NO_2 in such systems. However, it is more likely that NO_2 is formed directly by reaction of one or more of the oxidizing species H_2O^+, OH, or O^-. Kevan[7] has presented kinetic evidence in favor of reaction 3, and the

$$\begin{tikzcd} H_2O^+ + NO_3^- \arrow[rr] & & NO_3^* + H_2O \arrow[dl] \arrow[d] \\ & NO_3 & NO_2 + O \end{tikzcd} \quad (3)$$

observation of NO_3, NO_2, and OH in neutral systems supports this view. However, the formation of NO_3 would be explained equally well by reaction 4 for which there is direct evidence in the work of Ershov, *et al.*[13] These workers observed the conversion of OH to NO_3 during the thermal annealing of frozen neutral nitrate solutions. It may be significant that no NO_3 is found

$$OH + NO_3^- \longrightarrow NO_3 + OH^- \quad (4)$$

in strongly alkaline systems in which OH is likely to be converted largely to O^-. This suggests that the formation of NO_2 from H_2O^+ should be written according to (5), without NO_3^+ as an intermediate, and that all of the NO_3 arises from (4). This view is supported

$$H_2O^+ + NO_3^- \longrightarrow NO_2 + 2OH \text{ (or } H_2O + O) \quad (5)$$

by evidence from the gas-phase decomposition of N_2O_5 in which intermediate NO_3 decomposes into NO + O_2 rather than NO_2 + O. (OH radicals formed in (5) would, of course, appear as O^- in alkaline systems.)

Strictly analogous reactions may be written for neutral and alkaline glasses containing nitrite ions, though in these systems NO_2^{2-} ions do not appear to be

$$e^- + NO_2^- \longrightarrow NO_2^{2-} \quad (6)$$

$$H_2O^+ + NO_2^- \longrightarrow NO_2 + H_2O \quad (7)$$

$$OH + NO_2^- \longrightarrow NO_2 + OH^- \quad (8)$$

converted to NO_2 by ultraviolet irradiation. Thus, the slow formation of NO_2 in an ultraviolet-irradiated neutral ice containing nitrite and ferrocyanide ions presents a problem. There is evidently no trace of NO_2^{2-} and it is believed that the only oxidizing species present is $Fe(CN)_6^{3-}(aq)$. While it is well known that

$$Fe(CN)_6^{3-} + NO_2^- \longrightarrow Fe(CN)_6^{4-} + NO_2 \quad (9)$$

reaction 9 takes place in aqueous solution at room temperature, it is surprising that it can occur at 77°K where both species are thought to be immobile. However, there is evidence to suggest that electron transfer processes occur in the solid state between reactants separated by a considerable distance. For example, of the α' peaks in acetylene decomposition (which are, however, markedly smaller for acetylene than for ethylene), and the observed α'/β' peak height ratio is greater at 300°K than at 100°K, not less as the model implies. The model also fails to account for the appearance of methane in the flash decomposition products from ethylene; since the methane is a minor product, this failure is less serious. The appearance of acetylene and ethylene at low flash temperatures is easily accounted for by desorption of physically adsorbed species, and the appearance of ethylene in flash desorption products from ethylene-dosed filaments over the temperature range 400–600°K may be most simply attributed to desorption of chemisorbed ethylene.

The reaction sequence 1–3 can be readily modified to account semiquantitatively for the discrepancies between its predictions and observations. Suppose that there are two principal faces (*e.g.*, (111) and (100)) on the metal surface and that on one of them, say face A, the reaction proceeds as indicated in reactions 1–3. On the other face, say face B, the reaction sequence is

$$\mathrm{CH_2{=}CH_2} \longrightarrow \mathrm{C_2(adsorbed)} + 4\underset{*}{\mathrm{H}} \tag{1'}$$

$$\mathrm{CH{\equiv}CH} \longrightarrow \mathrm{C_2(adsorbed)} + 2\underset{*}{\mathrm{H}} \tag{3'}$$

$$2\underset{*}{\mathrm{H}} \longrightarrow \mathrm{H_2} \tag{2}$$

This reaction sequence is intended to imply that ethylene and acetylene chemisorb with complete dissociation of hydrogen at temperatures substantially below the temperature of rapid hydrogen desorption. It is known[2] that the chemisorbed hydrocarbons are immobile on iridium at least up to 700°K, so that equilibration of hydrocarbon between faces A and B would not be expected. On the other hand, hydrogen is completely mobile on iridium above 200°K, so that equilibration of hydrogen between faces A and B would be expected and desorption of hydrogen would occur in the α' peak whether dosed on face A or face B. Suppose equal amounts of ethylene were chemisorbed on faces A and B; the α'/β' peak height ratio on flash desorption would be 3. For the case of acetylene, the corresponding ratio would be 1. These ratios are approximately those observed. Further, since the chemisorption reaction on face B is more extensive, it is not unreasonable to suppose its rate slower at 100°K than the chemisorption rate on face A. Hence, when the filament is flashed after a given dosing period, desorption of physically adsorbed hydrocarbon would occur principally from face B, and so the α'/β' peak height ratio would be less for 100°K dosing than for 300°K dosing.

Roberts[3] has reported the decomposition of ethylene on clean iridium films at 27 and 100°, finding methane and ethane as principal products with only a small amount of hydrogen appearing during the early part of the reaction. These results are radically different from ours, but Roberts' reaction conditions are likewise radically different; for the dosing conditions cited, his ambient pressures must have been in the region of 10^{-3} torr whereas ours were of the order 10^{-8} torr. Under these circumstances, rates of impact of gaseous species with the surface would be greater in his experiments by a factor 10^5 than in ours. The difference in results suggests a mechanism for catalytic hydrogenation which, so far as we are aware, has not previously been proposed. The proposed sequence is

$$\underset{****}{\mathrm{CHCH}} + \mathrm{CH_2{=}CH_2(g)} \longrightarrow \mathrm{C_2(adsorbed)} + \mathrm{C_2H_6(g)} \tag{4}$$

$$2\underset{*}{\mathrm{H}} + \mathrm{C_2(adsorbed)} \longrightarrow \underset{****}{\mathrm{CHCH}} \tag{5}$$

This is intended to imply a direct transfer of hydrogen atoms from chemisorbed acetylene to an ethylene molecule colliding with it from the gas phase. The reaction would be somewhat analogous to diimine hydrogenation of olefins, which has been recently reviewed by Hünig, Müller, and Thier.[14] The $\mathrm{C_2}$(adsorbed) residue would then react with chemisorbed hydrogen by the reverse of reaction 3 to regenerate chemisorbed acetylene. Obviously, a similar set of reactions could be based on chemisorbed ethylene rather than on chemisorbed acetylene. This mechanism accounts readily for the fact that Roberts observed ethane and little hydrogen, whereas we observed hydrogen but not ethane, in the decomposition of ethylene on iridium. According to the mechanism, the rate of ethane production in Roberts' experiments would be greater than in ours by a factor 10^5.

---

(14) S. Hünig, H. R. Müller, and W. Thier, *Angew. Chem.*, **4**, 271 (1965).

electric constant. Since the process of proton transfer in HF leaves an excess of fluoride ions, a solution of sodium fluoride was studied as a control.

Experimental Section

In general, techniques for the vacuum line manipulation and optical studies with anhydrous hydrogen fluoride have been reported elsewhere,[3] and material reporting the latest refinements developed at Argonne is in preparation. For the research described in this paper, a rather simple Raman cell was used, fabricated from some 0.75-in. o.d. polychlorotrifluoroethylene extruded tubing 0.030 in. thick. Split-ring metal compression type of fittings permitted the attachment of a valve fabricated from the same plastic to one end and a sapphire window to the other end of the tubing so that no metal was in contact with the solution. This tube was then used with the 19-mm standard optics for the Cary 81 Raman spectrophotometer.

The hydrogen fluoride was distilled as described elsewhere.[4] The organic materials were reagent grade chemicals. The diethyl ether and dioxane were dried with lithium aluminum hydride and were distilled, and the absolute alcohol was dried with calcium oxide and was similarly purified. Solutions were prepared in a vacuum line largely fabricated from polychlorotrifluoroethylene, much as described in references cited above. Solutions were made up by weight and transferred directly into the Raman cell connected to the vacuum line through a Y arrangement.

Observations

The observations of the Raman spectrum of anhydrous HF have often been obscured by the presence of a broad fluorescent band. When the 4358-A Hg line is employed, as in this work, the maximum is found at a Raman displacement of about 3000 cm^{-1}. A number of additives, particularly such reactive halogen fluorides as BrF_5 and the noble gas compound XeF_4, have been observed to repress this fluorescence. Until very recently, we were not able to establish to what extent this behavior was inherent in hydrogen fluoride and to what extent it was a function of fluorescent impurity in the reagent. Recently, samples of pure anhydrous hydrogen fluoride have been obtained with very much lower intensities observed for this fluorescent peak, and we now believe that pure anhydrous hydrogen fluoride is essentially free of fluorescence radiation.

Most of the batches of hydrogen fluoride used in this series of measurements did have an appreciable fluorescence background, and intensities in general were measured above this background.

The observation that there is no identifiable band spectrum in anhydrous hydrogen fluoride is equivalent to suggesting the absence of a reasonable concentration of any single identifiable species. Presumably, the individual hydrogen fluoride fragments are associated and are in reasonably mobile equilibrium. For many organic solutes added to hydrogen fluoride, the most important chemical process is the proton transfer leaving an excess of solvated fluoride ion, *e.g.*, $C_2H_5OH + (HF)_n \rightarrow C_2H_5OH_2^+ + (HF)_{n-1}F^-$. The possible spectrum of such a solvated fluoride ion can be readily studied by adding sodium fluoride. We did, indeed, look at the Raman spectrum of such solutions and found they were indistinguishable from that of pure hydrogen fluoride; that is to say, there were no identifiable bands. We then conclude that the presence of fluoride ions in the system is not associated with the production of any identifiable molecule, although additional infrared bands are observed associated with the expected shifts in hydrogen fluoride bonding.[3c]

Raman spectra were recorded for mixtures of anhydrous hydrogen fluoride and diethyl ether, ethyl alcohol, dioxane, and tetrahydrofuran. For diethyl ether and ethyl alcohol, the entire range of concentration was successfully explored. For dioxane, good Raman spectra were observed in the organic-rich end, but with high concentrations of hydrogen fluoride the background was high, and most weak Raman bands could not be observed. Similarly with tetrahydrofuran, solutions containing more than about 50 mole % hydrogen fluoride could not be adequately studied, in this case because the solutions were colored (from pale yellow to deep red depending on time and concentration).

Complete tables of the observed Raman bands are available.[5] A few of the bands noted in diethyl ether and ethanol solutions are cited in Tables I and II to illustrate the correlation of Raman spectrum and proton transfer.

Discussion

The analysis of the Raman spectrum of a 15-atom molecule (diethyl ether) is complex[6] and the rather subtle effect of an acidic environment on this spectrum is being considered in detail and will be reported elsewhere.

---

[3] (a) J. J. Katz, and H. H. Hyman, *Rev. Sci. Instr.*, **24**, 1066 (1953); (b) R. H. Mayberry, J. J. Katz, and S. Gordon, *ibid.*, **25**, 1133 (1954); (c) R. M. Adams and J. J. Katz, *J. Mol. Spectry.*, **1**, 306 (1957); (d) H. H. Hyman, L. A. Quarterman, M. Kilpatrick, and J. J. Katz, *J. Phys. Chem.*, **65**, 123 (1961); (e) H. H. Hyman and J. J. Katz, "Non-Aqueous Solvent Systems," T. C. Waddington, Ed., Academic Press Inc., London, 1965, p 47.

[4] L. A. Quarterman, H. H. Hyman, and J. J. Katz, *J. Phys. Chem.*, **61**, 912 (1957).

[5] Copies may be obtained from H. H. Hyman, Argonne National Laboratory, 9700 South Cass Ave, Argonne, Ill. 60439.

[6] Y. Mashiko, *Nippon Kagaku Zasshi*, **80**, 593 (1959).

Table I: Changes in Relative Intensity of Raman Bands Associated with Proton Transfer in Anhydrous Hydrogen Fluoride Solutions of Diethyl Ether

	Relative intensity[a]			
	Concn of diethyl ether, mole %			
$\Delta\nu$	100	34	20	5
380	14	5	N.O.[b]	N.O.
390	N.O.	N.O.	28	36
442	113	47	12	9
790	N.O.	N.O.	12	26
1000	N.O.	N.O.	16	24
1155	59	19	N.O.	N.O.

[a] I at $\Delta\nu$ = 1460 taken as 100. [b] N.O. = not observed.

Table II: Changes in Relative Intensity of Raman Bands Associated with Proton Transfer in Anhydrous Hydrogen Fluoride Solutions of Ethanol

	Relative intensity[a]		
	Concn of ethanol, mole %		
$\Delta\nu$	100	66	30
350	N.O.[b]	2.5	10
395	N.O.	5	13
450	14	N.O.	N.O.

[a] I at $\Delta\nu$ = 890 taken as 100. [b] N.O. = not observed.

This discussion will be confined to the effects of proton transfer. We note that for diethyl ether, a solution containing 34 mole % ether shows no Raman bands attributable to a spectroscopically identifiable ion. The electrical conductivity observations[7] indicate a concentration of protonated ether ions well under 0.01 M, so that this observation is not surprising. This does not imply the absence of a significant interaction between diethyl ether and hydrogen fluoride. However it will take the form

$$(C_2H_5)_2O + (HF)_n \rightleftharpoons (C_2H_5)_2O\cdots H\cdots F(HF)_{n-1}$$

rather than $(C_2H_5)_2OH^+ + F(HF)_{n=1}^-$.

The 20 mole % ether, with about 20 times this ionic concentration, has a readily identifiable ionic Raman spectrum. The bands whose intensities are substantially reduced are bands which have been attributed to bending or stretching vibrations involving the C–O–C bonds. Presumably, the new bands derive from similar vibrations of the protonated molecules.

In the solvent of higher dielectric constant, ethanol, even a 66 mole % solution and an effective ionic concentration of perhaps 0.05 M seems to provide an adequate concentration of identifiable ionic species.

As mentioned above, neither dioxane nor tetrahydrofuran is a satisfactory solute for Raman studies in the high HF concentration region. Colored solutions are found with the latter and a high background with the former. In each case it is presumed that some reaction is involved in addition to proton transfer. It is worth noting however, that in the concentration regions studied, dioxane, as expected, shows only the slight modification of intensity and frequency shift associated with hydrogen bonding to the oxygen, while tetrahydrofuran is like alcohol and some additional lines are observed, presumably associated with proton transfer and ionization.

---

(7) L. A. Quarterman, H. H. Hyman, and J. J. Katz, *J. Phys. Chem.*, 65, 90 (1961).

Reversing Intramolecular Kinetic Carbon Isotope Effect in the Gas Phase Decomposition of Oxalic Acid

by Gabriel Lapidus,[1a] Donald Barton,[1b] and Peter E. Yankwich

Noyes Laboratory of Chemistry, University of Illinois, Urbana, Illinois 61801 *(Received March 28, 1966)*

The intramolecular C^{13} kinetic isotope effect has been measured between 127 and 180° in the decomposition to carbon dioxide and formic acid of oxalic acid-h_2 vapor at an initial pressure of 0.9 mm. This isotope effect, like that observed with oxalic acid-d_2, and like the intermolecular hydrogen isotope effect, is small and is so strongly temperature dependent that it inverts within the experimental range. The carbon isotope effect for the ordinary acid decomposition appears to be simple above 156°. The similarity of the inversion temperatures of the carbon and hydrogen isotope effects lends support to the postulate that the inversion phenomenon arises in the accessibility to the reaction of more than one path, not in isotopic differential effects themselves.

Introduction

Recently, we have reported on the hydrogen[2a] and carbon[2b] kinetic isotope effects in the vapor phase decomposition of oxalic acid. Though the hydrogen intermolecular isotope effect was measured *comparatively*, and the carbon intramolecular effect *competitively* on $(COOD)_2$, both exhibited similar characteristics: they were found to be relatively small, to have anomalously large temperature dependence, and, because of the latter, to invert in sense within the experimental temperature range. The deuterated acid was employed in the earlier carbon isotope effect study to eliminate or reduce to insignificance the possible influence of a statistical inverse isotope effect, should the *ca.* 1-mm initial pressure of the vapor lie well into the *low-pressure* region for the reaction. In this paper we report the extension of these experiments to ordinary oxalic acid, $(COOH)_2$.

Experimental Section

Reagent. Fisher analytical grade anhydrous oxalic acid was purified further by vacuum sublimation at 110°; samples were stored *in vacuo* over magnesium perchlorate until used.

Apparatus, Procedure, and Isotope Analyses. These were identical with those employed in the study of the oxalic acid-d_2 decomposition.[2b]

Notation and Calculations. The isotopic rate constant ratio sought was $(k_2/k_3)_H$ in the notation of Lindsay, McElcheran, and Thode.[3]

$$\begin{array}{ll} C^{13}OOH \xrightarrow{(k_2)_H} C^{13}O_2 + HC^{12}OOH & (1) \\ \vert & \\ C^{12}OOH \xrightarrow{(k_3)_H} C^{12}O_2 + HC^{13}OOH & (2) \end{array}$$

Though the reaction was run essentially to completion, it can be shown that for product collection up to any time t

$$\frac{(X_C)_t}{(X_F)_t} = (k_2/k_3)_H \qquad (3)$$

where $(X_C)_t$ is the mole fraction of $C^{13}O_2$ in carbon dioxide product collected up to t, and $(X_F)_t$ is the corresponding mole fraction of $HC^{13}OOH$ derived from measurements on carbon dioxide obtained by combustion (in a Pregl-like apparatus) of the formic acid product.

Results

The results obtained at seven temperatures are collected in Table I. The first figure at each tempera-

---

[1] (a) Research associate, 1960–1963; (b) visiting assistant professor, 1960–1962.

[2] (a) G. Lapidus, D. Barton, and P. E. Yankwich, *J. Phys. Chem.*, **70**, 407 (1966); (b) *ibid.*, **70**, 1575 (1966).

[3] J. G. Lindsay, D. E. McElcheran, and H. G. Thode, *J. Chem. Phys.*, **17**, 589 (1949).

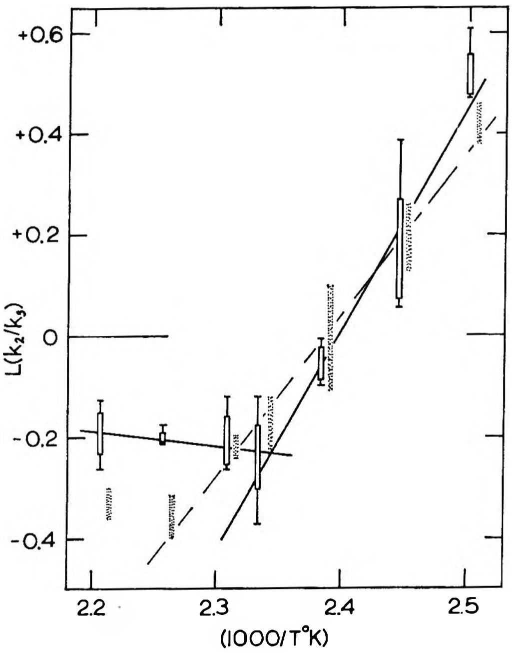

Figure 1. Influence of temperature on $(k_2/k_3)_{\rm obsd}$: ———, oxalic acid-h_2 (open rectangles encompass the average deviations; short horizontal bars indicate the extremal results at each temperature); – – – –, oxalic acid-d_2 (shaded rectangles, shifted 0.008 to right to avoid overlap, encompass average deviations).

ture in the last column refers to the present experiments on oxalic acid-h_2; the second figure (in parentheses) is for oxalic acid-d_2.[2b] The appended errors are average deviations from the mean. All of these results are plotted in Figure 1 as $L(k_2/k_3)$[4] *vs.* $(1000/T)$; the open points represent the data for the ordinary oxalic acid; the shaded points represent results obtained with the deuterated acid and have been shifted 0.008 to the right to eliminate the overlap arising in the use of identical run temperatures in the two investigations. The mean precision of individual $(k_2/k_3)_{\rm H}$ values is estimated to be ±0.0005.

Several least-squares fitted lines are drawn through the data plotted in Figure 1. The light dashed line through the oxalic acid-d_2 results has the equation[4]

$$L(k_2/k_3)_{\rm D} = (3.20 \pm 0.14)\theta - (7.61 \pm 0.34) \quad (4)$$

(The point at 180° was considered deviant and ignored in the calculation of this equation.) The heavier solid lines represent the results for $L(k_2/k_3)_{\rm H}$ derived from Table I for the four lowest and the four highest temperatures; their equations are
low temperatures

$$L(k_2/k_3)_{\rm H} = (4.37 \pm 0.32)\theta - (10.46 \pm 0.77) \quad (5)$$

high temperatures

$$L(k_2/k_3)_{\rm H} = -(0.32 \pm 0.26)\theta + (0.51 \pm 0.59) \quad (6)$$

$$= -(0.070 \pm 0.057)\theta^2 + (0.15_0 \pm 0.29_6) \quad (7)$$

Within the respective temperature ranges, the mean deviations of the experimental points from the least-squares lines are ±0.08 in L for eq 5 and ±0.04 in L for eq 6; from eq 4, one can calculate the apparent inversion temperature to be 145 ± 8°.

Table I: Intramolecular Isotope Effect in $(\text{COOH})_2(g)$ Decomposition

Run temp, °C	$(k_2/k_3)_{\rm H}$	Av $(k_2/k_3)_{\rm H}$ (Av $(k_2/k_3)_{\rm D}$)
126.6	1.0060_6	
	1.0047_2	
	1.0050_5	
	1.0049_5	
	1.0048_4	$1.0051_7 \pm 0.0004_0$
	1.0053_7	$(1.0041_7 \pm 0.0004_0)$
134.1	1.0009_8	
	1.0019_8	
	1.0007_8	
	1.0038_8	
	1.0022_6	
	1.0006_1	
	1.0005_7	$1.0017_2 \pm 0.0009_8$
	1.0026_8	$(1.0019_4 \pm 0.0006_3)$
146.4	0.9999_3	
	0.9990_3	$0.9994_5 \pm 0.0003_2$
	0.9993_8	$(0.9999_6 \pm 0.0010_2)$
155.6	0.9974_1	
	0.9979_5	
	0.9975_8	
	0.9962_9	$0.9976_0 \pm 0.0006_2$
	0.9987_9	$(0.9982_5 \pm 0.0005_1)$
160.0	0.9988_0	
	0.9973_7	
	0.9982_4	
	0.9973_8	$0.9979_3 \pm 0.0004_7$
	0.9978_6	$(0.9978_2 \pm 0.0002_0)$
170.0	0.9978_8	
	0.9978_8	
	0.9982_5	
	0.9979_1	$0.9979_8 \pm 0.0001_1$
	0.9979_9	$(0.9964_1 \pm 0.0004_1)$
180.0	0.9985_8	
	0.9977_5	
	0.9979_5	
	0.9987_3	$0.9980_8 \pm 0.0004_0$
	0.9973_8	$(0.9966_9 \pm 0.0003_0)$

---

(4) $L(x) = 100 \ln (x)$; $\theta = 1000/T(°\text{K})$.

spherical molecules equivalent to the hard-sphere or 6–12 potential fluids characterized by the fluid branch of the molecular dynamics and Monte Carlo calculations. The diffusion process in this model is assumed to occur by "jumps" of molecular dimensions made possible by the momentary increase in size of the "cage" of neighboring molecules in which the molecules are normally confined. The increase in cage dimensions to the critical size necessary for diffusion to occur arises by the redistribution of "free volume." When the free volume is defined as that volume which can be redistributed among the "cages" without change in over-all energy, it is possible to evaluate the transition (or jump) probability and thereby to arrive at the relation, eq 3, which is nearly equivalent to the empirical Doolittle equation for viscosity

$$D = D_0 \exp\left(-\frac{\gamma v^*}{v_f}\right) \tag{3}$$

where γ is a cage volume overlap factor, v^* is the critical increase in cage volume, and v_f is the total free volume. By making the additional intuitively satisfying assumption that the glass transition arises from the effective disappearance of free volume ($v_f \rightarrow 0$; $\therefore D \rightarrow 0$, $\eta \rightarrow \infty$) which occurs at T_0, and identifying v_f with the total thermal expansion of the liquid above T_0, eq 2 in the form

$$D = D_0 \exp\left[-\frac{\gamma v^*}{\bar{v}_m \alpha (T - T_{0p})}\right] \tag{4}$$

results. ($\bar{v}_m$ is the mean molecular volume; α is the mean coefficient of expansion over the range $T - T_0$).

The above concept of free volume and free volume disappearance is easy to accept for the hard-sphere fluid where all nonoverlapping configurations have the same energy. Here $v_f = 0$ would correspond to the close-packed volume ($p_{T=\mathrm{const}} \rightarrow \infty$) of the *fluid* branch. It can also be rationalized for the 6–12 potential liquid[7b] and, by analogy, for the simple ionic liquid.[3b] We have previously sought to interpret the validity of eq 2 for the ionic liquid systems we have studied in terms of this model, but have had difficulty in reconciling the experimental value of k (eq 2) with the value expected from eq 4 and the measured expansion coefficient. Also, it is difficult to see why k should be constant when the expansion coefficients vary from system to system, although a possible rationalization has been suggested.[3d] Measurements of the effect of pressure on relaxation properties have not been in accord with free volume model predictions.[22,23] The model may be criticized for considering only the contribution to diffusion of molecular diameter sized jumps; the criticism is strengthened by the most recent molecular dynamics result which shows that at least for hard spheres, there is no characteristic jump distance in fluid diffusion.[24] Also, it is difficult to see how the zero energy free volume redistribution concept can apply to molecularly complex systems (*e.g.*, with chain molecules). Such systems are nevertheless those whose conformity to eq 2, or to the equivalent WLF equation, is best documented.

An alternative theory leading to eq 2, which cannot be criticized either on the grounds of restrictive mechanisms or of inapplicability to complex systems, has recently been proposed by Adam and Gibbs.[6c] In this theory, the intuitive appeal of Cohen and Turnbull's idea connecting glass transition and free volume disappearance at T_0 has not been lost. Rather, it is replaced by the even more appealing proposition that the essential liquid state characteristic which becomes zero at the temperature T_0 is the *configurational entropy* of the liquid. Furthermore, where the free volume disappearance at T_0 was an assumption in Cohen and Turnbull's model, in the Adam–Gibbs theory the vanishing entropy comes as a central result of a successful statistical mechanical theory of chain polymer liquids at high particle densities,[6a,25] which can presumably be generalized to include nonpolymeric liquids.

In the development of their theory for relaxation properties of glass-forming liquids in the neighborhood of the glass transition temperature, Adam and Gibbs took the view that translational motion of a given molecule (or segment of a molecule) occurs, in a manner which need not be specified, by the cooperative rearrangement of a group of molecules. The temperature dependence of the translational process was then shown to be the result of the effect of temperature on the minimum size of the cooperatively rearranging groups. By making only the assumption that the cooperatively rearranging groups operated independently, *i.e.*, did not interact significantly, it was possible to show that the minimum (critical) size of the cooperatively rearranging group could be expressed in terms of the

---

[22] A. Gilchrist, J. E. Early, and R. H. Cole, *J. Chem. Phys.*, **26**, 196 (1957).

[23] S. B. Brummer, *ibid.*, **42**, 1636 (1965).

[24] B. J. Alder and T. Einwohner, *ibid.*, **43**, 3399 (1965).

[25] In this theory, the disappearance of the configurational entropy produces a second-order thermodynamic transition, which was shown to have all the characteristics of the glass transition. The fact that particular second-order transition equations are obeyed at the glass transition temperature[8,10] lends some support to the theory. Its success in predicting the dependence of T_g on molecular properties in polymer systems has been striking.[6a,9]

macroscopic configurational entropy. On showing that this smallest cooperative region must be that involved in the great majority of transitions, there resulted for the average transition probability, $\bar{w}(T)$, the expression

$$\bar{w}(T) = \bar{A} \exp\left(-\frac{C}{TS_c}\right) \qquad (5)$$

where $\bar{A}$ and C are constants, T is the absolute temperature, and S_c is the configurational entropy. This expression should therefore contain the important part of the temperature dependence of any of the familiar mass transport processes.

Introducing the experimental fact that the specific heats of the glass-forming liquids are approximately independent of temperature, and the theoretical result that $S_c = 0$ at T_0, it could then be shown that, for $[(T - T_0)/T_0]^2 << 1$

$$D, \Lambda T, \phi T, \text{etc.} \propto w(T) = A \exp\left(-\frac{C}{\Delta C_p(T - T_0)}\right) \equiv A \exp\left(-\frac{k}{(T - T_0)}\right) \qquad (6)$$

with

$$C = \frac{\Delta\mu s_c^*}{R/N} \qquad (7)$$

where ΔC_p is the difference in glassy and liquid state specific heats, $\Delta\mu$ is taken as the potential energy hindering the cooperative rearrangement, s_c^* is the configurational entropy of the critical-size cooperative region, and R/N is the Boltzmann constant.

Equation 2 ($\equiv$eq 6[26]) is thus seen to be the necessary consequence of the effect of temperature on the thermodynamic state of the liquid (which may or may not be in a metastable state with respect to some crystalline state) *and should therefore apply irrespective of specific liquid structure.* Although, in the Cohen–Turnbull model, the $1/(T - T_0)$ temperature dependence arises in essentially the same way through the disappearance at T_0 of a vital liquid-state characteristic, the above conclusion would not follow unless the free volume redistribution energy could be shown to be zero, independent of structure. An important feature of the Adam–Gibbs theory is therefore that it shows that any distinction between crystallizing and noncrystallizing liquids, on the basis of structural complexity, is largely irrelevant as far as the use of the noncrystallizing liquids to obtain information on "low-temperature" transport behavior is concerned. The validity of eq 2 for a variety of ionic[3] and complex molecular[6c] liquids is good evidence for this point.

With this point in mind, it is possible to say that, if Gibbs and co-workers are correct, then molten salt chemists seeking to establish rules governing the transport behavior of ionic liquids in the "normal" temperature range have been working at a serious disadvantage. *If the essential characteristic of the liquid state, viz. its configurational entropy, does not vanish before T_0, then the temperature range from the melting point down to T_0 is as equally valid a part of the liquid state as the range melting point to boiling point: to date, then, investigators of the post-melting point range have not had the benefit of any understanding of the behavior of this lower part of the ionic liquid range on which to build.* A parallel, which will be explored in more detail in a subsequent publication, may be drawn to the difficulties of understanding the specific heat of solids without information covering the range 0–200°K. An immediate suggestion of this line of thought is that the usual distinction made between the behavior of glass-forming oxide melts and that of common molten salts is largely artificial. At thermodynamically equivalent temperatures (see below), fused salts and oxide melts in fact behave in much the same way, but while the oxide melts have, for practical reasons, been much studied in their "low-temperature regions," fused salt studies have been confined principally to the high-temperature (post-melting point) range.

Let us therefore reproduce in summary what has been learned about transport behavior in the "lower half" of the ionic liquid state by the studies referred to in the opening paragraph, and consider to what extent the Adam–Gibbs theory can be used, through these data, to give perspective to previous observations on high temperature behavior.

In Figure 1 the slope of the ordinary Arrhenius plot for electrical conductance, in the familiar guise of an "activation energy," is plotted as a function of temperature for various systems, some of which are glass-forming. Were the Arrhenius equation to be obeyed, these plots would, of course, be straight lines parallel to the abscissa, as is approximately the case at the high temperatures. In Figure 2, we show how all the curves of Figure 1 coincide when the "activation energies," in this case corrected by an amount of the order of 1 kcal to correspond to the temperature dependence of a diffusion process,[3b] are plotted against the function T/T_0, where T_0 is obtained from the best

---

[26] R. Araujo (*J. Chem. Phys.*, **44**, 1299 (1966)) has now shown that using eq 5, *i.e.*, avoiding the approximations made in the subsequent derivation of eq 6, the viscosity of B_2O_3 (which has abnormal specific heat characteristics) may be described accurately over a much wider temperature range (800°) than is possible using eq 2. This success with B_2O_3, which had previously seemed an anomalous case, encourages belief in the validity of the Adam–Gibbs approach.

To reproduce the isotope effects observed in the inversion region, there must compete with the high-temperature path one or more others with which are associated isotope effects of the sense and magnitude of those characteristic of models near A-1; in no other way can one obtain the drastic temperature dependence observed in the region of reversal.[2b] We have not carried out calculations more sophisticated than the above, and these simple results do nothing to establish that a possible heterogeneous mechanism involve transition states like those of types A or B. However, the importance of planarity to the suggested models increases in the order B-1 → B-2 → A-1 → A-2; further, a heterogeneous mechanism dependent upon adsorption would decrease in importance with increasing temperature. These two considerations interact to lead one to the conclusion that a path through an activated complex like A-1 might well be favored on a surface, while a path through a transition state configuration approximately B-1.2 is more likely to be typical of reaction in the body of the gas.

The original kinetics investigations[2a,12] covered the short temperature range 127–157° while the carbon isotope effect experiments extend to 180°; there is in the former thus no reflection of the kinetic complexity postulated to account for the results reported here. The present results support the conclusion that the large temperature dependences which lead to reversal of the carbon and hydrogen isotope effects arise not in isotopic differential phenomena but in mechanistic complexity.[21]

Acknowledgments. Mrs. Nancy Neilson performed the mass spectrometric analyses. The assistance of Mr. James E. Harmon and Mr. Lawrence E. Kraut in bringing this and the two preceding publications[2] to the submission stage is deeply appreciated. This research was supported by the U. S. Atomic Energy Commission, COO-1142-66.

---

[20] The structures A-1 and B-1 are conventional in that bonds affected by the reaction are shown with orders halfway between those characteristic of the reagent and the product states. Transition states more reagent-like yield isotope effects closer to zero for both types of structures. Transition states more product-like and having the A-type reaction coordinate yield isotope effects larger than those shown for A-1. For the B-type reaction coordinate, increasing the product likeness of the transition state moves the predicted value of $L(k_2/k_3)$ downward from the band shown for B-1 toward a limit lying somewhat above the band for B-2; the vicinity of this limit is indicated by the light dashed line in Figure 2.

[21] The fact that both the carbon and the hydrogen isotope effects exhibit inversion with increasing temperature is likely an accident; there is no *a priori* expectation that the sense of a hydrogen intermolecular isotope effect and that of its carbon intramolecular relative will correspond. The fact that the inversion temperature for (k_H/k_D) and those for the (k_2/k_3) are similar is likely another accident; such similarity requires symmetry in the senses and relative magnitudes of the two kinds of isotope effects, a situation likely to be unusual of occurrence.

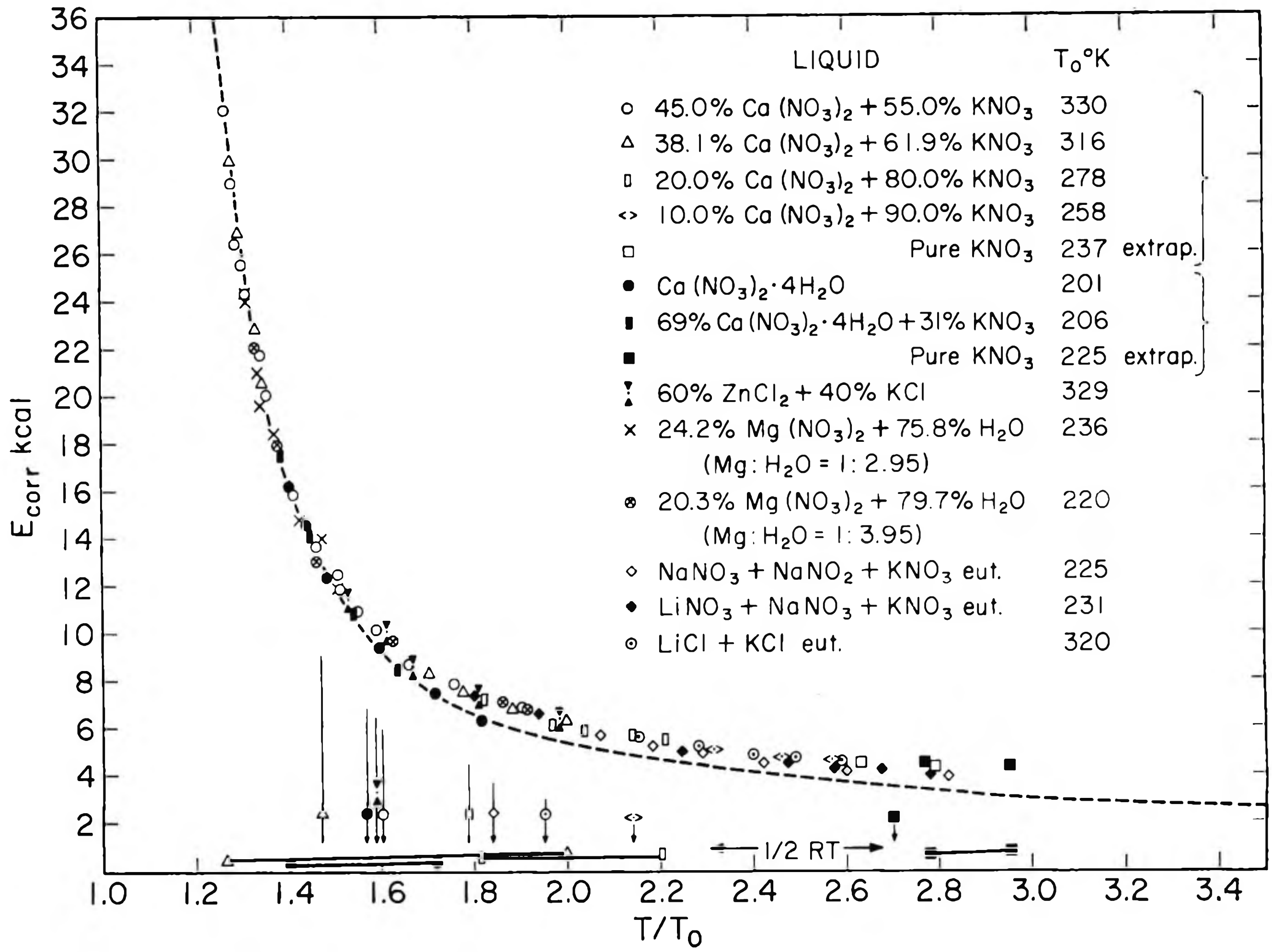

Figure 2. Plot of temperature dependence of electrical conductance, represented by E_{cor}, as a function of T/T_0 for various fused salt systems: dashed line is plot predicted by eq 2 for k = 680°K. For some of the melts T/T_0 values at the liquidus temperature are indicated by arrows. Effect of $T^{1/2}$ term in preexponential on computed E_{cor} shown at base of diagram.

some vindication of the previously empirical use of the T_0-based corresponding temperature scale in a discussion of diffusion–conductance relations in fused salts.[31] The general usefulness of such a corresponding temperature scale, however, remains to be demonstrated; the possibilities will be touched on in the concluding remarks.

With the help of Figure 2, we can now explain our use of the term "low temperature" in connection with the region of the liquid state whose importance we are attempting to establish. A liquid can, arbitrarily, be thought of as being in its "low-temperature region" when $T/T_0 \lesssim 2$. Consequently, a given Centigrade temperature may be "low" for one liquid but not for another, depending on the relative T_0 values. In view of the above discussion, "low temperature" in this sense would clearly be better read as "low entropy." Liquidus temperatures below $T/T_0 = 2$ are uncommon but are presumably a feature of all of the systems of Table I.

It remains to consider how general the ability of the Adam and Gibbs equations to describe transport in ionic liquids may prove. For instance, the plots of Figure 1 can only be expected to superpose as in Figure 2 if the constant k of eq 2 has the same value for the different systems. In the Adam–Gibbs theory, this constant contains the energy term $\Delta\mu$, (eq 7) and Gibbs suggests[32] that for ionic liquids $\Delta\mu$ should be a suitable function of the relevant cation–cation and cation–anion pair interaction energies and an effective coordination number. There is therefore some question as to why the coincidence should be as good as it appears to be. To account for the similar consistency

---

[31] C. A. Angell, *J. Phys. Chem.*, **69**, 399 (1965).

[32] J. H. Gibbs, private communication.

was calibrated by measurement of the vapor pressures of silver and gold. A combined cell-torsion constant was assigned by comparison of results with published data for silver:[12] 4.27×10^{-4} (cell 3), 5.47×10^{-4} (cell 4), and 1.725×10^{-4} (cell 6) atm radian^{-1}, respectively. When these values were used to convert torsion angles measured for gold to vapor pressure equivalents, results were found to agree reasonably well (*ca.* 5%) with published data.[13] Silver and gold were particularly convenient for calibration since their vapor pressures lie in the effusion range at temperatures of interest in the present studies.

HfO_2 (99.9%, Fairmount Chemical) and graphite (National Carbon, spectroscopic grade powder, L 4118) were mixed in a 1:3 mole ratio, thoroughly ground together, and pressed (0.5 ton) into small pellets. Between 2 and 3 g of the reaction mixture was placed in the cell for each series of runs. After bringing the cell to reaction temperature slowly, to permit gradual degassing, displacement angles, usually beginning at the highest temperature, were monitored continuously for periods of 5–12 hr, during which the temperatures were varied from point to point in a random manner over the range giving measurable angles. The vacuum external to the cell was always maintained below 10^{-4} torr and usually below 10^{-5} torr. Results were reproducible though a slight general falloff was noted (up to a total of about 20%) over the total heating period. It was observed, when the mixture was removed, reground, and repressed, that pressures resumed their initially higher values, but then again fell slowly with time. The total loss of CO at the end of a typical series of measurements, indicated by weight loss of the cell as well as estimated from the time and rate of escape of CO, averaged over the temperature interval, corresponded to conversion of about 35 mole % of the reactants initially present.

UO_2 (depleted, W. R. Grace and Co., 87.75% U (theory, 88.02%; principal impurities (ppm): Al, 6; Cr, 22; Fe, 10; Mg, 25; Ni, 23; Si, 11; Zn, 25), of 0.81-μ particle size, was similarly pressed into pellets in a 1:4 mole ratio with graphite. Runs were conducted as described above; conversion of the sample, based on the stoichiometry of eq 2, corresponded, at the end of a typical series of measurements, to about 40% conversion. On exposure of the UO_2 reaction product to air, an acetylene-like odor was easily detected.

To aid in identification of phases present, room-temperature Debye–Scherrer powder photographs were taken of the reactant mixtures before heating and of the products after completion of the effusion measurements.

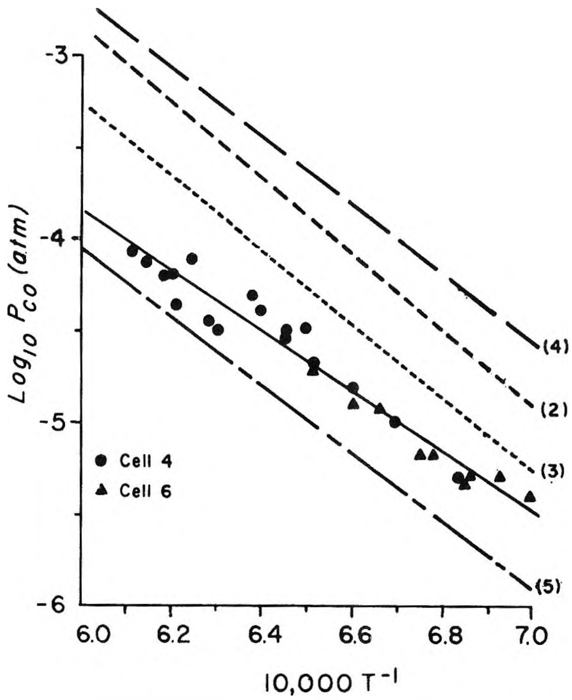

Figure 1. Effusion pressures for the UO_2–graphite system in comparison with predicted values for various reactions.

Results and Discussion

The UO_2–Graphite Reaction. The effusion studies on the UO_2–graphite reaction gave results suggestive of a well-behaved equilibrium system. CO pressures are shown in Figure 1. Our results lead to the equation $\log P_{CO(atm)} = -16.600T^{-1} - 6.1$ for the temperature interval 1430–1640°K. Pressures were consistent when a given point was approached from higher or lower temperatures and no significant change was seen during conversion of about 40% of the initial reactants. X-Ray powder patterns of the reaction product showed lines of UO_2 (a_0 = 5.46 A), UC_2 (a_0 = 3.52, c_0 = 6.00 A; this phase is reported[5] not to be stoichiometric, with composition *ca.* $UC_{1.86}$; we, however, for simplicity, represent it as UC_2), UC (a_0 = 4.95 A), and graphite phases, respectively; the given cell parameters for the carbide phases were not established with sufficient accuracy for a meaningful estimate of possible oxygen and/or carbon content; such an interpretation is made difficult by the fact that cell parameters also appear to be sensitive to thermal history and stresses in the samples.[5,14]

---

[12] P. Grieveson, G. W. Hooper, and C. B. Alcock, "Physical Chemistry of Process Metallurgy," Interscience Publishers, Inc., New York, N. Y., 1961, pp 341-352.

[13] D. L. Hildenbrand and W. F. Hall, *J. Phys. Chem.*, **66**, 754 (1962).

[14] S. Namba, S. Imoto, and T. Sano, *Technol. Rept. Osaka Univ.*, **12** (529) 429 (1962).

The patterns clearly demonstrate the presence of the indicated phases, however. The UC pattern was by far the most intense of the mixture and appeared to be the major product. All four solid phases indicated by the room-temperature X-ray pattern and CO cannot simultaneously be in equilibrium over the temperature interval studied (phase rule). The observed behavior could be explained if the carbides were in a single solid-solution phase at the reaction temperature and subsequently separated on cooling; such a stable solid solution is not indicated for our temperature range on currently proposed phase diagrams for the U–C system, however.[5] The existence of U_2C_3 has been suggested by a number of authors;[5] we did not find evidence for this phase in room-temperature X-ray data, however. An alternative possibility is that one or more of the solid phases is not in actual equilibrium with the others in the effusion cell. Various possible reactions, suggested by phases observed by us and by previous workers, will be considered below. The equilibrium-like behavior of the CO pressures suggests that some reasonably well-defined reaction may establish the steady-state CO pressures; it is possible that the solid-state product of this reaction may be metastable but that its conversion to the stable product and the interaction of the latter with carbon monoxide is kinetically slow.

The thermodynamic properties of the uranium carbides are found not to be sufficiently dissimilar or well enough established to serve as a means of positive identification of the reaction responsible for controlling the CO pressure in the effusion cell. However, some general conclusions can be drawn. Constants tabulated in standard references such as ref 2c differ considerably from those accepted by most of the authors in ref 5. Representative of the latter, which seem to be based on more recent experimental data, are the equations summarized by Alexander, Ward, Ogden, and Cunningham,[5] from which we have deduced the values in Table I for 1500°K, the mean temperature of our study.

Data in Table I, together with values for graphite and CO from the "JANAF Tables,"[4] were used to calculate equilibrium carbon monoxide pressures for the reactions (considered separately)

$$^1/_2UO_2(s) + {}^3/_2C(gr) = {}^1/_2UC(s) + CO(g) \quad (3)$$

$$^1/_2UO_2(s) + {}^7/_2C(gr) = {}^1/_4U_2C_3(s) + CO(g) \quad (4)$$

$$^1/_2UO_2(s) + {}^3/_2UC_2(a_2) = 2UC(a_1) + CO(g) \quad (5)$$

in addition to reaction 2. Results, if the solids are assumed to be at unit activity, are shown in comparison with the effusion data in Figure 1. All reactions give pressures within a factor of 20 with (3) and (5) quite close to the experimental values. Calculated results for (2) and (3) yield even higher CO pressures (deviate more) if the activities of the carbides are assumed reduced by formation of solid solutions. On the other hand, the calculated ($\Delta G°$ (Table I) $= -RT \ln K$) CO pressure for reaction 5 is in good agreement with experiment if the $a_1^2/a_2^{3/2}$ ratio is taken as *ca* 0.5 and $a_{UO_2} = 1$. Graphite does not appear in (5), however, and the carbide activities necessary for (5) to fit the effusion data are not those predicted from Table I for equilibrium between UC, C, and UC_2; if this were so, (2) and (3) would also give the same CO pressures and, of course, (2), (3), and (5) would all lead to the same equilibrium CO pressure. If the effusion data are assumed characteristic of such a general equillibrium system (with the carbides in a single solid solution phase), *i.e.*, disregarding values in Table I, an unreasonably small standard free energy of formation of UC and UC_2 (*ca.* −12 kcal $mole^{-1}$) is predicted. Hence it appears that graphite forms the carbide phase by reaction with UO_2, but not at a sufficient rate to establish the higher CO pressures necessary for equilibrium with graphite. The observed steady-state CO pressure is more nearly that expected for an equilibrium such as (5). The apparent enthalpy change and entropy change, deduced from the dependence of CO pressure on temperature (76 kcal and 28 cal deg^{-1} $mole^{-1}$ of CO), are also reasonably close to those predicted from Table I for (5) (83 kcal and 31 cal deg^{-1}, with no allowance for possible solid-solution effects).

Table I

Substance	$\Delta G°$, cal $mole^{-1}$	$\Delta H°$, cal $mole^{-1}$
$UO_2(s)$	−196,700	−260,800
$UC_2(s)$	−23,500	−19,000
$UC(s)$	−19,800	−24,000
$U_2C_3(s)$	−52,000	−72,000

Stoops and Hamme[9] report CO pressures in equilibrium with UO_2, U(l), and an oxycarbide phase for which they report the composition $UC_{0.75}O_{0.25}$. They propose a phase diagram which shows a three-phase equilibrium region, connecting UO_2, their oxycarbide phase, and a UC_{1+x} phase, adjacent to the region they have studied. Whereas their experiments were conducted at a higher temperature (1700–1900°) than ours, it is of interest to compare an extrapolation of their results with ours to see if the effusion reaction may involve the same oxycarbide phase. If one takes as their reaction

$$UO_2(s) + 4UC_{0.75}O_{0.25}(s) = 5U(l) + 3CO(g) \quad (6)$$

and as our reaction

$$2UO_2(s) + 5UC_2(a_2) = 8UC_{0.75}O_{0.25}(s) + 4CO(g) \quad (7)$$

where a_2 represents the activity of UC_2 in the UC_{1+x} phase, then, if the oxycarbide phases are in fact the same in the two cases, the two reactions may be suitably combined to give

$$^1/_2UO_2 + {}^1/_2UC_2(a_2) = U(l) + CO(g) \quad (8)$$

The experimental free energies may then be combined and compared with the value expected for (8); this eliminates the need for knowledge of the properties of the oxycarbide phase. For the results to give the standard free energy of UC_2 in Table I, the activity a_2 for UC_2 in the UC_{1+x} phase must be around 0.02, which is, perhaps, not unreasonable. This value is, of course, sensitive to uncertainty in the standard free energy of UC_2; if, for example, Alcock and Grieveson's value ($\Delta G° = -27{,}200$, $\Delta H° = 32{,}600$ cal mole^{-1})[5,15] is used, a_2 is predicted to be around 0.1. Also, if the activities in the oxycarbide phase of Stoops and Hamme are not the same as those of a similar phase formed at the lower temperatures of the effusion experiments, a correction for this difference will be needed. Hence, one can say only that the two experimental results seem generally compatible. Reaction 7 is, in effect, an alternative form of (5) but with UC present in an oxycarbide as well as a carbide phase.

It is interesting to note that if the oxycarbide phase is assumed to have a composition of $UC_{0.5}O_{0.5}$ in both Stoops and Hamme's and our experiment, combination of the results in a form similar to (6) and (7) leads to results for (8) in excellent agreement with the free energy (54 *vs.* 53.6 kcal), enthalpy (122 *vs.* 119 kcal), and entropy (45 *vs.* 44 eu) changes based on Alcock and Grieveson's values for UC_2; the latter, in this case, appears to be at or near unit activity.

In summary, the effusion study of the reaction of graphite and UO_2 yields CO pressures which behave in an equilibrium-like manner; existing thermodynamic data are not sufficiently well established to permit certain identification of the process controlling the CO pressure. Several possibilities appear consistent with the experimental results. The reaction product seems likely to be a solid solution and it appears that graphite is not in equilibrium with UO_2 and the principal product of its reduction.

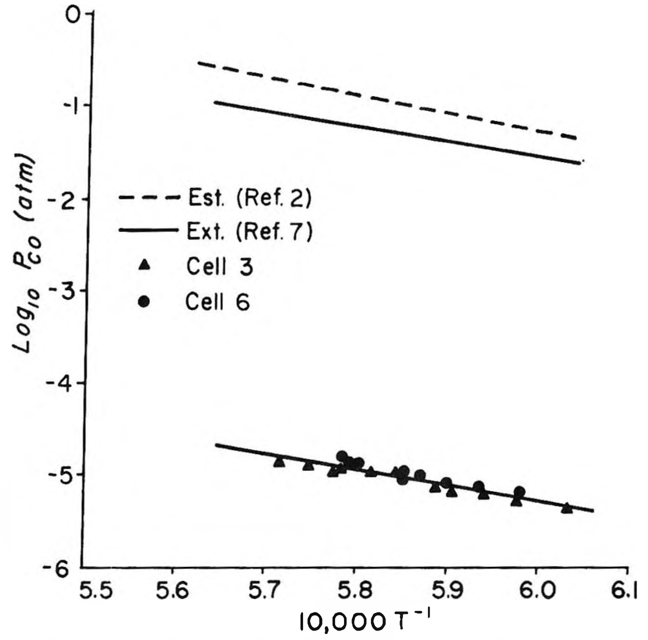

Figure 2. Effusion pressures for the HfO_2–graphite system in comparison with predicted values.

The HfO_2–Graphite Reaction. Torsion effusion pressures, based on data from two cells, are shown in Figure 2. The steady-state pressures are far below (a factor between 10^3 and 10^4) equilibrium pressures predicted from estimated thermodynamic properties[2] ($\Delta G_1° = 159{,}000 - 80T$, estimated for (1) in the vicinity of 1700°K) or from extrapolated data of the Russian workers[7] ($\Delta G_1° = 136{,}000 - 68T$, in the vicinity of 1900°K). A mean of our results from the two cells over the temperature interval 1650–1750°K can be represented by the equation

$$\log P_{CO(atm)} = -16{,}650T^{-1} + 4.75$$

If the CO pressures are taken as a measure of an equilibrium constant for (1), the expression $\Delta G°_1 = 153{,}000 - 44T$ is obtained. Although the apparent heat of reaction is quite close to the expected value, the entropy change is so low that reaction 1 cannot be near equilibrium in the effusion cell. However, the system behaves as though some reasonably well-defined equilibrium process is controlling the CO pressure. For example, the rate of escape of CO from cell 6 is nearly four times greater than that from cell 3; this would not be expected if the rate of effusion is determined solely by the forward rate of (1); the latter should be essentially the same in the two cells. Furthermore, although fairly large samples, *ca.* 2 g, were required to

---

(15) C. B. Alcock and P. Grieveson, "Thermodynamics of Nuclear Materials," IAEA, Vienna, 1962, p 563.

maintain the pressures at the reproducible values reported, when amounts larger than this were used, the observed steady-state CO pressures did not vary in proportion to the quantity of reactant mixture. Hence it appears that the steady-state pressure is not determined solely by the area of interfacial contact of the reacting solid phases.

Work reported in ref 6 and 7 shows that HfC, prepared under conditions comparable to our experiment may be expected to have appreciable oxygen content. The Russian workers[7] report a composition of the order of $HfC_{0.95}O_{0.05}$ for the phase in equilibrium with HfO_2 and graphite at temperatures between 1800 and 2800°. They also report the dependence of CO pressures on the composition of the oxycarbide phase in the presence of graphite but in the absence of HfO_2. The equilibrium CO pressures in this divariant system decreased as the carbon content approached the limiting value for HfC. They demonstrate that equilibrium can be approached from higher and lower CO pressures at values considerably below the equilibrium CO pressure found when HfO_2 is present. They conclude that at temperatures above 2300°K variation of the pressure of CO between 20 and 700 torr is without significant effect on the composition of the carbide phase which, under these conditions, is virtually oxygen free.

Cotter and Kohn[6] report preparation of a continuous series of solid solutions from HfC down to mixtures containing about one-half the theoretical amount of carbon. They heated graphite–HfO_2 pressed mixtures in a protective atmosphere of helium to temperatures between 1500 and 2800° but did not specify the partial pressures of CO in their systems. They report a cubic cell dimension of 4.641 A for pure HfC; most of their preparations gave a cell dimension around 4.632 A. These were found to contain *ca.* 4.9% combined carbon, which corresponds to $HfC_{0.78}O_{0.22}$. In an experiment in which the dioxide was heated in a graphite crucible without prior formation of a graphite–oxide pressed pellet, they obtained a phase which appeared to be near HfO in composition (cell parameter 4.584 A).

X-Ray patterns of our products (cooled to room temperature) showed lines of HfO_2, graphite, and a HfC phase, respectively. The former two appeared to be essentially pure; the latter gave a cubic cell parameter (4.634) near that of Cotter and Kohn's 4.632 phase; however, from the results of the Russian workers one would expect our product to have a relatively low oxygen content since the CO pressures in the effusion cell were materially below that expected for equilibrium between HfO_2 and graphite.

Formation of a carbide phase with some HfO dissolved in it does not explain the low CO pressures in the effusion cell on the basis of reaction 1 alone. The expected CO pressures for the equilibrium reduction of HfO_2 to HfO in such a solid solution are also much higher than the observed pressures. A materially reduced activity of the reactants in (1) is needed; however, X-ray evidence indicates that HfO_2 and graphite phases remain in essentially pure form.

Possibly the equilibrium-like behavior of the CO pressures in the effusion cell results from a secondary but relatively rapid "equilibration" of CO with the oxycarbide solid solution in which the monoxide and carbide are interconverted, *i.e.*

$$HfO(a_o) + 2C(gr) = HfC(a_c) + CO(g) \qquad (9)$$

a_o and a_c represent the activities of HfO and HfC, respectively, in the solid solution. Reaction 9, presumably, is the same kind of reaction occurring in the divariant equilibrium observed by the Russian workers, even though, in our case, HfO_2 is also present. Thus we must assume that the initial reduction of HfO_2 to form the HfC–HfO mixture does not proceed rapidly enough to build up the CO pressure to the point where reversal of (1) and normal equilibration occurs. The dilemma in the present case is that the effusion results are not indicative of such a rate-controlled process. A readily reversible process such as (9) may provide a sort of "buffering" action. An "excessive" rate of production of CO by (1) could be offset by conversion of some of the HfC to HfO; a "deficiency" in rate could be made up by the reduction of some of the HfO. Reaction 9 involves equilibration of only two solid phases (possibly only one if the reactant carbon is dissolved or effectively dispersed in a reactive manner in the oxycarbide phase) with CO, whereas (1) involves equilibration of three solid phases. One also expects from (9) that as the CO pressure diminishes, the oxycarbide phase tends more nearly to pure HfC, in accord with the observations of the Russian workers.[7]

For (9) to lead to a CO pressure roughly independent of the fraction of HfO_2 which has been reduced, the activities a_o and a_c must remain nearly constant. This would be expected if the oxycarbide phase is at a saturation limit or perhaps it may result fortuitously from the steady-state balance in the system. The slow falloff of pressures with time which was observed may reflect a gradually changing ratio of activities. If (9) effectively controls the magnitude of the CO pressure and its temperature dependence, the thermodynamic properties estimated therefrom should be more nearly those of (9) than of (1). An estimated standard entropy of HfO of 35 eu at 1700°K, *i.e.*,

Table I: Rates of Reaction of Atoms with Olefins at Room Temperature

	$10^{-10}k$, cm^3 $mole^{-1}$ sec^{-1}	Relative k					
	N^a	N^a	H^b	O^c	S^d	Se^e	Br^f
Ethylene	~1.0 ± 0.5	~0.5	0.56	0.17	0.28	0.38	0.57
Propene	1.9 ± 0.6	1.0	1.00	1.00	1.00	1.00	1.00
Butene-1	2.0 ± 0.4	1.1	1.08	1.04	1.0	2.7	1.28
t-Butene-2	1.7 ± 0.4	0.9	0.59	4.90		21.6	5.56
Isobutene	4.2 ± 1.0	2.2	2.47	4.35		17.2	21.7
2,3-Dimethyl-butene-2	2.4 ± 0.6	1.3	0.81	18.2	>20		
1,3-Butadiene	3.5 ± 1.0	1.8	4.85	5.9		37.8	

[a] This work (estimated uncertainties). [b] K. R. Jenning and R. J. Cvetanovic, *J. Chem. Phys.*, **35,** 1233 (1961). [c] R. J. Cvetanovic, *ibid.*, **30,** 19 (1959). [d] H. E. Gunning and O. P. Strausz, *Advan. Photochem.*, **1,** 248 (1963). [e] A. B. Callear and W. J. R. Tyerman, *Proc. Chem. Soc.*, 296 (1964). [f] P. I. Abell, *Trans. Faraday Soc.*, **60,** 2214 (1964).

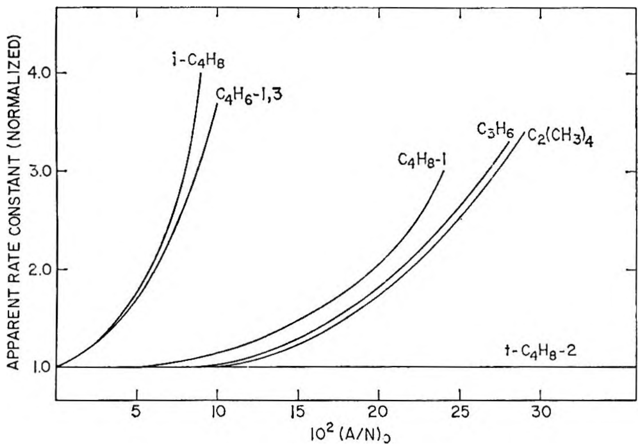

Figure 2. Apparent rate constants for a series of olefins as functions of $(A/N)_0$, normalized to a common origin. (The data for ethylene were too uncertain to be meaningful and have been omitted.)

of hydrogen atoms in addition to nitrogen atoms and hence to an increase in the apparent rate constant. Such an effect is observed as shown in Figure 3 where the apparent rate constant for the propene reaction is given as a function of $(C_3H_6/N)_0$ for differing amounts of added hydrogen. The most interesting feature of these experiments is that even with relatively large amounts of added hydrogen, the limiting value of the rate constant, *i.e.*, k at $(C_3H_6/N)_0 = 0$, is unaffected. By analogy with the mechanism postulated for the ethylene reaction (reactions 1–6), this would imply that propene is regenerated.[8] The following general mechanism is proposed to account for these observations.[9]

$$N + \text{olefin} \longrightarrow \text{products} + H? \qquad (7)$$

$$N + \text{products} \longrightarrow \text{products}' + H \qquad (8)$$

$$H + \text{olefin} \longrightarrow R \qquad (9)$$

$$H + R \longrightarrow RH \qquad (10)$$

$$N + R \longrightarrow \text{olefin} + NH \qquad (11)$$

$$R + R \longrightarrow \text{recombination and disproportionation products} \qquad (12)$$

$$N + NH \longrightarrow N_2 + H \qquad (13)$$

At low conversion where H/N is very small, reaction 11 predominates over (10) and olefin lost in reaction 9 is regenerated. At higher conversions reactions 10 and 12 become more important and olefin is lost, leading to an increase in the apparent rate constant.

On the basis of this mechanism, the true rate constant of the reaction would be the value of k obtained under conditions such that H/N approaches 0, *i.e.*, at (A/N) = 0. Rate constants derived by extrapolating the apparent rate constants to (A/N) = 0 are given in Table I, column 2, for a series of olefins. The experimental data for the propene reaction are shown in Figure 1, curve C. Curve shapes for the other olefins studied are shown in Figure 3.

This mechanism is, of course, quite speculative. However, it may be noted that for very small values of $(A/N)_0$ the rate expression reduces to the usual approximation for a bimolecular rate constant with one reactant in great excess, *i.e.*

$$k = \ln (A)_0/(A)_t/(N)t$$

---

[8] In studying the C_3D_6 reaction in the presence of added hydrogen, the formation of C_3D_5H is observed. It is not certain how much of the C_3D_5H is formed by reactions 9 and 11 and how much by reaction 12 or by simple isotopic exchange.

[9] This is a greatly simplified mechanism in which reactions 9 and 10 have been written only in terms of the formation of pressure stabilized products. For olefins other than ethylene this is approximately correct.

Gas Phase Dipole Moments of a Series of Terminal 1-Bromoalkanes

by Shmuel Weiss[1]

Department of Physical Chemistry, The Hebrew University, Jerusalem, Israe *(Received April 11, 1966)*

The dipole moments of ethyl, *n*-propyl, *n*-butyl, *n*-amyl, and *n*-hexyl bromide have been measured in the gas phase at 35°. The dipole moments were found to increase with increasing chain length up to and including the hexyl derivative. The increase in dipole moment up to such high members of the homologous series was explained as due to conformations in which the "tail" of the molecule comes quite close to the C–Br group. Calculations for a highly simplified model gave increases of dipole moment with chain length of the right order of magnitude.

Introduction

The dipole moments of *n*-alkanes bearing a terminal dipolar substituent have been studied widely in the past[2] and are an important means of determining the extent and range of the inductive effect. In recent years, the dipole moments of a series of *n*-alkyl bromides in benzene solution[3] and of *n*-alkynes in the gaseous state[4] were determined in this laboratory in connection with studies of the dipole moments of the corresponding α,ω-disubstituted *n*-alkanes.

It has been stated in the literature that the increase in dipole moment with chain length, in a homologous series, does not extend appreciably beyond the propyl derivative.[2] This statement, however, is based largely on measurements in solution, where the solvent would be expected to suppress the effect of increasing chain length. Also, many of the available dipole moment values have been reported with a precision of a few hundredths of a Debye unit only, so that further increase in dipole moment with increasing chain length, beyond the propyl derivative, cannot be considered ruled out. Such small increases in dipole moment with chain length as are thus still possible are not unimportant in relation to the problem of the dipole moments of α,ω-disubstituted alkanes and also to the theory of the inductive effect in general.

Published theories of the inductive effect range from consideration of electrostatically induced moments through semiempirical methods to quantum mechanical calculations.[5] The most widely considered model in recent years[2] was that of a dipolar substituent polarizing the nearest C–C bond which, in turn, polarizes to a smaller extent its next neighbor, and so on. The induced moments decrease rapidly along the chain and semiempirical calculations show that they become indeed very small after the third carbon atom. However, it would seem that, especially for flexible molecules, the direct induction of moments by the dipolar substituent (the so-called "field effect") in parts of the molecule farther along the chain cannot be neglected since, in certain conformations, these parts might come quite close to the dipolar group. If this effect is important, one might well expect the dipole moment to increase beyond the propyl derivative.

Recently, Hayman and Weiss remeasured the dipole moments of some terminal monoacetylenes in the gas phase[4] and did indeed find an increase in dipole moment with increasing chain length up to the amyl derivative.

We considered it, therefore, of interest to study this problem further by measuring the dipole moments of a homologous series with a more strongly dipolar substituent so that the inductive effect would be more pronounced. The bromoalkyl series seemed most suitable to us for technical reasons and also because the

---

[1] Department of Chemistry, Princeton University, Princeton, N. J.

[2] See, *e.g.*, C. P. Smyth, "Dielectric Behavior and Structure," McGraw-Hill Book Co., Inc., New York, N. Y., 1955, Chapters 8 and 9; J. W. Smith, "Electric Dipole Moments," Butterworth and Co. Ltd., London, 1955, Chapter 7.

[3] H. J. G. Hayman and I. Eliezer, *J. Chem. Phys.*, **35**, 644 (1961).

[4] H. J. G. Hayman and S. Weiss, *ibid.*, **42**, 3701 (1965).

[5] See references mentioned in ref 2 and, more recently, R. P. Smith and E. M. Mortensen, *J. Am. Chem. Soc.*, **78**, 3932 (1956); S. Maeda, *Bull. Chem. Soc. Japan*, **31**, 260 (1958).

Table I: Densities, Refractive Indices, and Polarizations of the Various Bromides Measured

Compound	Density, g/ml	Refractive index[a] D line	Refractive index[a] g line	P_E, cc[b]	P_A, cc[c]	P_O, cc[d]	P_T, cc[e]
Ethyl bromide	1.4518 (1.4492)	1.4211 (1.4210)	1.4332	18.49	0.96	84.68	104.13
n-Propyl bromide	1.3463 (1.3452)	1.4310 (1.4317)	1.4429	23.00	1.03	87.83	111.86
n-Butyl bromide	1.2685 (1.2687)	1.4369 (1.4378)	1.4485	27.55	1.10	87.27	115.92
n-Amyl bromide	1.2124 (1.2119)	1.4419 (1.4420)	1.4535	32.10	1.17	90.04	123.31
n-Hexyl bromide	1.1690 (1.1687)	1.4452 (1.4454)	1.4569	36.62	1.24	91.86	129.72

[a] Densities and refractive indices are at 25°. The values in parentheses are from R. R. Dreisbach, "Physical Properties of Chemical Compounds, II," American Chemical Society, Washington, D. C., 1959. [b] Molar refractions extrapolated to infinite wavelength. [c] Empirical values based on considerations given in the text. [d] Orientation polarizations are at 35°. [e] Total molar polarizations are at 35°.

alkyl bromides and dibromides have been so widely studied in solution. The dipole moments of these compounds have been measured before[6] (except for the hexyl derivative) but not with sufficient precision for the purpose of this study. (All of these measurements are about 30 years old.)

Experimental Section

The heterodyne beat apparatus used to determine the dielectric constants and the experimental procedure as well as the methods employed to obtain the electronic polarizations have been described previously.[4]

Ethyl bromide was obtained from the Hopkin and Williams Co. (England) and the rest of the bromides from Fluka (Switzerland). Each of the substances was dried and purified by distillation from anhydrous calcium sulfate through a Todd distilling column[7] with spiral packing using reduced pressures where necessary to avoid elevated temperatures (where the effectiveness of the calcium sulfate falls off). The substances were then further purified and their dryness was checked during the measurement as has been described.[4]

Results

Table I gives the measured values for the densities and refractive indices of the various monobromides (in the liquid form) together with the corresponding extrapolated values for the electronic polarization. The standard deviation of the electronic polarization (calculated from those of the densities and refractive indices) was 0.15%.

The total polarizations tended to increase slightly with pressure and were therefore extrapolated graphically to zero pressure (except for the two highest members for which measurements were carried out at only one pressure because of low volatility). The extrapolated polarization always agreed to within 0.3% with that measured at low pressure. The results thus obtained are listed in Table I. The standard deviation in the measurement of the total polarization was 0.3% except for 1-bromohexane, where, because of low volatility, the standard deviation was somewhat higher.

Atomic polarizations have been estimated by a method we have used before.[4] The atomic polarization of methyl bromide can be evaluated using the value reported for its dipole moment which has been measured rather accurately by the microwave Stark effect technique,[6] values for the total polarization reported in the literature,[8] and a value for the electronic polarization which can be deduced from our measurements on the other bromides by the additivity rule. Combining all these results we obtained the value 0.89 cc for the atomic polarization of methyl bromide. The atomic polarizations of the higher bromides were then evaluated by adding a constant increment of 0.07 cc/CH_2 group as recommended by Smyth.[9] The values of the atomic polarizations obtained in this way are listed in Table I.

The dipole moments of the various monobromides were then calculated from the total, electronic, and

---

[6] See A. A. Maryott and F. Buckley, National Bureau of Standards Circular 537, U. S. Government Printing Office, Washington, D. C., 1953.

[7] F. Todd, *Ind. Eng. Chem., Anal. Ed.*, **17**, 175 (1945).

[8] C. P. Smyth and K. B. McAlpine, *J. Chem. Phys.*, **2**, 499 (1934); L. G. Groves and S. Sugden, *J. Chem. Soc.*, 158 (1937); K. L. Ramaswamy, *Proc. Indian Acad. Sci.*, **A4**, 108 (1936); A. D. Buckingham and R. J. W. Le Fevre, *J. Chem. Soc.*, 3432 (1953).

[9] C. P. Smyth, "Dielectric Behavior and Structure," McGraw-Hill Book Co., Inc., New York, N. Y., 1955, pp 419, 420, and 422. This is based on the average increment found for the *n*-alkane series and the assumption that it will be of comparable magnitude for a similar series.

Iron(III) chloride solutions in concentrated HCl have long been of interest because of the ability of iron(III) and numerous other metal(III) ions to be extracted from such solutions into organic solvents[7] such as diethyl ether. The species present in iron(III) chloride-hydrochloric acid solutions have been investigated[8,9] electrometrically and spectrophotometrically as well as by solvent distribution. It is believed that the lower chloro complexes are predominantly octahedral with water molecules occupying the sites not filled by chloride ions, while the tetrachloro species is tetrahedral. Evidence has been presented that the tetrachloro complex is the highest one formed in aqueous HCl solutions.[10-12] Friedman[12] has given the most definitive evidence for four-coordination from ultraviolet and visible spectra of solid tetrachloroferrates, ethylene bromide, diisopropyl and diethyl ether solutions, aqueous HCl solutions, and ether extracts of the latter.

Recently, the spectral evidence for complex configurations[13] has been interpreted to suggest that the trichloroiron(III) species in HCl solutions is also four-coordinated and tetrahedral. The arguments presented there are somewhat indicative, but hardly conclusive. We must assume that the configuration of the trichloro species is not well established, and consider the possibility that both octahedral and tetrahedral species may be present, depending upon circumstances.

In the interpretation of results of the work reported here, we have relied upon the formation constants of Gamlen and Jordan[9] for the trichloro and tetrachloroiron(III) species, and those of Rabinowitch and Stockmayer[8] for monochloro and dichloro species. Activities of HCl are those listed by Robinson and Stokes,[14] which are sufficiently close to those used[15] by Gamlen and Jordan to ensure that the calculation of species concentrations is not seriously in error. The assumptions made in the calculations were the same as those used in obtaining the constants, the most notable of which is that the ratio of activity coefficients of successive members of the coordination series is a constant.[16,17] Thus the formation constants are not thermodynamic. However, since our principal interest is in recovering the species concentrations from the constants listed by Gamlen and Jordan, it is only necessary that we follow the same procedures and assumptions they did.

In the following sections we report the results of experimental investigation, by magnetic resonance methods, of iron(III) chloride solutions in 0.85-13.6 *M* HCl.

Experimental Section

Reagents. Iron(III) perchlorate was prepared by dissolving chemically pure iron in concentrated perchloric acid. Small amounts of iron(II) ion were oxidized to iron(III) by addition of hydrogen peroxide, the excess of which was destroyed by heating. Crystals of iron(III) perchlorate separated from the solution and were recrystallized from perchloric acid solution. Analysis of the salt corresponded to the formula: $Fe(ClO_4)_3 \cdot 10.5H_2O \cdot 0.65HClO_4$. Concentrated HCl, Baker Analyzed, was used in the preparation of all solutions except 13.6 *M* HCl, which was prepared by supersaturating H_2O^{17} with Matheson tank HCl gas. H_2O^{17} was prepared from NO^{17} by reaction with hot copper to form CuO^{17}, followed by reduction with H_2 to form H_2O^{17} which was redistilled after addition of a small amount of metallic sodium to remove acidic impurities. Analysis for oxygen isotopes 16, 17, and 18 was made mass spectrometrically after complete conversion of samples of water to CO_2.

Nuclear Measurements. All measurements were made using a Varian wide-line nuclear resonance spectrometer. Both O^{17} and Cl^{35} resonances were observed by phase detection with the spectrometer frequency locked on 8 and 5 Mc/sec, respectively, with either 20- or 40-cps field modulation. The Cl^{35} resonance was broadened by the modulation frequency in the most dilute HCl blanks when phase detection was used even at 20 cps. Therefore, the side-band technique as de-

---

(4) R. E. Connick and C. P. Coppel, *J. Am. Chem. Soc.*, **81**, 6389 (1959).

(5) E. Blatt, Ph.D. Thesis, University of California, Aug 1964 (UCRL-11584, Lawrence Radiation Laboratory). We were unaware of the part of that research dealing with HCl solutions at high concentrations until this work was completed, and are indebted to Professor R. E. Connick for supplying us with a copy of the thesis.

(6) E. C. Blatt and R. E. Connick, Proceedings of the 8th International Congress on Coordination Chemistry, Vienna, 1964, p 284.

(7) See, for instance, R. M. Diamond, and D. G. Tuck, *Progr. Inorg. Chem.*, **2**, 158 (1960).

(8) E. Rabinowitch and W. H. Stockmayer, *J. Am. Chem. Soc.*, **64**, 335 (1942).

(9) G. A. Gamlen and D. O. Jordan, *J. Chem. Soc.*, 1435 (1953), and references cited therein.

(10) N. H. Nachtrieb and J. G. Conway, *J. Am. Chem. Soc.*, **70**, 3547 (1948).

(11) R. J. Myers, D. E. Metzler, and E. H. Swift, *ibid.*, **72**, 3767 (1950).

(12) H. L. Friedman, *ibid.*, **74**, 5 (1952).

(13) I. I. Antipova-Karataeva, Yu. A. Zolotov, and I. V. Seryakova, *Zh. Neorg. Khim.*, **9**, 1712 (1964) [*Russ. J. Inorg. Chem.*, **9**, 927 (1964)].

(14) R. A. Robinson and R. H. Stokes, "Electrolyte Solutions," 2nd ed, Academic Press, Inc., New York, N. Y., 1959, pp 491, 504.

(15) G. Åkerlöf and J. W. Teare, *J. Am. Chem. Soc.*, **59**, 1855 (1937).

(16) J. Bjerrum, *Kgl. Danske Videnskab. Selskab., Mat.-fys. Medd.*, **22**, No. 18 (1946).

(17) R. Näsänen, *Acta Chem. Scand.*, **4**, 140, 816 (1950).

For the electrostatic calculations some more drastic approximations are needed. We first approximate the actual dipole by a point dipole located on the C–Br axis. Second, since a dipole field will obviously be a poor approximation for near atoms, we consider our point dipole to include the moments induced in the Br and adjacent CH_2 group; that is, we consider it to represent the primary moment and induced moments of an isolated $-CH_2Br$ group. As an approximation for its actual magnitude, we take the value of 1.80 D., the dipole moment of CH_3Br.[6]

Next, we have no reliable way to determine where on the C–Br axis the dipole should be, and so we shall have to calculate its effect for different locations on that axis.

Though, in principle, calculations can be carried out on the basis of the above assumptions, the mathematics is still rather complicated. We shall therefore make some further rather drastic approximations noting that we do not aim at a quantitative prediction of our dipole moments, but only at a test of whether our qualitative explanations can lead to predictions of the right order of magnitude. We thus consider moments induced in carbon atoms only (making their polarizabilities, however, equal to those of CH_2 groups (18.2×10^{-25} cgs) or CH_3 groups (22.4×10^{-25} cgs[12]), as the case may be). We neglect moments induced by induced moments and, finally, consider only moments induced in the direction of the primary moment. This last approximation seems reasonable in view of the first two noting that a small moment perpendicular to a large one gives rise to a total moment which is not very different from the large one. The small dipole moments connected with the alkyl residue (as evidenced, *e.g.*, by the dipole moment observed for propane, 0.08 D.[13]) are also neglected. Representative results of these calculations[14] for various locations of the inducing point dipole are listed in Table II. The peculiarities of the measured values, such as the equality (within experimental error) of the dipole moments of the propyl and the butyl derivative, are not reflected in the calculated values as can hardly be expected considering the many approximations made. It is, however, shown that the increase in dipole moment with increasing chain length might indeed be temporarily halted and that our model does lead to increase in dipole moment with chain length of the order found experimentally.

Acknowledgments. The author is greatly indebted to Dr. H. J. G. Hayman for many fruitful discussions. He is also grateful to the National Science Foundation (Contract No. NSF GP-5366 3748-4 with Brown University) for making computer time available to him.

---

[12] Calculated from P_E values given by Landolt-Börnstein, "Physikalisch-Chemische Tabellen," Vol. I, Part 3, Julius Springer, Berlin, 1951, p 515, plus our correction for atomic polarization.

[13] D. R. Lide, Jr., *J. Chem. Phys.*, **33**, 1514 (1960).

[14] Computations were performed on the Brown University IBM 7070 computer.

Double-Layer Impedance of Electrodes with Charge-Transfer Reaction

by Paul Delahay and Gilles G. Susbielles

Department of Chemistry, New York University, New York, New York 10003 *(Received April 19, 1966)*

Equations for the electrode impedance are derived for metal ion–amalgam electrodes and other electrode reactions without *a priori* separation of faradaic and double-layer charging processes. Derivation starts with the three general equations for nonsteady-state processes previously derived. The electrode impedance is equivalent to an RC parallel circuit involving the *experimental* quantities R and C. This impedance is *formally* separated in the usual faradaic impedance and a double-layer impedance in parallel. The latter is equivalent to a resistance and a capacity C_{dl} in parallel. Properties of the double-layer impedance are derived and discussed, particularly for C_{dl}. It is shown that, for any finite exchange current density, C_{dl} approaches the capacity of an ideal polarized electrode at infinite frequency. Conversely, C_{dl} approaches the capacity of an ideal reversible electrode at zero frequency. The latter behavior prevails at any frequency for an infinite exchange current. The zero-frequency capacity is derived independently by thermodynamic argument for the conditions prevailing in electrode-impedance measurements. The double-layer capacity is frequency dependent between $\omega = 0$ and $\omega \rightarrow \infty$. Frequency dependence of C_{dl} can be pronounced at the usual frequencies used in bridge measurements. Determination of C_{dl} and the exchange current densities is discussed, and conditions for practical validity of Sluyters' analysis of experimental data are established. The Tl^{+}–Tl(Hg) and $\mathrm{Hg_2}^{+2}$–Hg electrodes are discussed in particular.

The theory of the electrode impedance[1] was developed on the assumption that faradaic and double-layer charging processes can be separated *a priori*. It was recently pointed out[2] that such *a priori* separation does not correspond to any conceivable physical operation for nonsteady-state processes. Separation for such processes is not justified because there is charge separation or recombination, without external current, at nonideal polarized electrodes. Three general equations were also given which should allow, after solution, detailed analysis of transitory and periodic electrode processes. Application is made here to the electrode impedance. The double-layer impedance is derived for electrodes with charge-transfer reaction, and experimental conditions for electrode impedance measurements are reexamined with some emphasis on Sluyters' method[3] for separation of the double-layer capacity. Results are derived for metal ion–amalgam electrodes, and other types of electrode reactions are discussed afterward.

Derivation of the Electrode Impedance

Boundary Value Problem. We consider the reaction $\mathrm{M}^{+z} + ze = \mathrm{M(Hg)}$ for the usual conditions of electrode impedance measurements: mass transfer controlled by semiinfinite linear diffusion in the presence of a large excess of supporting electrolyte and low overvoltage allowing the use of a linearized current–overvoltage characteristic. The first two general equations previously given[2] state the balance conditions at the interface for the production and accumulation of M^{+z} and M. Thus we have the following relationships

---

[1] Reviewed, *e.g.*, by P. Delahay, *Advan. Electrochem. Electrochem. Eng.*, **1**, 233 (1961).

[2] P. Delahay, *J. Phys. Chem.*, **70**, 2373 (1966).

[3] M. Sluyters-Rehbach and J. H. Sluyters, *Rec. Trav. Chim.*, **82**, 525 (1963).

$$i_0\left[\left(\frac{c_{\mathrm{M}}}{c^{\mathrm{s}}_{\mathrm{M}}}\right)_{x=0} - \left(\frac{c_+}{c^{\mathrm{s}}_+}\right)_{x=0} + \frac{zF}{RT}\eta\right] = -zFD_+\left(\frac{\partial c_+}{\partial x}\right)_{x=0} + zF\left[\left(\frac{\partial \Gamma_+}{\partial E}\right)_{c^{\mathrm{s}}_{\mathrm{M}}} + \left(\frac{\partial \Gamma_+}{\partial E}\right)_{c^{\mathrm{s}}_+}\right]_{\eta=0}\frac{\mathrm{d}\eta}{\mathrm{d}t} \tag{1}$$

$$-D_{\mathrm{M}}\left(\frac{\partial c_{\mathrm{M}}}{\partial x}\right)_{x=0} = -D_+\left(\frac{\partial c_+}{\partial x}\right)_{x=0} + \left\{\left[\frac{\partial(\Gamma_+ + \Gamma_{\mathrm{M}})}{\partial E}\right]_{c^{\mathrm{s}}_{\mathrm{M}}} + \left[\frac{\partial(\Gamma_+ + \Gamma_{\mathrm{M}})}{\partial E}\right]_{c^{\mathrm{s}}_+}\right\}_{\eta=0}\frac{\mathrm{d}\eta}{\mathrm{d}t} \tag{2}$$

where i_0 is the exchange current density; the c's are the concentrations; the c^{s}'s are the bulk concentrations; the D's are the diffusion coefficients; x is the distance from the electrode with $x \geqslant 0$ in solution and $x \leqslant 0$ in the amalgam; t is the time; the Γ's are the surface excesses (true ones identified with relative surface excesses; dilute solution and amalgam); and η is the overvoltage ($\eta = E - E_{\mathrm{e}}$, E being the potential and E_{e} the equilibrium potential). The faradaic current, as expressed by eq 1, is positive for a net anodic process ($\eta > 0$) and negative for a net cathodic process ($\eta < 0$). Equations 1 and 2 are written on the assumption that the thicknesses of the double layer in solution and the amalgam can be neglected in comparison with the diffusion layer thicknesses. This assumption is entirely justified, even for the highest frequencies used in impedance measurements.

The derivatives of Γ_+ and Γ_{M} are written in the form appearing in eq 1 and 2 for the following reasons.[2] (a) The concentrations c_+ and c_{M} at $x = 0$ are not independent since they are related by eq 2. Hence E is the sole independent variable in the writing of $\mathrm{d}\Gamma_+/\mathrm{d}t$ and $\mathrm{d}\Gamma_{\mathrm{M}}/\mathrm{d}t$ in terms of $\mathrm{d}\eta/\mathrm{d}t$. (b) In expressing the variations of Γ_+ or Γ_{M} with E at the equilibrium potential, we note that the Γ's under equilibrium conditions depend on c^{s}_+ and $c^{\mathrm{s}}_{\mathrm{M}}$. Consequently we introduce the two derivatives $(\partial\Gamma/\partial E)_{c^{\mathrm{s}}_+}$ and $(\partial\Gamma/\partial E)_{c^{\mathrm{s}}_{\mathrm{M}}}$ at the equilibrium potential. We note in passing that since these derivatives may vary rapidly with E, the low-overvoltage approximation of eq 1 and 2 may require experimental η's lower that the usual (and perhaps unduly high) upper limit of 5 mv.

Equations 1 and 2 are the boundary conditions which must be solved for

$$\eta = \eta_{\mathrm{a}} \exp(j\omega t) \tag{3}$$

where η_{a} is the overvoltage amplitude, $j = (-1)^{1/2}$, and $\omega = 2\pi f$, f being the frequency. Furthermore, we prescribe $c_+ \rightarrow c^{\mathrm{s}}_+$ and $c_{\mathrm{M}} \rightarrow c^{\mathrm{s}}_{\mathrm{M}}$ for $x \rightarrow \infty$ for $t \geqslant 0$.

Solution of this boundary value problem yields the flux of M^{+z} at $x = 0$ which can now be introduced in the third general equation,[2] relationship 4 above

$$i = -zFD_+\left(\frac{\partial c_+}{\partial x}\right)_{x=0} + \left\{\left[\frac{\partial(q + zF\Gamma_+)}{\partial E}\right]_{c^{\mathrm{s}}_{\mathrm{M}}} + \left[\frac{\partial(q + zF\Gamma_+)}{\partial E}\right]_{c^{\mathrm{s}}_+}\right\}_{\eta=0}\frac{\mathrm{d}\eta}{\mathrm{d}t} \tag{4}$$

where i is the current density being measured and q the surface charge density on the electrode. It is supposed in the writing of eq 4 that diffusion need be considered only for species M^{+z} and M. There appear in eq 4 the derivatives of $q + zF\Gamma_+$ with respect to E at the equilibrium potential for $c^{\mathrm{s}}_{\mathrm{M}}$ or c^{s}_+ constant.

Electrode Impedance. We solve the above problem for the steady-state periodic current by setting the concentrations as[4]

$$c_+ = c^{\mathrm{s}}_+\{1 - P \exp[-(\omega/2D_+)^{1/2} \times (1 + j)x] \exp(j\omega t)\} \tag{5}$$

$$c_{\mathrm{M}} = c^{\mathrm{s}}_{\mathrm{M}}\{1 + N \exp[(\omega/2D_{\mathrm{M}})^{1/2} \times (1 + j)x] \exp(j\omega t)\} \tag{6}$$

The factors P and N are determined by introducing c_+ and c_{M} from eq 5 and 6 into the boundary conditions 1 and 2 (Appendix). The current density being measured, as given by eq 4, is

$$i = \left\{-zF\left(\frac{\omega D_+}{2}\right)^{1/2} c^{\mathrm{s}}_+P(1 + j) + j\omega\eta_{\mathrm{a}}\left\{\left[\frac{\partial(q + zF\Gamma_+)}{\partial E}\right]_{c^{\mathrm{s}}_{\mathrm{M}}} + \left[\frac{\partial(q + zF\Gamma_+)}{\partial E}\right]_{c^{\mathrm{s}}_+}\right\}_{\eta=0}\right\} \times \exp(j\omega t) \tag{7}$$

The electrode impedance is equivalent to a capacity C and a resistance R in parallel. The product ωC is equal to the coefficient of the imaginary term between braces in eq 7, and R is the reciprocal of the real term between braces in that equation. One has after introduction of P and N

$$R = \frac{[\lambda_+\lambda_{\mathrm{M}} - (\lambda_+ + \lambda_{\mathrm{M}})i_0]^2 + (\lambda_+\lambda_{\mathrm{M}})^2}{i_0\lambda_+\lambda_{\mathrm{M}}[\lambda_+(\mu_+ + \mu_{\mathrm{M}} + 2\gamma\lambda_{\mathrm{M}}) - (\lambda_+ + \lambda_{\mathrm{M}})(\gamma i_0 + \mu_+)]} \tag{8}$$

$$C = (\lambda_+/\omega) \times \frac{\lambda_+\lambda_{\mathrm{M}}[i_0(\mu_+ + \mu_{\mathrm{M}}) - 2\lambda_{\mathrm{M}}\mu_+] - i_0(\lambda_+ + \lambda_{\mathrm{M}})[i_0(\mu_+ + \mu_{\mathrm{M}}) + \lambda_{\mathrm{M}}(\gamma i_0 - \mu_+)]}{[\lambda_+\lambda_{\mathrm{M}} - (\lambda_+ + \lambda_{\mathrm{M}})i_0]^2 + (\lambda_+\lambda_{\mathrm{M}})^2} + \left\{\left[\frac{\partial(q + zF\Gamma_+)}{\partial E}\right]_{c^{\mathrm{s}}_+} + \left[\frac{\partial(q + zF\Gamma_+)}{\partial E}\right]_{c^{\mathrm{s}}_{\mathrm{M}}}\right\}_{\eta=0} \tag{9}$$

where

$$\gamma = zF/BT \tag{10}$$

---

[4] H. Gerischer, *Z. Physik. Chem.* (Leipzig), **198**, 286 (1951).

$$\lambda_+ = -zFc^{s}{}_{+}(\omega D_+/2)^{1/2} \tag{11}$$

$$\lambda_M = -zFc^{s}{}_{M}(\omega D_M/2)^{1/2} \tag{12}$$

$$\mu_+ = zF\omega[(\partial\Gamma_+/\partial E)_{c^{s}{}_{M}} + (\partial\Gamma_+/\partial E)_{c^{s}{}_{+}}]_{\eta=0} \tag{13}$$

$$\mu_M = zF\omega[(\partial\Gamma_M/\partial E)_{c^{s}{}_{M}} + (\partial\Gamma_M/\partial E)_{c^{s}{}_{+}}]_{\eta=0} \tag{14}$$

It may be noted that R and C can of course be converted to an equivalent circuit composed of a resistance and capacity in series, but equations are cumbersome and the parallel circuit is more convenient.

A Posteriori Separation of Faradaic and Double-Layer Impedance

Significance. The resistance R and C of eq 8 and 9 are experimental quantities which can be determined from the cell impedance after correction for the electrolyte resistance. (The impedance of the counterelectrode is generally negligible.) A series resistance–capacity combination may actually be used in the bridge, but measurements can be converted to the parallel circuit involving R and C of eq 8 and 9. This circuit represents the electrode impedance.

We *formally* divide the electrode impedance into two parts: (a) the classical faradaic impedance which is derived by neglecting double-layer charging and (b) the remaining part which is the double-layer impedance. It should be stressed that this *a posteriori* separation does not correspond to any conceivable physical operation because the faradaic process and double-layer charging cannot be separated.[2] *Only the total electrode impedance has an experimental significance.* However, such a separation is useful in bringing out the features of double-layer charging in terms of the familiar model in which the faradaic impedance and the double layer are separated.

Faradaic Impedance. The elements R_f and C_f of the equivalent parallel circuit of the faradaic impedance are derived by conversion of the series equivalent circuit composed of the charge-transfer resistance and the Warburg resistance and capacity. Values of R_f and C_f derived in this way are those given by eq 8 and 9 in which μ_+ and μ_M are set equal to zero and the last term on the right-hand side is dropped (no double layer). Thus

$$R_f = \frac{[\lambda_+\lambda_M - (\lambda_+ + \lambda_M)i_0]^2 + (\lambda_+\lambda_M)^2}{\gamma\lambda_+\lambda_M i_0[2\lambda_+\lambda_M - i_0(\lambda_+ + \lambda_M)]} \tag{15}$$

$$C_f = -\left(\frac{\lambda_+}{\omega}\right)\frac{\gamma\lambda_M(\lambda_+ + \lambda_M)i_0{}^2}{[\lambda_+\lambda_M - (\lambda_+ + \lambda_M)i_0]^2 + (\lambda_+\lambda_M)^2} \tag{16}$$

The parallel R_fC_f equivalent circuit of the faradaic impedance is well known[1,4] and need not be discussed.

Double-Layer Impedance. The terms containing μ_+ and μ_M in eq 8 and 9 and the last term on the right-hand side correspond to charging of the double layer. Thus

$$R_{dl} = \frac{[\lambda_+\lambda_M - (\lambda_+ + \lambda_M)i_0]^2 + (\lambda_+\lambda_M)^2}{\lambda_+\lambda_M(\lambda_+\mu_M - \lambda_M\mu_+)i_0} \tag{17}$$

$$C_{dl} = (\lambda_+/\omega) \times \frac{\lambda_+\lambda_M[(\mu_+ + \mu_M)i_0 - 2\lambda_M\mu_+] - (\lambda_+ + \lambda_M)[(\mu_+ + \mu_M)i_0 - \lambda_M\mu_+]i_0}{[\lambda_+\lambda_M - (\lambda_+ + \lambda_M)i_0]^2 + (\lambda_+\lambda_M)^2} + \left\{\left[\frac{\partial(q + zF\Gamma_+)}{\partial E}\right]_{c^{s}{}_{+}} + \left[\frac{\partial(q + zF\Gamma_+)}{\partial E}\right]_{c^{s}{}_{M}}\right\}_{\eta=0} \tag{18}$$

According to classical views, one would write $R_{dl} \to \infty$ and $C_{dl} = (\mathrm{d}q/\mathrm{d}E)_{\eta=0}$ (neglecting the fact that E depends on $c^{s}{}_{+}$ and $c^{s}{}_{M}$) for an ideal polarized electrode; *i.e.*, C_{dl} would be frequency independent. Equations 17 and 18 show that R_{dl} and C_{dl} are frequency dependent. This frequency effect results from the interplay of diffusion of M^{+z} and M and the charge-transfer reaction in double-layer charging.

The equivalent circuit for the electrode impedance is shown in Figure 1 as the parallel combination of the faradaic and double-layer impedance.

Double-Layer Impedance

Limiting Values of the Capacity C_{dl}. One would expect from a previous paper[2] that C_{dl} approaches a capacity similar to that for an ideal polarized electrode at infinite frequency for any finite i_0 and approaches the capacity for an ideal reversible electrode at zero frequency. This is indeed the case. Thus, the ratio of the terms of the highest degree in ω ($\omega^{5/2}$) in the numerator and denominator in eq 18 is equal to

$$-zF[(\partial\Gamma_+/\partial E)_{c^{s}{}_{+}} + (\partial\Gamma_+/\partial E)_{c^{s}{}_{M}}]_{\eta=0}$$

and consequently, for any finite frequency

$$(C_{dl})_{\omega\to\infty} = \left[\left(\frac{\partial q}{\partial E}\right)_{c^{s}{}_{+}} + \left(\frac{\partial q}{\partial E}\right)_{c^{s}{}_{M}}\right]_{\eta=0} \tag{19}$$

where the derivatives are taken at the equilibrium potential. This capacity is the same as for an ideal polarized electrode, except that E now depends on $c^{s}{}_{+}$

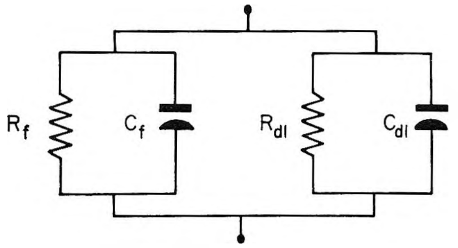

Figure 1. Equivalent parallel circuit for the electrode impedance.

and $c^s{}_M$. Hence two derivatives appear in eq 19, whereas one simply has dq/dE for an ideal polarized electrode.

Conversely, the ratio of the terms of lowest degree in ω ($\omega^{3/2}$) in the numerator and denominator in eq 18 is equal to $-[\lambda_+/(\lambda_+ + \lambda_M)][(\mu_+ + \mu_M)/\omega]$ for any finite i_0.

$$(C_{dl})_{\omega\to 0} = \left\{\left[\frac{\partial(q + zF\Gamma_+)}{\partial E}\right]_{c^s{}_+} + \left[\frac{\partial(q + zF\Gamma_+)}{\partial E}\right]_{c^s{}_M}\right\}_{\eta=0} - \frac{zF}{1 + \frac{c^s{}_M}{c^s{}_+}\left(\frac{D_M}{D_+}\right)^{1/2}} \times \left\{\left[\frac{\partial(\Gamma_+ + \Gamma_M)}{\partial E}\right]_{c^s{}_+} + \left[\frac{\partial(\Gamma_+ + \Gamma_M)}{\partial E}\right]_{c^s{}_M}\right\}_{\eta=0} \quad (20)$$

When $i_0 \to \infty$, C_{dl} at any frequency is always given by eq 20, and this process exhibits charging behavior as an ideal reversible electrode, regardless of the frequency. This is not surprising.

The physical interpretation of the limiting values of eq 19 and 20 is identical with the one previously advanced:[2] there is no time for charge separation or recombination to occur for $\omega \to \infty$ and for a finite i_0; conversely, double-layer charging occurs entirely by charge separation or recombination for $\omega \to 0$.

Differential Capacity of the Ideal Reversible Electrode. Equation 20 is a significant result because it gives the differential capacity of an ideal reversible electrode for the conditions prevailing in electrode impedance measurements. This result can be derived directly by starting with the basic thermodynamic equation[5,6] for an ideal polarized electrode as written for a constant chemical potential of the supporting electrolyte. Thus

$$d\sigma = -(q + zF\Gamma_+)\, dE - (\Gamma_+ + \Gamma_M)RT\, d \ln c_M \quad (21)$$

where dE results from a variation of c_+ at constant c_M. There σ is the interfacial tension, R the gas constant, and T the absolute temperature; the Γ's are the relative surface excesses with respect to the solvent and mercury. Equation 21 is written with c_M rather than the activity of M, in agreement with the use of concentrations rather than activities in the writing of the faradaic current of eq. 1. Since the concentrations of M^{+z} and M at the interface are not independent, we express d ln c_M at $x = 0$ as a function of dE for impedance measurements for $\omega \to 0$. The derivation is as follows.

We express $(c_M)_{x=0}$ for a simple Warburg impedance and for $\omega \to 0$; that is, we write eq 6 for $x = 0$, $\mu_+ = \mu_M = 0$, and $i_0 \to \infty$. Thus

$$[(c_M)_{x=0}]_{\omega\to 0} = c^s{}_M\left\{1 - \gamma\eta_a\frac{\lambda_+}{\lambda_+ + \lambda_M}\right\}\exp(j\omega t) \quad (22)$$

One obtains after replacing η, γ, and the λ's from eq 3 and 10–12

$$RT\, d \ln [(c_M)_{x=0}]_{\omega=0} = -\frac{zF}{1 + \frac{c^s{}_M}{c^s{}_+}\left(\frac{D_M}{D_+}\right)^{1/2}}dE \quad (23)$$

Hence eq 21 becomes

$$d\sigma = -\left\{(q + zF\Gamma_+) - \frac{zF(\Gamma_+ + \Gamma_M)}{1 + \frac{c^s{}_M}{c^s{}_+}\left(\frac{D_M}{D_+}\right)^{1/2}}\right\}dE \quad (24)$$

The second derivative of σ with respect to E is, by definition, the differential capacity of the ideal reversible electrode. This capacity is exactly that given by eq 20 provided one notes that

$$d^2\sigma/d\eta^2 = (\partial^2\sigma/\partial\eta^2)_{c^s{}_+} + (\partial^2\sigma/\partial\eta^2)_{c^s{}_M}$$

Equation 20 does not have the customary thermodynamic form for an ideal reversible electrode because both concentrations of M^{+z} and M vary simultaneously whereas only one of these concentrations varies in the usual treatment. Furthermore, D_+ and D_M appear in eq 20 because the concentrations at $x = 0$ depend on these diffusion coefficients.

The difference between the values of C_{dl} given by eq 19 and 20 depends on the quantity ρ defined by

$$\frac{\rho}{zF} = \left[\left(\frac{\partial\Gamma_+}{\partial E}\right)_{c^s{}_+} + \left(\frac{\partial\Gamma_+}{\partial E}\right)_{c^s{}_M}\right]_{\eta=0} - \frac{\left\{\left[\frac{\partial(\Gamma_+ + \Gamma_M)}{\partial E}\right]_{c^s{}_+} + \left[\frac{\partial(\Gamma_+ + \Gamma_M)}{\partial E}\right]_{c^s{}_M}\right\}_{\eta=0}}{1 + \frac{c^s{}_M}{c^s{}_+}\left(\frac{D_M}{D_+}\right)^{1/2}} \quad (25)$$

The quantity $[(\partial\Gamma_+/\partial E)_{c^s{}_+} + (\partial\Gamma_+/\partial E)_{c^s{}_M})_{\eta=0}$ can be evaluated from the diffuse double-layer theory (no specific adsorption of M^{+z}) as shown in the Appendix, but the $\partial\Gamma_M/\partial E$'s are not known in general. If we momentarily neglected the $\partial\Gamma_M/\partial E$ terms and assume $c^s{}_M = c^s{}_+$ and $D_M = D_+$, we find (Appendix) that ρ can easily be of the order of 100 μf cm^{-2} in 0.1 M univalent supporting electrolyte and about 7 μf cm^{-2} in 1 M univalent supporting electrolyte. Actual values of ρ should be different because of the contributions from the $\partial\Gamma_M/\partial E$ terms and may be smaller (or larger!) than the above values. Anyhow, it appears that the difference between the infinite frequency (eq 19) and zero frequency (eq 20) capacities, *in the absence of specific adsorption,* can be significant or even large

---

(5) D. C. Grahame and R. R. Whitney, *J. Am. Chem. Soc.*, **64**, 1548 (1942).

(6) D. M. Mohilner, *J. Phys. Chem.*, **66**, 724 (1962).

(for 0.1 M supporting electrolyte). Specific adsorption of M^{+z} probably enhances ρ and renders the difference between the capacities of eq 19 and 20 even more significant than in the absence of specific adsorption.

High values of ρ, in the absence of specific adsorption, are surprising upon superficial examination because c^{s}_{+} is quite small in comparison with the supporting electrolyte concentration. Hence $zF\Gamma_{+}$ is small in comparison with q. However, c^{s}_{+}, at constant c^{s}_{M}, varies rapidly with E (Nernst equation), and consequently it is not surprising that ρ, which depends on the derivatives of the Γ's with respect to E, can be quite comparable to q.

It should also be noted that ρ in eq 25 may not have the same sign as q. Indeed the case may be encountered where q and ρ change sign at different potentials. In that event the capacity of eq 20 may exhibit a complicated and perhaps rapid variation with potential.

Frequency Dependence of C_{dl}. Variations of C_{dl} with frequency are shown in Figure 2 for conditions similar to those in actual measurements. The corresponding faradaic capacity of eq 16 is plotted in Figure 3 for comparison purpose. We note that charging as an ideal polarized electrode nearly prevails for $i_0 \leqslant 10^{-3}$ amp cm^{-2} at or above 10^3 Hz and that the faradaic capacity (Figure 3) is then quite negligible. Conversely, charging as an ideal reversible electrode practically holds up to 10^5 Hz for $i_0 \geqslant 1$ amp cm^{-2}. Moreover, there is a pronounced frequency dependence of C_{dl}, especially for $10^{-3} < i_0 \leqslant 10^{-1}$ amp cm^{-2}, in the usual frequency range (10^2–10^6 Hz) used in electrode-impedance measurements. This range of i_0 precisely corresponds to a number of processes which have been studied by this method.

Selection of Experimental Frequencies. Analysis is simplified when C_{dl} can be assumed to be frequency independent for all practical purposes since the Sluyters method[3] then can be applied (see below). Furthermore, in the determination of i_0, the Warburg resistance should not overwhelm the charge-transfer resistance; *i.e.*, sufficiently high frequencies should be used since the Warburg resistance vanishes for $\omega \rightarrow \infty$. These two requirements are met for usual electrode impedance bridges (up to 100 kHz) for rather slow charge-transfer reaction (*e.g.*, $i_0 = 10^{-3}$ amp cm^{-2} in Figure 2). Faster processes require frequencies too high for usual bridges[7,8] if the C_{dl} for $\omega \rightarrow \infty$ is to be reached. Frequencies low enough to allow the use of C_{dl} for $\omega \rightarrow 0$ may unfortunately be in a range where the Warburg impedance is prohibitively high in comparison with the charge-transfer resistance. If the two limiting values of C_{dl} are quite different, complete analysis, including the frequency dependence of the double-layer impedance, cannot be avoided. This cumbersome problem is now being examined.

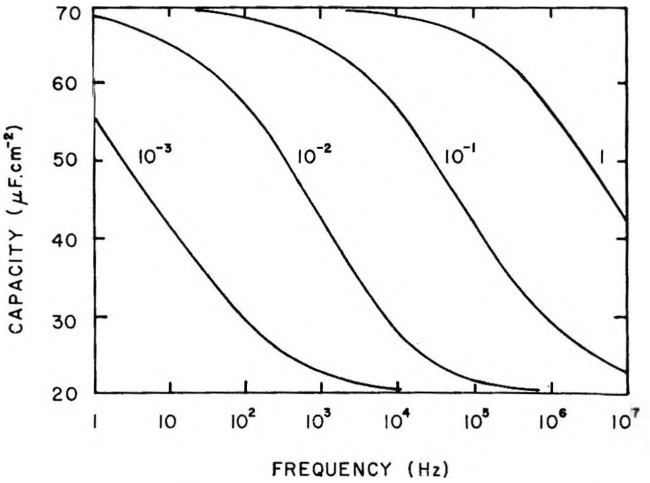

Figure 2. Capacity C_{dl} of the double-layer impedance as a function of frequency for different i_0's (amp cm^{-2}) and for the following data: $z = 2$, $T = 25°$, $c^{s}_{+} = c^{s}_{M} = 10^{-6}$ mole l.$^{-1}$, $D_{+} = D_{M} = 10^{-5}$ cm^2 sec^{-1}. $[(\partial q/\partial E)_{c^{s}_{+}} + (\partial q/\partial E)_{c^{s}_{M}}]_{\eta=0} = 20\ \mu$f cm^{-2}, $zF[(\partial\Gamma_{+}/\partial E)_{c^{s}_{+}} + (\partial\Gamma_{+}/\partial E)_{c^{s}_{M}}]_{\eta=0} = 50\ \mu$f cm^{-2}, $\partial\Gamma_{M}/\partial E = 0$ at c^{s}_{+} or c^{s}_{M} constant.

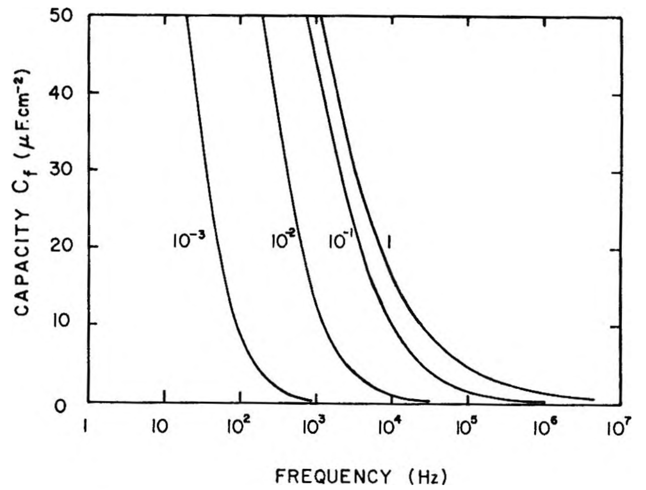

Figure 3. Capacity C_f of the faradaic impedance as a function of frequency for the data of Figure 2.

Phase Shift. The phase shift φ for the double-layer impedance which is defined by

$$\tan \varphi = \omega R_{dl} C_{dl} \qquad (26)$$

can be readily calculated from eq 17 and 18. One finds that $\tan \varphi \rightarrow \infty$ both for $\omega \rightarrow 0$ and $\omega \rightarrow \infty$; *i.e.*,

---

(7) Electrode impedances have been measured up to 1 MHz (approximately) by means of a T bridge.[8]

(8) W. Lorenz, *Z. Physik. Chem.* (Frankfurt), **26**, 424 (1960).

the double-layer impedance is purely capacitive for these two limits. Tan φ as a function of ω exhibits a minimum for

$$\omega_{\min} = \frac{i_0^2}{2}\left(\frac{1}{\lambda_+} + \frac{1}{\lambda_M}\right)^2 \frac{(C_{dj})_{\omega=0}}{(C_{dl})_{\omega\to\infty}} \tag{27}$$

By introducing $\omega_{\min}$ in eq 17, 18, and 26 one finds that tan φ at $\omega_{\min}$ is independent of i_0. For instance, tan $\varphi_{\min} = 7$ for the data of Figure 2, and consequently the capacitive component of the double-layer impedance is predominant. In that example $\omega_{\min}$ corresponds to $f = 14.4$ Hz, 1.44 kHz, and 144 kHz for $i_0 = 10^{-3}$, 10^{-2}, and 10^{-1} amp cm^{-2}, respectively.

One can also show that tan $\varphi \to \infty$ for $\omega \to 0$ and $\omega \to \infty$ from the limits of R_{dl} of eq 17 and C_{dl} for $\omega \to 0$ and $\omega \to \infty$. Thus, $R_{dl} \to \infty$ for $\omega \to 0$, whereas C_{dl} is finite; *i.e.*, tan $\varphi \to \infty$ for $\omega \to \infty$. Conversely, R_{dl} for $\omega \to \infty$ is proportional to $\omega^{-1/2}$, whereas C_{dl} is finite, and tan $\varphi \to \infty$ for $\omega \to \infty$.

Metal Ion–Pure Metal Electrodes and Other Electrode Reactions

The foregoing treatment can be applied directly to an oxidation–reduction electrode reaction involving two soluble species in solution. Transposition to the metal ion–pure metal electrode reaction, $M^{+z} + ze = M$, is immediate by letting $\lambda_M \to \infty$, $\mu_M \to 0$, and $(d\Gamma_+/dE)_{c^s_M} \to 0$. One can also derive the impedance directly as follows: the boundary condition is identical with eq 1 in which $(c^s_M/c^s_+)_{x=0}$ is set equal to unity and $(d\Gamma_+/dE)_{c^s_+}$ vanishes. The concentration c_+ is given by eq 5 where P is determined by satisfying the boundary condition. Thus eq 8 and 9 are replaced by

$$R = \frac{(\lambda_+ - i_0)^2 + \lambda_+^2}{i_0\lambda_+[2\gamma\lambda_+ - (\gamma i_0 + \mu_+)]} \tag{28}$$

$$C = -\left(\frac{\lambda_+}{\omega}\right)\frac{2\lambda_+\mu_+ + \gamma c_0^2 - \mu_+ i_0}{(\lambda_+ - i_0)^2 + \lambda_+^2} + \left[\frac{d(q + zF\Gamma_+)}{dE}\right]_{\eta=0} \tag{29}$$

where μ_+ is given by eq 13 in which $(d\Gamma_+/dE)_{c^s_+}$ vanishes. The double-layer impedance is represented by the parallel circuit composed of

$$R_{dl} = -\frac{(\lambda_+ - i_0)^2 + \lambda_+^2}{\lambda_+\mu_+ i_0} \tag{30}$$

$$C_{dl} = -\frac{\lambda_+\mu_+(2\lambda_+ - i_0)}{\omega[(\lambda_+ - i_0)^2 + \lambda_+^2]} + \left[\frac{d(q + zF\Gamma_+)}{dE}\right]_{\eta=0} \tag{31}$$

One readily verifies that the limiting value of C_{dl} for $\omega \to \infty$ is that of an ideal polarized electrode (dq/dE), whereas the limit for $\omega \to 0$ is $[d(q + zF\Gamma_+)/dE]_{\eta=0}$, in agreement with thermodynamics (see eq 21 without the term d ln c_M). Previous comments about the frequency dependence of the double-layer impedance can be transposed to this case.

Reexamination of the Sluyters Method and Some Results Obtained by It

Conditions for Validity of the Method. The Sluyters analysis[3] of experimental data for separation of the faradaic impedance from the double-layer impedance is based on the assumption that the latter involves only a frequency-independent capacity. The faradaic impedance is supposed to obey the classical treatment. This method and its extension using graphic analysis of data[9] represent a definite progress over previous work in which the double-layer capacity with M^{+z} was supposed to be the same as for the supporting electrolyte. We conclude from the theory in this paper that the basic assumption of a frequency-independent capacity made by Sluyters is valid under the following conditions: (a) rigorously only for $\omega = 0$ and $\omega \to \infty$; (b) practically when $(C_{dl})_{\omega=0}$ and $(C_{dl})_{\omega\to\infty}$ are the same for all practical purposes; (c) when experimental data are obtained in a range of frequency in which C_{dl} remains close to $(C_{dl})_{\omega=0}$ or $(C_{dl})_{\omega=\infty}$. The Sluyters method cannot be applied in its present form whenever C_{dl} varies significantly with frequency.

The previous analysis also accounts for some results obtained by Sluyters which however had not been interpreted by him. Some of Sluyters' inferences (double-pulse galvanostatic method, faradaic rectification), based on his results, must be reexamined in the light of the above theory.

Analysis of Tl^+ Data. Kinetic and double-layer data reported by Sluyters and co-workers can be divided into two groups: those for which C_{dl} is essentially that of the supporting electrolyte alone and those for which C_{dl} is significantly higher. To group I correspond Zn^{+2} in 1 *M* KCl or 1 *M* KI and Cd^{+2} in 1 *M* KCl;[10] in these cases, $(C_{dl})_{\omega=0} \approx (C_{dl})_{\omega=\infty}$[11] except for Cd^{+2} in 1 *M* KCl for which C_{dl} exceeded somewhat the capacity of the supporting electrolyte for $E < -0.7$ v *vs.* nce. To group II belong[12,13] the discharge on Tl^+ and Hg_2^{+2}. Since these processes are very fast, we can tentatively

---

(9) R. de Levie, *Electrochim. Acta*, **10**, 395 (1965).

(10) M. Sluyters-Rehbach and J. H. Sluyters, *Rec. Trav. Chim.*, **82**, 535 (1963).

(11) This should not be the case for 0.1 *M* KCl; measurements are now being made.

(12) M. Sluyters-Rehbach, B. Timmer, and J. H. Sluyters, *Rec. Trav. Chim.*, **82**, 553 (1963).

(13) M. Sluyters-Rehbach and J. H. Sluyters, *ibid.*, **83**, 217, 967 (1963).

assume that the double-layer capacities obtained by Sluyters, *et al.*, for the frequency range he used are nearly the ideal reversible electrode capacities $(C_{\mathrm{dl}})_{\omega=0}$. Equation 20 then applies to the capacity for Tl^+ and the capacity for $\mathrm{Hg_2}^{+2}$ is equal to $\mathrm{d}(q + zF\Gamma_+)/\mathrm{d}E$ (and not to $\mathrm{d}q/\mathrm{d}E$!). Results for Tl^+ will be examined first.

Equation 20 will first be written in the form

$$(C_{\mathrm{dl}})_{\omega=0} = -\left\{\frac{\partial}{\partial E}\left[szF(\Gamma_+ + \Gamma_{\mathrm{M}}) + \sum_{j\neq \mathrm{M}^{+2}} z_jF\Gamma_j\right]\right\}_{c^{s}_{+}} - \left\{\frac{\partial}{\partial E}\left[szF(\Gamma_+ + \Gamma_{\mathrm{M}}) + \sum_{j\neq \mathrm{M}^{+2}} z_jF\Gamma_j\right]\right\}_{c^{s}_{\mathrm{M}}} \quad (32)$$

with

$$s = \{1 + \exp[-(zF/RT)(E - E^{1/2})]\}^{-1} \quad (33)$$

where $E_{1/2}$ is the half-wave potential and z_j is the ionic valence of each ion, except M^{+z}, as taken with its sign. The value of s in eq 33 is written for generation of M *in situ* under reversible polarographic conditions. The Σ terms correspond to the supporting electrolyte alone and the anion of the salt of M^{+z}.

For $E > E_{1/2}$ with $E - E_{1/2} \gg RT/zE$, one has $s \rightarrow 1$, $\Gamma_{\mathrm{M}} \rightarrow 0$ (hardly any metal deposition). The terms in Γ_+ in eq 32 become significant when specific adsorption of Tl^+ becomes strong enough for the low concentrations (10^{-5} to 10^{-3} *M*) in Sluyters work. This occurs at potentials more negative than -0.3 v *vs.* nce.

Conversely, for $E < E^{1/2}$ with $|E - E_{1/2}| \gg RT/zF$, one has $s \rightarrow 0$ and $\Gamma_+ \rightarrow 0$ (diffusion current range). The capacity $(\mathrm{C_{dl}})_{\omega\,=\,0}$ is essentially that of the supporting electrolyte except if $zF\Gamma_{\mathrm{M}}$ is significant. In the case of Tl(Hg), $\Gamma_{\mathrm{Tl}} < 0$ at sufficiently negative potentials, and $(C_{\mathrm{dl}})_{\omega=0}$ is slightly larger than for the supporting electrolyte (see eq 32).

Sluyters, *et al.*,[12] found that the increase of capacity due to the presence of Tl^+ is proportional to the bulk concentration of Tl^+ at constant potential. They interpreted this linear relationship as the isotherm for adsorption of Tl^+. Actually, matters are more complex for two reasons: (a) $(C_{\mathrm{dl}})_{\omega=0}$ depends on Γ_+ and Γ_{M} which both are probably significant, except for the limiting cases discussed above; (b) specific adsorption of Tl^+ enhances anion adsorption, and consequently the Γ_j corresponding to the anion in eq 32 also changes when the Tl^+ concentration is varied. If one assumes linearity, which is reasonable at low concentration for all specific adsorption processes (M^{+z}, M, and anion enhanced adsorption), one indeed can account for experiment. This idea can be expressed quantitatively by using as variables the bulk concentration of Tl^+ and E. This will not be done here because application to the available experimental data would be difficult. The supporting electrolyte used by Sluyters, *et al.* (1 *M* $\mathrm{KNO_3}$ + 0.1 *M* KCl), exhibits strong anion specific adsorption which immediately complicates the analysis of adsorption. The experiment should be repeated with TlF in NaF.

Analysis of $Hg_2{}^{+2}$ Data.[13] If one assumes that $\mathrm{Hg_2}^{+2}$ is the sole mercury species in solution, one has

$$(C_{\mathrm{dl}})_{\omega=0} = \frac{\mathrm{d}(q + zF\Gamma_+)}{\mathrm{d}E} \quad (34\mathrm{a})$$

$$= -\frac{\mathrm{d}}{\mathrm{d}E}\sum_{j\neq \mathrm{M}^{+2}} z_jF\Gamma_j \quad (34\mathrm{b})$$

i.e., the surface excess of $\mathrm{Hg_2}^{+2}$ does not appear in eq 34b. If one assumes that Γ_j of the anion ($\mathrm{ClO_4}^-$) increases linearly with Γ_+ of $\mathrm{Hg_2}^{+2}$ one finds by application of the Nernst equation that the increase of capacity due to the presence of $\mathrm{Hg_2}^{+2}$ is proportional to $\exp[(zF/RT)E]$. This relationship is only very approximate. It involves the above rather drastic assumption and, moreover, correction for the supporting electrolyte alone is quite uncertain. Anyhow, the correct trend in the data of Sluyters, *et al.*, is obtained.

Use of $(C_{\mathrm{dl}})_{\omega=0}$ at High Frequencies or Short Pulses. Sluyters and co-workers used their measured capacities for $\mathrm{Hg_2}^{+2}$ in an analysis of previous results obtained by the double-pulse galvanostatic and faradaic rectification methods.[14,15] It is possible that i_0 for the discharge of $\mathrm{Hg_2}^{+2}$ is so high that the use of $(C_{\mathrm{dl}})_{\omega=0}$ in the analysis of data obtained in the microsecond range or up to 50 MHz is justified (see Figure 2). However, the exchange current densities that have been reported, and which are certainly open to question, are too low to justify the use of $(C_{\mathrm{dl}})_{\omega=0}$ under these conditions. This remark also applies to a similar comparison made for K^+ discharge[16] on Hg. In general, it seems necessary to take into account the frequency dependence of the double-layer impedance in the interpretation of faradaic rectification measurements, and this will complicate matters. Further comment must await the revision of the theory of these methods.

Acknowledgment. This work was supported in part by the Office of Naval Research.

Appendix

Derivation of the Electrode Impedance. The boundary

---

(14) M. Sluyters-Rehbach and J. H. Sluyters, *Rec. Trav. Chim.*, **83**, 983 (1964).

(15) D. J. Kooijman and J. H. Sluyters, *J. Electroanal. Chem.*, in press. Manuscript kindly supplied by one of the authors (J. H. S.).

(16) M. Sluyters-Rehbach and J. H. Sluyters, *Electrochim. Acta*, **11**, 73 (1966).

conditions of eq 1 and 2 become after introduction of c_+ and c_M at $x = 0$ from eq 5 and 6

$$i_0(N + P + \gamma\eta_a) = (1 + j)\lambda_+P + j\mu_+\eta_a \qquad (35)$$

$$(1 + j)\lambda_MN = (1 + j)\lambda_+P + j(\mu_+ + \mu_M)\eta_a \qquad (36)$$

Hence, after elimination of N

$$P = \frac{\eta_a}{2}\,\frac{2\lambda_M(\gamma i_0 - j\mu_+) + i_0(\mu_+ + \mu_M)(1 + j)}{\lambda_+\lambda_M - i_0(\lambda_+ + \lambda_M) + j\lambda_+\lambda_M} \qquad (37)$$

or, after separation of the real and imaginary parts

$$P = (\eta_a/2)(P_1/P_2) \qquad (38)$$

with

$$\begin{aligned} P_1 = {} & i_0(2\gamma\lambda_M + \mu_+ + \mu_M)[\lambda_+\lambda_M - i_0(\lambda_+ + \lambda_M)] - \\ & \lambda_+\lambda_M[2\lambda_M\mu_+ - i_0(\mu_+ + \mu_M)] - \\ & j\{[2\lambda_M\mu_+ - i_0(\mu_+ + \mu_M)][\lambda_+\lambda_M - \\ & i_0(\lambda_+ + \lambda_M)] + i_0\lambda_+\lambda_M(2\gamma\lambda_M + \mu_+ + \lambda_M)\} \qquad (39) \end{aligned}$$

$$P_2 = [\lambda_+\lambda_M - i_0(\lambda_+ + \lambda_M)]^2 + (\lambda_+\lambda_M)^2 \qquad (40)$$

Evaluation of ρ of Eq 25 in the Absence of Specific Adsorption. We evaluate ρ for attraction of M^{+z} in the diffuse double layer in the absence of specific adsorption. One has[17]

$$zF\Gamma_+ = A\left[\exp\left(-\frac{zF}{2RT}\phi_2\right) - 1\right] \qquad (41)$$

with

$$A = \left(\frac{RT\epsilon c^s_+}{2\pi}\right)^{1/2} \qquad (42)$$

where ϕ_2 is the potential in the plane of closest approach and ϵ is the dielectric constant in the diffuse double layer. One has at 25°, $A = 5.87(c^s_+)^{1/2}$ with $zF\Gamma_+$ in μcoulomb cm^{-2} and c^s_+ in mole l.$^{-1}$. Since both c^s_+ and ϕ_2 vary with E, one has at constant c^s_M

$$\left(\frac{\partial\Gamma_+}{\partial E}\right)_{c^s_M} = \left(\frac{\partial\Gamma_+}{\partial c^s_+}\right)_{\phi_2,c^s_M}\frac{dc^s_+}{dE} + \left(\frac{\partial\Gamma_+}{\partial\phi_2}\right)_{c^s_+,c^s_M}\frac{d\phi_2}{dE} \qquad (43)$$

At constant c^s_+ and for varying c^s_M only the term with $d\phi_2/dE$ in the equation similar to eq 43 needs be retained since the derivative $(\partial\Gamma_+/\partial c^s_M)_{\phi_2,c^s_M}$ should generally be small in comparison with $(\partial\Gamma_+/\partial c^s_+)_{\phi_2,c^s_+}$. Hence

$$\left(\frac{\partial\Gamma_+}{\partial E}\right)_{c^s_M} + \left(\frac{\partial\Gamma_+}{\partial E}\right)_{c^s_+} = \left(\frac{\partial\Gamma_+}{\partial c^s_+}\right)_{\phi_2,c^s_M}\frac{dc^s_+}{dE} + 2\left(\frac{\partial\Gamma_+}{\partial\phi_2}\right)_{c^s_+,c^s_M}\frac{d\phi_2}{dE} \qquad (44)$$

The derivative $d\phi_2/dE$ is known from double-layer studies and $dc^s_+/dE = (zF/RT)c^s_+$ from the Nernst equation. Thus

$$zF\left[\left(\frac{\partial\Gamma_+}{\partial E}\right)_{c^s_M} + \left(\frac{\partial\Gamma_+}{\partial E}\right)_{c^s_+}\right] = A\frac{zF}{2RT}\left[\left(1 - 2\frac{d\phi_2}{dE}\right)\exp\left(-\frac{zF}{2RT}\phi_2\right) - 1\right] \qquad (45)$$

As an example we take the following data which correspond approximately to Zn^{+2} discharge on zinc amalgam in a 0.1 M univalent supporting electrolyte (no complex formation): $z = 2$, $c^s_+ = 10^{-3}$ mole l.$^{-1}$, $\phi_2 = -0.09$ v, $d\phi_2/dE = 0.08$. Then $zF[(\partial\Gamma_+/\partial E)_{c^s_M} + (\partial\Gamma_+/\partial E)]_{c^s_+} = 194$ μf cm^{-3}. For a 1 M univalent supporting electrolyte ($\phi_2 = -0.03$ v, $d\phi_2/dE = 0.05$), the corresponding capacity is 13.9 μf cm^{-2}.

---

(17) See, *e.g.*, P. Delahay, "Double Layer and Electrode Kinetics," Interscience Publishers, Inc., New York, N. Y., 1965, p 47. The more general equation for electrolyte mixtures should be applied but eq 41 suffices, as a first approximation, since c_+ is quite small in comparison with the supporting electrolyte concentration.

The ($^3P_1$) Mercury-Photosensitized Decomposition of Monogermane

by Yves Rousseau and Gilbert J. Mains[1]

Department of Chemistry, Carnegie Institute of Technology, Pittsburgh, Pennsylvania 15213

(Received April 25, 1966)

The Hg6($^3P_1$)-photosensitized decomposition of GeH_4 appears to proceed by rupture of a Ge–H bond. Hydrogen, digermane, trigermane, tetragermane, and polymer were observed products. The H atoms formed in the primary process were not scavenged by 5% added propylene. The effect of added helium on the (HD)/(H_2) ratio obtained from the photolysis of a GeH_4–C_2D_6 system suggests the participation of "hot" hydrogen atoms in the reaction mechanism.

Introduction

Studies of the mercury-photosensitized decompositiln of paraffin-type hydrocarbons have revealed quantum efficiencies near unity at pressures corresponding to almost complete quenching.[2-4] A notable exception is methane for which the quantum yields of product formation are quite low.[5-7] Recent investigations of the mercury-photosensitized decomposition of monosilane in this laboratory[8] and elsewhere[9] have shown that this silicon analog behaves very differently from methane, the quantum yields of product formation exceeding unity. In order to extend this sequence of investigations[6,8] to additional group IV hydrides, the mercury-photosensitized decomposition of monogermane was studied. The most recent study of the mercury-photosensitized decomposition of monogermane, aside from a preparative investigation,[10] was reported by Romeyn and Noyes[11] in 1932.

Romeyn and Noyes proposed the following *over-all* equation to describe the photodecomposition of monogermane in the pressure range 0.01–5 torr

$$GeH_4 \xrightarrow{Hg(^3P_1)} Ge + 2H_2 \qquad (1)$$

The rate of the proposed primary process, *viz.*

$$Hg6(^3P_1) + GeH_4 \longrightarrow GeH_3 + H + Hg6(^1S_0) \qquad (2)$$

suggested a quenching cross section of GeH_4 for Hg6 ($^3P_1$) atoms of 140 A^2.

The present study was undertaken to extend the investigation of Romeyn and Noyes to a wider range of experimental conditions and, using GeD_4 as a tracer, to determine whether or not the primary process involved the production of hydrogen atoms as proposed.

Experimental Section

The cylindrical quartz reaction vessels, 7 cm in diameter and 10 cm long, were filled with GeH_4 to the desired pressure after addition of a drop of clean mercury and evacuation using a high-vacuum apparatus. The filled vessels were irradiated with a low-pressure mercury lamp, Hanovia SC 2537, described previously.[8] The temperature of the reaction vessel was maintained at 25° by flowing air from the air-conditioned laboratory over the cell–lamp system. Unless stated otherwise, all experiments were performed in duplicate. A neutral density filter and a Vycor no. 7910 filter were interposed between the reaction vessel and the lamp to reduce the light flux and to prevent appreciable 1849-A radiation from entering the reaction vessel. Using a nitrous oxide–butane actinometer, the 2537-A radiation absorbed in the vessel was found to be 0.16 μeinstein/min. A

---

(1) Department of Chemistry, University of Detroit, Detroit, Mich.

(2) R. A. Back, *Trans. Faraday Soc.*, **54**, 512 (1958).

(3) R. A. Back, *Can. J. Chem.*, **37**, 1834 (1959).

(4) R. J. Cvetanovic, W. E. Falconer, and K. R. Jennings, *J. Chem. Phys.*, **35**, 1225 (1961).

(5) K. Morikawa, W. S. Benedict, and H. S. Taylor, *ibid.*, **5**, 212 (1937).

(6) G. J. Mains and A. S. Newton, *J. Phys. Chem.*, **65**, 212 (1961).

(7) R. A. Back and D. van der Auwera, *Can. J. Chem.*, **40**, 2339 (1962).

(8) H. Niki and G. J. Mains, *J. Phys. Chem.*, **68**, 304 (1964).

(9) M. A. Nay, G. N. C. Woodall, O. P. Strausz, and H. E. Gunning, *J. Am. Chem. Soc.*, **87**, 179 (1965).

(10) G. Gibbon, Y. Rousseau, C. H. Van Dyke, and G. J. Mains, *Inorg. Chem.*, **5**, 114 (1966).

(11) H. Romeyn and W. A. Noyes, Jr., *J. Am. Chem. Soc.*, **54**, 4143 (1932).

experimentally determined value[11] of $\psi = (\kappa - \kappa_s)/(1 - \alpha)$, for tobacco mosaic virus, together with the same value of β_J^0, gave a value of 0.125 g/cm^{-4} for the effective density gradient.

Because values of ψ were not available in KBr and RbBr solutions for any protein and because the gradients obtained by the two procedures outlined above for CsCl were substantially the same, the effective density gradients for the first three salts listed in Table VIII were computed using the separate terms in eq 4.

The molecular weight of the solvated protein–salt complex was calculated from the relation[9]

$$M_{s,0} = \frac{RT\rho_0}{\sigma^2(\mathrm{d}\rho/\mathrm{d}r)_{\mathrm{eff}}\omega^2 r_0} \tag{20}$$

where ρ_0 is the density at the actual pressure in the experiment of the solution at band center. It is recognized that a term which expresses the variation of z_{XY} with distance in the band should have been included in the formulation of the effective density gradient. The salt binding increases with distance in the band and causes the species to become denser on the dense side and lighter on the light side than at band center. The anticipated effect is thus to lower the effective density gradient. This effect has not been included in the numerical calculations of the molecular weight. The magnitude of the errors incurred are estimated in the discussion. The molecular weight of the anhydrous protein was calculated from the equation

$$M_a = \frac{M_{s,0}}{1 + \Gamma_*' + z_{XY}} \tag{21}$$

Results

Anion Binding. The results of the anion binding experiments are collected in Table IV. The densities of the solutions in which measurements were performed are given in the second column. These correspond to within 0.010 g/ml of the buoyant densities. In concentrated salt solutions the anion binding by bovine albumin is relatively insensitive to salt concentration.[21]

The results for CsBr and RbBr are the least accurate. Two sets of ΔpH's differing by about 0.2 pH unit were obtained in each case. The value selected for CsBr was that given by three out of five measurements. The value given for RbBr was that which was consistent with the other two bromides. Scatchard and Black[8] have shown that the nature of the alkali cation has little effect on the extent of anion binding.

Refractive Index–Density Relations. The refractive index–density relations are presented in Table V as coefficients of the linear relation $\rho^{25} = a(n^{25}\mathrm{D}) - b$. Equations for KBr and RbBr give densities accurate to ±0.001 g/ml. The precision for the other salts is ±0.002 g/ml.

Table IV: Anion Binding from pH Shifts in Isoionic Protein Solutions

Salt	ρ	$\sqrt{I}$	w	ΔpH	$\bar{\nu}$	No. of anions bound
CsCl	1.278	2.22	0.0153	0.71	53	53
KBr	1.306	2.98	0.0138	0.81	67	67
RbBr	1.315	2.40	0.0149	0.85	66	66
CsBr	1.306	2.04	0.0158	0.96	70	70
CsI	1.331	1.93	0.0162	1.10	78	78
Cs_2SO_4	1.237	2.31	0.0151	0.64	49	25

Table V: Density *vs.* Refractive Index Relations for Several Aqueous Salt Solutions

$$\rho^{25} = a(n^{25}\mathrm{D}) - b$$

Salt	Parameters of equations		Density range
	a	b	
CsCl	10.8601	13.4974	1.25–1.90[a]
KBr	6.4786	7.6431	1.10–1.35
RbBr	9.1750	11.2410	1.15–1.65
CsBr	9.9667	12.2876	1.25–1.35
CsI	8.8757	10.8381	1.20–1.55
Cs_2SO_4	12.1200	15.1662	1.15–1.40

[a] A more accurate relation for 1.10 < ρ 1.38, ρ_4^{25} 10.2402, $n^{25}\mathrm{D}$ −12.6483, has recently been evaluated for CsCl solutions: R. Bruner and J. Vinograd, *Biochim. Biophys. Acta*, **108**, 18 (1965).

Density Gradient Experiments. The buoyant densities, standard deviations, and the net hydration of salt-free protein for the six salts are given in Table VI.

Table VI: Buoyant Densities, Standard Deviation, and Net Hydrations of BMA in Several Salt Solutions

Salt	ρ_0^0	ρ_0	σ_{av}	Γ'
CsCl	1.278	1.282	0.106	0.200
CsAc	1.291	. . .	. . .	. . .
KBr	1.295	1.302	0.147	0.138
RbBr	1.302	1.310	0.103	0.115
	1.302	1.310	0.106	0.115
CsBr	1.306	1.315	0.084	0.102
CsI	1.331	1.347	0.071	0.025
Cs_2SO_4	1.237	1.241	0.071	0.359

---

(21) G. Scatchard, Y. V. Wu, and A. L. Shen, *J. Am. Chem. Soc.*, 81, 6014 (1959).

cross section is as high as the 140 A^2 suggested by Romeyn and Noyes.

The rate of formation of Ge_2H_6 as a function of irradiation time is plotted in Figure 3 along with the rate of formation of hydrogen for comparison. These data suggest that the *initial* rates of hydrogen and digermane production are equal. The decrease in the rate of Ge_2H_6 production may be attributed to the consumption of this compound in the formation of trigermane, tetragermane, and polymer.

Table I shows the effect of propylene on the rate of hydrogen production. It should be noted that the addition of 5.3% propylene has little effect on the rate of hydrogen formation. Table II reports the isotopic distribution of hydrogens obtained from the irradiation of GD_4 and a mixture of GeH_4 and GeD_4. Figure 4 depicts the effect of helium on the ratio of H_2 to HD obtained from the mercury-photosensitized decomposition of a mixture of GeH_4 and C_2D_6. The significance of these observations will be treated in the subsequent discussion.

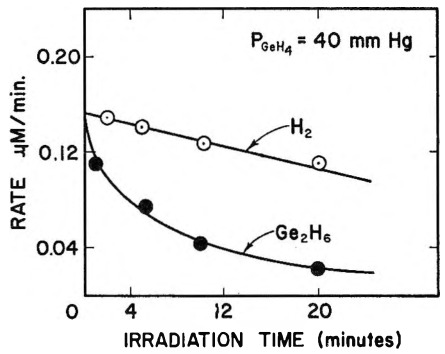

Figure 3. Effect of irradiation time on the rates of H_2 and GeH_4 production at 25°.

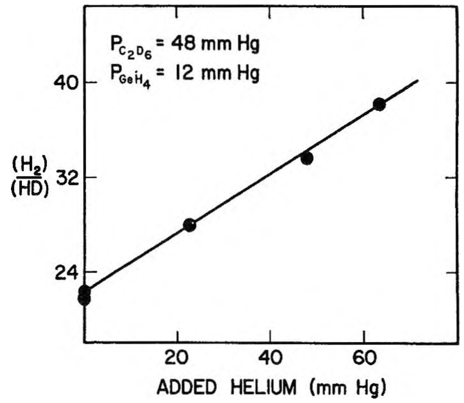

Figure 4. Effect of He pressure on the ratio $(H_2)/(HD)$ at 25°.

Table I: Effect of Propylene on H_2 in ($^3P_1$) Hg-Sensitized Photolysis of GeH_4 at 25°

p_{GeH_4}, torr	$p_{C_3H_6}$, torr	% decomposition	p_{H_2}, µmole/min
43	0	0.07	0.152
44	5.3	0.07	0.147

Table II: Isotopic Hydrogen Yields in the ($^3P_1$)Hg-Sensitized Photolysis of a GeH_4-GeD_4 Mixture at 25°

p_{GeD_4}, torr	p_{GeH_4}, torr	%H_2	%HD	%D_2	% decomposition
17	. . .	2.3	4.0	93.7	0.2
15.9	14.8	30.7	46.2	23.1	0.1

Discussion

The primary process, *i.e.*, the quenching of $6(^3P_1)Hg$ atoms by GeH_4, could conceivably be represented by any of the following reactions as they are all energetically feasible.

$$6(^3P_1)Hg + GeH_4 \longrightarrow GeH_3 + H + 6(^1S_0)Hg \quad (2)$$

$$\longrightarrow GeH_2 + H_2 + 6(^1S_0)Hg \quad (3)$$

$$\longrightarrow GeH + H_2 + H + 6(^1S_0)Hg \quad (4)$$

$$\longrightarrow Ge + 2H_2 + 6(^1S_0)Hg \quad (5)$$

Since there is no evidence for (or against) the participation of $6(^3P_0)Hg$ atoms in this system, these metastable atoms are not included in the reaction sequence.

The observed quantum yield of hydrogen, 0.92, rules out reactions 4 and 5 as the *exclusive* primary reactions since these would result in quantum yields in excess of unity. Furthermore, the significant yield of HD observed from the irradiation of a 1:1 mixture of GeH_4 and GD_4 (Table II) also rules out hydrogen production by either reaction 3 or 5 alone and suggests that the primary quenching act is best represented by reactions 2 and 4. Since the distribution of H_2, HD, and D_2 observed from irradiation of the GeH_4-GeD_4 mixture is nearly random (see Table II), it would appear that reaction 2, as postulated by Romeyn and Noyes, best represents the primary chemical quenching process. However, contributions of a few per cent from reactions 3, 4, and 5 cannot be ruled out.

Acceptance of reaction 2 as the primary process requires the participation of hydrogen atoms in the photolysis mechanism and suggests that the following abstraction reaction, proposed by Romeyn and Noyes

$$H + GeH_4 \longrightarrow H_2 + GeH_3 \qquad (6)$$

must occur with high collision efficiency to produce the observed 0.92 quantum yield for H_2 production in the presence of 5.3% propylene (Table I). Niki and Mains[8] found that olefins were also ineffective in scavenging hydrogen atoms in their SiH_4 study and suggested that the silane analog of reaction 6 was rapid because of a very low activation energy. Gunning, *et al.*,[9] on the other hand, supported an activation energy for the silane analog which was only a few kilocalories per mole lower than reported for alkanes. Since the question of the activation energy for the silane analog of reaction 6 is controversial, the interpretation of the high collision efficiency for the germane system merits further consideration here.

A high collision efficiency for reaction 6 may be due to a low activation energy, as suggested by Niki and Mains, if thermal H atoms are involved or the high efficiency may not depend upon the activation energy at all if energetic, *i.e.*, "hot" hydrogen atoms are postulated. The latter explanation, the participation of "hot" hydrogen atoms in these systems, is not entirely unreasonable since the rupture of a Ge–H bond requires only 70 kcal/mole and rupture of the Si–H bond requires approximately 75 kcal/mole.[13–15] Thus, about 42 kcal/mole must appear as translational energy of H, GeH_3, and Hg, and as internal energy of GeH_3 as a result of the chemical quenching of 6($^3P_1$)Hg by GeH_4 as postulated in reaction 2. Under these circumstances, the production of hydrogen atoms with energies in excess of 10 kcal/mole is quite conceivable.

In order to distinguish between the above possible alternative explanations for the high collision efficiency of reaction 2, it is necessary to resort to a test which is unique to "hot" atom reactions, such as collisional deactivation

$$H^* + He \longrightarrow H + He \qquad (7)$$

because the absence of a temperature coefficient is not definitive. The effect of helium in the mercury-photosensitized decomposition of GeH_4 in the presence of C_2D_6 provides such a test. Since the quenching cross sections of C_2D_6 and He are very small,[16] reaction 2 represents the primary process in this mixture. In addition to reaction 7, the following reactions may be expected to occur

$$H^* + GeH_4 \longrightarrow H + GeH_4 \qquad (8)$$

$$H^* + GeH_4 \longrightarrow H_2 + GeH_3 \qquad (9)$$

$$H + GeH_4 \longrightarrow H_2 + GeH_3 \qquad (6)$$

$$H^* + C_2D_6 \longrightarrow H + C_2D_6 \qquad (10)$$

$$H^* + C_2D_6 \longrightarrow HD + C_2D_5 \qquad (11)$$

$$H + C_2D_6 \longrightarrow HD + C_2D_5 \qquad (12)$$

Reactions 7, 8, and 10 are deactivation processes and probably occur through a sequence of collisions of the "hot" hydrogen atom, H*. If thermal hydrogen atoms are solely responsible for the hydrogen production, only reactions 6 and 12 need be considered and, since reaction 12 has an activation energy of 13 kcal/mole,[17] the ratio of H_2 to HD would be expected to be quite large and independent of added He. If "hot" hydrogen atoms participate in the formation of hydrogen, the ratio of H_2 to HD should be smaller and increase with the addition of helium. The results are shown in Figure 4. It should be noted that D_2 was not detected among the hydrogen products.

The $(H_2)/(HD)$ ratio does increase as the pressure of He is increased as predicted if "hot" hydrogen atoms are involved in the system. The mechanism cited above predicts a linear increase if it is assumed that reaction 12 is negligible, *i.e.*, $(H_2)/(HD) = [k_7(He) + (k_8 + k_9)(GeH_4) + k_{10}(C_2D_6)]/k_{11}(C_2D_6)$. Thus, it seems reasonable to conclude that "hot" hydrogen atoms are present in the mercury photosensitization of GeH_4 and may be cited to explain the high collision efficiency of reaction 2. We have attempted to obtain further evidence for "hot" hydrogen atoms by adding large amounts of helium to a mixture of GeH_4 and propylene (20:1). The results of the latter experiments were inconclusive because of the analytical problems involved. If, as the above results suggest, "hot" hydrogen atoms are involved in the mercury-photosensitized decomposition of GeH_4, a similar mechanism may be invoked in the controversial SiH_4 experiments and this system should be reexamined.

The formation of digermane, trigermane, and tetragermane probably involves a sequence of radical combination and hydrogen abstraction steps as postulated for the SiH_4 and CH_4 analogs, *viz.*

$$2GeH_3 \longrightarrow Ge_2H_6 \qquad (13)$$

$$H + Ge_2H_6 \longrightarrow Ge_2H_5 + H_2 \qquad (14)$$

$$GeH_3 + Ge_2H_5 \longrightarrow Ge_3H_8 \qquad (15)$$

$$2Ge_2H_5 \longrightarrow Ge_4H_{10} \qquad (16)$$

etc. to polymer deposition.

---

(13) F. E. Saalfeld and H. J. Svec, *Inorg. Chem.*, **2**, 46 (1963).

(14) S. R. Gunn and L. G. Green, *J. Phys. Chem.*, **65**, 729 (1961).

(15) M. L. Huggins, *J. Am. Chem. Soc.*, **78**, 546 (1956).

(16) Y. Rousseau and H. Gunning, *Can. J. Chem.*, **41**, 465 (1963).

(17) V. V. Voevodsky and V. N. Kondratiev, *Progr. Reaction Kinetics*, **1**, 54 (1961).

While the above sequence qualitatively describes the system, it should be emphasized that further study is required before the reaction sequence is accepted in detail. For example, the isotopic distributions of deuterium in digermane and trigermane products from the irradiation of the GeH_4–GeD_4 mixture strongly suggest formation *via* reactions 13 and 15. However, the abstraction reaction which produces Ge_2H_5 could involve GeH_3 as well as the H atoms as suggested in reaction 14.

Examination of the mass spectrum of GeH_4–GeD_4 *after* irradiation should, in principle, permit a decision as to whether GeH_3 radicals were involved in abstraction reactions. Because of the low conversions used in these experiments and the large number of isotopes of germanium, we could not find evidence for GeH_3D and GeD_3H formation. Future experiments, utilizing a high-resolution mass spectrometer, may permit a conclusion regarding the participation of GeH_4 in abstraction reactions.

Acknowledgments. The authors wish to thank Mr. Eric Daby for assistance with some experiments and Mr. Wrbican for determining the mass spectra. The financial support of the U. S. Atomic Energy Commission (Contract No. AT(30-1-3007)) and the U. S. Air Force Office of Scientific Research is gratefully acknowledged.

Cohesive Energies in Polar Organic Liquids

by Edwin F. Meyer[1] and Robert E. Wagner

U. S. Army Coating & Chemical Laboratory, Aberdeen Proving Ground, Maryland *(Received May 2, 1966)*

A method which allows quantitative estimation of the dipole–dipole (orientation), dipole–induced dipole (induction), and dispersion energies in polar organic liquids is presented and illustrated with the methyl *n*-alkyl ketones. Use is made of the temperature variation of density and vapor pressure for homologous series of organic compounds. Data were obtained for the odd-numbered 2-ketones from C_5 to C_{13}. As an example of the results, it is estimated that the cohesion in liquid 2-butanone at 40° is comprised of 8% orientation, 14% induction, and 78% dispersion energies. The relatively high value for induction is surprising in view of the general opinion in the literature, but reconsideration of the usual expressions for these energies as applied to the liquids in question makes it not unreasonable. The contribution of induction to cohesion is larger than is generally appreciated.

A knowledge of the relative amounts of the different types of cohesive energies in liquids will lead to a better understanding of liquid properties, particularly solubilities, as well as provide necessary information for the development of a satisfactory theory of the liquid state. It can be shown that such knowledge is obtainable from the temperature dependence of vapor pressures and densities for homologous series of organic compounds.

Theoretical Section

We assume herein that the cohesive energy (the energy required to separate the component molecules to infinity without changing the average internal energy of

---

[1] Correspondence should be directed to Capt. E. F. Meyer, NAS-NRC Postdoctoral Research Associate, at the U. S. Naval Research Laboratory, Washington, D. C.

the individual molecules), E_c, may be approximated by the energy of vaporization. In cases where appreciable forces of attraction remain in the vapor phase, the additional energy needed to separate the molecules to infinity may be calculated from appropriate compressibility data.

Consider first a liquid composed of nonpolar molecules such as *n*-hexane. Its cohesive energy results from the attraction of the individual atoms of one molecule for those of another, the so-called dispersion attraction. By increasing the length of the hydrocarbon chain, more atoms per molecule attract each other, with the result that the molecules are drawn closer together and the cohesive energy is increased. The increment in E_c per CH_2 group inserted (the "CH_2 increment") is not constant for the paraffin series, since the energy of interaction depends heavily on the distances between interacting centers, and these decrease upon insertion of each CH_2 group at constant temperature. The CH_2 increment might be expected to be constant under the condition of constant time-average distances between interacting centers. This condition can be realized in two ways: by considering all molecules at absolute zero or by choosing a fixed molar volume per CH_2 group and adjusting the temperature of each homolog until this molar volume is achieved. That the former produces a constant CH_2 increment is known;[2] that the latter does the same is illustrated by the lower curve in Figure 1. The fixed molar volume per CH_2 has been arbitrarily set at 19.08 cc/mole, characteristic of *n*-hexane at 0°. The value is calculated from the molar volume, 127.3 cc/mole, and the relative van der Waals volumes for CH_3 and CH_2 (13.67 and 10.23, respectively) given by Bondi.[3] The temperatures at which each member of the series displays 19.08 cc/mole of CH_2 groups is calculated from thermal expansion data, and E_c is calculated for each member at its appropriate temperature. The contribution of each CH_2 group to E_c is given by the slope of the E_c *vs.* *n* curve, where *n* is the number of CH_2 groups in the molecule.

It should be pointed out that Hijmans[4] has developed a phenomenological approach to the principle of corresponding states for chain molecules, wherein thermodynamic properties may be expressed as linear functions of the number of segments in the chain. The results obtained with the simplified approach used here agree with those obtained with his more elaborate scheme. For example, his molecular units for volume as a function of chain length are compared in Table I to analogous figures obtained as described above. In addition, of course, the temperatures at which the alkanes display our values for the volumes correspond to the same reduced temperature in Hijmans' scheme. Thus a fixed volume per CH_2 group puts the alkanes in "corresponding states," and addition of a CH_2 group under this condition increases E_c by a fixed amount.

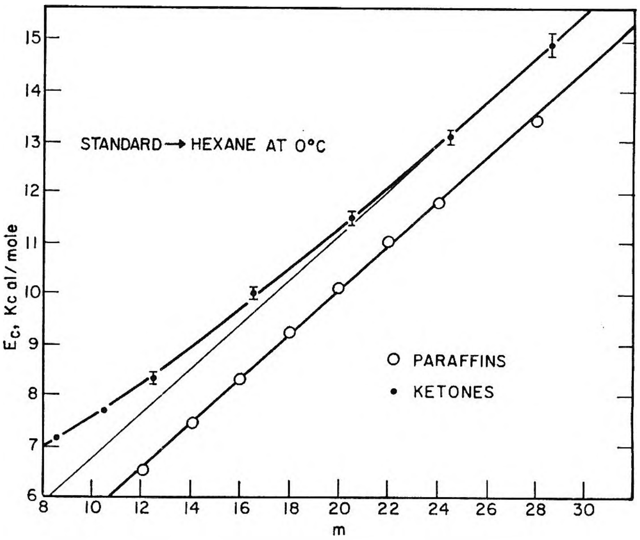

Figure 1. Paraffin densities from "International Critical Tables," vapor pressures from API Project 44.

Table I: Ratio of Molar Volume to That of *n*-Hexane for *n*-Alkanes in Corresponding States

	$V(n)/V(6)$	
n	Hijmans	This work
5	0.858	0.851
6	1.000	1.000
7	1.144	1.149
8	1.292	1.299
9	1.441	1.448
10	1.585	1.600
11	1.732	1.748

Consider now a liquid composed of polar molecules such as 2-pentanone. In addition to the dispersion energy present in the paraffins, orientation and induction energies contribute to cohesion. Stipulating the same volume per CH_2 group and assigning a consistent volume to the carbonyl group (11.70),[3] how might we expect these energies to vary with insertion of successive CH_2 groups to form higher 2-ketones?

The contribution of dispersion to the CH_2 increment should be the same as in the paraffin series, even though the absolute value of the dispersion energy for a ketone

---

(2) E. A. Moelwyn-Hughes, "Physical Chemistry," The Macmillan Co., New York, N. Y., 1964, p 702.

(3) A. Bondi, *J. Phys. Chem.*, **68**, 441 (1964).

(4) J. Hijmans, *Physica*, **27**, 433 (1961).

Techniques for the study of energy transfer from vibrationally excited species include sound dispersion,[9] kinetic spectroscopy,[10] and flash photolysis,[11] shock wave studies,[12] fluorescence stabilization,[13,14] photochemical systems,[15] and chemical activation[7,16] and low-pressure thermal unimolecular systems.[8,17] The existing information on the deactivation in binary collisions of complex molecules above the low-energy region may be readily summarized.

Fluorescence studies on aromatic species (at energies up to ~25 kcal $mole^{-1}$) indicate that amounts of energy up to several kcal $mole^{-1}$ may be transferred to foreign gases.[13] The amount of energy transferred seems to increase with increasing molecular weight and polarity of the deactivator (paralleling the thermal unimolecular reaction situation—see below). These results contrast with energy transfer studies with highly excited iodine[14a] which indicate, in part, that lighter molecules may be more effective in producing vibrational transitions (somewhat resembling sound dispersion results at low energies).

At still higher energies, chemically activated ethyl and *sec*-butyl radicals, vibrationally excited to ~40 kcal $mole^{-1}$, were found to lose ~2 kcal $mole^{-1}$ on collision with the rare gases, ~2.5 kcal $mole^{-1}$ on collision with diatomic gases, and $\geqslant$ 9 kcal $mole^{-1}$ on collision with polyatomic molecules.[7a] The deactivation of chemically activated vibrationally excited cyclopropane and dimethylcyclopropane ($\gtrsim$100 kcal $mole^{-1}$) by ethylene and butene[16] indicates that large amounts of energy may be transferred on collision, $\geqslant$ 12–15 kcal $mole^{-1}$.

The most definitive and outstanding thermal study has been that of Johnston and Volpe,[8b] who analyzed the effect of 16 chaperon gases on the unimolecular decomposition of nitryl chloride. In order to measure relative collisional transition probabilities most simply, they have pointed out that studies should be made in the low-pressure, second-order region of a thermal unimolecular reaction. In this nonequilibrium region, the rate of reaction is the rate of activation by collision. In practice, the behavior of inert molecules has usually been expressed as efficiency relative to the reactant itself. It was remarked by Trotman-Dickenson[18] that the maximum efficiency of energy transfer is reached for complex molecules. Johnston[19] has suggested that efficiency may be correlated with the boiling points of the inert gases and with Lennard-Jones parameters in terms of collision force. The deactivation probability per collision should be below unity (*i.e.*, far from saturation) to show direct proportionality to molecular parameters.

Up to the present time, most thermal studies of this kind have been relatively unproductive. The results of various workers have usually been obtained at diverse temperatures, total energy level, excess energy level, and energy distribution, and with reactant molecules of widely varying molecular complexity, frequency pattern, and polarity. Widely different systems have often been uncritically compared and no systematic variation of reaction parameters has been investigated for a single system.[20] It has been pointed out and illustrated previously[7b] that the usual definition of inert gas efficiency is a pragmatic operational one; comparisons of efficiencies between various systems which ignore this limitation are not necessarily helpful. For example, scarcely any study in the literature has defined the average energy excess of the reacting molecules[20b] above the critical threshold; the comparisons in question thus have not been well defined. Usually, no attempt has been made to correlate data with molecular parameters or interaction potentials. Some experimental limitations in many existing studies should also be recognized: work in the higher regions of falloff just below the high-pressure limit may lead to incorrect results because the pressure dependence

---

[9] (a) T. L. Cottrell and J. C. McCoubrey, "Molecular Energy Transfer in Gases," Butterworth and Co. Ltd., London, 1961; (b) K. F. Herzfeld and T. A. Litovitz, "Absorption and Dispersion of Ultrasonic Waves," Academic Press Inc., New York, N. Y., 1959; (c) J. D. Lambert and R. Salter, *Proc. Roy. Soc.* (London), **A253**, 277 (1959); J. D. Lambert, D. G. Parks-Smith, and J. L. Stretton, *ibid.*, **A282**, 380 (1964).

[10] J. D. McKinley, Jr., D. Garvin, and M. Boudart, *J. Chem. Phys.*, **23**, 785 (1955); J. C. Polanyi, *ibid*, **31**, 1338 (1959).

[11] See, for example, the reviews by N. Basco and R. G. W. Norrish, *Can. J. Chem.*, **38**, 1769 (1960); *Discussions Faraday Soc.*, **33**, 99 (1962). For a summary of iodine atom recombination reactions, see G. Porter, *ibid.*, **33**, 198 (1962).

[12] R. C. Millikan and D. R. White, *J. Chem. Phys.*, **39**, 3209 (1963), and references cited; R. C. Millikan, *ibid.*, **40**, 2594 (1964).

[13] (a) B. Stevens, *Can. J. Chem.*, **37**, 831 (1959); *Mol. Phys.*, **3**, 589 (1960); (b) M. Boudart and J. T. Dubois, *J. Chem. Phys.*, **23**, 223 (1955); B. Stevens and M. Boudart, *Ann. N. Y. Acad. Sci.*, **67**, 570 (1957); B. S. Neporent and S. O. Mirumyants, *Opt. Spectry. (USSR)*, **8**, 336, 414 (1960); (c) E. J. Bowen and S. Veljkovic, *Proc. Roy. Soc.* (London), **A236**, 1 (1956).

[14] (a) R. L. Brown and W. Klemperer, *J. Chem. Phys.*, **41**, 3072 (1964); J. I. Steinfeld and W. Klemperer, *ibid.*, **42**, 3475 (1965); (b) R. C. Millikan, *ibid.*, **38**, 2855 (1963).

[15] G. A. Taylor and G. B. Porter, *ibid.*, **36**, 1353 (1962).

[16] D. W. Setser, J. W. Simons, and B. S. Rabinovitch, *Bull. Soc. Chim. Belges*, 71, 662 (1962); *J. Chem. Phys.*, **40**, 1751 (1965); **41**, 800 (1965).

[17] D. E. Hoare, J. B. Protheroe, and A. D. Walsh, *Trans. Faraday Soc.*, **55**, 548 (1959); R. R. Baldwin and D. Brattan, 8th Combustion Symposium, Pasadena, Calif., 1960, p 110; W. Forst, *Can. J. Chem.*, **36**, 1308 (1958).

[18] A. F. Trotman-Dickenson, "Gas Kinetics," Butterworth and Co. Ltd., London, 1955.

[19] H. S. Johnston, *Ann. Rev. Phys. Chem.*, **8**, 249 (1957).

[20] (a) For a comparison table of relative collision efficiencies in thermal unimolecular reactions, see ref 9a, p 186; (b) see D. W. Placzek, B. S. Rabinovitch, G. Z. Whitten, and E. Tschuikow-Roux, *J. Chem. Phys.*, **43**, 4071 (1965), for some delineation of excess energy.

of conventional unimolecular reactions is insensitive to collisional transition probabilities,[21] and only indirectly related to these,[8] and because of experimental inaccuracy.[22-24]

At the low-pressure limit the situation is vastly improved, but still not simple, and must be treated on a stochastic model.[25a] However, the low-pressure rates can, in principle, be made to yield a connection between the amount of energy transferred on the average per collision and the measured efficiencies of activation.[25b]

Earlier work from this laboratory[26] has shown that the thermal unimolecular isomerization of methyl isocyanide to acetonitrile is a simple, clean, and homogeneous reaction. This reaction offers unique advantages in that a systematic variation of many reaction parameters is possible.[26-28] Variation of temperature will be attempted over the widest accessible range. More important, the structure of the reactant molecule as well as the nature of the deactivator can be altered, without altering significantly the reaction parameters, to provide an internally consistent reaction series, *e.g.*, CH_3NC, C_2H_5NC, CF_3CH_2NC, and the effects of the frequency pattern change, internal rotation, and low-frequency bending modes, total number of vibration modes, etc., on the collisional transition probabilities can be quantitatively evaluated.

The present paper dealing with the $CH_3NC \rightarrow CH_3CN$ reaction presents the first in a series which utilizes these systems.

Experimental Section

Materials. Methyl isocyanide was prepared by the general method of dehydration of an N-substituted formamide by an acid halide in the presence of a base.[29] N-Methylformamide (Fluka A.G. pure grade) was slowly added to a warm mixture of quinoline (Matheson Coleman and Bell refined grade, vacuum distilled from zinc dust) and *p*-toluenesulfonyl chloride (Eastman White Label). After purification by gas chromatography, no impurities could be detected.

Helium, neon, argon, krypton, xenon, hydrogen, nitrogen, and carbon dioxide were assayed reagent grade gases of the Air Reduction Co. Helium contained 0.017% nitrogen as an impurity. Krypton contained 0.008% xenon, and xenon contained 0.01% krypton. These gases were used without further purification.

Methane (Phillips Petroleum Co., research grade) of stated purity 99.58% was used without purification. Fluoroform (Matheson Co. Inc.) when analyzed by chromatography showed the presence of 6% of noninterfering side product (mainly CH_2F_2). Tetrafluoromethane (Matheson Co. Inc.) showed no impurities by chromatography. Methyl fluoride-d_3 of 95% isotopic purity was checked by chromatography for interfering side products and was estimated to be of 99% chemical purity. Trifluoroacetonitrile (Columbia Chemicals) contained <1% impurity when analyzed by chromatography. Propionitrile (Eastman White Label, free from isonitrile) and *n*-butyronitrile (Matheson Coleman and Bell) showed no impurities on chromatographic analysis. All of these gases were vacuum distilled and outgassed.

Other inert gases were purified by chromatography prior to use and subjected to the usual vacuum manipulations. All condensible gases were deoxygenated by the freeze–pump–melt method and small amounts of impurity other than oxygen will have a negligible effect on the energy transfer efficiencies.

Apparatus and Procedure. A static method was used for the rate determinations. A 12-l. Pyrex bulb, heated in an air furnace, served as the reactor. Temperature was regulated by a proportional controller and was measured with three calibrated chromel–alumel thermocouples located at different positions in the furnace. During a run the temperature was constant to ±0.1° and was uniform over the bulb to ±0.1°. Over the entire series of runs, temperatures between 279 and 282.5° were used and all rate constants were corrected to a standard temperature of 280.5° with use of the energies of activation at the pressure of the run, as given in I.[26]

The reactor was initially seasoned with a few millimeters of methyl isocyanide for 12 hr and was re-

---

(21) F. P. Buff and D. J. Wilson, *J. Chem. Phys.*, **32**, 677 (1960).

(22) Studies of inert gas efficiencies in the isomerization of cyclopropane,[23a] of methylcyclopropane,[24a] of 1,1-dimethylcyclopropane,[24b] and the decomposition of cyclobutane[23b] suffer from this problem: cyclopropane k/k_∞ was studied down to ~0.1; for $\triangledown CH_3$, $\triangledown (CH_3)_2$, and □, k/k_∞ was studied only down to ~0.5. This grouping is otherwise the only candidate as a consistent set of substrate species.

(23) (a) H. O. Pritchard, R. G. Sowden, and A. F. Trotman-Dickenson, *Proc. Roy. Soc.* (London), **A217**, 563 (1953); (b) H. O. Pritchard, R. G. Sowden, and A. F. Trotman-Dickenson, *ibid.*, **A218**, 416 (1953).

(24) (a) J. P. Chesick, *J. Am. Chem. Soc.*, **82**, 3277 (1960); (b) M. C. Flowers and H. M. Frey, *J. Chem. Soc.*, 1157 (1962).

(25) (a) E. W. Montroll and K. E. Shuler, *Advan. Chem. Phys.*, **1**, 361 (1958); (b) B. S. Rabinovitch and D. C. Tardy, *Science*, 150, 382 (1965); *J. Chem. Phys.*, in press.

(26) F. W. Schneider and B. S. Rabinovitch, *J. Am. Chem. Soc.*, **84**, 4215 (1962); called I.

(27) F. W. Schneider and B. S. Rabinovitch, *ibid.*, **85**, 2365 (1963); called II.

(28) B. S. Rabinovitch, P. W. Gilderson, and F. W. Schneider, *ibid.*, **87**, 158 (1965); called III.

(29) The method of I. Ugi and R. Meyr, *Chem. Ber.*, **93**, 239 (1960), as modified by J. Casanova, Jr. We thank Dr. Casanova for helpful advice on synthesis.

Table IV: Contributions to Total Cohesion (in kcal/mole)

Compound	Temp, °C	E_c	E_{disp}	E_{ind}	E_{orien}	% disp	% ind	% orien
2-Propanone	14	7.08	5.04	1.1	0.94	71.2	15.5	13.3
	51	6.81	4.68	1.1	1.03	68.8	16.2	15.0
2-Butanone	40	7.62	5.91	1.1	0.61	77.6	14.4	8.0
	80	7.19	5.49	1.1	0.60	76.4	15.3	8.3
2-Pentanone	51	8.29	6.79	1.1	0.40	81.9	13.3	4.8
	93	7.84	6.29	1.1	0.45	80.2	14.0	5.8
2-Heptanone	78	9.99	8.53	1.1	0.36	85.5	11.0	3.5
	122	9.24	7.90	1.1	0.24	85.5	11.9	2.6
2-Nonanone	96	11.48	10.27	1.1	0.11	89.5	9.6	0.9
	143	10.71	9.51	1.1	0.10	88.8	10.3	0.9
2-Undecanone	111	13.09	12.01	1.1	...	91.6	8.4	...
	162	12.09	11.13	1.1	...	91.0	9.0	...
2-Tridecanone	123	14.89	13.76	1.1	...	92.6	7.4	...
	176	14.02	12.74	1.1	...	92.0	8.0	...

the value of m corresponding to the ketone of interest, the dispersion energy is given by the paraffin curve; the induction energy is the vertical distance between the paraffin curve and the asymptote; and the orientation energy is the distance from the asymptote to the ketone curve.

It should be emphasized that each point of the graph corresponds to a temperature characteristic of the compound it represents; these are not isotherms in any sense.

Some arbitrariness cannot be avoided in drawing the asymptote to the ketone curve, since the probable error is larger for the higher boiling compounds. It was decided, in the light of the rapid disappearance of curvature, to assume that there is no orientation contribution in the C_{11} and C_{13} ketones and to take as the induction energy the average of the difference between E_c and E_{disp} for these two compounds. This procedure gave 1.1 kcal/mole at all temperatures. The equations for E_c for the paraffins at the lowest and highest temperatures are, respectively

$$E_c = 1.34 + 0.4357m \pm 0.10$$

$$E_c = 1.26 + 0.4028m \pm 0.06$$

making the equations for the asymptotes

$$E_{disp+ind} = 2.44 + 0.4357m$$

$$E_{disp+ind} = 2.36 + 0.4028m$$

Since the temperature dependence is slight for each type of cohesive energy, only the results for the lowest and highest temperatures are presented, with the temperature for each compound, in Table IV. The root-mean-square deviation in E_c for the ketones whose properties we measured is indicated in Figure 1.

Discussion

Estimates in the literature of the contributions of dispersion, induction, and orientation to cohesion in fluids are generally limited to very simple molecules in the gas phase.[14] However, the conclusions drawn are frequently applied to the liquid state. For example, Hildebrand and Scott[15] say, "...the induction forces are always small compared with the other two...," and Hirschfelder, Curtiss, and Bird[16] comment, "It is apparent that the induction effect is never important in the interaction of neutral molecules." These statements are made subsequent to an examination of the theoretical expressions for each type of energy

$$E_{disp} = -\frac{3}{4}\frac{\alpha^2}{r^6}I$$

$$E_{ind} = -\frac{2\alpha\mu^2}{r^6}$$

$$E_{orien} = -\frac{2\mu^4}{3kTr^6}$$

where α is the polarizability, μ is the dipole moment, I is the ionization potential, and r is the distance between interacting centers. Tables of calculated energies[15,16] for some simple molecules with dipole moments show

---

[14] P. A. Small, *J. Appl. Chem.*, **3**, 71 (1953), however, has calculated a dipole contribution parameter for liquid acetone from heats of mixing with nonpolar liquids. He estimates the dipole contributes but 4% to cohesion, unrealistically low considering the 66° difference in boiling point between acetone and isobutylene.

[15] J. H. Hildebrand and R. L. Scott, "The Solubility of Nonelectrolytes," Dover Publications, Inc., New York, N. Y., 1964, p 167.

[16] J. O. Hirschfelder, C. F. Curtiss, and R. B. Bird, "Molecular Theory of Gases and Liquids," John Wiley and Sons, Inc., New York, N. Y., 1954, p 988.

add a constant term to eq 2 and the low-pressure limit would become

$$k_0 = k^a C_M + k_{het} \tag{3}$$

Below 6 × 10^{-3} mm, the isocyanide rate constants very obviously began to deviate positively, indicating that surface effects were significant at that pressure; this was confirmed by packed vessel runs which gave evidence of increased rate at pressures below 10^{-2} mm. (A larger vessel is needed to extend the measurements to even lower pressures, and to this end measurements will be made in a 200-l. vessel.) In order to avoid this doubtful pressure region, a standard reactant pressure of ~1.4 × 10^{-2} mm was used for the present experiments.

A plot of the isocyanide rate data above 10^{-2} mm against pressure gave a zero pressure intercept on the k axis of ~0.1 (±0.1) × 10^{-5} $\sec^{-1}$. Relative to the value of k at 1.4 × 10^{-2} mm, which is 1.75 × 10^{-5} $\sec^{-1}$, this reveals possible heterogeneity of 6% which would be quite negligible at the higher inert gas pressures actually used.

Second-Order Requirement. For the case where M is a gas other than reactant, the first-order rate constant depends on the nature of M as well as on its concentration, and k may be written as[8]

$$k_{uni} = \sum_i \frac{k_i K_i \sum_m k_{mi}{}^d C_M}{\sum_m k_{mi}{}^d C_M + k_i} \tag{4}$$

where m denotes the possible dependence of the specific rate constants on the nature of M and, by detailed balance, $k_{mi}{}^a = k_{mi}{}^d K_i$, where K_i is the equilibrium fraction of reactant molecules in the excited state i.

It can be seen from eq 4 that, at higher pressures, the ratio of rate constants for different gases does not necessarily have a simple interpretation. It is only at the low-pressure limit that the relative values of rate constants for different foreign gases directly give the relative values of the activating efficiencies of these gases. The simplest condition arises if the relative efficiencies of inert gases are measured in large excess over the reactant concentration, and also if the inert gas pressure approachs zero; both simplifications together are impracticable.

The reaction order becomes second at zero pressure in the Lindemann mechanism but, experimentally, the order is always somewhat less than 2. However, if functional plots of k vs. C_M show little or no curvature, then it may be inferred that eq 2 is substantially obeyed. The plot of the present methyl isocyanide data in Figure 1 is a line of slope 0.96 ± 0.02, so that the reaction is almost in the second-order region. From the more sensitive plot of k vs. p, which shows little curvature, one finds (Figure 2) that the slope scarcely declines over the range 10^{-2} to 0.4 mm, the highest effective pressure used in this study. Thus our data were taken in a region at or near the second-order region.

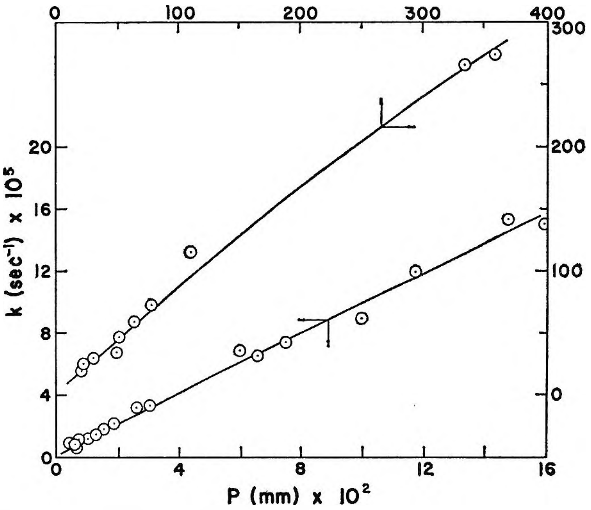

Figure 2. Low-pressure plot of k vs. pressure for methyl isocyanide at 280.5°.

Further confirmation of this conclusion is given by a plot of the Arrhenius activation energy, E_a, obtained in I, against log (pressure), as shown in Figure 3. It can be seen that E_a does not begin to increase until a pressure of at least 5 mm. Since the present total effective pressure was always less than 0.4 mm, the energy distribution of the reacting molecules was substantially close to the low-pressure limiting distribution.

RRKM Description of the Isomerization of Methyl Isocyanide. In Figure 4, a plot of falloff, log (k/k_∞) vs. log (pressure), is given for the low-pressure region, including earlier data from I at various temperatures. A recalculation of the falloff of CH_3NC has been carried out on the RRKM basis. The original calculation in I at 230° was based on the frequency assignment of Pillai and Cleveland.[31] Subsequent results in II[27] for CD_3NC were treated on the basis of the frequency assignment for this molecule which had been given in the interim by Mottern and Fletcher.[32] The rather heavy calculations in I for CH_3NC were not redone at that time, although the product rule ratio for the heavy and light molecules and activated complexes

---

[31] M. E. K. Pillai and F. F. Cleveland, *J. Mol. Spectry.*, 5, 212 (1960).

[32] J. G. Mottern and W. H. Fletcher, *Spectrochim. Acta*, 18, 995 (1962).

Conclusion

A method for quantitative estimation of the contributions of dispersion, induction, and orientation energies to cohesion in polar organic liquids has been proposed and illustrated with the methyl *n*-alkyl ketones. Dispersion always predominates, with induction in a minor, but constant, role. Orientation rapidly loses significance as the hydrocarbon side chain is increased. Induction energy is more important than is generally appreciated, contributing 5–10% to the total cohesion of the higher, "mostly nonpolar" 2-ketones.

Acknowledgment. We acknowledge many stimulating discussions with Dr. Myer Rosenfeld and thank the Director of the U. S. Army Coating & Chemical Laboratory for permission to publish this work.

Infrared Study of Adsorption of Carbon Dioxide, Hydrogen Chloride, and Other Molecules on "Acid" Sites on Dry Silica–Alumina and γ-Alumina[1]

by J. B. Peri

Research and Development Department, American Oil Company, Whiting, Indiana *(Received May 3, 1966)*

The adsorption of various molecules on specially prepared transparent plates of dry, high-area silica–alumina and γ-alumina was studied by infrared and gravimetric techniques. Carbon dioxide was selectively and reversibly adsorbed on a few so-called "acid" sites on both silica–alumina and γ-alumina, producing an infrared band near 2375 cm^{-1} for the former and near 2370 cm^{-1} for the latter. Use of adsorbed CO_2 as an indicator allowed titration of these sites, tentatively named "α sites," with other adsorbates which displaced carbon dioxide. The α sites on silica–alumina selectively adsorbed carbon dioxide, acetylene, butene, benzene, and hydrogen chloride. They also strongly adsorbed ammonia and water, but these adsorbates were also held by many other sites. Their reaction with hydrogen chloride produced hydroxyl groups. Their surface concentration fell in the range $3\text{–}9 \times 10^{12}/\text{cm}^2$. Similar sites on γ-alumina predried at 800° had a surface concentration of about $5 \times 10^{12}/\text{cm}^2$. The α sites are apparently formed by condensation of Al–OH groups during dehydration of the surface. They contain a reactive oxide ion (or ions) in close proximity to an exposed aluminum ion. Their role in catalysis is not yet clear.

Introduction

Although the important "acidic oxide" catalysts have been studied intensively for many years, little is known about the surface sites responsible for their activity.[2,3] Active sites are usually thought to be acidic, but the exact nature of the acidity remains controversial.[3,4]

Numerous attempts have been made to measure and characterize the acidity by adsorption of NH_3, butylamine, or other bases, often using organic indicators. While such methods show wide variations among sites on a given catalyst and among distributions of sites on

---

[1] Presented in part at 145th National Meeting of the American Chemical Society, New York, N. Y., Sept 1963.

[2] L. B. Ryland, M. W. Tamele, and J. N. Wilson, "Catalysis," Vol. 7, P. H. Emmett, Ed., Reinhold Publishing Corp., New York, N. Y., 1960.

different catalysts, the results usually correlate poorly with catalytic properties, particularly when different types of catalysts are compared.

Silica–alumina cracking catalysts represent a wide range of compositions but usually exhibit similar catalytic properties. γ-Alumina also develops cracking activity after it has been dried above 400°, but it is very easily poisoned by H_2O.[5] Although these catalysts must differ considerably in surface structure, there is reason to expect that the active sites have common structural features which can be demonstrated and identified.

Only a small fraction of the acid sites on the surface of silica–alumina catalysts are active for cracking,[6] and even these may be atypical. Special sites which may be catalytically important appear to exist at surface concentrations of 10^{13} sites/cm^2 or less,[6,7] although this has been questioned.[4]

Infrared studies of γ-alumina,[8,9] silica,[10,11] and silica–alumina[12] have provided some information about the surface structure of these oxides, but many questions remain. Infrared studies of NH_3 adsorbed on dry γ-alumina[13] and silica–alumina,[14,15] of CO_2 on silica[16] and alumina,[17] of butene on alumina[18] and silica–alumina,[19] and of acetylene on alumina[20] and silica–alumina[19] have also been reported.

Because a better understanding of the nature of the active sites on acidic oxides is greatly needed, further infrared study of silica–alumina and dry γ-alumina was undertaken using various adsorbed molecules as "probes" to identify and characterize adsorption sites. To facilitate study of molecules covering less than 1% of the surface, the oxides were prepared in the form of transparent aerogel plates.

Experimental Section

Most of the cells, equipment, and procedures have been described.[8,18] Perkin-Elmer Model 12C and 112 spectrometers (equipped with CaF_2 and LiF prisms) were supplemented with a Beckman IR-9 (prism-grating) spectrometer. The cell most frequently used (cell C[18]) permitted sample weight changes and spectral changes to be measured concurrently. In experiments involving reaction of $AlCl_3$ vapor with silica, the special cell shown in Figure 1 was used. It is entirely of glass and fused quartz. Connections to the cell (numbered in Figure 1) were sealed off as will be described.

The preparations of γ-alumina[9] and silica[11] aerogel plates have been described, as have the sources and purification of NH_3, HCl, CO_2, 1-butene, D_2, and D_2O.[8,18,19] Acetylene was prepared from calcium carbide and dried with P_2O_5. All other chemicals were commercial materials of high purity and were usually dried with P_2O_5.

Preparation and Properties of Silica–Alumina Aerogels. Silica–alumina aerogel plates were prepared both by reaction of "dry" silica with $AlCl_3$ vapor (followed by hydrolysis and redrying) and by reaction of silica hydrogel with solutions of $AlCl_3$ or $Al(NO_3)_3$ to which NH_4OH had been added (followed by established procedures for converting the hydrogel to a transparent aerogel).[19] Because the surface characteristics as well as the optical and mechanical properties of aerogel plates may be influenced by the method of preparation, preparative procedures are given in detail.

Samples SAV-1 and SAV-2 were made from the same batch of silica aerogel plates, whose original surface area (after calcination in O_2 and drying by evacuation for 2 hr at 600°) was 785 m^2/g as measured by N_2 adsorption. Evacuation for 1 hr at 800°, rehydration for 8 hr at 100° in 15 torr of H_2O vapor, and subsequent evacuation for 1 hr at 600° and 1 hr at 800° reduced this to 750 m^2/g.

The $AlCl_3$ was purified by repeated sublimation under vacuum and sealed off in tube A (shown in Figure 1). A silica aerogel plate was placed in a quartz holder in tube B and was then calcined in 200 torr of O_2 at 600° for 1 hr and dried by evacuation at either 600° (SAV-1) or 800° (SAV-2) for 1 hr. The cell was sealed off at 1 (Figure 1), and the break-seal between tubes A and B

---

(3) K. V. Topchieva, G. M. Panchenkov, M. A. Kaliko, A. V. Agafonov, L. I. Pigusova, N. M. Kamakin, and Ya. V. Mirsky, Proceedings of the Fifth World Petroleum Congress, Section III, New York, N. Y., 1959, p 133.

(4) A. E. Hirschler and J. O. Hudson, *J. Catalysis*, **3**, 239 (1964).

(5) W. K. Hall, F. E. Lutinski, and H. R. Gerberich, *ibid.*, **3**, 512 (1964).

(6) G. A. Mills, E. R. Boedeker, and A. G. Oblad, *J. Am. Chem. Soc.*, **72**, 1554 (1950).

(7) H. P. Leftin and W. K. Hall, *Actes Congr. Intern. Catalyse, 2e, Paris, 1960*, **1**, 1353 (1961).

(8) J. B. Peri and R. B. Hannan, *J. Phys. Chem.*, **64**, 1526 (1960).

(9) J. B. Peri, *ibid.*, **69**, 211 (1965).

(10) R. S. McDonald, *ibid.*, **62**, 1168 (1958).

(11) J. B. Peri, *ibid.*, in press.

(12) M. R. Basila, *ibid.*, **66**, 2223 (1962).

(13) J. B. Peri, *ibid.*, **69**, 220 (1965).

(14) J. E. Mapes and R. P. Eischens, *ibid.*, **58**, 1059 (1954).

(15) D. E. Nicholson, *Nature*, **186**, 630 (1960).

(16) R. P. Eischens and W. A. Pliskin, *Advan. Catalysis*, **9**, 662 (1957).

(17) N. D. Parkyns, "Third Congress on Catalysis," Vol. II, North-Holland Publishing Co., Amsterdam, 1965, p 914.

(18) J. B. Peri, *Actes Congr. Intern. Catalyse, 2e, Paris*, **1**, 1353 (1961).

(19) J. B. Peri, "Third Congress on Catalysis," Vol. II, North-Holland Publishing Co., Amsterdam, 1965, p 1100.

(20) D. J. C. Yates and P. J. Lucchesi, *J. Chem. Phys.*, **35**, 243 (1961).

was opened. Then the $AlCl_3$ was sublimed back and forth between A and C through the heated (600°) cell until spectra showed that all OH groups had been removed from the silica surface. The evolved HCl was collected and sealed off in C for later measurement. All glass external to the furnace was flamed to drive excess $AlCl_3$ back into A (cooled with liquid N_2) which was then sealed off. The cell was again connected to the vacuum system through a break-seal, and hydrolysis was carried out by repeated admission of small doses of H_2O vapor at 100°, with intervening heating at 400 to 600° to desorb HCl + H_2O. The evolved HCl was collected and dried with P_2O_5 before subsequent measurement.

Data obtained in preparation of the two SAV samples are shown in Table I. Analyses for Al_2O_3 were obtained on final samples. The calculated per cent Al_2O_3 for SAV-1 assumes that each $AlCl_3$ molecule reacted with two OH groups. The higher value "found" indicates that some 1:1 reaction occurred.

Table I: Data from Preparation of SAV Aerogels

	HCl recovered, cm^3 (STP)		% Al_2O_3 on final gel	
Sample	From initial $AlCl_3$ reaction	On hydrolysis	Calcd	Found
SAV-1	8.6	Estd ~4.3	(8.9)	9.5
SAV-2	4.6	5.9	6.3	6.2

The final samples were too small to permit chloride analyses, but analyses of similar preparations indicated that very little chloride was left after hydrolysis. In preparation of SAV-1, some of the HCl evolved on hydrolysis was accidentally lost, preventing independent check on chloride retention, but the amount of HCl recovered in preparation of SAV-2 was in agreement with that expected from removal of all chloride.

Surface areas were not determined directly for SAV-1 and SAV-2. The areas were assumed to be the same as those determined after similar treatment, except for $AlCl_3$ reaction, for the silica aerogel (SAV-1, 780 m^2/g; SAV-2, 750 m^2/g). Surface areas obtained for other preparations of silica-alumina made by similar procedures support this assumption. Dry weights for the silica plates used in preparation of SAV samples were SAV-1, 0.110 g, and SAV-2, 0.113 g.

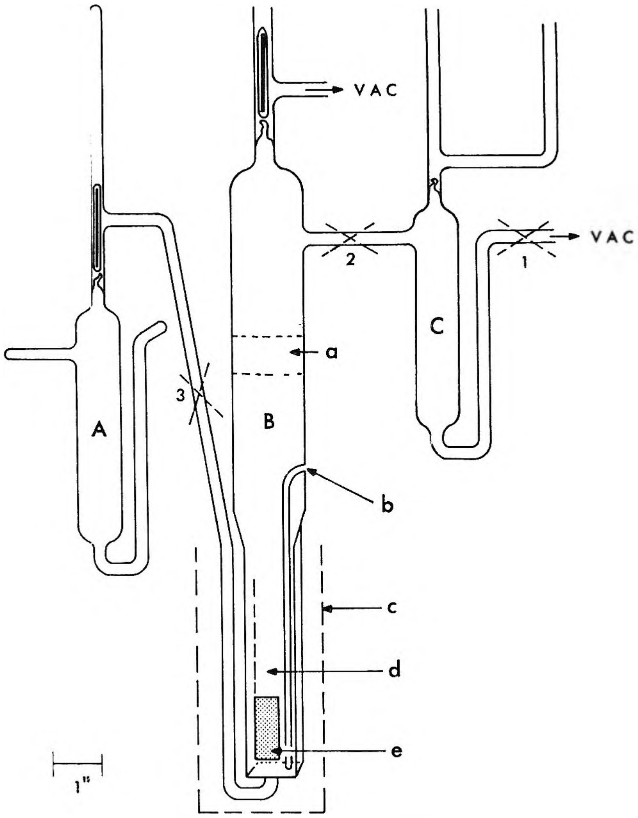

Figure 1. Cell used in studying reaction of $AlCl_3$ with surface OH groups: a, Pyrex-to-quartz graded seal; b, thermowell; c, furnace; d, cell body of 1-in. square fused-quartz tubing; e, aerogel plate.

The SAA samples were prepared from silica hydrogel plates that were repeatedly washed in distilled H_2O and then equilibrated with solutions of $AlCl_3$ (SAA-1 and -2) or $Al(NO_3)_3$ (SAA-3) which either had been (SAA-2 and -3) or were subsequently (SAA-1) titrated with NH_4OH solution to a final pH of ~3.5. Final solutions were clear. After equilibration for several days, the gel was heated in the solution for 6 hr at 100° in an autoclave. During the following week, it was washed six to eight times with H_2O and four or five times with methanol, which was then removed above its critical temperature in an autoclave. The final plates were almost as transparent as typical silica aerogel plates. The dry weights of the plates studied were 0.21 ± 0.01 g.

Differences in pH, concentration of solutions, and other variables gave gels having the compositions and surface areas listed in Table II.

A commercial silica-alumina (Nalco HA-1), containing 26% Al_2O_3 and having a surface area of 495 m^2/g, was also studied briefly. It was pressed at 12,000 psi into a thin (~28 mg/cm^2) self-supporting wafer for infrared study with the Beckman IR-9.

After drying at 600° or higher, all silica-alumina catalysts were active for butene isomerization and polymerization, and there is little doubt that the aero-

Table III: Collision and Intermolecular Parameters for Various Gases

Molecule	σ, A[a]	ϵ/k, °K[a]	σ_{AM}, A	ϵ_{AM}/k, °K	μ', D.[40]	$\Omega^{2,2*}$, kT/ϵ_{AM}	s_{AM}, A	s_{AA}^2/s_{AM}^2
CH_3NC	4.47[b]	380[b]	4.47		3.83	1.330	5.15	1.00
He	2.56	10.2	3.52	62		0.839	3.22	2.56
Ne	2.79	36	3.63	117		0.937	3.51	2.15
Ar	3.42	124	3.95	217		1.087	4.12	1.57
Kr	3.61	190	4.04	268		1.162	4.36	1.40
Xe	4.06	229	4.27	296		1.204	4.69	1.21
H_2	2.93	37	3.70	117		0.937	3.58	2.07
N_2	3.68	92	4.08	186		1.042	4.17	1.53
CO_2	4.00	190	4.24	268		1.162	4.57	1.27
CH_4	3.80	144	4.14	234		1.113	4.37	1.39
CD_3F	4.10[c]	200[c]	4.29	276		1.174	4.65	
	3.73[d]	333[d]	4.10	356	1.81	1.295	4.67	1.22
CHF_3	4.38[e]	254[e]	4.43	311	1.63	1.226	4.90	1.10
CF_4	4.70	153	4.59	242		1.124	4.86	1.12
	4.70[e]	179[e]	4.59	260		1.151	4.92	1.09
C_2H_6[f]	4.42	230	4.45	296		1.204	4.88	1.11
HCN[g]	3.93[g]	320	4.20	348.7	2.95	1.282	4.75	1.17
CF_3CN[h]	4.80	300	4.64	337.7	2.1[i]	1.267	5.22	0.973
C_2H_5CN[h]	5.00	400	4.74	389.8	4.04	1.345	5.50	0.879
C_3H_7CN[h]	5.50	400	4.98	389.8	4.07	1.345	5.78	0.796
CH_3CCH[j]	4.60	250	4.54	308.2	0.75	1.221	5.02	1.06
C_2H_5CCH[j]	5.20	300	4.84	337.7	0.81	1.267	5.45	0.895

[a] All values are from ref 35 unless otherwise specified and are derived from viscosity data where possible. [b] From ref 34; See text for discussion of this quantity. [c] See ref 7a. [d] J. L. Stretton, *Trans. Faraday Soc.*, **61,** 1053 (1965); G. A. Miller and R. B. Bernstein, *J. Phys. Chem.*, **63,** 710 (1959). [e] R. R. Boade and S. Legvold, *J. Chem. Phys.*, **42,** 569 (1965); values derived from a Lennard-Jones 7–28 potential. [f] Data from I—approximate value only. [g] σ(HCN) was calculated from viscosity data,[35] assuming a spherical molecule. In view of the similarity of HCN to H_2O where the values of ϵ/k vary widely according to the method of calculation,[36] the estimated value of ϵ/k of 320 for HCN must only be regarded as a reasonable estimate; the HCl–alkylhalide series behavior[d] is comparable. [h] Values of σ and ϵ/k for the higher nitriles were interpolated from the alkyl chloride and alcohol series listed by Mason.[36] [i] Calculated value. [j] Parameters for the higher acetylenes were interpolated from the corresponding hydrocarbon values[35] and are merely reasonable estimates.

cross sections for the energy transfer process under consideration here.

Nonpolar Gases. The collision cross sections and their temperature dependence were obtained from transport properties with the use of the 6–12 Lennard-Jones potential, $V(r) = 4\epsilon[(\sigma/r)^{12} - (\sigma/r)^6]$. The usual combining rules were employed for the force constants

$$\sigma_{AM} = (\sigma_A + \sigma_M)/2; \quad \epsilon_{AM} = (\epsilon_A\epsilon_M)^{1/2}$$

The temperature-dependent collision diameter, $s_{AM}^2 = \sigma_{AM}^2\Omega^{(2,2)*}$, was evaluated from the integrals $\Omega^{(2,2)*}(kT/\epsilon_{AM})$ which are tabulated[36] as a function of the reduced temperature, $T^* = kT/\epsilon_{AM}$. Collision cross sections at the reaction temperature 280° were used to calculate β_c. The results are tabulated in Table III.

An alternative approach to the temperature variation of cross section has been made by Rowlinson,[37] who derived a potential-dependent expression for molecules which approach to a distance, d, or less; d is the maximum internuclear distance which is to be counted as a collision. For $d = \sigma$, the collision number is just the rate of collisions of hypothetical spheres of this diameter and is proportional to $T^{1/2}$. For $d = r_m$ (where $r_m = 2^{1/6}\sigma$, and $V(r_m) = \epsilon$, the depth of the potential well defined by a Lennard-Jones function) an expression is obtained which is the analog of the Sutherland equation for a hard sphere with an attractive potential. The collision number is increased not only by a factor of $(r_m/\sigma)^2$ over $Z_{\text{hard sphere}}$, but also by a temperature-dependent factor $(1 + \epsilon/kT)$. Depending on the importance of the attractive or repulsive part of the potential for energy exchange, the collision cross section should be defined accordingly. The attractive part is important for the duration of a collision, the repulsive part for the perturbation of the internal states brought about by a collision. The use of s_{AM} considers both features.

Polar Inert Gases. For polar gases, the interaction potential is angular dependent. The most successful

---

(37) J. S. Rowlinson, *Mol. Phys.*, **4,** 317 (1961).

Table IV: Measured Collision Efficiencies for Various Gases

Molecule	$k_m{}^a \times 10^5$, mm^{-1} sec^{-1}	β_p	$(\mu_{AM}/\mu_{AA})^{1/2}$	β_μ	β_c
CH_3NC	96.0	(1.00)	1.00	(1.00)	(1.00)
He	12.0	0.125	0.422	0.055	0.14
Ne	9.06	0.094	0.813	0.076	0.16
Ar	10.6	0.110	0.993	0.11	0.17
Kr	10.5	0.109	0.158	0.13	0.18
Xe	9.50	0.099	1.234	0.12	0.15
H_2	23.4	0.244	0.306	0.074	0.15
N_2	16.4	0.171	0.900	0.15	0.24
CO_2	44.3	0.462	1.017	0.47	0.60
CH_4	32.7	0.341	0.749	0.26	0.35
CD_3F	37.3	0.389	0.974	0.38	0.46
CHF_3	40.4	0.421	1.123	0.47	0.52
CF_4	27.7	0.289	1.168	0.34	0.38
$C_2H_6\theta$	...	...	...	...	~0.6
HCN	50.6	0.527	0.861	0.45	0.53
C_2H_5CN	67.5	0.703	1.07	0.75	0.66
n-C_3H_7CN	89.9	0.937	1.12	1.05	0.84
CF_3CN	42.2	0.440	1.181	0.52	0.51
CH_3CCH	46.5	0.484	0.994	0.48	0.51
C_2H_5CCH	65.0	0.685	1.064	0.73	0.66

[a] Data from I.[26]

potential for polar gases is that of Stockmayer (the 12–6–3 potential)

$$V(r) = 4\epsilon\left[\left(\frac{\sigma}{r}\right)^{12} - \left(\frac{\sigma}{r}\right)^{6}\right] - \frac{\mu'_A\mu'_M\zeta}{r^3}$$

where μ'_A and μ'_M are the dipole moments of the two interacting molecules and the angular dependent factor is $\zeta = 2\cos\theta_A\cos\theta_M - \sin\theta_A\sin\theta_M\cos\phi$. In the limit, as μ'_A or $\mu'_M \rightarrow 0$, the 12–6 potential is recovered.

Hirschfelder, *et al.*,[35] and Rowlinson[38] have used second virial coefficient data to calculate σ and ϵ/k from the polar potential, but the values obtained sometimes show great inconsistency when examined in homologous or related series of molecules, as compared with values obtained from the 12–6 potential. These discrepancies have been considered by Monchick and Mason,[36] who have calculated the potential parameters σ and ϵ/k for a series of molecules from experimental viscosity coefficients with the 12–6–3 potential. The values so obtained proved to be fairly consistent with those derived from the 12–6 potential. Their σ parameters show reasonable trends in homologous series and correspond fairly closely (±0.1 A) to those obtained from the nonpolar potential. The parameters deduced from second virial coefficients are very sensitive to dipolar forces, indicating that the point dipole model used may be too artificial. These authors conclude that viscosity-derived parameters should be given preference. On this basis, only slight differences arise between polar and nonpolar molecules of related structure, *e.g.*, CF_3H and CF_4. They have tabulated accurate values of the collision integrals $\Omega^{(2,2)*}$ calculated from the 12–6–3 potential, for a range of values of the angle-dependent function, including zero.

The value of σ for CH_3CN calculated by Rowlinson[38] from virial coefficient data, using $\mu' = 3.5$ D., is given as 4.02 A; a recalculation[39] using the accepted value[40] of $\mu' = 3.92$ D. yields a value of $\sigma = 4.42$ A.

Using the same method as Rowlinson with the virial coefficient data of CH_3CN, $\sigma(CH_3NC)$ is calculated to be 4.33 A with use of $\mu' = 3.83$ D.; also ϵ/k is found to be 310°K.

However, for continuity with earlier work and in line with the above discussion, the value of $\sigma(CH_3CN) = 4.47$ A ($\epsilon/k = 380$°K), as calculated from viscosity measurements and the 12–6 potential by Craven and Lambert,[34] was also used for CH_3NC and for the calculation of s_{AM} values at 280° for methyl isocyanide-inert gas pairs.

In cases where viscosity data were not available for polar molecules to allow calculation of the potential parameters by the method of Monchick and Mason,[36] and because the parameters derived by the 12–6–3

---

(38) J. S. Rowlinson, *Trans. Faraday Soc.*, **45**, 972 (1949).

(39) See ref 35, following the method on p 215.

(40) A. L. McClellan, "Experimental Dipole Moments," W. H. Freeman and Co., San Francisco, Calif., 1963.

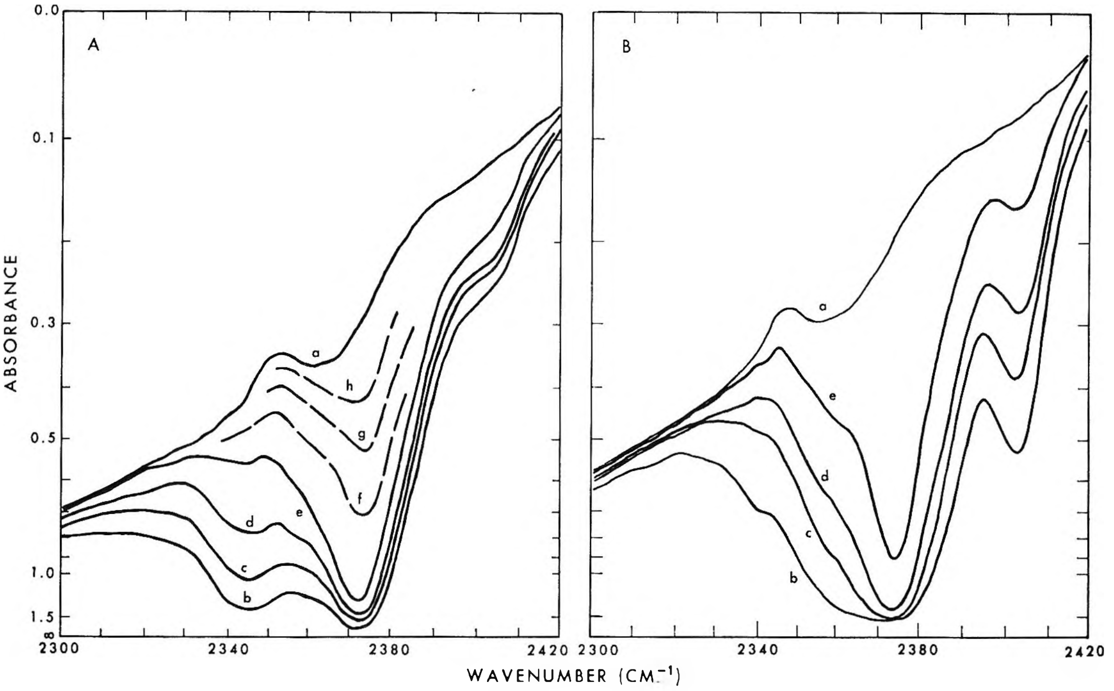

Figure 4. Spectra of CO_2 adsorbed on silica–alumina. A. SAA-1: a, after drying at 600°; b, after CO_2 addition, $P = 30$ torr; c, 19.0 torr; d, 9.8 torr; e, 2.5 torr; f, 4.4×10^{-2} torr; g, 1.0×10^{-2} torr; h, 3.5×10^{-3} torr. B. SAA-3: a, after drying at 800°; b, after CO_2 addition, $P = 4.2$ torr; c, 0.2 torr; d, 1.0×10^{-2} torr; e, 5.0×10^{-4} torr (12C spectrometer, LiF prism).

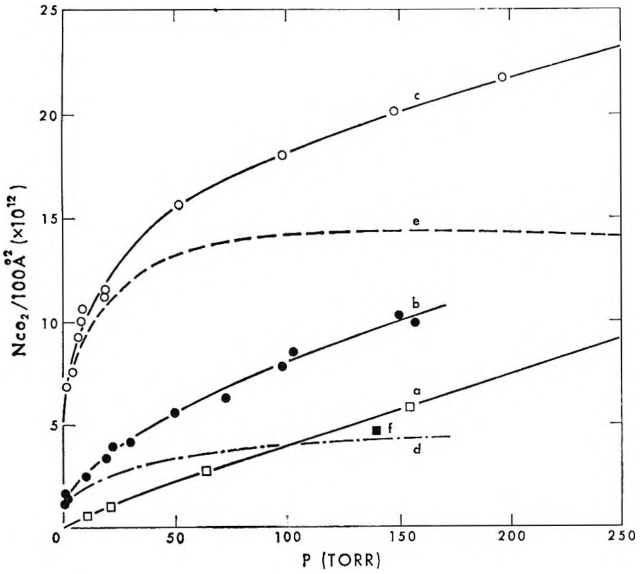

Figure 5. Adsorption of CO_2 on silica aerogel and on silica–aluminas (~35°): a, on silica aerogel; b, on SAA-1; c, on SAA-3; d, difference between adsorption on silica and on SAA-1 (= b − a); e, difference between adsorption on silica and on SAA-3 (= c − a); f, adsorption on SAA-1 after chemisorption of HCl.

dashed curves (~5×10^{12}/cm^2 for SAA-1 and ~16×10^{12}/cm^2 for SAA-3). The existence of an upper limit for the concentration of these sites was also established by blocking them with adsorbates held more strongly than CO_2, as will be shown. For SAA-1 the "net" adsorption approximates a Langmuir isotherm for a surface containing about 5×10^{12} sites/cm^2. The plot of P/weight adsorbed *vs.* P does not give a straight line, however, being instead concave downward, particularly at lower pressures. Similar curvature was obtained by plotting P/absorbance *vs.* P using intensities of the 2375-cm^{-1} band at pressures between 2 torr and 3.5×10^{-3} torr. The adsorption sites thus apparently vary in strength as also indicated by the shift in frequency of the 2375-cm^{-1} band as surface coverage decreased. The heat of adsorption of CO_2 at low coverage on these sites was estimated as roughly 15 kcal/mole from spectra and pressure measurements at 40, 80, and 120° (using the Clausius–Clapeyron equation). The sites on which CO_2 giving a band in the 2360–2380-cm^{-1} region is held will be called α sites.

Adsorption of HCl. On all of the silica-aluminas, some HCl was chemisorbed to form new OH groups. This was evidenced either by a marked increase in the H-bonded "tail" below the isolated OH band at 3750 cm^{-1} or by a distinct band near 3610 cm^{-1}, as shown in Figure 6. The intensity of the 3750-cm^{-1} band was not reduced. When DCl was added, a new OD band was produced near 2660 cm^{-1}.

Chemisorption was rapid at room temperature but

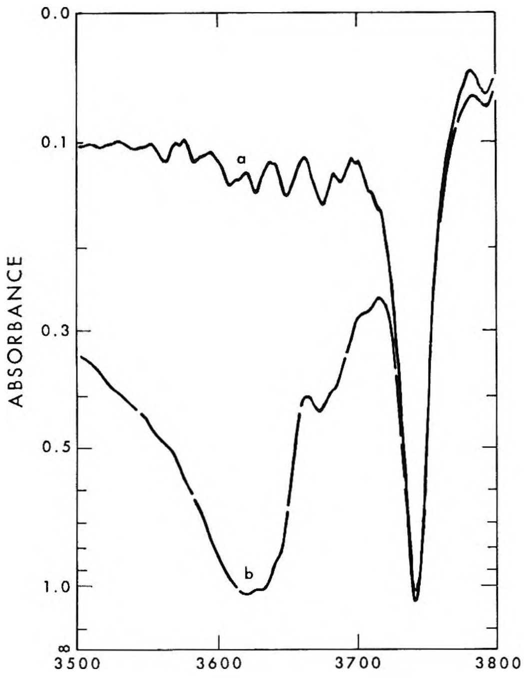

Figure 6. Hydroxyl bands on SAA-3: a, after drying at 800°; b, after subsequent chemisorption of HCl (12C spectrometer, LiF prism).

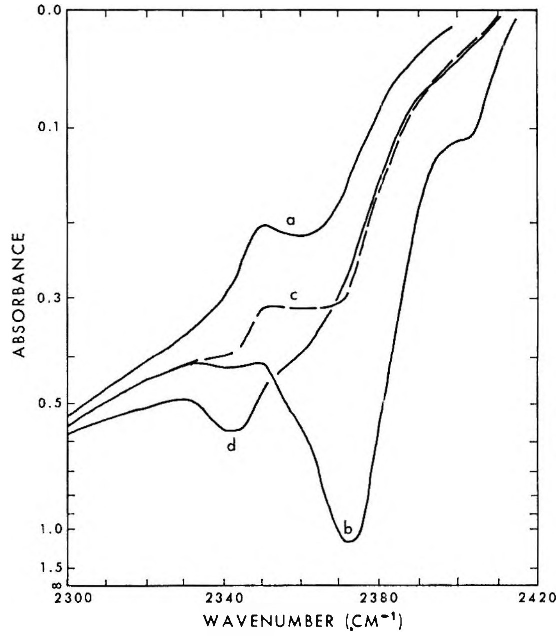

Figure 7. Spectra showing effect on CO_2 adsorption of prior chemisorption of HCl: a, SAA-1 dried at 600°; b, after addition of CO_2 (~3 torr); c, after evacuation, adsorption of 0.4 cm³ (STP) of HCl, and readdition of CO_2 (~3 torr); d, after evacuation, further adsorption of HCl, and readdition of CO_2 (12 torr) (12C spectrometer, LiF prism).

not extensive even with large additions of HCl. The extent varied with silica-alumina sample, with predrying temperature, and with contact time but after short contact was usually less than 2×10^{13} molecules/cm².

Chemisorption of HCl completely blocked subsequent adsorption of CO_2 on α sites. Following the experiments on CO_2 adsorption, SAA-1 was redried under vacuum at 600° (1 hr) and exposed to about 3 torr of CO_2 at room temperature. No major change was noted in the number of α sites. After a 15-min evacuation to remove adsorbed CO_2, a small dose (0.48 cm³ (STP)) of HCl was admitted to the cell, and it was adsorbed almost completely. After evacuation for 5 min, 83% of the HCl remained on the aerogel. When CO_2 was then added as before, the spectrum, shown in Figure 7, indicated only a small fraction of the original CO_2 adsorption. The adsorbed CO_2 was again removed by evacuation and a large dose (5.35 cm³ (STP)) of HCl was admitted. This addition increased retention of HCl after 5 min evacuation by 33%. When CO_2 was then admitted at 12 torr, none was adsorbed on the α sites. Maximum chemisorption of HCl was 1.1×10^{13} molecules/cm². The number of α sites was evidently somewhat lower than this; from the extent of site-blocking by the first addition of HCl, the maximum was estimated as 9×10^{12}/cm². After reevacuation at 600°, the plate was exposed to 5 torr of HCl for 15 min. Permanent retention of HCl in this instance was nearly 1.6×10^{13} molecules/cm². Thus after the rapid and fairly selective blocking of the α sites, HCl continued to chemisorb, but more slowly.

For comparison, SAA-3 (predried at 800°) was later *slowly* titrated with just enough HCl to displace the CO_2 held after a 5-min evacuation. The apparent number of α sites was 2.6×10^{13}/cm².

Blocking of α Sites by NH_3 or H_2O. Compared with HCl, two to four times as many molecules of NH_3 were required to block the α sites for subsequent adsorption of CO_2. This was partly caused by slow rearrangement of adsorbed NH_3 on the surface. Equilibration overnight at room temperature or heating to 200° and slow cooling somewhat decreased the amount of NH_3 required. Equilibration for 0.5 hr at room temperature was, however, normally allowed.

Figure 8 illustrates data obtained on SAA-1. As shown in curve d, the complete adsorption of 1.0 cm³ (STP) of NH_3 failed to block CO_2 adsorption completely after 0.5-hr equilibration. After 16 hr, however, CO_2 was no longer adsorbed. The NH_3 added corresponded to 2.0×10^{13} molecules/cm². Over three times this amount was retained after the sample had been exposed to 50 torr of NH_3 followed by evacuation for 0.5 hr at room temperature.

data with the turbidity. However, for reasons which are discussed below, it was not possible to do this.

Experimental Section

Materials. Several commercial samples of TSA were used (Fisher Certified reagent, Baker and Adamson reagent). These were purified by repeated extractions of the acid from aqueous solution with ether and hydrochloric acid, as described elsewhere.[9] For the Baker and Adamson acid, the purification did not affect the results, whereas Fisher samples, with one exception, had to be purified before reproducible results could be obtained. Most of the experiments were performed with the Fisher sample that was not influenced by the purification. The solutions of the purified samples were colorless and clear even at concentrations approaching saturation (about 2.3 g/ml). Other chemicals were of the highest grade and were used as received. The doubly distilled water was obtained from an all-Pyrex still.

Preparation of Solutions. The procedure described previously[4] was followed except that the dilutions of the ternary solutions for light scattering measurements were carried out by the addition of clarified NaCl solution directly into the light scattering cell. The initial stock solution also contained the same concentration of sodium chloride so that this quantity remained constant in the course of a series of dilutions. The concentration of the diluted solutions was then determined by weight. This concentration was checked at frequent intervals, usually every third dilution, by refractometry. The concentration of the stock solution was determined in the same way from the known value of the refractive index increment. The diluted solutions prepared in this manner were refiltered whenever necessary. The more dilute ternary solutions were clarified after every addition of NaCl solution. The dilutions were prepared from several stock solutions of different initial concentration of TSA, so that a great deal of overlapping data at close intervals was assured.

Solutions were clarified by repeated filtration directly into the cell through Millipore filters under slight nitrogen pressure. Filters of 220- and 450-mμ porosity were used simultaneously. All solutions were carefully inspected visually in a strong beam of light at low angles. The cell was tightly covered with several layers of Parafilm.

Light Scattering and Refractive Index Measurements. Essentially, technique A of the previous paper[4] was utilized. This technique, with small modifications, was critically tested recently in the determination of the Rayleigh ratio and depolarization of such weakly scattering liquids as water and CCl_4,[11] and the determination of the absolute angular intensities of monodisperse Dow polystyrene latexes.[12] The standard 1.2-cm slit system, defining the incident beam of a Brice-Phoenix light scattering photometer, and a Pyrex 2.4-cm square cell or a 4.0-cm semioctagonal cell were used. The instrument was calibrated at frequent intervals using the standard opal diffusors supplied by the manufacturer. The reliability of this calibration procedure for obtaining absolute scattering intensities has been recently discussed in detail.[13,14] Changes in the calibration constant between determinations were small, usually less than 1%. Polarization measurements were made using Glan-Thompson prisms.

Refractive index measurements were obtained at 25° with a Brice-Phoenix differential refractometer, as described earlier.[4]

Vapor Pressure Measurements. Vapor pressure measurements were obtained with a Mechrolab Model 301A vapor pressure osmometer at 25°. The temperature was controlled by the thermostating unit supplied by the Mechrolab Co. A water-cooled metal jacket surrounded the chamber block of the instrument. It was found that a temperature difference of at least 3° between the working temperature (25°) and the surroundings was needed in order to assure proper thermostating. The instrument was calibrated with aqueous NaCl solutions. A plot of the resistance change, ΔR, against the activity of water for these solutions was made, using the values given by Robinson and Stokes.[15] The calibration curve did not change over a period of 9 months. The calibration curve of activity of water *vs.* ΔR was made from 65 determinations of ΔR on 12 different solutions of NaCl. The data could be represented by the linear equation $a_W = -0.3660 \times 10^{-3}\Delta R + 0.9999$. The standard deviations of the slope and intercept were 1.38×10^{-6} and $\pm 0.95 \times 10^{-4}$, respectively. The standard deviation of the fit was 3.50×10^{-4}.

Since ΔR varies with time, it was necessary to choose an optimum time for taking the readings. The criterion chosen was the time at which the change of ΔR for the NaCl solutions was the slowest. This was found to be 10 min after the solution was placed on the thermistor bead, and all readings were taken at this time. In order to check the consistency of the method, a calibration curve was also prepared for a time of 5 min.

---

(11) J. P. Kratohvil, M. Kerker, and L. E. Oppenheimer, *J. Chem. Phys.*, **43**, 914 (1965).

(12) J. P. Kratohvil and C. Smart, *J. Colloid Sci.*, **20**, 875 (1965).

(13) J. P. Kratohvil, Gj. Deželić, M. Kerker, and E. Matijević, *J. Polymer Sci.*, **57**, 59 (1962).

(14) J. P. Kratohvil, *Anal. Chem.*, **36**, 458R (1964).

(15) R. A. Robinson and R. H. Stokes, "Electrolyte Solutions," Butterworth and Co. Ltd., London, 1959.

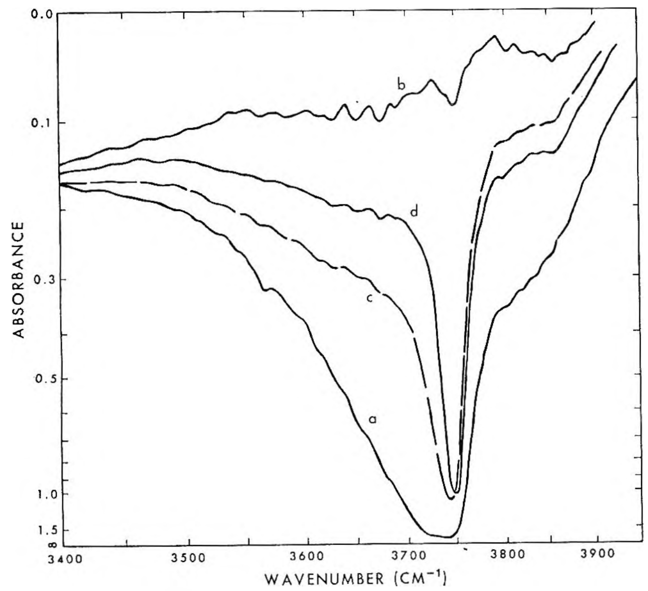

Figure 9. Spectra recorded during preparation of SAV-1: a, silica predried at 600°; b, all OH groups removed by reaction with $AlCl_3$; c, after hydrolysis and redrying at 600° following b; d, after final drying at 800° (12C spectrometer, LiF prism).

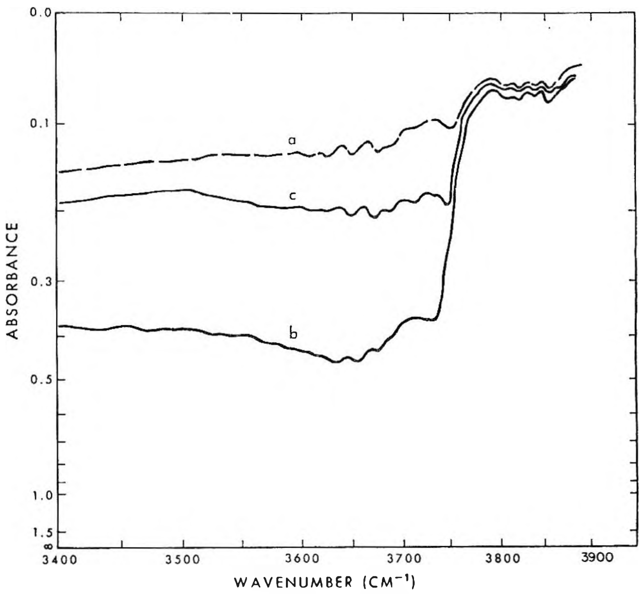

Figure 10. Spectra recorded during the hydrolysis procedure in preparation of SAV-1: a, after reaction of all hydroxyl groups with $AlCl_3$; b, after first addition of H_2O; c, after drying at 600° following b (12C spectrometer, LiF prism).

Further Evidence on the Genesis and Nature of α Sites on Silica–Alumina. Typical spectra recorded during the preparation of SAV-1 are shown in Figure 9. As evidenced by the greatly decreased intensity of the hydroxyl stretching band after $AlCl_3$ treatment, hydrolysis, and redrying, SAV-1 held markedly fewer OH groups than the original silica. The spectra of OH groups on SAV-1 and SAV-2 after hydrolysis plus final drying at 800° were virtually identical, revealing no difference in the number of the residual OH groups.

During the preparation of SAV-1, CO_2 adsorption was checked at various stages to determine at what point the α sites were first created. No α sites were detected after complete removal of OH groups by reaction with $AlCl_3$ and evacuation at 600°, but admission of a dose of H_2O (<20% monolayer) at 100° followed by reevacuation at 600° produced many sites ($^1/_3$ to $^1/_2$ of the number ultimately obtained after final hydrolysis and 600° drying). When first added, the H_2O produced a broad H-bonded OH band extending below 3750 cm^{-1}, as shown in Figure 10. Drying at 600° removed most of this band and left a very small isolated OH band at 3750 cm^{-1}. Addition of H_2O at 100° followed by redrying at 600° was repeated until no more HCl was produced. The number of α sites present after drying at 600° increased during the process as did the intensities of the isolated OH band at 3750 cm^{-1} and the tail below this band. The OH bands, however, never regained the intensities shown after original evacuation at 600°, as illustrated in Figure 9.

After hydrolysis was complete, the SAV-1 was dried at 600° and titrated with butene and NH_3. Then it was repeatedly exposed to hydrocarbons and other adsorbates, calcined in O_2, and dried under vacuum at 600°. Virtually constant intensity of the 2375-cm^{-1} band (at 3 torr of CO_2) showed that the number of α sites (after drying at 600°) did not change significantly throughout these experiments. However, when the sample was dried under vacuum at 800° for 0.5 hr, the number of α sites increased by approximately 50%, as indicated both by the increase in the intensity of the 2375-cm^{-1} band on adsorption of CO_2 and by subsequent titration with butene.

Table IV shows results of titration of selected samples with *n*-butylamine and Hammett indicators.[21] No correspondence is apparent between any of the types of acid sites measured by butylamine titration and the α sites (Table III). Even the relative numbers of α sites on different catalysts cannot be compared on the basis of butylamine titration. For SAV-2, only strong acid sites ($pK_a = -5.6$) were present, whereas SAV-1 also had weaker acid sites. The strongest ($pK_a < -8.0$) acid sites were found only on SAA-3.

α Sites on γ-Alumina. Drying γ-alumina by evacuation at 600° or higher produced sites which strongly

---

(21) R. J. Bertolacini, *Anal. Chem.*, **35**, 599 (1963).

Table IV: Acidity by Butylamine Titration

Sample	pK_a	m equiv/g	Sites/cm² × 10^{-13}
SAV-1	<−8.0	0	0
	−5.6	0.48	3.8
	−3.0	0.26	2.0
	1.5	0	0
	Total	0.74	5.8
SAV-2	<−8.0	0	0
	−5.6	0.32	2.5
	−3.0	0	0
	1.5	0	0
	Total	0.32	2.5
SAA-2	<−8.0	0	0
	−5.6	0.53	5.2
	−3.0	Not determined	
	1.5	Not determined	
SAA-3	<−8.0	0.71	8.3
	−5.6	0	0
	−3.0	0.03	0.4
	1.5	0	0
	Total	0.74	8.7

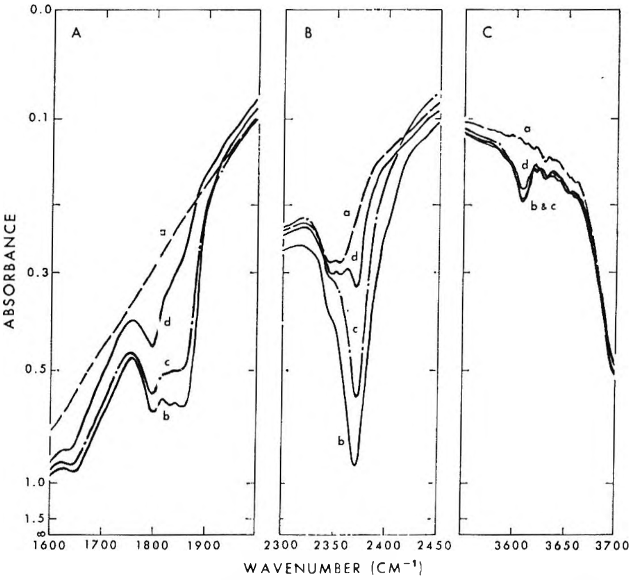

Figure 11. Spectral changes resulting from adsorption of CO_2 on γ-alumina: a, alumina predried at 800°; b, exposed at room temperature to CO_2 at 2 torr followed by 1-min evacuation; c, after 15-min evacuation at room temperature; d, after 30-min evacuation at 100° (IR-9 spectrometer, single-beam operation).

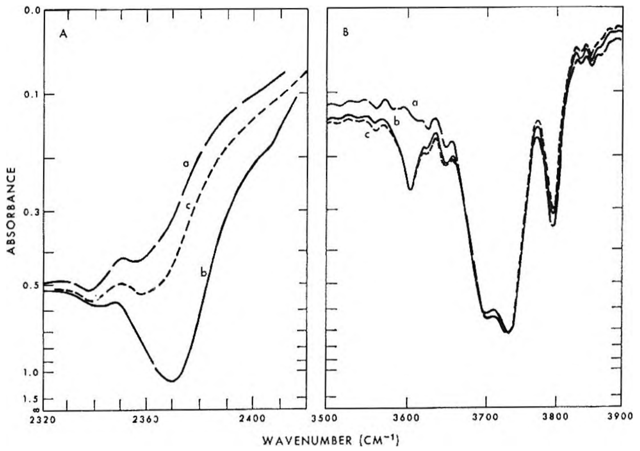

Figure 12. Spectra showing displacement of CO_2 from γ-alumina by butene (A) and its failure to affect OH stretching bands (B): a, alumina dried at 800°; b, after exposure to CO_2 and evacuation for 1 min; c, after small addition of butene.

adsorbed molecular CO_2 in a manner similar to that described for silica–alumina. Figure 11 illustrates some of the spectral changes for γ-alumina (predried at 800° for 1 hr) when CO_2 was adsorbed and desorbed. Several bands (not all shown) that were also produced in the region from 1350 to 1750 cm^{-1} apparently represent relatively stable carboxylate or carbonate structures. The bands observed near 1800–1870 cm^{-1}, however, arise from a more weakly adsorbed form of CO_2 and may be related to that near 2370 cm^{-1} (molecular CO_2). One form of adsorbed CO_2 produces a band at 3610 cm^{-1} which apparently reflects strong interaction (probably bicarbonate formation) with a surface OH ion. A similar band is produced near 2665 cm^{-1} on similarly dry deuterated alumina.

The independence of various types of CO_2 adsorption was demonstrated by independent changes in corresponding bands either on progressive desorption of CO_2 by heating and evacuation or on displacement of adsorbed CO_2 from the α sites with 1-butene. As illustrated in Figure 12, the "bicarbonate" OH band at 3610 cm^{-1} remained unaffected after displacement of the CO_2 causing the 2370-cm^{-1} band. The surface concentration of α sites—5.2×10^{12} sites/cm² by titration with 1-butene—found here was similar to that found on comparably dried silica–alumina.

Because HCl, NH_3, and many other adsorbates react extensively with the surface of dry γ-alumina, no attempt was made to titrate α sites on alumina with compounds other than 1-butene. Adsorption of acetylene, for example, colored the dry alumina light brown and produced new OH groups. (No color changes or other evidence for complex reaction had been noted for acetylene on silica–alumina.)

Discussion

The conclusion[12,22] that most of the residual OH groups on very dry silica–alumina are attached to silicon rather than to aluminum atoms has been supported. On less thoroughly dried silica–aluminas, however, many OH groups, particularly those giving a band in the 3600–3650-cm^{-1} region, must be attached to aluminum atoms. Elimination of these groups through condensation to form H_2O evidently creates the α sites which strongly hold molecular CO_2.

Description of these sites as "acid" sites is misleading. They hold HCl more selectively than they do NH_3. The formation of OH groups when HCl is chemisorbed indicates that a reactive oxide ion, of a type not present on pure silica, is part of the site, while strong adsorption of butene, benzene, NH_3, etc., argues that the site also contains an exposed metal ion (Lewis acid). The α site appears, therefore, to be a grouping structured either as

$$Al^+O^{2-}Al^+ \text{ or } Al^+O^-\text{–}Si$$

Possibly it is a "strained" oxide link similar to that postulated by Cornelius, *et al.*,[23] for γ-alumina. Chemisorption of HCl probably forms Al–OH · · · Cl–Al groups in which the OH group is affected by an adjacent chlorine atom.

The evidence obtained during preparation of the SAV samples suggests that the α sites on silica–alumina are probably $Al^+O^{2-}Al^+$ rather than Al^+O^-–Si. The Al–Cl bonds are probably hydrolyzed more easily than are the Al–O–Si links. Nearly all of the OH groups should be attached to Al atoms following initial hydrolysis of the surface =AlCl groups, and condensation of =AlOH with either =AlCl or another =AlOH would give $Al^+O^{2-}Al^+$. However, the argument is not conclusive because, as indicated by Figure 9, some isolated Si–OH groups do result from rehydration and strong drying.

The characteristics of the CO_2 band near 2375 cm^{-1} (ν_3) shed some additional light on the nature of the α sites. The CO_2 held on these sites remains as linear CO_2, although it no longer freely rotates. Possible evidence for limited rotation or vibration is, however, seen in the presence of the weak bands near 2405 and 2355 cm^{-1}. The frequency shift *vs.* the ν_3 band for gaseous CO_2 is opposite to shifts observed when CO_2 is liquefied or solidified. The increased frequency shown by CO_2 on α sites can possibly be explained by weak bonding to surface ions—which effectively have infinite mass. In the case of bonding through one end, the C–O force constant could appear to be increased, as suggested by Overend,[24] because the weak bond to the surface must also be stretched and compressed during the CO_2 vibration. On this basis, the frequency shift should increase with increasing force constant for the O-surface bond, but the same qualitative argument could also apply to other types of CO_2 attachment to the surface. Because CO_2 has a high quadrupole moment, the strong adsorption of CO_2 on α sites is probably best explained by ion–quadrupole interaction. On this basis, adsorption by one end seems less likely than lateral attachment at an ionic site ($Al^+O^{2-}Al^+$). The CO_2 band at 2375 cm^{-1} (+ associated shoulders) on silica–alumina seems unrelated to any other bands in the spectrum, and there is apparently little or no formation of surface "carbonates" or similar structures. On γ-alumina, however, a connection may exist between the CO_2 band (2370 cm^{-1}) and bands in the 1800–1870-cm^{-1} range. Such bands are found in spectra of organic carbonates and can be attributed to C=O stretching in $\begin{smallmatrix}-O\\-O\end{smallmatrix}\!>C{=}O$ groups.[25] Possibly, the 2370-cm^{-1} and 1870-cm^{-1} bands are related through an equilibrium such as

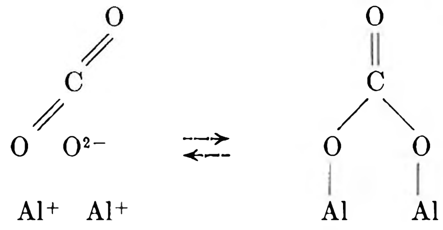

The concentration of α sites on silica–alumina is known within fairly narrow limits. It can hardly be greater than that indicated by HCl chemisorption and hardly less than that indicated gravimetrically at pressures below 2 torr. Steric factors[4] cannot explain the low concentrations of α sites found in this study, because CO_2 and the other molecules used as titrants are all fairly small. The NH_3 titrations show, moreover, that the α sites represent only a fraction of a larger group of sites which are virtually equivalent for adsorption of NH_3 and presumably also of *n*-butylamine. Thus, a large steric factor is not required to explain differences in the number of sites measured by Hirschler[4] and by Leftin and Hall.[7] Characterization of the strength and number of acid sites by titration with *n*-butylamine using organic indicators may be very misleading. If the acid color of the indicator is produced

---

(22) A. Terenin and V. Filimonov, "Hydrogen Bonding," D. Hadzi, Ed., Pergamon Press, Inc., New York, N. Y., 1959, p 545.

(23) E. B. Cornelius, T. H. Milliken, G. A. Mills, and A. G. Oblad, *J. Phys. Chem.*, 59, 809 (1955).

(24) J. Overend, private discussion.

(25) B. M. Gatehouse, S. E. Livingstone, and R. S. Nyholm, *J. Chem. Soc.*, 3137 (1958).

on only a few sites belonging to a large class wherein all sites hold butylamine strongly, titration will falsely indicate that all sites in the class are as strong as those holding the indicator. The difference between the acid sites on the SAA-2 and SAA-3 shown in Table IV apparently does not fairly reflect differences between these catalysts. Probably the presence of a few very strong acid sites on SAA-3 has in this instance caused classification as $pK_a < -8.0$ of sites which would otherwise have been titrated as $pK_a = -5.6$ sites. Description as $pK_a = -5.6$, moreover, may properly apply to only a small fraction of the sites normally so characterized.

The α sites show important adsorptive properties, but although these sites are either active or similar in nature to sites which are active, they are not essential for catalytic activity. Blocking all α sites by chemisorption of HCl increases activity for polymerization of butene.[19] Possibly, slow desorption of products normally limits the catalytic contribution of the α sites, while similar sites which hold olefins less strongly are responsible for most of the catalyzed reaction. Possibly, a cooperative effect is needed between an α site and an adjacent Brønsted acid site, but no direct evidence presently supports such speculation.

The α sites, which preferentially and strongly adsorb many unsaturated or polar molecules, are evidently ionic and therefore should promote the ionic dissociation of adsorbed hydrocarbons. Yet butene and acetylene seem to be held on such sites on silica–alumina with relatively little change in their character; there is no spectral evidence for hydride or proton abstraction (or for proton addition) to form organic ions. Ions of such hydrocarbons are probably formed only transiently on active sites and readily escape detection because of their very low steady-state concentration.

The ability to identify and study separate types of surface sites and to establish the type of site on which adsorption of a given molecule occurs is essential for ultimate solution of the complex problems presented by oxide catalysts. Some progress has been made in this direction, but much more remains to be done in relating individual types of sites, or combinations of these, to the actual catalytic behavior of a surface.

Acknowledgments. Special acknowledgment is made of the contribution of R. J. Bertolacini, who measured the acidities given in Table IV. The assistance of J. Kekich in most of the experimental work is also gratefully acknowledged.

Heats and Entropies of Dissociation of Sodium Salts of Aromatic Radical Anions in Tetrahydrofuran and Dimethoxyethane. The Limitation and Generalization of the Concepts of Contact and Solvent-Separated Ion Pairs

by P. Chang, R. V. Slates, and M. Szwarc

Department of Chemistry, State University College of Forestry at Syracuse University, Syracuse, New York
(Received May 5, 1966)

Conductance of sodium salts of aromatic radical anions was investigated in tetrahydrofuran (THF) and in dimethoxyethane (DME) at temperatures ranging from −70 to 25°. The results provided the respective dissociation constants of ion pairs and the mobilities of the ions as functions of temperature. The heats and entropies of dissociation of the investigated ion pairs have been calculated. Contrary to some claims reported in the literature, the sodium salts are associated into pairs even in DME, the dissociation constants being smaller than 10^{-5} M. Moreover, for ion pairs which may be classified as solvent-separated pairs, the dissociation is slightly *more* extensive in THF than in DME. The sodium ion is larger when coordinated with THF than with DME and therefore the latter forms a tighter pair than the former. Finally, the concept of contact and solvent-separated ion pairs is reviewed. Its limitations are outlined and a more general treatment is suggested.

The results of conductance studies of sodium salts of aromatic radical ions in tetrahydrofuran (THF) at 25° were reported in an earlier paper.[1] The present investigation extends the data to other temperatures (−70 to 25°) and to dimethoxyethane (DME) solution. This was done for two reasons. (1) A more accurate determination of Λ_0 was necessary because any uncertainties in their values are amplified in the calculation of the corresponding dissociation constants, K_{diss}. The latter are given by the reciprocal of the product (slope of Fuoss' line) × Λ_0^2. The present work provides additional means of ascertaining the accuracy of the determined Λ_0 values and, hence, of K_{diss}. (2) Study of the equilibria over a wide temperature range permits us to determine the heats and entropies of the dissociation of the respective ion pairs.

Experimental Section

The method of preparation of sodium salts of aromatic radical ions was fully described elsewhere.[1] The technique used for the studies of conductance was given in previous papers.[2,3] The former[2] includes a diagram of the apparatus used in the conductance study and gives details of the method of diluting the investigated solutions. It suffices to say that the dilution was accomplished by removal of the solute and not by the addition of solvent, and therefore, no impurities were introduced in the process. The concentrations of the aromatic radical ions (ion pairs + free ions) were determined *in situ* at 25°, using a spectrophotometric technique. The relevant absorption maxima and extinction coefficients are given in Table I. The contraction of the solution, caused by lowering the temperature, was accounted for in the calculations.

Any possible difference in the absorption of ion pairs and of free ions may affect the spectrophotometrically determined concentration of radical ions, particularly at high dilutions. It is believed, however, that these changes are negligible. The reliability of the spectro-

---

[1] R. V. Slates and M. Szwarc, *J. Phys. Chem.*, 69, 4124 (1965).

[2] D. N. Bhattacharyya, C. L. Lee, J. Smid, and M. Szwarc, *ibid.*, 69, 612 (1965).

[3] C. Carvajal, K. J. Tölle, J. Smid, and M. Szwarc, *J. Am. Chem. Soc.*, 87, 5548 (1965).

fining membrane, which is only of incidental interest here. A considerable number of experiments using different kinds and thicknesses of cellophane membranes has further demonstrated that the value of the diffusion coefficient so found is independent of membrane thickness. Since this point is fundamental to the experiment, the evidence for it is given in Table I, which also shows the precision attainable in D, about 1%.

Confining membranes used are various forms of unwater proofed cellophane, kindly given to us by the Du Pont Co., and here denoted by the manufacturer's symbols. The wet thicknesses (b, mm) of these materials are approximately as follows: experimental, 0.024; 300-PUD, 0.053; 300-NR, 0.050; 300-GF, 0.125. These numbers are given merely as an indication that the materials were in fact of different thicknesses; the thickness parameter, ξ, significant to our experiment, depends on b through the relation

$$\xi = b\frac{Dc}{D_m c_m}$$

in which D and D_m are the diffusion coefficients in the confined gel and in the confining membrane for the corresponding salt concentrations c and c_m. Since the computation treats ξ as an adjustable parameter in a least-squares procedure, we do not need individual values for b, D_m, or c_m.

Table I: Self-Diffusion Coefficients with Various Confining Membranes[a]

Membrane	$D \times 10^5$, cm²/sec	ξ, cm	$10^3\sigma$
Experimental	1.227	0.0084	1.7
	1.221	0.0087	1.5
	1.231	0.0068	1.3
	1.207	0.0081	1.7
	1.222 ± 0.008		
300 PUD	1.222	0.0166	1.4
	1.215	0.0168	1.3
	1.238	0.0161	1.4
	1.242	0.0168	1.4
	1.227	0.0154	...
	1.229 ± 0.009		
300 NR	1.206	0.0130	1.4
	1.212	0.0118	1.5
	1.209		
300 GF	1.204	0.0132	1.6
	1.212	0.0131	1.6
	1.208		
Av (13)	1.220 ± 0.010		

[a] Conditions: 0.0100 M NaCl; 2% agar; 25°.

The fourth column of Table I gives the root-mean-square deviations for the observed values of (count at time t)/(initial count) from those computed for the least-square "best" values of D and ξ, namely, those given in the table. (The details of these computations are described by Allen, *et al.*[5]) Counting statistics at about half-time correspond to $10^3\sigma = 3$.

A total of 79 diffusion runs was made for gels containing 1–4 wt % agar with 0.01 and 0.05 M NaCl using the four types of cellophane. The results given in Table I are typical.

In all of our work the gels were from a single preparation of agar, Purified Agar, Difco Certified, Control No. 437,277.[6] An appropriate quantity was placed in a 10-ml volumetric flask to which was added exactly 5 ml of a solution of twice the salt concentration desired together with the necessary amount of carrier-free tracer (Na^{22} or Cs^{134}). After dilution to the mark the mixture was slowly warmed and gently stirred. When clear and homogeneous the gel was transferred to ten or twelve small test tubes and tightly stoppered. These portions were used in separate diffusion runs. Most gels were used within 1 week of preparation; none was allowed to stand more than 1 month. The details of filling the cell have been described.[5] The reproducibility of the preparation of these gels, insofar as self-diffusion in them is concerned, is indicated by the following results for three different preparations on each of which three or four diffusion runs were made. (These gels all contained 1% agar with 0.01 M NaCl.)

	$D \times 10^5$, cm²/sec				Av
A	1.239	1.245	1.246		1.242
B	1.253	1.249	1.244		1.248
C	1.248	1.240	1.252	1.249	1.247

Av (10) 1.246; max dev 0.007; av dev 0.004

Results

In Tables II and III are given the averages of the values found for the self-diffusion coefficients of sodium and cesium under the various conditions with the mean deviations between independent runs, the number of these being given in parentheses.

To be able to make a comparison with a somewhat different transport phenomenon, the conductances of two series of agar gels and of the solutions from which they were prepared have been measured. These gels

---

[6] From Difco Laboratories, Inc., Detroit, Mich.

Table II: Self-Diffusion Coefficients of Sodium in Agar Gels with NaCl Solutions

% agar	$D \times 10^5$, cm²/sec		
	10°		
	0.001 M	0.01 M	0.05 M
1	0.859 ± 0.006 (4)	0.859 ± 0.002 (3)	0.866 ± 0.002 (3)
2	0.837 ± 0.010 (4)	0.840 ± 0.009 (3)	0.848 ± 0.005 (2)
3	0.810 ± 0.006 (3)	0.816 ± 0.003 (3)	0.819 ± 0.004 (3)
4	0.790 ± 0.004 (3)	0.800 ± 0.004 (5)	0.802 ± 0.002 (3)
	25°		
	0.001 M	0.01 M	0.05 M
1	1.282 ± 0.004 (4)	1.247 ± 0.004 (15)	1.247 ± 0.006 (7)
2	1.229 ± 0.013 (5)	1.220 ± 0.010 (13)	1.219 ± 0.004 (9)
3	1.193 ± 0.006 (4)	1.183 ± 0.007 (12)	1.183 ± 0.012 (7)
4	1.143 ± 0.003 (3)	1.158 ± 0.008 (8)	1.150 ± 0.008 (8)
	0.1 M	0.25 M	
1	1.280 ± 0.006 (3)	1.315 ± 0.006 (5)	
2	1.267 ± 0.004 (3)	1.288 ± 0.005 (3)	
3	1.245 ± 0.002 (3)	1.254 ± 0.006 (3)	
4	...	1.234 ± 0.004 (2)	

Table III: Self-Diffusion Coefficients of Cesium in Agar Gels with CsCl

% agar	$D \times 10^5$, cm²/sec	
	10°	
	0.001 M	0.05 M
0.5	...	1.420 ± 0.009 (2)
1	1.379 ± 0.013 (3)	1.398 ± 0.012 (3)
2.5	1.342 ± 0.019 (3)	1.344 ± 0.004 (4)
4	1.293 ± 0.012 (3)	1.297 ± 0.001 (4)
	25°	
0.5	...	1.989 ± 0.011 (2)
1	1.968 ± 0.020 (5)	2.014 ± 0.018 (3)
2.5	1.919 ± 0.024 (5)	1.927 ± 0.003 (4)
4	1.851 ± 0.003 (4)	1.862 ± 0.009 (3)

contained either 3 or 4% agar with no and approximately 0.01, 0.02, 0.03, 0.05, and 0.1 M NaCl. The measurements were made at 1000 cps using a Hewlett-Packard wide-range oscillator, a Leeds and Northrup shielded ratio box, air capacitor, and a Leeds and Northrup No. 4755 AC resistance box in conjunction with a tuned amplifier-detector of 1-μ sensitivity. A Leeds and Northrup dipping conductance cell was slowly immersed in the freshly prepared, molten gel and brought to 25° for measurement. The results are shown in Figure 1 as relations between $K_s - K_g$ and K_s, conductivities of solution and gel, respectively. These are accurately straight lines and correspond to constant formation factors according to the relation

$$K_g = \frac{K_s}{F} + \Delta K$$

which may be taken as a definition of an excess conductance, ΔK, for a heterogeneous system, in terms of a constant F. The constancy of F for a given agar content must be verified to make this definition meaningful. This is done in the plots of Figure 1, which correspond to the relation

$$K_s - K_g = \left(\frac{F - 1}{F}\right)K_s - \Delta K$$

The slopes of the lines measure F and the intercepts give ΔK for the two gels studied.

Over the range of agar content studied, the observed diffusion coefficients vary linearly with the weight fraction of agar. The accuracy of this linearity seems to be well established. For twelve such lines, involving 45 values of D (determined by a total of 189 runs), three values of D deviate from the lines by about 1%, two by about 0.5%, and the remainder by less than 0.5%, with an average deviation of 0.25%. Table IV gives the constants D_0 and a for these lines; $D = D_0 - aw$. Inspection of this table discloses the fact that all of the results, regardless of nature of ion or of the other conditions of the experiment, can be expressed by the relation

$$\frac{D(t,c,w)}{D_0(t,c)} = 1 - 0.023w$$

Table IV: Heats and Entropies of Dissociation at 15 and −65° in THF Solution[a]

	Naphthalene·⁻	Biphenyl·⁻	Triphenylene·⁻	Anthracene·⁻	Perylene·⁻
ΔH_{15}, kcal/mole	−8.2	−7.3	−5.2	−6.1	−2.2
$\Delta S°_{15}$, cal/deg mole	−58	−52	−42	−45	−29
ΔH_{-65}, kcal/mole	−1.8	−1.6	−0.4	0.0	0.0
$\Delta S°_{-65}$, cal/deg mole	−30	−28	−23	−21	−21

[a] Standard state: 1 M solution.

Table V: Experimental Λ_0 Values and the Walden Products for Sodium Salts of Aromatic Radical Ions in DME

T, °C	Biphenyl·⁻ Λ_0	Biphenyl·⁻ $\eta\Lambda_0$	Triphenylene·⁻ Λ_0	Triphenylene·⁻ $\eta\Lambda_0$	Perylene·⁻ Λ_0	Perylene·⁻ $\eta\Lambda_0$
25	160	0.724	130	0.600	143	0.645
15	143	0.720	125	0.630	125	0.630
5	125	0.714	105	0.597	118	0.670
−5	111	0.707	91	0.591	100	0.650
−15	95	0.714	77	0.576	83	0.620
−25	82	0.715	66.7	0.582	71.5	0.623
−35	69	0.711 (?)	55.6	0.574	59	0.610
−45	(53)	0.65	45.5	0.561	50	0.615
−55	(40)	0.60	38.5	0.577	38.5	0.580
−65	...	...	28.5	0.53	(25)	(0.46)
−75	...	...	...	...	(18?)	...
Averaged (smoothed) Walden product, $\eta\Lambda_0$[a]		0.715		0.580		0.633
Λ_0^- at 25°, calcd from smoothed $\eta\Lambda_0$	103		77		84	

[a] Below −45°, progressively lower values were used for the "smoothed" Walden products. All of the conductance data are given in cm²/ohm mole.

Table VI: Dissociation Constants and "Smoothed" Λ_0 Values of Sodium Salts of Aromatic Radical Ions in DME[a]

T, °C	Biphenyl·⁻ Λ_0	Biphenyl·⁻ 10^6K_{diss}, M	Triphenylene·⁻ Λ_0	Triphenylene·⁻ 10^6K_{diss}, M	Perylene·⁻ Λ_0	Perylene·⁻ 10^6K_{diss}, M
25	159	4.6	133	5.6	140	6.0
15	142	6.2	119	6.3	125	7.1
5	125	7.2	105	7.5	111	8.1
−5	110	8.3	91	9.1	97.5	9.6
−15	95	10.0 (?)	77	11.4	84.5	11.8
−25	82	11.0	66	13.1	72.5	12.7
−35	69	11.5	55.5	14.6	61.5	14.6
−45	53	14.0	45.5	16.7	51.5	15.1
−55	40	17.0	36.8	14.8	38.5	18.8
−65	...	...	29.5	15.0	...	...
Difference between "smoothed" $(\eta\Lambda_0)_{\text{DME}}$ and $(\eta\Lambda_0)_{\text{THF}}$	0.095		0.125		0.143	

[a] All of the conductance data are given in cm²/ohm mole.

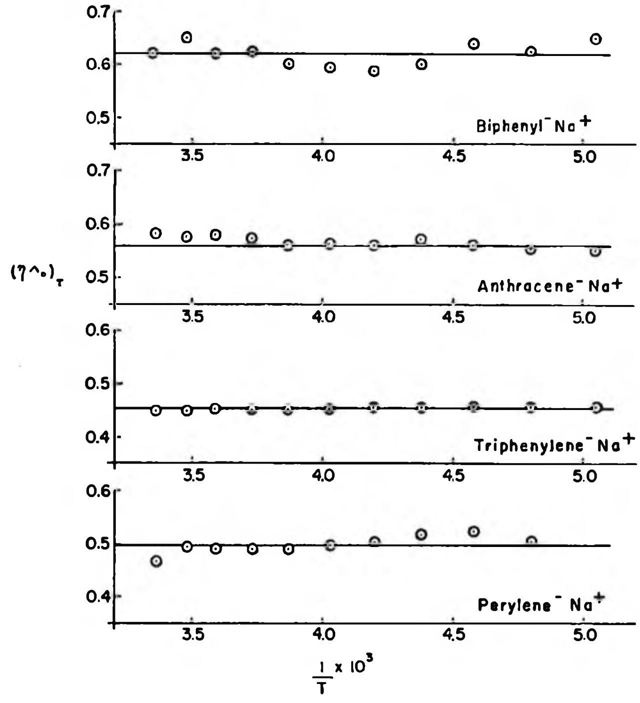

Figure 1. Plot of the Walden product of sodium salts of radical ions in THF *vs.* $1/T$.

temperatures, because their degree of coordination with the solvent molecules increases, whereas the contributions of the negative radical ions, which do not coordinate with the solvent, are likely to increase because the dielectric constant then becomes larger.[6-8] From the plots shown in Figures 1 and 2, the "smoothed" values of the Walden products are derived. A greater weight is attributed to those Λ_0 which are experimentally more reliable. This preference affects only slightly the proposed values (see Tables II and V). From the "smoothed" Walden products the values of Λ_0 listed in Tables III and VI were calculated. The Fuoss parameters were then recomputed and the plots of F/Λ *vs.*

---

(6) R. M. Fuoss, *Proc. Natl. Acad. Sci. U. S.*, **45**, 807 (1959).

(7) R. H. Boyd, *J. Chem. Phys.*, **35**, 1281 (1961).

(8) R. Zwanzig, *ibid.*, **38**, 1603 (1963).

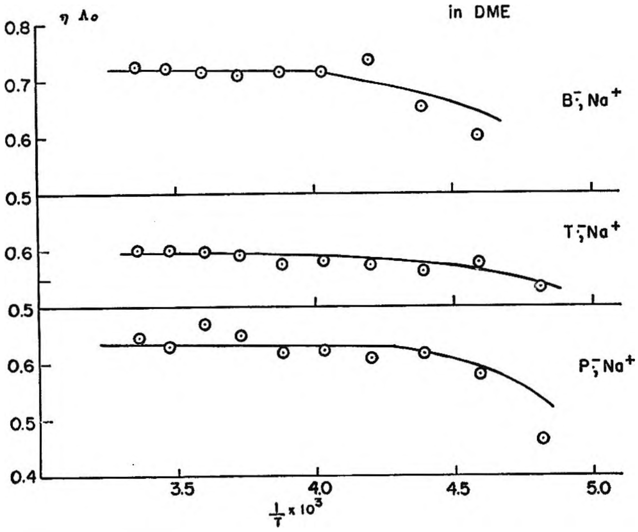

Figure 2. Plot of the Walden product of sodium salts of radical ion in DME *vs.* $1/T$.

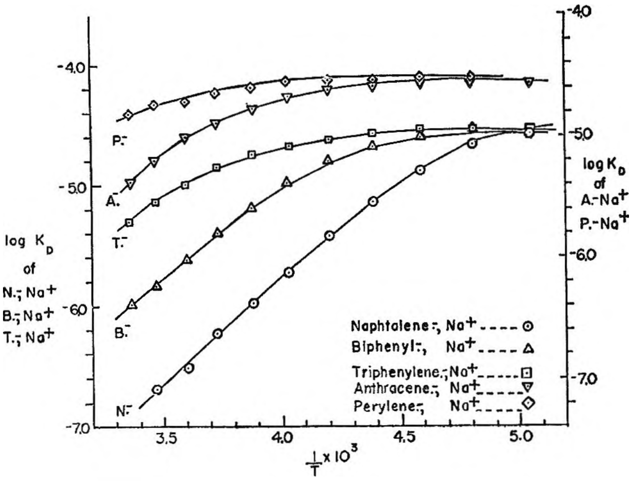

Figure 3. Plot of the log K_{diss} of sodium salts of radical ions in THF *vs.* $1/T$. Notice that the results for anthracene$\cdot^-$, Na^+ and perylene$\cdot^-$, Na^+ are shifted up by 0.4 unit. In fact, all K_{diss} become virtually identical at the lowest temperatures.

$\Lambda cf^2/F$ were redrawn. These plots were used in the final calculations, the results of which are listed in Tables III and VI.

Plots of log K_{diss} *vs.* $1/T$ are shown in Figures 3 and 4, and from these the ΔH and ΔS values, given in Tables IV and VII, were obtained.

Discussion

Inspection of Tables II and V shows that the individually determined Λ_0 values may be uncertain within 4–10%, although the "smoothing" procedure improves their reliability significantly. The presently recommended values of Λ_0 differ somewhat from those reported in ref 1, the differences being 6% for sodium naphthalene (the value given in ref 1 was assumed and not determined), 6% for sodium biphenyl, −13% for sodium triphenylene, −4% for sodium anthracene, and 12% for sodium perylene. These changes affect the slopes of the Fuoss lines causing deviations of the same order of magnitude as those found for Λ_0. The net effect of these errors usually leads to an error of less than 10% in the values of dissociation constants, the sodium perylene case being exceptional. It is thought that the present result is more reliable and that the previously reported value is much too high (~48%). The reason for this discrepancy is not obvious.

Table VII: Heats and Entropies of Dissociation at 20 and −55° in DME Solution[a]

	Biphenyl$\cdot^-$	Triphenylene$\cdot^-$	Perylene$\cdot^-$
ΔH_{20}, kcal/mole	−2.1	−2.4	−2.5
$\Delta S°_{20}$, cal/deg mole	−31.5	−32.5	−32.5
ΔH_{-55}, kcal/mole	0	0	0
$\Delta S°_{-55}$, cal/deg mole	−22.0	−22.0	−21.5

[a] Standard state: 1 M solution.

Our present values of Λ_0, in conjunction with the value for $\lambda_0(Na^+)$ reported in ref 3, give the mobilities of the negative radical ions. These are greater than those found for the sodium ions, implying no coordination between the negative ions and the ethers. This conclusion was reached previously,[1] because the mobilities of naphthalene$\cdot^-$ and anthracene$\cdot^-$ radical ions were found to be comparable to those calculated from the diffusion constants of the respective hydrocarbons.

The λ_0^- of the individual radical anions form an interesting pattern. Their mobilities are apparently determined by the area of their smallest cross section, *i.e.*, that perpendicular to the plane of the molecule. Thus, the biphenyl$\cdot^-$ radical ion should be the most mobile; its λ_0^- in THF is 88. The naphthalene$\cdot^-$ and anthracene$\cdot^-$ radical ions should be less mobile, the respective λ_0^- values being 83 and 75, the mobility of perylene$\cdot^-$ should be substantially lower, $\lambda_0^- = 61$, and that of the triphenylene$\cdot^-$ radical ion should be the lowest, in agreement with the observation, $\lambda_0^- = 52$. The mobilities are related to the respective self-diffusion constants through the equation $u = \mathfrak{D}/kT$. Its application leads to the self-diffusion constants, $\mathfrak{D}$, listed in Table II.

Similar results were obtained in DME. The biphenyl$\cdot^-$ ion is the most mobile ($\lambda_0^- = 103$), the triphenylene$\cdot^-$ the least ($\lambda_0^- = 77$), and the perylene$\cdot^-$

Absorption Spectra of Octahedral Lanthanide Hexahalides

by Jack L. Ryan

Battelle Pacific Northwest Laboratory, Richland, Washington[1]

and Chr. Klixbüll Jørgensen

Cyanamid European Research Institute, Cologny (Geneva), Switzerland *(Received February 18, 1966)*

Hexahalide 4f group complexes can be prepared in aprotic solvents such as nitriles and in triphenylphosphonium and pyridinium salts. The internal transitions in the partly filled 4f shell correspond to absorption bands much weaker than for the corresponding aqua ions (except the hypersenitive pseudoquadrupolar transitions) and show the vibrational structure characteristic for octahedral complexes with a center of inversion. The nephelauxetic effect is much stronger than for the same central ions in $LaCl_3$ but not as pronounced as for the oxides. The electron-transfer spectra observed in Ce(IV), Sm(III), Eu(III), Tm(III), and Yb(III) hexahalides are discussed; the apparent optical electronegativities are somewhat higher than for the analogous halide complexes in ethanolic solution. The 4f → 5d transitions observed in Ce(III) hexahalides show that the subshell energy difference Δ is larger than 15 kK. The similar transitions in Tb(III) hexahalides seem to involve a spin-forbidden absorption band at relatively low wavenumber and indicate slightly smaller exchange integrals K(4f, 5d) than in the isoelectronic Gd^{+2}.

Introduction

The octahedral symmetry of hexahalides MX_6^{+z-6} allow many group-theoretical arguments to be applied to the energy levels. In particular, the excited levels of the detailed electron-transfer spectra have been classified, using inductive MO theory, in a large number of 4d and 5d group complexes.[2-4] Because of chemical problems, the study of the hexahalides of the other transition groups is far more difficult. Thus, the 5f group hexahalides cannot normally be studied in aqueous solution. However, using anhydrous acetonitrile CH_3CN as solvent, we obtained the absorption spectra of various U(IV), Np(IV), and Pu(IV) hexahalides and identified internal transitions in the partly filled 5f shell, 5f → 6d transitions, and electron transfer $\pi \rightarrow$ 5f.[5] Similar techniques allow the study of $CeCl_6^{-2}$ and the much less stable $CeBr_6^{-2}$. The situation is even more difficult in the case of trivalent lanthanides.

Until recently, many scientists believed that 6 is a common coordination number N for lanthanides. Actually, N = 8, 9, 10, or even 12 seems to be far more typical.[6] For instance, hexanitrates such as $U(NO_3)_6^{-2}$ or $Pu(NO_3)_6^{-2}$ (ref 7) may not necessarily have N = 6 but may contain bidentate nitrate groups. Thus, the crystal structure[8] of $[Mg(H_2O)_6]_3[Ce(NO_3)_6]_2 \cdot 6H_2O$ confirmed Judd's spectroscopic prediction[9] of somewhat distorted, icosahedral groups $Ce(NO_3)_6^{-3}$ with N = 12. X-Ray diffraction studies of aqueous solutions of $Ce(NO_3)_6^{-2}$ (ref 10) seem to show N = 12. As seen in the Experimental Section, the organic cation $P(C_6H_5)_3H^+$

---

[1] The work done at this laboratory was performed under Contract No. AT(45-1)-1830 for the U. S. Atomic Energy Commission.

[2] C. K. Jørgensen, *Mol. Phys.*, **2**, 309 (1959).

[3] C. K. Jørgensen, *Acta Chem. Scand.*, **17**, 1034 (1963).

[4] C. K. Jørgensen and K. Schwochau, *Z. Naturforsch.*, 20a, 65 (1965).

[5] J. L. Ryan and C. K. Jørgensen, *Mol. Phys.*, **7**, 17 (1963).

[6] C. K. Jørgensen, "Inorganic Complexes," Academic Press Inc., London, 1963.

[7] W. E. Keder, J. L. Ryan, and A. S. Wilson, *J. Inorg. Nucl. Chem.*, **20**, 131 (1961).

[8] A. Zalkin, J. D. Forrester, and D. H. Templeton, *J. Chem. Phys.*, **39**, 2881 (1963).

[9] B. R. Judd, *Proc. Roy. Soc.* (London), **A241**, 122 (1957).

[10] R. D. Larsen and G. H. Brown, *J. Phys. Chem.*, **68**, 3060 (1964).

The sodium ion is larger when coordinated with THF than with DME. Therefore, the latter approaches closer to the aromatic moiety than the former. Consequently, at low temperatures, or for perylene$\cdot^-$ radical ion, the dissociation constants of ion pairs are *greater* in THF than in DME (see Tables III and VI). However, for salts resembling contact ion pairs, the reverse is observed; *e.g.*, at 25° the dissociation constant of biphenyl$\cdot^-$, sodium$^+$ is substantially lower in THF than in DME.

It is obvious that the respective K_{diss} of a solvent-separated ion pair increases with the thickness of the anion. For example, tetraphenylboride anion, or tetraphenylethylene radical ion, are substantially "thicker" than the planar aromatic negative ions, and indeed, the dissociation constants of their sodium salts in THF at $-70°$ are 150 and 180.10^{-6} M, respectively,[11] *i.e.*, about six times higher than those of the planar radical anions or carbanions.

The dissociation constant of ion pairs composed of large spherical ions was calculated by Fuoss.[13] His equation

$$K_{\text{diss}} = (3000/4\pi a^3N)\exp(-e^2/aDkT)$$

is based on the thermodynamic approach proposed by Denison and Ramsey,[14] and its preexponential factor, $3000/4\pi a^3N$, is derived by assuming the volumes of all the spheres representing the two ions in physical contact to be excluded for the free ions. There is some doubt about the validity of this derivation, and this point will be discussed elsewhere. It seems that the proper expression should contain a term $4\pi a^2\cdot\Delta a$ instead of $4\pi a^3/3$, where Δa is the average thickness of the layer within which the two ions of a pair may vibrate. However, the two expressions become identical for $\Delta a = a/3$. In systems involving nonspherical ions, *e.g.*, for salts of fluorenyl carbanion, the preexponential factor may significantly differ from that derived from the Fuoss equation.

Heat and Entropy of Dissociation of Ion Pairs into Free Ions. Inspection of Figures 3 and 4 shows striking differences in the behavior of the various ion pairs in THF and in DME. The exothermicity of dissociation of naphthalene$\cdot^-$,Na$^+$ and biphenyl$\cdot^-$,Na$^+$ in THF is high at 25° and amounts to 8.2 and 7.3 kcal/mole, respectively, whereas that of perylene$\cdot^-$, Na$^+$ is low, 1.5 kcal/mole. For the salts of anthracene$\cdot^-$ and triphenylene$\cdot^-$, intermediate values were found, *viz.*, 6.1 and 5.2 kcal/mole, respectively. All of these data seem reliable within ±0.5 kcal/mole.

On the basis of the equation $\Delta H = (e^2/aD)(1 + \partial \ln D/\partial \ln T)$, the exothermicity of the dissociation of perylene$\cdot^-$,Na$^+$ in THF at 25° is about 1 kcal/mole (observed 1.5 kcal/mole) for the interionic distance of 6.5 A. This justifies the classification of that ion pair as a virtually solvent separated. In DME at 25° this approach leads to $-\Delta H$ of about 2.1 kcal/mole (observed 2.5 kcal/mole) for the interionic distance of 6.0 A (the term $1 + \partial \ln D/\partial \ln T$ is -0.16 for THF and -0.28 for DME), again indicating that all the investigated salts form virtually solvent-separated pairs in the latter solvent.

The high exothermicity of dissociation observed in THF for the salts of naphthalene$\cdot^-$ and biphenyl$\cdot^-$, and to a lesser extent for those of anthracene$\cdot^-$ and triphenylene$\cdot^-$, indicates that these species exist under those conditions mainly as contact ion pairs. Increase in the extent of sodium ion solvation on the dissociation of the pair contributes to the exothermicity of the process. However, at lower temperatures the heat of dissociation approaches zero and this behavior may be accounted for by two hypotheses. (1) The contact ion pairs and solvent-separated pairs exist in equilibrium, each species being a distinct thermodynamic component of the system. At lower temperature, the position of the equilibrium shifts toward solvent-separated species. (2) The potential energy curve, representing the energy of the pair as a function of its separation, varies with temperature. This idea and its implication will be discussed in the last part of this paper.

The entropies of dissociation are negative and the observed changes of their values are to be expected. The coordination of solvent molecules with sodium ions probably is the main factor responsible for a decrease in the entropy of the system. This is less important at lower temperatures as the ion pairs become solvated and the ordering of solvent molecules in the bulk of the liquid becomes more pronounced. The loss of vibrational entropy of the pair, which may be quite large in view of the "softness" of such a vibration, may also add appreciably to the increase of entropy of dissociation.

The conductance studies of alkali salts of aromatic radical anions were reported by Hoijtink and his associates.[4] The ambiguity of their approach was discussed previously.[1] The dependence of conductance, measured at constant salt concentration, on solution temperature is determined by the "activation energy" of viscosity and by the heat of dissociation. Our present data prove that Λ determined at constant salt concentration may monotonically decrease with temperature even if the electrolyte is only slightly

---

[13] R. M. Fuoss, *J. Am. Chem. Soc.*, **80**, 5059 (1958).

[14] J. T. Denison and J. B. Ramsey, *ibid.*, **77**, 2615 (1955).

dissociated. Hence, the monotonic decrease of Λ does not provide any impelling evidence for a complete dissociation.

The dissociation constant of biphenyl$\cdot^-$,Na$^+$ in THF at room temperature was determined by Dieleman (Ph.D. Thesis, Amsterdam, Holland, 1962) to be about 1.5×10^{-5} *M*. His conductance was measured at too high concentrations (10^{-4} to 10^{-3} *M*) and consequently the reported value is too high by a factor of 10. Nevertheless, the temperature dependence of the relative dissociation constant, measured by the variation of conductance with temperature at constant salt concentration, seems to be reliable and the reported heat of dissociation of −8.1 kcal/mole compares reasonably well with our value of −7.3 kcal/mole.

A novel and important approach to studies of free ion–ion pairs equilibria was developed by Atherton and Weissman.[15] They demonstrated that the additional splits of the esr signals of sodium$^+$, naphthalene$\cdot^-$ arise from the association of the radical anion with the Na$^+$ ion, the magnetic moment of the latter nucleus being responsible for the observed phenomenon. In THF solution, the degree of splitting decreases virtually to zero at −70°, and no splitting is observed in DME. These facts indicate that the interaction with sodium ion vanishes as the ions of the pair become more separated by solvent molecules. The intensities of the "split" and "nonsplit" spectra lead to the dissociation constant of the Na$^+$,naphthalene$\cdot^-$ ion pair in THF. Although the observed heat of dissociation, −7.5 ± 1.5 kcal/mole, agrees satisfactorily with our determination (−8.2 ± 0.5 kcal/mole), the absolute value of K_{diss} is substantially larger than that derived from the conductance study. A possible explanation of this discrepancy may be given in a recent work of Chang and Johnson.[16]

The heat of dissociation determined by Weissman in tetrahydropyran and in MeTHF is less negative. Apparently, the free sodium ions are less strongly coordinated with these solvents than with THF. These results agree again with preliminary data obtained in this laboratory through studies of conductance.

From the esr line breadth, the lifetime of the pair was determined as at least $>10^{-6}$ sec and probably $>10^{-5}$ sec at 25°.

Recently, the temperature dependence of the Na$^+$ splitting was investigated by Hirota and Kreilick.[17] They concluded that the changes in the coupling observed in Na$^+$,anthracene$\cdot^-$ in MeTHF and in Na$^+$, di-*t*-butylnaphthalene$\cdot^-$ in THF are due to the conversion of contact ion pairs into solvent separated pairs, and estimated the heats of these processes to be −4.5 and −4.6 kcal/mole, respectively. The lifetimes of the respective species were determined at about 10^{-8} sec.

Comparison of THF and DME as Ionizing Solvents. In general, DME promotes ionic dissociation better than THF. The greater ionizing power of DME is not due to its higher dielectric constant but to its bidentate structure which allows for a claw-shape coordination with the cation.[18] In fact, at 25° the dielectric constant of DME (7.2) is slightly *lower* than that of THF (7.4), although the relation is reversed at −70° (11.75 and 11.6, respectively). Thus, for lithium or sodium salts having structures described as contact-ion pairs, the dissociation into free "solvated" ions is greatly enhanced in DME. This effect is shown even more dramatically in salts of Cs$^+$ because this ion does not coordinate with THF molecules, whereas it does coordinate with molecules of DME (see ref 3).

However, for cations which are fully solvated in the ion pair, the dissociation is *more* extensive in THF than in DME. This, as we pointed out earlier, is due to the smaller size of the DME-coordinated sodium ion (and probably also Li$^+$) than of the THF coordinated cation. Hence, the former associates tighter into the (still solvent-separated) ion pair than the latter. Our data confirm this conclusion.

Validity of the Concept of Contact Ion Pairs and Solvent Separated Ion Pairs. As early as 1954, Sadek and Fuoss[19] pointed out that association of free ions into ion pairs may involve two distinct steps. An ion coordinated with solvent molecules is surrounded by a relatively rigid solvent shell. Such an ion approaches its counterion without any hindrance until its solvation shell contacts its partner. Further approach is hindered—it requires squeezing out a coordinated solvent molecule, or molecules, and therefore this stage of the association process, which leads to the formation of a contact ion pairs, is distinct from the previous one. This idea has been now fully confirmed by studies of Eigen and his co-workers[20] who observed two relaxation times in many association processes involving hydrated ions. Hence, two types of ion pairs apparently coexist in such solutions, each representing a distinct thermodynamic species.

---

(15) N. M. Atherton and S. I. Weissman, *J. Am. Chem. Soc.*, **83**, 1330 (1961).

(16) R. Chang and C. S. Johnson, *ibid*, **88**, 2338 (1966).

(17) N. Hirota and R. Kreilick, *ibid.*, **88**, 614 (1966).

(18) B. R. Sundheim and K. F. A. Cafasso, *J. Chem. Phys.*, **31**, 809 (1959); *Ann. N. Y. Acad. Sci.*, 21 281 (1959).

(19) H. Sadek and R. M. Fuoss, *ibid.*, **76**, 5905 (1954).

(20) See, *e.g.*, a recent review by M. Eigen, W. Kruse, G. Maass, and L. De Mayer, *Progr. Chem. Kinetics*, **2**, 285 (1964).

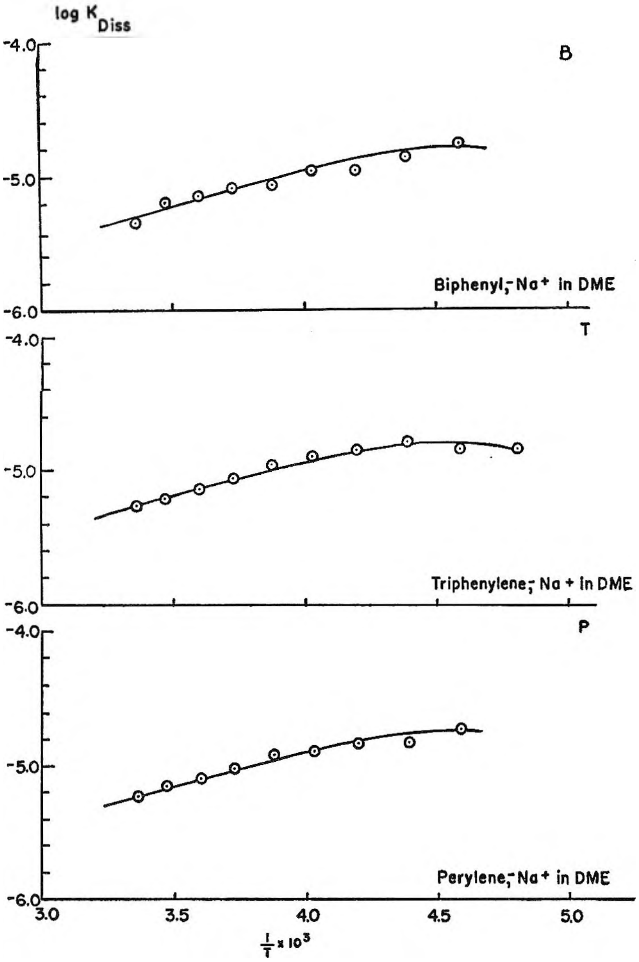

Figure 4. Plot of the log K_{diss} of sodium salts of radical ions in DME *vs.* $1/T$.

Kinetic studies of some solvolytic processes led Winstein[21] to postulate that two distinct ion pairs participate in those reactions, each characterized by its own rate constant and stereochemical requirement. This hypothesis has proved to be most valuable and applicable to many systems. It has been formalized by Grunwald[22] who described the potential energy of the system A^+, B^- as a function of their separation distance, r. In his model, the potential energy shows two minima—one for r equal to the separation distance of a contact ion pair, the other appearing when the interionic distance is sufficiently large to accommodate just one solvent molecule between the ions. The maximum separating the two minima reflects the unfavorable situation of the system when the two ions are still apart but the space separating them is too narrow to accommodate even one solvent molecule.

The existence of two types of ion pairs of fluorenyl salts has been demonstrated in this laboratory by Hogen-Esch and Smid.[23] In THF, and in a few other ethereal solvents, sodium and lithium fluorenyl show two absorption peaks in the near-ultraviolet region. Their relative intensities change with temperature, but not with concentration, indicating that two interconvertible species, convincingly identified by Hogen-Esch and Smid as contact and solvent-separated ion pairs, coexist in these solutions. The proposed assignment gained further support from the conductance studies of these salts.[9]

The following question now arises. Is the concept of two types of ion pairs applicable to all systems containing associated ions? There are, of course, systems in which only one type of ion pair may exist. For example, for free ions which are not coordinated or only weakly coordinated with solvent molecules, the association gives contact ion pairs only; no solvent-separated ion pairs can exist in such solutions. On the other hand, for a very strong coordination and for a sufficiently bulky counterion, the possible gain in coulombic energy arising from the conversion of solvent-separated ion pair into contact ion pair may be much too small to permit squeezing out the solvent molecules. In such systems, only solvent-separated ion pairs exist. This point was fully discussed by Roberts and Szwarc.[11]

These are rather obvious limitations which do not deny the virtual existence of two types of ion pairs; they show only that the concentration of one form may become vanishingly small under some conditions. However, in many systems the concept of two ion pairs may be unattainable and the description of such systems cannot be achieved in these terms. To clarify the problem, let us return to the model proposed by Grunwald.[23]

Grunwald's model is static in nature; the potential energy of the ion pair is assumed to be uniquely determined by the interionic distance, r. The situation is, however, more complex. The ion pair is embedded in a fluctuating environment of solvent molecules; it vibrates and the environment participates in this motion. The potential energy depends, therefore, on solvent because interaction with its molecules provides an average force field superimposed upon the interaction field of the pair. Such a field changes with temperature because the temperature affects the average configuration of solvent molecules with respect to the pair, and hence the shape of the potential energy curve

---

[21] S. Winstein, E. Clippinger, A. H. Fainberg, and G. C. Robinson, *J. Am. Chem. Soc.*, **76**, 2597 (1954).

[22] E. Grunwald, *Anal. Chem.*, **26**, 1696 (1954).

[23] T. E. Hogen-Esch and J. Smid, *J. Am. Chem. Soc.*, **88**, 307 (1966).

Also the dielectric constant as a function of temperature shows no discontinuity at the freezing point (54.5°).[18] If it is assumed that the dielectric constants of these very similar solvents are additive, a mixed-nitrile solvent containing 85% succinonitrile and 15% acetonitrile would have a dielectric constant of about 62 at 25°. This is a considerably higher dielectric constant than those for nitromethane or acetonitrile (~38). This mixture has been found to be a very effective noncomplexing solvent for salts such as Cs_2UCl_6, $Cs_2UO_2Cl_4$, and $[(C_2H_5)_4N]_4UO_2(SO_4)_3$ which are not appreciably soluble in acetonitrile or nitromethane.[19] The triphenylphosphonium salts used in this work were more soluble in this solvent than in acetonitrile. Acetonitrile was obtained as Spectrograde from Eastman. The succinonitrile (also Eastman), although inherently colorless, was not Spectrograde and was found to be light yellow. The mixed solvent (85 vol. % succinonitrile–15 vol. % acetonitrile) was dried and purified by passing it through a bed of neutral-type activated alumina. This treatment removed the color sufficiently that the mixed-nitrile solvent was usable down to 220 mμ in 0.1-cm cells and to 260 mμ in 1.0-cm cells.

The solubilities of the triphenylphosphonium salts in the mixed-nitrile solvent were sufficient to obtain good absorption spectra in the region of the internal 4f transitions ($\epsilon < 1$) using 10-cm cells. The hypersensitive transitions ($\epsilon \sim 10$) could be obtained in the mixed-nitrile solvent with 1.0- or 2.0-cm cells or in acetonitrile with 10-cm cells. It should be noted that these solutions usually supersaturated readily and spectra of solutions could be obtained from which crystals later formed. Both the MCl_6^{-3} and MBr_6^{-3} complexes partially dissociate in acetonitrile or in the mixed-nitrile solvent. This dissociation is easily prevented in the case of the chloride by a small excess of chloride as $(C_2H_5)_4NCl$ or even $(C_2H_5)_3NHCl$. After a small excess of Cl^- has been added, further large additions cause no further change in the spectra, and the spectra become essentially identical with those of the solid triphenylphosphonium salts. With the MBr_6^{-3} complexes, the tendency to dissociate is greater. If the system is kept dry the $[(C_6H_5)_3PH]_3MBr_6 \cdot (C_6H_5)_3PHBr$ salts can be dissolved in the nitrile solvents containing a large excess of Bu_4NBr without dissociation of the MBr_6^{-3} complexes. The MBr_6^{-3} complexes are very markedly stabilized by addition of HBr gas to the nitrile solutions. This is because it reacts readily with water to form H_3O^+ and with other electron-donor groups in similar manner. This significantly decreases their coordinating power and decreases competition with Br^-. If a large amount of HBr is added, a solid product is formed because of reaction with the nitrile. Reaction of hydrogen halides with nitriles reportedly produces R—CX=NH.[20] This reaction of the HBr with the solvent was found not to affect the MBr_6^{-3} spectra. Addition of a large excess of HCl to the MCl_6^{-3} solutions actually destroys rather than stabilizes the MCl_6^{-3} complexes. This is probably due to the greater tendency for Cl^- to hydrogen bond producing HCl_2^-, thus removing Cl^- from MCl_6^{-3}. The weaker bonding of H^+ to Br^- makes HBr a more powerful dehydrating agent than HCl in these solutions.

Since the phenyl and pyridinium groups absorb strongly in the ultraviolet region, the MX_6^{-3} salts cannot be used (with the exception of the $EuBr_6^{-3}$) to obtain the $\pi \rightarrow 4f$ spectra. The hydrated rare earth chlorides can be dissolved in the nitrile solvents containing a large excess of R_4NCl to produce the MCl_6^{-3} complexes as determined by comparison of the internal 4f spectra of these solutions with those of the solid MCl_6^{-3} salts and the salts in nitrile solutions containing excess Cl^-. With the bromides, a similar situation exists except that HBr gas must be added to dehydrate the solution. Much higher concentrations of MX_6^{-3} in acetonitrile can be obtained in this manner than with the triphenylphosphonium salts. These solutions were used to obtain the electron-transfer spectra of $EuCl_6^{-3}$, $YbCl_6^{-3}$, $SmCl_6^{-3}$, $EuBr_6^{-3}$, $YbBr_6^{-3}$, $SmBr_6^{-3}$, and $TmBr_6^{-3}$ and the $4f \rightarrow 5d$ transitions of $TbCl_6^{-3}$, $TbBr_6^{-3}$, $CeCl_6^{-3}$, and $CeBr_6^{-3}$.

The procedure for obtaining the MCl_6^{-3} electron-transfer spectra was as follows. A concentrated lanthanide chloride solution in aqueous HCl was diluted about two- to threefold with ethanol, and a large volume of acetone was added rapidly with stirring. The resulting crystals of $MCl_3 . xH_2O$ were acetone washed and dried lightly under a heat lamp. They were then dissolved in a saturated solution of $(C_2H_5)_4NCl$ in acetonitrile, and the absorption spectra were obtained in 0.01- to 0.1-cm cells to minimize absorption by impurities. The reference cells contained the same solutions without rare earth present.

The procedure for obtaining the MBr_6^{-3} electron-transfer spectra was as follows. A concentrated lanthanide solution in aqueous HBr was diluted about twofold with ethanol and saturated with Bu_4NBr, and a large volume of acetone was added. The hydrated bromides precipitated (very slowly after seeding

---

[19] J. L. Ryan, unpublished results.

[20] M. Silman, "Organic Chemistry, An Advanced Treatise," Vol. II, 2nd ed, John Wiley and Sons, Inc., New York, N. Y., 1943, p 107.

by the addition of an inert diluent, gradually varies the shape of the surface. Consequently, the height of potential energy barrier, which determines the activation energy of the process, varies with the nature of the solvent and becomes a function of the medium. Nevertheless, one should not suppose that the potential energy barrier becomes negative if the modification of a reaction's milieu speeds up the process.

The properties of the solvent are modified by changing its temperature. In fact, a solvent at low temperature forms a different medium than the same solvent at high temperature. Therefore, it is possible to encounter systems for which the potential energy barrier decreases sufficiently on lowering the temperature to cause an increase in the rate of investigated reaction. This leads to an apparent negative activation energy, although the system has to surmount a *positive* potential energy barrier at each temperature. It is likely that the apparent negative activation energy observed in the polymerization of sodium salt of living polystyrene in tetrahydrofuran[10] is due to such a phenomenon.

Acknowledgment. This research was supported by the Petroleum Research Fund administered by the American Chemical Society, by the U. S. Army Research Office (Durham), and by the National Science Foundation. This support is gratefully acknowledged

---

Vibrational Spectra of Organophosphorus Compounds. II. Infrared and Raman Spectra of CH_3POF_2 and CH_3POFCl

by J. R. Durig, B. R. Mitchell, and J. S. DiYorio,

Department of Chemistry, University of South Carolina, Columbia, South Carolina

and F. Block

Research Laboratories, U. S. Army Edgewood Arsenal, Edgewood Arsenal, Maryland

(Received May 5, 1966)

The infrared spectra of gaseous and liquid CH_3POF_2 and CH_3POFCl have been recorded from 4000 to 250 cm^{-1}. The Raman spectra of the liquids have been recorded and depolarization values measured. Assignment of the fundamentals based on position, depolarization values, and band contours is given. Comparison of the spectra to that of the CH_3POCl_2 molecule is made and discussed.

Introduction

Recently, we reported a complete vibrational analysis for the molecules CH_3PCl_2, CH_3POCl_2, and CH_3PSCl_2.[1] A similar study has also been reported for the two molecules CH_3PCl_2 and CF_3PCl_2.[2] As an extension of our previous work, the infrared and Raman spectra of methylphosphonic difluoride and methylphosphonic fluorochloride have been recorded. To the best of our knowledge, no previous infrared or Raman study of either CH_3POF_2 or CH_3POFCl has been discussed. Vibrational spectra of these two

---

(1) Part I of this series: J. R. Durig, F. Block, and I. W. Levin, *Spectrochim. Acta*, 21, 1105 (1965).

(2) J. E. Griffiths, *ibid.*, 21, 1135 (1965).

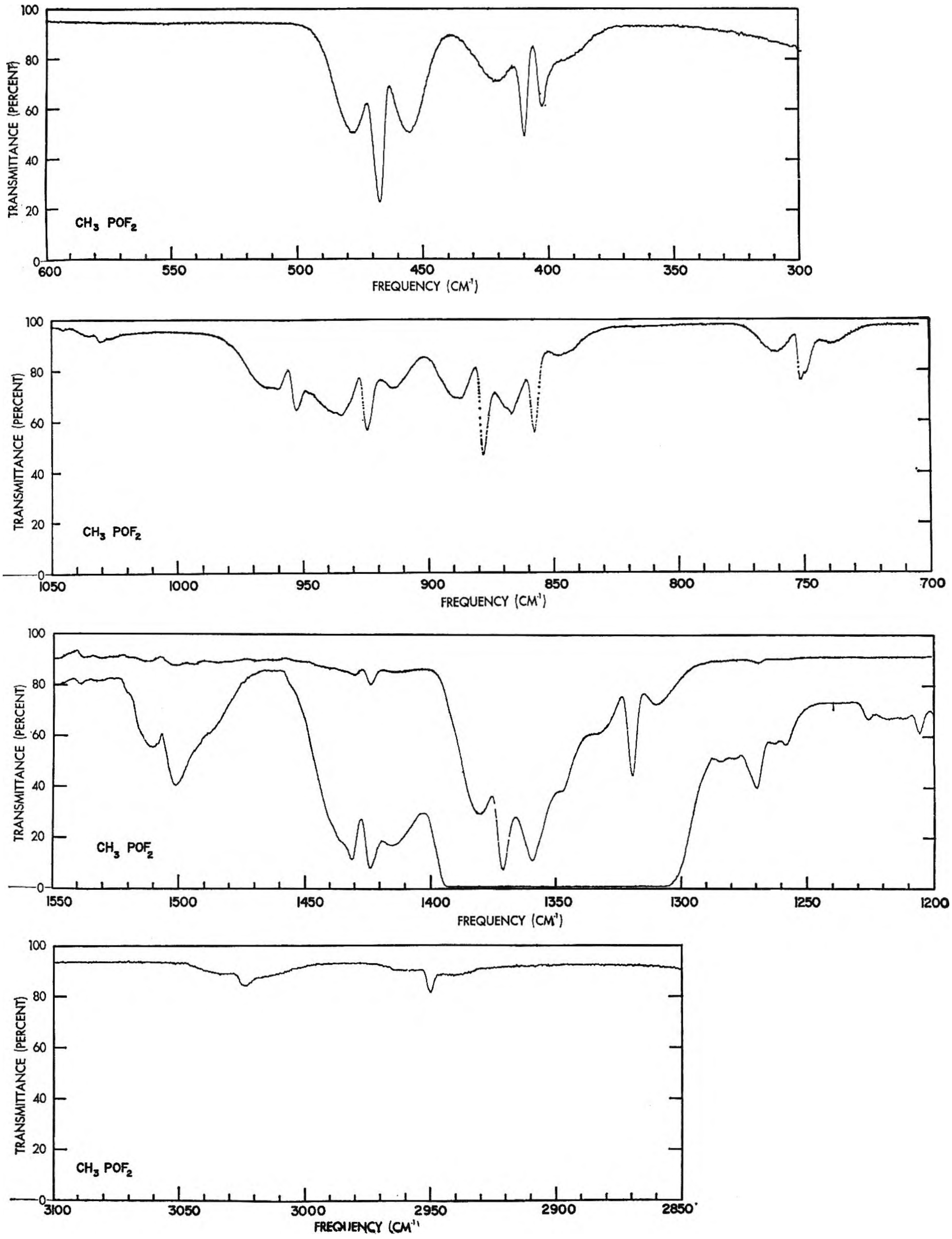

Figure 1. Infrared gas-phase spectrum of CH_3POF_2 (expanded scale).

molecules are compared with that previously reported for CH_3POCl_2.[1]

Experimental Section

The sample of methylphosphonic difluoride was distilled using a Teflon annular still and an intermediate fraction with a constant boiling point of 54° at 150 mm pressure was used in this study. The methylphosphonic fluorochloride was prepared by heating an equimolar mixture of methylphosphonic difluoride and methylphosphonic dichloride in a sealed tube at 100° for 2 weeks. The production of methylphosphonic fluorochloride was followed by the nmr spectrum of P^{31}. The sample of CH_3POFCl was removed from the reaction mixture by fractional distillation with a yield of approximately 23%. The CH_3POFCl sample was

Table I: Internal $4f^2$ Transitions in Praseodymium(III) Complexes[a]

	$PrCl_6^{-3}$			$PrBr_6^{-3}$			$Pr(H_2O)_9^{+3}$		Pr^{III}-$LaCl_3$	Pr^{III}-$GdCl_3$	Pr^{III}-$LaBr_3$
	λ_J	σ_J	ϵ_{max}	λ_J	σ_J	ϵ_{max}	σ_J	ϵ_{max}	σ_J	σ_J	σ_J
$^1D_2$	592	16.89	0.09	595	16.81	0.14	16.78	1.9	16.73	16.69	16.67
$^3P_0$	485	20.61	0.94	487.6	20.50	1.0	20.69	4.0	20.47	20.41	20.37
$^3P_1$	475	21.05	0.40	477	20.96	0.59	21.29	4.6	21.08	21.01	20.98
$^3P_2$	450	22.22	0.34	455.5	21.95	0.45	22.43	10.5	22.23	22.16	22.13

[a] λ_J is the wavelength in mμ and σ_J the wavenumber in kK of the baricenter of the band group corresponding to the excited J level indicated. ϵ_{max} is the molar extinction coefficient of the highest band of each group in the solution absorption spectra; the wavenumber of this band does not necessarily coincide with σ_J.

Table II: Internal $4f^3$ Transitions in Neodymium(III) Complexes[a]

	$NdCl_6^{-3}$			$NdBr_6^{-3}$			$Nd(H_2O)_9^{+3}$		Nd^{III}-$LaCl_3$	A-Nd_2O_3
	λ_J	σ_J	ϵ_{max}	λ_J	σ_J	ϵ_{max}	σ_J	ϵ_{max}	σ_J	σ_J
$^4F_{3/2}$	881	11.35	0.31	878	11.39	0.38	11.58	3.6	11.44	11.19
$^4F_{5/2}$	808	12.38	0.65	803	12.45	0.94	12.62	11.8	12.48	12.27
$^4F_{7/2}$	747	13.39	0.56	748	13.37	0.68	13.58	7.2	13.44	13.25
$^4F_{9/2}$	~686	14.58	0.05	685	14.56	0.07	14.84	0.4	14.72	14.47
$^4G_{5/2}$	590	16.95	5.6	587	17.04	10.0	17.40	7.0	17.21	16.72
$^4G_{7/2}$	534	18.73	0.72	533	18.76	1.5	19.18	4.4	19.03	18.60
$^4G_{9/2}$	517	19.34	0.27	520	19.23	0.40	19.63	1.7	19.44	19.17
$^2P_{1/2}$	434	23.04	0.11	434	23.04	0.12	23.40	0.6	23.21	22.84
$^4D_{3/2}$	358	27.93	~1.0	...	...	...	28.28	5.2	27.97	27.20

[a] Notation as in Table I.

Table III: Internal $4f^5$ Transitions in Samarium(III) Complexes[a]

	$[P(C_6H_5)_3H]_3SmCl_6$			$SmCl_6^{-3}$	$Sm(H_2O)_9^{+3}$		Sm^{III}-$LaCl_3$	B-Sm_2O_3
	λ_J	σ_J		ϵ_{max}	σ_J	ϵ_{max}	σ_J	σ_J
$^6F_{5/2}$	~1420	7.04	Strong	...	7.15	1.6	7.05	7.34
$^6F_{7/2}$	1255	7.97		...	8.0	2.1	8.00	8.05
$^6F_{9/2}$	1090	9.17		...	9.25	1.8	9.08	9.22
$^4G_{5/2}$	562	17.79	Very weak	0.02	17.9	0.04	17.86	17.57
$^4F_{3/2}$	531	18.83	Very weak	0.01	18.6	0.02	18.86	18.87
...	491	20.37	Weak	0.03	20.02	0.08	...	...
...	478	20.92	Weak	0.04	20.88	0.6	20.60	20.75
$^4I_{13/2}$	465	21.51	Weak	0.025	21.55	0.5	21.56	21.41
$^6P_{5/2}$	422	23.70		0.15	24.0	0.5	23.78	23.64
^6P	410	24.39		0.67	24.9	3.3	24.54	24.39

[a] Notation as in Table I.

in the 3d, 4d, and 5d transition groups.[29] Keating and Drickamer[30] studied the nephelauxetic effect of high pressures applied to 4f group compounds. A more chemical technique for modifying the internuclear distances was applied by McLaughlin and Conway[31] studying Pr(III) in $LaCl_3$, $CeCl_3$, $NdCl_3$, $SmCl_3$, and $GdCl_3$. The gradually decreasing Pr–Cl distances produce a strongly increasing nephelauxetic effect, dβ in Table VIII going from 0.8 to 1.2%. On the other

---

(29) C. K. Jørgensen, "Orbitals in Atoms and Molecules," Academic Press Inc., London, 1962.

(30) K. B. Keating and H. G. Drickamer, *J. Chem. Phys.*, **34**, 143 (1961).

(31) R. D. McLaughlin and J. G. Conway, *ibid.*, **38**, 1037 (1963).

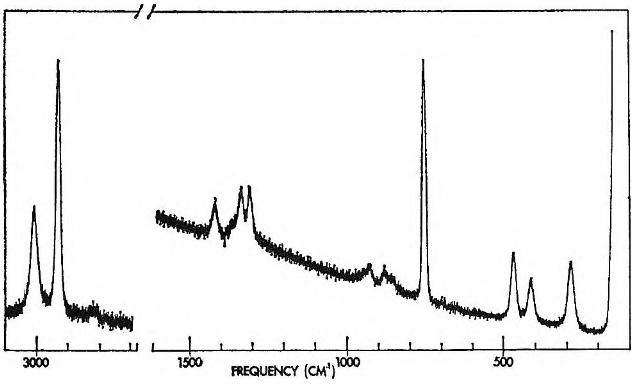

Figure 3. Raman spectrum of CH_3POF_2; cell, 5 ml and 7-mm diameter; slit, double 10 cm × 10 cm^{-1}; sensitivity, 1.7 × 200; period, 0.5; scan, 0.5 cm^{-1}/sec.

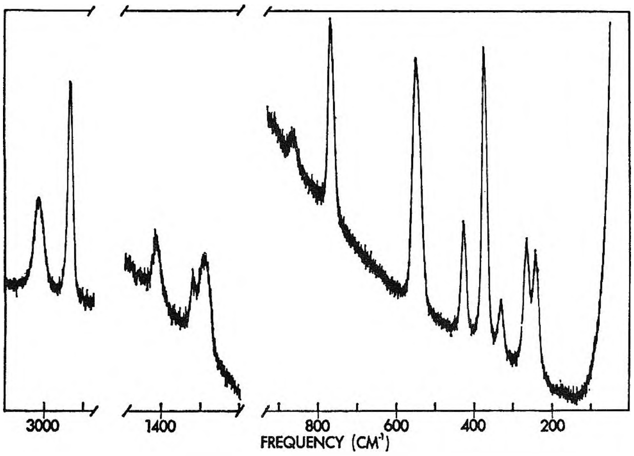

Figure 4. Raman spectrum of CH_3POFCl; cell 5, ml and 7-mm diameter; slit double 10 cm × 10 cm^{-1}; sensitivity, 2 × 2000; period, 2; scan, 0.5 cm^{-1}/sec.

are shown in Figures 3 and 4 and the frequencies are recorded in Tables I and II. All Raman frequencies are believed to be accurate to ±3 cm^{-1}.

Results and Discussion

CH_3POF_2. Methylphosphonic difluoride can have at most a plane of symmetry in which case it belongs to the point group C_s. The molecule has 18 fundamental vibrations, 11 of which are of the symmetric species a′ and give rise to polarized Raman lines. The seven remaining vibrations belong to the a″ species and produce depolarized Raman lines. The 18 vibrations can be further characterized as nine fundamentals resulting from the CH_3 motions and nine fundamentals which result from the motions of the $CPOF_2$ skeleton. The assignment of all the vibrations of the CH_3 group with the exception of the torsion can be made using previous assignments for the methyl group with C_{3v} symmetry. These include two carbon-hydrogen stretching vibrations, one of which belongs to the degenerate e species and usually falls near 3000 cm^{-1}, while the other one belongs to species a_1 and is usually found around 2900 cm^{-1}. Although the lower C_s symmetry would be expected to split the degenerate vibration, only one band was found in both the infrared and Raman spectra near 3000 cm^{-1}. The band at 3005 cm^{-1} in the Raman spectrum is broad and depolarized, and the carbon-hydrogen antisymmetric stretching vibrations of both species a′ and a″ are assigned to this frequency. The corresponding band in the infrared spectrum of the gas is found at 3020 cm^{-1}. The most intense Raman line is found at 2933 cm^{-1} and is strongly polarized. The line is conclusively assigned to the CH_3 symmetric stretching vibration with the corresponding band found at 2950 cm^{-1} in the infrared spectrum of the gas.

The methyl group with C_{3v} symmetry has two deformations, one of which will belong to the degenerate e species, and it has the higher frequency. The Raman spectrum of CH_3POF_2 has a line of medium intensity at 1419 cm^{-1} which is depolarized, and it is thus assigned to the CH_3 antisymmetric deformation. The infrared band centered at 1428 cm^{-1} has a "B" type band contour, and there is no indication that the degeneracy has been removed. Therefore, the CH_3 antisymmetric deformations of both species a′ and a″ are assigned to the same bands in the infrared and Raman spectra. Similar assignments have been given for the corresponding vibrations for the CH_3PCl_2 and CH_3POCl_2 molecules.[1] The CH_3 symmetric deformation is assigned to the polarized Raman line of medium intensity at 1333 cm^{-1}. The symmetric deformation is expected to have a type "A" band contour, and a band of strong intensity with a strong Q branch is observed in the infrared spectrum of the gas at 1372 cm^{-1}. The shift is much larger than that observed for the CH_3 antisymmetric deformation, and there is considerable doubt as to whether this band should be assigned to the P=O stretching vibration or the CH_3 symmetric deformation. The P=O stretching vibration has been assigned to a band at 1415 cm^{-1} for the OPF_3 molecule.[6] It has also been shown that the P=O stretching vibration normally falls in the range 1310 to 1275 cm^{-1},[7] and the frequency is highly dependent on the electronegative substituents on the phosphorus atom. In previous work on the organophosphorus molecules,[1] it was found that the P=O stretching vibration gave a

---

(6) H. S. Gutowsky and A. D. Liehr, *J. Chem. Phys.*, **20**, 1652 (1952).

(7) L. J. Bellamy, "The Infra-red Spectra of Complex Molecules," John Wiley and Sons, Inc., New York, N. Y., 1957, p 312.

to allow the Pr–O distances to achieve the same, most favored, values. A similar effect was found for Er(III)[26] having dβ 3 times larger in the six-coordinated YCl_3 with relatively short Er–Cl distances than in the nine-coordinated $LaCl_3$. There is little doubt that our MX_6^{-3} exemplify a similar behavior. In particular, the M–X distances are probably even smaller in organic solvents[13] such as acetonitrile than they would be in aqueous solution if the complexes did not immediately exchange their halide ligands for water. The molar extinction coefficients of the normal, not hypersensitive, transitions increase from some 0.04 times the intensities of the aqua ion in $PrCl_6^{-3}$ to about one-tenth of $ErCl_6^{-3}$. This may suggest that the cubic symmetry of $ErCl_6^{-3}$ is perhaps slightly less nearly perfect.

Recently, Sugar[27] (who also was so kind as to supply this information at an early stage) found 12 of the 13 levels of the configuration $4f^2$ of gaseous Pr^{+3}. The four levels of Table I are situated at 17.33, 21.39, 22.01, and 23.16 kK. The blue shift of these J levels relative to the aqua ion would indicate that dβ of Pr^{+3} is some −4.3%, though the relative shifts are smaller than expected in the infrared. As also discussed by Sinha and Schmidtke,[32] this effect may be connected with a relatively smaller variation of the Landé parameter ζ_{4f}, say 1.5%, than the variation of the parameters of interelectronic repulsion.

Electron-Transfer Spectra. In the ultraviolet, the hexahalide complexes of the reducible central ions Sm(III), Eu(III), Tm(III), and Yb(III) show broad, moderately strong, absorption bands (Figure 3) which can be ascribed to electron transfer from the highest filled MO, mainly localized on the halide ligands, to the partly filled 4f shell.[16] Table IX gives data for those absorption bands and for the only two lanthanide(IV) hexahalides we have been able to study, $CeCl_6^{-2}$ and $CeBr_6^{-2}$. The bands are much more intense in the latter case, the empty 4f orbitals probably being somewhat more delocalized out on the ligands. Surprisingly enough, the intensities of $CeCl_6^{-2}$ and $CeBr_6^{-2}$ are even larger than those of UI_6^{-2} and the Np(IV) and Pu(IV) hexahalides previously studied.[5]

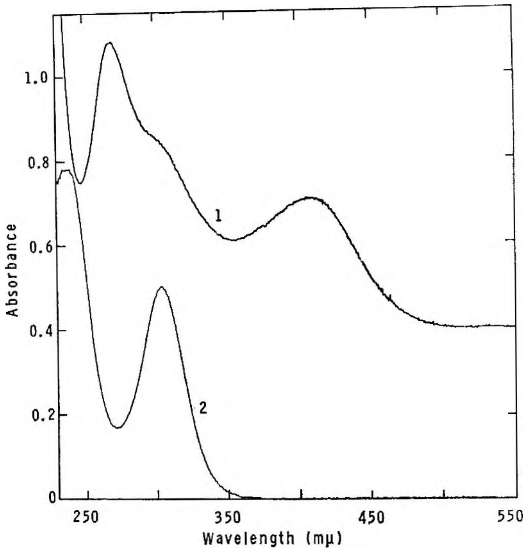

Figure 3. Electron-transfer spectra of europium(III) hexahalides: (1) 0.114 *M* $EuBr_6^{-3}$ in acetonitrile containing excess $(C_4H_9)_4NBr$ and HBr in 0.0108-cm cell (absorbance scale displaced 0.4) and (2) 0.0125 *M* $EuCl_6^{-3}$ in $(C_2H_5)_4NCl$-saturated acetonitrile in 0.10-cm cell.

Table IX: Electron-Transfer Spectra of Hexahalides in Nitrile Solution[a]

	λ	σ	ϵ	$\delta(-)$
$SmCl_6^{-3}$	232	43.1	930	2.3
$SmBr_6^{-3}$	286	35.0	1,050	2.4
$EuCl_6^{-3}$	301	33.2	400	2.1
	234.5	42.6	640	(3.8)
$EuBr_6^{-3}$	409	24.5	250	2.0
	(309)	(32.4)	(340)	...
	270	37.0	540	...
$TmBr_6^{-3}$	~260	~38.6	~300	...
$YbCl_6^{-3}$	272.5	36.7	160	1.7
$YbBr_6^{-3}$	342	29.2	105	2.4
	(240)	(41.7)	(450)	...
$CeCl_6^{-2}$	376	26.6	5,200	2.9
	255	39.2	13,800	3.2
$CeBr_6^{-2}$	522	19.2	~5,700	2.5

[a] The wavelengths λ in mμ, wavenumbers σ in kK, and molar extinction coefficients ϵ are given for maxima (shoulders in parentheses). $\delta(-)$ is the half-width in kK toward smaller wavenumbers.

Since the theory for the variation of the optical electronegativity x_{opt} of 4f and 5f group elements has been discussed elsewhere,[5,16,33] we are here restricting ourselves to the much simpler equation

$$\sigma_{obsd} = [x_{opt}(X) - x_{uncor}(M)] \cdot 30 \text{ kK} \qquad (3)$$

where the wavenumber σ_{obsd} of the first electron-transfer band is related to the optical electronegativity of the ligand $x_{opt}(X)$ and the *uncorrected* value, not taking spin-pairing energy or other forms of interelectronic repulsion effects nor relativistic effects into account, $x_{uncor}(M)$ for the central atom in a definite oxidation state.

Table X gives the values of $x_{uncor}(M)$ obtained in a variety of cases. It is seen that the hexabromides

---

(32) S. P. Sinha and H. H. Schmidtke, *Mol. Phys.*, **10**, 7 (1965).

(33) C. K. Jørgensen, "Lanthanides of 5f Elements," Academic Press Inc., London, 1966.

Table II: Infrared and Raman Spectra of Methylphosphonic Fluorochloride[a]

Infrared (gas), cm^{-1}		Intensity	Infrared (liquid), cm^{-1}	Intensity	Raman (liquid), cm^{-1}	Intensity	Depolarization	Assignment
			3009	M	3007	36	$^6/_7$ dp	ν_2 CH$_3$ antisymmetric stretching
2924		W	2929	M	2925	100	0.23 p	ν_3 CH$_3$ symmetric stretching
			1516	W				$2 \times \nu_{11} = 1506$
			1406	M	1407	15	$^6/_7$ dp	ν_4 CH$_3$ antisymmetric deformation
1373		M						impurity ?
1346	R							
1338	Q	S	1317	S	1320	18	0.69 p	ν_6 CH$_3$ symmetric deformation
1328	P							
1313		W						$\nu_9 + \nu_{13} = 1316$
1301		W	1289	S	1294	27	0.51 p	ν_7 P=O stretching
			1005	W				$\nu_{11} + \nu_{16} = 1019$
950	Q	W						$\nu_{12} + \nu_{13} = 967$
931	R							
922sh								$\nu_{12} + \nu_{14} = 911$
920	Q	S	918	S				ν_8 CH$_3$ antisymmetric rocking
910	P, R							
895	Q	S	898	S				ν_9 CH$_3$ symmetric rocking
888	P							
876	Q	W						$\nu_{15} + \nu_{12} = 876$
865	R							
855	Q	S	855	S	850	1	. . .	ν_{10} P–F stretching
762	R							
755	Q	S	753	S	762	52	0.52 p	ν_{11} P–C stretching
745	P							
552	R							
546	Q	S	539	S	545	61	0.41 p	ν_{12} P–Cl stretching
541	Q							
536	P							
467		W	469	W				$2 \times \nu_{17} = 478$
427	R							
421	Q	M	421	S	424	24	$^6/_7$ dp	ν_{13} P–F bending
413	P							
365		W	368	M	371	64	0.74 p	ν_{14} P=O bending-in-plane
337		VW						
330		VW	324	W	331	9	$^6/_7$ dp	ν_{15} P=O bending-out-of-plane
					262	27	$^6/_7$ dp	ν_{16} F–P–Cl bending
					239	24	$^6/_7$ dp	ν_{17} P–Cl bending

[a] Abbreviations used: S, M, W, V, p, and dp denote strong, medium, weak, very, polarized, and depolarized, respectively; P, Q, and R refer to the branches of an individual band.

relatively strong Raman line which was strongly polarized. Thus, the depolarization value and intensity of the 1306-cm^{-1} Raman line slightly favored the assignment of this lower frequency band to the P=O stretching vibration and the 1333-cm^{-1} band to the CH$_3$ symmetric deformation. Both fundamentals belong to symmetry species a′ and the vibrations are probably mixed so that describing one as a CH$_3$ motion, or the other as a P=O motion, is very likely a poor approximation. The Raman lines are of comparable intensity, lending further support that these two fundamentals are well mixed. Association in the liquid accounts for the large shift noted between the gas and liquid phase frequencies of both the CH$_3$ and P=O stretching vibrations. However, the larger shift is found for the higher frequency band which would favor the assignment of the 1372-cm^{-1} to the P=O stretching vibration. The conclusion is that either the 1333- or 1306-cm^{-1} Raman line could be equally well assigned as the P=O stretching mode and the latter line has been chosen rather arbitrarily.

The methyl group has a degenerate rocking vibration, and the frequency ranged from 867 to 927 cm^{-1} in the previous organophosphorus compounds studied.[1] The assignment of the CH$_3$ rocking vibration in methylphosphoric difluoride is complicated because the phosto a decreasing number of angular node-planes. An important negative result of our measurements is that no weak electron-transfer bands have been observed before the first strong bands.

Crystalline $[P(C_6H_5)_3H]_3EuBr_6 \cdot [P(C_6H_5)_3H]Br$ shows nearly the same absorption spectrum as the solution of $EuBr_6^{-3}$ with a maximum at 24.6 kK. The half-width $\delta(-) = 2.4$ kK is not directly comparable, because the optical density of solids observed by our technique usually increases less strongly than the actual ϵ. The transition $^7F_0 \rightarrow {}^5D_2$ corresponding to a very sharp little hump at 465.2 mμ is somewhat intensified as in the orange dialkyldithiocarbamates.[16]

The measurements in the ultraviolet were made on solutions containing only "aliphatic" constituents and not $P(C_6H_5)_3H^+$. Another experimental problem was constituted by the danger of forming Br_3^- by oxidation of bromide solutions. This species[42,43] has an extremely intense band ($\epsilon \sim 50{,}000$) at 37 kK but does not seem to have perturbed our results, largely because of the technique of using very thin cells.

As discussed in the Experimental Section, $CeBr_6^{-2}$ has only a transient existence at room temperature, and the molar extinction coefficient $\epsilon \sim 5700$ of the wine-red solution was obtained by extrapolation toward the time zero.

It may be worthwhile to make the chemical comment that, until recently, octahedral lanthanide complexes in solution were exceedingly rare. There exist some oxides[24] and sulfides[44] with distorted octahedral coordination of 4f group atoms. There appear also to exist a few cases of tetrahedrally coordinated sulfides.[44]

The 4f → 5d Transitions in Cerium(III) and Terbium(III) Hexahalides. When $CeCl_6^{-3}$ and $CeBr_6^{-3}$ are prepared according to the same techniques as the other MX_6^{-3}, they show some tendency in acetonitrile solution toward oxidation to $CeCl_6^{-2}$ and $CeBr_6^{-2}$. However, the original spectra can readily be obtained and consist in both cases of a single strong band as seen from Table XI and Figure 4. This band is 2 to 3 times narrower than the electron-transfer bands given in Table IX, and there is every reason to believe that it is the transition from the ground-state $^2F_{5/2}$ of [Xe] 4f to the excited configuration [Xe] $(5d\gamma_5)$ containing one electron in the lower subshell of octahedral MX_6 chromophores. The weak red shift from the chloride to the bromide is quite compatible with such an interpretation.[5,35] It may be mentioned that Feofilov[45] reported a similar band at 32.7 kK for Ce(III) in the cubic, eight-coordinated position in CaF_2. However, a much weaker band seems to occur already at 30.3 kK.[45,46]

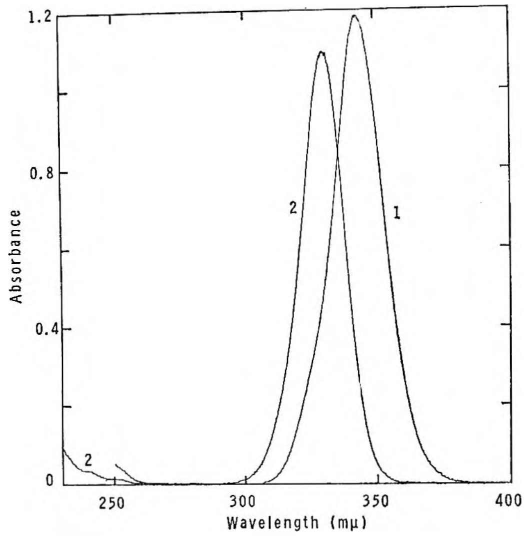

Figure 4. Absorption spectra of cerium(III) hexahalides: (1) 6.8 × 10^{-2} *M* $CeBr_6^{-3}$ in acetonitrile containing excess $(C_4H_9)_4NBr$ and HBr in 0.0108-cm cell and (2) 6.4 × 10^{-2} *M* $CeCl_6^{-3}$ in acetonitrile containing excess $(C_2H_5)_4NCl$ in 0.0108-cm cell.

Table XI: 4f → 5d Transitions in Cerium(III) and Terbium(III) Hexahalides[a]

	λ	σ	ε	δ(−)	δ(+)
$CeCl_6^{-3}$	330	30.3	1600	0.8	1.05
$CeBr_6^{-3}$	343	29.15	1600	1.05	1.05
$TbCl_6^{-3}$	271.5	36.8	28	1.2	...
	233.8	42.75	1500	0.65	1.1
$TbBr_6^{-3}$	278	36.0	Weak	0.9	...

[a] Notation as in Table IX; δ(+) is the half-width in kK toward higher wavenumbers.

The most interesting feature of our spectra is perhaps the absence of any other absorption bands in the measured range, up to 45 kK in $CeCl_6^{-3}$ and 40 kK in $CeBr_6^{-3}$. This sets a lower limit of some 15 kK for the energy difference Δ between the two 5d subshells γ_5 and γ_3. This figure may be compared with $\Delta = 20.4$ kK in $RhCl_6^{-3}$ and 25.0 kK in $IrCl_6^{-3}$,[29] and suggests a strong σ-antibonding influence on the upper subshell though the Ce–Cl distance must be considerably larger than, say, the Ir–Cl distance.

---

[42] A. I. Popov and R. F. Swensen, *J. Am. Chem. Soc.*, **77**, 3724 (1955).

[43] J. E. Dubois and H. Herzog, *Bull. Soc. Chim. France*, 57 (1963).

[44] C. K. Jørgensen, R. Pappalardo, and J. Flahaut, *J. Chim. Phys.*, **62**, 444 (1965).

[45] P. P. Feofilov, *Opt. Spectry.* (USSR), **6**, 150 (1959).

[46] P. P. Sorokin, M. J. Stevenson, J. R. Lankard, and G. D. Pettit, *Phys. Rev.*, **127**, 503 (1962).

Table III: Summary of the Fundamental Frequencies of CH_3POF_2, CH_3POFCl, and CH_3POCl_2 Molecules

Approximate description	Species[a]	CH_3POF_2	CH_3POFCl	CH_3POCl_2, (ref 1)
CH_3 antisymmetric stretching	a''	3020	3007[b]	3005
CH_3 antisymmetric stretching	a'	3020	3007[b]	2998
CH_3 symmetric stretching	a'	2950	2924	2918
CH_3 antisymmetric deformation	a''	1428	1407[b]	1416
CH_3 antisymmetric deformation	a'	1428	1407[b]	1416
CH_3 symmetric deformation	a'	1372	1330	1316
CH_3 antisymmetric rocking	a''	953	920	902
CH_3 symmetric rocking	a'	925	895	894
P=O stretching	a'	1320	1313	1297
P—C stretching	a'	752	755	757
PX_2 antisymmetric stretching	a''	878	855[c]	552
PX_2 symmetric stretching	a'	858	546[c]	497
PX_2 wagging	a'	469	421	285[b]
PX_2 twisting	a''	408	262[b]	226[b]
PX_2 deformation	a'	287	239[b]	200[b]
P=O in-plane bending	a'	408	365	349
P=O out-of-plane bending	a''	287	330	325
Torsion	a''	?	?	?

[a] Species designation does not apply for the CH_3POFCl molecule. [b] Liquid phase Raman frequencies, all other values are gas phase infrared frequencies. [c] The 855-cm^{-1} band is P–F stretching and the 546-cm^{-1} band is P–Cl stretching.

The assignment of the vibrations of the CH_3 group follows directly from those given for the corresponding vibrations of the CH_3POF_2 molecule. The CH_3 antisymmetric stretching vibration is assigned to the Raman line at 3007 cm^{-1} which is depolarized. The infrared band at 3009 cm^{-1} is very broad, but two discernible bands were not observed. The CH_3 symmetric stretching vibration is assigned to the very strong Raman line at 2925 cm^{-1} and the band is strongly polarized. Similarly, the CH_3 antisymmetric deformation is assigned to the depolarized Raman line at 1407 cm^{-1}, and the CH_3 symmetric deformation to the polarized Raman line at 1320 cm^{-1}. The infrared spectrum had a band of strong intensity, at 1330 cm^{-1}, and because of its intensity this band is assigned to the CH_3 symmetric deformation rather than the P=O stretching vibration. The P=O stretching fundamental is assigned to the polarized Raman line at 1294 cm^{-1}. The infrared spectrum of the liquid had a strong band at 1289 cm^{-1}, but the infrared spectrum of the gaseous material showed only weak bands at 1301 and 1313 cm^{-1}. Again, these two fundamentals are expected to be strongly mixed and the descriptions are probably rather poor. The CH_3 antisymmetric and symmetric rocking vibrations are readily assigned to the infrared bands at 920 and 895 cm^{-1}, respectively. The P–F stretching vibration is assigned to the 855-cm^{-1} Q branch with the corresponding Raman band observed at 850 cm^{-1}. The P–C stretching is observed at 762 cm^{-1} in the infrared spectrum. The P–Cl stretching is assigned to the Q branch at 546 cm^{-1} (545 cm^{-1} in the Raman effect), and the band shows an additional Q branch at 541 cm^{-1} which probably corresponds to the $v = 1$ to $v = 2$ vibrational transition. The P–F bending vibration is assigned to the Q branch at 421 cm^{-1} (Raman line at 424 cm^{-1}), the PFCl bending to the Raman line at 262 cm^{-1}, and the PCl bending to the Raman line at 239 cm^{-1}. The P=O bending vibrations are assigned based on the previous assignments given for the CH_3POCl_2 molecule.[1] The P=O in-plane bending for the CH_3POCl_2 molecule was assigned to the polarized Raman line at 356 cm^{-1} and the out-of-plane bending was assigned to the depolarized Raman line at 334 cm^{-1}. Thus, the two Raman lines at 371 and 331 cm^{-1} in the spectrum of CH_3POFCl are similarly assigned. Weak bands were observed in the infrared spectrum at 365 and 330 cm^{-1}, indicating that both of these vibrations are active in the infrared and Raman spectra, which is in direct contrast to what was observed in the vibrational spectrum of CH_3POF_2. Table III gives a summary of the fundamental frequencies for the CH_3POF_2, CH_3POFCl, and CH_3POCl_2 molecules. All of the fundamentals have been assigned for these molecules with the exception of the torsional vibration. The torsional modes are expected to lie well below 250 cm^{-1}, which was beyond the limit of our current infrared instrumentation, and they are normally too weak to be detected in the Raman effect. Due to the low symmetry of the molecules, all combination and overtone frequencies are permitted. Therefore, several weak bands observed in the infrared and Raman spectra could not be uniquely assigned, but a few reasonable assignments are given in Tables I and II. The data do not justify a detailed discussion of these assignments.

Acknowledgment. We wish to thank Mr. Harold Klapper for recording the nmr data and the National Science Foundation for support of this research.

Kinetics of the Solid-State Reaction between Magnesium Oxide and Ferric Oxide

by Donald L. Fresh[1] and J. Stuart Dooling

Department of Chemistry, Catholic University of America, Washington, D. C.

(Received May 5, 1966)

The reaction between equimolar amounts of intimately mixed powders of magnesium oxide and ferric oxide at elevated temperatures to form magnesium ferrite was studied considering the variables of temperature, time, and particle size of the oxide powders. The reaction mixtures were analyzed by X-ray diffractometry employing a spectrogoniometer. After a rapid initial reaction period, which was attributed to surface diffusion, the reaction was expressed by Jander's diffusion equation. The controlling process was the diffusion of the oxide components through the ferrite product layer. The solid-state reaction rate constants were calculated, and the temperature dependence of the rate constants was studied. Activation energies were found to be 117 kcal/mole.

Introduction

Although solid-state reactions were recognized during the 1800's and early 1900's, as evidenced by work of Faraday,[2] Spring,[3] and Cobb,[4] very little was done toward understanding the mechanisms until after 1910. Some of the earliest quantitative work on the kinetics of solid-phase reactions was done by Hedvall,[5] Tammann,[6] and Jander.[7] Jander conducted experiments on the solid-phase reaction between crystalline solids and concluded that the square of the thickness of the reaction layer of the new-formed product is proportional to time. The differential equation representing the reaction is

$$\frac{\mathrm{d}y}{\mathrm{d}t} = \frac{k}{y} \tag{1}$$

Equation 1 states that the rate of thickening of the product layer is inversely proportional to the thickness of the layer, y, at time, t. The product layer may be considered as a diffusion barrier which tends to retard the reaction as the layer thickens.

A number of experimental methods have been employed in following solid-state reactions. Chemical analytical techniques meet with only limited use when the reactions do not involve a change in chemical composition but merely a change in crystalline configuration. This is the case in the reaction

$$\mathrm{MgO} + \mathrm{Fe_2O_3} \longrightarrow \mathrm{MgFe_2O_4}$$

---

(1) General Precision Inc., Librascope Group, Glendale, Calif.

(2) M. Faraday and J. Stodart, *Quart. J. Sci.*, **9**, 319 (1820).

(3) W. Spring, *Z. Physik. Chem.*, **2**, 535 (1888).

(4) J. Cobb, *J. Soc. Chem. Ind.*, **29**, 69, 250, 399, 608, 799 (1910).

(5) J. A. Hedvall, "Reaktionshahigkeit Fester Stoff," J. Barth Co., Leipzig, 1938.

(6) G. Tammann, *Z. Anorg. Allgem. Chem.*, **111**, 78 (1921); **123**, 196 (1922); **149**, 21 (1925).

(7) (a) W. Jander, *ibid.*, **163**, 1 (1927); **166**, 31 (1927); **214**, 55 (1933); (b) W. Jander, *Z. Ver. Deut. Ing.*, **80**, 506 (1936).

Although X-ray diffraction, principally camera techniques, has been used for a number of years to measure crystalline structures, only recently have methods been available that provide the degree of accuracy required to follow a reaction of this type quantitatively.

Experimental Section

The particle method, as applied in this study, includes the following experimental steps: selection and preparation of the reactant oxides; preparation of large particles of MgO by comminuting and sizing; preparation of the reaction specimens by intimately mixing the two oxides and compacting the mixtures into disk shapes; heat-treating the shapes; preparation of the heat-treated shapes for X-ray diffraction analysis by pulverizing to fine powders; and analysis by X-ray diffractometry.

For the finely divided ferric oxide, Grade 2199 of the C. K. Williams Co., Easton, Pa., was selected on the basis of purity and particle size. A spectrographic analysis of the material indicated a purity of 99.2% and an electron micrograph of the material showed the particles to be in the vicinity of 0.05 μ. A high purity (99.5%) "optical fused grade" of magnesium oxide in the form of large crystals (5- to 50-mm diameter) available from the Norton Co. of Worcester, Mass., was used as the source of the other reactant particles.

In order to obtain the various coarse particle-size ranges, the large crystals of magnesium oxide were comminuted into three particle-size ranges. An upper limit of about 0.25-mm cross-sectional dimension was felt sufficiently large to guarantee that complete reaction would not occur even after exposure to high temperatures for long periods of time. The ranges of 177 to 210, 88 to 105, and 44 to 53 μ were then selected on the basis of available Tyler Standard Sieves. Crushing was accomplished between two hardened steel plates on a mechanical press. A slow stream of dry argon was introduced into the crushing assembly and into containers used in all subsequent steps to minimize hydroxide and carbonate formation.

Three reaction specimen types were prepared by combining equimolar amounts of each of the particle-size ranges of magnesium oxide with the finely divided ferric oxide as shown in Table I. The weighed amounts of each of the two oxides were placed in glass jars with plastic screw caps and were shaken to promote dry mixing. Additional mixing was performed by shaking after the addition of stainless steel balls. Next, an amount of anhydrous ethanol, sufficient to produce a good mixing consistency, was added and the jars and balls were again shaken and then revolved on a ball-mill roller until a mixture was obtained that appeared uniform by microscopic examination. This examination also showed that the original size of the coarse particles had not been reduced by the mixing operation.

Table I: Particle size of Reaction Specimens

Specimen no.	MgO	Fe_2O_3
1	1 mole 44–53 μ	1 mole 0.05 μ
2	1 mole 88–105 μ	1 mole 0.05 μ
3	1 mole 177–210 μ	1 mole 0.05 μ

Rapid drying was accomplished by placing the jars under heat lamps while gently blowing argon into each jar to remove the alcohol vapor. The drying was rapid enough to minimize preferential settling of heavy particles in the slurries. The specimen powders were pressed into disks in order to force the particles closer together and thereby obtain a higher degree of intimacy between the reactants and to provide a convenient shape to facilitate handling during the heat-treating step. Disks, with dimensions 5-mm thickness by 17.5-mm diameter, were formed with 10,000 kg of force.

The three reaction disks (plus individual MgO and Fe_2O_3 disks and crucibles of powders for use in preparing X-ray standards) were placed in procelain boats lined with platinum foil in preparation for heat treatment. A preheating furnace was used to heat the boats of specimens before placing them in the heat-treating furnace. This served to prevent any drastic lowering of the temperature in the heat-treating furnace and permit rapid attainment of the desired peak temperatures. At the completion of the heat-treatment period, the boats of specimens were removed from the furnace and rapidly cooled by air quenching. Electronic measuring and controlling apparatus maintained the zone used in the heat-treating furnace within ±2° of the desired value. The reaction specimens were fired at four temperatures (1000, 1100, 1200, and 1300°) for seven periods of time (0.25, 0.5, 1, 2, 4, 8, and 20 hr).

X-Ray diffraction was used to follow the reaction by measuring the amount of ferric oxide remaining in a specimen. The ferric oxide crystal provides a strong diffraction line that receives no interference from the patterns of the other constituents in the way of line superposition or adjacency. The intensity of this ferric oxide line was measured in each specimen and the amount of reactant remaining was thereby determined. Apparatus utilized was a Norelco dif-

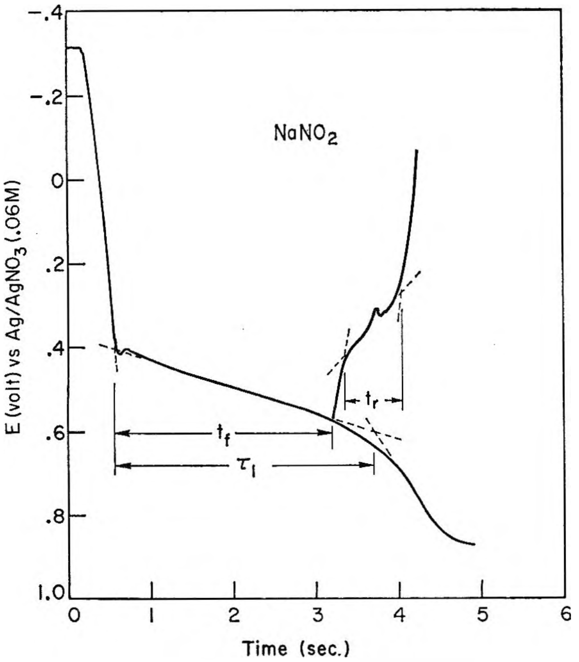

Figure 2. Chronopotentiograms for $NaNO_2$ solution in $NaNO_3$–KNO_3 at 290°: τ_1, anodic transition time; t_f, time of forward (anodic) current; t_r, transition time for reverse (cathodic) process.

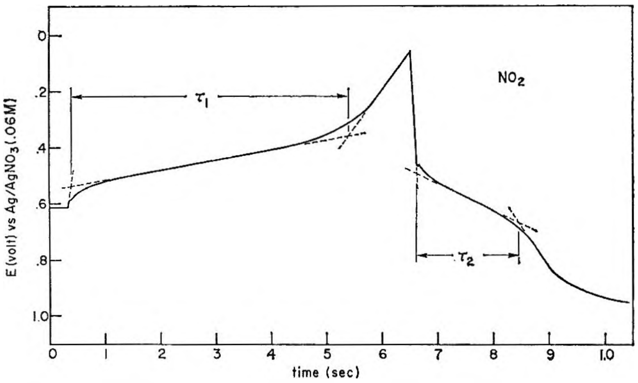

Figure 3. Chronopotentiograms for dissolved NO_2 in $NaNO_3$–KNO_3 melt: τ_1, cathodic transition time; τ_2, transition time for reverse (anodic) process due to oxidation of products formed during τ_1.

Table II: Average $E_{1/4}$ Values at Pt Electrode (*vs.* Ag|$AgNO_3$ (0.06 *M*) Reference) in $NaNO_3$–KNO_3 at 300°

Solute	$E_{1/4}$, v^a Cathodic	Anodic
$NaNO_2$	0.44 (r)	0.47 (f)
NO_2	0.42 (f)	0.45 (r)
$K_2S_2O_7$	0.42 (f)	0.47 (r)
$KHSO_4$	0.41 (f)	0.45 (r)

^{a} f = forward wave, r = reverse wave.

the O^{2-}. Swofford and McCormick apparently found a single wave, but it is not clear from their presentation if a second wave may have existed. The Na_2CO_3 and NaOH solutions each produced one wave at about +0.4 and −0.3 v, respectively. On reversal of current after these waves, single reduction waves at −0.6 to −0.9 v were found in all these melts. (When the electrode potential was cycled between +0.1 and −0.6 v, anodic waves due to a solid on the electrode were frequently found at about 0.0 v.) Solutions containing $NaNO_2$ + Na_2CO_3 or $NaNO_2$ + Na_2O_2 (Figure 5) were titrated with $K_2S_2O_7$. It was observed that both the carbonate and peroxide, being stronger bases than nitrite, were neutralized before the nitrite. However, the expected stoichiometry did not seem to be obeyed. Figure 6 shows the neutralization of a Na_2O_2 melt by purging with NO_2.

Addition of NO and Oxygen. When nitric oxide was bubbled through the nitrate melt, the only electrochemical reaction observed was an oxidation; linear voltammetric and chronopotentiometric measurements were the same as for solutions to which NO_2^- had been added. These results indicated that a reaction took place between NO and the nitrate melt (see below).

Attempts to reduce gaseous oxygen in these melts were unsuccessful. This result differs from that of Kust and Duke[15] but is in agreement with the findings of Swofford and McCormick.[14]

Discussion

For the $NaNO_3$–KNO_3 melt the limiting reactions at −1.6 (cathodic) and +1.2 v (anodic) have been attributed to the reduction of NO_3^- to NO_2^- and O^{2-} and the oxidation of NO_3^- to NO_2 and O_2, respectively.[12] The anodic wave at −0.3 v can be ascribed to oxidation of the Pt electrode and/or of oxide ion formed during the reduction of NO_3^-. Nitrate solutions containing various bases show anodic waves which may involve the same over-all oxidation process, *i.e.*, depolarization of the platinum electrode by oxide. The difference in potentials at which these processes occur in the various solutions may be indicative of the different basic characteristics of the oxide donors.

The electrochemical studies demonstrate that the species NO_2^+, assumed to exist in measurable concentration[15] in acidic nitrate melts, cannot be detected by the techniques employed above. The same electrochemical techniques have been utilized successfully in a recent study[16] of NO^+ and NO_2^+ in concentrated

---

(15) R. N. Kust and F. R. Duke, *J. Am. Chem. Soc.*, **85**, 3338 (1963).

(16) L. E. Topol, R. A. Osteryoung, and J. H. Christie, *J. Electrochem. Soc.*, **112**, 861 (1965).

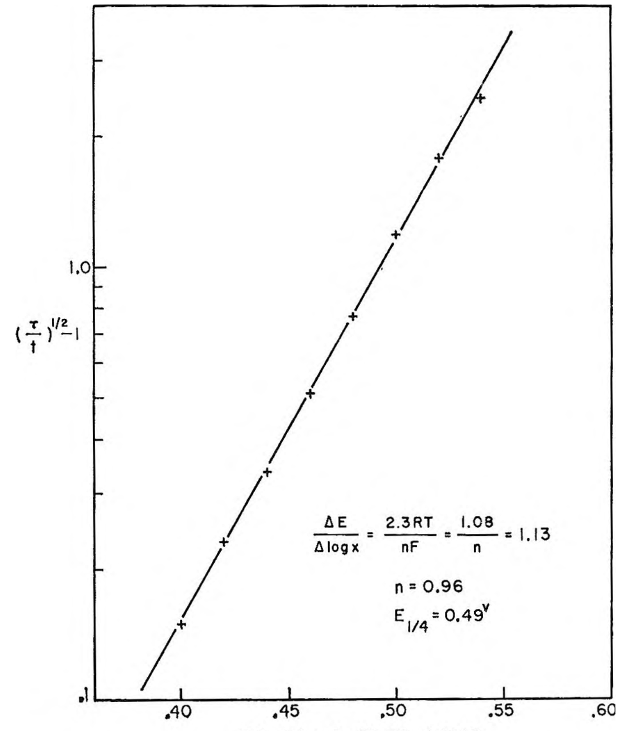

Figure 4. Log $[(\tau/t)^{1/2} - 1]$ *vs.* E for the electrode reaction $NO_2 + e \rightarrow NO_2^-$.

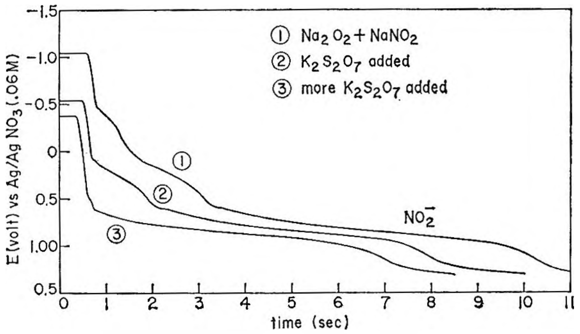

Figure 5. Reaction of $Na_2O_2 + NaNO_2$ with $K_2S_2O_7$ in $NaNO_3$-KNO_3 at 300°.

sulfuric acid. Attempts to oxidize NO_2 and NO at Pt electrodes in the molten nitrates were also unsuccessful. Furthermore, recent thin-film infrared-emission measurements[17] of acidic nitrate melts yielded no evidence of the existence of NO_2^+. These results are in disagreement with Delarue,[5] who reported the coulometric production of NO_2^+ by the reaction

$$NO_3^- - 2e \longrightarrow NO_2^+ + {}^1/_2O_2 \qquad (4)$$

and claimed to have identified the electrode reaction

$$NO_2^+ + 2e \longrightarrow NO_2^- \qquad (5)$$

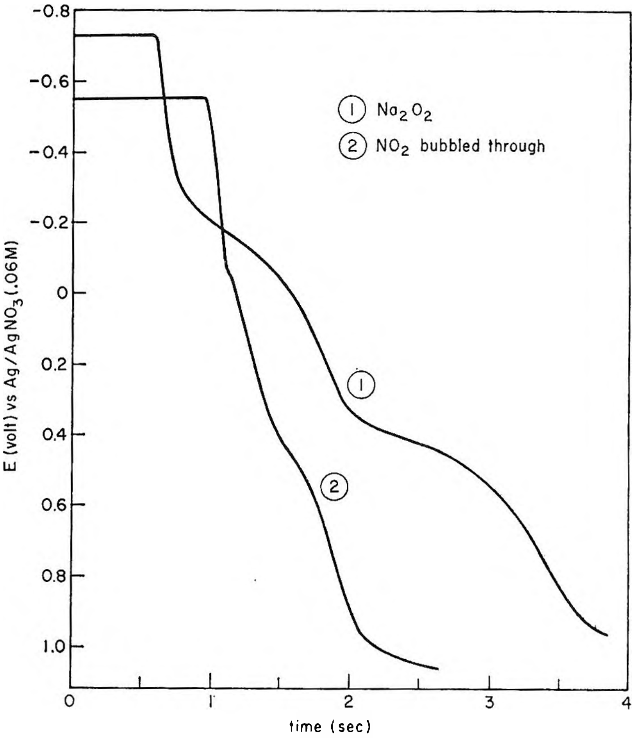

Figure 6. Reaction of Na_2O_2 with NO_2 in $NaNO_3$-KNO_3 at 300°.

Our results regarding the electrochemical behavior of NO_2 are in opposition to those of Swofford and McCormick, who state that NO_2 "exhibits no significant electrochemical activity." We are in agreement regarding the existence of a reversible one-electron oxidation of NO_2^- to NO_2. The voltammetry and reverse-current chronopotentiometry on nitrite as well as NO_2 support the reversibility of reaction 3. Certainly, Swofford and McCormick's conclusion regarding a reversible couple requires that NO_2 be reducible to NO_2^-, and we are unable to suggest a cause for their finding NO_2 electrochemically inert.

Kust and Duke,[15] using an oxygen electrode in acid nitrate melts, claim to have measured the dissociation constant for reaction 1. However, their dissociation constant increased with time and it may be that here, as well as in previous kinetic studies,[4] the reaction observed was

$$2NO_3^- = 2NO_2 + {}^1/_2O_2 + O^{2-} \qquad (6)$$

or in the presence of acids, *e.g.*, $S_2O_7^{2-}$

$$S_2O_7^{2-} + 2NO_3^- \longrightarrow 2SO_4^{2-} + 2NO_2 + {}^1/_2O_2 \qquad (7)$$

The present electrochemical studies have shown that

---

[17] J. R. Moyer, Dow Chemical Co., private communication.

the NO_2–NO_2^- couple is reversible on Pt and that the only detectable electroactive species in solution upon the addition of strong acids to nitrates is NO_2. The diffusion coefficient of NO_2 dissolved in these melts could not be determined from eq 2 since the gas concentration or solubility is not known. If one assumes that the diffusion coefficients of NO_2 and NO_2^- are approximately equal, the solubility of NO_2 in $NaNO_3$–KNO_3 is calculated to be about $(5 \pm 3) \times 10^{-3}$ mole/l. at 300°.

It was further demonstrated that NO_2 itself behaves as an acid, reacting with strong bases and nitrite and converting chromate to dichromate, posssibly *via* the following reactions.

$$2NO_2 + O^{2-} = NO_3^- + NO_2^- \quad (8)$$

$$NO_2 + NO_2^- = NO_3^- + NO \quad (9)$$

$$2NO_2 + 2CrO_4^{2-} = NO_3^- + NO_2^- + Cr_2O_7^{2-} \quad (10)$$

In an equilibrium study, reaction 9 was found to proceed far to the right as written. However, the reverse reaction can also be observed by bubbling NO through a nitrate melt as was demonstrated by the electrochemical results. This also appears to disagree with the findings of Swofford and McCormick, although their experimental conditions may preclude comparison with our data. It was also found that equilibrating nitrite with an acid such as $K_2S_2O_7$ or $K_2Cr_2O_7$ in a nitrate melt always resulted in the formation of a gaseous mixture of NO and NO_2. The relative amounts of the two gases varied with the acid used, the percentage of NO decreasing from over 90% with $K_2Cr_2O_7$ to about 50% with $K_2S_2O_7$ at 275°. If NO_2^+ were the acid species, then one would expect to find NO_2 primarily, according to the reactions

$$NO_2^+ + NO_2^- \longrightarrow 2NO_2 \quad (11)$$

and

$$NO_2^+ + NO_3^- \longrightarrow 2NO_2 + {}^1/_2O_2 \quad (12)$$

However, the reaction occurring appears complicated but may be

$$S_2O_7^{2-} + 2NO_2^- = 2SO_4^{2-} + NO + NO_2 \quad (13)$$

or may also involve reactions 7 and 9. With dichromate the reaction would be similar to (13) except that chromate would be formed instead of sulfate, and reaction 10 must also be considered. These reactions with the appropriate equilibrium constants could account for the low NO_2 concentration at equilibrium in the dichromate system. In any event it is difficult to reconcile these results with the assumption of NO_2^+ as the acid species.

Finally, NO_2^+ has been postulated as the intermediate in the acid oxidation of bromide ion,[4b] *i.e.*

$$NO_2^+ + Br^- \longrightarrow NO_2 + {}^1/_2Br_2 \quad (14)$$

and also, oxidation of iodide[3] has been found in metaphosphate-containing melts, the reaction suggested as

$$NO_3^- + PO_3^- + I^- \longrightarrow PO_4^{3-} + {}^1/_2I_2 + NO_2 \quad (15)$$

It was decided to check these reactions and to see if NO_2 could oxidize these halide ions. Solutions of KI and $K_2Cr_2O_7$ in $NaNO_3$–KNO_3 were equilibrated overnight *in vacuo* and the reaction was found to be complex in that it required about four parts of dichromate to one of iodide for complete iodide oxidation. The gas phase was analyzed by mass spectrometry and consisted entirely of NO in every case in contrast to NO_2 reported and postulated earlier.[3,4b] To test the effect of nitrogen dioxide, some experiments were run in which NO_2 was bubbled through nitrate melts containing Br^- or I^-. Both halogen and NO were found indicating the over-all reaction to be

$$2NO_2 + X^- \longrightarrow {}^1/_2X_2 + NO + NO_3^- \quad (16)$$

Thus, here again the observed behavior of NO_2 is equivalent to that attributed to NO_2^+ in acidified melts, and although the chemical evidence above does not preclude the existence of NO_2^+, it certainly favors NO_2 as an acid intermediate, if one is required, rather than NO_2^+.

Acknowledgments. This work was supported in part by the U. S. Atomic Energy Commission and was presented at the molten salt session of the Electrochemical Society Meeting, San Francisco, Calif., May 9–13, 1965.

The activation energies and constants were obtained from the graphs of the temperature dependence of the rate constant (Figure 5). Table III lists these values. Activation energies were also calculated from the slopes of plots of ln $(1 - \sqrt[3]{1 - x})^2$ against $1/T$. These were in agreement with the values of Q listed in Table III.

On the Irradiation of *n*-Heptadecane

by R. Salovey and W. E. Falconer

Bell Telephone Laboratories, Incorporated, Murray Hill, New Jersey *(Received May 10, 1966)*

Radiolyses of *n*-heptadecane in the pure state and in the presence of iodine are examined and compared with those of *n*-hexadecane. In general, similar irradiation behavior is noted. However, differences are observed in radiolyses of the respective crystalline solids. Lower cross-linking yields and an unsymmetrical distribution of low molecular weight products result from irradiated solid *n*-heptadecane as compared to solid *n*-hexadecane. These differences are associated with poorer molecular coupling in the orthorhombic structure of odd *n*-alkanes than in the triclinic habit of even homologs. The end-linking yield in solid *n*-heptadecane is larger than in solid *n*-hexadecane. The combination of heptadecyl radicals yields at least 35 and 80% of the tetratriacontane isomers on irradiation of pure *n*-heptadecane in solid and liquid states, respectively.

Introduction

Detailed studies of the irradiation behavior of *n*-hexadecane[1,2] lead to conclusions on the radiolysis of long-chain paraffins. To explore the generality of these results, the next higher homolog (containing an odd number of carbon atoms), *n*-heptadecane, was examined.

There is an even–odd alternation in the crystallographic properties of normal paraffins.[3] Even *n*-alkanes of carbon numbers 8 through 24 crystallize in a triclinic modification, with layers of parallel molecules obliquely inclined to layer planes drawn through chain ends. Just below their melting points, odd linear paraffins between C_9 and C_{35} assume rotational crystalline structures in which molecules rotate about their long axes. At lower temperatures, these odd *n*-alkanes crystallize in orthorhombic habit with molecular axes normal to "end planes."[4]

Radiolyses of solid and liquid *n*-hexadecane are sensitive to physical state.[1] Cage recombination of radical fragments from main-chain scission in the crystalline solid was adduced to explain differences in product yields in different states. Since molecular packing in solid paraffins is altered by crystalline modification, it is of interest to examine the effect of crystal state on radiation behavior. The importance of crystalline modification in *n*-hexadecane radiolysis was indicated by the observation that cross linking was affected by the addition of specific impurities which cause *n*-hexadecane to assume an orthorhombic form.[1,5]

Another reason for studying the importance of crystal habit is to ascertain the validity of considering *n*-hexadecane as a polyethylene analog. Linear poly-

---

(1) R. Salovey and W. E. Falconer, *J. Phys. Chem.*, **69**, 2345 (1965).

(2) W. E. Falconer and R. Salovey, *J. Chem. Phys.*, **44**, 3151 (1966).

(3) A. I. Kitiagorodskii, "Organic Chemical Crystallography," Consultants Bureau, New York, N. Y., 1961.

(4) Yu. V. Mnyukh, *J. Phys. Chem. Solids*, **24**, 631 (1963).

(5) A. Müller and K. Lonsdale, *Acta Cryst.*, **1**, 129 (1948).

Table I: Photolysis of 1,3-Dioxolane

Press., mm	11.0	20.0	20.0	20.0	46.5	50.0	50.0	50.0	50.0	50.0	61.0	73.0	81.0	82.0
Temp, °C	27	27	81	110	110	27	27	27	27	27	80	27	110	80
Exposure time, min	120	120	120	121.5	120.0	19.0	30.0	58.0	120.7	183.8	122.2	50.0	120.0	120.0
Products	µmoles													
H_2	2.90	3.82	4.72	5.62	7.58	0.64	1.08	2.21	4.63	7.01	6.85	3.36	9.60	7.64
CO	2.60	3.45	3.12	3.49	4.63	0.41	0.72	1.53	3.64	5.86	4.79	2.77	5.81	5.29
CH_4	0.39	0.48	0.61	0.89	1.34	0.09	0.12	0.27	0.62	1.02	1.12	0.36	1.80	1.31
C_2H_6	0.26	0.29	0.27	0.37	0.53	Trace	0.03	0.08	0.20	0.37	0.43	n	0.70	0.35
CO_2	1.89	2.51	3.20	4.48	5.37	0.47	0.59	1.11	2.38	3.49	4.82	n	7.34	4.48
C_2H_4	2.10	2.89	3.13	4.21	5.44	0.64	0.80	1.52	3.22	4.80	5.40	n	7.14	5.21
C_4H_{10}	n[a]		0.31	0.29	0.31	n	n	0.09	0.17	0.33	0.39	n	0.28	n
CH_2O	n	2.51	2.47	2.64	n	0.74	n	1.73	2.99	3.96	3.70	2.55	4.05	n

[a] n = not analyzed.

After each run the products were condensed at −196° and then distilled through two LeRoy traps at −196° and a solid nitrogen trap (−210°). In experiments in which oxygen was added to the reactant, the noncondensable gases were pumped off, while in runs which were performed without oxygen, the noncondensable gases were measured in a Toepler pump–gas buret. The noncondensable fraction which contained H_2, CH_4, and CO was analyzed by a mass spectrometer. The condensable fraction was transferred quantitatively into an ampoule and then introduced into the inlet system of a dual-column, dual-detector gas chromatograph. The two columns and the detectors were connected in series, and the electrical signals from the detectors were fed into a double-pen recorder. One of the columns was 2 m long, packed with 25 wt % Carbowax 600 on Chromosorb, while the other was 1.5 m long and packed with silica gel. Ethane, carbon dioxide, ethylene, and butane were all resolved very well in the silica gel column. The Carbowax column could resolve acetaldehyde, ethylene oxide, and 1,3-dioxolane. The columns were calibrated using known quantities of authentic samples. Since it was not possible to analyze formaldehyde by gas chromatography, it was estimated quantitatively by the color reaction.[3] In order to analyze all of the products, two runs were carried out under identical conditions, of which one was used for analysis of formaldehyde while the other one was used for analysis of all other products.

Results

Within the decomposition range 0.5–2.5%, the principal products of the reaction were hydrogen, carbon monoxide, carbon dioxide, methane, ethane, ethylene, *n*-butane, and formaldehyde (Table I). Acetaldehyde was not detected as a product, and, if it were present at all, it could not be more than a few per cent of the total products.

The product yields at different exposure times are shown in Figures 1 and 2, which demonstrate the leveling off of formaldehyde at longer exposure while the other products were linearly proportional with time except carbon monoxide, the rate of which increased with time.

The scavenging effect of ethylene-d_4 (Table II) on the hydrogen yield is prominent in Figure 3. The purpose of added ethylene-d_4 was dual. First, it acted as a scavenger of the hydrogen atom. Second, it acted as a detector of shorter wavelengths since

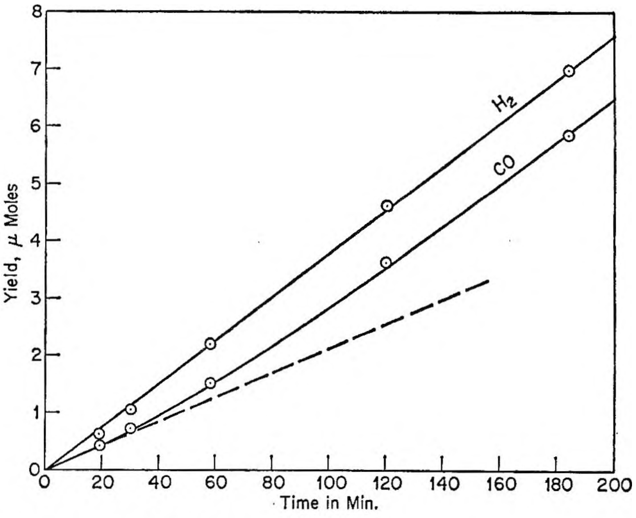

Figure 1. Yield of CO and H_2 *vs.* time.

---

[3] D. Matsukawa, *J. Biochem.* (Tokyo), **30**, 386 (1939).

Table II: Yields of Low and Intermediate Molecular Weight Products in the Radiolysis of *Liquid* n-Heptadecane (4.0 Mrads)

Carbon no.	Hydrocarbons			Iodoalkanes	
	Pure	+0.6% I	+1.2% I	+0.6% I	+1.2% I
4	0.091	0.061	0.056		
5	0.117	0.075	0.062	0.077	0.072
6	0.130	0.085	0.072	0.060	0.066
7	0.122	0.076	0.062	0.052	0.054
8	0.101	0.059	0.049	0.054	0.056
9	0.082	0.047	0.037	0.062	0.063
10	0.070	0.035	0.029	0.057	0.057
11	0.069	0.035	0.030	0.048	0.046
12	0.073	0.037	0.031		
13	0.065	0.035	0.025		
14	0.070	0.042	0.033		
15	0.066	0.042	0.032		
16	0.021[a]	0.003[a]	0[a]		
17				1.11	1.16
17				0.51	0.61
n-17				0.152	0.176
Av C_9–C_{15}	0.071	0.039	0.031		
$\Sigma G(C_1$–$C_{16})$[b]	1.03	0.55	0.43		
ΣG(intermediate)[a,c]	0.29	0.07	0.06		

[a] Reduced precision because of impurities. [b] 14 × average value + 2 × C_{16} yield. [c] Estimate from most reliable data excluding $C_{17}I$.

radiolysis of n-heptadecane in Table I and for the irradiation of liquid n-heptadecane in Table II. Radiation yields of tetratriacontanes are listed in Table III. All results are averages of repeated analyses; pure paraffins were irradiated and analyzed at least in triplicate, and scavenged radiolyses were in duplicate.

Table III: Yields of Tetratriacontane in the Radiolysis of n-Heptadecane (4.0 Mrads)

State	Additive	G(dimer)	G(linear dimer)
Solid		1.13	0.043
	0.6% iodine	0.75	0.042
	1.2% iodine	0.732	0.042
Liquid		1.63	0.0045
	0.6% iodine	0.368	0
	1.2% iodine	0.307	0

Low molecular weight hydrocarbons identified in Tables I and II are linear paraffins and olefins. Normal alkanes and alkenes with the same number of carbon atoms were not resolved. Branched hydrocarbons would have eluted significantly earlier than linear isomers and were not detected.

By injecting samples into the chromatograph immediately upon opening sealed irradiation tubes, products as low as C_4 were determined. However, the derivation of concentrations from peak heights becomes increasingly unreliable below C_8 (*cf.* Figure 1 in ref 2). Moreover, in the scavenged radiolysis of the liquid, peaks from C_8 to C_4 are not resolved from iodoalkanes. Consequently in the low molecular weight region, the accuracy of radiation yields decreases from C_8 to C_4, and the most reliable hydrocarbon yields are C_9 to C_{15}. Only these will be discussed; lower hydrocarbon yields are included for cautioned comparison. In the irradiation of hexadecane,[2] yields for each of the C_9 to C_{14} hydrocarbons were approximately equal with an average $G = 0.036$ for solid and $G = 0.073$ for liquid radiolyses. Yields of each of the C_9 to C_{15} hydrocarbons from the irradiation of liquid n-heptadecane are also nearly equal with an average G value of 0.071. In the solid radiolysis, however, an unmistakable minimum yield is observed at C_{10} with $G = 0.024$ as compared to C_{15} with $G = 0.053$. These products are linear paraffins and olefins from main-chain scission. A preferential depletion of certain scission fragments by secondary cleavage may account for these results. When chain scission produces fragments of comparable size, excess energy is not removed by a small particle and further fragmentation may ensue, creating an unsymmetrical product distribution. That this is observed in solid n-heptadecane but not in n-hexadecane suggests that excess energy associated with energetic fragmentation of a C–C bond may be more effectively dissipated in the triclinic than in the orthorhombic crystal modification. Because some product yields are higher in n-heptadecane than in n-hexadecane, it is further inferred that primary scission is enhanced by poorer coupling of heptadecane molecules in the orthorhombic habit. Relatively lower yields of C_{16} hydrocarbons are a consequence of the reduced probability of terminal relative to internal carbon–carbon scission.[2,8]

Yields of low molecular weight products from irradiated solid n-heptadecane are unaffected by the presence of 0.6 or 1.2 mole % iodine. This is consistent with the view that these products result from molecular reactions.[2,9] However, chromatograms of products eluting before n-heptadecane in the irradiated liquid are considerably altered by the presence of iodine. The average radiation yield of each linear hydrocarbon is reduced from 0.071 to 0.039 with 0.6% iodine and to 0.031 by 1.2% iodine. As with hexadecane irradiation, about half of this region in the liquid results from radical reactions, largely disproportionation of radical fragments from main-chain scission with n-heptadecyl radicals.[2] In addition to the reduction in yield of linear hydrocarbons, a series of peaks corresponding to 1-iodoalkanes is observed.

Intermediate hydrocarbon products, comprising carbon numbers C_{18} to C_{33}, were not specifically identified. Total radiation yields for the entire group, excluding iodoheptadecanes which elute in this region, were estimated using the same calibration as for low molecular weight products. Allowance was made for C_{18} and C_{19} impurities. Since this region is characterized by a series of similar peaks, an average peak height calculated from the most reliable chromatographic data was multiplied by the total number of major peaks in the intermediate region. In the radiolysis of solid n-heptadecane, intermediate hydrocarbons are produced with a G value of 0.05. The yield for liquid n-heptadecane irradiation is 0.29. Corresponding values for n-hexadecane radiolysis are very similar, 0.05 and 0.31, respectively.[2] In the presence of iodine, intermediate region yields are unaffected in the solid but reduced in the liquid irradiation to approximately solid-state values. Intermediate region hydrocarbons in irradiated liquid n-heptadecane are largely combination products of radical fragments from main-chain scission with heptadecyl radicals.[2]

The yield of C_1 to C_{16} 1-iodoalkanes may be related to the scavenged portion of low and intermediate products in the irradiated liquid. Most of the radical fragments from main-chain scission react with heptadecyl radicals.[2] In solid n-heptadecane, as in solid n-hexadecane,[2] radical reactions leading to intermediate and low molecular weight products are suppressed by cage recombination of radical fragments from main-chain scission, and no 1-iodoalkanes below C_{17} are anticipated or found.

Yields of tetratriacontane from irradiated n-heptadecane measure the cross-linking reaction and are referred to as G(dimer). For irradiated liquid n-heptadecane the radiation yield of total dimer (Table III) is very close to the cross-linking yield in n-hexadecane liquid ($G = 1.7$).[2] However, whereas no linear "dimer" resulted from irradiation of liquid n-hexadecane, about 0.3% of the total dimer from liquid n-heptadecane was linear tetratriacontane. The cross-linking yield of solid n-heptadecane is, however, considerably different from the analogous reaction in irradiated solid n-hexadecane. The radiation yield of dimer, 1.13, is lower than for n-hexadecane where $G = 1.6$. Moreover, the proportion of linear dimer is almost 4% as compared to 1% in n-hexadecane radiolysis.[10] The enhancement of linear dimer is related to crystal structure, and was demonstrated in doped n-hexadecane radiolysis.[1] Although there is closer molecular packing in the triclinic structure of even n-paraffins than in the orthorhombic modification of odd homologs, layers of odd n-paraffins are rectangular whereas even n-paraffins have an oblique layer structure.[4] This difference in end-group packing is reflected in the efficiency of the end-linking reaction to form linear dimer; that is, terminal radicals apparently combine more readily in the rectangular structure. Poorer molecular packing of crystalline n-heptadecane compared to n-hexadecane may account for the reduced yield of total dimer. The presence of iodine reduces cross-linking yields in the irradiation of n-heptadecane (Table III). For solid n-heptadecane the yield of tetratriacontane is reduced 35% by the addition of 1.2% iodine. The comparable figure for the suppression of dimer in liquid radiolysis is 80%. In the irradiation of solid and

---

[8] A. V. Topchiev, "Radiolysis of Hydrocarbons," Elsevier Publishing Co., Amsterdam, 1964.

[9] L. Kevan and W. F. Libby, *J. Chem. Phys.*, **39**, 1288 (1963).

[10] A ratio of 8% linear dimer/total dimer for n-hexane[9,11] is consistent with 1% for this ratio in n-hexadecane. Assuming primary C–H rupture is half as probable as secondary C–H scission, and neglecting differences in disproportionation, random combination gives 7 and 1% for linear dimer/total dimer for C_6 and C_{16} paraffins, respectively; that is, the fraction of linear dimer for these triclinic crystalline solids is that predicted by random cross linking, whereas in the orthorhombic C_{17} it is enhanced by a factor of 4.

[11] H. Widmer and T. Gäumann, *Helv. Chim. Acta*, **46**, 944 (1963).

of ethylene was due to the addition of the hydrogen atom to the ethylene double bond. As is evident from Figure 3, the hydrogen yield was reduced to about 55% by the addition of 7.5% of ethylene. Extrapolation of the linear part of the curve in Figure 3 to infinite concentration of ethylene showed that about 33% of hydrogen from 1,3-dioxolane decomposition was produced as molecular hydrogen and therefore was unscavengable by ethylene.

Both ethylene and carbon dioxide were produced in abundant quantities in the presence of oxygen (Table II). This indicated that a major portion of ethylene and carbon dioxide was formed in a direct molecular process. The persistent production of formaldehyde in large amounts, even in the presence of oxygen and ethylene, indicated that perhaps it was formed by a direct molecular process and may, in fact, be the same process which yielded CH_3, CO, and part of the hydrogen atom. The presence of methyl radical in the photolysis was obvious. The formation of methane and ethane in the pure 1,3-dioxolane and removal of C_2H_6 by the addition of oxygen can only be explained by the reactions of methyl radical. Since no acetaldehyde was detected as a product, the diradical $\dot{C}H_2\text{-}CH_2\text{-}\dot{O}$, a possible intermediate formed after the elimination of formaldehyde, could decompose after the migration of a hydrogen atom into CH_3, CO, and H. On the other hand, the diradical could split to give $CH_2{=}CH_2$ and the O atom. In the flash photolysis of ethylene oxide we have observed such a process.[4] In addition, the data of Table I show that, at a pressure of 50 mm of dioxolane and at 27°, the ethylene yield is greater than CO_2. This may indicate that excess ethylene might have come from such a process as

$$\dot{C}H_2{-}CH_2{-}\dot{O} \longrightarrow CH_2{=}CH_2 + O$$

Then the number of oxygen atoms is given by $[C_2H_4] - [CO_2]$; at higher conversion this difference is a large number. Thus, all of these oxygen atoms could react with the substrate by some radical mechanism to produce the observed products.

The decrease in the formaldehyde rate with reaction time (Figure 1) indicates consumption of the product formaldehyde in secondary reactions. Since the carbon monoxide rate increased with time, it is certain that a portion of CO has been formed by the secondary decomposition of formaldehyde

$$HCHO \xrightarrow{h\nu} H + CHO$$

$$2CHO \longrightarrow CH_2O + CO$$

An approximate estimate indicates that at least 35% of the decomposition proceeds *via* process A and the rest *via* process B, provided, of course, no other primary processes are involved.

The decrease in the yield of CO_2 and C_2H_4 by the addition of 3 mm of oxygen in 20 mm of 1,3-dioxolane suggests that perhaps the triplet state was the precursor of about 28% of the CO_2 and C_2H_4 formed in the system. Further addition of oxygen (10 mm) did not quench the products CO_2 and C_2H_4 anymore within experimental errors. This is in contrast to the decomposition of acetone[5] where very small amounts of oxygen were very effective in removing the triplet state. It is possible that the major part of CO_2 and C_2H_4 originated *via* singlet state and that is why they are not quenched completely. However, it has been indicated that the diagnostic test of triplet by the use of oxygen is not effective in every case.[6]

The existence of diradicals in the present system cannot be ignored and requires some comment. It is possible that the initial act of a photon in this system might lead to the formation of diradicals such as $\dot{C}H_2\text{-}CH_2\text{-}O\text{-}CH_2\text{-}\dot{O}$ (I) and/or $\dot{O}\text{-}CH_2\text{-}CH_2\text{-}O\text{-}\dot{C}H_2$ (II) and these could decompose to yield observed products or re-form the starting compound. Since the C–O bond in 1,3-dioxolane is of the order of 75–80 kcal/mole[7] and since the radiation absorbed corresponds to 144 kcal/mole or greater, the diradical formed will be highly energetic and might decompose to give the observed products. The temperature dependence of the product yield (Figure 4) indicates that the decomposition of diradical I into C_2H_4, CO_2, and H_2 (and/or 2H) was favored by higher temperatures whereas the breakdown of diradical II into CH_2O, CO, CH_3, and H atom was almost independent of temperature in spite of the fact that in both cases the rupture of C–O bond(s) was essential. Owing to the polychromatic nature of the light source, photons with varying amounts of energies are absorbed in the system. Thus, it is possible that the diradicals I and II, formed by primary process, have different lifetimes and consequently behave differently with increasing temperature. Since quantum yields are not measured, it was virtually impossible to ascertain as to what extent these diradicals re-formed 1,3-dioxolane. Finally the formation of *n*-butane in this system could be explained as the result of the reaction of ethyl radicals which were formed by addition of H atom to ethylene

---

(4) B. C. Roquitte, *J. Phys. Chem.*, **70**, 2699 (1966).

(5) G. W. Luckey and W. A. Noyes, Jr., *J. Chem. Phys.*, **19**, 227 (1951); J. Heicklen, *J. Am. Chem. Soc.*, **81**, 3863 (1959).

(6) D. W. Setser, D. W. Placzek, *et al.*, *Can. J. Chem.*, **40**, 2179 (1962).

(7) P. Gray and A. Williams, *Chem. Rev.*, **59**, 239 (1959).

linking but enhance both primary main chain scission and secondary cleavage of scission fragments. The proportion of linear dimer produced on irradiation of solid *n*-heptadecane (4%) exceeds that for solid *n*-hexadecane (1%).[2] Differences in end linking are a consequence of variations in the environment of chain ends in the two crystalline modifications. Iodoheptadecane yields from scavenged radiolyses of *n*-heptadecane are lower than corresponding products from *n*-hexadecane, particularly for solid-state irradiation.

Infrared Spectra of Some Alkaline Earth Halides by the Matrix Isolation Technique

by Alan Snelson

IIT Research Institute, Chicago, Illinois 60616 *(Received February 28, 1966)*

The infrared spectra of beryllium fluoride, beryllium chloride, magnesium fluoride, calcium fluoride, strontium fluoride, and barium fluoride were observed in matrices of neon, argon, and krypton over the wavelength region 2.5 to 50 μ. For beryllium fluoride and magnesium fluoride the asymmetric stretching and the bending frequencies were observed, while for beryllium chloride the asymmetric stretching mode only was observed. These molecules are assigned a linear configuration. There is a discrepancy between the experimentally determined entropy of magnesium fluoride and that calculated using the new frequency assignment. For each of the remaining fluorides of calcium, strontium, and barium, the symmetric and asymmetric stretching modes were observed. These molecules are assigned a nonlinear configuration.

Introduction

At the present time there is considerable uncertainty concerning molecular configurations and spectroscopic constants of many inorganic dihalide gas-phase species existing at high temperature. This uncertainty largely reflects the experimental difficulties in determining these parameters for high-temperature systems.

Brewer, *et al.*,[1] reviewed the existing data on internuclear distances, vibrational frequencies, and molecular geometries of the inorganic dihalides. The paucity of experimental data is such that of the 72 compounds considered, a complete vibrational assignment was available for 3, a partial vibrational assignment for 16, and estimated values only for the remainder.

Several experimental studies on group II dihalides indicate that some of the molecular parameters in Brewer's tabulation may be in error. Hildenbrand and Theard[2,3] used vapor pressure and mass spectrographic data to determine the gaseous entropies of all the alkaline earth difluorides and some of the chlorides. In all cases the experimentally determined entropies were larger than those tabulated by Brewer. In some cases the discrepancy was of the order of 5 to 6 eu. Hildenbrand[2] suggested that the values assigned to the vibrational constants of the molecules, together

---

(1) L. Brewer, G. R. Somayajula, and E. Brackett, *Chem. Rev.*, **111**, 63 (1963).

(2) D. L. Hildenbrand, Aeronutronic Report No. U-3183, June 30, 1965.

(3) D. L. Hildenbrand and L. P. Theard, *J. Chem. Phys.*, **42**, 3230 (1965).

with the possibility that some of them might not be linear, was the most likely source of this difference.

Brewer assumed a linear structure for most of the dihalides, largely on the basis of electron diffraction work by Akishin and Spiridonov.[4] Klemperer,[5,6] however, in experiments using the deflection of molecular beams by inhomogeneous electric fields to determine the geometry of the gaseous alkaline earth dihalides, obtained results indicating that beryllium fluoride and magnesium fluoride are linear and that calcium fluoride, strontium fluoride, and barium fluoride are bent. The apex angle, though not determined explicitly, increased in the order barium > strontium > calcium. These results conflict with those of the electron diffraction experiments on the same molecules, but Klemperer[5] noted that the precision of Akishin and Spiridonov's measurements does not preclude a bent structure for at least some of the molecules.

In an attempt to clarify the present confusion over the molecular geometries and the spectroscopic constants of the alkaline earth dihalides, the infrared spectra of these molecules were investigated by the matrix isolation technique. The infrared spectra of the following molecules were examined: beryllium fluoride, beryllium chloride, magnesium fluoride, calcium fluoride, strontium fluoride, and barium fluoride.

Procedures

A matrix isolation cryostat of conventional design was used in conjunction with an inductively heated high-temperature molecular-beam furnace. The refrigerant was liquid helium. The Knudsen cells were cylindrical, 0.75 in. long and 0.75 in. in diameter, and were made of graphite, platinum, or nickel. For double-oven experiments, a graphite tube 0.5 in. in diameter was used. Diffusion barriers were screwed into the tube to form two compartments, one to contain the sample and the other to superheat the vapor. Only the superheated region of the tube was heated directly. The sample compartment was heated by thermal conduction along the tube. By varying the position of the sample compartment with respect to the heated zone, the degree of superheating could be easily changed.

The matrix gases, neon, argon, and krypton, were research grade supplied by the Matheson Co. and were used without further treatment.

Perkin-Elmer spectrometers were used to record the infrared spectra. The spectral region from 4000 to 200 cm^{-1} was examined. A 521 double-beam spectrophotometer was used for the region 4000 to 250 cm^{-1} and a 112 single-beam spectrophotometer equipped with cesium iodide optics for the region 250 to 200 cm^{-1}. After experiments each instrument was calibrated against atmospheric water and carbon dioxide bands.

The matrix isolation technique has been fully described previously.[7,8] It was used essentially unchanged in this study with one exception: the matrix was not annealed after deposition. Instead, the concentration of the active species in the matrix was varied on deposition. As previous studies[8] have shown, both procedures produce similar effects.

The ratio M/H, where M is the number of moles of matrix gas condensed on the window and H is the number of moles of trapped species in the matrix, was calculated as described in an earlier paper.[8] The matrix was usually deposited over a period of 60 min at a rate of approximately 5×10^{-8} mole of halide/min and 2×10^{-4} to 5×10^{-5} mole of matrix gas/min. Although the deposition rates of both the halide and the matrix gas were varied by a factor of 10, the spectra did not differ noticeably.[9]

Table I lists the source of the alkaline earth halides, the type of Knudsen cell materials, and the experimental effusion temperatures. At the lowest and the highest effusion temperature, the main features of the spectra were unchanged regardless of sample origin or Knudsen cell material. Accordingly, the spectra were assumed to be those of the alkaline halides only, not those of sample impurities or of species formed by interaction of the sample with its container.

Results and Discussion

Two factors affect all halide spectra: varying the M/H ratio and superheating the vapor. These factors were examined in order to facilitate the assignment of absorption bands to specific molecular species.

As an example, Figure 1 shows the calcium fluoride spectra obtained under three different sets of conditions in an argon matrix. Figure 1A, the spectrum of calcium fluoride deposited at its saturated vapor pressure under conditions of good isolation, exhibits one strong absorption band, at 561 cm^{-1}, and three much weaker bands at 528, 489, and 370 cm^{-1}. Figure 1B, the spectrum of the vapor deposited in a matrix, the dilution reduced by about one-third, shows little, if any, change in the relative intensity of the bands at 561 and

---

[4] P. A. Akishin and V. P. Spiridonov, *Kristallografiya*, **2**, 475 (1957).

[5] L. Wharton, R. A. Berg, and W. Klemperer, *J. Chem. Phys.*, **39**, 2023 (1963).

[6] A. Buchler, J. L. Stauffer, and W. Klemperer, *J. Am. Chem. Soc.*, **86**, 4544 (1964).

[7] M. J. Linevsky, *J. Chem. Phys.*, **25**, 224 (1961).

[8] A. Snelson and K. S. Pitzer, *J. Phys. Chem.*, **67**, 882 (1963).

[9] G. E. Levoi, G. L. Ewing, and G. C. Pimentel, *J. Chem. Phys.*, **40**, 2298 (1964).

Table I: Materials and Effusion Conditions

Compound	Source of compound	Knudsen cell material	Effusion temp, °C
BeF_2	A. D. Mackay	Nickel or platinum	600 1000
$BeCl_2$	A. D. Mackay	Nickel or platinum	500 1000
MgF_2	Nassau Chemical Works, optical grade Baker and Adamson, reagent grade	Platinum or graphite	1300
CaF_2	Baker and Adamson, reagent grade Harshaw Chemical Co., optical grade $C^{44}F_2$ prepared by treating $Ca^{44}CO_3$, enriched 79% with Ca^{44}, with HF acid	Platinum or graphite	1400 1900
SrF_2	Baker and Adamson, reagent grade	Graphite	1350
BaF_2	Baker and Adamson, reagent grade Harshaw Chemical Co., optical grade	Platinum or graphite	1200 1850

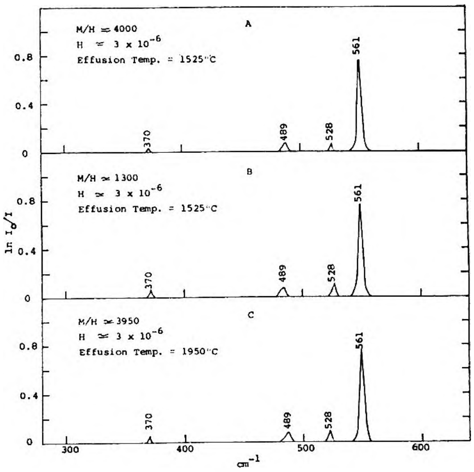

Figure 1. Infrared spectra of CaF_2 in an argon matrix.

489 cm^{-1} but a noticeable increase in the intensity of the bands at 528 and 370 cm^{-1}. Figure 1C, the spectrum of the vapor superheated at about 1950° and deposited in a matrix of the same dilution as that in Figure 1A, shows the same relative intensity of the bands at 561 and 489 cm^{-1} but, compared to Figure 1A, an enhanced intensity of the bands at 528 and 370 cm^{-1}.

Measurements of the relative absorption intensity of the peaks at 561 and 489 cm^{-1} under the three different sets of conditions were constant to within ±10%. This is about the estimated precision of the measurements; the large differences in absorption intensity of the two bands makes precise measurement difficult. The results suggest that these two bands may originate from the same molecule. Further, since the band at 561 cm^{-1} is the most intense band under all conditions, it is assigned to monomeric calcium fluoride.

The variation in intensity of the bands at 370 and 528 cm^{-1} with matrix dilution indicates that these bands can be assigned to polymeric or agglomerate species since their absorption intensity increases under conditions of poor isolation. At M/H ratios <500 these two peaks appeared at about 30% of the intensity of the absorption band at 561 cm^{-1}, while under the best isolation conditions the same figure was only about 9%. Mass spectrographic studies[10] have shown that the amount of polymeric species present in the high-temperature vapor of calcium fluoride is negligible. Hence the presence of peaks at 370 and 528 cm^{-1} suggests that if this is polymeric or agglomerate material it must be formed during deposition of the matrix. Presumably the finite time required to trap the high-temperature species effectively in the inert gas host lattice permits diffusion of the fluoride species and resultant interaction. Support for this idea is obtained from the experiments in which the unsaturated vapor is superheated. If the absorption bands at 370 and 528 cm^{-1} were due to polymeric material vaporizing from the sample, the superheating treatment could be expected to reduce the concentration of such species. In Figure 1C the absorption intensity of the bands at 370 and 528 cm^{-1} actually increases slightly over the corresponding peaks in Figure 1A, even though the matrix dilution is approximately the same for both. Therefore these absorption bands cannot be ascribed to a polymeric species vaporizing for the sample. Rather, they are the result of agglomeration during the trapping of the species. The higher temperature due to superheating requires a longer time for effective trapping of the fluoride molecules in the inert gas lattice. With the present experimental arrangement agglomeration of the high-temperature species in the inert gas matrices cannot be completely eliminated.

In contrast to calcium fluoride, the beryllium halide spectra showed a marked reduction in the intensity of some of the absorption bands on superheating the vapor, indicating the presence of vaporizing polymeric species.

---

(10) G. D. Blue, J. W. Green, R. G. Bautista, and J. L. Margrave, *J. Phys. Chem.*, **67**, 877 (1963).

Table I: Electromotive Force of the Cell: Pt; H_2 (g, 1 atm), $\underbrace{(CH_2)_2O(CH_2)_2NH_2}Cl$ (m_1), $\underbrace{(CH_2)_2O(CH_2)_2NH}$ (m_2), AgCl; Ag from 0 to 50° (in v)

m_1	m_2	0°	5°	10°	15°	20°	25°	30°	35°	40°	45°	50°
0.10082	0.04334	0.77859	0.77881	0.77878	0.77859	0.77818	0.77752	0.77686	0.77588	0.77482	0.77360	0.77218
0.09024	0.07330	0.79542	0.79593	0.79621	0.79635	0.79627	0.79599	0.79555	0.79497	0.79420	0.79332	0.79224
0.08599	0.04446	...	...	...	...	...	0.78541	...	0.78403	0.78308	0.78200	0.78062
0.07955	0.03420	0.78279	0.78309	0.78318	0.78303	0.78271	0.78218	0.78156	0.78068	0.77974	0.77857	0.77727
0.07858	0.03860	0.78622	0.78657	0.78669	0.78663	0.78637	0.78590	0.78533	0.78442	0.78353	0.78240	0.78114
0.07271	0.03760	...	...	...	...	...	0.78876	...	0.78750	0.78661	0.78555	0.78432
0.06962	0.05655	0.80000	0.80068	0.80105	0.80127	0.80130	0.80102	0.80081	...	...	...	...
0.06542	0.03213	0.78943	0.78990	0.79007	0.79011	0.78995	0.78956	0.78904	0.78825	0.78736	0.78635	0.78508
0.05966	0.02565	0.78800	0.78842	0.78852	0.78855	0.78829	0.78787	0.78736	0.78654	0.78554	0.78444	0.78319
0.05513	0.02851	...	...	...	...	...	0.79441	...	0.79323	0.79251	0.79145	0.79035
0.05066	0.02488	0.79424	0.79479	0.79509	0.79523	0.79515	0.79484	0.79437	0.79368	0.79290	0.79178	0.79057
0.04989	0.04053	0.80628	0.80715	0.80772	0.80806	0.80821	0.80814	0.80798	0.80757	0.80704	0.80632	0.80544
0.03965	0.017047	0.79581	0.79637	0.79674	0.79687	0.79683	0.79656	0.79623	0.79562	0.79489	0.79397	0.79290
0.03475	0.017968	...	...	...	...	...	0.80409	...	0.80341	0.80284	0.80204	0.80111
0.02905	0.014267	0.80511	0.80585	0.80626	0.80655	0.80667	0.80658	0.80639	0.80585	0.80529	0.80450	0.80359
0.02068	0.008890	0.80875	0.80954	0.81014	0.81052	0.81069	0.81070	0.81047	0.81012	0.80958	0.80887	0.80808
0.017231	0.008910	...	...	...	...	...	0.81940	...	0.81911	0.81873	0.81822	0.81752
0.014732	0.007236	0.81861	0.81962	0.82031	0.82091	0.82129	0.82141	0.82147	0.82114	0.82077	0.82026	0.81961
0.009693	0.007873	0.83949	0.84087	0.84202	0.84295	0.84369	0.84418	0.84460	0.84475	0.84477	0.84459	0.84426

Table II: Values of pK_a from 0 to 50°

t, °C	pK_a (exptl)	pK_a (calcd)[a]
0	9.108	9.108
5	8.978	8.977
10	8.850	8.851
15	8.727	8.728
20	8.608	8.608
25	8.492	8.492
30	8.380	8.379
35	8.268	8.269
40	8.161	8.161
45	8.056	8.057
50	7.955	7.955

[a] $pK_a = 1663.29/T + 4.1724 - 0.0042239T$.

Table III

	pK_a	$\Delta H°$, joules mole^{-1}	$\Delta S°$, joules deg^{-1} mole^{-1}	$\Delta C_p°$, joules deg^{-1} mole^{-1}
Morpholinium	8.492	39,030	−31.7	48
Piperidinium	11.123	53,390	−33.9	88
Pyrrolidinium	11.305	54,470	−33.7	68

there are marked differences both in pK_a and in the enthalpy change. Thus, not only is there a large difference (2.813) in pK_a between morpholinium ion and pyrrolidinium ion at 25° but the difference changes with temperature in a manner consistent with the differences in the other thermodynamic quantities. The pK_a values of morpholinium ion decrease with increased temperature less rapidly than do those of pyrrolidinium ion. Thus the difference in pK_a is only 2.601 at 50°.

While mixtures of morpholine and morpholinium hydrochloride are not proposed as pH standards, they may have some uses in biochemical work when a medium of controlled pH is needed. We have, therefore, interpolated in Table I to obtain values of p($a_H\gamma_{Cl}$) ($\equiv -\log a_{H^+}\gamma_{Cl^-}$) and have derived the corre-

Table IV: Values of p($a_H\gamma_{Cl}$) and pa_H for a Buffer Solution Composed of Morpholine Hydrochloride (0.1 m) and Morpholine (0.05 m) from 0 to 50°

t, °C	p($a_H\gamma_{Cl}$)	pa_H
0	9.068	8.963
5	8.934	8.828
10	8.809	8.702
15	8.687	8.579
20	8.567	8.458
25	8.453	8.343
30	8.341	8.231
35	8.231	8.120
40	8.125	8.013
45	8.021	7.908
50	7.921	7.806

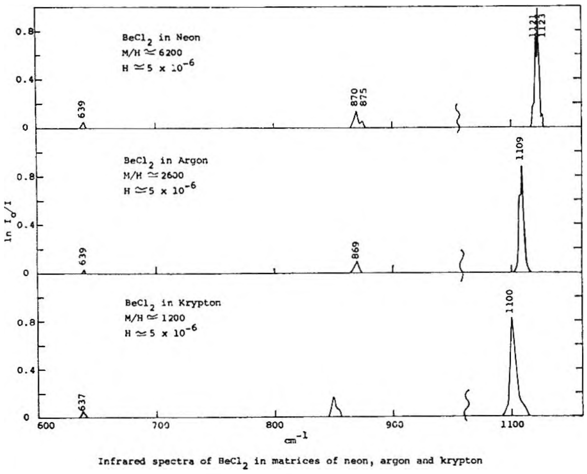

Figure 3. Infrared spectra of $BeCl_2$ in matrices of neon, argon, and krypton.

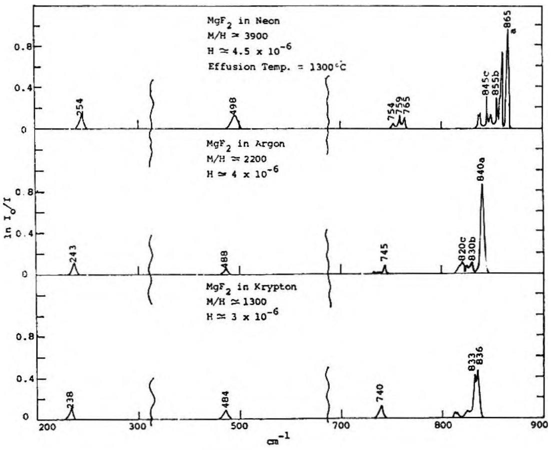

Figure 4. Infrared spectra of MgF_2 in matrices of neon, argon, and krypton.

cm^{-1} in the matrix study correspond to the band observed at 825 cm^{-1} in the gas-phase study.

That a weak absorption band at 1250 cm^{-1} was observed in the matrix spectra but not in the gas-phase study is difficult to explain. Possibly the relative insensitivity of the high-temperature infrared study did not allow its detection. Evidence in favor of assigning this band and those at 790 and 825 cm^{-1} to polymeric material vaporizing from the sample came from experiments in which the vapor was superheated, since under these conditions the intensity of these bands was much reduced.

Beryllium Chloride (*Figure 3*). Only one strong absorption band appeared, at approximately 1110 cm^{-1}. Weaker bands at 870 and 640 cm^{-1} were dependent on the M/H ratio and the degree of vapor superheating. This latter dependence would indicate that these bands are due to polymeric material vaporizing from the sample.

The frequency at 1110 cm^{-1} was assigned to ν_3 of beryllium chloride assuming a linear configuration. This value is in good agreement with the 1113 cm^{-1} reported by Buchler and Klemperer[14] in their high-temperature gas-phase study. The bands at 870 and 640 cm^{-1} probably correspond to the 856- and 608-cm^{-1} bands reported by Buchler and Klemperer.[14] They assigned these bands to dimeric beryllium chloride.

They observed an additional band, at 482 cm^{-1}, which was assigned to ν_2. From the matrix spectra and the thermodynamic arguments to be given later, it is believed the previous assignment of the bending frequency at 482 cm^{-1} is in error. It is difficult to account for the presence of this absorption band in the gas-phase spectra but not in the matrix spectra. Both studies indicate it is not a polymeric species. The only alternative is to postulate an impurity in the halide sample used in the high-temperature study, possibly an oxy or hydroxy chloride of beryllium.

Magnesium Fluoride (*Figure 4*). Bands at approximately 850 and 250 cm^{-1} were present in all spectra, their relative intensities being insensitive to the M/H ratio or to the degree of vapor superheating. They were assigned to ν_3 and ν_2, respectively, of magnesium fluoride with a linear configuration.

Since there have been no other infrared studies on this molecule, comparison with other frequency assignments is not possible. Some support for a linear assignment is obtained from the magnitude of the frequency shifts of magnesium fluoride containing the three isotopes Mg^{24}, Mg^{25}, and Mg^{26}. The approximate natural abundance is 79, 10, and 11%, respectively. The calculated values for $\nu_3(Mg^{24}F_2)/\nu_3(M^{25}F_2)$ and $\nu_3(Mg^{24}F_2)/\nu_3(Mg^{26}F_2)$ are 1.0124 and 1.0245, respectively. The corresponding experimental values for the same ratios, obtained from the frequencies appearing in the neon and the argon spectra, for the peaks labeled a, b, and c in Figure 4, were 1.012 and 1.023, respectively. These are in excellent agreement with the calculated values within the precision of the experimental measurement of ±1 cm^{-1}.

It was not possible to obtain the isotope shift for the band assigned to the bending frequency at 250 cm^{-1}. The poor sensitivity of the spectrometer in this wavelength region precluded measurement of closely spaced relatively weak absorption maxima.

The bands at approximately 750 and 490 cm^{-1} were assigned to polymeric or agglomerate material since their absorption intensity showed considerable dependence on matrix dilution. Mass spectroscopic studies[15] of magnesium fluoride indicated that the dimer is present at less than 1 mole % in the vapor phase.

Calcium Fluoride (*Figure 5*). The details of the calcium fluoride spectra in an argon matrix were discussed earlier in this paper. The results for $Ca^{44}F_2$ and $Ca^{40}F_2$ of about 98% isotopic purity, shown in Figure 5, in no way alter those conclusions. The two weaker absorption bands in the neon matrix, at 547 and 377 cm^{-1}, and the corresponding peaks in the other matrices were assigned to agglomerate or polymeric material. The strong absorption maximum, at approximately 567 cm^{-1} ($Ca^{44}F_2$), is assigned to ν_3 of monomeric calcium fluoride. If a linear configuration is assumed, the calculated isotope ratio $\nu_3(Ca^{40}F_2)/\nu_3(Ca^{44}F_2)$ is 1.023, which agrees fairly well with the values of 1.019, 1.020, and 1.021 obtained in the different matrices.

An assignment for the remaining absorption bands, at 504 cm^{-1} ($Ca^{40}F_2$) and 502 cm^{-1} ($Ca^{44}F_2$) in the neon matrix, and of the corresponding bands in the other matrices, is less certain. Earlier it was noted that the relative intensity of this band and that assigned to ν_3 of calcium fluoride showed no significant change under different experimental conditions and that the two peaks might be assigned to the same molecular species. If this conclusion is correct, it may be inferred that calcium fluoride has a nonlinear configuration, the band at about 500 cm^{-1} corresponding to ν_1. It is observed that this frequency of the four bands in the calcium fluoride spectra is the least sensitive to isotopic substitution of the calcium atom. In a linear molecule the totally symmetric stretching mode is independent of isotopic substitution of the central metal atom in the absence of interactions between ν_1 and ν_2. In the present case ν_2 is considerably lower than ν_1, and these modes are expected to be nearly separable. Making this approximation it may be shown that an angle of about 145° would result in the observed frequency shift of about 2 cm^{-1} for ν_1. That the observed values of the isotope ratio $\nu_3(Ca^{40}F_2)/\nu_3(Ca^{44}F_2)$ are all lower than the calculated value by a margin slightly larger than can be accounted for by experimental error lends support to a nonlinear configuration.

Alternatively, the apparent constancy in the relative intensity measurements of these two peaks may be misleading. In this event, the weaker absorption band would be assigned to polymeric or agglomerate material.

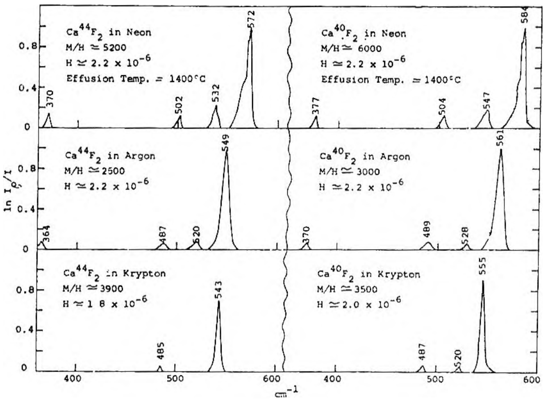

Figure 5. Infrared spectra of $Ca^{40}F_2$ and $Ca^{44}F_2$ in matrices of neon, argon, and krypton.

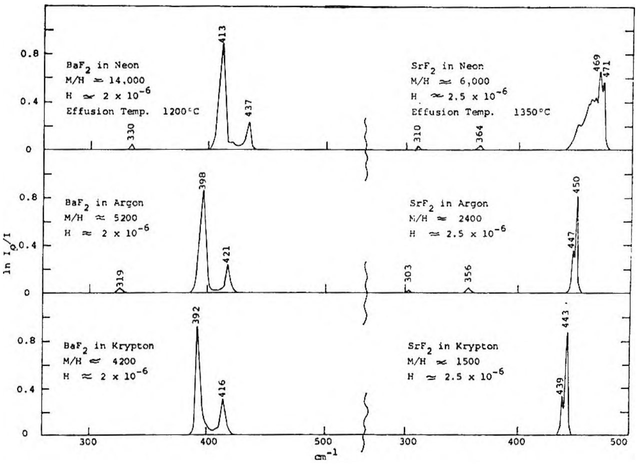

Figure 6. Infrared spectra of SrF_2 and BaF_2 in matrices of neon, argon, and krypton.

Strontium Fluoride (*Figure 6*). The peak intensities, at about 360 and 305 cm^{-1}, were strongly dependent on matrix dilution. In the krypton matrix the peaks could be eliminated completely. They were assigned to polymeric or agglomerate species.

The absorption band at about 450 cm^{-1} is split into a doublet in all the matrices, the maxima being separated by about 3 cm^{-1}. In the argon and krypton matrices the stronger feature had the higher frequency, whereas in the neon matrix this situation was reversed. However, in the neon matrix the entire absorption band envelope was much broader, and hence the true relative intensity of the two bands could not be resolved.

Two assignments for these absorption bands are possible. (1) The appearance of two maxima in the absorption band envelope is due to matrix effects. It is not uncommon in matrix experiments to have a single absorption band split into several closely spaced maxima. The small energy separation of 3 cm^{-1}

---

[15] J. Berkowitz and J. Marquardt, *J. Chem. Phys.*, **37**, 1853 (1962).

observed for the band makes this a distinct possibility and in this event assignment of the band to ν_3, the asymmetric stretching mode, is entirely feasible. (2) The two absorption maxima represent different fundamental frequencies, the lower being assigned to the symmetric stretching mode, ν_1, of strontium fluoride assuming a bent configuration and the higher, more intense frequency (argon and krypton matrices) to the asymmetric stretching mode, ν_3.

Because of the proximity of the two maxima it was not possible to make reliable intensity measurements to give more weight to the latter assignment, but comparison of these spectra with those of calcium fluoride and barium fluoride indicates that strontium fluoride is probably nonlinear.

Barium Fluoride (*Figure 6*). With the exception of the weak absorption at about 325 cm^{-1}, appearing only in the neon and the argon matrices, the other bands, at approximately 400 and 425 cm^{-1}, showed no intensity dependence on the M/H ratio or the degree of superheating of the vapor. The weak absorption feature was assigned to polymeric or agglomerate material.

There is little doubt the bands at 400 and 425 cm^{-1} represent two fundamental frequencies of barium fluoride since in each matrix the bands had the same well-defined form. If the two maxima were due to matrix splitting of a single frequency, the bands might be expected to take different forms in the three matrices. The absorption maximum at 400 cm^{-1} was assigned to ν_3 since this mode would be expected to have the greater absorption intensity, while the band at 425 cm^{-1} was assigned to ν_1, the molecule having a nonlinear configuration.

Molecular Geometries

In the preceding discussion, the magnitude of the frequency shift caused by isotopic substitution of the central metal atom was used to infer molecular geometries for some of the alkaline earth halides. The experimental isotopic frequency ratio was compared with that calculated from the well-known expression[12]

$$\frac{(\nu_3^{\mathrm{i}})^2}{\nu_3} = \frac{M_{\mathrm{m}}(M_{\mathrm{m}}^{\mathrm{i}} + 2M_{\mathrm{F}} \sin^2 \theta/2)}{M_{\mathrm{m}}^{\mathrm{i}}(M_{\mathrm{m}} + 2M_{\mathrm{F}} \sin^2 \theta/2)}$$

where the superscript i and the subscripts m and F denote isotope, alkaline earth metal, and fluorine, respectively, and θ refers to the apex angle.

Unfortunately, the magnitude of the frequency shift is not a very sensitive function of the apex angle. As an illustration, in Table II the calculated values of $\nu_3(\mathrm{Ca^{40}F_2})$ are given as a function of θ based on a value of $\nu_3(\mathrm{Ca^{44}F_2})$ = 550 cm^{-1}. It is immediately apparent that frequency measurements must be accurate to at least 0.1 cm^{-1} if a reliable decision is to be made concerning the molecular geometry of a bent molecule on the basis of such measurements. In this investigation the frequency measurements were accurate to ±1 cm^{-1}, resulting in a precision of only ±30° in the calculated apex angle for calcium fluoride and magnesium fluoride.

Table II: Frequency Difference between Isotopes of Calcium Fluoride as a Function of Apex Angle Based on $\mathrm{Ca^{44}F_2}$ = 550 cm^{-1}

θ	$\gamma_3(\mathrm{Ca^{40}F_2})$	$\Delta\upsilon$ = $\gamma_3(\mathrm{Ca^{40}F_2})$ − $\gamma_3(\mathrm{Ca^{44}F_2})$
180	562.6	12.6
160	562.4	12.4
120	560.7	10.7
80	557.2	7.2

The other criterion that can be used to distinguish the linearity or nonlinearity of the alkaline earth fluorides is the number of infrared-active frequencies. Since two frequencies of appropriate order of magnitude for ν_1 and ν_3 in a nonlinear molecule can be assigned to calcium, strontium, and barium fluorides from their spectra, nonlinearity for these molecules is inferred. Further support for this assignment would be available if the bending frequencies of all these molecules had been observed, but because of instrument limitations this was not possible.

Two frequencies are assigned to beryllium fluoride and magnesium fluoride. Their magnitude is such that they are undoubtedly the unsymmetrical stretching and the bending modes, ν_3 and ν_2, respectively. No absorption band was observed that could be assigned to ν_1, the symmetrical stretching mode, which would be infrared active if the molecule were bent. This might be taken as evidence that these molecules are linear. However, as noted previously, in a slightly bent molecule the ν_1 absorption intensity might be very weak and escape observation. Attempts were made to find an absorption band assignable to ν_1 by observing the spectra of large samples, but no absorption features that could be interpreted in this way were found.

On the basis of the spectral measurements it is concluded that the most probable molecular configurations for the halides investigated are: beryllium fluoride, beryllium chloride, and magnesium fluoride, linear; calcium fluoride, strontium fluoride, and barium fluoride, nonlinear.

Table III: Frequencies of the Group II-a Halides

	BeF_2		$BeCl_2$	MgF_2		CaF_2		SrF_2		BaF_2		LiF	AlF
	ν_2	ν_3	ν_3	ν_2	ν_3	ν_1	ν_3	ν_1	ν_3	ν_1	ν_3	ν	υ
	Observed Matrix Frequencies (cm^{-1})												
Neon	330	1542	1122	254	862	504	581	468	471	437	413	868	785
Argon	309	1528	1108	243	840	489	561	447	450	421	398	835	774
Krypton	302	1524	1100	238	834	487	555	439	443	416	392	820	768
	Differences in Frequencies												
Δv^{NA}	21	24	14	11	22	15	23	21	21	16	15	33	11
Δv^{AK}	7	4	8	5	6	2	6	8	7	5	6	15	6
	Corrected Frequencies												
	345	1555	1135	270	875	520	595	485	490	450	430	890[a]	798[a]

[a] Experimentally observed gas-phase frequencies.

Matrix Effects

Most of the absorption bands exhibited splitting, due to the matrix environment.[8] In beryllium fluoride and magnesium fluoride it was particularly pronounced. Since this splitting was present under all conditions of matrix dilution, it is attributed to the trapped species occupying more than one site in the matrix lattice.

More troublesome than the splitting of an absorption band is the effect of the matrix environment on the frequency of a given vibration. Depending on the particular matrix, the band center is shifted from the true gas-phase value to some other frequency. This effect is well illustrated in Table III, in which the observed frequencies of the alkaline earth halides are tabulated together with the frequency shifts, Δv, between the neon and argon and the argon and krypton matrices. In all the halides Δv^{NA} is greater than Δv^{AK}. Δv^{NA} ranges from about 1.6- to $6\Delta v^{AK}$. In all cases the shift is toward lower frequencies, in going from the neon to argon and the argon to krypton matrices. The behavior is paralleled by lithium monofluoride[16] and aluminum monofluoride; in these compounds Δv^{NA} lies between 1.8- and $2.2\Delta v^{AK}$.

The frequency shift due to the matrix environment could not be calculated directly because the necessary data are not available. Instead, an empirical approach was used to estimate the gas-phase frequencies from the matrix spectra, the frequency shifts of some monofluorides being used for comparison. The infrared gas and matrix spectra of lithium monofluoride and aluminum monofluoride are accurately known. The frequency shift from the gas-phase value in the neon matrix is about -22 and -13 cm^{-1}, respectively, for the two compounds. The alkaline earth halides are probably largely ionic compounds, and in this respect they resemble lithium monofluoride and aluminum monofluoride. The former is completely ionic and the latter largely ionic.[17] In view of the similarities of these compounds, it is suggested that the neon matrix frequencies of the alkaline earth halides be increased by 15 cm^{-1} in order to give a more realistic gas-phase frequency assignment.

Table III lists the frequencies corrected and rounded off to the nearest 5 cm^{-1} together with assignments to specific vibrational modes. An error limit for the adjusted frequencies is difficult to estimate, but a value of ± 10 cm^{-1} is probably good.

Force Constants and Thermodynamic Considerations

Since it was not possible to observe all the fundamental frequencies of any of the alkaline earth fluorides examined, a detailed force constant analysis is not possible. For beryllium fluoride and magnesium fluoride, however, the simple valence force-field method was applied.[12] Table IV gives the results of such a calculation. The symmetric bending frequency, ν_2, of beryllium chloride was calculated on the assumption that the ratio of the bond-stretching to bond-bending force constant, $k_1/(k/l^2)$, of beryllium fluoride is the same for beryllium chloride.[1] Table IV also lists the experimentally determined entropies as well as those calculated by using standard statistical methods and the new vibration frequency assignments. In this calculation, a ground-state quantum weight of unity was assumed and the bond distances listed in the

---

[16] To be published.

[17] D. R. Lide, National Bureau of Standards, Annual Report, No. 8504, U. S. Government Printing Office, Washington, D. C., 1964, p 57.

JANAF[18] thermochemical tables were used. The experimentally determined entropies of Hildenbrand[19] were used and are believed to be accurate to ±2.0 eu.

Table IV: Force Constants of Some Alkaline Earth Halides[a]

Halide	Cm^{-1}			10^5 dynes/cm		cal/°K mole		Temp, °K
	ν_1	ν_2	ν_3	k_1	k/l^2	S_{calcd}	S_{obsd}	
BeF_2	(680)	345	1555	5.15	0.12	68.3	69.0	880
$BeCl_2$	(380)	(240)	1135	3.28	0.08	66.7	69.2	500
MgF_2	(540)	270	875	3.00	0.07	78.8	82.4	1400

[a] The values in parentheses were calculated.

The observed and the calculated entropies of beryllium fluoride[11] are in good agreement, well within the experimental error of both sets of measurements. The molecular constants for this compound can be considered satisfactory.

The disagreement between the observed and the calculated entropies of beryllium chloride[11] and magnesium fluoride[2] is larger than the assigned experimental error of ±2.0 eu. In the case of beryllium chloride this is not unexpected. The calculated value of the bending frequency, ν_2, is obviously in error since no absorption band corresponding to this frequency was observed in the experimental determination, which extended to 200 cm^{-1}. When the observed entropy was used to derive the bending frequency of beryllium chloride, a value of about 150 cm^{-1} was obtained. The error limits on this value are large, of the order of ±40 cm^{-1}. The difference of ±3.6 eu between the observed[20] and the calculated entropies of magnesium fluoride is difficult to explain if the observed value is assumed to be correct.

There are two possibilities. (1) The calculated value of ν_1 is too large. This implies that the simple two potential constant valence force-field approximation is not adequate for this molecule. A large value of ν_1 would result in the calculated entropy being too low. To bring the calculated entropy to within the range of the experimental determination, ν_1 would have to be about 270 cm^{-1}, or half the value calculated using the two-force constants potential function. (2) The discrepancy between the observed and the calculated entropy could be eliminated if the calculated entropy of magnesium fluoride were based on a nonlinear model with an apex angle between 160 and 170°. Such a configuration, however, would have permitted observation of ν_1. As noted earlier, this absorption band may have a very low absorption intensity, which might account for its not being observed experimentally. From the available data it is not possible to favor one of these alternatives more than the other.

Calculation of the force constants in the remaining fluorides, of calcium, strontium, and barium, was not possible because the apex angle could not be determined with sufficient accuracy and the bending frequencies were not observed.

Conclusions

Although the results of this study were not as conclusive as anticipated, the following points were established.

(1) The new frequency assignment for beryllium fluoride is in excellent agreement with recently determined thermodynamic data for this compound.

(2) The frequency of the bending mode of beryllium chloride, though not observed experimentally, is considerably lower than the previously assigned value[14] of 482 cm^{-1}. On thermodynamic grounds this frequency is estimated to be 150 ± 40 cm^{-1}.

(3) Infrared and electric deflection experiments predict a linear configuration for beryllium fluoride and beryllium chloride, in agreement with the results of this investigation.

(4) The new frequency assignment for magnesium fluoride is not consistent with existing thermodynamic data. The reason for this discrepancy has been discussed, and it is possible the molecule may be nonlinear. This conflicts with the findings of Klemperer,[14] who assigned a linear structure to this molecule from electron-deflection experiments. However, for a slightly bent molecule the resultant dipole moment may be too small to allow detection in the electron-deflection experiments; hence, a nonlinear structure for this compound cannot be entirely eliminated on the basis of these experiments.

(5) The spectrum of barium fluoride can only be satisfactorily interpreted in terms of a molecule with a bent configuration. The arguments in favor of a similar structure for calcium and strontium fluoride from their spectra are less rigorous, but taken in conjunction with the findings of Klemperer[14] do not appear unreasonable.

(6) With the exception of beryllium fluoride and magnesium fluoride, the bending frequencies of group II-a halides may be expected to lie below 200 cm^{-1}. Tabulated thermodynamic functions for these com-

---

(18) "JANAF Thermochemical Tables," The Dow Chemical Co., Midland, Mich.

(19) D. L. Hildenbrand, Aeronutronic Report No. U-1606, 1965.

(20) J. Berkowitz and J. Marquardt, *J. Chem. Phys.*, **37**, 1853 (1962).

Waals forces between ions or between ions and solvent molecules, these should cause marked changes in the parameters of the equation since these forces are not directly related to the dielectric constant and the viscosity.

Experimental Section

Tetra-*n*-butylammonium fluoroborate was prepared by titrating a methanolic solution of tetrabutylammonium hydroxide with an aqueous solution of fluoroboric acid. The salt was recrystallized three times from 1:1 methanol–water mixtures and dried at 70° under vacuum to constant weight. The melting point was 161°. Fluorine analyses yielded 22.99 and 22.86% compared to the theoretical 23.08%.

The phenylacetonitrile was dried over molecular sieves and carefully fractionated. The specific conductance was less than 0.3×10^{-7} mho/cm and the refractive index was $n^{25}\text{D}$ 1.5208. The dielectric constants of the solvent were measured on a General Radio 716-C Schering bridge equipped with a 716-P4 guard circuit. To reduce the effects of the higher solvent conductances at high temperature, measurements were made at 263 kHz and checked at 100 kHz. The capacitance cell consisted of an inner high potential electrode $1^1/_8$ in. in diameter and $5^9/_{16}$ in. long which was suspended in a deep cup leaving an annulus of $^3/_{16}$ in. The cup was the grounded electrode and the top inch of it was a guard ring. All metal parts were of stainless steel and the insulation was Supramica. The capacitance cell was calibrated at 25° with nitrobenzene and ethylene dichloride whose dielectric constants are 34.82 and 10.36, respectively.[5] The nitrobenzene was purified by the method[6] used previously, yielding a specific conductance of less than 7×10^{-9} mho/cm. The Eastman Spectrograde ethylene dichloride was redistilled and had a specific conductance of much less than 2×10^{-9} mho/cm. The cell constant was 0.04213 which was independent of temperature within the precision of the measurements. The results in Table I agree with the approximate value of Grimm and Patrick[5,7] and are about 1–2% above those of Walden.[8]

The viscosities were measured under argon in Ubbelohde viscometers. The densities were measured in a Sprengle-type pycnometer on which the two arms were interconnected and the whole pycnometer was completely submerged in the thermostat. The small vapor space required a maximum correction for the vapor volume of 0.03% at 200°.

The conductance bridge, the method of calibration, and the technique for the conductance measurements were similar to those used by one of the authors previously.[6] The cells used were two erlenmeyer cells whose cell constants were 0.15591 ± 0.00002 and 2.0714 ± 0.0003 cm^{-1}. Both cells were calibrated directly with KCl. A small cell with a volume of about 20 ml was also used for the high-temperature runs and the cell constant was 2.8278 ± 0.0003. The temperatures were measured by a platinum resistance thermometer and the variation was no greater than ±0.03° at the highest temperature. All runs were performed with the solutions under an atmosphere of argon. The runs at 25 and 100° were performed by diluting the solutions in the erlenmeyer cell. The run at 75° was made in the same cell by diluting the solution successively in a flask at room temperature and then transferring a portion of the solution by a syringe to the cell. This could be done easily because the vapor pressure of the solvent at room temperature was so low that there was no significant amount of solvent lost through evaporation. This technique had to be used for the runs at 150 and 175° since decomposition was noticeable and thus a single sample could not be diluted for measurement at five different compositions. The small cell was used for these two high-temperature runs and the vapor space at equilibrium was only about 1 ml, so that no correction for the amount of solvent in the vapor space was needed. The decomposition at 150° caused a resistance change of 0.1% in 30 min and at 175° the change was 1% in the same period. For these two runs the resistance was measured only at 10 kHz since the runs at lower temperature indicated that the value extrapolated to infinite frequency differed by only about 0.01%.

Table I: Dielectric Constant of Solvent

Temp, °C	Dielectric constant
24.9	18.77
58.9	16.57
78.6	15.46
99.0	14.45
117.7	13.53
138.9	12.69
162.8	11.86
185.4	11.14
201.4	10.72

---

(5) A. A. Maryott and E. R. Smith, "Tables of Dielectric Constants of Pure Liquids," National Bureau of Standards Circular 514, U. S. Government Printing Office, Washington, D. C., 1951.

(6) J. E. Lind, Jr., and R. M. Fuoss, *J. Phys. Chem.*, **65**, 999 (1961).

(7) F. V. Grimm and W. A. Patrick, *J. Am. Chem. Soc.*, **45**, 2794 (1923).

(8) P. Walden, *Z. Physik. Chem.*, **70**, 569 (1910).

frequently differ markedly from data obtained on gaseous molecules.

The method proposed here is designed to obviate all of these objections. A linear interpolation of data is used, which is expected to be linear; the Kirkwood-Onsager equation for dielectric constants of liquids is used, and the polar solute is dissolved in a solvent of equal polarity, thus assuring more ideal behavior. As expected, there is better agreement between results in the liquid and gaseous state.

A crucial part of this new approach was the choice of a solvent whose dielectric constant may be varied to match the molar polarization of solutes. The solvent consists of mixtures of dioxane and cyclic ethylene carbonate, with variation of dielectric constant from 2.3 to about 60. These two compounds have the added advantage of having molecular weights which differ by only 0.06%, so that the molecular weight of mixtures is always constant.

Theoretical Development

The Kirkwood-Onsager equation[4]

$$P = \frac{(\epsilon - 1)(2\epsilon + 1)}{9\epsilon}\frac{M}{d} = \frac{4\pi N}{3}\alpha + \frac{g\mu^2}{3kT} = P\alpha + \frac{4\pi N g \mu^2}{9kT} = P\alpha + P\mu \quad (1)$$

is applicable to liquids since it takes into account the hindrance of rotation due to neighboring molecules. The correlation parameter g shows this hindering effect. However, the evaluation of g requires a knowledge of the structure of a liquid, which in general is not available. Consequently, the Kirkwood-Onsager equation *per se* is not in general a valid way to calculate dipole moments when applied to pure liquids.

Oster[5] has concluded, for polar solutes in nonpolar solvents, that the correlation parameter of the solute is a smooth function of mole fraction of solute and approaches the value 1 in dilute solutions.[6] We shall use such graphs of correlation parameter in the computation of dipole moments.

We choose a solvent of such dielectric constant that there is no change in the dielectric constant on adding the solute. We assume that the molar polarizations of solvent and solute are additive. For the solvent

$$P_1 = \frac{(\epsilon - 1)(2\epsilon + 1)}{9\epsilon}\frac{M_1}{d_1} \quad (2)$$

For the solution

$$P_{12} = \frac{(\epsilon - 1)(2\epsilon + 1)}{9\epsilon}\frac{M_{12}}{d_{12}} = X_1P_1 + X_2P_2 \quad (3)$$

In these equations the subscripts 1, 2, and 12 refer to solvent, solute, and solution, respectively, and X is the mole fraction. Substituting (2) into (3), remembering that $M_{12} = X_1M_1 + X_2M_2$ and rearranging, yields

$$P_2/M_2 = \frac{(\epsilon - 1)(2\epsilon + 1)}{9\epsilon d_{12}}\left(1 + \frac{X_1M_1}{X_2M_2}\frac{d_1 - d_{12}}{d_1}\right) \quad (4)$$

It will be noted that the left side of the above equation contains quantities pertaining only to the solute and the right side contains only experimentally determined quantities. By use of eq 1 we can calculate the value of the dipole moment of the solute, provided that g is known. The dipole moment of the molecule in solution is calculated from the gas value by the Onsager equation.[7]

$$\mu = \mu_0\frac{(\epsilon_\infty + 2)(2\epsilon + 1)}{3(2\epsilon + \epsilon_\infty)} \quad (5)$$

It was stated previously that a linear interpolation of data is used to obtain figures to be used in the calculations. (For details see the Experimental Section.) This graph for interpolation can be shown to be linear. For the solvent mixture

$$P_1 = \frac{(\epsilon_1 - 1)(2\epsilon_1 + 1)M_1}{9\epsilon_1 d_1} = \frac{[2\epsilon_1 - 1 - (1/\epsilon_1)]M_1}{9d_1} = \frac{2\epsilon_1 M_1}{9d_1} \quad (6)$$

or $P_1 \propto \epsilon_1$, if ϵ is fairly large. Likewise for the solution, $P_{12} \propto \epsilon_2$. However, we have assumed molar polarizations to be additive, so

$$\Delta P = P_{12} - P_1 = X_1P_1 + X_2P_2 - P_1 = P_1(X_1 - 1) + X_2P_2 \quad (7)$$

However, X_1 and X_2 are constant in any series of measurements, and X_2P_2 is constant, so ΔP is a linear function of P_1. It follows from the previous relations that $\Delta\epsilon$ is a linear function of ϵ_1.

Experimental Section

The measurement of dielectric constant was made by using a General Radio Co. Type 821-A Twin-T impedance circuit and Type 1330-A bridge oscillator, and Hallicrafters' S-85 receiver as detector. The Twin-T bridge was calibrated by the General Radio Co.

The dielectric constant cell followed the design of

---

(4) J. G. Kirkwood, *J. Chem. Phys.*, 7, 911 (1939).

(5) G. Oster, *J. Am. Chem. Soc.*, 68, 2036 (1946).

(6) The true situation is somewhat different from the conclusions of Oster. This will be the subject of a separate communication.

(7) L. Onsager, *J. Am. Chem. Soc.*, 58, 1486 (1936).

Conner, Clark, and Smyth.[8] The inner surfaces of the cell were gold plated. The cell was calibrated by use of air and pure water, dichloromethane, dioxane, 1-propanol, dimethylformamide, 1,2-dichloroethane, acetone, and methanol. A graph of dielectric constant against capacity of the cell was linear, with the point for water on the line. Subsequent checks on the calibration curve were made by merely measuring the capacity of the empty cell and that of the cell when filled with water. It was found that if the cell was left plugged into the capacity bridge connector at all times, except when in use, its capacity remained constant, within experimental error. In fact, over a period of 3 years the measured capacitance of the cell filled with water was 512.7 ± 0.2 pf.

Refractive index was measured with a Bausch and Lomb precision Abbé refractometer. Refractive indices of solid solutes, which cannot be measured directly by use of the refractometer, were calculated from refractive index and density of solutions. The Lorenz-Lorentz molar refraction of the solution was calculated and assumed to be the sum of solvent and solute, respectively. The density for solute was calculated on the assumption that molar volumes are also additive. The result is the refractive index for a hypothetical pure liquid solute at 25°. The validity of this procedure is shown in Table I. Small errors in refractive index have little effect on calculations using eq 5.

Temperature was maintained at 25 ± 0.03°.

A 10-cc hypodermic syringe was used for transferring samples in order to protect them from moisture of the air. It was especially useful for filling the pycnometer.

All materials (except ethylene carbonate) were of reagent or spectroscopic grade from Eastman or Matheson Coleman and Bell. The ethylene carbonate was recrystallized by cooling to −15° at least three times from a 1.05:1 by volume mixture of chloroform and carbon tetrachloride. (A typical crystallization used 210 ml of chloroform, 200 ml of carbon tetrachloride, and 200 ml of ethylene carbonate.) In order to prevent condensation of moisture on the cold crystals, an atmosphere of very low humidity was maintained in the Büchner funnel until the crystals came to room temperature. Excess solvent clinging to the crystals was removed in a vacuum desiccator by use of a water aspirator or by evaporation in the room if the humidity was below 30%. If the conductances of the solutions of ethylene carbonate in dioxane were too high to permit measurement of dielectric constant, then it was recrystallized until a product of suitably low conductance was obtained. It appeared that absence of moisture was the most important factor.

A solvent mixture was made up whose dielectric constant was expected to be near the correct value, and its dielectric constant, density, and refractive index were measured. (The dielectric constant of the solvent mixture is near that of the solute if the latter is liquid. Solid solutes require more experimentation to obtain solvent mixtures of suitable dielectric constant.) Then a fixed mole percentage (either 4 or 10%) of solute was added, and the measurements were repeated. The difference in dielectric constant, $\Delta\epsilon = \epsilon_{12} - \epsilon_1$, was determined. The measurements were repeated for at least two other solvent mixtures of slightly different composition, preferably including one with $\Delta\epsilon$ of opposite sign. Graphs of $\Delta\epsilon$, d_1, d_{12}, $(n^{25}\text{D})_1$, and $(n^{25}\text{D})_{12}$ against ϵ_1 were constructed, and the values of the variables were read off where $\Delta\epsilon$ is zero. This will then fit the conditions imposed in eq 4. These graphs were always linear, provided $\Delta\epsilon$ was no larger than ±0.5.

Table I: Summary of Experimental Results Obtained from Graphs of Data for Individual Compounds: 4 Mole % of Solutes

Compd	ϵ	$d^{25}{}_4$ of solvent d_1	$d^{25}{}_4$ of soln, d_{12}	$n^{25}\text{D}$ of solute
n-$C_6H_{13}Br$	6.38	1.0548	1.0611	1.4572
n-C_4H_9Br	7.28	1.0595	1.0696	1.4368
n-$C_5H_{11}Br$	7.78	1.0623	1.0703	1.4412
p-$ClC_6H_4CH_3$	7.00	1.0572	1.0572	1.5180
CH_2Cl_2	9.95	1.0732	1.0808	1.4213
p-$ClC_6H_4NO_2$	11.72	1.0864	1.0968	1.588[a]
$(C_6H_5)_2CO$	14.20	1.0928	1.0937	1.618[b]
$C_6H_5COCH_3$	17.75	1.1089	1.1042	1.5299
CH_3COCH_3	22.75	1.1279	1.1161	1.3563
CH_3NO_2	39.25	1.1859	1.1844	1.3799[c]
$C_6H_5NO_2$	38.5	1.1836	1.1846	1.5499

[a] Calculated from molar refraction, as indicated in text. [b] Calculated from molar refraction. Agrees fairly well with value of 1.605 interpolated from data for the supercooled liquid, taken from Beilstein. [c] J. Timmermans, "Physico-Chemical Constants of Pure Organic Compounds," Elsevier Publishing Co., New York, N. Y., 1950, p 578.

In practice we chose several solutes of known dipole moment (in the gaseous state) and calculated P_2/M_2. This was then plotted against the experimentally determined quantity on the right side of eq 4 called the ϵ function. These compounds of known dipole moment were used to establish an empirical test of eq 4. We may assume that the correlation parameter of the solute was essentially the same as that for the ethylene carbonate in the solvent, since the structure of the solvent is to a large extent determined by the ethylene carbon-

---

[8] W. P. Conner, R. P. Clark, and C. P. Smyth, *J. Am. Chem. Soc.*, 72, 2071 (1950).

Multipulse Potentiodynamic Studies of the Competitive Adsorption of Neutral Organic Molecules and Anions on Platinum Electrodes. I. Competitive Adsorption of Carbon Monoxide and Chloride Ions[1]

by S. Gilman

General Electric Research & Development Center, Schenectady, New York *(Received March 7, 1966)*

In the absence of Cl^- and in the potential range −0.1 to 0.6 v, the structure of the adlayer, the maximum coverage, and the experimental rate of adsorption (initially diffusion controlled) remain constant for the adsorption of CO from 1 *N* $HClO_4$ solution. In the presence of any extent of initial surface coverage with Cl^- in this potential range, the characteristics of the CO adsorption remain unchanged. Therefore, the system tends toward full coverage with CO and very small residual coverage with Cl^-. For any transient coverage with CO, there is an equilibrium coverage with Cl^- which is rapidly (probably transport limited) established by either desorption or adsorption of the ions. There is a simple linear relationship between equilibrium coverage with Cl^- and transient coverage with CO. It is possible to explain the inhibitive effect of dissolved chloride ions on the "polarization curve" on the basis of the findings of the competitive adsorption studies.

Introduction

It has long been recognized that the adsorption of anions can have profound effects on the adsorption and reaction of neutral molecules.[2-4] Quantitative determinations of mixed surface coverages would seem a necessary prerequisite toward the understanding of such effects. Such determinations appear to be lacking, although there have been considerable studies of individual adsorbates.[2]

Since (on platinum) adsorbed organic and anionic species have distinctly different voltammetric properties, it is possible to devise a multipulse potentiodynamic (MPP) sequence which permits quantitative study of competitive adsorption. For the first study, CO and Cl^- were chosen because of availability of considerable previous information for these adsorbates.[5-11]

Experimental Section

The glassware, electronic equipment, etc. have been described previously.[6] The electrolyte was 1 *N* perchloric acid, prepared from the AR grade acid and quartz-distilled water. The hydrochloric acid was AR grade. Gas mixtures of CO and argon were prepared, bottled, and analyzed by the Matheson Co., using CP grade CO and "prepurified" grade argon. The working electrode was a length of CP grade platinum wire which was annealed in a hydrogen flame and sealed in a soft-glass tube so that a geometric area of 0.071 cm² was exposed to the electrolyte. The "saturation hydrogen coverage," $_sQ_H$, measured using a linear cathodic sweep[5] was 0.29 mcoulomb/

---

[1] This paper was presented at the spring meeting of the Electrochemical Society, Cleveland, Ohio, May 1-6, 1966.

[2] (a) A. N. Frumkin in "Modern Aspects of Electrochemistry," Vol. 3, J. O'M. Bockris and B. E. Conway, Ed., Butterworth Inc., Washington, D. C., 1964, Chapter 3; (b) P. Delahay, "Double Layer and Electrode Kinetics," Interscience Publishers, Inc., New York, N. Y., 1965.

[3] M. W. Breiter, *Electrochim. Acta*, **9**, 827 (1964).

[4] B. I. Podlovchenko and Z. A. Iofa, *Zh. Fiz. Khim.*, **38**, 211 (1964).

[5] S. Gilman, *J. Phys. Chem.*, **66**, 2657 (1962).

[6] S. Gilman, *ibid.*, **67**, 78 (1963).

[7] S. Gilman, *ibid.*, **68**, 2098 (1964).

[8] S. Gilman, *ibid.*, **68**, 2112 (1964).

[9] T. B. Warner and S. Schuldiner, *J. Electrochem. Soc.*, **111**, 992 (1964).

[10] R. A. Munson, *J. Electroanal. Chem.*, **5**, 292 (1963).

[11] S. B. Brummer and J. I. Ford, *J. Phys. Chem.*, **69**, 1355 (1965).

Table VI: Comparison of Accuracy of Dipole Moments Determined in Solution, as Compared to Moment Determined in Gas

Substance	μ_0 (lit.)	μ_0 (4 mole %), present method	% dev	μ_0 (10 mole %), present method	% dev	μ in benzene[a]	% dev
n-$C_6H_{13}Br$	2.17	2.22	+2.3	2.15	−0.9	1.99	−8.3
n-$C_5H_{11}Br$	2.20	2.32	+5.4	2.16	−1.8	2.00	−9.1
n-C_4H_9Br	2.17	2.08	−4.1	2.11	−2.8	1.97	−8.3
n-C_3H_7Br	2.17	...	...	2.09	−3.8	1.97	−9.2
p-$ClC_6H_4CH_3$	2.16	1.97	−8.8	1.96	−9.3	1.89	−12.5
$(C_6H_5)_2CO$	3.06[b]	3.20	+4.6	3.17	+3.6	2.98	−2.6
$C_6H_5COCH_3$	3.06	3.18	+3.9	3.19	+4.2	2.93	−4.2
CH_3COCH_3	2.88	3.08	+6.9	3.10	+7.6	2.69	−6.6
CH_3NO_2	3.46	3.26	−5.8	3.27	−5.5	3.13	−9.5
$C_6H_5NO_2$	4.25	4.20	−1.2	4.18	−1.6	3.93	−7.5
CH_2Cl_2	1.62	1.91	+17.9	1.90	+17.3	1.53	−5.9
p-$ClC_6H_4NO_2$	2.77	2.73	−1.4	2.53	−8.7	2.60	−6.1

[a] From McClellan's compilation, ref 11. [b] Estimated; see text.

method of Oster.[9] The high value of the correlation parameter at 5 mole % is no doubt real.

One of the difficulties of the present research was finding suitable solutes. These must first of all have accurately measured values for dipole moment in the gas phase and give a good range for P_2/M_2. In addition they must not tend to form hydrogen bonds[10] with the solvent and should have varied shapes and sizes. One can find few compounds meeting these criteria and, therefore, giving a valid test of the method. It was necessary to use one compound (benzophenone) with estimated dipole moment.

The accuracy of the procedure is demonstrated in the following way. The values of P_2/M_2 for each compound were calculated, assuming that the correlation parameter for the solute was the same as that of the ethylene carbonate in the solution. Correlation parameters were interpolated from a graph of data from Table V. The moment of ethylene carbonate was assumed for this purpose to be 5.25. If this were the correct moment for ethylene carbonate then the result should be a straight line through the origin with a slope of 1. In practice, the data were fitted by the method of least squares to an equation of the form $P_2/M_2 = M(\epsilon$ function). The values of M were 1.04 and 1.07 for 4 and 10 mole % solute, respectively.

Then the experimental ϵ function was assumed to be correct, and the corresponding value of P_2/M_2 was calculated, *i.e.*, as if the point lay on the line. From this the moment in the gas phase was computed. These calculated moments are compared to literature values of moments[11] in the gas phase in Table VI. In the same place a comparison is also made with the average moment[11] of the compounds as obtained in benzene solution.

It can be seen that the present method gives results for dipole moment which are closer to the values in the gas phase. This is even more impressive when one realizes that the figures given for the moment in benzene solution are an average for several investigators. On examining the individual values making up any one of these averages one observes very wide deviations. This either indicates that the extrapolation is not linear, in which case different experimenters arrive at different extrapolated values, or means that errors in measurement are so high at the low concentrations used that the exact position of the straight line is in doubt. In any event the precision of measurements by different investigators is not high. On the other hand, the close agreement of moments determined by the present interpolation method with the *average* dipole moment is good indication of its high precision. It also appears that the method given here has nearly reached the maximum accuracy, or, in other words, averaging the results for several investigators will not give much improvement. This is clearly shown by the good agreement between the moments calculated for the 4 and 10 mole % solutions. One possible way to improve the accuracy may be to go to smaller concentrations of

---

[9] G. Oster, *J. Am. Chem. Soc.*, **68**, 2036 (1946).

[10] Solutes which may form hydrogen bonds will be the subject of a separate study. Oster's calculations show greater variability for the correlation parameter for hydrogen-bonding solutes.

[11] Practically all the moments used were obtained from A. L. McClellan, "Tables of Experimental Dipole Moments," W. H. Freeman and Co., San Francisco, Calif., 1963.

solute; however, there is the limitation in the ability to measure accurately the change in dielectric constant.

The advantages of the method are: dipole moments are obtained which are more nearly equal to values obtained on the gaseous compound; extreme accuracy is not needed for dielectric constants; the data are treated in a simple and straightforward way (in particular an interpolation is used instead of an extrapolation); and, apparently, high precision of measured dipole moment. Possible disadvantages are: insufficient solubility of compound being measured, and reaction of compound with solvent (*e.g.*, if it is a strong Lewis acid or can hydrogen bond with solvent). These can be obviated in many cases by changing the solvent system

---

Rates of Hydrogen Abstraction from Methanol by CF_3 Radicals

by Terry S. Carlton, J. Rodger Steeper, and Ronald L. Christensen

Department of Chemistry, Oberlin College, Oberlin, Ohio 44074 *(Received March 21, 1966)*

Hexafluoroazomethane was photolyzed in the presence of gaseous CH_3OH plus CD_3OD, CH_3OD plus CD_3OD, CH_4 plus CD_3OD, and CD_3OH. From the relative rates of formation of CF_3H and CF_3D, rate constants and Arrhenius parameters were determined for abstraction by CF_3 radicals of the hydroxyl and alkyl hydrogens in CH_3OH. The activation energy for abstraction of each kind of hydrogen is 8.3 kcal/mole. The preexponential factor for alkyl hydrogen abstraction is 10 times the factor for hydroxyl hydrogen. The results are compared with those for abstraction from CH_3OH by CH_3 and CD_3 radicals. A dipolar model is used to explain trends in the relative activation energies for abstractions by CH_3 and CF_3.

Introduction

Arrhenius parameters have been reported for a large number of reactions in which CH_3 abstracts hydrogen atoms from substrate molecules[1] and for a smaller number of reactions in which CF_3 abstracts hydrogen.[2] None of the CF_3 reactions involved hydrogen abstraction from a functional group. This paper reports the Arrhenius parameters for abstraction by CF_3 of the hydroxyl and alkyl hydrogens of methanol and compares these parameters with those for the corresponding abstractions by CH_3.

Experimental Section

The CH_3OH (Baker and Adamson reagent grade) was dried by passing the vapor through Drierite and purified by bulb-to-bulb distillations. The CD_3OD, CH_3OD, CD_3OH, and hexafluoroazomethane (Merck Sharp and Dohme) were used without further purification. Nmr showed that 0.3% of the methyl hydrogen in CD_3OD and CD_3OH was protium, as was 0.4% of the hydroxyl hydrogen in CD_3OD and 0.3% in CH_3OD. CF_3H and CH_4 (Matheson) were used without further purification, since the infrared spectra revealed no impurities.[3,4] CF_3D was synthesized from CF_3H by shaking the latter with two successive por-

---

(1) See, for example: (a) A. F. Trotman-Dickenson, "Gas Kinetics," Butterworth and Co. Ltd., London, 1955, p 199; (b) S. W. Benson and W. B. DeMore, *Ann. Rev. Phys. Chem.*, **16**, 397 (1965).

(2) See, for example: (a) H. Carmichael and H. S. Johnston, *J. Chem. Phys.*, **41**, 1975 (1964); (b) G. O. Pritchard, H. O. Pritchard, H. I. Schiff, and A. F. Trotman-Dickenson, *Trans. Faraday Soc.*, **52**, 849 (1956); (c) W. G. Alcock and E. Whittle, *ibid.*, **61**, 244 (1965); (d) W. G. Alcock and E. Whittle, *ibid.*, **62**, 134 (1966).

(3) (a) E. K. Plyler and W. S. Benedict, *J. Res. Natl. Bur. Std.*, **47**, 202 (1951); (b) H. D. Rix, *J. Chem. Phys.*, **21**, 1077 (1953).

(4) American Petroleum Institute, Research Project 44, Infrared Absorption Spectrogram No. 528, 1946.

tions of 1.8 *M* NaOD at 75 to 115° for about 2 days each time. Infrared analysis showed CF_3H contamination in the CF_3D to be less than 1%.[5]

Hexafluoroazomethane was used as the source of CF_3 radicals because it does not react with methanol, whereas hexafluoroacetone does. When hexafluoroazomethane at 25.8 torr was mixed at 25° with methanol at 23.6 torr, the pressures were additive to within the total experimental uncertainty of 0.3 torr; but when hexafluoroacetone and methanol were mixed at 100°, there was a markedly negative deviation from pressure additivity.

Reaction mixtures were prepared separately for each run. A check showed that isotopic exchange with the walls during mixture preparation was negligible. The pressure of hexafluoroazomethane was 0.4–1.6 torr, and the pressure of the alcohol in each run was between 8 and 70 torr. The maximum percentages of substrate molecules which reacted in a single run were as follows: 4.9% for CH_3OH, 2.7% for CH_3OD, 1.4% for CD_3OD, 1.9% for CD_3OH, and 0.3% for CH_4. The temperature throughout the cylindrical Pyrex reaction vessel was maintained within 1° of its nominal value. Collimated light from a high-pressure mercury lamp was filtered by soda glass before entering the reaction vessel to prevent mercury-photosensitized reactions.

After fractionation of the reaction mixture, CF_3H, CF_3D, and C_2F_6 were analyzed with a Perkin-Elmer 621 infrared spectrophotometer. Air was added to make the pressure the same for each spectrum. Spectrophotometric analyses of known mixtures of CF_3H and CF_3D gave 4.4% as the root-mean-square deviation from the true pressure ratios. Absorbances were measured at 1152 and 1210 cm^{-1}, and in the few runs in which appreciable C_2F_6 was formed a correction was made for its absorbance at these frequencies.

Results

In runs with mixtures of CH_3OH plus CD_3OD, CF_3H and CF_3D were produced by the reactions

$$CF_3 + CH_3OH \longrightarrow CF_3H + \begin{Bmatrix} CH_3O \\ CH_2OH \end{Bmatrix} \quad (1)$$

and

$$CF_3 + CD_3OD \longrightarrow CF_3D + \begin{Bmatrix} CD_3O \\ CD_2OD \end{Bmatrix} \quad (2)$$

Since the alcohol concentrations remained essentially constant throughout a run

$$\frac{k_1}{k_2} = \frac{[CF_3H][CD_3OD]}{[CF_3D][CH_3OH]} \quad (3)$$

Experimental values of k_1/k_2 are shown in Table I and Figure 1.

Table I: Results from Mixtures of CH_3OH and CD_3OD

Temp, °K	$[CD_3OD]/[CH_3OH]$	Time, min	$[CF_3H]/[CF_3D]$	k_1/k_2
388.4	5.01	492	1.61	8.06
404.8	5.06	510	1.49	7.54
424.4	4.27	332	1.554	6.64
450.2	4.40	371	1.39	6.12
473.7	5.86	285	0.934	5.47
522.3	5.57	385	0.810	4.51
527.7	4.73	273	0.935	4.42

In runs with mixtures of CH_3OD plus CD_3OD, CF_3H was produced by the reaction

$$CF_3 + CH_3OD \longrightarrow CF_3H + CH_2OD \quad (4)$$

In addition, runs at 300 and 532°K with CH_3OD as the only substrate produced negligible amounts of CF_3D relative to CF_3H. Therefore reaction 2 must have been the source of virtually all the CF_3D in runs with mixtures of CH_3OD and CD_3OD, and

$$\frac{k_4}{k_2} = \frac{[CF_3H][CD_3OD]}{[CF_3D][CH_3OD]}$$

Experimental values of k_4/k_2 are shown in Table II and Figure 1.

Table II: Results from Mixtures of CH_3OD and CD_3OD

Temp, °K	$[CD_3OD]/[CH_3OD]$	Time, min	$[CF_3H]/[CF_3D]$	k_4/k_2
407.3	4.02	314	1.63	6.55
437.8	5.00	385	1.155	5.78
478.0	3.61	344	1.31	4.73
525.2	4.34	194	0.938	4.07

Reaction 1 is composed of the two concurrent reactions

$$CF_3 + CH_3OH \longrightarrow CF_3H + CH_3O \quad (5)$$

and

$$CF_3 + CH_3OH \longrightarrow CF_3H + CH_2OH \quad (6)$$

We shall assume that k_6 equals k_4, since evidence from several systems indicates that secondary isotope effects are negligible in hydrogen abstraction reactions;[6] therefore

---

[5] S. R. Polo and M. K. Wilson, *J. Chem. Phys.*, **21**, 1129 (1953).

[6] (a) J. R. McNesby, *J. Phys. Chem.*, **64**, 1671 (1960); (b) P. Gray and J. C. J. Thynne, *Trans. Faraday Soc.*, **59**, 2275 (1963); (c) T. E. Sharp and H. S. Johnston, *J. Chem. Phys.*, **37**, 1541 (1962).

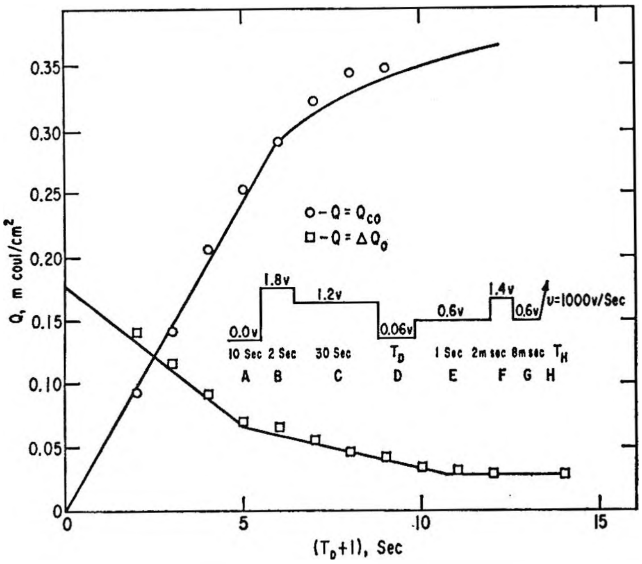

Figure 5. Sequential mixed adsorption of CO and Cl^-. The 1 *N* $HClO_4$ contained 10^{-4} *M* HCl, was saturated with a gas mixture of 1% CO and 99% argon (30°)- and was paddle stirred (360 rpm). Adsorption of CO occurs during both steps D and E for $T_D + 1$ sec. Adsorption of Cl^- occurs only during step E (for 1 sec). Q_{CO} is related to absolute and relative coverages with CO by eq 4 and 6, respectively. ΔQ_O is related to absolute and relative coverages with Cl^- by eq 2 and 7, respectively. ΔQ_O and Q_{CO} were evaluated from traces similar to those of Figure 2.

above, adsorption was conducted at potential *U* so that CO and Cl^- could adsorb *simultaneously*. In the experiments described below, CO was first adsorbed at a potential (0.06 v) at which only CO could adsorb. After achieving a desired CO coverage, the potential was then raised to 0.6 v, at which potential both CO and Cl^- could adsorb.

Procedure. The pulse sequence used appears in Figure 5. Steps A–C of the sequence are identical with those employed in section II above. In step D, CO only was adsorbed for time interval T_D. In step E, further adsorption of CO could occur at 0.6 v, along with adsorption of Cl^-. The rest of the sequence served to obtain ΔQ_O and Q_{CO}, as described in the previous section.

Results. Values of charge are plotted against the total time ($T_D + 1$) allowed for CO adsorption in Figure 5. The solid curves passing through the data points are identical with those measured in the previous section, for adsorption at 0.6 v.

IV. The "Polarization Curve" for CO. The linear anodic sweep (las) traces of Figures 1 and 2 correspond to CO adsorbed *before* the application of the rapid sweep. There is thus no appreciable "turnover" (additional adsorption and reaction) during the sweep. For examination of the qualitative effects of Cl^- adsorption on steady-state anode performance, a slow periodic triangular sweep was applied alternatively in the presence and absence of dissolved Cl^-. The results appear in Figure 6.

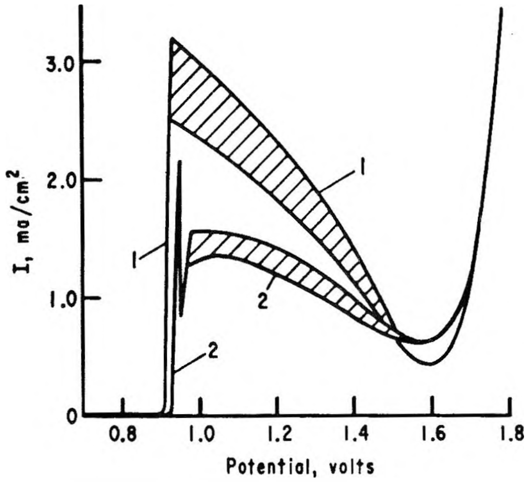

Figure 6. Anodic "polarization curves" for CO. The traces were recorded during the positive-going portion of a periodic triangular sweep (sweep speed, v = 0.04 v/sec) operating between 0.4 and 1.8 v. Trace 1 was obtained in the absence and trace 2 in the presence of 10^{-4} *M* HCl. The 1 *N* $HClO_4$ electrolyte was saturated with pure CO (30°) for both traces and was paddle stirred (360 rpm). The hatched areas correspond to regions of oscillation of the current.

Discussion

I. Adsorption of CO in the Absence of Cl^-. Structure of the Adsorbed Layer. Previous studies of the CO adlayer at 0.4 v[6] suggested that the adsorbed layer retained the *composition* of the adsorbate in the gas phase. The results were also consistent with the conclusion that the adlayer comprised CO bonded to the surface in both bridged and linear configurations. The las traces measured for $-0.1 \text{ v} \leqslant U \leqslant 0.7$ v after 10-sec adsorption time (trace 2, Figure 1) are identical. This suggests that the adlayer formed over this range is constant in composition and structure. On the other hand, the trace obtained at −0.2 v is noticeably shifted to the left on the potential axis (trace 3, Figure 1). At medium potentials (*e.g.*, 0.4 v, ref 6), such shifts sometimes correspond to decreasing coverage for an adsorbed phase of constant composition.[12] However, since the oxidative charge corresponding to trace 3 is almost identical with that for trace 2, the observed potential shift is not simply a surface coverage effect but must likely represent a change in composition or

---

(12) S. Gilman, *J. Phys. Chem.*, **67**, 1898 (1963); **68**, 70 (1964).

structure of the adlayer (*e.g.*, partial reduction at highly cathodic potentials).

It is the opposing rate of oxidation of CO (to CO_2) which prevents buildup of CO surface coverage at potentials much above 0.7 v. If, for the conditions of Figure 1, the adsorption time is increased to 100 sec, it is possible to compare the las traces for as high as 0.8 v. It is then found that the traces for potentials between 0.1 and 0.8 v are identical. The traces for lower potentials are similar, but the traces for the clean surface (trace 1 of Figure 1) and that for the CO-covered surface no longer merge in the high-potential region. This effect may again be due to the final buildup of some small quantity of refractory reduction product or may be due to the accumulation of a small amount of an (cationic) impurity.

The over-all results suggest that the structure of the adlayer remains constant over a range of potentials extending from -0.1 to 0.8 v.

Rate of Adsorption of CO. It has already been shown[6] that, at 0.4 v, the adsorption of CO from a quiescent or paddle-stirred solution is transport controlled until almost full coverage is achieved. The constancy of Q_{CO} after 1.0 sec of adsorption over a range of -0.1–0.6 v (Table I) suggests that the adsorption is transport controlled over this entire range.

At 0.0 and -0.1 v, the solution adjacent to the electrode is saturated with H_2 (perhaps supersaturated at the lower potential). Hence, the observation of transport-controlled CO adsorption at these potentials implies a relatively slow rate of displacement of dissolved CO by dissolved H_2 (in a region extending from the surface through the diffusion layer and into the bulk of the solution). The lower rate of CO adsorption at -0.2 v might, on the other hand, be due to an appreciable rate of displacement of CO in the solution phase, by very vigorously evolved H_2, rather than to slow adsorption kinetics.

The lower values of Q_{CO} for $U = 0.7$ and 0.8 v are likely due to the oxidation of some CO to CO_2. For the 10- and 100-sec points of Table I, it may be seen that even $U = 0.7$ and 0.8 v fall within the region of constancy. This is because the adsorption is no longer transport controlled in the higher range of coverage[5] and there is sufficient transport of CO to the surface to allow both further adsorption and oxidation of CO.

Maximum Surface Coverage with CO. After the region of transport-controlled adsorption (approximately 85% of full coverage for a quiescent solution with 1 atm partial pressure of CO, ref 5; approximately 75% of full coverage for a stirred solution with 0.01 atm partial pressure of CO, Figure 3), the adsorption becomes activation controlled and changes gradually with time. After 100 sec, approximately the same maximum charge was obtained for 0.01 and 0.1 atm partial pressure of CO. This charge, $(Q_{CO})_{max}$, has the value 0.38 mcoulomb/cm^2 (geometric area). We may obtain the charge per unit of "hydrogen area" by dividing by the "roughness factor." Hence, $(Q_{CO})_{max}/RF = 0.28$ mcoulomb/cm^2 ("hydrogen area"). As previously pointed out[6] "full coverage" is not meant to imply that all (hydrogen) sites are occupied. In fact, hydrogen-codeposition experiments suggest that 10–20% of the hydrogen sites are still vacant. (Hydrogen-codeposition experiments are not sensitive at very high coverages with CO. Determinations suggest 20% of the hydrogen sites remain vacant, but a value of only 10% would be in better agreement with the apparent ratio of bridged to linear CO.[6]) It is also possible even higher coverages would very slowly result if the adsorption were continued over much longer periods of time. Without considerable improvements in the level of solution purity such measurements would be suspect.[6]

Validity of CO-Coverage Determinations. There are some working assumptions implicit in MPP determinations of surface coverage[5,6] as is generally the case with quantitative voltammetric measurements of other types. The validity of the final results for this particular system, however, is best supported by the good quantitative agreement between adsorption rates and diffusion theory which applies until full coverage is almost complete.[6] Although this paper relies mainly on the low-coverage data, it seems justifiable to make comparison with the full-coverage values of others, in view of current interest.

Munson[10] measured medium- to low-current galvanostatic transients (after adsorption at 0.40) for 0.1 *N* perchloric acid saturated with CO at 25°. After graphically eliminating mass-transport contributions to the measured transition times, Munson obtained a coverage with CO approximately 30% higher than corresponding adsorption of hydrogen. This is equivalent to $(Q_{CO})_{max}/RF = 0.27$, which is in good agreement with the value 0.28 mcoulomb/cm^2 ("hydrogen area") offered here. Warner and Schuldiner[9] report values (sulfuric acid), which are over 50% higher than those reported here. Brummer and Ford[11] have already suggested that these values are in error owing to faulty evaluation of the transition time. Brummer and Ford[11] have offered (1 *N* $HClO_4$, 40°, 0.3 v) the value of 0.365 mcoulomb/cm^2 (32% higher than reported here) for Q_{CO}/RF and have suggested that the value offered in a previous paper[5] and here is in error owing to improper correction for "oxygen adsorption." Although several rather arbitrary corrections were made by Brummer and Ford in arriving at their final value, the main issue is whether they have made a proper correction for "oxygen adsorption" using their particular cathodic reduction scheme. Vetter and Berndt,[13] Laitinen and Enke,[14] and Feldberg, Enke, and Bricker[15] have all concluded that balance could not be attained between the charges passed in oxidizing and reducing the surface. Gilman[16] showed that charge balance (within 10%) could be attained by reducing the surface at 0.4 v. However, the reduction followed an exponential decay law so that from 200 msec (for small oxygen coverage) to 10 sec (for large coverage) was required to achieve charge balance. Brummer and Ford's[11] typical reduction was made in only *ca.* 3 msec, making it likely that the surface was only partially reduced. This would have lead to undercorrection for "oxygen" and values of Q_{CO} which are too high.

II. Proof of the Thermodynamic Dependence of Chloride Ion Surface Coverage on the Instantaneous Coverage of the Surface with Carbon Monoxide. The data of Figure 3 correspond to the following experimental situation. (1) Adsorption (step D) occurs when passive film is reduced. (2) The concentration of dissolved chloride ion is approximately 10 times higher than that of dissolved CO and the rate of transport of the two species to the surface is in approximately the same ratio. (3) The initial value of θ_{CO} is zero. (4) The initial value of chloride coverage is very low ($\theta_{Cl^-} = 0.04$).

The experimental results appearing in Figure 3 may be summarized as follows. (1) The adsorption of CO follows the same law over the entire range of potentials studied (activation controlled at high coverage; transport controlled at lower coverage) in the presence of adsorbed chloride ion. This law is identical with that observed in the absence of Cl^-. (2) Within 1 sec (the approximate time required for transport control), the adsorption of Cl^- reaches a maximum value close to the equilibrium value measured in the absence of CO.[8] The Cl^- coverage then decreases linearly as CO coverage increases. Extrapolation of the linear θ_{Cl^-}–time plots back to zero adsorption time yields intercepts which agree (within a few per cent) with the equilibrium values measured on this electrode in the absence of CO. Agreement with equilibrium values previously determined on another electrode[8] is within 8%.

The results suggest that the *experimental* rate of CO adsorption is unaffected by the presence of adsorbed Cl^-. Since this rate is transport controlled (through most of the range of coverage), this does not preclude the possibility that the large *kinetic* rate *is* affected. The adsorption of CO goes to the usual state of completion, causing the gradual desorption of chloride ions. There are two possible explanations for the observed *experimental* rate of desorption of Cl^-. (1) The desorption may be an activated process, and the rate of Cl^- desorption may reflect *kinetics* of desorption. (2) There may be an *equilibrium* value of Cl^- surface coverage (with kinetics of adsorption and desorption both rapid, compared with mass transport) corresponding to each value of CO surface coverage. The apparent rate of desorption of Cl^- may reflect only an *indirect* dependence on the rate of CO adsorption. The experimental results presented in Figure 5 establish that possibility 2 is the correct intrepretation.

The data of Figure 5 correspond to the following experimental conditions. (1) Adsorption of CO is allowed to proceed for time T_D at 0.06 v. Because of the low potential, θ_{Cl^-} remains zero.[7] (2) The potential is then raised to 0.6 v for 1.0 sec. During this time both CO and Cl^- may adsorb. In Figure 5, values of ΔQ_O and Q_{CO} are plotted against CO adsorption time (T_D + 1). For each point, the total adsorption time for Cl^- is, however, only 1.0 sec. The results are in good agreement with those obtained when the adsorption is conducted entirely at 0.6 v (Figure 3). When we recall that all of the values of ΔQ_O for Figure 5 are arrived at by *adsorption* of Cl^- in just 1.0 sec and that all of the corresponding values in Figure 3 are obtained by gradual *desorption* of Cl^-, this constitutes proof that the measured Cl^- coverages bear a *thermodynamic* relationship to the CO coverages.

III. Quantitative Dependence of Cl^- Coverage on CO Coverage, Electrode Potential, and Concentration of Dissolved Cl^-. In the last section, we established that Cl^- adsorption–desorption is a reversible process with the equilibrium Cl^- coverage dependent on the instantaneous CO surface coverage. Previous results[8] show that Cl^- adsorption is also reversibly dependent on the potential. The thermodynamic data are presented in a convenient form in Figure 4. We see that for any value of $\theta_{CO} \leqslant 0.6$, the Cl^- coverage decreases linearly with decrease in potential. For $\theta_{CO} = 0.7$, the Cl^- coverage decreases linearly with decreasing potential at first but does not drop below $\theta_{Cl^-} = 0.04$, which seems to be the minimum attainable (by displacement with CO) Cl^- coverage. Hence, for

---

[13] K. J. Vetter and D. Berndt, *Z. Elektrochem.*, **62**, 378 (1958).

[14] H. A. Laitinen and C. G. Enke, *J. Electrochem. Soc.*, **107**, 773 (1960).

[15] S. W. Feldberg, C. G. Enke, and C. E. Bricker, *ibid.*, **110**, 826 (1963).

[16] S. Gilman, *Electrochim. Acta*, **9**, 1025 (1964).

Table I: Frequencies and ϵ^a for Alcohol OH Stretch Vibrations at Various Temperatures

Alcohol	Wavelength		ϵ^a			
	μ	(cm^{-1})	21.7°	30.2°	39.1°	48.1°
Methyl	2.745 ± 2	(3643 ± 3)	60.6 ± 2.8[a] (60.4)[b]	56.4 ± 3.0 (56.8)	52.3 ± 2.8 (53.4)	48.3 ± 2.8 (49.8)
Ethyl	2.752 ± 2	(3634 ± 3)	56.9 ± 1.6 (56.7)	53.8 ± 1.4 (54.3)	50.9 ± 1.5 (51.9)	48.6 ± 1.8 (50.1)
n-Propyl	2.750 ± 2	(3636 ± 3)	58.3 ± 1.9 (58.1)	56.4 ± 1.7 (56.8)	53.8 ± 1.6 (54.6)	51.6 ± 1.3 (53.3)
Isopropyl	2.757 ± 2	(3627 ± 3)	59.7 ± 2.1 (59.6)	56.2 ± 2.4 (56.6)	52.6 ± 2.4 (53.5)	49.3 ± 2.0 (50.9)
n-Butyl	2.748 ± 1	(3639 ± 2)	59.5 ± 1.1 (59.4)	56.8 ± 1.2 (57.3)	54.7 ± 1.0 (55.8)	52.8 ± 1.1 (54.4)
Isobutyl	2.747 ± 1	(3640 ± 2)	64.1 ± 1.4 (63.9)	61.1 ± 1.5 (61.5)	58.5 ± 2.1 (59.6)	56.4 ± 2.1 (58.2)
t-Butyl	2.766 ± 1	(3615 ± 2)	66.7 ± 2.5 (66.5)	66.7 ± 2.5 (63.3)	59.1 ± 1.3 (60.2)	56.2 ± 1.7 (58.0)
Neopentyl	2.744 ± 1	(3644 ± 2)	72.1 ± 2.8 (71.6)	69.1 ± 2.7 (69.4)	66.2 ± 2.7 (67.2)	63.4 ± 2.0 (65.1)

[a] Calculated using the density of carbon tetrachloride at 24°. [b] Values in parentheses are corrected for changes in solution density with temperature.

with open window brass screw caps to secure the assembly. Teflon gaskets prevented the end caps from damaging the salt windows. The brass shells were provided with tubular inlets and outlets placed at opposite ends and at 180°. Both sample and reference cells were temperature regulated with a Haake Series F circulator–heater which was coupled with a Brinkman Thermo-Cool heat pump. This system controlled cell temperature to ±0.1°. In changing temperature a 15-min equilibration period was used.

Materials. The solvent used was carbon tetrachloride. Ordinary spectroscopic grade carbon tetrachloride contains too much water for use with long-path cells. To eliminate error due to hydrogen bonding between water and alcohol and to prevent loss of energy in the critical spectral region, the solvent was rendered completely anhydrous (no absorbance above base line in the 4000–3000 cm^{-1} range). To obtain this level of desiccation the carbon tetrachloride was shaken with Woelm neutral alumina, decanted into a phosphorus pentoxide containing distilling flask, and distilled into phosphorus pentoxide. All further solvent transfers were carried out in a phosphorus pentoxide dried glove box. Just prior to use, it was passed through an 8 × 2 cm column of Woelm neutral alumina and collected in a flask closed with a hollow, phosphorus pentoxide containing stopper.

The solute alcohols were purified by ordinary methods.[4] Additionally, they were distilled from sodium in a desiccated, all-glass system, just prior to use. To avoid adsorption of atmospheric water, all transfers were carried out in the drybox. Alcohol solutions were prepared gravimetrically by using samples sealed in melting point capillaries. The capillaries were crushed in suitably sized volumetric flasks containing a small volume of carbon tetrachloride. The samples were made to volume at 24°. Each value of ϵ^a appearing in Table I represents eight individual samples. The concentrations of alcohols ranged from slightly over 0.002 *M* to just under 0.004 *M*. At each temperature three to five separate spectra were made for each sample. In each case the recorded curves were symmetrical and very sharp. The values of ϵ^a were calculated using the usual relationships. Values of B^0 were calculated from gravimetrically measured integrated absorbancies and approximate integrated absorbancies derived from area measurements based on triangles.

Results and Discussion

Table I summarizes the ϵ^a data for the eight alcohols. Figure 1 contains plots of the average ϵ^a values as a function of temperature. At the concentrations used (>0.002 and <0.004 *M*) there was no spectroscopic evidence for the existence of alcohol dimer in the 3500-cm^{-1} region or polymer in the 3350-cm^{-1} region at any of the temperatures. The values of ϵ^a are independent of concentration and vary linearly with temperature, a phenomenon observed previously.[2f] The linear relationship between ϵ^a and temperature may be expressed by the equation: $\epsilon^a = -at + b$, where the factors a and b were calculated by the method of least squares. The data appear in Table II. The values of slope a are in terms of ϵ^a units per degree and the values of intercept b are the ϵ^a values at 0°. An interesting relationship appears on extrapolation to the boiling temperatures of the solutes. These points in Figure 1 are indicated by open circles. From these data it appears that regardless of whether an alcohol is primary, secondary, or tertiary and regardless of its boiling point, the ϵ^a at that temperature will be approximately 42. This predicts that high molecular weight and high boiling point alcohols may have low values of a. Alternatively, their ϵ^a values at low temperatures may exceed the ranges usually quoted for

---

[4] A. Weissberger, "Technique of Organic Chemistry," Vol. 7, Interscience Publishers, Inc., New York, N. Y., 1955.

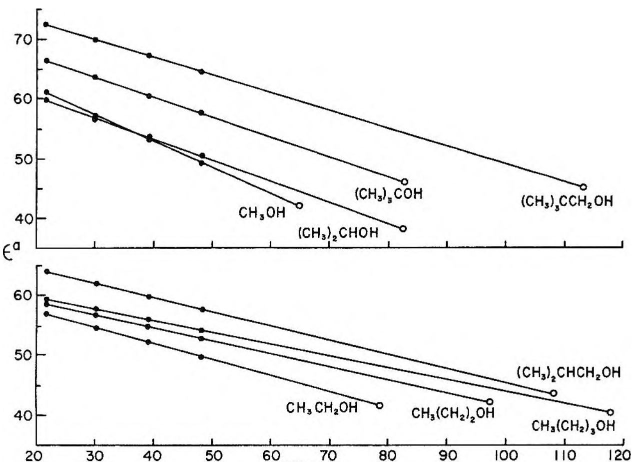

Figure 1. Temperature dependency of ϵ^a for alcohol OH stretching fundamentals.

particular structural types. On the limited experience provided by neopentyl alcohol, ϵ^a values for higher alcohols will be greater than expected.

There are few ϵ^a values in the literature with which to compare these results. They are in general agreement with those recently published by Ungenade[5] and the earlier data of Liddel and Becker,[6] but in the case of *t*-butyl alcohol there is disagreement. Our value of ϵ^a, as obtained at high dilution and rigid temperature control, are intermediate between those of the other two groups. However, comparisons are difficult because the former work does not cite the temperatures of experimentation and the latter was conducted on solutions which were a minimum of 0.01 *M* in *t*-butyl alcohol.

Table II: Boiling Point Values of ϵ^a as Calculated by the Equation $\epsilon^a = -at + b$

Alcohol	Bp, °C	a	b	ϵ^a (bp)
Methyl	64.72	0.438	70.4	42.0
Ethyl	78.32	0.269	62.6	41.5
n-Propyl	97.18	0.219	63.3	42.0
Isopropyl	82.40	0.356	67.5	38.2
n-Butyl	117.7	0.197	63.6	40.4
Isobutyl	107.9	0.236	69.0	43.4
t-Butyl	82.50	0.336	73.7	46.0
Neopentyl	113.0	0.299	78.7	45.0

We have not observed a temperature dependence for the hydroxyl bands described here. The dependency of such bands on temperature has previously been noted to be slight.[2f] Because of this it appears that our experimental error would obscure any very small shifts in λ_{max} with temperature.

If the series of methyl, ethyl, isopropyl, and *t*-butyl alcohols is considered, it is apparent that the inductive effect of added methyls at the carbon α to the hydroxyl groups shifts λ_{max} to higher values. A plot of λ_{max} in terms of log (cm^{-1}) *vs.* number of methyl groups is linear and serves to indicate the changes in hydroxyl group electrical environment as a consequence of methyl substitutions. If substitution effects are considered on a broader basis and the series of ethyl, *n*-propyl, *n*-butyl, isobutyl, and neopentyl alcohols is examined, it is seen that substitution at the carbon β to the hydroxyl group shifts λ_{max} to lower wavelengths. A plot of λ_{max} as cm^{-1} *vs.* number of added carbon atoms is linear, indicating no changing electrical environment at the hydroxyl group but rather a mass effect.

Acknowledgments. This work was supported in part by National Science Foundation Grant GB 2044, National Institutes of Health Grant GM 10363, and the Upjohn Co.

---

[5] H. E. Ungenade, E. M. Roberts, and L. W. Kissinger, *J. Phys. Chem.*, **68**, 3225 (1964).

[6] U. Liddel and E. D. Becker, *J. Chem. Phys.*, **25**, 173 (1956).

Self-Diffusion in Suspensions. Sodium in Montmorillonite at Equilibrium

by Adrien Cremers[1] and Henry C. Thomas

Department of Chemistry, University of North Carolina, Chapel Hill, North Carolina *(Received March 29, 1966)*

A surface excess coefficient of self-diffusion for an ion is defined for a suspension of colloidal material capable of sorbing that ion. Four independent experimental quantities are necessary: the coefficient for the solution in dialytic equilibrium with the suspension, the gross coefficient for the suspension, the surface excess of ions for the suspended material, and the formation factor of the suspension as determined by measurements of conductivity. These surface diffusion coefficients are produced for suspensions of a highly purified montmorillonite clay in solutions of sodium chloride, over a range of concentrations of salt, for a variety of clay contents up to 5% by weight, and at three temperatures. The surface coefficients are shown to be independent of clay content, to vary exponentially with the square root of the salt concentration, and to give an energy of activation near that for self-diffusion in pure solution.

We here define and present measurements of a quantity which describes the self-diffusion of an ion in the neighborhood of the surfaces of a siliceous ion exchanger dispersed in an aqueous solution. This surface self-diffusion coefficient is a typical excess quantity and receives its definition in an almost purely operational fashion. The reason for the qualification will become apparent. For the case at hand, sodium ion in suspensions of montmorillonite, the quantity will be seen to be independent of the extent of the surface, but strongly dependent on the concentration of the neighboring solution and on the temperature. Tentative suggestions are offered in explanation of the behavior of these quantities.

The surface diffusion coefficient derives its meaning, in part, from the possibility of establishing the existence and value of a "formation factor" for the suspension. The formation factor is an average over the suspension of a measure of the angle between the true flux and the macroscopic gradient producing it. (The actual form of this measure is unimportant; it is, however, the reciprocal of the average square of the cosine of the angle mentioned.) We determine the formation factor by measurements of conductance, that is, for a flux in an applied electrical gradient, and use these results in treating measurements of flux in a gradient of isotopic concentration. The nature of the case at hand is such that this step cannot be completely justified, although evidence is adduced in support of its plausibility. The procedure may be taken as part of our definition of the surface coefficient. In addition, the surface diffusion coefficient depends very directly on the fraction of ions counted as belonging to the surface. This fraction, of cations in the present case, is defined in terms of the base exchange capacity of the suspended mineral. It will be shown that any ambiguity in the definition of this quantity is less than a rather small experimental uncertainty. Thus the excess diffusion coefficient measures the difference between the rate of transport through a suspension and the rate through an equilibrium dialyzate in terms of the geometry of the gel and its surface excess of ions. The diffusion coefficient in pure solution and the concentration of that solution are taken as points of reference.

It is necessary to distinguish four diffusion coefficients with the following meanings: D, the directly observed self-diffusion coefficient for the suspension or gel; D_0, the diffusion coefficient for a fictitious suspension in which all surfaces are oriented parallel to the macroscopic gradient (In terms of the formation factor, F, $D_0 = FD$.); D_s, the diffusion coefficient for the dialyzate in equilibrium with the suspension; D_σ, the surface excess diffusion coefficient to be defined.

We consider a suspension through which a diffusive flow, J, due to an isotopic gradient is taking place along

---

[1] Visiting Fellow. Research Fellow of the Fonds National de la Recherche Scientifique, Belgium, Catholic University of Louvain.

an axis, z, determined by the equipment. The suspended particles, with ion-exchange characteristics, are in chemical equilibrium with a dialyzate of concentration c_s. In addition, the particles are in isotopic equilibrium with neighboring solution but only in layers perpendicular to the average flux. If $\bar{c}$ is the concentration of all ions free to move, averaged through the volume available for motion, and θ is the fraction of these isotopically tagged, then $\bar{c}$ is constant throughout, and θ is constant in layers perpendicular to the flux but varies with z. The observed flux can then be written

$$-J = D\bar{c}\frac{\partial\theta}{\partial z} = \frac{D_0}{F}\bar{c}\frac{\partial\theta}{\partial z} = \frac{D_\sigma X_\sigma + D_s X_s}{F}\bar{c}\frac{\partial\theta}{\partial z}$$

The surface coefficient D_σ is here defined through the relation involving the four independent experimental quantities D, D_s, F, and X_σ, the surface excess ionic fraction

$$DF = D_\sigma X_\sigma + D_s(1 - X_\sigma) \tag{1}$$

Of these four quantities the meanings of D and D_s are unambiguous; X_σ and particularly F require comment.

The fraction of cations in the suspension to be associated with the surface is determined by isotopic distribution through a membrane impermeable to the clay particles. The weight of the clay and the total weight of material within the membrane are measured. The solution within is conventionally taken to be of the same concentration as the dialyzate without. Isotopic dilution then gives directly the base exchange capacity, q, as defined by this convention, and hence

$$X_\sigma = (\text{weight of clay} \times q)/(\text{solution volume in suspension} \times c_s + \text{weight of clay} \times q)$$

The extent of anion exclusion from the suspension is a measure of the ambiguity of this definition. Anion exclusion for suspensions of the clay we here use has been measured.[2]

For our most concentrated suspension (5% clay) in 0.1 M solution, where the effect is greatest, neglect of anion exclusion corresponds to an uncertainty in X_σ of 1.3%. In all other cases the effect is less than the experimental uncertainty in the distribution experiment (1–2%) which determines the error in X_σ.

Our use of the formation factor from measurements of conductance is more open to attack. The theory of transport through heterogeneous materials and in particular through dilute suspensions of disordered particles produces a relation between a formation factor and the porosity, ϕ.[3] Nothing in the theory predicts the range of validity of this relation. For these dilute suspensions the relation is simple.

$$F - 1 = k\frac{1 - \phi}{\phi} \tag{2}$$

in which ϕ is the volume fraction of solvent and k depends only on the shapes of the particles and not on their sizes. For a suspension of stationary particles bearing a surface charge and characterized by a formation factor F, the conductance may be written

$$K_g = \frac{K_s}{F} + K_\sigma \tag{3}$$

where the quantity K_σ, *defined* by this equation, results from the contribution to the conductance of the counterions. In terms of equivalent conductances, $\Lambda_g = K_g/(q + \phi c_s)$, $\Lambda_\sigma = FK_\sigma/q$, and $\Lambda_s = K_s/c_s$, this definition has the same form as that adopted for D_σ.

$$F\Lambda_g = \Lambda_\sigma X_\sigma + \Lambda_s(1 - X_\sigma) \tag{4}$$

The applicability of these relations has been quite extensively examined for different clay minerals.[4] In particular, for the montmorillonite used in the present study (the purified mineral from Camp Berteau, Morocco) the measurements have now been extended, for sodium chloride solutions, to cover the range from 0.001 to 2.2 M. Over a wide range of salt content (0.025–2.2 M), constant values of F are obtained which are related to the porosities by eq 2 with the shape factor $k = 8.6$. In the model which pictures the clay particle as an oblate ellipsoid, this value of k corresponds to an axial ratio of 36.

A sensitive representation of these measurements of conductance is afforded by a plot of $K_s - K_g$ *vs.* K_s. If the surface contribution is small or constant, a straight line will be obtained, the slope of which is $(F - 1)/F$. Deviations from this line might be caused by a varying surface contribution or to a failure in the constancy of F. We return later to this important point.

Experimental Section

1. *Preparation of the Clay.* The crude montmorillonite from Camp Berteau, Morocco, was immersed in 1 M NaCl. The solution was renewed several times, and after a third or fourth change the suspension was washed with distilled water and allowed to stand for several hours. The supernatant was removed, fresh water added, and the procedure repeated until spontaneous peptization occurred. A fine fraction separated by decantation was again treated with 1 M NaCl and washed with water in a centrifuge. The speed of the

---

(2) H. Laudelout, *Bull. Groupe Franc. Argiles*, **9**, 61 (1957).

(3) See, *e.g.*, H. Fricke, *Phys. Rev.*, **24**, 575 (1924).

(4) A. Cremers and H. Laudelout, *J. Chim. Phys.*, **62**, 1155 (1965).

centrifuge and the extent of washing were adjusted to allow the separation of a fraction finer than 0.2 μ *equivalent spherical diameter.* This suspension was concentrated to about 4% using a Sharples "Supercentrifuge." The 4% suspension was dialyzed against 0.001 M NaCl for about a week, with renewal of the dialyzate several times a day and occasional shaking. From this preparation three stock suspensions were prepared containing 1.21, 2.43, and 3.80% clay. Each of these was divided into nine portions, to which were added appropriate amounts of NaCl so as to obtain a series at concentrations of 0.001 to 0.1 M. Each suspension was dialyzed to equilibrium with its corresponding solution, shaking continuously. Dry weights in each series were rechecked after the conductivity measurements. After correction for the salt present these were found to be within 1% of the original values. Porosities were based on d = 2.5 g/cm³ for the density of the clay.

2. Conductivity Measurements. The conductivities of the equilibrated suspensions and their dialyzates were measured at 25°; those of the 2.43% series were also measured at 15 and 35° to search for any possible dependence on temperature of the formation factor. The conductivities were determined at 1000 cps using a Hewlett–Packard wide-range oscillator with a Leeds and Northrup shielded ratio box, an air capacitor, and a No. 4755 ac resistance box. A tuned amplifier detector with a sensitivity of 1 μv determined bridge balance. Measurements were made in a No. 4920 Leeds and Northrup conductivity cell, the constant of which was determined with standard KCl solutions.

3. Cation-Exchange Capacity. The base exchange capacity of the clay has been determined by several variants of the experiment which consists essentially of bringing a known weight of a suspension to isotopic equilibrium, through a dialysis membrane, with its chemically equilibrated solution. The results are based on the weight of the sodium form of the clay found after 14–15 hr at 110°. (No further change in weight was found after 2–3 days at this temperature.) The results obtained show a distinct dependence on the concentration of the solution, which cannot be accounted for by anion exclusion. This variation in capacity has, however, a nearly negligible influence on the values of D_σ. We find for the capacity

NaCl, M	q, mequiv/g of Na clay
0.001	0.802 ± 0.011
0.002	0.900 ± 0.013
0.006	0.985 ± 0.025
0.010	1.000 ± 0.020

4. The Diffusion Experiment. The method for the determination of the self-diffusion coefficients has been described in detail and the treatment of the data discussed.[5,6] The method is applicable to γ-emitting ions in gels or viscous suspensions at equilibrium with known solutions. The results of the present work are strongly dependent on the values used for D_s, the coefficients for the equilibrium solutions. We have here used those obtained by Slade, *et al.*,[6] who state the accuracy to be 1% or better.

In the early stages of the work with the clay suspensions the ^{22}Na tag was added in the form of a few drops of carrier-free solution carefully adjusted to the same salt concentration as that of the suspension in question. The clay content of the suspension was corrected for this addition. The small uncertainties involved in this procedure were later avoided by evaporating appropriate amounts of carrier-free ^{22}NaCl to dryness and taking up the residue directly into the suspension. The spiked suspensions were allowed to stand for a few days, with occasional shaking, to ensure isotopic mixing.

The diffusion cell used in this work was the piece of equipment described by Slade.[7] The cavity was filled until a small inverted meniscus of suspension was obtained, great care being taken to avoid air bubbles. A Plexiglas plate lightly lubricated with silicone grease was slowly pushed across the metal surface of the cell to remove extra suspension and to close the bottom of the cell. Traces of extra suspension were mopped up with cotton. That this technique gives a reproducible filling is demonstrated by the following initial counts for eight fillings, each of which is the average of ten to twelve 1-min counts: 287,417, 287,862, 286,592, 287,964, 283,448, 288,370, 288,319, and 287,316. After assembling the cell, it was put into the thermostat for 10 min before installing in the counter well.

It has been demonstrated[5–7] that diffusion coefficients obtained by this method are independent of the thickness of the cellophane membrane through which the diffusion takes place into the moving solution. We have used the samples of cellophane designated 300 NR and 300 PUD, as described by Slade.[7] Diffusion runs required from 8 to 16 hr according to the magnitude of D. Each result is based on a least-

---

[5] G. F. Allen, H. Schurig, L. Slade, and H. C. Thomas, *J. Phys. Chem.*, **67**, 1402 (1963).

[6] A. L. Slade, A. E. Cremers, and H. C. Thomas, *ibid.*, **70**, 2840 (1966).

[7] A. L. Slade, Ph.D. Dissertation, University of North Carolina, Chapel Hill, N. C., 1964.

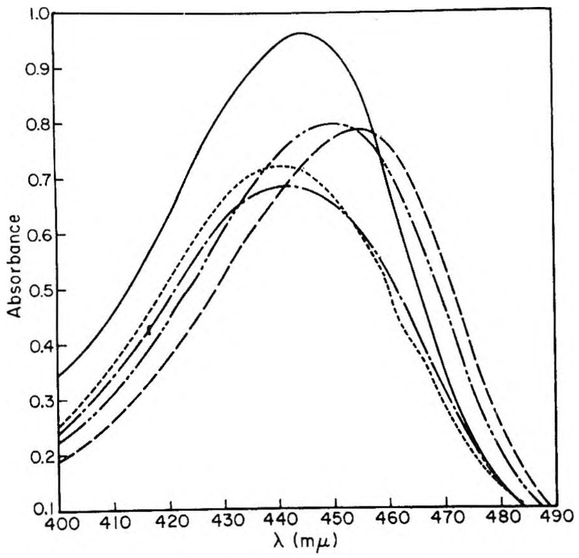

Figure 2. Spectra of poly A–PR solutions at pH 7.5, 25.0°, ionic strength = 0.1 M, [PR] = 2.5 × 10^{-5} M: ———, [poly A] = 0 M; — —, [poly A] = 1.82 × 10^{-3} M; —··—, [poly A] = 7.28 × 10^{-4} M; - - - -, [poly A] = 1.82 × 10^{-4} M; — · —, [poly A] = 2.28 × 10^{-5} M.

ing value of this relaxation process at infinite time. A plot of the logarithm of the amplitude against t is linear. Figure 3 shows a typical oscilloscope trace and the semilogarithmic plot extracted from it by the above procedure. The relaxation time obtained in this manner is to a good approximation independent of the concentrations of poly A and AO (in the limited concentration range of the latter employed) and appears to be independent of the ionic strength of the solution. However, when the value of [poly A]/[AO] is reduced to less than about 6, a faster relaxation process can be distinguished. The method given above was applied to evaluation of the relaxation times of both processes, the faster of which is of the order of 0.7 msec, while the magnitude of the slower relaxation is of the same order of magnitude as its counterpart at high poly A concentrations. The precision with which the relaxation times can be measured is very poor when both processes are observed; this is due to the fact that the amplitude of the faster process is very small and that both processes have relaxation times of the same order of magnitude. In view of the small concentration range in which the faster process can be distinguished, and the polydisperse nature of the poly A, a detailed interpretation will not be attempted. The faster relaxation process is probably always part of the over-all relaxation spectrum but only becomes discernible at very low concentrations of poly A. The complexity of the relaxation spectrum prevents a more exact evaluation of the relaxation parameters.

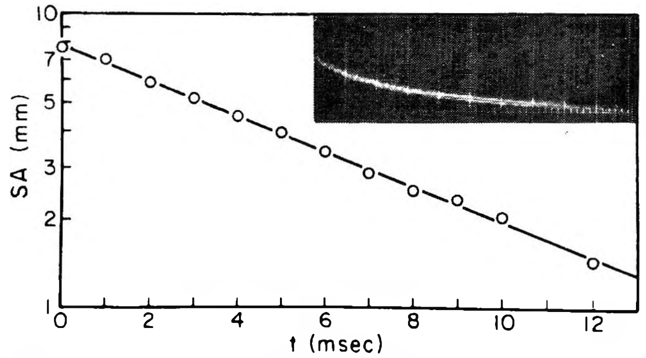

Figure 3. A typical relaxation effect and plot of logarithm of amplitude of light intensity change, SA, *vs.* time. [Poly A] = 4.24 × 10^{-3} M, [AO] = 2.5 × 10^{-5} M, pH 7.5, τ = 6.05 msec. The time scale on the photograph is one large division of the horizontal axis = 2 msec. Details of the method for obtaining the plot are described in the text.

Measurement of the relaxation time characterizing the slowest part of the over-all relaxation effect was attempted by use of both the Guggenheim[13] and the Swinborne methods,[14] but the difficulty of distinguishing between chemical relaxation effects and absorption changes of the solution due to convection within the temperature-jump cell after 200 msec has elapsed after the temperature jump makes any estimate extremely dubious. Attempts to characterize quantitatively the slowest part of the relaxation spectrum by a concentration-jump method and by direct mixing of polymer and dye in a flow apparatus were not successful because of the very small amplitude of the relaxation effect in the former experiments and because of the lack of reproducibility in measurement of the slow reactions in the latter method. However, the results indicate a relaxation process with a relaxation time of approximately 0.5 to 2.0 sec is occurring. The fact that only an order of magnitude can be placed upon the relaxation time of the slowest part of the relaxation effect prevents evaluation of its dependence on the reactant concentrations and the molecularity of the process involved. Therefore, attention is confined to the faster relaxation process.

Qualitatively, the observed relaxation effect for the poly A–PR system is similar to that for the poly A–AO system in that it is a spectrum which extends over the time range measurable by the temperature-jump technique, and has a step in the first part of the spectrum which yields a linear semilogarithmic plot obtained in the manner already described. Nevertheless, significant differences from the poly A–AO system

---

[13] E. A. Guggenheim, *Phil. Mag.*, **2**, 538 (1926).

[14] E. S. Swinborne, *J. Chem. Soc.*, 2371 (1960).

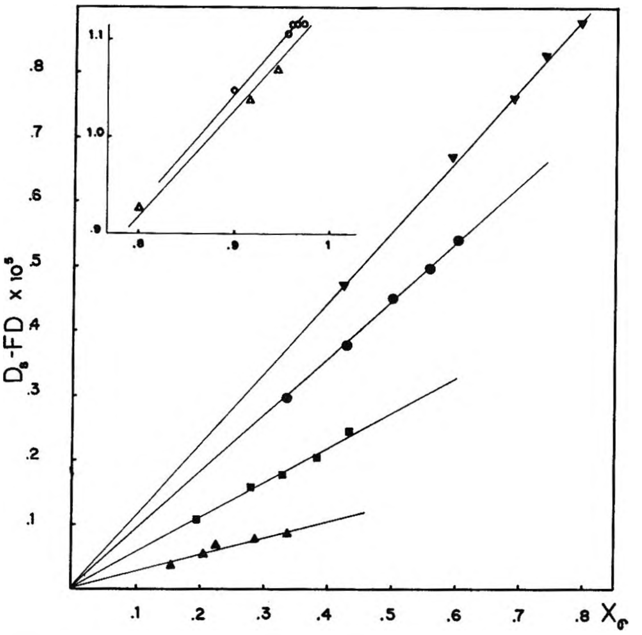

Figure 3. Excess self-diffusion coefficients for montmorillonite in NaCl solutions according to eq 5: ▲, 0.1 M; ■, 0.05 M; ●, 0.025 M; ▼, 0.0107 M; △, 0.002 M; O, 0.001 M. (To spread out the lines the ordinates, from top to bottom, have been divided by 1/1.1, 1, 1.5, 3.)

have been made at 15 and 35° only at 0.001, 0.002, and 0.01 M. The lines for these are entirely similar to those of Figure 3. Table III gives all the results for D_σ, the average deviations being computed regardless of clay content.

Table III: Surface Excess Self-Diffusion Coefficients for Sodium Ion in Montmorillonite–Sodium Chloride Suspensions[a]

Concn of equilibrium dialyzate, mequiv/l.	$D_\sigma \times 10^6$ cm^2 sec^{-1} 15°	25°	35°
1.00	1.25 ± 0.05	1.65 ± 0.08	2.19 ± 0.04
2.00	1.41 ± 0.03	1.80 ± 0.13	2.41 ± 0.08
10.70	2.05 ± 0.14	2.43 ± 0.09	3.28 ± 0.24
25.00		3.85 ± 0.07	
50.00		4.64 ± 0.24	
100.00		5.15 ± 0.39	

[a] All D_σ for 0.0107 M and greater concentrations are derived from the best lines of Figure 3, not forced through the origin.

Discussion

The marked departure of the conductance from simple behavior at low concentrations (Figure 1) must be ascribed at least in part to a decrease in the contribution of the surface excess conductance. As is seen from eq 4, if the effect were solely due to a change in the formation factor, this would necessarily be a decrease with decreasing concentration of salt. The opposite, if anything, is to be expected; peptization is taking place and the clay platelets are bcoming more eccentric—the shape factor, k, should become larger. If there were no change in surface conductance below the minima of the curves of Figure 1, the corresponding values of F would be less than unity, an absurdity.

Over a wide range of concentration (0.025–2.2 M) the conductance data are represented by constant values of K_σ and F.[4] Unless an extraordinary compensation is present, equally effective at three temperatures, the pertinent geometry of the suspension remains unchanged over this range of concentration. It does not follow that the same is true at lower concentrations. Some indirect support for the assumption of the constancy of F in this region is to be found in measurements of the viscosity of salt-free suspensions.[4] From such work is deduced a value for the shape factor in close agreement with that obtained from high salt conductivity. Nevertheless, in the absence of direct proof of the constancy of F at low salt concentrations, we are forced to adopt this only as a not unreasonable assumption. In eq 2 and 3 we have a method of extrapolating the formation factor into the dilute region. All of our computations are made on this basis. It is in this regard that our definition of D_σ is not strictly operational: D_σ cannot be deduced solely from measurements made on the system at hand. With this qualification in mind, we examine some of the properties of the excess self-diffusion coefficients. The behavior of these is far less complex than that of the Λ_σ (obtainable from eq 4); among other things, the latter depend on the clay content of the suspensions, whereas the values of D_σ do not.

In Figure 4 are given the lines depicting the dependence of ln D_σ on $1/T$; these are seen to be quite accurately straight for the two lower concentrations, 0.001 and 0.002 M. The data for the line at 0.0107 M probably reflect the accumulation of errors unavoidable at the higher concentrations. (The line for the salt-free suspensions was obtained by the extrapolation of Figure 5.) The corresponding values of the energy of activation are, for increasing concentration, 5.10 (at $c_s = 0$), 4.90, 4.71, 3.97 kcal/mole. These are seen to be but little different from those found for the self-diffusion of sodium in aqueous solution; the data of Slade, *et al.*,[6] at 0.001 M give 4.45 kcal/mole.

From these results one may estimate the value of $\lambda^2 \exp(\Delta S^\dagger/R)$ in the Eyring equation as applied to D_σ. Further discussion hinges on the choice of λ,

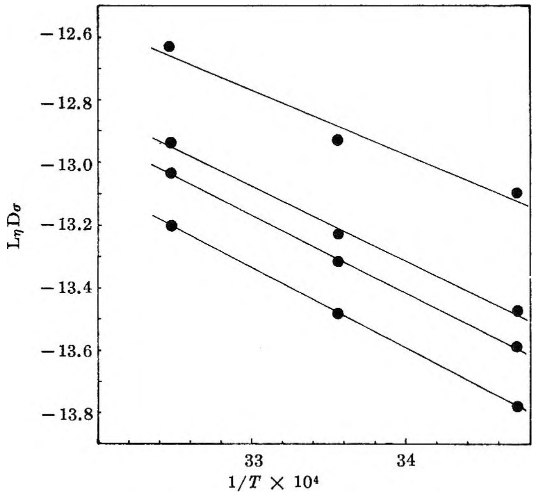

Figure 4. Arrhenius plots for the surface excess self-diffusion coefficient. From top to bottom: 0.0107, 0.002, 0.001 M NaCl. The lowest line is from the extrapolation to zero salt of Figure 5.

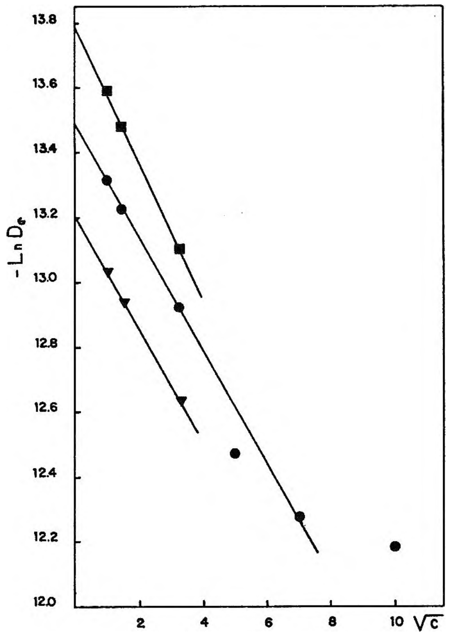

Figure 5. The dependence of the surface excess diffusion coefficient on the concentration of the equilibrium dialyzate; ln D_σ *vs.* the square root of c_s in mequiv/l.: ■, 15°; ●, 25°; ▼, 35°.

the "jump distance" for the elementary diffusional process. A minimum value for λ might reasonably be taken as the average distance between exchange sites on a clay platelet. For the Camp Berteau montmorillonite this distance is near 10.9 A.[8,9] This choice corresponds to $-\Delta S^\dagger = 7.0, 7.3, 9.1$ cal/mole deg for the three concentrations. Since little or nothing is known about the distribution of *sizes* of the clay particles or about their arrangement in suspension, we can make no estimate of the *average* jump distance for the process. It does appear reasonable to suppose that the activated complex is formed with a fall in entropy greater than 7 units.

One is led to speculate that the ordering effect in the surface diffusion process is associated with a rehydration, in the bulk solution, of ions from the surface where they had lost part of their shell of water molecules. The gain in energy due to such an effect helps to explain what otherwise appears to be an unaccountably low value for the energy of activation. It will be interesting to see if this speculation can survive a test with ions known to be less hydrated than sodium.

To discuss the concentration dependence of D_σ, we need the form of the Eyring equation with activity coefficients explicitly expressed. To arrive at this, we note merely that the thermodynamic activity of the activated complex must be a constant: the complex is in equilibrium with a saturated surface. Thus $c^\dagger\gamma^\dagger$ is constant, and if, with Eyring, we put D_σ proportional to $c^\dagger$ we have at once

$$\ln D_\sigma(c_s) = -\ln \gamma^\dagger + \ln D_\sigma(0)$$

Here $\gamma^\dagger$ is the single-ion activity coefficient for, perhaps, $Na_2^{2+}\cdot(aq)$ in a solution of concentration c_s. One is led at once to make plots of ln D_σ *vs.* $\sqrt{c_s}$. These are given in Figure 5, where ln D_σ is seen to be linear at low concentration. For these solutions a semiquantitative estimate of ln $\gamma^\dagger$ can be obtained from the Debye–Hückel limiting law, $\ln \gamma^\dagger = -Z^2A\cdot\sqrt{c_s}$ with $Z = 2$. The slopes of the lines of Figure 5 are thereby predicted to be 4.6, 4.7, 4.8. The least-squares best lines through the three points at the lower concentrations have slopes of 6.6, 5.4, and 5.5. The character of this somewhat better than qualitative agreement lends verisimilitude to an otherwise unconvincing picture for the activation process. Clearly a severe test of this idea will be possible only with data for an ion of multiple charge.

Acknowledgment. We are much indebted to the Petroleum Research Fund of the American Chemical Society and to the National Science Foundation for grants which have made this work possible.

---

[8] J. J. Fripiat, *Bull. Groupe Franc. Argiles*, 4, 23 (1957).

[9] J. J. Fripiat, "Proceedings of the 12th National Conference on Clays and Clay Minerals," Pergamon Press, New York, N. Y., 1964, p 327.

Characterization of Graft Copolymers of Methylated Xylan and Polystyrene

by James J. O'Malley and R. H. Marchessault

Cellulose Research Institute and Chemistry Department, State University College of Forestry, Syracuse, New York

(Received April 11, 1966)

The preparation and characterization of graft copolymers of methylated xylan and polystyrene are described. The copolymers were prepared anionically by reaction between "living" polystyrene and the methyl glucuronate moiety to give well-defined comblike structures. Infrared analysis indicated that all ester functions reacted. Copolymer compositions were determined by oxygen analyses and optical rotation measurements. The grafted structures were established through molecular weight analysis which showed that on the average each ester had reacted at least once. The intrinsic viscosity was found to decrease with increasing branch density. Contrary to predictions for homopolymer grafts, the osmotic second virial coefficient increased with branch density.

Introduction

This report is concerned with the physicochemical characterization of methylated xylan–polystyrene graft copolymers. A previous note[1] reported the synthesis of this type of graft copolymer which is summarized in Figure 1, where X stands for a monomer unit in the linear backbone of poly-β-D-anhydroxylose. The actual grafting site is on the ester grouping of the methylated glucuronate moiety which occurs randomly along the backbone. The substrate is essentially a linear copolysaccharide of a simple carbohydrate—2,3-dimethylxylose—and a disaccharide—3-methyl-2-O-(methyl 2,3,4-trimethylglucuronate)xylose. A question raised by the data in the previous paper concerns the extent of reactivity of the ester group and whether one or two living polystyrene chains react with each ester group. Korotkov, *et al.*, have suggested that the second reaction can take place but their results with the poly(methyl methacrylate)–polystyrene system provide no evidence of its occurrence. The controlling factor in the second-stage reaction is more likely steric rather than electronic since the preparation of an alcohol *via* nucleophilic attack on the ester carbonyl is a classical organic reaction. Evidence that the grafting efficiency (number of polystyrene chains per ester) is greater than unity necessitates a careful analysis of the reaction product. The present copolymer, because of the unique structure of its polysaccharide backbone, lends itself to a rather complete characterization which is described herein.

Experimental Section and Results

Synthesis. Polystyrylpotassium was prepared by conventional high-vacuum techniques in tetrahydrofuran (THF) solution with cumylpotassium as initiator.[2] Its molecular weight was calculated[3] as 1100 and by measurement in a Mechrolab vapor pressure osmometer in chloroform at 37° it was experimentally found to be 1070. The polystyrylpotassium "living end" concentration was determined spectrophotometrically at 340 mμ.

The 4-O-methyl glucuronoxylan from Aspen[4] was methylated and esterified by well known procedures.[5,6] Complete methylation and esterification was established by methoxyl, oxygen, and infrared analysis. The number-average molecular weight of this sample as measured in chlorobenzene in a Mechrolab membrane osmometer was 15,500. The xylan solution in THF was prepared by freeze drying a weighed amount of xylan in thiophene-free benzene in an ampoule with attached break-seal, evacuating it for an additional

---

[1] J. J. O'Malley and R. H. Marchessault, *J. Polymer Sci.*, **B3**, 685 (1965).

[2] R. Asami, M. Levy, and M. Szwarc, *J. Chem. Soc.*, 361 (1962).

[3] R. Waach, A. Rembaum, J. D. Coombes, and M. Szwarc, *J. Am. Chem. Soc.*, **79**, 2026 (1957).

[4] J. K. N. Jones, C. B. Purves, and T. E. Timell, *Can. J. Chem.*, **39**, 1059 (1961).

[5] W. N. Haworth, *J. Chem. Soc.*, **107**, 8 (1915).

[6] R. Kuhn, H. Tirschman, and I. Löw, *Angew. Chem.*, **67**, 32 (1955).

48 hr, and finally distilling THF into the ampoule to make the desired concentration.

The graft copolymers were prepared by adding a THF solution of xylan to stirred "living" polystyrylpotassium at room temperature. The molar ratio of "living ends" to ester functions was 2.0 in the reaction mixture. The reaction was terminated after 1 hr by the addition of methanol. The graft copolymers were recovered by precipitation in methanol and subsequent freeze drying from benzene.

A comment regarding the visual observations made on the grafting reaction may be in order. Upon addition of the xylan solution to the "living" polystyrene solution, the intense red color diminished considerably and determination of the "living end" concentration indicated that approximately 80% of the "living" polymer had reacted. The viscosity of the reacting solution increased to a viscous syrup and after 10 min reaction time, a gellike precipitate appeared followed by a decrease in the viscosity of the solution. The viscous syrup was probably due to intermolecular ionic association of the molecules in solution[7] which is destroyed by the precipitation of the potassium methoxide salt. The reddish orange color of the reaction medium persisted during this period and upon addition of methanol and opening of the apparatus to the atmosphere there was no change in this color. The fact that neither methanol nor oxygen decolorized the solution indicates the color cannot be due to unreacted polystyrene "living ends." The gellike precipitate is thought to be potassium methoxide because of its solubility in methanol, a nonsolvent for both polymers used.

Fractionation and Composition of Graft Fraction. The graft copolymer was fractionated from benzene solution by the addition of petroleum ether and fractions containing varying amounts of xylan were isolated. These fractions were characterized according to their polystyrene composition, optical rotation, number-average molecular weight, and intrinsic viscosity.

The polystyrene content of the fractions was determined by oxygen analysis. Initially, it was thought that the specific optical rotation of a 1% solution of the graft in chloroform at a wavelength of 589 mμ could also be used for this determination since only the xylan is optically active. The composition data, based on oxygen analysis and optical rotation, are shown in Table I.

Table I: Composition Analysis of Graft Fractions[a] Based on Oxygen Analysis and Optical Rotation

Fraction	Wt, g	$[\alpha]^{28}D$ (c = 1%, in $CHCl_3$)	% oxygen	% xylan from	
				Rotation	Oxygen
Reference xylan	...	−63.0	40.34	100	100
1	0.5	Insol	...	...	...
2	1.1	−78.2	34.75	124	86.1
3	0.58	−74.3	35.07	118	86.8
4	0.82	−58.6	29.14	92.8	72.2
5	0.5	−40.0	24.57	62.5	60.9
6	0.3	−34.5	21.76	54.8	53.9
7	0.5	−33.9	21.32	53.8	52.8
8	0.3	−30.9	17.83	49.0	44.2
9	0.75	−27.4	19.95	43.5	49.5
10	1.0	−2.9	...	4.6	
11	0.3	−3.1	...	4.9	

[a] The fractionation yielded a total of 6.8 g or an 89% recovery of the material fractionated.

A large discrepancy is apparent between the analytical results for the two methods used for determining the composition. Oxygen analysis is clearly more absolute than the specific rotation analysis. The latter method involves the assumption that all fractions of the methylated xylan chains are equally substituted in 4-O-methylglucuronic acid residues. This assumption is questionable since previous studies have shown that fractions with different uronic acid content can be isolated from a given xylan sample or a given wood source.[8] Since the xylan rotation is increasingly negative for lower uronic acid content, the greater than 100% xylan contents calculated for fractions 2 and 3 from the observed rotations are best explained in terms of a "lower than average uronic content." Only oxygen analysis was relied on for determining the composition of the graft fractions.

In another respect the optical activity of the polysaccharide backbone proved to be uniquely valuable as an analytical tool. The specific rotation of acidic xylan is a function of uronic acid content.[9] The reason for this dependence is the opposite rotatory contributions of the β linkages in the backbone and the α linkages of the uronic acid side groups to the specific rotation. The specific rotation decreases; that is, it has a larger negative value, as the number of uronic acid groups on a given chain decreases. This is also true of methylated xylan. This dependency enables one to determine the number of uronic esters per xylose unit in xylan by setting up a calibration curve of specific rotation *vs.* the number of uronic esters per xylose and

---

(7) D. H. Richards and M. Szwarc, *Trans. Faraday Soc.*, **55**, 1644 (1959).

(8) I. Croon and B. F. Enström, *Tappi*, **44**, 870 (1961).

(9) R. H. Marchessault, T. E. Timell, and H. Holava, *Can. J. Chem.*, **41**, 1912 (1963).

then measuring the specific rotation of the xylan. The curve has been constructed using values of $[\alpha]_D$ reported in the literature for methylated xylans having different degrees of uronic acid substitution. A linear relationship was found as has been realized previously in the case of the unmethylated xylans.[8,9] The linear relation is given by

$$[\alpha]_D = +249(1/\sigma) - 91 \quad (1)$$

where σ is the ratio of xylose to ester groups in the methylated xylan.

To use the calibration curve for analyzing the uronic acid content of xylan in graft copolymers, it is necessary to correct the measured specific rotation of the graft copolymer for the polystyrene content which contributes nothing to the rotation. To do so, the measured specific rotation is divided by the per cent xylan in the graft copolymer as found by oxygen analysis. If the xylan used in the grafting reaction was homogeneous with respect to uronic acid composition, the corrected values for the specific rotation of the xylan in each graft fraction should be −63.0° which corresponds to 1 acid per 9 xylose units. However, the initial xylan was heterogeneous with respect to uronic acid substitution, and therefore the corrected specific rotations deviate from this value. The corrected specific rotations and the number of xylose units per uronic ester are given in Table II for fractions 4, 5, 6, 7, and 9 which were chosen for more extensive study because they exhibited good solubility properties.

Table II: Uronic Acid Substitution of Xylan in Graft Fractions

Fraction	$[\alpha]_D$	% xylan by O_2 anal.	$[\alpha]_D$ (cor)	No. of xylose units/ uronic ester
4	−58.6	72.2	−81.1	25.0
5	−40.0	60.9	−65.7	9.8
6	−34.5	53.9	−64.0	9.2
7	−33.9	52.8	−64.1	9.2
9	−27.4	49.5	−55.3	7.0

It is readily seen from the data in the last column of Table II that the xylan chains used in the grafting experiment are heterogeneous in uronic ester composition. The fraction containing the lowest amount of polystyrene also has the lowest uronic ester substitution.

Molecular Weight Analysis of Graft Fractions. Molecular weight measurements have always been an important aspect of graft copolymer characterization.[1,10,11] Only molecular size distinguishes a graft copolymer sample and a physical mixture of the same two polymers. The number-average molecular weights were measured in chlorobenzene at 37° in a Mechrolab (Model 501) membrane osmometer.

Knowing the number-average molecular weight ($\bar{M}_n$) of the graft copolymer and its composition, one is able to calculate the $\bar{M}_n$ of the xylan in each graft fraction. Although the number-average molecular weight of the xylan used in the grafting reaction was 15,500, the heterogeneity in molecular weight of the xylan will cause the calculated $\bar{M}_n$ of the xylan in each fraction to vary. By difference one also obtains the summative $\bar{M}_n$ of the grafted polystyrene in the fraction. It is then simple to calculate the average number of polystyrene chains per substrate molecule since the $\bar{M}_n$ of each polystyrene chain is 1100. The data are shown in Table III.

Table III: Molecular Weight Analysis of Graft Fractions

Fraction	$10^{-4}\bar{M}_n$	% xylan	$10^{-4}\bar{M}_n$ (xylan)	$10^{-4}\bar{M}_n$ (polystyrene)	No. of graft chains
4	2.77	72.2	1.96	0.81	7.4
5	2.78	60.1	1.70	1.08	9.8
6	3.06	53.9	1.65	1.41	12.8
7	2.78	52.8	1.47	1.31	11.9
9	2.58	49.5	1.28	1.30	11.8

From Table III the following conclusions seem reasonable. (a) The $\bar{M}_n$ of our graft fractions are very similar, the highest and lowest differing by about 15%. (b) The calculated $\bar{M}_n$ of xylan in each fraction indicates the xylan is somewhat heterogeneous in molecular weight. (c) The number of grafted polystyrene chains appears to be independent of the xylan $\bar{M}_n$. The last conclusion merits further comment. Both Rempp[10] and Korotkov[12] have found that for a polydisperse backbone polymer (*i.e.*, PMMA), the efficiency or degree of grafting (ratio of reacted sites to total sites available for reaction) is highest for the lowest molecular weight backbone polymer. Rempp also comments that for a monodisperse backbone there is little, if any, fluctuation in the degree of grafting. From the data in Table III we see that the molecular

---

[10] Y. Gallot, P. Rempp, and J. Parrod, *J. Polymer Sci.*, **B1**, 329 (1963).

[11] C. P. J. Glaudemans and E. Passaglia, *ibid.*, **C2**, 189 (1963).

[12] S. P. Mitsengendler, G. A. Andreyeva, K. I. Sokolava, and A. A. Korotkov, *Vysokomolekul. Soedin.*, **4**, 1366 (1962).

the coefficient of the quadratic term is extremely small (0.0003), and the average deviation remains ±0.0002. Increasing the degree of the polynomial to 3 or 4 (*i.e.*, $n = 3$ or 4 in eq 9) does not improve the fit. Thus, our data show no evidence for association of water molecules in benzene solution.

The situation in chloroform solutions of water is quite different. Fitting the data to an equation of the same form as (10) gives

$$C_w = 0.0729a_w \qquad (12)$$

The average deviation here is ±0.0006, three times the estimated error in C_w. Moreover, the deviations at low water activities (<0.8) are all negative, while those at higher values of a_w are positive. This suggests that a second-degree polynomial of the form of (11) would give a better fit. Least-squares treatment gives

$$C_w = 0.0691a_w + 0.0045a_w^2 \qquad (13)$$

The average deviation is now reduced to ±0.0002; positive and negative deviations occur randomly. Statistical analysis[12] reveals that the coefficient of the quadratic term is significant at the 99.5% confidence limit. We conclude that significant association of water molecules occurs in chloroform solution.

On the basis of our data, it is not necessary to postulate the presence of polymeric water species higher than dimers in chloroform solution. Fitting the data to an equation of the form of (9) with $n = 3$ gives

$$C_w = 0.0707a_w + 0.0030a_w^3 \qquad (14)$$

The average deviation in this case is ±0.0002, precisely that obtained with eq 13.

The conclusions reached with chloroform solutions are equally valid for solutions of water in 1,2-dichloroethane. The relations between concentration and activity of water are best expressed by the second-degree polynomials

$$(25°) \quad C_w = 0.1131a_w + 0.0138a_w^2 \quad \text{(av dev } \pm 0.0002) \qquad (15)$$

$$(5°) \quad C_w = 0.0639a_w + 0.0049a_w^2 \quad \text{(av dev } \pm 0.0004) \qquad (16)$$

The increased scatter of the data at 5° may reflect errors in estimating the activity of water in calcium chloride solutions at this temperature. Statistical analysis shows that the coefficients of the quadratic terms in (15) and (16) are significant at the 99.5 and 98% confidence limits, respectively. Third-degree equations similar to (14) do not improve the fit; the average deviations between experimental and calculated values of C_w remain ±0.0002 at 25° and ±0.0004 at 5°.

Equilibrium constants for dimer formation can be calculated from the coefficients of the linear and quadratic terms of eq 13, 15, and 16. Comparison of eq 7 and 11 shows that

$$K = \frac{B}{2A^2} \qquad (17)$$

It is evident from Table III that, at a given temperature and concentration, water is associated to approximately the same extent in chloroform as in 1,2-dichloroethane. The relatively small change with temperature of the equilibrium constant for association of water in 1,2-dichloroethane is rather surprising. It is difficult, however, to attribute too much significance to this because of the uncertainties in the values of a_w at 5°. One can calculate that a change of 20% in the value of the heat of dilution could increase K at 5° to about 0.7 l. mole^{-1}.

Table III: Equilibrium Constants for $2H_2O \rightleftharpoons (H_2O)_2$

Solvent	Temp, °C	K, l. mole^{-1}
Chloroform	25	0.47
1,2-Dichloroethane	25	0.54
1,2-Dichloroethane	5	0.6

It should be emphasized that the equilibrium constants reported in Table III correspond to relatively small amounts of association. One can calculate, for example, that in a saturated solution of water in chloroform at 25°, only about 6% of the water molecules would be associated.

Christian, *et al.*,[6] found somewhat larger deviations from Henry's law in solutions of water in 1,2-dichloroethane than those reported here. Likewise, they observed a larger temperature dependence of the association constant for this system.

Acknowledgment. This work was supported, in part, by a grant from the Research Foundation of the University of Connecticut. We are indebted to Mr. Peter Skribanowitz for constructing the apparatus used to determine dissolved water and to Miss Lillian Acayan for assisting in the statistical analysis.

---

[12] F. Graybill, "An Introduction to Linear Statistical Models," Vol. I, McGraw-Hill Book Co., Inc., New York, N. Y., 1961, p 166.

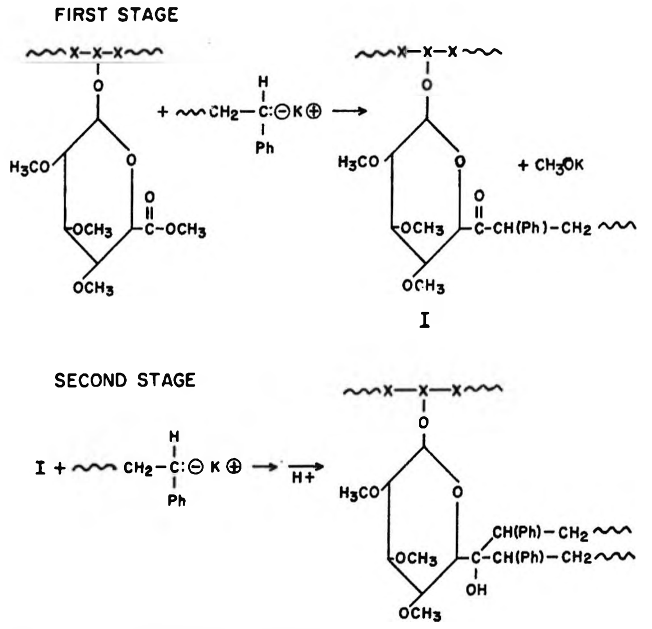

Figure 1. Reaction scheme for coupling of "living" polystyrene and methyl glucuronate ester of completely methylated xylan.

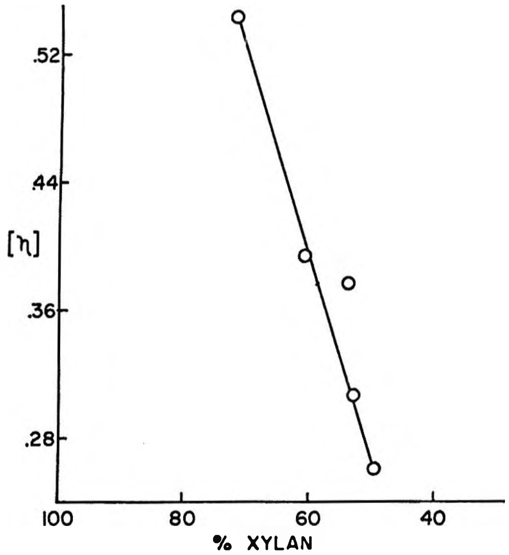

Figure 2. Effect of copolymer composition on the intrinsic viscosity in chlorobenzene measured at 37°.

system, α has been assumed to be equal to 1.0 and K has been calculated using the intrinsic viscosity and number-average molecular weight measured in this work. The value of K was found experimentally to be about 2.8×10^{-5}. The data are shown in Figure 3 and the observed decrease in the ratio $[\eta]_B/[\eta]_L$ is in agreement with theoretical predictions of the effect of branching on viscosity. In fact, several theoretical treatments[14,17,18] of the hydrodynamic properties of

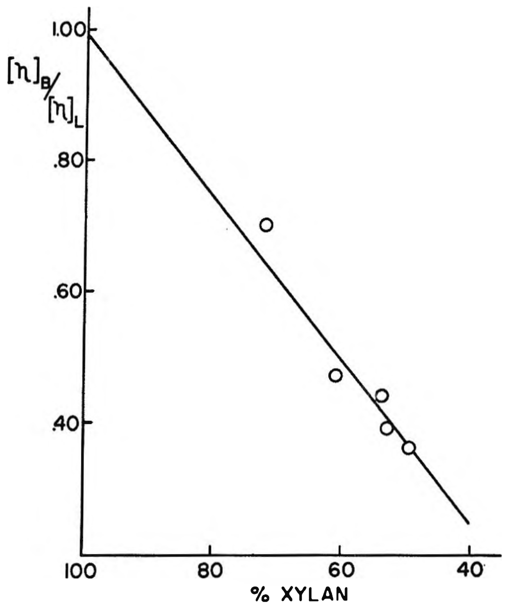

Figure 3. Effect of copolymer composition on the viscosity ratio of graft to equivalent linear methylated xylan.

branched homopolymers attempt to relate a parameter "g," defined as the ratio of the mean-square radii of gyration of a branched and linear polymer of the same molecular weight to some function of the above-mentioned viscosity ratio. Unfortunately, there is no equivalent parameter which can be used to characterize branched copolymers.

Preliminary experiments on the solubility characteristics of the graft copolymers indicate the polystyrene grafts exert considerable influence on the solubility of the copolymers. Xylan is swollen by dimethylformamide (DMF) and is insoluble in cyclohexane, yet fraction 9 is easily dissolved in pure DMF and 80% cyclohexane–20% chlorobenzene with no change in the intrinsic viscosity as measured in pure chlorobenzene. More extensive measurements will be communicated at a later date.

The Second Virial Coefficients. The second virial coefficient, A_2, was obtained for the fractions from the slope of the reduced osmotic pressure–concentration plots. Figure 4 shows A_2 plotted against the composition of the graft fractions. Theory predicts[17] a decrease in A_2 as a result of branching, and this is observed in the present study since the ungrafted methylated xylan has $A_2 = 2.65 \times 10^{-3}$ in chlorobenzene. Also plotted in Figure 4 is Γ_2 *vs.* composition.

---

[17] W. H. Stockmayer and M. Fixman, *Ann. N. Y. Acad. Sci.*, **57**, 334 (1954).

[18] C. D. Thurmond and B. H. Zimm, *J. Polymer Sci.*, **8**, 477 (1952); B. H. Zimm and R. W. Kilb, *ibid.*, **37**, 19 (1959).

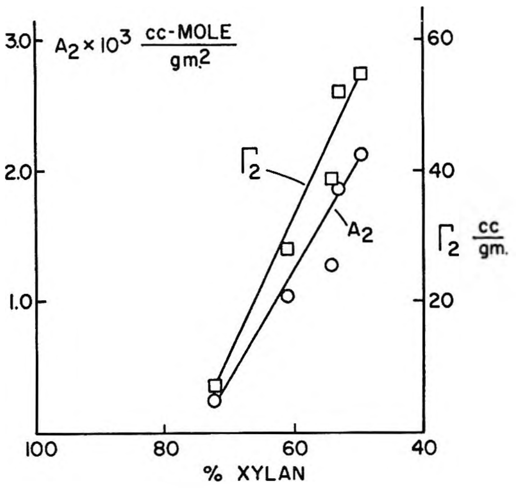

Figure 4. Effect of copolymer composition on the osmotic second virial coefficient. Γ_2 is the product of A_2 with the number-average molecular weight.

This quantity is related to the virial coefficient by the relationship, $\Gamma_2 = A_2\bar{M}_n$. The trend in Γ_2 with composition is similar to that of A_2, since the molecular weight of each fraction is similar and it can be interpreted in the same manner.

In addition, however, the data of Figure 4 show a significant rise in A_2 as a function of the branch density along the backbone. Since all fractions have nearly the same molecular weight, it appears that the increase in A_2 is best explained in terms of repulsive interactions between the two dissimilar segments of the graft copolymer.[19] Although seldom considered, these extra interactions would seem to be the reason for some of the favorable solubility properties of grafts compared to their component homopolymers or compared to compositionally equivalent block and statistical copolymers.[20] Qualitatively, these interactions should expand the polymer coil and cause $[\eta]_B$ to be larger than would be observed in a θ solvent, $[\eta]_{B\theta}$. In the preceding section it was shown that $[\eta]_B$ decreases over the same range of composition for which A_2 increases. This was inevitable since the shape factor far outweighs the interaction factor with increasing degree of branching. What must be compared is the ratio $[\eta]_B/[\eta]_{B\theta}$ at each grafting level and this should increase in parallel with A_2 as a function of composition.[21] Such measurements are in progress; however, calculation of $[\eta]_{B\theta}$ using Krigbaum's[22] semiempirical equation which related intrinsic viscosity to A_2 shows that considerable coil contraction is to be expected for the more highly grafted fractions. French workers[23] have already made observations of this phenomenon and have referred to the tightly coiled molecules as "molecular micelles" or "internally precipitated."

Conclusions

The physicochemical characterization of well-defined graft copolymers of methylated xylan and polystyrene has been presented. Heretofore, such analyses of graft copolymers, especially in the polysaccharide field, have been hampered by the ill-defined structures synthesized. We have succeeded in allowing each potential grafting site to react at least once and, as a result, have obtained predictable structures. Dilute solution measurements were made, but their quantitative interpretation is premature since no theories exist for heteropolymer constructs. The expected decrease in viscosity due to branching has been observed. The parallel increase in the second virial coefficient data with branch density is not predicted by theory and constitutes one area where existing theories on homopolymer constructs are not applicable to the present case.

Although only briefly mentioned, another interesting observation was the solubilizing effect exerted by polystyrene on the xylan part of the copolymer in solvents which do not dissolve the ungrafted xylan derivative. Further study is being conducted in this area.

Acknowledgment. This project was supported by a grant from the Army Research Office (Durham).

---

(19) W. H. Stockmayer, L. D. Moore, Jr., M. Fixman, and B. N. Epstein, *J. Polymer Sci.*, **36**, 517 (1955).

(20) Y. Gallot, M. Leng, H. Benoit, and P. Rempp, *J. Chim. Phys.*, 1093 (1962).

(21) D. Froelick, G. Boeckel, and H. Benoit, *Compt. Rend.*, **259**, 4675 (1964).

(22) W. R. Krigbaum and Q. A. Trementozzi, *J. Polymer Sci.*, **28**, 295 (1958).

(23) A. Dondos, P. Rempp, and H. Benoit, *J. Chim. Phys.*, 821 (1965).

The Hydrogen Fluoride Solvent System. IX.[1,2] Potentiometric Study of the Systems: (1) $Cu(s),CuF_2(s)|TlF(HF)|TlF_3(s)(Pt)$; (2) $Ag(s)|AgF,TlF(HF)|TlF_3(s)(Pt)$; (3) $Ag(s)|AgF(HF)|AgF_2(s)(Pt)$

by A. F. Clifford,[3] W. D. Pardieck, and M. W. Wadley

Department of Chemistry, Purdue University, Lafayette, Indiana *(Received April 14, 1966)*

The emf's of the systems given in the title, measured potentiometrically, have the values for $E°_{273}$ of 0.9269 ± 0.0019, 1.3816 ± 0.0071, and 0.5654 ± 0.0069 v and the values for $\Delta G°_{273}$ of −42.7 ± 0.1, −31.8 ± 0.2, and −26.1 ± 0.3 kcal/mole, respectively. From the same data, the thermodynamic ionization constants $K_{b(\text{apparent})}$ and $K_{b(\text{molar})}$ were calculated for the reactions $AgF \rightleftharpoons Ag^+ + F^-$ and $TlF \rightleftharpoons Tl^+ + F^-$ in HF at 0°. The apparent and molar activity coefficients for the electrolytes above were also calculated.

Introduction

Data on cell potentials in liquid hydrogen fluoride have been reported in only a few instances. They are of considerable interest, however, because of the information which they can give, not only on the free energies of the cell reactions but also on activity coefficients, equilibrium constants, and the like, and also for the contributions which they can make toward determination of other thermodynamic properties.

In a continuation of the potentiometric studies in liquid HF reported earlier,[4] the standard electrode potentials were determined for the systems mentioned in the title. Using these data, the Gibbs free energies for the cell reactions were calculated and also the basic ionization constants and apparent and molar activity coefficients of the electrolytes AgF and TlF in HF at 0°.

The standard electrode potential of the single-compartment cell

$$Cu(s),CuF_2(s)|TlF(HF)|TlF_3(s)(Pt)$$

was redetermined and found to be 0.9269 ± 0.0019 v, which differs by 1.3 mv from the previously reported value.[4]

The potentials for the cell

$$Ag(s)|AgF,TlF(HF)|TlF_3(s)(Pt)$$

could also be determined in a single compartment, since neither of the electrolytes in solution could be oxidized by TlF_3 or reduced by silver metal. The standard electrode potential of the cell at 0° was found to be 0.5654 ± 0.0069 v.

Similarly, a single compartment sufficed for the cell

$$Ag(s)|AgF(HF)|AgF_2(s)(Pt)$$

for which $E°_{273}$ was found to be 1.3816 ± 0.0071 v. Great difficulty was experienced in obtaining stable and consistent potentials in this last case until methods were developed for the purification of the silver fluorides. In all three cases the oxidizing fluorides (TlF_3 and AgF_2) were prepared or purified externally and were transferred in an anhydrous atmosphere to a platinum-cup electrode, as described in ref 4.

Experimental Section

Apparatus. The experimental apparatus was essentially as previously described.[4]

---

[1] Work supported by U. S. Atomic Energy Commission under Contract No. AT(11-1)-620; paper No. COO-620-2.

[2] Taken from the thesis submitted to the faculty of Purdue University in partial fulfillment of the requirements for the degree of Doctor of Philosophy of M. W. Wadley, and for the degree of Master of Science of W. D. Pardieck.

[3] Department of Chemistry, Virginia Polytechnic Institute, Blacksburg, Va. 24061.

[4] A. F. Clifford and E. R. Zamora, *Trans. Faraday Soc.*, **57**, 1963 (1961).

Reagents. Thallium(I) fluoride, purchased from K & K Laboratories (Jamaica, N. Y.), was analyzed for thallium content using the method of Smith and Wilcox.[5] The fluoride content was determined by titration with an aqueous solution of thorium(IV) nitrate previously standardized against a solution of accurately weighed KF using alizarin red S indicator (Found: Tl, 90.6%; F, 8.4%). The thallium(III) fluoride used was that prepared by Zamora.[4] The silver(I) fluoride, purchased from Harshaw Chemical Co., Cleveland, Ohio, was purified by recrystallization from liquid hydrogen fluoride to obtain the white salt $AgHF_2$, which was either used as such or was heated in a platinum evaporating dish to obtain the yellow-orange AgF. This had a silver fluoride content of 99.66%. The silver(II) fluoride, also from Harshaw Chemical Co., was purified by stirring it in liquid HF for 8 hr, filtering off the bulk of the liquid, and repeating the process twice more on the residue. This procedure removed any silver(I) fluoride and any oxide as water.

General Procedure. The system was first rinsed with liquid hydrogen fluoride and this liquid was discarded. In a drybox the electrolyte was weighed into the vessel containing a Teflon-coated magnetic stirring bar. The vessel was removed from the drybox in a polyethylene bag containing a desiccant and was quickly put in place after the TlF_3 or AgF_2 was placed in the platinum-cup electrode, while being flooded with dry nitrogen. The cell was flushed with dry nitrogen for at least 0.5 hr and finally with HF vapors. Liquid hydrogen fluoride, doubly distilled into the reservoir and having a conductivity varying from 1.54 to 5.72×10^{-3} ohm^{-1} cm^{-1} corresponding to water concentrations of 0.01 *M* or less, was allowed to flow into the cell with the magnetic stirrer in operation. After thorough stirring to dissolve the electrolyte, the potentials were measured by a digital voltmeter which was frequently compared with a K-2 potentiometer (Leeds and Northrup). The largest deviation was 0.07 mv. Samples were removed from the cell by forcing liquid into the buret using nitrogen pressure after the system had attained the "steady-state potential," that is, when the potential changed less than 1 mv/hr. These were evaporated and analyzed for concentration of electrolyte.

By a method of successive dilutions, further potentials at various concentrations were obtained.

Treatment of Data. All calculations were performed on the IBM 7090 computer. In the treatment of data, two assumptions were made which seemed justified by the results. They are (1) that the electrolyte was completely dissociated at all concentrations and (2) that molarity rather than molality may be used for expressing concentrations. If the first of these assumptions is not correct, the slope of the line obtained by plotting the square root of the ionic strength *vs.* calculated potentials will differ from that which would be obtained if it is correct, but the intercept at infinite dilution should not change, unless dissociation at infinite dilution is incomplete. However, judging from the observed trends of the activity coefficients, this is not the case. As to the latter assumption, in solutions for which the density is very nearly the same as that of the pure solvent, and the density of pure solvent is near unity—as it is for HF—the terms may be used interchangeably without appreciable error.

The calculated potentials were obtained using the equation

$$E^{\circ\prime} = E_{\text{obsd}} + \frac{2RT}{nF} \ln m_{\pm} \tag{1}$$

which for the cells having $n = 2$ becomes

$$E^{\circ\prime} = E_{\text{obsd}} + 0.0542[{}^1/_2(\log\,[\mathrm{M}^+] + \log\,[\mathrm{F}^-])] \tag{2}$$

The apparent activity coefficients were calculated from the cell potentials according to the method used in ref 4 using the equation

$$\log \gamma_{\pm(\text{apparent})} = \frac{1}{k}(E^{\circ} - E^{\circ\prime}) \tag{3}$$

"Molar" activity coefficients were also calculated using the equation

$$\log \gamma_{\pm(\text{molar})} = \frac{-S\alpha^{1/2}}{1 + A\alpha^{1/2}} - \log\left(1 + \frac{\beta\mu M_1}{1000}\right) \tag{4}$$

where S is a function of valence and number of ions, dielectric constant of the solvent, and absolute temperature; $\alpha = \Sigma c_i z_i^2$ (*i.e.*, 2μ); A is a function of ionic size, dielectric constant of the solvent, and absolute temperature; β is the number of ionic species produced by the dissociation of one molecule of electrolyte; and M_1 is the molecular weight of the solvent. These, however, showed no greater internal consistency than the apparent activity coefficients and were not used in the final interpretation.

All fluoride ion concentrations included the contribution from the solvolysis of water (not exceeding 0.01 *M*) according to the equation

$$\mathrm{HF} + \mathrm{H_2O} \rightleftharpoons \mathrm{H_3O^+} + \mathrm{F^-} \tag{5}$$

The basic ionization constant for water in HF has been found by Kongpricha and Clifford[6] to have the value 0.55, for the equilibrium given in eq 6.

---

[5] G. F. Smith and C. S. Wilcox, *Ind. Eng. Chem., Anal. Ed.*, **14**, 49 (1942).

[6] S. Kongpricha and A. F. Clifford, *J. Inorg. Nucl. Chem.*, **18**, 270 (1961).

$$K_b = \frac{[H_3O^+][F^-]}{[H_2O]} \qquad (6)$$

In this equation $[F^-]$ represents total fluoride ion concentration from all sources, but $[H_2O]$ represents undissociated water only. Equation 6 may be expressed for this work as

$$K_b = \frac{[H_3O^+]([\text{sum of other cations}] + [H_3O^+])}{(0.01 - [H_3O^+])} = 0.55 \qquad (7)$$

Letting $X = [H_3O^+]$, this becomes the quadratic

$$X^2 + ([\text{sum of other cations}] + 0.55)X - 0.0055 = 0 \qquad (8)$$

This total fluoride ion concentration is the sum of the concentrations of all cations in the solution including oxonium ion concentration obtained by solving eq 8 for each set of data.

The basic ionization constant of the electrolyte may be calculated using the equations

$$MF(HF) \rightleftharpoons M^+ + F^- \qquad (9)$$

and

$$K_b = \frac{[M^+]\gamma_M[F^-]\gamma_F}{[MF]\gamma_{MF}} \qquad (10)$$

where the symbols have their usual meanings and where [MF] is the concentration of un-ionized metal fluoride, *i.e.*, the stoichiometric concentration of metal fluoride minus $[M^+]$. To take the effect of the ionization of water into account

$$[F^-] = [M^+] + [H_3O^+] \qquad (11)$$

the water content of the HF was always determined conductometrically immediately before each run.

If now the assumption is made that the activity coefficients actually represent the degree of ionization, an apparent K_B' can be calculated for each electrolyte concentration (taken as the ionic strength). Extrapolation by the IBM 7090 of $-1/\log K_B'$ *vs.* $\mu^{1/2}$ to zero ionic strength gave the thermodynamic K_B for the metal fluoride.

Results

The $E°_{273}$ reported by Clifford and Zamora[4] for the $Cu(s),CuF_2(s)|TlF(HF)|TlF_3(s)(Pt)$ system was corroborated. The cell potentials were found to obey the equation

$$E°' = 0.9269 + 0.1002\mu^{1/2} \qquad (12)$$

The dissociation constant of TlF in HF was found to be 1.04 ± 0.03, several orders of magnitude greater than reported in ref 4.

The system $Ag(s)|AgF(HF)|AgF_2(s)(Pt)$ was found to follow the equation

$$E°' = 1.3816 + 0.09526\mu^{1/2} \qquad (13)$$

The dissociation constant of AgF in HF was calculated to be 0.087 ± 0.0025.

The system $Ag(s)|AgF,TlF(HF)|TlF_3(s)(Pt)$ followed the equation

$$E°' = 0.5654 \pm 0.047\mu^{1/2} \qquad (14)$$

The data are summarized in Table I and Figure 1.

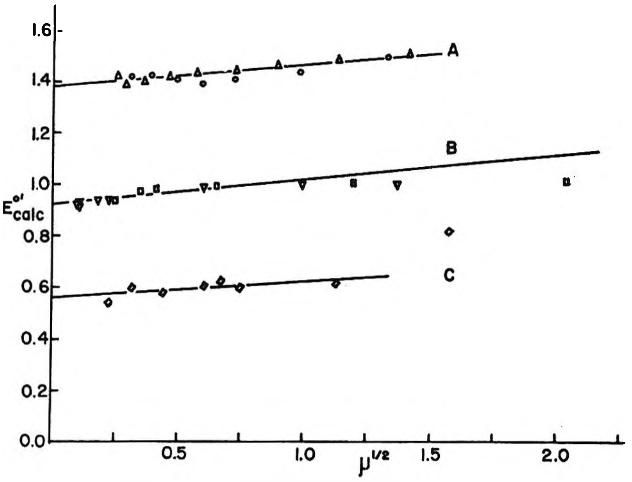

Figure 1. Oxidation potential *vs.* (ionic strength)$^{1/2}$. A: $Ag(s)|AgF(HF)|AgF_2(s)$ (Pt); ○, run 1, △, run 2; curve drawn for run 2 only. B: $Cu(s),CuF_2(s)|TlF(HF)|TlF_3(s)(Pt)$; ▽, this work; □, ref 4. C: $Ag(s)|AgF,TlF(HF)|TlF_3(s)(Pt)$; curve omits highest point.

Discussion

Dissociation Constants. The value of 1.04 found for the K_B of TlF in HF at 0° may be compared with that of TlOH in water, which was measured by Bell, *et al.*, as 0.151,[7] 0.141,[8] or 0.151[9] at 25°, the last two values being corrected to zero ionic strength. Bell and George[7] found very little variation with temperature, the value measured at 0° being 0.155. Thallium fluoride, TlF, was found by these same workers to have a dissociation constant of 0.79 in water at 25°.

The value of 0.087 found for the K_B of AgF in HF at 0° may be compared with that of AgOH in water at

---

[7] R. P. Bell and J. H. B. George, *Trans. Faraday Soc.*, **49**, 619 (1953).

[8] R. P. Bell and M. H. Panckhurst, *J. Chem. Soc.*, 2836 (1956).

[9] R. P. Bell and M. H. Panckhurst, *Rec. Trav. Chim.*, **75**, 725 (1956).

Table I: Data for the Cell Reactions

A. The System Cu(s),CuF_2(s)|TlF(HF)|TlF_3(s)(Pt)

[TlF]	$\gamma_\pm$(app)	$\gamma_\pm$(molar)	$[\mathrm{F}^-]_{\mathrm{total}}$	$\mu^{1/2}$	E_{obsd}	$E^{\circ\prime}$	K_B(app)
0.0032	1.1117	0.7527	0.0130	0.0899	1.0425	0.9238	...
0.0061	1.2399	0.7384	0.0158	0.1047	1.0299	0.9212	...
0.0082	0.8892	0.7300	0.0179	0.1142	1.0329	0.9290	1.2774×10^{-1}
0.0277	0.6275	0.6850	0.0371	0.1800	1.0182	0.9372	3.7977×10^{-2}
0.0348	0.6244	0.6751	0.0441	0.1986	1.0136	0.9442	4.5776×10^{-2} [a]
0.0450	0.4708	0.6635	0.0541	0.2226	1.0148	0.9440	2.2659×10^{-2}
0.1038	0.1384	0.6237	0.1121	0.3286	1.0252	0.9746	2.4921×10^{-3} [a]
0.1518	0.0976	0.6048	0.1596	0.3946	1.0248	0.9819	1.6847×10^{-3} [a]
0.3560	0.0620	0.5589	0.3620	0.5992	1.0158	0.9917	1.4835×10^{-3}
0.4134	0.0146	0.5500	0.4191	0.6452	1.0464	0.9987	9.065×10^{-5} [a]
0.9760	0.0079	0.4892	0.9796	0.9888	1.0408	1.0403	6.162×10^{-5}
0.0450	0.0080	0.4594	1.3620	1.1664	1.0728	1.0402	8.787×10^{-6} [a]
1.8610	0.0043	0.4269	1.8633	1.3646	1.0399	1.0545	5.317×10^{-6}
1.2102	0.0003	0.3298	4.0639	2.0158	1.0985	1.1172	3.6×10^{-7} [a]

$$-1/\log K_B(\mathrm{TlF}) = 1.0415 - 0.77037\mu^{1/2}$$

B. The System Ag(s)|AgF(HF)|AgF_2(s)(Pt)[b]

[AgF]	$\gamma_\pm$(app)	$[\mathrm{F}^-]_{\mathrm{total}}$	$\mu^{1/2}$	E_{obsd}	$E^{\circ\prime}$	K_B(app)
1.7580	0.07244	1.7628	1.3268	1.4506	1.5038	*c*
0.9622	0.2504	0.9694	0.9828	1.4487	1.4454	*c*
0.5152	0.4587	0.5254	0.7213	1.4784	1.4169	*c*
0.3495	0.7211	0.3616	0.5963	1.4930	1.3956	*c*
0.2384	0.4867	0.2521	0.4592	1.5462	1.4141	*c*
0.1440	0.3444	0.1595	0.3896	1.6080	1.4304	*c*
0.8687	0.3971	0.1037	0.3087	1.6454	1.4237	*c*
2.0094	0.06167	2.0116	1.4179	1.4455	1.5113	8.840×10^{-3}
1.2829	0.08997	1.2859	1.1333	1.4700	1.4936	1.2451×10^{-2}
0.8001	0.1420	0.8042	0.8957	1.4929	1.4721	2.0762×10^{-2}
0.5219	0.2252	0.5270	0.7242	1.5112	1.4504	3.8117×10^{-2}
0.3254	0.2802	0.3317	0.5732	1.5449	1.4401	4.0686×10^{-2}
0.2136	0.3870	0.2208	0.4660	1.5687	1.4249	6.1241×10^{-2}
0.1291	0.5553	0.1371	0.3648	1.5978	1.4079	1.09381×10^{-1} [d]
0.07970	0.7603	0.08830	0.2898	1.6264	1.3931	2.56566×10^{-1} [d]
0.06092	0.3928	0.06977	0.2556	1.6813	1.4242	2.2776×10^{-2} [d]

$$-1/\log K_B(\mathrm{AgF}) = 0.94335 - 0.34653\mu^{1/2}$$

C. The System Ag(s)|AgF,TlF(HF)|TlF_3(s)(Pt)

[AgF]	$\gamma_\pm$(app)	[TlF]	$\gamma_\pm$*TlF	$[\mathrm{F}^-]_{\mathrm{total}}$	$\mu^{1/2}$	E_{obsd}	$E^{\circ\prime}$
0.017	1.7590	0.029	0.685	0.055	0.2248	0.7854	0.5455
0.032	0.3780	0.065	0.645	0.105	0.3181	0.7924	0.5998
0.064	0.6718	0.128	0.615	0.199	0.4423	0.7253	0.5795
0.117	0.3472	0.250	0.580	0.373	0.6083	0.7044	0.6028
0.139	0.1926	0.306	0.575	0.450	0.6691	0.7121	0.6236
0.219	0.3807	0.498	0.500	0.721	0.8480	0.6550	0.5995
0.464	0.2780	1.027	0.485	1.494	1.2216	0.6142	0.6106
0.781		1.692	0.435	2.475	1.5729	0.7883	0.8207

[a] See ref 4. [b] W. D. Pardieck. [c] Run 1. Data not used for calculation of E° and K_B. [d] Not used for calculation of K_B.

25°, which was determined by Johnston, *et al.*,[10] and again by Beck[11] to be 2.0×10^{-3}. Silver fluoride, AgF, was found by Paul[12] to have a dissociation constant of 0.44 in water at 25°.

The fluorides in HF are thus seen to be considerably more highly dissociated than the corresponding hydroxides in water. (They are stronger "solvo bases"

---

(10) H. L. Johnston, F. Cuta, and A. B. Garrett, *J. Am. Chem. Soc.*, 55, 2311 (1933).

(11) M. T. Beck, *Acta Chim. Acad. Sci. Hung.*, 4, 227 (1954).

Table II: Electromotive Series at 0° in Liquid HF

In *HF*			In water	
Couple	$E°_{273}$	Ref	Couple	$E°_{273}$[a]
$Cd(s)-CdF_2(s)$	0.29	14	$Cd-Cd^{2+}$	0.41
$Pb(s)-PbF_2 \cdot {}^5/_2HF(s)$	0.26	14		
$Pb(s)-PbF_2(s)$	0.17	14	$Pb-Pb^{2+}$	0.12
$H_2(g)-HF(l)$	0	15	H_2-H^+	0.00
$Cu(s)-CuF_2(s)$	−0.52	14	$Cu-Cu^{2+}$	−0.34
$FeF_2(s)-FeF_3(s)$[b]	−0.58	15	$Fe^{2+}-Fe^{3+}$	−0.77
$Hg(l)-Hg_2F_2(s)$	−0.80	Assumed	$Hg(l)-Hg_2^{2+}$	−0.79
$Ag(s)-AgF(HF)$	−0.88	This work	$Ag-Ag^+$	−0.80
$Ag(s)-AgF(HF,satd)$	−0.94	14		
$TlF(HF)-TlF_3(s)$	−1.45	This work	Tl^+-Tl^{3+}	−1.25
$AgF(HF)-AgF_2(s)$	−2.27	This work	Ag^+-Ag^{2+}	−1.96
$F^-(HF)-F_2(g)$	−2.708	*c*	$F^--F_2(g)$	−2.87

[a] W. M. Latimer, "Oxidation Potentials," 2nd ed, Prentice-Hall, Inc., New York, N. Y., 1952. [b] In 2.76 *M* KF. [c] K. Fredenhagen and C. Kreft, *Z. Elektrochem.*, **35**, 670 (1929).

than the hydroxides are.) Since the dielectric constants of the two solvents are nearly the same, this probably reflects the much greater solvating power of HF for anions compared with water. Since, however, there is as yet no information on the enthalpies and entropies of solvation of these fluorides in HF, the true cause of the greater dissociation can only be surmised.

Oxidation Potentials. The cell potentials available through this and other work now make possible the beginnings of an electromotive series for the hydrogen fluoride solvent system. From the three cells studied, two derived potentials can be obtained such that all of the thallium and silver couples can be compared to the $Cu-CuF_2$ couple. Thus

$$Cu(s) + TlF_3(s) \longrightarrow CuF_2(s) + TlF(HF) \qquad E° = 0.9269 \text{ v}$$

$$Cu(s) + 2AgF(HF) \longrightarrow CuF_2(s) + 2Ag(s) \qquad E° = 0.3615 \text{ v}$$

$$Cu(s) + 2AgF_2(s) \longrightarrow CuF_2(s) + 2AgF(HF) \qquad E° = 1.7431 \text{ v}$$

Koerber and De Vries[13] have studied the potential of the cell

$$Cu(s) + Hg_2F_2(s) \longrightarrow CuF_2(s) + 2Hg(l)$$

and found its potential, $E°_{273} = 0.277$ v. From the very scanty evidence[14] on the cell system $H_2(g) + Hg_2F_2(s) \rightarrow 2HF(l) + 2Hg(l)$, the potential for this reaction appears to be about 0.8 v. For purposes of comparison, therefore, we shall define the potential of the $Hg-Hg_2F_2$ couple to be −0.80 v. From the available cell potentials the electromotive series in Table II can be generated. Potentials for the couples of ref 13 at different temperatures and for the corresponding reactions involving the amalgamated metals are also given in ref 13.

It can be seen from Table II that, although the actual values vary somewhat, the trend in potentials is the same in HF and in water. The spread in HF from the cadmium couple to the Ag(I)–Ag(II) couple is slightly, but not significantly, greater than in water. If the series for HF involved ions in solution for the higher oxidation states rather than solids, the potentials would all shift to somewhat more negative values relative to hydrogen, but there is no reason to believe that the order or the spread would change significantly. This points out the great similarity between water and HF as solvents and contrasts strongly with the considerable difference between water and liquid ammonia.[15]

The more negative potential obtained by Koerber and deVries[14] for the Ag(s)–AgF couple is to be expected from their higher AgF concentration.

---

(12) A. D. Paul, Thesis, University of California, Berkeley, Calif., 1955; UCRL 2926.

(13) G. G. Koerber and T. De Vries, *J. Am. Chem. Soc.*, **74**, 5008 (1952).

(14) A. F. Clifford and G. Balog, *U. S. At. Energy Comm., Nucl. Sci. Abstr.*, **5**, 694 (1951); AECU 1491 (nd); and A. F. Clifford and E. M. Jeram, unpublished work.

(15) V. A. Pleskov and A. M. Monoszon, *Acta Physicochim. U.R.S.S.*, **2**, 615 (1935).

Kinetics of Diffusion-Controlled Reactions. An Experimental Test of the Theory as Applied to Fluorescence Quenching

by William R. Ware and Joel S. Novros

Department of Chemistry, San Diego State College, San Diego, California 92115 *(Received April 14, 1966)*

An experimental test of the theory of diffusion-controlled reactions as applied to fluorescence quenching is described. Both steady-state fluorescence quenching measurements and fluorescence lifetime studies with a nanosecond flash have been made. It was found that departures from Stern-Volmer kinetics are satisfactorily accounted for by the theory based on Fick's laws, including transient term, for the system of anthracene quenched by carbon tetrabromide. The sum of the collision radii was taken as an adjustable parameter and it was found that the steady-state quenching data could be explained with values falling between 6 and 7.5 A. Radii in this range were also consistent with the lifetime measurements. The possibility of static quenching is also discussed.

Introduction

The problem of diffusion-controlled reactions has received considerable theoretical attention in the past several decades.[1] Theoretical treatments of the problem may be divided into two categories, one involving a consideration of the concentration gradients in the system[2-6] and the other involving an analysis of the behavior of a pair of diffusing molecules.[1,7] This latter approach, which utilizes the probability of reencounter derived from the theory of random walks, has been developed over the past 10 years by Noyes, whereas the development based on concentration gradients had its origin in the work of Smoluchowski, who applied Fick's laws to the problem of the rate of coagulation of colloidal particles. Smoluchowski[2] solved Fick's second law

$$\partial C/\partial t = D\nabla^2 C \tag{1}$$

subject to the boundary conditions

$$\begin{aligned} C(r, 0) &= C_0 \\ C(\infty, t) &= C_0 \\ C(R, t) &= 0 \end{aligned} \tag{2}$$

where R is the sum of the collision radii and C_0 is the initial concentration of the diffusing species. The problem of the relative motion of the particles in question was taken into account by adding the individual diffusion coefficients, *i.e.*, $D = D_A + D_B$. The solution to eq 1 is

$$C(r, t) = C_0\left[1 - \frac{R}{r}\,\text{erfc}\left(\frac{r - R}{2\sqrt{Dt}}\right)\right] \tag{3}$$

where

$$\text{erfc}(x) = \frac{2}{\sqrt{\pi}}\int_x^\infty e^{-\lambda^2}d\lambda$$

Equation 3 yields for the flux at R

$$\Phi = 4\pi RDN'C_0(1 + R/\sqrt{\pi Dt}) \tag{4}$$

which leads to the familiar equation

$$\Phi/C_0 = 4\pi RDN' \tag{5}$$

for the rate constant for a diffusion-controlled reaction in the absence of transient effects. N' is the number of molecules in 1 mmole.

The boundary condition, $C(R, t) = 0$, has been the

---

[1] R. M. Noyes *Progr. Reaction Kinetics*, **1**, 131 (1961).

[2] M. v. Smoluchowski, *Z. Physik. Chem.*, **92**, 129 (1917).

[3] E. W. Montrol, *J. Chem. Phys.*, **14**, 202 (1946).

[4] T. R. Waite, *ibid.*, **28**, 103 (1958); **32**, 21 (1960).

[5] A. Weller, *Z. Physik. Chem.* (Frankfurt), **13**, 335 (1957).

[6] J. Yguerabide, M. A. Dillon, and M. Burton, *J. Chem. Phys.*, **40**, 3040 (1964).

[7] R. M. Noyes, *J. Phys. Chem.*, **65**, 763 (1961).

subject of much discussion,[1,8,9] and it is now generally recognized that one must use instead

$$\Phi = kC_R \tag{6}$$

or its equivalent

$$C_R = \frac{D}{k}\left(\frac{\partial C}{\partial r}\right)_R \tag{7}$$

where k is the rate constant that would pertain if the equilibrium concentration of encounter pairs were maintained. The subscript R refers to evaluation at a distance R from the species considered fixed.

The flux now becomes

$$\Phi = \frac{4\pi RDC_0N'}{1 + \dfrac{4\pi RD}{k}}\left[1 + \frac{k}{4\pi RD}\ \exp(x^2)\mathrm{erfc}(x)\right] \tag{8}$$

where

$$x = (\sqrt{Dt}/R)(1 + k/4\pi RD) \tag{9}$$

At times greater than 10^{-11} sec for ordinary values of D and R, $\exp(x^2)\mathrm{erfc}(x)$ may be expanded in a series with retention only of the first term, giving[1]

$$k(t) = \Phi/C_0 = 4\pi R'DN'\left(1 + \frac{R'}{\sqrt{\pi Dt}}\right) \tag{10}$$

where

$$R' = R/(1 + 4\pi RD/k) \tag{11}$$

Collins,[9] using random-walk considerations, has obtained a similar relationship for R'

$$R' = \alpha R^2/(\alpha R + \rho) \tag{12}$$

where α is the reaction probability and ρ is related to the average diffusive displacement. Equation 10 is of the form of Smoluchowski's solution and approaches it as $k >> 4\pi RD$.

The application of eq 10 to fluorescence quenching is straightforward.[3,5,6] For the mechanism

Process	Rate	
$A \longrightarrow A^*$	$\propto F(t)$	(a)
$A^* \longrightarrow A + h\nu$	$[A^*]/\tau_0$	(b)
$A^* \longrightarrow A$		(c)
$A^* + Q \longrightarrow$ products	$k(t)[A^*][Q]$	(d)

one obtains the decay law from eq 10 for instantaneous excitation. This is given by the expression

$$I(t) =$$
$$I_0 \exp\left\{-\frac{t}{\tau_0} - 4\pi R'DN'[Q]t[1 + 2R'/\sqrt{\pi Dt}]\right\} \tag{13}$$

The application of eq 13 to experimental results requires the evaluation of a superposition integral of F(t), the excitation function, and G(t), the decay function of A^* for instantaneous excitation, *i.e.*

$$J(t) = \int_0^t F(t)G(t - \lambda)d\lambda \tag{14}$$

J(t) gives the time dependence of the fluorescence intensity anticipated experimentally. The steady-state solution is obtained by considering the response to excitation by a step function. The result is

$$(I_0/I)_{ss} = (1 + 4\pi R'DN'[Q]\tau_0)Y^{-1} \tag{15}$$

where

$$Y = 1 - (b/a^{1/2})\pi^{1/2} \exp(b^2/a)\ \mathrm{erfc}(b/a^{1/2})$$

and

$$a = 1/\tau_0 + 4\pi R'DN'[Q]$$
$$b = 4R'^2\sqrt{\pi D}N'[Q]$$

This development, based on the questionable application of a continuum theory to the diffusion of two species through a solvent composed of molecules of similar size, remains essentially unverified experimentally. The recently reported results of Noyes[10,11] on the rate of recombination of iodine atoms in carbon tetrachloride are encouraging, but the test suffers somewhat from a lack of accurate diffusion coefficients.

This paper reports an attempt to test experimentally the theory (including transient term) as outlined above. Steady-state and transient measurements have been made on a fluorescence quenching system of high efficiency, the quenching of anthracene fluorescence by carbon tetrabromide. This system has been reported by Bowen and Metcalf[12] to depart significantly from Stern–Volmer kinetics. Bowen and Metcalf attributed this behavior to static quenching, but Noyes[13] adopted the view that the observed concentration dependence of the Stern–Volmer constant was due to transient effects in the diffusion-controlled kinetics. However, Noyes had no transient studies available to use in reinterpreting the data.

Experimental Section

Fluorescence decay measurements were made with a photocurrent-sampling apparatus similar to that de-

---

[8] F. C. Collins and G. E. Kimball, *J. Colloid Sci.*, **4**, 425 (1949).

[9] F. C. Collins, *ibid.*, **5**, 499 (1950).

[10] R. M. Noyes, *J. Am. Chem. Soc.*, **86**, 4529 (1964).

[11] R. M. Noyes, *J. Phys. Chem.*, **69**, 3182 (1965).

[12] E. J. Bowen and W. S. Metcalf, *Proc. Roy. Soc.* (London), **A206**, 437 (1951).

[13] R. M. Noyes, *J. Am. Chem. Soc.*, **79**, 551 (1957).

scribed by Bennett.[14-16] Fluorescence was excited with a nanosecond flash lamp operated at a repetition rate of 5–7 kc. The flashing gas was air, the emission originating primarily from the $C^3\pi_u \rightarrow B^3\pi_g$ fluorescence of nitrogen quenched by oxygen. The time base was set by a variable delay line, which determined the time interval between the pulsing of the lamp and the pulsing of the photomultiplier tube. This variable-delay line was calibrated against the speed of light and was found to be linear and accurate to better than 2.5%.

In the past decade a number of investigators have made fluorescence lifetime measurements, and there is some overlap regarding the compounds measured and the solvent used. If one compares the measurements of Ware,[16] Ware and Baldwin,[15] Birks and Dyson,[17] Metcalf,[18] and Lumry, Kokubun, and Müller[19] on compounds such as acridone, quinine bisulfate, fluorescein, anthracene, perylene, and 9,10-diphenylanthracene, one finds that the agreement between investigators is on the average within 2.5% for a given compound. This comparison includes measurements made with both the phase-shift technique and the direct-observation nanosecond-flash method. Thus we have apparently reached the point where considerable confidence may be placed in such measurements.

Steady-state measurements of fluorescence intensity ratios were accomplished with the apparatus illustrated in Figure 1. The instrument utilizes the double-beam method described by Bowen and Metcalf[12] and is quite insensitive to variations in lamp intensity. Measurements were made in 1-cm cells. Oxygen was carefully removed from all solutions. In obtaining $(I_0/I)_{ss}$, corrections were made for dark current and scattered light. Care was exercised to limit the exposure time in the steady-state measurements in order to prevent the photochemical disappearance of anthracene from introducing an error.

Zone-refined anthracene was used for all experiments. The carbon tetrabromide (Matheson Scientific Co.) was vacuum sublimed until white crystals were obtained. Carbon and bromine microanalyses indicated better than 99% purity. The solvents heptane and acetonitrile were spectroscopic grade. Isobutyl alcohol was distilled prior to use.

Representative solutions containing anthracene and carbon tetrabromide were examined with a Cary 14 spectrophotometer and the resultant spectra compared with spectra of the individual components. No evidence was obtained to suggest ground-state complex formation.

Results and Discussion

The comparison of experimental results with the theory of diffusion-controlled reactions involved two different approaches. The first, which will be referred to as method A, was as follows. Equation 15 was fit to the $(I_0/I)_{ss}$ data, using R' as an adjustable parameter. The value of R' which gave the best fit for each solvent was then used in the analysis of the fluorescence decay data to produce a comparison between $(\Delta(1/\tau)/\Delta[Q]_{obsd}$ and the theory.

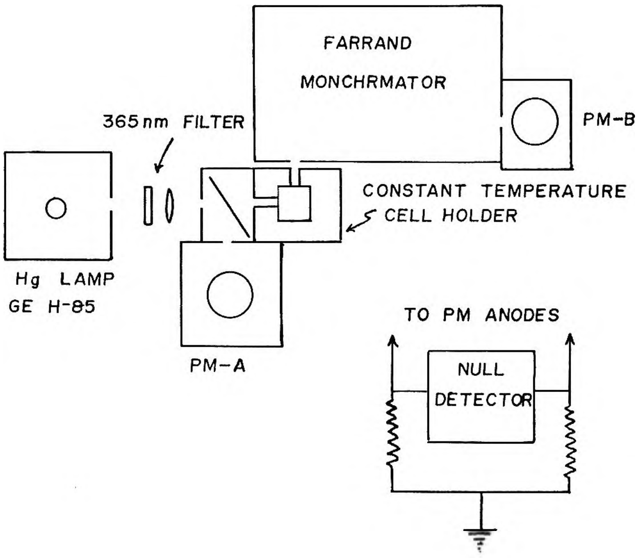

Figure 1. Steady-state fluorescence apparatus.

In method B, the results of the fluorescence lifetime measurements were also used directly to interpret the steady-state results by making the following modifications of eq. 15

$$(I_0/I)_{ss} = (1 + k'[Q]\tau_0)Y^{-1} \qquad (16)$$

with

$$a = 1/\tau_0 + k'[Q]$$

$$b = k'[Q]R'/\sqrt{\pi D}$$

The value of k' was obtained from the superposition integral calculations; *i.e.*, the decay law was taken to be

$$I(t) = I_0 \exp\{-t/\tau_0 - k'[Q]t[1 + 2R'/\sqrt{\pi D t}]\} \qquad (17)$$

and k' was varied until agreement with the measured variation of the lifetime with concentrations was ob-

---

(14) R. G. Bennett, *Rev. Sci. Instr.*, **31**, 1275 (1960).

(15) W. R. Ware and B. A. Baldwin, *J. Chem. Phys.*, **40**, 1703 (1964).

(16) W. Ware, *J. Am. Chem. Soc.*, **83**, 4374 (1961).

(17) J. B. Birks and D. J. Dyson, *Proc. Roy. Soc.* (London), **A275**, 135 (1963).

(18) W. S. Metcalf, *J. Sci. Instr.*, **42**, 603 (1965).

(19) A. Müller, R. Lumry, and H. Kokubun, *Rev. Sci. Instr.*, **36**, 1214 (1965).

tained. This fit was not particularly sensitive to the value of R', and k' was thus easily found. R' in eq 16 was then varied to obtain a fit with the steady-state data. The decay law calculations were then checked to see if the new R' caused a significant change in k'.

These two methods will now be discussed in detail. Steady-state measurements produced values of $(I_0/I)_{ss}$ and K_{sv}, where

$$K_{sv} = \frac{1}{[Q]}\left(\frac{I_0}{I} - 1\right)_{ss} \qquad (18)$$

To compare the results with eq 15, values for the diffusion coefficients of anthracene and carbon tetrabromide were required. Diffusion coefficients were estimated from values of $D\eta/T$, where η is the solvent viscosity, reported in the literature for phenanthrene and carbon tetrabromide[20] in benzene. To obtain values of the diffusion coefficient in heptane and acetonitrile, it was assumed that $D\eta/T = C$. For isobutyl alcohol, account was taken of the fact that the value of C is different from that appropriate to benzene or heptane, and a correction was applied based on the diffusion coefficient for bromoform in various alcohols.[20] The resultant diffusion coefficients listed in Table I were within 20% of the values predicted from the nomographs of Othmer and Thaker[21] and are in fair agreement with the tracer measurements recently reported,[22] although these latter measurements appear to give somewhat high results.

Examples of the degree to which eq 15 fits the experimental data are shown in Figures 2–4, and the results for all systems studied are contained in Table I. Equation 15 is clearly quite sensitive to the value of R', as is indicated by the ranges given on the theoretical curves.

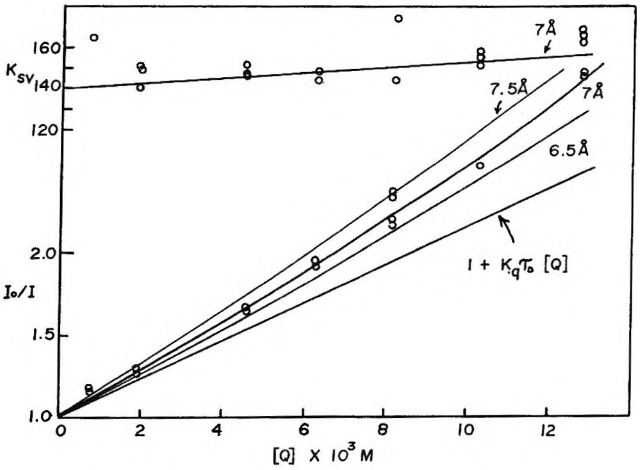

Figure 2. Steady-state results in heptane at 25°

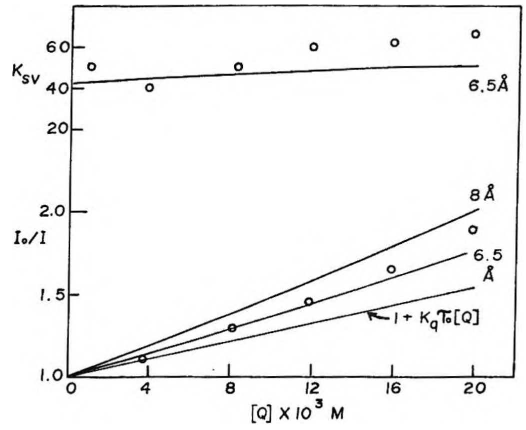

Figure 3. Steady-state results in isobutyl alcohol (low concentration) at 25°.

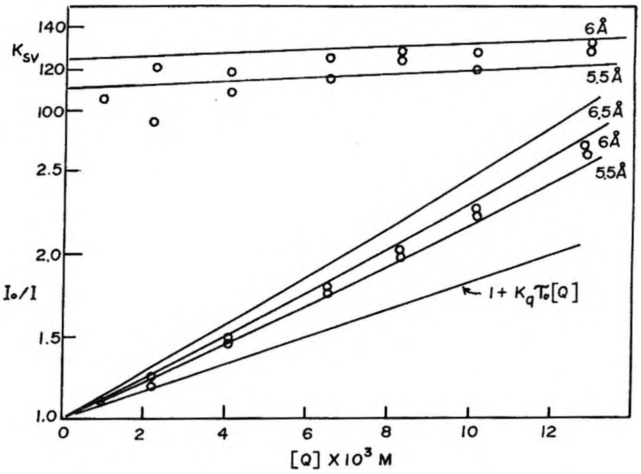

Figure 4. Steady-state results in acetonitrile at 25°.

The values of R' found to produce a fit with the steady-state data were then used to calculate the fluorescence decay behavior, J(t), anticipated theoretically. The superposition integral

$$\mathrm{J}(t) = \int_0^t \exp\left\{-\frac{\lambda}{\tau_0} - 4\pi R'DN'[\mathrm{Q}]\lambda[1 + 2R/\sqrt{\pi D\lambda}]\right\}\mathrm{F}(t - \lambda)\mathrm{d}\lambda \qquad (19)$$

where F(t) is the empirical lamp intensity function, was calculated numerically. The lamp function had a rise time (10–90%) of about 2 nsec, a width at half-

---

[20] A. E. Stearn, E. M. Irish, and H. Eyring, *J. Phys. Chem.*, **44**, 981 (1940).

[21] D. F. Othmer and M. S. Thakar, *Ind. Eng. Chem.*, **45**, 589 (1953).

[22] T. A. Miller, *et al.*, *J. Am. Chem. Soc.*, **87**, 121 (1965).

Table I: Results of Analysis of Data by Method A[a]

Solvent	T, °C	10^5D, cm² sec⁻¹	$10^{-8}/\tau_0$, sec⁻¹	R', A	$10^{-10}\Delta(1/\tau)/\Delta[Q]$, M^{-1} sec⁻¹ Theoret	Exptl	K_{sv}^0, M^{-1} Theoret	Exptl
Heptane	10	3.59	1.79 (±0.009)	7.0	1.99	1.74 (±0.013)	125	118 (±3)
Heptane	25	4.35	1.81 (±0.007)	7.0	2.38	2.13 (±0.023)	140	140 (±2)
Heptane	40	5.36	1.82 (±0.011)	7.0	2.97	2.37 (±0.037)	170	160 (±20)
Acetonitrile	25	5.07	2.07 (±0.17)	6.0	2.33	1.76 (±0.36)	120	107 (±2)
Isobutyl alcohol	25	1.10	1.95 (±0.018)	6.5	0.59	0.54 (±0.023)	35	25[b] (±1)

[a] Experimental errors listed are probable errors from least-squares analysis. [b] Low-concentration value.

maximum of 4.4 nsec, and a decay time given by $\exp(-5.55 \times 10^8 t)$. $J(t)$ was calculated from $t = 0$ to $t = 30$ nsec with values of [Q] from 3.00×10^{-3} to 1.10×10^{-2} M. The decay portion of $J(t)$ became exponential soon after the maximum was passed and was exponential for 4–6 half-lives. It was thus possible to associate with each [Q] value a value of the apparent lifetime, τ_{app}. The range over which $\Delta \log J(t)/\Delta t$ was computed corresponded to the range used in the analysis of the experimental decay curves. Plots of $1/\tau_{app}$ *vs.* [Q] were linear below 7×10^{-3} M and this slope was used to obtain a theoretical value for $\Delta(1/\tau)/\Delta[Q]$. The exponential decay predicted theoretically was observed experimentally in all cases. The results of the lifetime measurements are given in Table I, along with the theoretical predictions.

From the experimental value of $\Delta(1/\tau)/\Delta[Q]$ it was possible to construct a Stern–Volmer line on the I_0/I plots from

$$(I_0/I)_{ss} = 1 + (\Delta(1/\tau)/\Delta[Q])_{exptl}\tau_0[Q] \quad (20)$$

The results are shown in Figures 2–5 to emphasize the magnitude of the departures from the anticipated behavior if Stern–Volmer kinetics had been obeyed in both the transient and steady-state studies.

The results of the calculations following method B are given in Table II. It should be noted that in method B, k' is held constant while R' is varied in order to fit the steady-state data. This is, of course, not strictly valid since k' is a function of R', but one can argue that this approach makes maximum use of the experimental data and leaves only part of the R' dependence of the correction factor b to be determined. It can be seen that method B produces results that are not significantly different from those of method A.

Table II: Analysis of Data by Method B[a]

Solvent	T, °C	$10^{-10}k'$, M^{-1} sec⁻¹	R', A	K_{sv}^0, M^{-1} Theoret	Exptl
Heptane	10	1.68	8.0	139	118 (±3)
Heptane	25	2.05	7.0	143	140 (±2)
Heptane	40	2.30	7.0	173	160 (±20)
Acetonitrile	25	1.70	6.0	120	107 (±2)
Isobutyl alcohol	25	0.50	6.0	32	28[b] (±1)

[a] Experimental errors listed are probable errors from least-squares analysis. [b] Low-concentration value.

The values of R' obtained are reasonable since the sum of the collision radii must fall somewhere between 6 and 8 A. In addition, since according to eq 11, $R' < R_A + R_B$, it is encouraging that the values of R' are found to be in the range of 6–7 A. For example, if one calculates k from the kinetic theory of gases, then eq 11 gives $R' \cong R/1.2$ for low-viscosity solvents.

The agreement between $\Delta(1/\tau)/\Delta[Q]$ obtained by method A and the experimental results of the lifetime measurements given in Table I would appear to be satisfactory when one considers that, once the value of R' is fixed by the fit to the steady-state data, there are no adjustable parameters. The agreement between the value of K_{sv} obtained by extrapolating the theoretical calculations to zero concentration

$$K_{sv}^0 = \lim_{[Q]\to 0} K_{sv} = 4\pi R'DN'\tau_0\left(1 + \frac{R'}{\sqrt{D\tau_0}}\right) \quad (21)$$

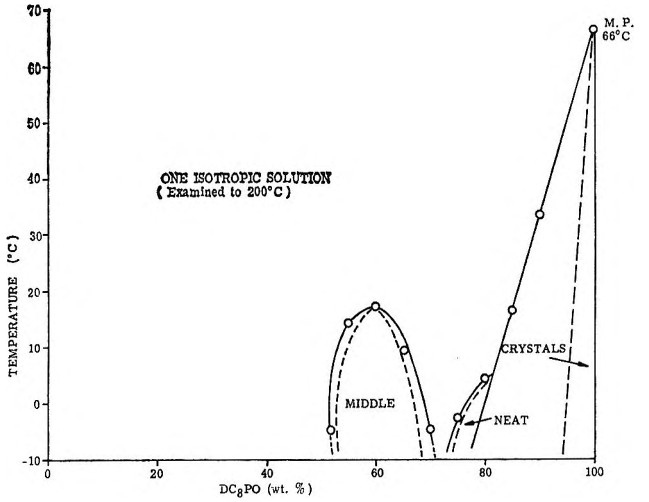

Figure 1. Phase diagram for dimethyloctylphosphine oxide–water.

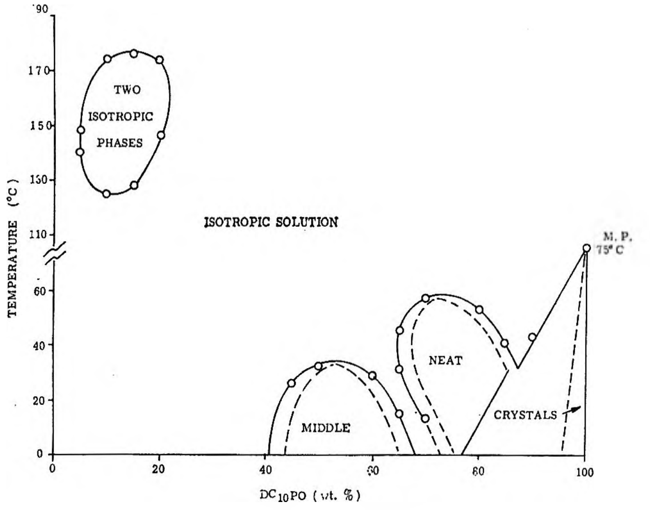

Figure 2. Phase diagram for dimethyldecylphosphine oxide–water.

and will not be considered any further in this paper. The part of the phase diagram of particular interest here is the region where two immiscible isotropic solutions coexist (Figures 2 and 3). In binary solution terminology,[21] the two immiscible isotropic solutions are referred to as conjugate solutions. The temperature at which phase separation occurs is called an upper consolute temperature when a maximum occurs in the phase boundary. The surfactant concentration at which the maximum or minimum occurs is called the critical concentration. The temperature at which the maximum occurs in the consolute boundary is called an upper critical solution temperature, and the temperature at which the minimum occurs in the consolute temperature is called a lower critical solution temperature. Thus, while DC_8PO does not form immiscible isotropic solutions at the temperature examined, both the $DC_{10}PO$ and $DC_{12}PO$ binary systems do exhibit critical solution behavior. If one examines phase data for ethylene oxide surfactant–water systems published in the literature,[11,12] it can be seen that the term "cloud point," as used by the authors, is really the lower consolute temperature of the system. Hence, we equate the term "cloud point" and lower consolute temperature.

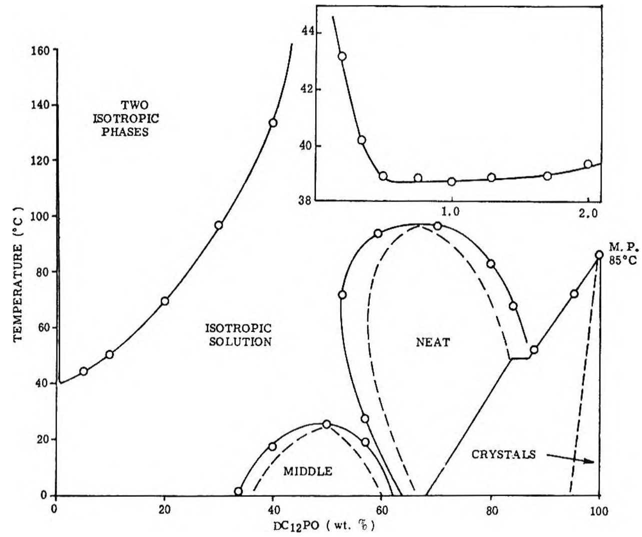

Figure 3. Phase diagram for dimethyldodecylphosphine oxide–water. Insert shows consolute boundary at low concentrations.

The temperature and composition ranges over which conjugate solutions exist in the dimethylalkylphosphine oxide–water systems decrease with decreased alkyl chain length in the surfactant (see Figures 1, 2, and 3). Only $DC_{12}PO$ exhibits a lower consolute boundary which extends over a wide range of temperatures and compositions; the critical solution temperature and concentration were visually estimated to be approximately 38.8° and about 0.7% $DC_{12}PO$, respectively. The $DC_{10}PO$ system exhibits both an upper and lower consolute boundary with critical temperatures of about 177 and 124°, respectively, and critical concentrations between 10 and 15% $DC_{10}PO$. Considerable pressure must have developed in the sealed phase tubes at the temperatures where the conjugate solutions of $DC_{10}PO$ were observed; the effect of pressure on this type of phase separation is unknown. The DC_8PO system does not form conjugate solutions below 200°.

General Light-Scattering Properties and Theory.

---

[21] S. Glasstone, "Textbook of Physical Chemistry," 2nd ed, D. Van Nostrand Co., Inc., New York, N. Y., 1946, Chapter X.

lated directly from the concentration dependence of K_{sv}. However, the slope and intercept of plots of K_{sv} *vs.* [Q] together provide sufficient information to permit calculation of both $k_q\tau_0$ and K'. It was found that the two methods are not consistent and that K' is not a constant at 25°. For isobutyl alcohol, the calculation was done only for the high concentration results since in the low-concentration range, $k_q\tau_0 \cong K_{sv}$. The results are listed in Table III.

Table III: Analysis of the Data According to Eq 22

Solvent	T, °C	K_{sv}^0, M^{-1} (exptl)	$\Delta K_{sv}/\Delta[Q]$, M^{-2} (exptl)	K'[a]	K'[b]	K'[c]
Heptane	10	118	2570	29	21	26
Heptane	25	140	1770	14	23	16
Heptane	40	160	2200	16	30	17
Acetonitrile	25	107	1830	21	23	17
Isobutyl alcohol	25	39[d]	300	11	11	8.6

[a] From slope and intercept. [b] From assumed $k_q\tau_0$ and intercept. [c] From assumed $k_q\tau_0$ and slope. [d] High-concentration intercept.

We have attempted to fit eq 15 to the data of Bowen and Metcalf, using the least-squares slopes and intercepts quoted by Noyes[13] for the K_{sv} *cs.* [Q] plots of Bowen and Metcalf. Diffusion coefficients were estimated from the diffusion coefficient of toluene reported for a series of hydrocarbon solvents ranging from heptane to tridecane.[20] It was assumed that the D *vs.* T/η plot for $D = D_A + D_Q$ would be similar in shape but displaced upward. The curve was made consistent with the values of D quoted in Table I. This was taken as valid over the range of T/η of 5.8×10^{-4} to 1.25×10^{-4} deg/poise. The I_0/I plots were reconstructed from Bowen and Metcalf's K_{sv} data. The value of the unquenched lifetime was taken to be 5.5 nsec, since the lifetime of anthracene does not appear to vary significantly from one saturated hydrocarbon solvent to the next. Values of R' required to cause eq 15 to fit the I_0/I data were determined and are given in Table IV. The results of fitting to the low-concentration ($1\text{–}10 \times 10^{-3}$ M) portions of Bowen and Metcalf's I_0/I curves are in reasonable agreement with our own results, as can be seen from Table IV. The R' values are somewhat higher, but this is perhaps due to the fact that this analysis involves linear extrapolation of data obtained at higher quencher concentrations than used in most of the work reported above. Also listed in Table IV are the results of comparing the predicted slopes and intercepts of K_{sv} *vs.* [Q] plots with those observed experimentally by Bowen and Metcalf. Since both τ_0 and D are somewhat uncertain, the agreement seen in the values listed in Table IV is considered within the uncertainty of the calculations and the experimental data used.

Table IV: Analysis of the Data of Bowen and Metcalf[a]

$10^4T/\eta$, deg/poise	10^5D, cm^2 sec^{-1}	R', A	K_{sv}^0, M^{-1} Exptl	K_{sv}^0, M^{-1} Theoret	$\Delta K_{sv}/\Delta[Q]$, M^{-2} Exptl	$\Delta K_{sv}/\Delta[Q]$, M^{-2} Theoret
5.8	3.48	7.5	125	126	953	1000
4.8	2.96	7.5	110	109	785	950
3.5	2.20	8.0	93	91	857	700
2.4	1.50	8.0	76	64	468	350
1.25	0.85	8.5	49	48	355	300

[a] See ref 12 and 13.

Since we have seen no spectral evidence to suggest the existence of a complex between anthracene and carbon tetrabromide, and since eq 15 appears to fit the existing data better than eq 22, it is more reasonable to view the concentration dependence of K_{sv} as a result of the transient effects in diffusion-controlled reactions rather than as a result of static quenching.

Summary and Conclusions

The magnitude of the departures from Stern–Volmer kinetics leaves little doubt as to the existence of an "effect," whatever its origin might be. The theory of diffusion-controlled reactions based on Fick's laws has been found to fit the experimental data using reasonable values for the sum of the collision radii, provided transient terms in the flux equation are retained. Noyes,[10,11] using eq 10 (without the transient terms, which were unnecessary), was able to account within about 20% for the magnitude of the rate constant for iodine atom recombination in carbon tetrachloride. In the iodine system, the difference between the observed rate constant and $4\pi R'DN'$ again leaves little doubt as to the existence of an "effect" in spite of the uncertainty in the value of the diffusion coefficient. It would thus appear that a start has been made in the direction of providing experimental verification for the theory of diffusion controlled reactions. A variety of interesting experiments remains. For example, once quenching measurements with subnanosecond flash lamps become practical, it should be possible to test directly the validity of the decay law. In addition, a detailed steady-state and transient study should be made on an efficient quenching system where static quenching is well characterized (ϵ_A/ϵ_{AQ} and K known independently from spectral studies), since this would eliminate one of the minor uncertainties associated with the present system. It would also be of interest to establish, through the study of several efficient quenching systems, whether or not the high-concentration failure is indeed a characteristic of diffusion-controlled reactions. Furthermore, the quantitative characteristics of this failure at high concentrations should be investigated.

There are three mechanisms that have been frequently invoked to explain the mechanism of fluorescence quenching,[25] *i.e.*

$$^1A^* + Q \longrightarrow A^{\pm}\cdot Q^{\mp} \longrightarrow A + Q \qquad \text{(i)}$$

$$^1A^* + Q \longrightarrow A^{\pm}\cdot Q^{\mp} \longrightarrow {}^3A^* + Q \qquad \text{(j)}$$

$$^1A^* + Q \longrightarrow {}^1A^*\cdot Q \longrightarrow {}^3A^*\cdot Q \longrightarrow {}^3A^* + Q \qquad \text{(k)}$$

where $^1A^*$ and $^3A^*$ are the first excited singlet and lowest triplet states of the molecule, respectively. Wilkinson and Medinger[25] have recently presented experimental evidence that the triplet state is the product of the fluorescence quenching of anthracene by bromobenzene. They found no effect on the mechanism in going from a low to a moderate dielectric constant solvent and no evidence for charged species following flash excitation. This led them to favor process k over process j. We also find no dielectric constant effect; the rate appears to be controlled entirely by diffusion. Recent[26] work in our laboratory with aromatic hydrocarbons quenched by amines suggests that when a charge-transfer complex is involved in a fluorescence-quenching mechanism, low dielectric constant solvents can cause a reversal of the quenching process with the regeneration of $^1A^*$ and thus a nonexponential fluorescence decay. On the other hand, in solvents of high dielectric constant, the decay becomes exponential and the rate follows the inverse of the viscosity and is independent of the dielectric constant. This type of behavior has not been found with anthracene quenched by carbon tetrabromide, suggesting perhaps that process k is correct.

Acknowledgment. This research was supported by a grant from the National Science Foundation (GP-1619). The authors also wish to acknowledge the assistance of Michael Richter, who made some of the preliminary measurements on this system.

---

(25) T. Medinger and F. Wilkinson, *Trans. Faraday Soc.*, **61**, 620 (1965).

(26) W. R. Ware and H. P. Richter, unpublished results.

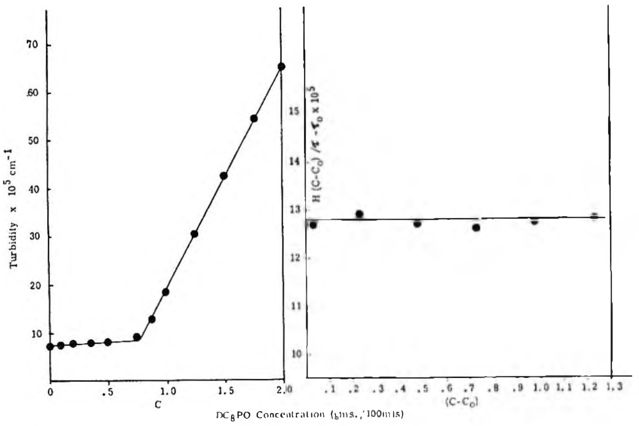

Figure 8. Light-scattering results for DC_8PO.

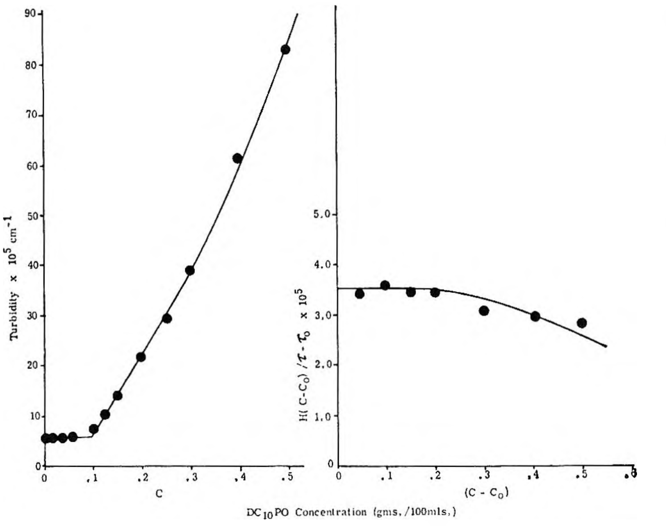

Figure 9. Light-scattering results for $DC_{10}PO$.

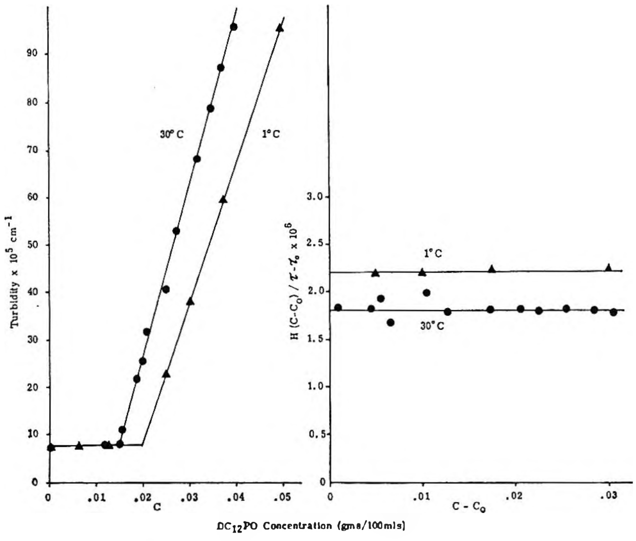

Figure 10. Light-scattering results for $DC_{12}PO$.

Table I: Micellar Properties of Some Dimethylalkylphosphine Oxide Surfactants

Surfactant	Temp, °C	Cmc, g/100 ml Light scattering	 Surface tension	dn/dc, ml/g	Mmw
DC_8PO	30	0.77	0.79	0.148	7,800
$DC_{10}PO$	30	0.10	0.082	0.144	28,600
$DC_{12}PO$	30	0.014	0.008	0.155	555,000
$DC_{12}PO$	1	0.020	...	...	458,000

mmw for a 29° reduction in temperature, a small temperature effect compared to those reported in the literature for other nonionic surfactants having a lower consolute boundary.[8,11,12,15] Unless there is a threshold temperature above which the micelle molecular weight increases exponentially,[15] and the existence of such a point above 30° cannot be ruled out on the basis of these experiments, the reported exponential increase in micelle molecular weight with temperature[8,11,12,15] may indeed only be reflecting the variation of $d\Pi/dc$ with temperature as the critical temperature is approached and not a true variation in molecular weight. Micelle molecular weights have sometimes been determined from the minimum in the Hc/τ plots[11] which presumably occur at or near the concentration where the minimum in the lower consolute boundary occurs. Based on the previous discussion and Figure 7, we would predict that $d\Pi/dc$ or Hc/τ at the critical concentration should decrease as the critical temperature is approached. This could make it appear that the temperature dependence of molecular weight is very large. If the molecular weights were compared at or near the cmc, as we have done, such a marked temperature dependence might not have been observed. We have concluded that the higher order concentration terms in the osmotic pressure equations are highly temperature dependent for systems having lower consolute boundaries and that it is, therefore, improper to interpret quantitatively light-scattering data for these systems in terms of micellar molecular weights at any concentration other than infinite dilution of the micelles, *i.e.*, at or very near the cmc.

It can be seen from the data in Table I that increasing the alkyl chain length attached to the hydrophilic head group decreases the cmc and increases the mmw. A decrease in free energy of micellization of $1.06kT$ is calculated from the light-scattering cmc data for an increase of one CH_2 group. This agrees well with values of this parameter obtained previously for other surfactants.[1] The very high micelle molecular weight found for the $DC_{12}PO$ surfactant as compared to the at 40°. The precipitate was washed with 4 l. of water by decantation and filtered; 500 ml of water was added to the precipitate, and concentrated aqueous ammonia was used to dissolve all of the silver oxalate. The solution was filtered, and concentrated perchloric acid was added dropwise with stirring to reprecipitate the silver oxalate. The solid was washed with 4 l. of water, filtered, and stored in a dessicator. It was hoped that this reprecipitation process would remove some of the adsorbed or occluded nitrate ions. Analysis showed that the nitrate ion concentration decreased from 0.22 to 0.09% while the ammonium and perchlorate ions were not detectable (less than 0.02%). For doped samples the following procedure was adopted. About 20 ml of water was used to cover approximately 7 g of the solid, and concentrated aqueous ammonia was added dropwise until all the silver oxalate dissolved. The solution was filtered and a solution of the appropriate dopant was added. The following millimoles of dopant were added: 2.9×10^{-3} rose bengal, 3.7×10^{-3} erythrosin B, 6.7×10^{-3} acridine orange, 6.5×10^{-3} rhodamine B, 5.8×10^{-3} tetracyanoethylene, and 6.5×10^{-3} triphenylamine. The silver oxalate was precipitated in each of the solutions by adding concentrated perchloric acid dropwise with rapid stirring. With the dye solutions the precipitate was colored and little color remained in the solution, indicating that the dyes were indeed incorporated in the crystals either by surface adsorption or in the bulk. It was assumed that the colorless additives were taken up in the same way. The precipitates were washed with 500 ml of water, filtered, and stored in a desiccator. An undoped sample of silver oxalate was prepared in the same manner except that the dopant was omitted from the solution. All of the samples were prepared the same day under identical conditions to ensure that differences other than doping could be minimized. Photomicrographs showed that in all of the preparations the crystals were reasonably well formed with little differences among the different preparations and were about 5×10^{-3} mm wide and about twice that in length. X-Ray powder diffraction studies on these doped crystals (and all the other crystals mentioned later) showed that the crystal structure was monoclinic in all cases with no detectable change in the d spacings with the addition of dopants or method of preparation. Some larger crystals were made to facilitate their study by microscopy. In this case equal volumes of 0.2 N oxalic acid and silver nitrate at 40° were simultaneously run into a beaker containing 400 ml of well-stirred water kept at 40° and 5 ml of a 0.1 N solution of rhodamine B dye. The colored precipitate was washed by decantation, filtered, and stored in a desiccator. The crystals were well formed and were about 0.125 mm wide and 0.2 mm long. There was a mixture of relatively flat, diamond-shaped crystals and what seemed to be the same type of crystal but more fully grown in three dimensions producing an imperfect octahedral-shaped form. Some undoped crystals of silver oxalate were prepared in the same manner, as well as some with an excess of oxalate by using a 0.4 N solution of oxalic acid for precipitation. These latter two crystal preparations were not as well formed and were about one-tenth as large, in general, compared to the rhodamine B doped sample. All of the preparations were conducted under darkroom conditions with only a weak amber safelight for illumination. The samples were stored and handled in the dark after preparation. All of the reagents used were of analytical grade except for the dopants. Acridine orange and rose bengal were obtained from Fisher Scientific, rhodamine B and erythrosin B were produced by Allied Chemical, and triphenylamine and tetracyanoethylene were obtained from K & K Laboratories. All of these materials were used without further purification. The ultraviolet light source used for photolyzing the crystals was a GE 100-w S-4 mercury arc lamp.

III. Results

(a) *Observations by Optical Microscopy.* The microscopic observations were begun with the large pure silver oxalate crystals. In general, these crystals were observed to turn brown when exposed to ultraviolet light in air. Under the microscope these crystals showed no structure due to decomposition but seemed to be uniformly darkened. The change in color indicated that some decomposition had taken place, and the uniform darkening showed that nucleation could have been rapid enough to produce many small nuclei which did not grow. An attempt was made to follow the extent of decomposition by a thermogravimetric-type technique. A sample suspended from a Mettler balance was placed in a Fisher Isotemp oven kept at 135°, and the weight change as a function of time was followed. *In vacuo* a similar sample would have fully decomposed in about 1 hr, but in air no weight change was noticed in several hours, although the sample had turned brown. With time the sample turned darker with some weight loss until it was almost black, and finally, after complete decomposition, to a gray powder after about 3 days in the oven. X-Ray diffraction analysis of some of the partially decomposed sample indicated that only silver and silver oxalate were present during the decomposition, proving that the desired reaction was progressing although at a greatly inhibited

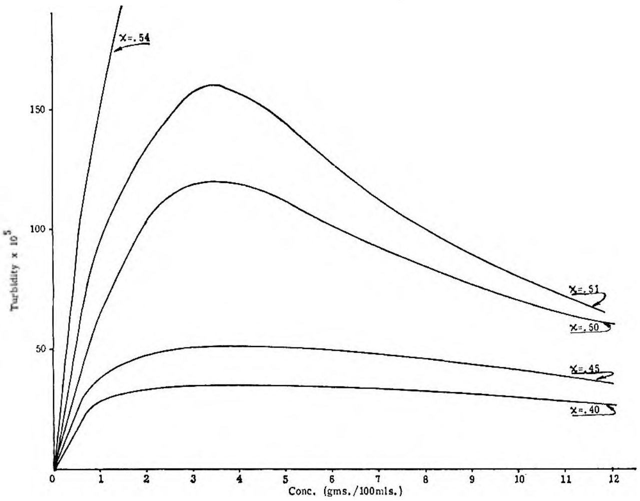

Figure 11. Theoretical curves calculated from eq 3; $V_1 = 18$, $M = 10{,}000$, $\bar{v} = 1.125$, $H = 6.9 \times 10^{-6}$.

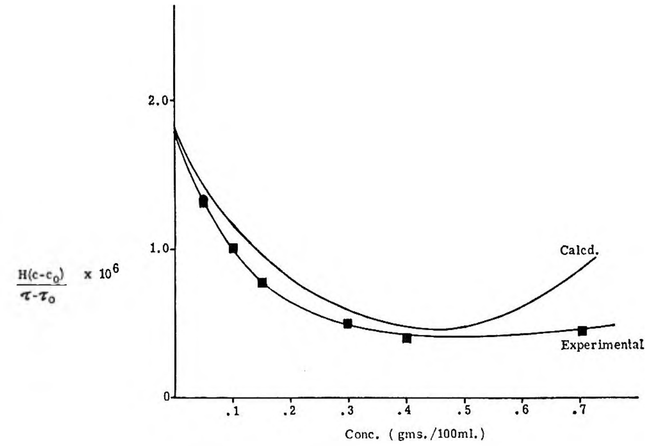

Figure 12. Comparison of theory and experiment for $DC_{12}PO$ solutions. Calculated curve from eq 3; $\bar{v} = 1.1$, $\chi = 0.5046$, $M = 555{,}000$.

dissymmetry maximum, and the critical temperature for separation of the system into two isotropic solutions will occur at the same concentration. Figures 2–5 show that these conditions are approximately met for $DC_{10}PO$ and $DC_{12}PO$. The magnitude of this turbidity maximum is strongly dependent upon temperature (the value of χ), and this does not necessarily mean that molecular weight is increasing rapidly with temperature.

To carry the application of this theory one step further, Figure 12 shows an Hc/τ *vs.* concentration curve for $DC_{12}PO$ and a theoretical curve calculated from eq 3 using the molecular weight found by extrapolation of the dilute solution light-scattering results and the other parameters shown in Figure 12. It is obvious that there is quite good qualitative agreement of the two curves. It therefore seems unnecessary, as has sometimes been done, to invoke an increase in micelle molecular weight with increasing concentration to account for the negative slope of an Hc/τ *vs.* concentration curve slightly above the cmc. It does not appear to be possible using light-scattering data alone to decide whether negative slopes in Hc/τ *vs.* concentration curves for surfactant–water systems are due to increasing molecular weight of the micelle or to contributions to nonideality of the solution at quite low concentrations due to solvent–solute, solute–solute, and solvent–solvent interactions.

It would appear that a Flory–Hildebrand type of mixing theory qualitatively predicts the behavior observed in surfactant–water systems, but quantitative agreement of experiment with theory must await the development of a more refined free energy of mixing expression for surfactant–water systems.

Critical Opalescence in $DC_{12}PO$–H_2O Solution. Figure 5 shows that the dissymetry (Z_{45}) exhibited by solutions of $DC_{12}PO$ at 30° has a maximum at a concentration of 0.5 g/100 ml, very close to the concentration at which a minimum occurs in the lower consolute boundary. This is believed to be due to critical opalescence, similar to that observed in high polymer solutions[29–34] and several other binary systems.[35–38] This phenomenon has received much experimental and theoretical attention in recent years. Debye[39] has generalized the light-scattering fluctuation theory of Smoluchowski–Einstein to present an explanation for the strong dissymmetry near the critical point and has extended the theory to binary critical mixtures.[31] Several other authors[40–42] have presented theoretical treatments which give results nearly equivalent to those of Debye. The Debye theory depends upon the fact that the

---

(29) P. Debye, H. Coll, and D. Woermann, *J. Chem. Phys.*, **33**, 1746 (1960).

(30) P. Debye, B. Chu, and D. Woermann, *ibid.*, **36**, 1803 (1962).

(31) P. Debye, *ibid.*, **31**, 680 (1959).

(32) D. McIntyre, A. Wims, and M. S. Green, *ibid.*, **37**, 3019 (1962).

(33) R. Fürth and C. L. Williams, *Proc. Roy. Soc.* (London), **A224**, 104 (1954).

(34) P. Debye, D. Woermann, and B. Chu, *J. Polymer Sci.*, **A1**, 255 (1963).

(35) B. Zimm, *J. Phys. Colloid Chem.*, **54**, 1306 (1950).

(36) B. Chu, *J. Chem. Phys.*, **41**, 226 (1964).

(37) B. Chu, *J. Am. Chem. Soc.*, **86**, 3557 (1964).

(38) B. Chu and W. P. Kao, *Can. J. Chem.*, **43**, 1803 (1965).

(39) P. Debye in "Scattering of Radiation by Noncrystalline Media in Noncrystalline Solids," V. D. Fechette, Ed., John Wiley and Sons, Inc., New York, N. Y., 1960, pp 1–25.

(40) M. Fixman, *J. Chem. Phys.*, **33**, 1357 (1960).

(41) A. Münster, *J. Chim. Phys.*, **57**, 492 (1960).

(42) E. W. Hart, *J. Chem. Phys.*, **34**, 1471 (1961).

position of this sample compared to previous ones, and the elongated areas were more prominent with very few round spots present. The mottled appearance of the decomposed areas indicated that the silver was not deposited in a uniform manner. The mottled pattern of the surface may have arisen from removal of carbon dioxide during the decomposition leaving the remaining silver deposited in an irregular pattern. The growth of the nuclei during photolysis could be observed using this microscope in conjunction with the spectrally sensitized rhodamine B dyed sample since the illuminating light was concentrated in a very small area. The thermal decomposition was unlikely since a temperature rise of 100° by the crystals suspended in the oil was not probable. As the crystal was viewed, the dark areas slowly disappeared and the light, decomposed areas grew until the entire crystal surface was filled with decomposition products after about 0.5 hr. Photomicrographs of a thermally decomposed crystal are shown in Figure 2 before and after illumination. This photolytic process could be observed since oxygen was excluded by the paraffin oil[7] used with the oil immersion objective. Similar observations on other dyed crystal preparations were precluded since the crystals were generally smaller and the magnification was insufficient to see a distinct growth of the nuclei.

Some of the large rhodamine B dyed silver oxalate crystals were exposed to sunlight in air and then were viewed with transmitted light on a Leitz microscope. It was seen that definite black spots were present after exposure, with some elongated areas as well. The edges of the crystal were outlined by black lines indicating that the silver deposited preferentially along crystal edges. In one crystal it was observed that the deposition of silver occurred in a very regular pattern along the lines of what might be a screw dislocation. In the case of this dyed sample the inhibiting effect of oxygen did not produce a uniform darkening, but this result may be connected with the increase of the growth rate by the presence of rhodamine B dye or a change in oxygen adsorption by the presence of the dye.

(*b*) *Observations by Electron Microscopy.* A replica of the surface of some of the large rhodamine B dyed crystals partially heat decomposed under vacuum, from the same batch as those observed using the Wild microscope, was examined by electron microscopy to determine the features of the decomposed surface and to confirm the earlier optical microscope observations at the higher magnifications possible with the electron microscope. The replica was made by dispersing the partially decomposed crystals on a plastic-coated slide and shadowing with palladium. Carbon was deposited on top of the palladium and the plastic was peeled off the slide. The plastic and silver oxalate then were dissolved away to produce a usable replica. The silver from the crystal surface adhered to the replica and could be seen on the electron micrographs as dark, nonuniform-appearing areas. A particularly large nonuniform area found on a crystal is shown in Figure 3. The silver could be seen often at crushed edges or corners of the crystals. More than one patch of silver could be seen on each crystal and the number and location (in the absence of obvious defects in the crystal) seemed to be quite random. Some crystals had a few large areas of silver while others had more and smaller ones. The decomposed areas had a distinctly mottled appearance as originally observed using the Wild microscope, indicating that growth proceeded along some short-range preferred path. The replica had small specks of dark material all over as well as the large dark areas on the crystal. These specks were examined by electron diffraction and found to be normal cubic silver, while the large, nonuniform-appearing areas showed a cubic structure as well, but the spacings were

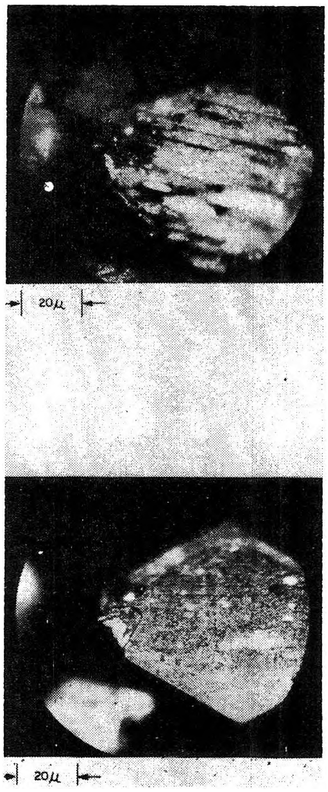

Figure 2. Silver oxalate doped with rhodamine B viewed with reflected light: top, original thermally decomposed crystal; bottom, after 30-min exposure to microscope-illuminating light.

---

(7) J. Y. Macdonald and R. Sandison, *Trans. Faraday Soc.*, **34**, 589 (1938).

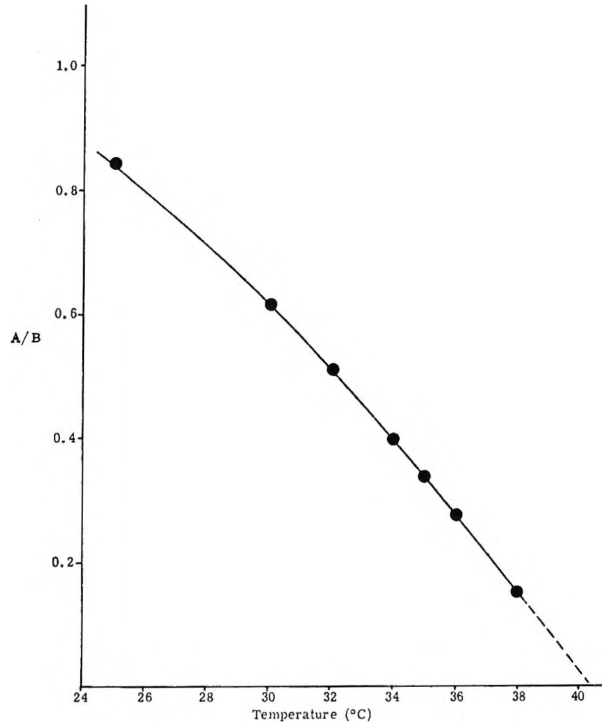

Figure 15. A/B *vs.* temperature.

concluded that it was not. In order to show this, a quantity S is defined, given in the simple theory described above by

$$S = (B/A)\Delta T = \frac{8\pi^2 l^2}{3\lambda^2} T_c \qquad (9)$$

Figure 16 is a plot of S *vs.* ΔT for the $DC_{12}PO-H_2O$ system. If l were temperature independent, this would be parallel to the abscissa. However, the fact that curvature is observed does not necessarily mean that l is temperature dependent, especially since the curve is parallel to the abscissa at small temperature distances from T_c. In the case of polystyrene–cyclohexane, where the polystyrene is of large enough molecular weight to contribute to the dissymmetry because of the extension of the polymer coil, Debye[30] showed that the quantity S, defined in eq 9, should really be written as

$$S = (B/A)\Delta T = \frac{8\pi^2 l^2}{3\lambda^2} T_c + \frac{16\pi^2 r^2}{3\lambda^2}\Delta T \qquad (10)$$

Since the radius of gyration (r) is temperature dependent for the polystyrene–cyclohexane case, the S–T curve for that system shows curvature of the kind shown in Figure 16 for our system. At large temperature distances from the critical point (1°), dissymmetry (Z_{45}) is still observed in a 0.5 g/100 ml solution of DC_{12}PO indicating that some theoretical equation similar to eq 10 should apply to our case rather than the simple theory represented by eq 9. Also, since the molecular weight of the micelle changes with temperature (Table I), the S–T curve should not be a straight line but should be curved owing to this temperature dependence. How this theory should be formulated to obtain both the range of molecular forces and the size of the micelles for a surfactant–water system is a difficult question, especially since the micellar aggregation number is probably both temperature and concentration dependent. In any case, the system qualitatively obeys the Debye critical opalescence theory. Results similar to those shown in Figures 13–16 were also obtained at a concentration of 1 g of $DC_{12}PO$/100 ml, which is well removed from the concentration at which the dissymmetry maximum occurs.

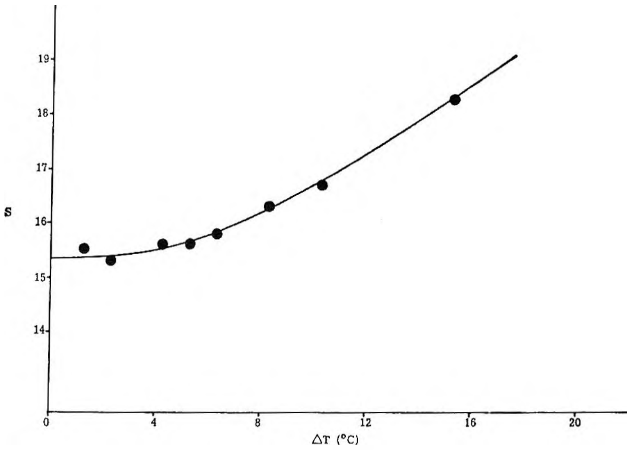

Figure 16. S *vs.* ΔT.

Acknowledgments. We gratefully acknowledge the assistance of Dr. R. G. Laughlin, who prepared the DC_nPO surfactants, and that of Dr. R. C. Mast, who determined the surface tension cmc values. We are especially indebted to Professor P. Debye for his encouragement and for many helpful discussions regarding the applicability of light-scattering and consolute-solution theory to the surfactant solutions studied.

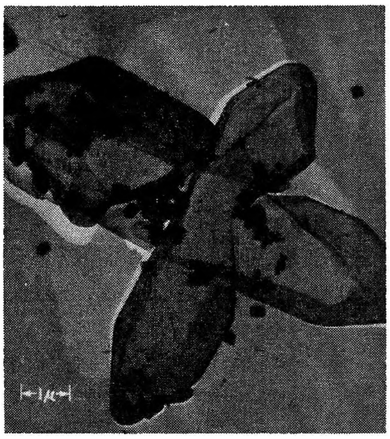

Figure 5. Surface replica of undoped silver oxalate thermally decomposed under vacuum.

Figure 6. Surface replica of silver oxalate doped with rose bengal thermally decomposed under vacuum.

could be seen from the electron diffraction pattern of the silver on the crystals, and the diffraction pattern showed only spacings characteristic of ordinary silver. The conversion process of metastable silver to ordinary cubic silver is not understood at the present time, but it may be that the treatment of these small crystals facilitated the conversion. It is possible that the presence of oxygen could affect the conversion of the silver. Further experiments have been initiated to examine the conditions needed for the conversion to cubic silver and the properties of the metastable silver. The growth of nuclei from the surface into the crystal could be seen by examination of stereo electron micrographs of the replicas. The decomposed areas appeared as irregular-shaped holes formed into the crystals.

IV. Conclusions

On the basis of these microscopic observations, it seems clear that the compact nuclei produced in both the photolytic and thermal decomposition of silver oxalate under vacuum are quite similar. The nuclei are produced on the surface and grow three dimensionally into the crystal. In cases where the crystals were prepared in the presence of the donors and acceptors, discrete nuclei, growing in three dimensions, could be seen even when these samples were photolyzed in air as well as by thermal decomposition under vacuum. The thermal and photolytic decomposition of pure silver oxalate in air was found to be greatly inhibited and no compact nuclei could be seen. In cases where compact nuclei were found, observations of both large and small crystals showed that the same type of nuclei were produced and three-dimensional growth took place in these crystals upon heating or exposure to light. A metastable form of silver was seen only in the large rhodamine B dyed crystals thermally decomposed under vacuum. The age and size of the crystals would not appear to be an important factor in explaining the variable kinetic behavior of the decomposition reaction, under vacuum, observed by others,[4,13] since similar compact nuclei, that grow three dimensionally, are observed in all these cases.

Acknowledgment. The author thanks Keith Johnson for obtaining the electron micrographs and Paul Cherin for his help with the X-ray and electron diffraction studies of the crystals.

---

(13) A. Finch, P. W. M. Jacobs, and F. C. Tompkins, *J. Chem. Soc.*, 2053 (1954).

Decomposition of Silver Oxalate. II. Kinetics of the Thermal Decomposition

by Algird G. Leiga

Xerox Corporation, Rochester, New York 14603 *(Received February 14, 1966)*

The thermal decomposition of silver oxalate between 115 and 135° was studied as a function of the adsorbed donors (triphenylamine, acridine orange, and rhodamine B) and the acceptors (tetracyanoethylene, rose bengal, and erythrosin B). The decomposition of all the samples was found to fit the equation $\alpha = Ct^n$, where α is the fractional decomposition, t is time, and C and n are constants. The constant C, containing the rate constant for growth of nuclei and nucleation, was found to increase as the temperature of the decomposition was increased. With donors present the constant was greater than for the undoped case, while with acceptors much smaller values were obtained. Values of n were not affected very much by donors, yielding values between about 3 and 4 depending on temperature, but the acceptor-doped samples yielded higher values up to about 5. The variation of n with dopants was interpreted as a change in the nucleation step of the reaction in the presence of the acceptors. Similarly, the change in C with dopants was attributed to an enhanced growth rate of nuclei with donors and a retarded growth rate with acceptors. The steps of the proposed reaction mechanism include the trapping of the excitation energy of the oxalate ion at the dopant sites on the crystal surface with the donors facilitating the electron-transfer reactions and the acceptors retarding them.

I. Introduction

The thermal decomposition of silver oxalate into silver and carbon dioxide has been studied extensively in recent years under varying conditions of preparation,[1,2] decomposition environment,[3] and preirradiation.[1,4-6] Quite early it was noticed that silver oxalate prepared in the presence of excess oxalate decomposed faster than a sample prepared with stoichiometric amounts of oxalate and silver ions.[7] Furthermore, the sample prepared in the presence of an excess of silver nitrate decomposed slower than the stoichiometrically produced material. In addition, Sheppard and Vanselow[8] showed that silver sulfide nuclei introduced into silver oxalate acted as catalysts for the thermal decomposition reaction. The crystal size and age were other important factors, and it has been suggested that some of the discrepancies among different workers may be resolved by a consideration of the age and crystal size.[1,4]

The marked influence of the surrounding environment of the decomposition of silver oxalate was demonstrated by several investigators. It was shown that oxygen exerts a very marked decrease in the decomposition rate, while carbon dioxide does not affect it at all.[7] Compared to the reaction *in vacuo* the decomposition under liquids such as paraffin, nitrobenzene, and dichlorobenzene was retarded, while the decomposition rate under liquids such as phenol, glucose syrup, aniline, and benzaldehyde was markedly increased.[3]

The diverse observed effects of the medium and impurities has been discussed by Boldyrev[9] in terms of the electronic theory of adsorption and catalysis. The observed facts of the thermal decomposition of a

---

(1) A. Finch, P. W. M. Jacobs, and F. C. Tompkins, *J. Chem. Soc.*, 2053 (1954).

(2) J. Y. Macdonald, *ibid.*, 832 (1936).

(3) J. Y. Macdonald and R. Sandison, *Trans. Faraday Soc.*, **34**, 589 (1938).

(4) R. M. Haynes and D. A. Young, *Discussions Faraday Soc.*, **31**, 229 (1961).

(5) F. C. Tompkins, *Trans. Faraday Soc.*, 44, 206 (1948).

(6) A. F. Benton and G. L. Cunningham, *J. Am. Chem. Soc.*, **57**, 2227 (1935).

(7) J. Y. Macdonald and C. N. Hinshelwood, *J. Chem. Soc.*, **127**, 2764 (1925).

(8) S. E. Sheppard and W. Vanselow, *J. Am. Chem. Soc.*, **52**, 3468 (1930).

(9) V. V. Boldyrev, *Zh. Fiz. Khim.*, **33**, 2539 (1959).

solid can be explained if the special features of the individual stages are taken into account. The decomposition of ionic crystals is assumed to begin with a splitting off of an electron from the anion and its transfer to the conduction band either directly or through an intermediate exciton state. The electron may be trapped at an impurity site or at an anion vacancy, and either interstitial cations or anion vacancies will be drawn to the trapped electron depending on whether Frenkel or Schottky defects predominate. The holes remaining after release of the electron would react to form one product and the trapped electron would ultimately react with the cations to form the other product. The successive alternation of the processes of trapping electrons, migration of cations, and reaction would produce the growth of the nucleus. On this basis Boldyrev can explain the effects of environment and impurities on the decomposition of solids such as silver oxalate. Since the mechanism involves conduction-band electrons, it should be possible to enhance the rate of reaction by adsorption of electron donors on the surface of the crystal; conversely, electron acceptors which would tend to decrease the electron concentration in the conduction band would retard the reaction. The observed effects of environment are then explained by assuming that materials such as hydrogen gas, excess oxalate ions, and glucose develop donor functions on silver oxalate while oxygen, nitrate ion, and nitrobenzene develop acceptor properties.

The rate of decomposition should depend on the concentration of ionic defects in the decomposing solid. If impurities are introduced into the lattice producing anion vacancies, the rate of thermal decomposition should increase since the conduction-band electrons or excitons would be readily trapped. If cation vacancies are formed, the positive holes produced after removal of the electron would be trapped and accumulate in the lattice, increasing the probability of their recombination with electrons, and hence the reaction rate should decrease. In support of these ideas it has been shown that introduction of Cd^{+2} ions into the silver oxalate lattice, producing additional cation vacancies, yields a decrease in the thermal decomposition rate.[10]

The mechanism organically suggested by Boldyrev was, however, in conflict with the known facts, since silver oxalate was purely an ionic conductor and showed no photoconductivity.[5,10] The mechanism was later modified[10] by considering that instead of conduction-band electrons mobile excitons were produced and trapped by interstitial silver ions to produce decomposition products, but then the effect of adsorbed impurities was not so readily explained.

A possible method of studying the effect of adsorbed impurities on the thermal decomposition of silver oxalate would be to determine the decomposition rate with known donors and acceptors adsorbed on the crystals. In the present experiments the thermal decomposition rate was determined using crystals with adsorbed donor and acceptor dyes and with triphenylamine and tetracyanoethylene.

II. Experimental Procedure

Samples of pure silver oxalate as well as donor- and acceptor-doped samples were prepared by precipitation of the salt from solution in the presence of the dopant. The detailed preparation has been described previously.[11] The dopants used in the experiments could be broadly classified into donors and acceptors based on Mulliken's classification.[12] The donors were triphenylamine (I), acridine orange, C.I. No. 46005 (II), and rhodamine B, C.I. No. 45170 (III), and the acceptors were tetracyanoethylene (IV), rose bengal, C.I. No. 45440 (V), and erythrosin B, C.I. No. 45430 (VI). The relative donor or acceptor strengths is an additional problem that is not readily solved since the orientation of the molecules in the adsorbed state and the actual amount adsorbed are not known exactly.

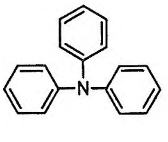
I

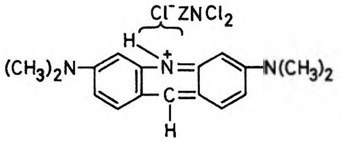
II

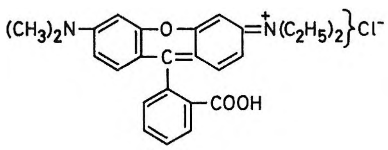
III

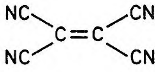
IV

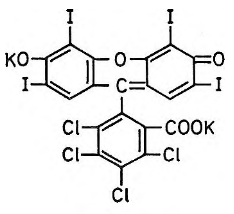
V

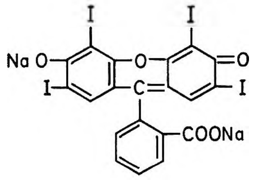
VI

---

(10) V. V. Boldyrev, Yu. A. Zakharov, V. M. Lykhin, and L. A. Votinova, *Kinetika i Kataliz*, **4**, 672 (1963).

(11) A. G. Leiga, *J. Phys. Chem.*, **70**, 3254 (1966).

(12) R. S. Mulliken, *J. Chim. Phys.*, **61**, 20 (1964).

Based on Mulliken's work and the results presented in the review by Parini,[13] it is possible to estimate that the best donors would be triphenylamine and acridine orange, while rhodamine B would be a weaker donor since it contains some electron-withdrawing substituents on the aromatic rings. Similarly, rose bengal would be expected to be a better acceptor than erythrosin B since it contains the additional electron-withdrawing chloro groups on one of the aromatic rings. The acceptor strength of tetracyanoethylene is not clear among these three compounds although it would certainly be expected to be an acceptor in these experiments.

The decompositions of the various samples were followed by measuring the pressure rise with time. Approximately a 0.05-g sample was weighed into a quartz tube attached to a mercury-free vacuum system by means of a greased standard taper and evacuated to a pressure of about 5 × 10^{-6} torr. An oil bath regulated to ±0.3° was raised until the sample tube was immersed in the hot oil. The time of the reaction was assumed to begin as soon as the sample was in the oil bath. The temperature of the sample within the cell was measured by a thermocouple and indicated that the desired decomposition temperature was reached within about 5 min. The pressure was measured by means of a Wallace and Tiernan gauge calibrated between 0 and 20 mm in 0.1-mm graduations. The volume of the decomposition cell, pressure gauge, and necessary tubing was 196.9 ml. An additional volume of 202.3 ml could be valved into the system to facilitate measuring higher pressures. The decompositions were studied at 115, 120, 125, 130, and 135°. The fractional decomposition, α, was obtained by determining the final pressure at the decomposition temperature and taking the ratio of the measured pressure at a particular time to the final pressure. All pressure measurements were corrected for the temperature difference between the decomposition cell volume and connecting tubing. The pressure was assumed to be constant at the end of a run when two successive 5-min readings showed no change.

III. Results

The present data for the decomposition of undoped silver oxalate are shown in Figure 1 plotted as fractional decomposition, α, against time, t, with temperature as a parameter. From these plots the time to reach a given percentage decomposition can be obtained at different temperatures, and from this value the temperature coefficient for a 10° rise in temperature can be calculated. The temperature coefficients obtained in this way are shown in Table I for different fractional decompositions and over several temperature ranges and indicate a coefficient of about 2. Macdonald[14] studied the decomposition of a sample of silver oxalate prepared with excess oxalate and found that the rate of reaction increased by a factor of about 3.0 for a 10° rise in temperature. Based on the higher figure of Macdonald and assuming a simple relationship between the variation in the rate and the temperature, a fluctuation of ±0.3° in the decomposition temperature would produce a maximum error of ±9% in the decomposition rate. All other errors, such as pressure readings, would be small and probably would contribute only ±1% additional error, yielding a total error of about ±10% in α. From a knowledge of the total error, analysis of the kinetic data could be made to decide whether a power or exponential decomposition law was followed in this instance. Since the model used to derive the equations[15] clearly would

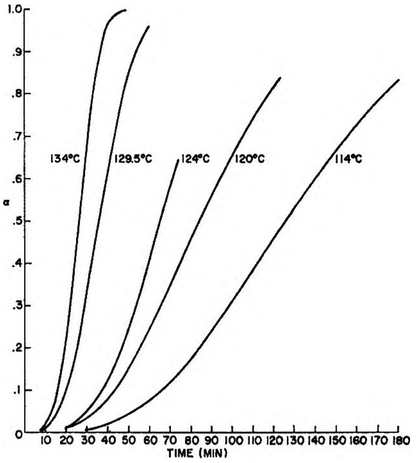

Figure 1. Thermal decomposition of undoped silver oxalate.

Table I: Temperature Coefficient for Decomposition of Silver Oxalate

Temp range, °C	Fractional decomposition					
	0.05	0.10	0.15	0.20	0.25	0.30
114–124	1.73	1.76	1.67	1.81	1.85	1.86
124–134	2.25	2.35	2.42	2.39	2.37	2.43
120–129.5	2.12	2.14	2.19	2.24	2.26	2.26
114–134	1.97	2.04	2.01	2.08	2.09	2.13

---

(13) V. P. Parini, *Russ. Chem. Rev.*, **31**, 408 (1962).

(14) J. Y. Macdonald, *J. Chem. Soc.*, 273 (1937).

(15) P. W. M. Jacobs and F. C. Tompkins, "Chemistry of the Solid State," W. E. Garner, Ed., Academic Press Inc., New York, N. Y., 1955, Chapter 7.

which may be compared with $G(C_6H_6) = 1.05$ obtained at $F = 0.007$ for the silica–alumina.[13] At the lower doses used in this work, decomposition of isopropylbenzene was of the order of 1%.

Discussion

A. The Reaction of Isopropylbenzene on Irradiated Silica Gel. In quartzes and silica-base glasses and gels, the mechanism of formation and the nature and interrelationships of the many color centers formed by high-energy radiation are not thoroughly understood.[4,5,15–18] Consequently, it would be premature to attempt the development of a unique and integrated interpretation of the chemical effects occurrent on interaction of isopropylbenzene and other substances with irradiated silica and silica–alumina gels. Nevertheless, certain color centers in silica-base solids have been rather thoroughly studied, and their behavior and nature have been established with reasonable certainty. By comparison of the behavior of such color centers with that of the isopropylbenzene dealkylation reaction on irradiated silica and silica–alumina gels, a strong correlation is established between these color centers and the excitations effective in dealkylation.

The Role of Impurities. The results in Table I are to be compared with benzene yields of 13–233 × 10^{17} molecules/g of solid obtained on silica–aluminas irradiated at room temperature to a saturation dose;[2,14] these silica–aluminas contained $\sim 1.2 \times 10^{21}$ atoms of Al/g of solid. For the room temperature irradiations, a qualitative correlation is observed between the yield of benzene and the aluminum or total impurity content.[19] Similar qualitative correlations have been reported between the aluminum content of irradiated silica gels and their visible color, H_2–D_2 exchange activity, and irreversible H_2 adsorption.[8,11] Nevertheless, the relationship between benzene yield and impurity content is quite evidently not a proportional one; certainly the aluminum content does not govern the limiting yield. Similarly, poor quantitative correlations have been obtained between aluminum content and the visible color of irradiated quartz and silica; this has been accounted for as owing to presence of part of the aluminum in interstitial sites,[20] rather than in substitutional sites where aluminum acts as a positive-hole trap and gives rise to the visible color[21] and a characteristic esr signal.[22] Such an explanation cannot account for the low benzene yields relative to aluminum content on the silica–aluminas for which a major fraction of the benzene yield has been associated with the visible color centers;[2] in such solids, the aluminum appears to be largely substitutional.[23] The benzene yield on silica–alumina may be limited by the availability of stable electron traps or of specific charge-compensation ions essential to stabilization of positive holes on substitutional aluminum.[4,5]

Although the aluminum content of the three silica gels is sufficient to account for the yields of benzene in room-temperature irradiation, the absence of significant visible coloration in the irradiated solids suggests that the traces of aluminum are not substitutional in these solids. On solids A and C irradiated at −196°, benzene yields actually exceed the aluminum content. One might argue that benzene yields on the irradiated silica gels are related to total impurity content, which may exceed the benzene yield even in the case of solid A irradiated at −196°. In the ensuing discussion, remarkably good correlations are established between the behavior of benzene yields on irradiated solid A and that of certain color centers, namely the E′ centers (trapped electrons) absorbing at $\sim 0.22\ \mu$, associated with specific vacancies in the silica matrix. It is our opionion that limiting benzene yields on the three silica gels are governed by the availability of defects inherent in the silica matrix and not by cationic impurities. The difference between the benzene yield on solid A and those on solids B and C may be attributable to the effect of the very different methods of preparation on the concentration of silica matrix defects produced; *e.g.*, it has been observed that anion impurities, particularly OH^-, may occupy oxygen vacancies and preclude formation of E′ centers on irradiation.[18] Solids B and C were prepared with $SiCl_4$ while the solid A preparation used ethyl silicate. Although the large difference in surface area of solid A as compared to solids B and C reflects an effect of preparation method on structure, it is evident that benzene yields are not directly related to surface area. It should be noted that an appreciable fraction of the benzene yield on irradiated silica–alumina was shown not to be associated with visible color centers;[2] it is probable that this yield of benzene arises from the same centers that are effective in the silica gels.

---

(15) *Cf.* the ten papers from the Mellon Institute Symposium on Defect Structure of Quartz and Glassy Silica, *J. Phys. Chem. Solids*, **13**, 271 (1960).

(16) W. D. Compton and G. W. Arnold, Jr., *Discussions Faraday Soc.*, **31**, 130 (1961).

(17) C. M. Nelson and R. A. Weeks, *J. Appl. Phys.*, **32**, 883 (1961).

(18) R. A. Weeks and E. Lell, *ibid.*, **35**, 1932 (1964).

(19) Other impurities—such as iron, magnesium, copper, calcium, and sodium—were present in silica gels A and B at about the same level as the aluminum.

(20) A. J. Cohen, *J. Phys. Chem. Solids*, **13**, 321 (1960).

(21) R. W. Ditchburn, E. W. J. Mitchell, E. G. S. Paige, J. F. Custers, H. B. Dyer, and C. D. Clark, Bristol Conference on Defects in Crystalline Solids, The Physical Society, London, 1955, p 92.

(22) M. C. M. O'Brien and M. H. L. Pryce, ref 21, p 88.

(23) A. Leonard, S. Suzuki, J. J. Fripiat, and C. DeKimpe, *J. Phys. Chem.*, **68**, 2608 (1964).

Correlations with the E′ Centers. In fused silicas of high purity, in which no visible color is produced by irradiation, certain radiation-induced ultraviolet absorption bands are enhanced by irradiation at $-196°$.[16,24,25] Arnold and Compton[25] report that on irradiation and measurement at 77°K, the intensity of the 0.215-μ band (an E′ center) was ~10 times greater than the intensity observed after an irradiation at ~300°K and measurement at 77°K. In addition, these authors observed that when the sample irradiated at 77°K is warmed to room temperature and then immediately remeasured at 77° K, the 0.215-μ absorption is reduced to about half its original value. Further loss in the 0.215-μ absorption was observed to occur slowly at room temperature and to approach the value obtained when the irradiation was made at room temperature. The parallel between these results and the benzene yield results is striking (*cf.* Figures 1 and 2).

The same limiting yield of benzene is attained in room-temperature irradiation as in the decay at room temperature of centers produced by a saturation dose at $-196°$; therefore, this limiting yield of benzene at room temperature must correspond to essentially complete population of certain silica matrix defects, rather than to attainment of a radiation-induced steady-state population of such defects. Furthermore, the annealing behavior suggests a quantitative conversion of centers formed on irradiation at $-196°$ into available room-temperature centers on warming. Again, a similar interconversion of electron-type centers has been observed in optical bleaching experiments on irradiated fused silicas;[26-29] *e.g.*, Nelson and Weeks observe that interconversion of E_1' and E_2' centers occurs with only a small loss of total intensity and conclude that it is easier to transfer electrons between electron-type centers than to cause electron-hole recombination at a hole center.

The results of Table II show that centers produced on irradiation at $-196°$ are converted into the room-temperature centers by irradiation at room temperature;[30] the loss in benzene yield due to the room-temperature irradiation corresponds to a $G(-C_6H_6) \approx 4$, which equals $G_0(C_6H_6)$ at $-196°$. Such a result suggests that the limiting yield of benzene in irradiation at $-196°$ corresponds to a steady-state population of the unstable (at room temperature) centers; these centers must have a negligible cross section for formation at room temperature. The $G_0(C_6H_6) \approx 4$ at $-196°$ corresponds to 25 ev per center, which is about what might be expected for the formation of free charge carriers in silica. Thus, at $-196°$ a high capture efficiency for the free charge carriers is indicated; that for formation of the room-temperature centers is ~60-fold smaller.

Correlation with Other Chemical Effects on Irradiated Silica Gels. The dealkylation of isopropylbenzene appears to occur on a variety of color centers produced by irradiation of silica and silica–alumina gels. The centers effective in dealkylation that are produced by irradiation of silica gel at $-196°$ seem to correspond to the acid centers of Barter and Wagner.[9] These authors observed no coloration of their irradiated silica gel and observed decay of the radiation-induced acid centers at room temperature. We suggest that such centers are associated with some kind of color center characteristic of the silica matrix. In addition, there are radiation-induced dealkylation centers in silica gel and in silica–alumina that are stable at room temperature and also do not absorb in the visible and, hence, are not associated with positive holes trapped on substitutional aluminum impurity. Such are the centers formed at room temperature in solid A and those which remain after a hydrogen or thermal bleach of visible color centers in silica–alumina.[2] These centers, to which $-196°$ centers convert on warming of a $-196°$ irradiated silica, also appear to be related to defects inherent in the silica matrix. Finally, in silica–alumina[2] dealkylation of isopropylbenzene has been shown to occur also on the visible color centers (stable at room temperature) identified as positive holes trapped on substitutional aluminum. Boreskov, *et al.*,[8] have demonstrated that in a silica gel that is colored by irradiation, such aluminum centers are responsible for the color, for the irreversible adsorption of hydrogen concomitant with bleaching of the color, and for a major part of the H_2–D_2 exchange activity measured at $-196°$. It has been noted previously[2] that dealkylation of isopropylbenzene does not occur on the radiation-induced H_2–D_2 exchange sites studied by Kohn and Taylor;[6] these sites do not absorb in the visible (they remain after hydrogen bleaching) and are poisoned by oxygen.

B. Irradiation of Isopropylbenzene Adsorbed on Silica

---

[24] P. W. Levy, *J. Phys. Chem. Solids*, **13**, 287 (1960).

[25] G. W. Arnold and W. D. Compton, *Phys. Rev.*, **116**, 802 (1959).

[26] F. S. Dainton and J. Rowbottom, *Trans. Faraday Soc.*, **50**, 480 (1954).

[27] C. M. Nelson and R. A. Weeks, *J. Am. Ceram. Soc.*, **43**, 396 (1960).

[28] C. M. Nelson and J. H. Crawford, Jr., *J. Phys. Chem. Solids*, **13**, 296 (1960).

[29] The existence of such interconversions in the alkali halides has been known for some time; *cf.* K. Przibram, "Irradiation Colours and Luminescence," Pergamon Press Ltd., London, 1956, p 72.

[30] A similar effect has been observed in KCl by H. U. Harten, *Z. Physik*, **126**, 619 (1949).

both k_2 and k increase normally with temperature. As expected on the basis of this explanation, pronounced dips in C were found only for the acceptor-doped cases. These samples had the largest increase of n between 115 and 124°, and as a result the greatest decrease in the apparent nucleation rate constant would be expected in these cases.

From the plots of n *vs.* various dopants (Figure 5), it can be seen that donors do not particularly change the nucleation step as compared to the undoped samples; however, acceptors clearly change the nucleation process. In general, nucleation requires several atoms to form a stable nucleus; however, in the present case it may be possible to consider that there are traps present which can help stabilize smaller nuclei. In addition the plot of C *vs.* dopant (Figure 4) shows that C markedly decreases when the dopants are changed from donors to acceptors. If the change in C as a function of dopant is more representative of growth changes rather than nucleation as would be expected by the cubic dependence of k_2, then these results can be interpreted to mean that acceptors favor some process that produces nuclei in a more complex manner involving two steps (or more) as the growth rate diminishes. The growth rate of nuclei with donors present is enhanced compared to the undoped material and retarded when acceptors are present.

(*b*) *Power Law or Exponential Law.* The discrepancy between the power law and exponential law decomposition has been thought[1] to result from the dislocation density. In highly disorganized crystals, where the dislocation density was high, the exponential law was found to hold, but in well-annealed crystals the power law was valid. Although the aging seemed to be a satisfactory explanation for the change from the exponential to the power law, Haynes and Young[4] found that freshly prepared silver oxalate was variable in its decomposition behavior, but for material that had been annealed at 80° for 1 hr the acceleratory period could be represented by the Prout and Tompkins expression,[16] which is basically decomposition according to an exponential law. The present samples could not be considered well-annealed crystals since they were used relatively fresh (all the runs were made within 5 months of their preparation with no special annealing procedures used). In addition, no systematic variation in the decomposition could be attributed to an aging of the crystals in the time of the experiments. A possible explanation for the variety of rate expressions may be attributed to the presence of silver at the start of the reaction from the slow room-temperature decomposition of the salt, especially on very small crystals. These nuclei could constitute the instantaneous nucleation observed in the kinetic analysis of the data and might lead to the observed power law decomposition.

V. Mechanism of the Decomposition Reaction

A reasonable mechanism for the decomposition of silver oxalate incorporating the experimental facts can now be written. The first step, the excitation of the crystal, has been considered to occur by means of excitons[1] in the photochemical decomposition. The thermal excitation process is not as clear, but the energy required would be less since the transition does not have to follow the Franck–Condon principle.[17,18] The thermal process does not necessarily involve an exciton and may simply involve a vibrationally excited oxalate ion lattice point that has sufficient energy to transfer an electron to a trap.

A potential energy *vs.* internuclear distance diagram may be drawn for a solid analogous to a diatomic molecule, but in the solid the internuclear distance coordinate would represent the configuration of the nuclei at the particular point in the crystal where the transition takes place. In silver oxalate the optical transition initially produces a vibrationally excited upper electronic state which then may decay rapidly to the ground vibrational state of the same electronic level, make a radiationless transition to another excited electronic level, or emit resonance fluorescence. The orange emission observed[19] at low temperatures when the pure compound is illuminated with 3650-A radiation indicates that a transition has occurred to a lower excited electronic level which ultimately can emit the orange light. At room temperature a weak purplish emission has been observed[19] as well. These results indicate that there are several excited electronic states in the pure solid below the energy of the exciting radiation, and it is possible that the photochemical decomposition of the solid may proceed through any or all of these excited states. Although the photochemical decomposition of silver oxalate usually has been carried out with ultraviolet radiation, the threshold of decomposition has been found[5] to be as high as 4920 A. This result could be interpreted to mean that absorption takes place at different upper electronic states from which radiationless transitions can occur, producing a lower excited state before decomposition occurs. The orange fluorescence from silver oxalate

---

[17] J. G. W. Thomas and F. C. Tompkins, *J. Chem. Phys.*, **20**, 662 (1952).

[18] N. F. Mott and R. W. Gurney, "Electronic Processes in Ionic Crystals," 2nd ed, Oxford University Press, London, 1948, pp 160–162.

[19] S. Makishima and T. Tomotsu, *Bull. Chem. Soc. Japan*, **27**, 70 (1954).

Pure Quadrupole Resonance of Halogens in Some Hexahalorhenates(IV)

by **Ryuichi Ikeda, Akinobu Sasane, Daiyu Nakamura, and Masaji Kubo**

Department of Chemistry, Nagoya University, Chikusa, Nagoya, Japan *(Received March 10, 1966)*

The nuclear quadrupole resonance of halogens in various hexahalorhenates(IV) $R_2[ReX_6]$ ($R = NH_4$, Rb, Cs; $X =$ Cl, Br, I) was observed at various temperatures. The change in the number of observed resonance lines reveals the existence of a phase transition of ammonium hexaiodorhenate(IV) at 44–46°. From the dependence of resonance frequencies on the kind of cations R, it is concluded that, in addition to the direct electrostatic effect of external charges, an indirect effect, due to neighboring ions, is significant on the field gradient at the resonant halogen nucleus. Sternheimer's antishielding accounts for the large field gradient amplification at least with regard to the sign and the order of magnitude of the indirect effect relative to the direct effect. All these complexes show a positive temperature coefficient of quadrupole resonance frequencies with the single exception of ammonium hexachlororhenate(IV). It is suggested that hydrogen bonding or some electrostatic interaction between hydrogen and chlorine atoms in crystals is responsible for the exceptional behavior of this complex.

Introduction

In a preceding paper,[1] we have reported that positive temperature coefficients of quadrupole resonance frequencies were found for potassium hexachlororhenate(IV), hexabromorhenate(IV), and hexachlorotungstate(IV). The temperature range was that in which these complexes show a single resonance line, *i.e.*, the range in which they form cubic crystals having the potassium hexachloroplatinate(IV) structure. A theoretical explanation was made in terms of the $d\pi$–$p\pi$ bond character of metal–ligand bonds in paramagnetic complexes having one or more vacancies in their $d\epsilon$ orbitals. However, the field gradient at the resonant nucleus leading to the positive temperature coefficient does not originate solely from the electron distribution within the complex ion containing the nucleus: charges on other ions should make an appreciable contribution as well. Therefore, we have undertaken a systematic study of the temperature coefficient of quadrupole resonance frequencies of hexachloro-, hexabromo-, and hexaiodorhenates(IV) having ammonium, rubidium, and cesium ions as cations. Potassium hexaiodorhenate(IV) has been already examined,[1] but it does not crystallize in a cubic structure at any accessible temperature. No reports have ever been published on the possible formation of lithium and sodium hexahalorhenates(IV).

Experimental Section

Apparatus. A Dean-type, self-quenching, superregenerative spectrometer, already described,[2] was used for the observation of quadrupole resonance frequencies of chlorine isotopes. For detecting the resonance absorptions of bromine and iodine isotopes, a self-quenching, superregenerative spectrometer[2] equipped with Lecher lines was employed. Resonance frequencies were determined at room, Dry Ice, and liquid nitrogen temperatures. For ammonium hexaiodorhenate(IV), frequency determination was extended up to about 100° in order to locate a possible phase transition to a cubic structure. For all of the complexes studied, the temperature coefficient of the resonance frequencies was determined between Dry Ice and room temperatures.

Materials. When ammonia solution was added to an aqueous solution of rhenium(VII) heptoxide, Re_2O_7, ammonium perrhenate(VII), $(NH_4)ReO_4$, separated as a white precipitate. It was dissolved in concentrated hydrochloric acid and reduced with hypophosphorous acid to prepare ammonium hexachlororhenate-

---

[1] R. Ikeda, D. Nakamura, and M. Kubo, *J. Phys. Chem.*, **69**, 2101 (1965).

[2] D. Nakamura, Y. Kurita, K. Ito, and M. Kubo, *J. Am. Chem. Soc.*, **82**, 5783 (1960).

All of these subsequent reactions would be fast compared to the production of initially excited oxalate ions. On the basis of this mechanism it can be seen that a temperature increase should increase the rate of production of excited oxalate ions as well as the mobility of Ag_i^+ ions, leading to further nucleation requiring only one step and a more rapid growth of these nuclei.

The addition of dopants produces additional traps on the crystals and most likely the adsorbed dopants are then the only effective traps. With donor molecules on the surface interstitial silver ions now would tend to be trapped at these sites since a charge-transfer complex could be formed with the Ag_i^+ ions. The formation and decomposition reactions of the complex would be quite rapid but would produce a net increase of Ag_i^+ ions at the donor impurity site.

$$\left.\begin{array}{l} Ag_i^+ + D \rightleftarrows Ag_i^+D \\ Ag_i^+D + Ag_i^+ \rightleftarrows (Ag_i^+)_2D \end{array}\right\} \text{fast} \qquad (7)$$

The limiting step in the reaction would still be the production of excited oxalate ions. The trapping of the excited species now would occur at the donor site at which there is an enrichment of interstitial silver ions leading to a rapid reaction to form the nucleus.

$$C_2O_4^{*2-} + (Ag_i^+)_2D \longrightarrow Ag_2D + 2CO_2 \qquad (8)$$

The growth of the nucleus would proceed by the same reaction and would be enhanced over that with the undoped material since there would be a greater concentration of Ag_i^+ ions at the donor site, and the donor would probably lower the energy barrier for transfer of electrons to the silver ions. An increase of temperature would produce the same results as with the undoped material.

In the acceptor-doped samples the reaction producing the excited ions is still slow, but now the trapping site is the acceptor impurity. With the acceptor the interstitial silver ions are not affected, therefore, as in the undoped case

$$C_2O_4^{2-} \rightleftarrows C_2O_4^{*2-} \quad \text{slow} \qquad (3)$$

$$C_2O_4^{*2-} + A \rightleftarrows [C_2O_4^{*2-}A] \quad \text{fast} \qquad (9)$$

The reaction with silver ions is the next step, but the presence of the acceptor raises the energy barrier to the electron transfer as compared to the undoped case leading to the slow reaction

$$[C_2O_4^{*2-}A] + 2Ag_i^+ \longrightarrow [Ag_2A] + 2CO_2 \qquad (10)$$

The combination of the slow, excited oxalate ion production step and the slow transfer of electrons to the silver ion requires that $\beta = 2$ in the nucleation step since the nucleation steps can now be considered the successive formation of the excited oxalate ion and the decomposition of the intermediate silver ion excited oxalate ion pair to form silver and carbon dioxide. The growth of the nucleus is also retarded since the silver nucleus has an acceptor associated with it; therefore, electron transfer to silver ions has a higher energy barrier. In this case, the back reactions of trapping and deactivation of the excited oxalate ion become important and the effective number of these species decreases. A rise in temperature would increase the number of excited oxalate ions and hence the rate of decomposition as well as the slow nucleation step. At the lower temperature some nuclei are produced rapidly, but as the temperature is raised the new nucleation step becomes more important, changing the time dependence.

Acknowledgment. The author thanks Roy Walder for his assistance in obtaining the kinetic data for the decomposition reactions.

Salt and Acid Effects in the Hydrolysis of N-Acylimidazolium Ions and the Role of Structured Water

by James A. Fee[1] and Thomas H. Fife

Department of Biochemistry, University of Southern California, Los Angeles, California

(Received May 2, 1966)

The effect of varying concentrations of NaCl, NaBr, and $NaClO_4$ at a constant HCl concentration of 0.1 *M* and the effect of increasing concentrations of HCl on the rate constants and activation parameters for hydrolysis of a series of N-acylimidazoles in water have been measured. The slopes of plots of log k_{obsd} *vs.* NaCl concentrations up to 5 *M* are nearly identical for all of the compounds in the series. Increasing concentrations of HCl, however, affect the compounds with branching at the β carbon of the acyl group differently from the compounds with branching at the α carbon, the rates of hydrolysis of β-branched compounds showing much less sensitivity to changes in acid concentration. The rate of hydrolysis of N-3,3-dimethylbutyrylimidazolium ion is unaffected by HCl concentrations up to 6.0 *M*. A plot of the logarithm of the rate constant for hydrolysis of N-isovalerylimidazolium ion *vs.* HCl concentration is curved at low concentrations of HCl. In the hydrolysis of N-acetylimidazolium ion, chloride and bromide ions act primarily to bring about an increase in ΔH^*, but perchlorate ion affects primarily ΔS^* at lower concentrations and ΔH^* at concentrations above 5 *M*. The acid effect on the rate of hydrolysis of both N-acetylimidazolium and N-3,3-dimethylbutyrylimidazolium ions is produced by a large linear compensation between ΔH^* and ΔS^*, both becoming more positive as the acid concentration is increased. The slopes of these plots are 385°K for N-acetylimidazolium ion and 303°K for N-3,3-dimethylbutyrylimidazolium ion. Thus, the effect of increasing HCl concentration on the hydrolysis of N-acylimidazoles is dependent on the structure of the acyl group and the temperature at which the rate measurements are made. In solutions of HCl and LiCl, such that the concentration of Cl^- and the activity of water are nearly constant, the rate constants for hydrolysis of both N-acetylimidazolium and N-3,3-dimethylbutyrylimidazolium ions increase at 30° as the concentration of acid increases. The hydronium ion, therefore, is exerting a rate-accelerating effect on the hydrolysis of these compounds, in opposition to the rate-retarding effect of Cl^-. The possibility that the alkyl groups of the N-acylimidazolium ions and hydronium ion are cooperating to structure water in a manner favorable for the reaction is considered.

The effects of a large number of different salts and acids on the rate of hydrolysis of N-acetylimidazolium ion were studied by Marburg and Jencks.[2] Increasing concentrations of both salts and acids, with the exception of F^- and SO_4^{2-}, produce large rate decreases.[2] The *w* plots of Bunnett[3] are curved with high initial slope which depends on the acid, thus showing no linear dependence on the activity of water in the solution. The salt effects are characterized by a specific anion effect with relatively minor specific influences due to the cation.

It is known that the hydrolysis of N-acetylimidazolium ion involves more than one water molecule in the transition state;[4-6] therefore, it is of particular interest

---

(1) This study represents part of the work to be submitted by J. A. Fee in partial fulfillment of the requirements for the Ph.D. degree, University of Southern California.

(2) S. Marburg and W. P. Jencks, *J. Am. Chem. Soc.*, **84**, 232 (1962).

(3) J. F. Bunnett, *ibid.*, **83**, 4956, 4958, 4973, 4978 (1961).

(4) J. A. Fee and T. H. Fife, *J. Org. Chem.*, **31**, 2343 (1966).

(5) R. Wolfenden and W. P. Jencks, *J. Am. Chem. Soc.*, **83**, 4390 (1961).

(6) W. P. Jencks and J. Carriuolo, *ibid.*, **83**, 1743 (1961).

that in the series of monoanions[2] the order of effectiveness in decreasing the rate of hydrolysis parallels the "water-structure" breaking properties of the anions.[7] It is likely that alkyl groups will cause water around a molecule to be more highly ordered.[8] Such water-structuring effects have been postulated to be important in determining protein behavior[8] and could explain in part the great efficiency of enzymatic catalysis. Certain nonenzymatic reactions have been found to proceed at faster rates in frozen systems than in water.[9] The demonstration of a role for structured solvent in a hydrolytic reaction in a nonfrozen system would, therefore, be of considerable interest, and it appeared that the hydrolysis of N-acylimidazolium ions having alkyl group branching in the acyl group might afford such an example. The present study is concerned with the effects of salt and acid on the activation parameters for the hydrolysis of a series of fully protonated N-acylimidazoles (eq 1) and with the effects of acid at constant ionic molarity and activity of water.

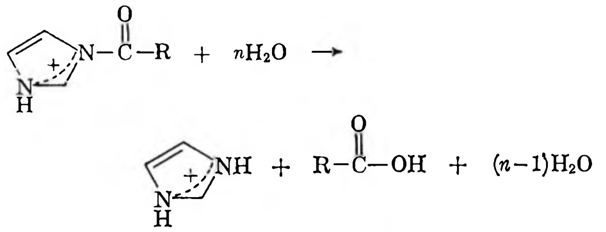

(1)

Experimental Section

Materials. The salts and acids were reagent grade and were used without further purification. Deionized water was used to prepare the solutions. The salt solutions were prepared by weighing out the correct amount of salt on a Mettler Model K-7 top-loading balance for the most concentrated solutions, and dilutions were made for the lower concentrations. All salt solutions were made up with 0.1 M HCl. The acid solutions were standardized by titration with base. The various N-acylimidazoles were the same as previously described.[4,10]

Kinetic Measurements. The rates in the acid and salt solutions were measured spectrophotometrically by following the decrease in absorption at 245 mμ with a Beckman DU spectrophotometer equipped with a Gilford Model 2000 recording attachment. The material was added, with vigorous stirring, by means of a microspatula. The rates were generally followed to 75% completion, and the infinity points were taken at roughly 10 half-lives. Pseudo-first-order rate constants were calculated using a computer program as previously described.[4]

Constant temperature was maintained during the kinetic runs by circulating water from a Precision Scientific Co. Temptrol Model 154 circulating bath around the cell compartment. The temperature of the cell compartment was measured with a temperature probe supplied with the Gilford instrument. The difference between the bath temperature and the temperature of the cell compartment was reduced by surrounding the exterior of the cell compartment with sheets of highly insulating Polycel 1202 foam obtained from Polytron Co., Richmond, Calif. All temperatures are reported to ±0.1° and were obtained from the probe reading.

The activation energies were calculated by means of a computer program designed to carry out least-squares evaluation of ln k_{obsd} *vs.* $1/T$°K. The output of interest consisted of the regression coefficient, the intercept value, and the correlation coefficient. The latter varied from 0.993 to 0.999 with the average value being about 0.998. The errors reported in ΔH^* and ΔS^* were calculated from the standard error of the regression coefficient of the plot of ln k_{obsd} *vs.* $1/T$°K.

The solvolysis product of N-3,3-dimethylbutyrylimidazole in 6.0 M HCl was shown to be imidazole by the method of Macpherson.[11] The analyses were made after the acid solution had remained in the dark for 24 hr at room temperature.

Results

Tables I–IV list the observed rate constants for the hydrolysis of the N-acylimidazoles at various salt and acid concentrations and at different temperatures. The rates were measured in duplicate or triplicate, and the average deviations for the rate constants in Tables III and IV are listed. Where deviations are not listed they are about 2%.

Table V gives the values of the slopes of plots of log k_{obsd} *vs.* molar concentration of electrolyte for the various N-acylimidazoles. It is seen that for NaCl all the values are the same within error. In the acid solutions, however, the differences are marked. The rates of hydrolysis of the compounds with branching at the β position of the acyl group show less sensitivity

---

[7] H. S. Frank and W. Wen, *Discussions Faraday Soc.*, **24**, 133 (1957); R. W. Gurney, "Ionic Processes in Solution," McGraw-Hill Book Co., Inc., New York, N. Y., 1953.

[8] H. S. Frank and M. W. Evans, *J. Chem. Phys.*, **13**, 507 (1945); I. M. Klotz, *Science*, **128**, 815 (1958); W. Kauzmann, *Advan. Protein Chem.*, **14**, 1 (1959); G. Nemethy and H. A. Scheraga, *J. Chem. Phys.*, **36**, 3382, 3401 (1962); *J. Phys. Chem.*, **66**, 1773 (1962).

[9] W. Prusoff, *Biochim. Biophys. Acta*, **68**, 302 (1963); N. H. Grant, D. E. Clark, and H. E. Alburn, *J. Am. Chem. Soc.*, **83**, 4476 (1961); A. R. Butler and T. C. Bruice, *ibid.*, **86**, 313 (1964); T. C. Bruice and A. R. Butler, *ibid.*, **86**, 4104 (1964).

[10] T. H. Fife, *ibid.*, **87**, 4597 (1965).

[11] H. T. Macpherson, *Biochem. J.*, **36**, 59 (1942).

Table I: Rate Constants (k_{obsd}, min^{-1}) for the Hydrolysis of the N-Acylimidazolium Ions at Various Concentrations of NaCl at 30°

	NaCl concentration, moles/l.[a]					
N-Acyl group	0.1[b]	1.0	2.0	3.0	4.0	5.0
Trimethylacetyl	31.6	26.1	15.9	13.2	9.42	6.19
Isobutyryl	7.57	5.47	4.06	2.76	1.91	1.18
Propionyl	4.54	3.08	2.55	1.49	1.08	0.683
Butyryl	2.74	2.29	1.43	1.10	0.700	0.493
3,3-Dimethylbutyryl	0.123	0.0843	0.0633	0.0406	0.0293	0.0200
Triethylacetyl	0.0101	0.00960	0.00598	0.00446	0.00262	0.00208

[a] All solutions made up with 0.1 M HCl. [b] 0.1 M HCl.

Table II: Rate Constants (k_{obsd}, min^{-1}) for the Hydrolysis of the N-Acylimidazolium Ions at Various Concentrations of HCl at 30°

	HCl concentration, moles/l.					
N-Acyl group	0.1	1.20	2.38	3.60	4.77	5.97
Trimethylacetyl	31.6	25.4	18.4	12.4	8.50	5.86
Isobutyryl	7.57	5.77	4.28	3.15	2.28	1.70
Propionyl	4.54	3.11	2.53	1.94	1.36	1.25
Butyryl	2.74	2.23	1.61	1.24	1.06	0.884
Isovaleryl	0.814		0.496	0.412	0.362	0.374
3,3-Dimethylbutyryl	0.123	0.127	0.129	0.123	0.125	0.125
Triethylacetyl	0.0101	0.00768	0.00663	0.00495	0.00282	0.00174

to changes in acid concentration than do the α-branched compounds. The rate of hydrolysis of N-3,3-dimethylbutyrylimidazolium ion is unaffected by HCl concentrations up to 6.0 M. Increasing the concentration of $HClO_4$, however, results in a decrease in rate of hydrolysis for this compound at 30°. The plot of log k_{obsd} *vs.* HCl concentration for N-isovalerylimidazolium ion is curved at low concentrations of HCl. In Figure 1 are plotted the logarithms of the observed rate constants *vs.* the concentration of electrolyte. The plots shown for N-isobutyrylimidazole are representative of the whole series in NaCl solution and of the α-branched series in acid solution.

Table VI lists the activation parameters for the hydrolysis of N-acetylimidazolium ion at various concentrations of different salts and hydrochloric acid. The results are plotted in Figures 2 and 3. The salts decrease the rate of hydrolysis in the order $NaClO_4$ > NaBr > NaCl. Figure 2 demonstrates how these relative effects are brought about. The chloride and bromide ions act primarily to increase ΔH^*, but the perchlorate ion affects primarily ΔS^* at the lower concentrations and ΔH^* at very high concentrations with the break occurring at approximately 5 M perchlorate ion. It is seen that the acid effect on the rate of hydrolysis is produced by a compensation between

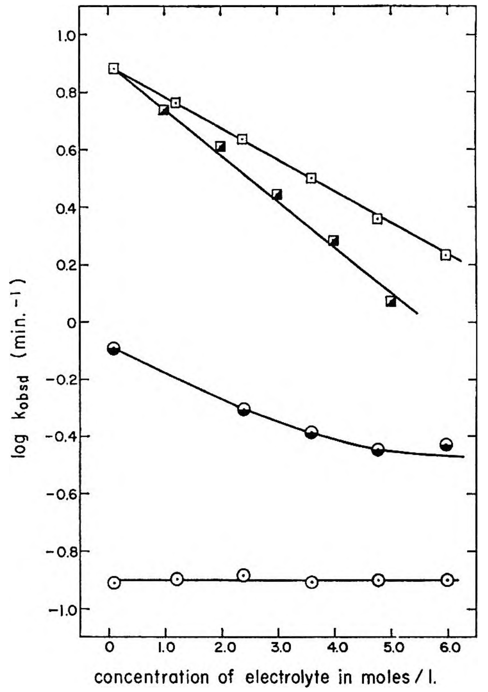

Figure 1. Plot of log k_{obsd} for hydrolysis of N-isobutyrylimidazolium ion in NaCl solutions (◪) and in HCl (⊡) and N-isovalerylimidazolium ion (◒) and N-3,3-dimethylbutyrylimidazolium ion (⊙) in HCl at 30° *vs.* the concentration of acid or salt in moles/liter.

Table III: Rate Constants (k_{obsd}, min^{-1}) for the Hydrolysis of N-Acetylimidazolium Ion at Various Temperatures and Concentrations of Electrolyte

0.1 *M* HCl		2.19	4.08	6.57	11.6
Temp, °C		20.6	30.0	39.3	49.0
2.37 *M* HCl	0.572	1.21	2.43	4.69	8.05
Temp, °C	10.8	20.8	30.0	39.2	49.4
3.57 *M* HCl	0.432	0.941	1.91	3.69	6.79
Temp, °C	10.8	20.8	30.0	39.2	49.4
4.77 *M* HCl	0.337	0.747	1.59	2.98	5.85
Temp, °C	10.8	20.8	30.0	39.2	48.8
5.74 *M* HCl	0.273	0.648	1.38	2.78	5.05
Temp, °C	10.8	20.8	30.0	39.2	48.8
% deviation from mean	0.5	0.5	1.1	1.2	2.1
1.0 *M* NaCl		1.52	2.85	4.87	8.19
Temp, °C		20.8	30.0	39.2	48.2
3.0 *M* NaCl		0.694	1.37	2.43	4.28
Temp, °C		20.8	30.0	39.2	48.2
5.0 *M* NaCl		0.299	0.557	1.06	1.89
Temp, °C		20.8	30.0	39.2	48.2
% deviation from mean		1.3	1.4	1.7	1.7
1.25 *M* NaBr		1.17	2.15	3.89	6.46
Temp, °C		20.8	30.0	39.0	48.6
2.50 *M* NaBr		0.617	1.18	2.07	3.64
Temp, °C		20.8	30.0	39.0	48.6
3.75 *M* NaBr		0.313	0.600	1.11	1.95
Temp, °C		20.8	30.0	39.0	48.6
5.0 *M* NaBr		0.151	0.287	0.536	0.988
Temp, °C		20.8	30.0	39.0	48.5
% deviation from mean		1.7	1.1	1.1	1.3
0.96 *M* $NaClO_4$		0.878	1.80	3.13	5.31
Temp, °C		20.2	30.0	40.0	49.4
1.92 *M* $NaClO_4$		0.482	0.956	1.66	2.85
Temp, °C		20.2	30.0	40.0	49.4
2.88 *M* $NaClO_4$		0.252	0.495	0.909	1.55
Temp, °C		20.2	30.0	40.0	49.4
3.74 *M* $NaClO_4$		0.159	0.327	0.552	
Temp, °C		20.0	30.0	40.0	
4.96 *M* $NaClO_4$		0.0635	0.113	0.219	0.368
Temp, °C		20.0	30.0	40.0	49.6
6.88 *M* $NaClO_4$		0.0127	0.0260	0.0489	0.0897
Temp, °C		20.1	30.0	40.0	49.6
8.0 *M* $NaClO_4$		0.00446	0.00967	0.0192	0.0358
Temp, °C		20.0	30.0	40.0	49.6
% deviation from mean		2.4	1.7	0.9	0.7

ΔH^* and ΔS^*, both becoming more positive as the acid concentration increases over a range of 3.1 kcal in ΔH^* and 8.2 eu in ΔS^*. The slope of the plot of ΔH^* *vs.* ΔS^* is 385°K.

Table VII lists the activation parameters for the hydrolysis of N-3,3-dimethylbutyrylimidazolium ion at different concentrations of HCl and NaCl. The results of the acid studies are plotted in Figure 3. In HCl solutions a large compensation occurs between ΔH^* and ΔS^*, such as to leave ΔF^* unchanged, over a range of 4.2 kcal in ΔH^* and 13.9 eu in ΔS^*. The major changes in these parameters occur at acid concentra-

The Melting Point and Decomposition Pressure of Neptunium Mononitride

by W. M. Olson and R. N. R. Mulford

University of California, Los Alamos Scientific Laboratory, Los Alamos, New Mexico *(Received March 11, 1966)*

Decomposition pressures for the reaction NpN(s) = Np(l) + $0.5N_2(g)$ in the temperature range 2210–2830° are presented. NpN melts congruently at 2830 ± 30° under a nitrogen pressure of about 10 atm. An equation, $\log p$ (atm) $= 8.193 - [(29.54 \times 10^3)/T] + 7.87 \times 10^{-18}T^5$, was found to describe the decomposition pressure–temperature relation for NpN. A lattice parameter of $a = 4.8987 \pm 0.0005$ A was measured for the cubic nitride.

Introduction

At ambient nitrogen pressures below the pressure where NpN melts congruently the following reaction occurs.

$$\text{NpN(s)} = \text{Np(l, saturated with N)} + 0.5\text{N}_2\text{(g)}$$

At sufficiently high temperatures the solid will liquefy as soon as the decomposition pressure exceeds the ambient nitrogen pressure. Therefore the decomposition pressure–temperature relation can be determined by observing the apparent melting point as a function of nitrogen pressure. If the ambient nitrogen pressure is high enough to suppress decomposition, the congruent melting point may be observed.

Experimental Section

Apparatus. The apparatus and procedure have been fully described previously.[1] Briefly, about 5 mg of NpN powder was placed in a 30° vee formed in a tungsten strip which was heated resistively. The sample was observed and its temperature determined by means of a calibrated Pyro micro optical pyrometer sighted through a quartz window and prism located at the top of the stainless steel vacuum-pressure can.

Temperatures were corrected for the absorption of the prism and window, and also for the emissivity of the tungsten vee. It is estimated that the accuracy of the temperatures reported is ±30°.

Preparation of NpN. Most of the NpN was made in the following manner. Neptunium metal, which contained 230 ppm of carbon as the principal impurity, was cleaned in an inert atmosphere by removing the surface with a file. The cleaned metal was reduced to filings which were placed in a tungsten vee and heated resistively under vacuum for approximately 5 min at about 500° to remove absorbed gases. The filings were then cooled to room temperature, and 1 atm of spectroscopic grade nitrogen, to which had been added about 0.5% hydrogen (Linde Ultra Pure) to serve as a catalyst, was introduced into the system.

The reaction between the neptunium filings and the gas was started by heating the filings to 600°. After the reaction appeared to be complete, the temperature was increased to 1500° and the gas was pumped off. This procedure decomposed any neptunium hydride which had not been converted to nitride during the heating at 600° and volatilized any unreacted neptunium metal. An X-ray diffraction pattern showed only NpN to be present. The resulting NpN powder was stored under vacuum, and small portions were used for the melting point determinations.

Procedure. In determining the melting point, or decomposition temperature, about 5 mg of NpN powder was placed in a tungsten vee, the apparatus was evacuated, and the sample heated to about 1000°. Spectroscopically pure nitrogen was then introduced into the system until the desired pressure was attained. Then the temperature was raised until the sample started to melt. Temperature and pressure readings were taken just before and just after melting had occurred, and the true values were assumed to be the averages. The before and after temperature readings were usually about 10° apart.

Results

The decomposition pressures obtained for NpN are plotted in Figure 1 as $\log p$ (atm) *vs.* $10{,}000/T$

---

[1] W. M. Olson and R. N. R. Mulford, *J. Phys. Chem.*, **67**, 952 (1963).

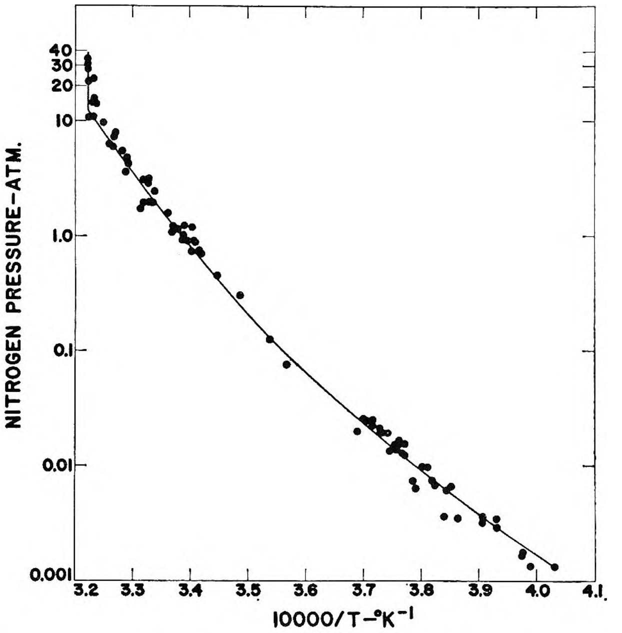

Figure 1. Decomposition pressure of NpN.

(°K). The data points are considerably scattered, but it is apparent that they fall along a gentle curve which intersects the vertical line representing congruent melting at a pressure of about 10 atm. The congruent melting point, as established by this vertical line on the plot, is 2830 ± 30°.

In previous work, oxygen impurity had been found to have considerable influence on the decomposition of ThN.[2] In the present work with NpN no clear influence of oxygen was detected. Some of the points in Figure 1 were obtained with nitride made from sawdust which definitely contained oxide as a result of the sparking and burning that accompanied the sawing process. The other points were obtained from nitride prepared from bulk metal by the method previously described. There was no apparent difference between the pressure–temperature results from the two nitride sources. No oxide was detected in X-ray patterns from the nitride made from the bulk metal.

Neptunium, like plutonium, forms only a mononitride. The lattice parameter of this cubic, sodium chloride type nitride was found to be $a = 4.8987 \pm 0.0005$ A which agrees well with the value reported by Zachariasen,[3] $a = 4.897 \pm 0.002$ A.

Discussion

Since the liquid neptunium in equilibrium with the nitride is saturated with nitrogen, and therefore its activity is some unknown value less than unity, the present data cannot be used to provide an accurate value for the standard heat of formation of NpN. The solubility of nitrogen in liquid neptunium presumably varies with temperature, the solubility increasing, and, consequently, the neptunium activity decreasing as the temperature increases. This temperature dependence of the solubility is reflected in the curvature shown by the data in Figure 1. A limit for $\Delta H°_{298}$ may be obtained from the lowest experimental point, where the activity of the neptunium was nearest to unity, by combining the experimental value with entropy and heat capacity estimates. If, for the formation of 1 mole of NpN from pure neptunium and nitrogen gas, we assume $\Delta S°_{298} = -20$ cal/deg mole and $\Delta C_p° = 1.5$ cal/deg mole as an average between 298 and 2500°K, the heat of formation at 298°K is found to be more negative than −61 kcal/mole. The entropy of formation is taken to be the same as that of UN, as calculated from the measured absolute entropy of UN.[4]

In previous similar work with UN,[1] PuN,[5] and ThN,[2] it was found that an equation of the form $\log p = A + (B/T) + CT^5$ fitted the experimental points well. This equation, which was derived empirically has the property of approaching a straight line as the temperature becomes lower. This behavior is plausible for the nitrogen pressure over a univariant mixture of liquid metal and nitride; that is, the deviation from linearity is caused by the lowering of the activity of the metal in the liquid phase. As the temperature decreases, less and less nitrogen remains in solution and the metal activity approaches unity. For the decomposition pressure of NpN, the data in Figure 1 are fitted by (T is in °K)

$$\log p \text{ (atm)} = 8.193 - [(29.54 \times 10^3)/T] + 7.87 \times 10^{-18}T^5$$

It is of some interest to compare the stability of NpN with the stabilities of the other actinide nitrides.[1,2,5] For accurate comparisons, the standard free energies of formation of the nitrides are needed, but these cannot be obtained because the activities of the metals in their liquid phases are unknown. One is thus forced to compare decomposition pressures. Small differences among the decomposition pressures may reflect only the variation of nitrogen solubility in the liquid metals, but it is likely that a large difference

---

(2) W. M. Olson and R. N. R. Mulford, *J. Phys. Chem.*, **69**, 1223 (1965).

(3) W. H. Zachariasen, *Acta Cryst.*, **2**, 388 (1949).

(4) E. F. Westrum, Jr., "International Symposium on Compounds of Interest in Nuclear Reactor Technology," University of Colorado, Boulder, Colo., Aug 3-5, 1964.

(5) W. M. Olson and R. N. R. Mulford, *J. Phys. Chem.*, **68**, 1048 (1964).

between the decomposition pressures of two nitrides is a true indication of different stabilities or bond strengths. Comparison of the known decomposition pressures of the actinide shows an increase in decomposition pressure at constant temperature as atomic number increases. At 2500°K, the lowest temperature for which measured pressures are available, comparison of the logarithms of the decomposition pressures calculated from the equations shows that, while UN, NpN, and PuN are not too dissimilar in stability, ThN is possibly significantly more stable than the other three. However, small differences in entropy or heat capacity or solubility of nitrogen in the liquid metal phase could easily account for the differences among observed pressures. Similarly, differences in stoichiometry of the nitride phases could affect the observed pressures. Benz and Bowman[6] have found a departure from stoichiometry at high temperatures for UN.

Acknowledgment. We are grateful to F. H. Ellinger for making the X-ray measurements on NpN. This work was performed under the auspices of the U. S. Atomic Energy Commission.

---

[6] R. Benz and M. G. Bowman, *J. Am. Chem. Soc.*, **88**, 264 (1966)

The Americium–Hydrogen System[1]

by W. M. Olson and R. N. R. Mulford

University of California, Los Alamos Scientific Laboratory, Los Alamos, New Mexico *(Received April 18, 1966)*

Pressure–temperature–composition measurements and X-ray data are presented for the americium–hydrogen system. Two hydride phases were found: one, face-centered cubic of composition AmH_{2+x}; the other, hexagonal of composition AmH_3. Both phases are isostructural with the corresponding plutonium and neptunium hydrides. The plateau pressures for the Am–AmH_2 univariant composition range are represented by $\log p(\text{atm}) = 7.190 - 8812/T(°\text{K})$. The derived heat of formation of AmH_2 is $\Delta H_f = -40.3$ kcal/mole.

Introduction

The uranium–hydrogen,[2] neptunium–hydrogen,[3] and plutonium–hydrogen[4,5] systems have been studied previously. Now, with sufficient americium metal available, it seemed appropriate to extend our knowledge of the hydrides to this seventh member of the actinide series. Such a study should be especially interesting because no very regular behavior, as is seen for the rare earth hydrides, has yet been found for the actinide hydrides.

Experimental Section

The apparatus and method have been described in detail previously.[3] Briefly, a sample of americium metal was contained in an yttria crucible which was placed in a silica tube attached to a standard Sievert's apparatus. The sample was out-gassed at 800°. Then, measured amounts of hydrogen were added to the sample, the pressure in the system being determined by means of a combination mercury manometer

---

[1] Work done under the auspices of the U. S. Atomic Energy Commission.

[2] F. H. Spedding, *et al.*, *Nucleonics*, **4**, 4 (1949).

[3] R. N. R. Mulford and T. A. Wiewandt, *J. Phys. Chem.*, **69**, 1641 (1965).

[4] R. N. R. Mulford and G. E. Sturdy, *J. Am. Chem. Soc.*, **77**, 3449 (1955).

[5] R. N. R. Mulford, *ibid.*, **78**, 3897 (1956).

(pressures above 2 torr) or a McLeod gauge (pressures below 2 torr). The accuracy of measurement of the hydrogen pressure was such that the H/Am atom ratio is believed to be known to ±0.02. The silica sample tube was enclosed within a silver block to smooth temperature variations in the sample, and an automatically controlled tube furnace able to maintain the sample temperature within ±0.1° was used. The sample temperature was determined with a calibrated Pt—Pt-10% Rh thermocouple having its measuring junction in a reentrant well in the sample bulb.

The Am^{241} isotope was used and contained 0.15% by weight of Ca and 0.20% La as the principal metallic impurities. A trace of AmO_2 was also detected in the X-ray diffraction pattern of the metal. The computed H/Am ratios were not corrected to take account of the impurities in the americium. Matheson Co. ultrapure grade hydrogen, claimed by the manufacturer to contain less than 10 ppm total impurities, was used directly from the cylinder.

The procedure consisted of adding small increments of hydrogen to the system, measuring the pressure and temperature after each increment until the highest H/Am ratio had been obtained, then removing the hydrogen in successive decrements and again measuring the pressure and temperature after each decrement. Since it was not possible to attain a predetermined temperature exactly, the isotherm points were obtained by short interpolations. The pressure–temperature curve for each amount of hydrogen in the system was obtained for both ascending and descending temperature. Hysteresis was observed, as described below, only for compositions close to AmH_3.

Results

The *P–T–C* data are plotted in Figures 1 and 2. The isotherm plots in Figure 1 show some solubility of hydrogen in americium at the higher temperatures, about 16 atom % being soluble at 800°. Figure 1 also reveals that the dihydride phase has a lower composition limit that is almost temperature independent over the range studied. The inference, if any, is that the phase becomes slightly hydrogen deficient as the temperature increases.

When the ratio of hydrogen to metal exceeded 2, hydrogen dissolved in the AmH_2 phase until a composition of about $AmH_{2.7}$ was reached. When more hydrogen was added, a hexagonal AmH_3 phase was found. However, this conversion is sluggish, and single-phase AmH_3 was not obtained. Up to $AmH_{2.7}$, good reproducibility in the pressure–temperature data was obtained, but some hysteresis was observed at higher hydrogen contents, as can be seen in Figure 2.

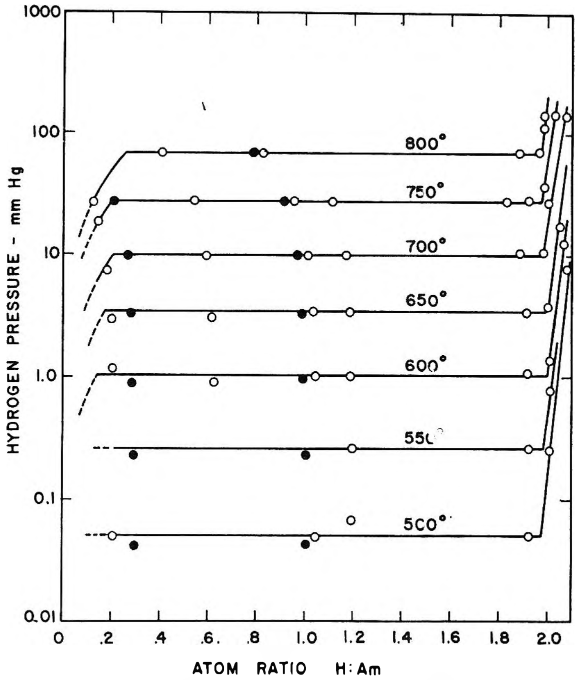

Figure 1. Pressure isotherms *vs.* sample composition for the range Am to AmH_2. Open circles are for addition of hydrogen, solid circles are for removal of hydrogen.

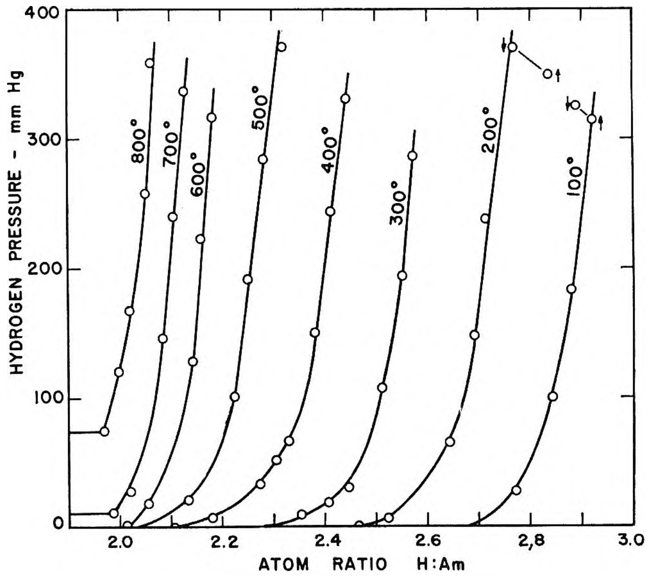

Figure 2. Pressure isotherms for the composition AmH_2 to AmH_3. Arrows show direction of temperature approach to the point.

Because of the extreme sluggishness of the reaction forming AmH_3, no well-defined hysteresis loops were observed.

In Table I, X-ray data for several compositions are presented. It was very difficult to obtain samples which could provide X-ray patterns sufficiently sharp to permit determination of the AmH_3 lattice parameters. A satisfactory pattern was finally obtained from a sample that had been annealed under 530 torr of hydrogen pressure for 40 hr at 100°.

Table I: X-Ray Data

Sample	H/Am ratio	Phases present		Lattice parameter, A
1	0.46	Cubic only		$a_0 = 5.347 \pm 0.001$
2	1.76	Cubic only		$a_0 = 5.349 \pm 0.001$
3	2.67	Cubic only		$a_0 = 5.338 \pm 0.004$
4	2.92	Cubic + hex	Cubic:	$a_0 = 5.340 \pm 0.005$
			Hex:	Poor pattern
5	2.96	Cubic + hex	Hex:	$a_0 = 3.77 \pm 0.01$
				$c_0 = 6.75 \pm 0.01$

The AmH_{2+x} ($0 \leq x \leq 0.7$) phase is face-centered cubic, presumably of the fluorite type, and is isostructural with PuH_{2+x}[6] and NpH_{2+x}[3] as well as with most of the rare earth dihydrides. The lattice parameters observed for the cubic phase are given in Table I; the calculated density of $AmH_{2.0}$ is 10.6 g/cm^3.

The AmH_3 phase is hexagonal and is isostructural with PuH_3,[6] NpH_3,[3] and the trihydrides of the heavy rare earths.[7] The calculated density of $AmH_{3.0}$ is 9.76 g/cm^3. As the hydrogen positions have not been determined for any of these compounds except CeH_2, the assumption that they are isostructural rests on their having similar metallic lattices.

It is seen from Table I that the lattice parameter shrinks as the hydrogen content of the cubic AmH_{2+x} phase increases. Similar behavior is exhibited by PuH_{2+x} and the rare earth hydrides of comparable structure. However, the lattice parameter of NpH_{2+x} expands with increasing hydrogen content.

When the logarithms of the plateau pressures of Figure 1 are plotted *vs.* the reciprocal of the temperature, a straight line is obtained whose slope gives the heat per mole of hydrogen gas for the formation of AmH_2 from americium and hydrogen. The americium and AmH_2 phases for which this heat is appropriate have compositions as defined by the ends of the plateau, but in view of the small solubility of hydrogen in americium and the small departure from stoichiometry of the AmH_2 on the hydrogen-poor side, the heat may be assumed to be close to that for the reaction involving the pure phases. The equation for the line is

$$\log p(\text{atm}) = 7.190 - 8812/T(°\text{K})$$

The slope, for the process

$$Am(s) + H_2(g) = AmH_2(s)$$

gives an enthalpy change

$$\Delta H = -40.3 \text{ kcal/mole } (773\text{–}1073°\text{K})$$

which should be nearly correct for the standard heat of formation of AmH_2 in the temperature range given.

A brief comparison of the actinide hydrides is of interest. Pertinent data are listed in Table II. Different crystal structures and compositions are found for the lower hydrides in the respective systems. Thus ThH_2 is tetragonal, PaH_3 and β-UH_3 are cubic, and NpH_2, PuH_2, and AmH_2, although also of cubic symmetry, are structurally different from PaH_3 and β-UH_3. If, however, the metal-hydrogen bond lengths are computed for each hydride, assuming that NpH_2, PuH_2, and AmH_2 have the fluorite structure from analogy to CeH_2, it is seen that for all except ThH_2 the distances are close to 2.32 A.

Table II

Compound	Structure	Lattice parameter, A	M–H distance, A	$-\Delta H_f$, kcal/mole of H_2
ThH_2	Tetragonal	$a = 4.10$, $c = 5.03$	2.41(?)	34
PaH_3	Cubic	6.648	2.33	..
β-UH_3	Cubic	6.631	2.32	20
NpH_2	Fcc	5.343	2.314	28
PuH_2	Fcc	5.359	2.320	37
AmH_2	Fcc	5.348	2.316	40

The heats of formation per mole of hydrogen gas show a fairly large increase with atomic number; ThH_2 is again an exception. Thus the actinide hydrides above thorium become more stable as atomic number increases, at least as far as americium. In the comparable fluorite-structure dihydrides formed by the rare earth series, no trend is evident in the heats of formation; all the known heats are close to −50 kcal/mole of H_2. In the rare earth hydrides the lanthanide contraction is clearly evident; that is, the metal–hydrogen distance decreases uniformly with atomic number.[7] The actinide hydrides, however, do not exhibit any effect that can be attributed to actinide contraction, although such contraction is clearly evidenced in other series of more ionic actinide compounds, the dioxides

---

(6) F. H. Ellinger in "The Metal Plutonium," A. S. Coffinberry and W. N. Miner, Ed., University of Chicago Press, Chicago, Ill., 1961, p 291.

(7) A. Pebler and W. E. Wallace, *J. Phys. Chem.*, **66**, 148 (1962).

Phase Separation of Poly-L-proline in Salt Solutions

by A. Ciferri and T. A. Orofino

Chemstrand Research Center, Inc., Durham, North Carolina *(Received May 6, 1966)*

Solutions of form II poly-L-proline in water and aqueous salt solutions exhibit a reversible phase change upon heating. Precipitation, viscosity, and light-scattering analyses have been carried out to elucidate the mechanism of the phase separation, to establish similarities with the heat precipitation of tropocollagen, and to determine the role of salts in the transformation. The precipitation and light-scattering results indicate that the phase change observed involves crystallization of the polypeptide units from solution. Great similarities to the behavior of collagen are exhibited. The effect of salts in increasing or decreasing the field of stability of the dissolved form is similar to that expected from the behavior of these salts in altering the activity coefficients of related substances which crystallize on cooling. The intrinsic viscosity, however, is decreased monotonically with increase in concentration of both salting-in and salting-out agents and thus is apparently responsive to other compensating effects. Some general thermodynamic considerations of the heat precipitation of polymers to form an amorphous or crystalline phase are presented.

Introduction

Poly-L-proline is known to exist in two forms, designated I and II, which apparently differ in the structural configuration[1-3] about the imide linkage in the polymer repeating unit

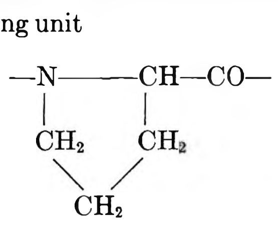

Isomerization of one form into the other can be accomplished in solutions of certain reagents. Crystallographic analysis of form II, believed to represent the *trans* isomer, indicates that the polypeptide chain is a helix with a 3.1-A monomer repeat distance. This conformational arrangement is also the basis for the structure of collagen, of which proline is the second most abundant constituent.[2] In contrast with form I (insoluble), II dissolves readily in water. Although the crystallographic helix is not stabilized by hydrogen bonds, a particularly rigid conformation would be expected in solution, owing to the decreased rotational freedom imposed by the ringed structure of the repeat unit and the resonance-stabilized *trans*-imide bond. Opportunity for internal rotation thus resides primarily in the C_α–carbonyl linkage.

Blout and Fasman,[1a] and Kurtz, Berger, and Katchalsky[1b] have reported that upon increase of temperature to about 65°, poly-L-proline precipitates from aqueous solution, the process being completely reversible on cooling. In the present communication we report the results of an extensive investigation of the solubility characteristics of this material in various aqueous salt solutions. Our purpose has been twofold: (1) to examine the general characteristics of the phase separation process, to investigate its origin, and to compare similarities noted with the heat precipitation of collagen;[4] (2) to study the effect of salts on the temperature of phase separation. For this purpose precipitation, intrinsic viscosity, and light-scattering studies on a single sample of form II poly-L-proline have been carried out.

---

(1) (a) E. R. Blout and G. D. Fasman, *Recent Advan. Gelatin Glue Res., Proc. Conf. Univ. Cambridge, 1957*, 122 (1958); (b) J. Kurtz, A. Berger, and E. Katchalsky, *ibid.*, 131 (1958).

(2) A. Veis, "The Macromolecular Chemistry of Gelatin," Academic Press Inc., New York, N. Y., 1964.

(3) W. F. Harrington and P. H. von Hippel, *Advan. Protein Chem.*, 16, 19 (1961).

(4) E. Bianchi, G. Conio, and A. Ciferri, *Biopolymers*, in press.

but some OH groups are retained very tenaciously.[3] Substitution of other groups for the OH groups is often sought to modify adsorptive and other properties of silicas.

Much of our present knowledge of their surface structure has come from infrared studies of high-area silicas.[4-18] Because typical silica gels scatter much radiation, special forms of high-area silica such as Aerosil (Cabosil) and microporous glass have been used in most studies to date. Neither of these materials represents typical silica gel. Microporous glass is, moreover, very impure (96% silica), containing boria, alumina, and other impurities. Only a few studies of more typical silica gels prepared by "wet" methods have been reported.[5,11,14] To minimize scattering losses, these silica gels have been studied as self-supporting pressed disks. The high pressures used in disk formation can apparently significantly alter the behavior of the silica, however.[5,16]

Considering the variety of materials studied, the major characteristics of their infrared spectra are remarkably similar. A sharp band at 3750 cm^{-1} is universally assigned to "isolated" (*i.e.*, not H-bonded) OH groups. A tail, or close-lying band, in the 3600-3750-cm^{-1} region appears to be caused by weakly H-bonded OH groups. Absorption centered in the 3400-3500-cm^{-1} region is attributed to strongly H-bonded OH groups and/or adsorbed H_2O. Because the bands in this region are generally associated with a band near 1630 cm^{-1} (presumably caused by H_2O deformation), assignment to H_2O is usually favored. Attribution of a band at 3500 cm^{-1} to geminal OH groups (*i.e.*, two groups attached to the same silicon atom) has been suggested, however.[2,11]

A band found at 4540 cm^{-1} on microporous glass has been assigned to the combination of isolated OH stretching with Si-O stretching vibrations,[13] while a similar band on silica gel has been assigned to the combination of OH stretching with Si-OH bending.[14] A band near 870 cm^{-1} has been assigned to deformation of surface OH groups.[9]

Bands at 1635, 1870, and 2000 cm^{-1} (shoulder) in the spectrum of dry silicas appear to arise from combinations and/or overtones of lattice vibrations,[9,10] as do weaker bands in the region from 2200 to 2950 cm^{-1} in the spectrum of microporous glass.[10,13,17]

Spectra in the H_2O deformation region indicate that little or no adsorbed H_2O remains after the silica has been dried above 250°[4,10] and that most H_2O can be eliminated at considerably lower temperatures. Evidence from reaction of silica gels with $AlCl_3$ and BCl_3 has, however, been interpreted to mean that molecular H_2O can be strongly held even after the silica has been dried under vacuum at 350° or higher.[19]

Prevailing opinion holds that most of the OH groups in silica gel are on the surface. Characteristically, however, a significant fraction of the OH content, even on silicas predried at 600°, is not removed by reaction with reagents such as diborane,[3,20] CH_3MgI, and CH_3Li,[4] suggesting that the groups are held internally rather than on the surface. Absence of reaction could, however, reflect steric factors, possibly arising from the presence of geminal OH groups.[2]

Little is presently known about the mobility, attachment, or arrangement of OH groups on the surface. It has even been suggested[5] that the OH groups left after the silica has been dried at very high temperatures may not actually exist on the hot surface but may reform only at lower temperatures as traces of H_2O are again chemisorbed.

Replacement of OH groups on microporous glass by NH_2 groups[15] and by fluoride[18] have been studied, but little infrared study of reactions of OH groups on pure silica has been reported to date. Some NH_3 is slowly chemisorbed on silica, but chemisorption never exceeds 1.5 molecules/100 A^2 of surface.[21] No infrared study of such adsorption has been reported, but physical adsorption of NH_3 has been investigated.[6-8]

---

(3) C. Naccache and B. Imelik, *Bull. Soc. Chim. France*, 553 (1961); C. Naccache, J. F. Rosetti, and B. Imelik, *ibid.*, 404 (1959).

(4) J. J. Fripiat and J. Uytterhoeven, *J. Phys. Chem.*, **66**, 800 (1962); J. J. Fripiat, M. C. Gastuche, and R. Brichard, *ibid.*, **66**, 805 (1962).

(5) R. S. McDonald, *ibid.*, **62**, 1168 (1958).

(6) A. N. Sidorov, *Dokl. Akad. Nauk SSSR*, **95**, 1235 (1954).

(7) N. W. Cant and L. H. Little, *Can. J. Chem.*, **42**, 803 (1964).

(8) M. Folman and D. J. C. Yates, *Proc. Roy. Soc.* (London), **A246**, 32 (1958); *J. Phys. Chem.*, **63**, 179 (1959).

(9) H. A. Benesi and A. C. Jones, *ibid.*, **63**, 179 (1959).

(10) L. H. Little and M. V. Mathieu, *Actes Intern. Congr. Catalyse, 2e, Paris*, **1**, 771 (1961).

(11) J. A. Hockey and B. A. Pethica, *Trans. Faraday Soc.*, **57**, 2247 (1961).

(12) G. J. Young, *J. Colloid Sci.*, **13**, 67 (1958).

(13) V. A. Nikitin, A. N. Sidorov, and A. V. Karyakin, *Zh. Fiz. Khim.*, **30**, 117 (1956).

(14) J. H. Anderson and K. A. Wickersheim, *Surface Sci.*, **2**, 252 (1964).

(15) M. Folman, *Trans. Faraday Soc.*, **57**, 2000 (1961).

(16) F. H. Hambleton, J. A. Hockey, and J. A. G. Taylor, *Nature*, **208**, 138 (1965).

(17) N. Sheppard and D. J. C. Yates, *Proc. Roy. Soc.* (London), **A238**, 69 (1956).

(18) T. H. Elmer, I. D. Chapman, and M. E. Nordberg, *J. Phys. Chem.*, **67**, 2219 (1963).

(19) H. P. Boehm, M. Schneider, and F. Arendt, *Z. Anorg. Allgem. Chem.*, **320**, 43 (1963).

(20) I. Shapiro and H. G. Weiss, *J. Phys. Chem.*, **57**, 219 (1953); H. G. Weiss, J. A. Knight, and I. Shapiro, *J. Am. Chem. Soc.*, **81**, 1823 (1959).

(21) V. W. Stober, *Kolloid-Z.*, **145**, 17 (1956).

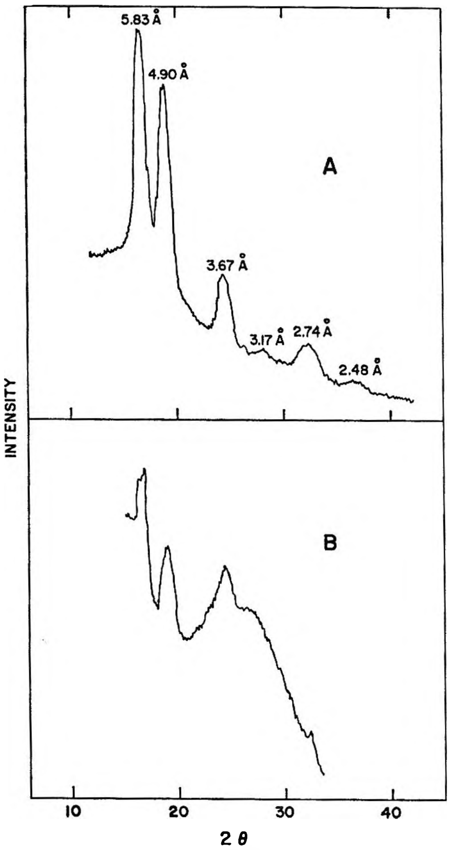

Figure 2. Photometric microdensitometer traces of relative intensity *vs.* scattering angle for poly-L-proline: (A) original dry sample, (B) precipitate from water solutions at 67° in the presence of supernatant solution.

appeared to consist of lamellae which exhibited only a very faint depolarization. Flat-plate X-ray diffraction patterns at 24° were obtained for the precipitate mixed with the supernatant (water) in a lead-free glass capillary. The X-ray tube was operated at 30 kv and 20 ma, the radiation being Ni-filtered Cu Kα (λ 1.54 A). An exposure time of about 2 hr was necessary. The films were scanned with a microdensitometer to obtain the intensity–scattering angle plot shown in Figure 2 and compared with the crystalline pattern obtained for a finely ground specimen of the original dry material. It is clear that the precipitate deposited from solution exhibits considerable crystalline order.

An infrared spectrum of the precipitate obtained from water solution, dried, and pressed into KBr disks was taken with a Perkin-Elmer 421 grating spectrometer. The curve is shown in Figure 1 and is compared with the spectrum for the original material. No adsorption bands at 900 and 1355 cm^{-1} have emerged as a result of the heat precipitation; accordingly, there is no indication that the phase change observed is attributable to the transition from form II to (insoluble) form I.

5. *Resolubilization Experiments.* Precipitates obtained with rates of heating of both 2°/hr and 1°/day generally would not redissolve on cooling at room temperature over a period of about 2 months. Precipitation could be arrested, however, by cooling to room temperature solutions where only incipient turbidity, or a very small amount of precipitation, had been effected by limiting the time during which the solution was maintained at a higher temperature. After long standing the turbid solution separated into a small quantity of precipitate and a clear supernatant which obviously contained most of the polymer. Neither further development of precipitate with time at room temperature nor further clarification was evident. If, starting from this "stable," partly precipitated solution, temperature was again increased, a precipitation value a few degrees lower than that observed starting from the clear solution (at a given rate of heating) was obtained. The only way in which the precipitate could be redissolved completely was by lowering the temperature to between 5 and −15°. Generally, the lower t_p the lower the temperature necessary for the resolubilization. The exact temperatures required for resolubilization as a function of salt concentration were not determined.

6. *Viscosity Measurements.* Intrinsic viscosity $[\eta]$ as a function of temperature ($\pm 0.1°$) in various aqueous salt solutions selected for this investigation was measured in a Cannon-Ubbelohde dilution viscometer chosen to provide solvent efflux times not less than 70 sec. Kinetic energy corrections were small and were ignored in treatment of the primary data. The viscosity of a given solution was measured first at 25°, then successively at higher temperatures. Upon cooling the solution to 25°, the original value could be reproduced. Prolonged exposure at the higher temperature was, however, avoided, the viscometer with the solution being stored in a cold room (*ca.* 1°) during the longer intervals between measurements. The customary extrapolation of reduced specific viscosity η_{sp}/c to zero polymer concentration, c, is illustrated in Figure 3 for various solvent media. The systems appear to exhibit normal behavior and show no anomalous trend with decreasing polymer concentration.

7. *Light-Scattering Studies.* Light-scattering intensities as a function of temperature and polymer concentration were measured in 1 *M* KSCN and in 0.44 and 0.5 *M* KCl solution. The apparatus consisted of a standard Brice-Phoenix photometer, Series 1999-108 (λ 4358 A, unpolarized), modified to provide tem-

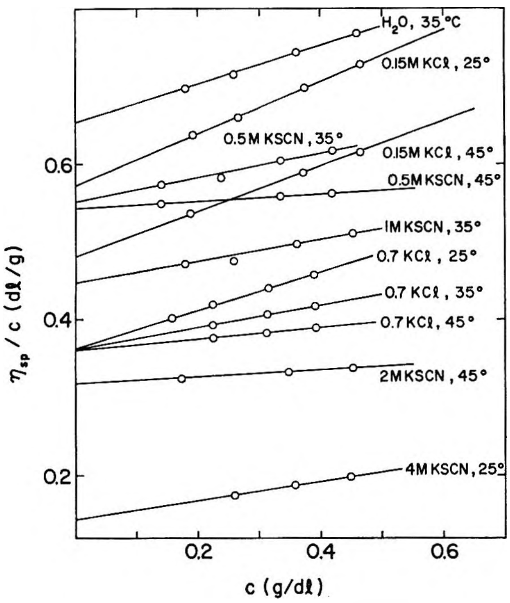

Figure 3. Representative plots of the reduced specific viscosity *vs.* poly-L-proline concentration at different temperatures and salt concentrations.

perature control of the cell by means of a surrounding water jacket. Calibration and general procedural details parallel those in a similar study reported elsewhere,[5] with the exception that measurements here were confined to the principal scattering angles (45, 90, 135°). All solutions were filtered through ultrafine glass frits under nitrogen pressure. In contrast with the viscosity measurements, intensities measured originally at the lowest temperature (25°) could be reproduced only when, upon completion of the sequence of measurements at progressively higher temperatures, the solutions were stored for several hours at *ca.* 1°. Moreover, the effects of differences in thermal history were revealed in the final data obtained. In particular, the results reported for 0.5 M KCl solutions can differ substantially from those for the 0.44 M solvent only on this account. It is significant that in the former measurements, a slight amount of precipitated material was observed just prior to the ultrafine filtration of the stock solution. The residue was removed by the clarification process, thus apparently yielding a solution free of aggregated solute constituents over the time scale of the experiment (*cf.* Discussion section).

The dissymmetry ratios d for the various solutions ranged from 1.2 to 1.8 in 1 M KSCN, from 1.0 to 1.4 in 0.44 M KCl (d increasing with increasing c in each instance), and were unity in the 0.5 M KCl solution. The intrinsic dissymmetries $[d]$, obtained by extrapolation of $(d - 1)^{-1}$ to zero polymer concentration, were 1.15, 1.02, and 1.00, respectively. Small contributions from fluorescent radiation in KCl solutions were observed. Appropriate corrections to the scattering intensities were made on the basis of data obtained with optical filters inserted in the path of the scattered beam. Depolarization corrections were ignored.

The refractive index increment for the polymer in 0.5 M KCl was measured at 25° with a Brice-Phoenix differential refractometer. With blue light, the value 0.195 was obtained.

Results

Plots of precipitation temperature *vs.* salt concentration, C_s, for the poly-L-proline sample in aqueous KF, KCl, and KSCN solutions are shown in Figure 4. Data for the intrinsic viscosity in the same media are collected in Table I, and the change in $[\eta]$ with C_s and temperature is illustrated in Figure 5. A decrease of $[\eta]$ with both variables is seen to be indicated. Plots of the reciprocal reduced scattering intensity at 90° (arbitrary units) *vs.* polymer concentration are shown in Figure 6. From the intercept for 0.5 M KCl and the corresponding refractive increment, a value for the weight-average molecular weight, $\bar{M}_w = 18{,}500$, is obtained. A comparable value seems to be indicated from the plot for the KSCN data, after taking into account corrections of the limiting reduced intensity

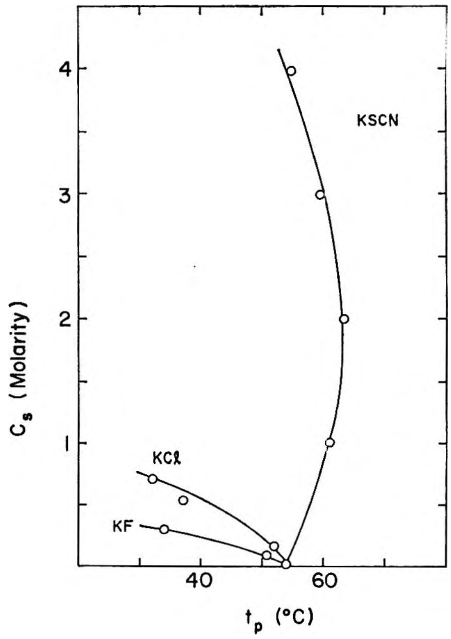

Figure 4. Variation of the precipitation temperature with salt concentration for poly-L-proline solutions containing 0.4% polymer.

---

[5] T. A. Orofino and F. Wenger, *J. Phys. Chem.*, **67**, 566 (1963).

Table I: Intrinsic Viscosity Results for Poly-L-proline Solutions

Solvent	Temp, °C	[η], dl/g	k'	$10^3 d[\eta]/dT$
Water	25	0.690	(0.69)	
	35	0.655	0.58	−4.4
	45	0.616	0.59	
	55	0.566	0.59	
KSCN, 0.5 *M*	25	0.605	0.33	
	35	0.547	0.57	−2.8
	45	0.540	0.45	
	55	0.528	0.05	
1 *M*	25	0.506	0.74	
	35	0.480	0.66	−2.8
	45	0.450	0.58	
2 *M*	25	0.316	2.1	
	35	0.314	1.4	0
	45	0.318	0.5	
4 *M*	25	(0.14)	...	
	35			0
	45			
KCl, 0.15 *M*	25	0.59	(0.8)	
	35	0.51		−4.4
	45	0.50		
0.5 *M*	25	0.61	(0.8)	
	35	0.56		−5.0
	45	0.50		
0.7 *M*	25	0.39	(1.7)	
	35			0
	45			

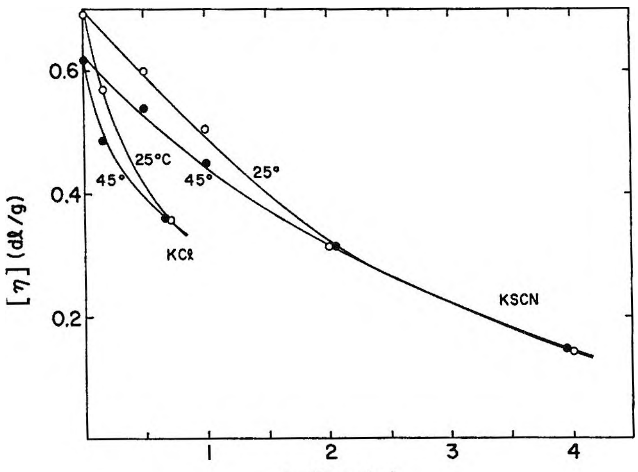

Figure 5. Variation of the intrinsic viscosity of poly-L-proline with salt concentration at different temperatures.

for dissymmetry effects and the somewhat smaller d*n*/d*c* value estimated for this system. Within experimental error, effects of temperature on the excess scattering intensities in 0.5 *M* KCl were not apparent in the range 25–35°.

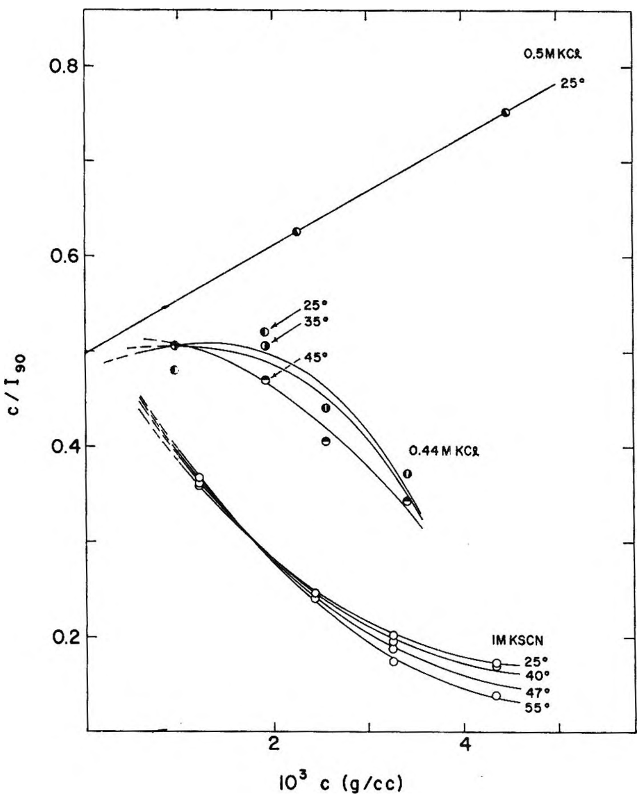

Figure 6. Reciprocal reduced excess scattering intensity *vs.* poly-L-proline concentration at different temperatures and salt concentrations.

Discussion

1. Characteristics of the Heat Precipitation. The observations reported in this investigation firmly establish that the phase transition effected by heating in poly-L-proline systems is a reversible process, in spite of the appreciable rate and hysteresis phenomena involved. Large time effects are commonly indicative of liquid–crystalline transitions; in contradistinction, equilibrium conditions are readily achieved with liquid–liquid separations encountered in conventional polymer systems. In any case, the observation that some birefringent fibers occur in the precipitate, together with the results of the X-ray analysis of the concentrated phase in the presence of the supernatant solution, offers strong indications that some crystallinity has developed in the precipitate. Since the infrared spectrum of the precipitate clearly shows that the material has remained in the original form II, the choice of possible mechanisms responsible for the heat precipitation is considerably limited. We shall consider and examine the evidence for the following interpretations: (1) the phase change involves the direct transformation of dissolved polymer to an ordered, crystalline material; (2) the change represents a liquid–liquid transition in the polymer–solvent system, with the concentrated phase subsequently acquiring partial crystalline order.

We examine first the thermodynamic requirements for the occurrence of liquid–liquid separation upon increasing temperature. The necessary condition here is that the interaction of the polymer with water or salt–water diluent (regarded as a single-component solvent) changes upon heating until a critical temperature is reached, at which a phase richer in amorphous polymer separates. According to current theories for binary polymer solutions[6] the partial molar free energy of mixing polymer molecules with solvent, $\Delta\bar{F}_1$, is given by the expression

$$\Delta\bar{F}_1/RT = -[v_2/x + (1/2 - \chi_1)v_2^2] + 0(v_2^3) \quad (1)$$

where v_2 is polymer concentration in volume fraction, x is proportional to polymer molecular weight, R is the gas constant, T is absolute temperature, and χ_1 is a parameter which expresses the degree of interaction of polymer with the solvent. At given molecular weight and solute concentration, the coefficient of the second term in parentheses in eq 1 alone dictates the relationship of $\Delta\bar{F}_1$ to the nature of the polymer–solvent pair. It may be alternatively expressed[6]

$$(1/2 - \chi_1) = \psi_1 - \kappa_1 = \psi_1(1 - \Theta/T) \quad (2)$$

where κ_1 and ψ_1 are the component enthalpy and entropy of dilution parameters, respectively, and Θ represents the quantity $T\kappa_1/\psi_1$. In order to characterize the systems under consideration, it is required that $\Delta\bar{F}_1$ given by eq 1 maintain a value less than zero for all values of $T < T_p$ ($\simeq\Theta$) and that $\Delta\bar{F}_1$, upon increase in temperature to or above T_p, exceed zero. The latter condition will correspond observationally to the onset of phase separation of amorphous polymer from solution. It is clear from inspection of eq 1 and 2 that, since T_p must remain within the range of observation, $\Theta > 0$ and thus the thermodynamic parameters ψ_1 and κ_1 are of the same algebraic sign. The additional condition $d\Delta\bar{F}_1/dT > 0$ requires that the pair assume negative values. Thus, in the binary solution approximation, a liquid–liquid separation upon increasing temperature may occur only when both the heat and entropy of dilution parameters for polymer–solvent interaction are negative. Reported examples of such systems are aqueous solutions of gelatin[7] and polymethacrylic acid[8a] (*cf.* also ref 8b). The appropriateness of a similar interpretation for the present system may be assessed through consideration of the viscosity and light-scattering data obtained.

We shall assume in the analysis following that poly-L-proline in dilute solution may be satisfactorily represented as a coiling, albeit relatively stiff, polymer. (The magnitude of $\bar{M}_w$ and the range of $[\eta]$ values encountered would appear to provide a basis for this assumption although the degree of validity of the approximation is in any case not critically relevant here.)

The dependence of the intrinsic viscosity upon pertinent chain parameters may be expressed,[6] for example, by the pair of relationships

$$[\eta] = \Phi(\overline{r_0^2}/M)^{3/2}M^{1/2}\alpha^p; \quad 2 < p \leqq 3 \quad (3)$$

$$\alpha^5 - \alpha^3 = C'(\overline{r_0^2}/M)^{-3/2}\psi_1(1 - \Theta/T)M^{1/2} \quad (4)$$

where M is polymer molecular weight, $\overline{r_0^2}$ is the mean-square unperturbed end-to-end distance of the polymer chain, α is the factor by which $(\overline{r_0^2})^{1/2}$ is expanded through interaction with solvent, and Φ and C' are constants. It is clear from eq 3 and 4 that $[\eta]$ will decrease with increasing temperature[9] only if either $\overline{r_0^2}$ or the quantity $\psi_1(1 - \Theta/T)$ decreases with increasing T. The experimental observation (Table I) is that $d[\eta]/dT < 0$. Quantitative assessment of the role of the thermodynamic parameters is, however, precluded since the extent to which the temperature coefficient of $\overline{r_0^2}$ contributes to $d[\eta]/dT$ is unknown. Qualitatively, a negative value might be expected if one assumes, for example, that the rigidity of poly-L-proline in aqueous solution is sufficient to permit representation of the chain dimensions according to the Bressler and Frenkel[10] formulation

$$\overline{r_0^2} = x'l^2(2V_0/kT - 1)(1 + \cos\beta)/(1 - \cos\beta) \quad (5)$$

in which x' is the number of inflexible links of length l, β is the complement of the valence angle, V_0 is the potential barrier for uncorrelated rotation of one link with respect to its neighbor, and k is the Boltzman constant. This equation is based upon the existence of only a single minimum in the potential and is seen

---

[6] P. J. Flory, "Principles of Polymer Chemistry," Cornell University Press, Ithaca, N. Y., 1953.

[7] L. V. Rajagh, D. Puett, and A. Ciferri, *Biopolymers*, **3**, 421 (1965).

[8] (a) J. Eliassaf and A. Silberberg, *Polymer*, **3**, 555 (1962); (b) H. Morawetz, "Macromolecules in Solution," Interscience Publishers, Inc., New York, N. Y., 1965, p 66.

[9] T. A. Orofino and A. Ciferri, *J. Phys. Chem.*, **68**, 3136 (1964).

[10] M. L. Volkenstein, "Conformational Statistics of Chain Molecules," Interscience Publishers, Inc., New York, N. Y., 1961, p 189; S. E. Bressler and Ya. I. Frenkel, *Zh. Eksperim. i Teor. Fiz.*, **9**, 1094 (1939).

to require that $\overline{r_0^2}$ decrease with increasing temperature.

It has been implicitly assumed in the foregoing discussion that intrinsic viscosity parameters measured for poly-L-proline in various media relate to the molecularly dispersed solute. The data depicted in Figure 6, taken together with the dissymmetry data presented in part 7 of the Experimental Section, reveal, however, the effects of various time-dependent factors upon the incipient precipitation of poly-L-proline from solution. The curve for 1 *M* KSCN exemplifies a character typical[11] of aggregated solute dispersions in which the extent of molecular dispersion increases progressively with decrease in polymer concentration and, in this case, with decrease in temperature. A similar behavior, although less pronounced, is shown in the case of the 0.44 *M* KCl solutions. It is noteworthy that the portions of the latter curves at low concentration, particularly at lower temperatures, begin to exhibit a dependence on *c* characteristic of dispersed polymers of moderate molecular weight in good solvent media (*i.e.*, far from the Θ point): the dissymmetries are essentially unity (small coil size) and the apparent values of the virial coefficient Γ_2 defined by the relation

$$\Gamma_2 = [\mathrm{d}(c/I_0)/\mathrm{d}c]_{c=0}/2(c/I_0)_{c=0}$$

are greater than zero. This behavior is fully evident in the case of the 0.5 *M* KCl curve in which no indication of solute aggregation is provided. The large differences in light-scattering characteristics among the three systems cannot reasonably be associated solely with intrinsic variations in solvent power in the media, two of which (KCl solutions) are virtually identical thermodynamically. Obviously, the differences observed reflect variations in the thermal history of the solutions and corresponding changes in the extent of incipient solute aggregation to which the light-scattering measurements (and indeed, on a lesser scale, the visual precipitation and viscosity studies) are responsive. To the extent that the data for 0.5 *M* KCl and the initial portions of the curves for 0.44 *M* KCl describe the inherent solution properties of the dispersed solute system, however, the following conclusion may be drawn: the solvent medium 0.5 *M* KCl is thermodynamically favorable toward poly-L-proline at 25° and does not change its characteristics appreciably with temperature. Thus, it appears likely that at the precipitation temperature for this system (*ca.* 45°, see Figure 4), the observed phase transition is not induced by liquid-liquid separation. The foregoing analysis lends, therefore, support to an interpretation of the observed phase changes in aqueous poly-L-proline based upon a liquid-crystal transition, *i.e.*, crystallization from dilute solution.

It is interesting to observe that the macroscopic precipitation seems to be preceded by the formation of aggregates. A similar effect was noted for cellulose derivatives[12a] and for polyglutamic acid.[12b] Additional investigations are required in order to establish whether the phenomenon is associated simply with the slow rate of crystallization or whether crystallites are indeed in equilibrium with aggregates rather than single molecules.

The occurrence of a direct liquid-crystal transition upon increase in temperature requires that the entropy and enthalpy of the polymer segments comprising the precipitated phase exceed the corresponding (partial molar) quantities for the polymer in solution. A net increase in the entropy per polymer unit upon transfer from solution to the precipitated form would imply that in the dispersed phase a substantial degree of order prevails, probably involving organization of solvent molecules with respect to the solute species. The required characteristics of the enthalpic process likewise comply with such an interpretation. Thus, viewed in this manner, the solvent species acquire increased mobility as the polymer separates from solution. Transitions of this kind are known: the aggregation of tobacco mosaic virus protein occurs, reversibly, on increasing temperature and the entropy contribution due to the release of bound water has been confirmed.[13] Indeed, simple substances like $NaI \cdot 2H_2O$ exhibit negative solubility-temperature coefficients.

The heat precipitation of poly-L-proline bears strong resemblance to the aggregation of tropocollagen helices on increasing temperature.[4] In both cases occurrence of a crystalline precipitate is observed.

Large time effects are as common to tropocollagen as to poly-L-proline[4,14,15] systems; in some cases aging of a clear tropocollagen solution results in isothermal crystallization, and the process appears irreversible. (The possible significance from the point of view of fibrogenesis is interesting.) The apparent irreversibility of the precipitation for tropocollagen can, however, be reconciled with the observations for poly-L-proline

---

[11] C. Tanford, "Physical Chemistry of Macromolecules," John Wiley and Sons, Inc., New York, N. Y., 1961; P. Doty and G. E. Myers, *Discussions Faraday Soc.*, **13**, 51 (1953).

[12] (a) S. Newman, W. R. Krigbaum, and D. K. Carpenter, *J. Phys. Chem.*, **60**, 648 (1956); (b) T. M. Schuster, *Biopolymers*, **3**, 681 (1965).

[13] C. L. Stevens and M. A. Lauffer, *Biochemistry*, **4**, 31 (1965).

[14] (a) J. Gross. *J. Exptl. Med.*, **108**, 215 (1958); (b) H. B. Bensusan and B. L. Hoyt, *J. Am. Chem. Soc.*, **80**, 719 (1958).

[15] J. H. Fessler, *Biochem. J.*, **76**, 452 (1960).

Lorentz shape for the central band. The separations in the P and R branch maxima were approximately 200 cm^{-1} for the OH band and 140 cm^{-1} for the OD band.

The separation $\Delta\nu$ (cm^{-1}) is given by

$$\Delta\nu = \sqrt{8kTB/hc} = 2.358\sqrt{TB}$$

where T is the absolute temperature, and B, the rotational constant, is equal to $h/8\pi^2cI_B$. For linear molecules, I_B is the moment of inertia about an axis perpendicular to the internuclear axis and going through the center of mass. For diatomic molecules, $I_B = \mu r^2$ where μ is the reduced mass and r is the distance between atom centers. The surface silicon atom to which an OH group is attached is also bound to three O atoms; it can probably be regarded as an essentially infinite mass. Only a single axis of rotation exists, passing through the Si atom and very close to the O atom. Assuming a bond angle >90°, the OH group was approximated as a diatomic molecule with the atomic masses of O and H rotating about the axis of rotation and separated from each other by $r_{eff} = r \cos(\phi - 90°)$, where ϕ is the angle between the axis of rotation and the O–H axis.

$$I_B = \mu r^2 \cos^2(\phi - 90°)$$

where $\mu = m_1m_2/(m_1 + m_2)$. Assuming an equilibrium O–H distance r (as in H_2O) $= 0.958 \times 10^{-8}$ cm, values were calculated for expected separations between P and R branch maxima as a function of the angle ϕ. For values of ϕ ranging from 90 to 125°, the separations ranged from 180 to 220 cm^{-1}. The observed separation ($\sim$200 cm^{-1}) falls in midrange–corresponding to roughly 115°; ϕ is slightly larger than θ, the true Si–OH bond angle. Calculations indicate that at ϕ = 115°, θ = 113°. The difference is less than the error involved in the approximations and in measuring the separations of the P and R branch maxima.

Similar calculations were made for OD groups, and the observed separation in P and R maxima ($\sim$140 cm^{-1}) again corresponded to a bond angle of $\sim$113°.

The calculated bond angle seems reasonable, but torsional oscillation (or possibly other causes) could give similar bands. Since I is the same for torsional oscillation as for free rotation, the branch maxima separations should be the same. The P and R branches are very weak compared to the strong central (Q branch) band. Perhaps rotation is strongly hindered.[17] Perhaps only some of the OH groups, situated differently from the rest, rotate freely while the others do not. If so, differences in the rate of exchange with D_2O, or in other chemical behavior, might alter the ratio of the intensities of the central and side branches. Although present data cannot exclude minor alterations in the relative intensity of the branches, no major differences were observed following D_2O exchange or during any of the other reactions described.

The bands reported between 2700 and 3000 cm^{-1} in the spectrum of microporous glass[10,13] may reflect impurities not present in silica, or possibly adsorbed hydrocarbons.[5] No such bands were found for silica aerogel.

As silica is dried at progressively higher temperatures, the "tail" below the 3750-cm^{-1} disappears more rapidly than does the 3750-cm^{-1} band itself. The H-bonded OH groups are thus eliminated more easily than those that are not H bonded. This indicates that these OH groups are bonded to other OH groups, because H bonding to an oxide ion should not, *per se*, promote elimination of the OH group (as H_2O).

The spectral changes observed for hot silica probably reflect changing interactions with the local environment as well as direct effects of temperature on the O–H bond vibrations. However, the OH and OD groups clearly remain on much the same type of sites at high temperature as those on which they are found after cooling. They are not desorbed as H_2O at high temperatures and reformed when H_2O readsorbs on cooling.

The evidence obtained from adsorption of ethyl ether or NH_3 on silica aerogel predried at 600° or above shows that all the OH groups remaining are surface groups.

Evidence from reaction with $SiCl_4$ suggests that steric factors are probably usually responsible for the incomplete reaction of OH groups. Even on silica holding <2 OH/100 A, a surprising number of the surface OH groups are sufficiently close together to permit two of them to react with one $SiCl_4$ molecule. Such close proximity of OH groups would probably make quantitative removal by reaction with diborane, CH_3MgI, or CH_3Li at low temperatures extremely difficult.

Boehm, *et al.*,[19] conclude that production of two molecules of HCl for each molecule of $AlCl_3$ which reacts with the silica surface results from the reaction

$$H_2O + AlCl_3 \longrightarrow AlOCl + 2HCl$$

A similar explanation does not appear possible for the results obtained with $SiCl_4$ in the present work, because $SiOCl_2$ is unknown,[29] and no spectroscopic evidence was found for H_2O (as such) on silica aerogel dried at 600° or above. Clearly, however, close proximity of two OH groups on the surface provides an alternative explanation in both cases.

Present evidence suggests that OH groups are vir-

---

(29) A. F. Wells, "Structural Inorganic Chemistry," Oxford University Press, Oxford, 1962, pp 776–778.

tually immobile on the surface of dry silica below 800°. Even at 900°, the groups remaining after the first hour of evacuation are eliminated only extremely slowly. Ready migration of OH groups or protons would presumably cause rapid formation and elimination of H_2O. Migration of OH as such requires that Si–O bonds be broken to form Si^+ sites or unsaturated valencies, and it would probably not occur much more readily than bulk rearrangement of the silica structure. Migration of protons might occur more easily, but if migration occurs very readily, it is hard to understand why NH_2 groups on silica are not more rapidly replaced by OH groups when exposed to H_2O vapor at elevated temperatures (and *vice versa*). If OH groups are very mobile, it is also difficult to see how those left on the surface after predrying at 800° could be paired in some cases and single in other cases as indicated by reaction with $SiCl_4$. The OH groups on silica appear less mobile than those on alumina.[26]

If surface OH groups are indeed relatively immobile, their arrangement must be very important in possible reactions with one another or with other molecules. Despite much speculation, there is no evidence to date concerning such arrangement. Isolated OH groups are not necessarily widely separated. The results of reaction of $SiCl_4$ indicate that, on the contrary, they are often close together. Vicinal OH groups, *i.e.*

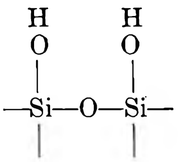

$$\begin{array}{ccc} \mathrm{H} & & \mathrm{H} \\ \mathrm{O} & & \mathrm{O} \\ | & & | \\ -\mathrm{Si} & -\mathrm{O}- & \mathrm{Si}- \\ | & & | \end{array}$$

are not necessarily H bonded and may be difficult to remove because removal requires edge linking of SiO_4 tetrahedra. Geminal OH groups ($=Si(OH)_2$) are probably not H bonded to their partners because a five- or six-member ring is normally needed for "intramolecular" H bonding.[30] Triplet OH groups ($-Si(OH)_3$) should be equally free of internal H bonding. Elimination of H_2O by internal condensation of geminal pairs or triplet OH groups would require formation of $=Si=O$ groups. Silicon is not believed to form such groups;[29] so, unless geminal or triplet OH groups adjoin OH groups on adjacent Si atoms, their removal through H_2O formation would probably be very difficult. Probably, particularly on fresh silica gels, geminal and triplet OH groups do exist, but this has not been proved. Interesting questions are raised by the fact that reaction with $SiCl_4$ plus hydrolysis and redrying fails to alter significantly either the number of surface OH groups or the appearance of the OH bands. The best apparent interpretation is as follows. During hydrolysis, $=Si(OH)_2$ or $-Si(OH)_3$ groups, which as initially produced protrude above the surface, are further hydrolyzed and migrate as $Si(OH)_4$ to other locations where they add to the existing structure in a more stable fashion, simply extending the original surface slightly without changing its character. It has not been established, nor is it evident, that geminal or triplet OH groups which are not H bonded can be readily distinguished spectroscopically from widely separated single OH groups.

The slow chemisorption of a limited amount of NH_3 or very dry silica implies the existence of a small number of highly strained[12] or ionic siloxane linkages on the surface which react with NH_3 to produce $-NH_2 + -OH$. As found here, the maximum number of such sites is about 1.4/100 A^2. Chemisorption of NH_3 on silica, as an alumina, appears to be analogous to chemisorption of H_2O. The failure of HCl to chemisorb similarly on dry silica is somewhat surprising.

Conclusion

Although infrared spectroscopic studies have provided considerable information about the surface of silica, many questions concerning the details of surface structure remain unanswered. Answers to most of these questions probably cannot be obtained without supporting studies with other techniques. Additional evidence seems particularly needed on the relative abundance of single, paired, and triplet hydroxyl groups. Evidence on this subject will be presented in a subsequent paper.

Acknowledgments. Discussions with A. L. Hensley, Jr., and Professor R. L. Burwell, Jr., were very helpful in this work. The assistance of J. Kekich in the experimental work is also gratefully acknowledged.

---

(30) G. C. Pimentel and A. L. McClellan, "The Hydrogen Bond," Reinhold Publishing Corp., New York, N. Y., 1960.

Sedimentation Equilibrium of Ovalbumin in Concentrated Cesium Chloride[1]

by Julie Hill and David J. Cox

Clayton Foundation Biochemical Institute and the Department of Chemistry, The University of Texas, Austin, Texas 78712 *(Received March 16, 1966)*

Ovalbumin has been examined in the ultracentrifuge at sedimentation equilibrium in concentrated cesium chloride. From the position of the band of protein in the density gradient generated by the redistribution of the salt in the centrifugal field, the buoyant density of ovalbumin was found to be 1.296 ± 0.003 g/cm^3. This value agrees quite well with the apparent hydrodynamic density of ovalbumin obtained by plotting the viscosity-corrected sedimentation coefficients observed at several cesium chloride concentrations against the density of the salt solutions, and extrapolating the resulting linear relation to $S = 0$. Sedimentation equilibrium experiments at different rotor speeds and with solution columns of different lengths indicate that the variation of the buoyant density of ovalbumin with hydrostatic pressure is small.

Introduction

A previous report has described measurements of the sedimentation velocity of ovalbumin in concentrated aqueous solutions of five different salts.[2] When the sedimentation coefficients, measured at several concentrations of a given salt, were corrected to a reference viscosity and plotted against the densities of the solvents, each set of points defined a straight line which, on extrapolation, crossed the density axis well below the reciprocal of the partial specific volume of the protein ($1/\bar{v}_p$). The discrepancy between the density intercept and $1/\bar{v}_p$ could be accounted for by variation of the frictional ratio of ovalbumin with salt concentration, by the binding of water in preference to salt of the protein, or by certain combinations of the two effects. For reasons cited previously, it seems improbable that either the molecular weight or the partial specific volume of ovalbumin varies in these solvents.

Cesium chloride was one of the salts in which the sedimentation velocity of ovalbumin was measured. In cesium chloride, a direct determination of the density of the sedimenting unit can be done—at one salt concentration—by means of the banding method developed by Meselson, Stahl, and Vinograd.[3,4] Comparison of the buoyant density of the protein measured by the banding method with the density intercept obtained from the sedimentation velocity measurements allows the elimination of several of the possible ways of accounting for the way in which the sedimentation coefficient of ovalbumin varies with the concentration of cesium chloride. For example, if variation of the frictional ratio alone were responsible for the observed dependence of the sedimentation coefficient on the density of the solvent, then the two densities could not agree. If the two values agree and the frictional ratio does change significantly with the composition of the solvent, then the protein must bind one component of the solvent in preference to the other and the degree of preferential solvation must also vary with salt concentration. The simplest explanation of the velocity experiments, that the protein binds water in preference to salt, and that neither the degree of preferential hydration nor the frictional ratio varies with salt concentration, would require agreement between the density intercept of the velocity data and the buoyant density measured by the banding method.

---

[1] This work was supported by Grant GM-11749 from the U. S. Public Health Service. Some of the work was reported at the Southwest-Southeast Regional Meeting of the American Chemical Society, Memphis, Tenn., Dec 8–10, 1965.

[2] J. Hill and D. J. Cox, *J. Phys. Chem.*, **69**, 3032 (1965).

[3] M. Meselson, F. W. Stahl, and J. Vinograd, *Proc. Natl. Acad. Sci. U. S.*, **43**, 581 (1957).

[4] J. Vinograd and J. E. Hearst, *Progr. Chem. Org. Natl. Prod.*, **20**, 372 (1962).

Experimental Section

Materials. The ovalbumin was twice-crystallized material purchased from Worthington Biochemical Corp. The protein was taken from the same lot used in previous work.[2] Cesium chloride was obtained from the Gallard-Schlesinger Chemical Manufacturing Corp. Salt solutions for the ultracentrifuge experiments were prepared by dissolving the appropriate amounts of cesium chloride in potassium phosphate buffer at pH 6.8. The buffer was 0.01 M with respect to phosphate and was prepared using glass-distilled water. Solvent densities were measured using 1-ml vented-cap pycnometers, and the results were reproducible within ±0.001 g/cm^3. A sample of the dense and insoluble fluorocarbon FC-43, produced by Minnesota Mining and Manufacturing Corp., was obtained from the Spinco Division of Beckman Instruments, Inc.

Ultracentrifugation. Solutions of ovalbumin in concentrated cesium chloride were brought to sedimentation equilibrium at 20° in a Spinco Model E analytical ultracentrifuge, and the experiments were observed using schlieren optics. The cesium chloride concentrations used were so selected that the position of the band of protein at equilibrium lay near the middle of the solution column. Ovalbumin, with a molecular weight of 45,000, formed relatively wide bands at sedimentation equilibrium and, in order to obtain bands that were sharp enough to be located accurately, it was necessary to operate the centrifuge at relatively high rotor speeds. Double-sector cells could not be used with dense solutions at high velocities, since these generally leaked across the partition between the sectors. The protein solutions and the solvents were, therefore, run separately in single sector cells equipped with 1° negative wedge windows.

In order to calculate the density gradient obtained at sedimentation equilibrium in any particular experiment, the schlieren photograph of water at the same rotor speed was required. In principle, the appropriate base line for the density gradient calculation would be derived from a photograph of the schlieren pattern of the salt solution taken as the rotor reaches the operating speed, but before the salt gradient has developed.[4,5] In practice, it was found that the gradient began to develop rapidly from the ends of the solution column during acceleration and, by the time the rotor reached top speed, no more than the central third of the schlieren pattern remained unperturbed by the redistribution of the salt.

Experiments were done in which the developing schlieren pattern of a cesium chloride solution was photographed at several angular velocities as the rotor was accelerated to 59,780 rpm. In separate experiments, the cell was filled to the same level with water, and its schlieren pattern was photographed at each of the rotor speeds at which the cesium chloride solution had been observed. The water and cesium chloride base lines both rose appreciably as the centrifugal field was increased. However, at a given angular velocity, the water pattern coincided quite closely with whatever portion of the cesium chloride base line was still unaffected by the development of the salt gradient. It was concluded that the schlieren pattern of water at the appropriate rotor speed could be used as the base line for the density gradient calculation in these particular measurements. This procedure might not be correct for other solvents, and its use would have to be justified experimentally in each case.

All three of the runs required for a given buoyant density measurement—protein and salt, salt alone, and water—were done in the same cell, using the same windows. The rotor speed, the schlieren bar angle, and the length of the solution column were carefully matched among the three runs. It was found that the column lengths could be reproduced most precisely by weighing the amounts of solutions or solvents introduced into the cell.

The relation between the density gradient at sedimentation equilibrium and the area under the schlieren pattern was determined in separate experiments using a valve-type synthetic boundary cell. A cesium chloride solution of known density (ρ_1) was introduced into the centerpiece of the cell, and a solution of lower density (ρ_2) was placed in the cup. The schlieren bar was set at the same position as was used for the equilibrium runs. The rotor was accelerated until the cup emptied, and the boundary was allowed to diffuse until the entire schlieren pattern was visible. The pattern was photographed, the area under the boundary ($A_{1,2}$) was measured, and the quantity $K = (\rho_1 - \rho_2)/A_{1,2}$ was calculated. The measurements were most conveniently done using pairs of solutions that differed in density by about 0.05 g/cm^3, and seven pairs were chosen which covered the range of densities encountered in the cell at sedimentation equilibrium. The precision (±2–3%) of the individual measurements of K was not sufficient to allow the detection of a significant trend in the values with density; a mean value was used in subsequent calculations. In a few cases, after the schlieren pattern had been photographed at a relatively low rotor speed, the rotor was accelerated to 59,780 rpm and the pattern was photo-

---

(5) J. E. Hearst, J. B. Ifft, and J. Vinograd, *Proc. Natl. Acad. Sci. U. S.*, **47**, 1015 (1961).

determined density was $1.00195_4 \pm 0.00000_5$ g/ml, while that calculated from the interpolated "Critical Table" data was 1.00195_2.

Conversion of Densities to Partial Specific Volumes. The apparent specific volume, Φ, of a solute at temperature, T, can be obtained from density data by use of the relationship

$$\Phi_T = \frac{1}{n_T}\left(\frac{1}{\rho_T} - \frac{1-n}{\rho_{0,T}}\right) \qquad (1)$$

where n is the weight fraction of solute, ρ_T is the density of the solution at temperature T, and $\rho_{0,T}$ is the density of the solvent at the same temperature. If the specific volume of the solute is not concentration dependent, the apparent specific volume is equal to the partial specific volume, $\bar{v}$.

The method described in this paper is not suitable for the study of solutes whose specific volume is concentration dependent. Since the diver has a particular density at any given temperature, only one concentration of solute will result in a solution which has the same density as the diver at that temperature (see Discussion).

Density of Sucrose at 20°. Accurate density data are available for sucrose at 20°.[10] Despite the fact that the specific volume of sucrose is concentration dependent, it was decided to investigate the density–temperature behavior of sucrose and compare the data at 20° with the published data.

Sucrose was dried in a vacuum oven at 70° for 4 hr and stored in a desiccator. A stock solution (2.53670 g/100 g of solution) was prepared and various weight dilutions of this solution placed in the test tube with the diver. The solution–diver isopycnic temperatures were determined and the densities of the sucrose solutions were obtained from the diver calibration curve. The apparent specific volume of the sucrose at the various temperatures was obtained from eq 1. Once an interpolated value for the apparent specific volume at 20° had been obtained from the experimental data, the concentration of sucrose which would give a solution of the same density as the diver at this temperature could be calculated by use of eq 1.

Ulrich, Kupke, and Beams[6] have calculated that the least-squares fit to the published sucrose density data can be expressed by the relationship

$$\rho_{20°} = 0.998238 + 0.386734n + 0.10624n^2 \qquad (2)$$

where n is the weight fraction of sucrose.

When the value for the sucrose concentration, which was obtained from eq 1, was incorporated into eq 2, a value of 1.00199_7 was obtained for the density of this concentration of sucrose at 20°. At this concentration of sucrose the solution and the diver should have the same density. The density of the diver at this temperature which was obtained from the KCl calibration curve was 1.00199_4. The good agreement between these two values for the density of the diver at 20° affords corroborative evidence for the reliability of the KCl calibration curve.

Determination of Density of Albumin Solutions. Stock albumin solutions of approximately 5 g/dl were prepared and dialyzed exhaustively against distilled water at +2°. They were then filtered through washed No. 1 Whatman paper to remove any lint or other suspended material and stored in a glass-stoppered bottle at +2°. Weight dilutions of the albumin were obtained by weighing aliquots of the stock solution and glass-distilled water into weighing bottles (final albumin concentrations, 0.9–1.5%). The diluted solution was mixed well, placed in the test tube with the diver, and the isopycnic temperature was determined. The density of the solution was obtained from the diver calibration curve.

Determination of Protein Concentration by Dry Weight Measurements. Triplicate dry weight measurements were made on 2-ml samples of the stock albumin solutions. To obtain dry weight data of an accuracy comparable to that of the density data, the error in the dry weight determinations would have to be less than one part per thousand. The triplicate samples were routinely in agreement to well within this limit. However, the actual value obtained depended on the method of drying which had been employed. Different drying conditions gave dry weights which varied up to almost one part in a hundred. The best conditions for obtaining the true dry weight of a protein are somewhat uncertain and probably vary from protein to protein.

The most common method of obtaining dry weight data is heating in air at 110° to constant weight,[11,12] but various other techniques have been used. A comparison was made of several of these methods, *viz.*, drying in air at 110 and 125°, drying in air at 110° over activated alumina,[6] drying over P_2O_5 at 110° *in vacuo* in an Aberhalden drying pistol,[13] and drying in a vacuum oven at 75, 95, 105, 110, and 115°. In all cases the samples were freeze dried prior to the final drying procedure. All measurements were repeated to constant weight (when possible) and all weighings were

---

[10] F. Plato, *Wiss. Abh.*, **2**, 153 (1900); quoted by F. J. Bates and Associates, "Polarimetry, Saccharimetry and the Sugars," U. S. Government Printing Office, Washington, D. C., 1942.

[11] M. O. Dayhoff, G. E. Perlmann, and D. A. MacInnes, *J. Am. Chem. Soc.*, **74**, 2515 (1952).

[12] P. A. Charlwood, *ibid.*, **79**, 776 (1957).

[13] S. E. Allerton, personal communication.

Table I: Dry Weights of Albumin Relative to Dry Weight at 75° *in Vacuo*

	$c(T)/c(75°, in\ vacuo)^a$				
	BMA	BPA	HMA I	HMA II	HMA III[b]
75° (*in vacuo*)	(1.0000)	(1.0000)	(1.0000)	(1.0000)	(1.0000)
95° (*in vacuo*)					0.9981
105° (*in vacuo*)					0.9967
110° (*in vacuo*)	0.9960	0.9962	0.9958	0.9954	
110° (*in vacuo* over P_2O_5)				0.9953	
110° (in air)				1.0053	
115° (*in vacuo*)					0.9947
125° (in air)					0.9929

[a] $c(T)/c(75°$, *in vacuo*) = concentration of albumin at $T°$ in grams/100 g of solution divided by concentration of the same sample at 75° *in vacuo*; 2-ml samples of approximately 5% protein were used for each determination. [b] BMA = bovine mercaptalbumin; BPA = bovine plasma albumin; HMA = human mercaptalbumin.

performed 45 min after removal of the samples from the heating chamber. Some of the data obtained by use of these various procedures are shown in Table I. For reasons which are discussed later in this paper, the method finally adopted was that of drying the protein in a vacuum oven at 110°. Details of the procedure are given in the following paragraphs.

Five clean glass weighing bottles were removed from the desiccator, wiped with lens paper, and placed in the microbalance. After 20-min equilibration the bottles were weighed, the first bottle (the tare) being reweighed after weighing of the other bottles had been completed. A mean value of the two weights was taken as the weight of the tare. The difference between the two weighings was almost always less than 10^{-5} g. The stock albumin solution (2 ml) was pipetted into three of the bottles and the five bottles were reweighed, the tare again being weighed first and last. The other empty bottle was used as a secondary tare to ensure that any change in weight of the tare due to contamination which had occurred during the various manipulations would be detected. If the weight of the tare had changed between the two sets of weighings due to differing environmental conditions, the difference in the weight of the tare was added to or subtracted from all of the weights obtained in the second set of weighings.

The lids of the bottles were placed at right angles on the top of the bottles and the bottles were placed in Dry Ice until the solutions had frozen. A copper block which contained holes slightly larger than the diameter of the weighing bottles and about one-third of their height had been precooled in Dry Ice. The weighing bottles were transferred to the cooled block and the block was placed in the vacuum oven. The samples were then freeze dried overnight *in vacuo*. In the morning, the temperature of the oven was raised to 110° and the oven was maintained at that temperature for 48 hr. After the vacuum pump had been turned off, the air inlet to which the drying tube filled with P_2O_5 had been attached was opened and air was allowed to enter the oven as rapidly as was possible without dislodging the dried protein from the weighing bottles. The bottles were capped as quickly as possible while still in the oven and transferred to a desiccator.

After 25 min the bottles were wiped with lens paper and transferred to the microbalance. After 20 min they were weighed in the same order and manner as described previously. The bottles were reweighed 30, 60, and 120 min after the initial time of the first weighing. The weights of the bottles were corrected for changes in the weight of the tare as previously described and the concentration of albumin (grams/g of solution) was calculated. The albumin could regain almost one-thousandth of its weight between the first and third weighing. The protein concentrations determined at 45, 75, 105, and 165 min were extrapolated to zero time.

The samples were reheated in the vacuum oven and reweighed at 24-hr intervals until constant weight was achieved. Mean zero time values which varied by less than one part per thousand were considered to be at constant weight. A mean of all the zero time data at constant weight was taken as the dry weight of the albumin.

Determination of Partial Specific Volume. The partial specific volume of the various albumin preparations was calculated by the use of eq 1. The data for human mercaptalbumin are plotted in Figure 3. The straight line on the graph is a calculated least-squares-fit line. The two triangles on the graph represent data obtained by pycnometry. A stock 5% albumin solution and 10-ml pycnometers were used in these determinations

Table II: Partial Specific Volume[a] of Bovine Plasma Albumin (BPA) at Various Temperatures

	Run I (9 data points)	Run II (8 data points)	Run III (10 data points)
$\bar{v}_{20°}$	$0.7331_1 \pm 0.0001_5$	$0.7329_1 \pm 0.0001_6$	$0.7329_6 \pm 0.0001_0$
$\bar{v}_{25°}$	$0.7348_9 \pm 0.0001_0$	$0.7347_5 \pm 0.0001_0$	$0.7348_4 \pm 0.0000_6$
$\bar{v}_{30°}$	$0.7366_6 \pm 0.0000_9$	$0.7365_9 \pm 0.0001_0$	$0.7367_2 \pm 0.0000_8$
$d\bar{v}/dT$	$0.00035_6 \pm 0.00001_6$	$0.00036_9 \pm 0.00001_9$	$0.00037_6 \pm 0.000014$

[a] The values shown are means and standard deviations of the experimental data. $\bar{v}$ has units of ml/g; $d\bar{v}/dT$ has units of ml/g deg.

Table III: Partial Specific Volume[a] of Bovine Plasma Albumin (BPA), Bovine Mercaptalbumin (BMA), and Human Mercaptalbumin (HMA) at Various Temperatures

	BPA (27 data points)	BMA (23 data points)	HMA (24 data points)
$\bar{v}_{20°}$	$0.7330_0 \pm 0.00027$	0.73305 ± 0.00024	$0.7328_0 \pm 0.00013$
$\bar{v}_{25°}$	$0.7348_2 \pm 0.00017$	0.73493 ± 0.00015	$0.7345_8 \pm 0.0000_8$
$\bar{v}_{30°}$	$0.7366_5 \pm 0.0001_9$	$0.7368_0 \pm 0.0001_8$	$0.73635 \pm 0.0000_9$
$d\bar{v}/dT$	$0.00036_6 \pm 0.000033$	$0.00037_5 \pm 0.00003_0$	$0.00035_5 \pm 0.00001_6$

[a] The values shown are means and standard deviations of the experimental data. $\bar{v}$ has units of ml/g; $d\bar{v}/dT$ has units of ml/g deg.

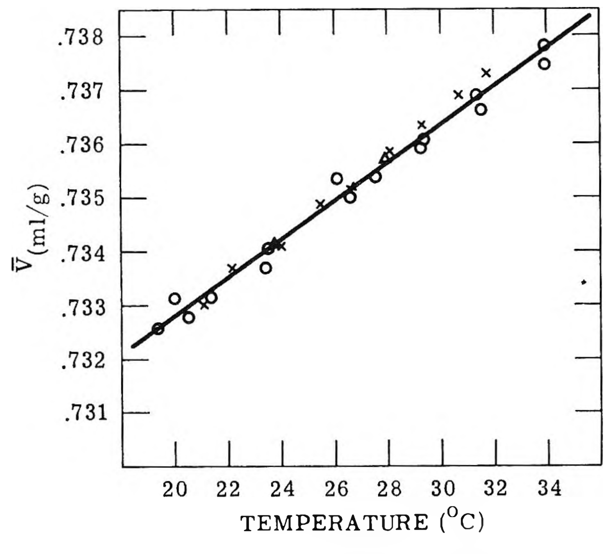

Figure 3. Partial specific volume of human mercaptalbumin at various temperatures: O, run I; ×, run II; △, pycnometric determinations.

which were performed in triplicate. The densities of the triplicates varied by less than ±1 × 10^{-5} g/ml.

Similar results were obtained with bovine plasma albumin and bovine mercaptalbumin. The variation in three experiments with bovine plasma albumin can be seen from the data in Table II. The standard deviations of the values are also listed. Similar results were obtained with the other albumin preparations.

Mean partial specific volume data for bovine plasma albumin, bovine mercaptalbumin, and human mercaptalbumin are summarized in Table III. If the densities of the KCl solutions used to calibrate the diver were in error by one in the fifth decimal place, $\bar{v}$ will be in error by 0.00034. An error of one part in a thousand in protein concentration will cause an error of approximately 0.0003 in $\bar{v}$, and an error of 0.01° in temperature will cause an error of 0.00014 in $\bar{v}$.

Discussion

The determination of partial specific volumes by measurement of solution–diver isopycnic temperatures has one intrinsic disadvantage: for a particular diver, only one concentration of solute will give any particular isopycnic temperature. The partial specific volume data at various temperatures are thus obtained from solutions of different solute concentration. If the partial specific volume of the solute is concentration dependent, a series of apparent specific volumes is obtained, and, unless density concentration data are available at several temperatures, the true partial specific volume cannot be determined. The necessary information could be obtained by the use of several divers of differing density. It is unlikely, however, that the concentration dependence of the partial specific volume is a serious problem when protein solutions of relatively low concentration (<5%) are being studied. The partial specific volume data of Dayhoff, Perlmann, also varies from salt to salt, and there is a smooth correlation between water activity and preferential hydration. On the basis of these data, each obtained in a different salt, Bruner and Vinograd[7] suggest that the preferential hydration of a macromolecule in a given salt should vary with salt concentration since the activity of water does so. Their interpretation would argue against the possibility that the sedimentation behavior of ovalbumin may be accounted for by the constancy with salt concentration of preferential hydration and the frictional ratio. It should be possible to approach the problem more directly by measuring the buoyant density of ovalbumin in cesium chloride and deuterium oxide. The salt concentration and thus the water activity at the protein band should be different in water and in deuterium oxide, and it should be possible, in this way, to determine whether or not the preferential solvation of the protein is the same at two different concentrations of the same salt.

The Radiolysis of Ethyl Mercaptan[1]

by J. J. J. Myron and R. H. Johnsen

Department of Chemistry and the Institute of Molecular Biophysics, Florida State University, Tallahassee, Florida *(Received March 21, 1966)*

A study of the radiolysis of liquid ethyl mercaptan has been undertaken. The data strongly suggest that the radiolytic behavior of the mercaptan differs significantly from that of the corresponding alcohol. A comparison of the two radiolyses in the light of the present results is presented.

Introduction

In the past, radiolytic studies of compounds containing sulfhydryl groups have generally been carried out on dilute aqueous solutions of polyfunctional thiols. Except for data on the esr spectra of irradiated methyl and ethyl mercaptan[2] taken at 77°K, no studies on the radiolytic behavior of these compounds appear to have been made. Investigation of simple mercaptans in the "pure" state should be of interest as a comparison to that of the corresponding aliphatic alcohols which have been extensively studied by various workers.[3-6]

The possible importance of thiol radiolysis studies is evidenced by the number of publications dealing with biological systems in which mercaptans were present as additives. Compounds such as cysteine,[7-9] cysteamine,[10] and glutathione[11,12] have been widely used as "protectors" of biologically significant systems against radiation damage. Oxidation of the thiol group by radiation-produced radicals from the other components of the system is probably an important mode of "protection" or "inhibition" afforded by the sulfur compound. The corresponding disulfide and small amounts of hydrogen sulfide are the usual products of oxidation.

---

(1) Research supported in part by A.E.C. Contract AT-(40-1)-2001 and in part by A.E.C. Contract AT-(40-1)-2690.

(2) C. L. Luck and W. Gordy, *J. Am. Chem. Soc.*, **78**, 3240 (1956).

(3) (a) W. McDonnell and A. S. Newton, *ibid.*, **76**, 4651 (1954); (b) I. A. Taub and L. M. Dorfman. *ibid.*, **84**, 4053 (1962).

(4) (a) J. G. Burr, *J. Phys. Chem.*, **61**, 1477 (1957); (b) G. E. Adams, J. H. Baxendale, and R. D. Sedgwick, *ibid.*, **63**, 854 (1959).

(5) E. M. Hayon and J. Weiss, *J. Chem. Soc.*, 3962 (1961).

(6) R. H. Johnsen, *J. Phys. Chem.*, **65**, 2144 (1961).

(7) S. L. Whitcher, M. Rotheram, and N. Todd, *Nucleonics*, **11**, 30 (1953).

(8) P. Riesz and B. E. Burr, *Radiation Res.*, **16**, 661 (1962).

(9) C. N. Trumbore, *et al.*, *J. Am. Chem. Soc.*, **86**, 3177 (1964).

(10) B. Shaprio and L. Eldjar, *Radiation Res.*, **3**, 225 (1955).

(11) G. E. Woodward, *Biochem. J.*, **27**, 1411 (1933).

(12) E. S. G. Barron and V. Flood, *J. Gen. Physiol.*, **33**, 229 (1950).

densities obtained from recently determined calibration curves. The magnitude of the change in the density of the diver was not great; for example, the density of the diver at 25° dropped from 1.00197_1 to 1.00192_9 during this time period.

With the present equipment, the volume of sample required for a density determination is slightly over 3 ml. This volume is necessary for the thermometer bulb and 0.5–1 cm of the stem to be immersed in the solution. If the thermometer were replaced by a small thermistor, the volume of solution required for the measurement could be decreased to less than 1 ml. With the equipment in its present form, about 200 mg of protein is required for a series of five density determinations.

Density measurements on albumin in the presence of KCl are in progress. These will be continued and extended by the concomitant addition of HCl or KOH in an attempt to determine the partial specific volume of nonisoionic protein components.

Acknowledgments. The author wishes to acknowledge the technical assistance of Miss Joanne Psenka and Mr. David Turk, who performed many of the density determinations. The author also wishes to thank Dr. G. L. Nordby for his help in obtaining the interpolated KCl data by the use of an IBM 7090 computer.

Spectroscopy and Franck–Condon Factors of Scandium Fluoride in Neon Matrices at 4°K

by Donald McLeod, Jr., and William Weltner, Jr.[1]

Union Carbide Research Institute, Tarrytown, New York 10591 *(Received May 16, 1966)*

The absorption and emission spectra of ScF in neon matrices at 4°K have been observed in the visible and near-infrared regions. The vapor that evolved from a mixture of solid Sc + ScF_3 at 1700°K was superheated to 2400°K before being trapped in the neon matrix; this was necessary to obtain a sufficient concentration of ScF molecules. Comparison of the matrix absorption spectrum with the analysis of the gas spectra by Barrow, *et al.*, shows that only transitions from the lowest $^1\Sigma^+$ state are occurring at 4°K and that it is the ground state. Gradual small shifts of the visible spectrum of ScF in the matrix when exposed to tungsten light (reversed on warming) indicate that new metastable sites are being formed in the neon lattice. Ratios of Franck–Condon factors have been derived from the relative intensities of the bands in two progressions of ScF in the matrix spectra ($E^1\Pi \leftarrow X^1\Sigma$ and $C^1\Sigma \leftarrow X^1\Sigma$). Values of Δr_e (the change in interatomic distance during excitation) derived from them are compared with those obtained from gas data and agree to better than 7%. Five bands in the infrared have been tentatively assigned to the ScF_2 and ScF_3 molecules.

Introduction

The ScF molecule is isoelectronic with TiO and, if inner shells are excluded, with ZrO. Each of these oxide molecules has been thoroughly investigated *via* gas[2] and matrix spectroscopy,[3] and TiO has also been studied theoretically.[4] TiO has a $^3\Delta_r$ ground state with low-lying $^1\Delta$ and $^1\Sigma^+$ electronic levels, while matrix studies of ZrO indicate that it has a $^1\Sigma^+$ ground state with low-lying $^3\Delta$ and $^1\Delta$ levels. The simplest criteria suggest that ScF would be more like TiO and so have a $^3\Delta_r$ ground state. Recently Barrow, Gissane, LeBargy, Rose, and Ross[5,6] have made a thorough analysis of the gas phase spectrum but are not able to unambiguously specify the lowest state. This matrix investigation was undertaken to allow a comparison of the absorption spectrum at 4°K with their analysis in order to determine the ground state of ScF. The result is that three singlet–singlet transitions are observed at 4°K and the lowest state is therefore $^1\Sigma^+$.

Because of the large changes in interatomic distance (Δr_e) occurring during the electronic transitions of ScF in the visible region,[6,7] long progressions of bands are observed in the spectrum. The relative intensities of the bands in a progression yield the ratios of Franck–Condon factors for transitions to the various excited vibrational levels in the upper electronic state. From these ratios the Δr_e value for an electronic transition can be derived. It is of interest to see how the Δr_e values derived from matrix spectra compare with those obtained from rotational analysis in the gas. In the case of ScF the agreement is found to be excellent.

---

[1] University of Florida, Gainesville, Fla.

[2] By J. G. Phillips, U. Uhler, L. Akerlind, and others. See R. W. B. Pearse and A. G. Gaydon, "The Identification of Molecular Spectra," 3rd ed, John Wiley and Sons, Inc., New York, N. Y., 1963.

[3] (a) W. Weltner, Jr., and D. McLeod, Jr., *J. Phys. Chem.*, **69**, 3488 (1965); (b) M. J. Linevsky, "Proceedings of the First Meeting of the Interagency Chemical Rocket Propulsion Group on Thermochemistry, New York, N. Y., 1963," Vol. 1, Chemical Propulsion Information Agency, Silver Spring, Md., 1964, p 11.

[4] K. D. Carlson and C. Moser, *J. Phys. Chem.*, **67**, 2644 (1963); K. D. Carlson and R. K. Nesbet, *J. Chem. Phys.*, **41**, 1051 (1964).

[5] R. F. Barrow, W. J. M. Gissane, R. C. LeBargy, G. V. M. Rose, and P. A. Ross, *Proc. Phys. Soc.* (London), **83**, 889 (1964).

[6] R. F. Barrow and W. J. M. Gissane, *ibid.* **84**, 615 (1964).

[7] Dr. R. F. Barrow kindly provided the latest results of his group's analysis of the singlet systems before publication. This included several excited states not given in ref 5 and 6.

However, in the ethanol system there is evidence that the reaction similar to (3) occurs to a significant extent in the liquid but not in the gas phase.[19] This appears to be due to the fact that the hydrogen bonding present in the liquid phase could not aid the formation of the transition complex I in the gas phase.[19]

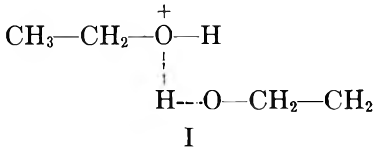

$$\begin{array}{l} CH_3—CH_2—\overset{+}{O}—H \\ \qquad\qquad\quad\; \vdots \\ \qquad\qquad\quad\; H\cdots O—CH_2—CH_2 \end{array}$$

I

Hydrogen bonding in ethyl mercaptan occurs to a much lesser extent than in ethyl alcohol due to the significantly smaller electronegativity of the sulfur atom as compared to the oxygen atom. Therefore, the formation of the transition complex necessary for reaction 3 is not as likely in liquid mercaptan as it is in liquid ethanol and, therefore, this mechanism for H_2 is relatively less important.

The various bond strengths (in kilocalories) that have been reported (or estimated) for the ethyl mercaptan and alcohol molecules are listed in Table I.[20,21] The bond strengths that were estimated for the ethanol molecule were arrived at as follows. The C–H value for the methyl group was assumed to be that quoted for ethane by Cottrell,[22] who also cited a 6-kcal difference in dissociation energy for the primary and secondary C–H bonds in propane. Hence, the approximate value of 90 kcal for the C–H bond in the methylene position for ethanol is given. The C–C bond strength is that quoted for ethane.[22] The corresponding bond strengths for the mercaptan molecule will, in all likelihood, be somewhat greater due to the sulfur atoms' smaller electronegativity. These figures, while approximate, should give a reasonable estimate of the relative bond strengths for the molecules.

Table I

Type of bond	Bond strength, kcal
Ethanol	
O–H	99[a]
C–O	90[a]
C–C	83[b]
C–H(methylene)	90[b]
C–H(methyl)	96[b]
Ethanethiol	
S–H	87[c]
C–S	73[c]

[a] See ref 20. [b] Estimated bond strength, see text. [c] See ref 21.

It thus appears that the O–H bond in the alcohol is the strongest and methylene C–H bond is the weakest among the bonds to hydrogen atoms. This supposition is supported by the esr spectra of ethyl alcohol[23,24] at 77°K and the nature of the major liquid products from the radiolysis.[3,16]

Both these types of data indicate that at some stage in the radiolysis CH_3CHOH is present in appreciable quantities. On the other hand, the S–H bond in the mercaptan appears to be the most labile of all bonds to hydrogen in both molecules. It is possible that the greater hydrogen yield is due to the relatively great ease of abstraction by hydrogen atoms (produced by reaction 5 and/or other reactions) from the S–H group.

The lability of the bond to the sulfhydryl hydrogen atom should result in products that attest to the presence of CH_3CH_2S radicals in the system. Diethyl disulfide and diethyl sulfide constitute 95% of the condensation products while the 1,2-dithiol was not observed. As the formation of these products is most easily explained by the combination of two ethylthiyl radicals and the combination of an ethylthiyl and an ethyl radical, respectively, the presence of thiyl radicals can be inferred.

Further evidence for the presence of thiyl radicals at some stage in the radiolysis can be obtained from data on mercaptan samples that were irradiated and subjected to esr analysis before and after photolysis with selected wavelengths at 77°K. These experiments show that the species giving rise to the original esr signal is converted by light to another paramagnetic intermediate which has been identified as CH_3CH_2S.[25] This interpretation is consistent with Truby's[26,27] work on disulfides in which he postulates that the esr spectrum of irradiated disulfides consists of contributions from ionic species (predominantly) and RS

---

(19) J. J. Myron and G. R. Freeman, *Can. J. Chem.*, **43**, 1484 (1965).

(20) P. Gray, *Trans. Faraday Soc.*, **52**, 344 (1956).

(21) J. L. Franklin and H. E. Lumpkin, *J. Am. Chem. Soc.*, **74**, 1023 (1952).

(22) T. L. Cottrell, "The Strengths of Chemical Bonds," Butterworth and Co. Ltd., London, 1958.

(23) H. Zeldes and R. Livingstone, *J. Chem. Phys.*, **30**, 40 (1959).

(24) B. Smaller and M. S. Matheson, *ibid.*, **28**, 1169 (1958).

(25) S. B. Milliken, K. Morgan, and R. H. Johnsen, to be published.

(26) F. K. Truby, *J. Chem. Phys.*, **40**, 2768 (1964).

(27) F. K. Truby, D. C. Wallace, and J. E. Hess, *ibid.*, **42**, 2845 (1965).

Observations

Near-Infrared and Visible Absorption Spectrum. Two strong systems and a weak one at longer wavelength were observed in the absorption spectrum of ScF in a neon matrix at 4°K. They are shown in Figure 1. The (0,0) transitions of these three progressions lie at 4792, 6227.5, and $\geq$9405 A. The observed transitions are listed in Table I along with the higher v' levels and derived vibrational frequencies in the upper electronic states. The rounded bands on the long-wavelength side of the bands in the infrared system (see Figure 1) are assumed to be a matrix effect because they have the same spacing as that system. However, it is possible that they are due to another lower-lying electronic state.

Table I: Observed Band Systems in the Absorption Spectrum of ScF in a Neon Matrix at 4°K

Band system	(v',v'')	λ, A	ν, cm^{-1}	$\Delta G_{v'+1/2}$
$E^1\Pi \leftarrow X^1\Sigma$	(0,0)	4792	20,862	605
	(1,0)	4657	21,467	597
	(2,0)	4531	22,064	
	(3,0)	4415		
$C^1\Sigma \leftarrow X^1\Sigma$	(0,0)	6227.5	16,053	580
	(1,0)	6010.5	16,633	574
	(2,0)	5810	17,207	571
	(3,0)	5623.5	17,778	566
	(4,0)	5450	18,344	560
	(5,0)	5288.5	18,904	553
	(6,0)	5138	19,457	547
	(7,0)	4997.5	20,004	~550
	(8,0)	~4864	~20,554	
$B^1\Pi \leftarrow X^1\Sigma$	(0,0)[a]	9405	10,630	592
	(1,0)	8909	11,222	584
	(2,0)	8468	11,806	568
	(3,0)	8079	12,374	564
	(4,0)	7727	12,938	563
	(5,0)	7405	13,501	558
	(6,0)	7111	14,059	

[a] The true (0,0) band of this system may be at longer wavelengths.

The ScF spectrum has been observed in the gas by Gurvich and Shenyavskaya[12] and investigated much more thoroughly by Barrow, *et al.*[5,6] Their analysis indicates that the three matrix systems are to be identified with transitions from a $^1\Sigma$ ground state. Table II gives a comparison of the gas and neon matrix data. Unfortunately, our instrumentation was as limited in the near-infrared as was that of Barrow, *et al.*, and we were not able to establish whether the band at 9405 A (10,630 cm^{-1}) was the (0,0) of the B $\leftarrow$ X system. The changes in the interatomic distances (Δr_0) in these transitions measured in the gas are also included in the table in order to suggest that extensive Franck–Condon envelopes are to be expected in the spectrum. The relative band intensities in these progressions will be discussed more fully below.

Table II: Comparison of Gas and Neon Matrix Data for the ScF Molecule

Transition[a]	Gas		Neon matrix		Δr_0 (gas),[b] A
	T_{00}, cm^{-1}	$\Delta G_{1/2}$, cm^{-1}	T_{00}, cm^{-1}	$\Delta G_{1/2}$, cm^{-1}	
$E^1\Pi \leftarrow X^1\Sigma$	20,326.8	614.7	20,862	605	0.078
$C^1\Sigma \leftarrow X^1\Sigma$	16,092.0	584.3	16,053	580	0.119
$B^1\Pi \leftarrow X^1\Sigma$	$\leq$10,661.3	$\geq$582.4	$\leq$10,630	$\geq$592	$\leq$0.132

[a] Assignments are those given in ref 5 and 7. The designation of the upper states as B, C, and E was suggested by Dr. Barrow. [b] From ref 5 and 7.

It was observed that the shapes of the bands in the $C^1\Sigma \leftarrow X^1\Sigma$ transition slowly changed while the absorption spectra were being measured. These bands are about 20 cm^{-1} wide at half-height. Irradiation with tungsten light caused a gradual decrease in the intensity of the main spike in each band and the successive appearance of new spikes about 13 cm^{-1} apart on the short-wavelength side of each band. The initial stage of this change in shape is illustrated in Figure 2. Although exact measurements were not made, there was not any noticeable decrease in the over-all intensity of each band, thus indicating the absence of diffusion. Upon warming the matrix to about 12°K and requenching to 4°K, the side spikes disappeared and the band reverted back almost to its initial appearance. It is therefore concluded that these side bands are due to the formation of new metastable sites for the ScF molecule in the matrix, formed as a result of electronic excitation. The $E^1\Pi \leftarrow X^1\Sigma^+$ progression has broader bands (~60 cm^{-1} wide at half-height), and it is difficult to choose the peak of a band to within $\pm$1.5 A. Because of this, the light effect becomes noticeable only after considerable changeover of intensity has taken place. The band peak positions appear to shift by as much as 70 cm^{-1} after irradiation but toward longer wavelengths.

The relative intensities of the bands in two progressions were measured as described in the Experimental Section and are given in Table III. Measurements on

---

(12) L. V. Gurvich and E. A. Shenyavskaya, *Opt. Spectry.* (USSR), **14**, 161 (1963).

Multiple Knudsen Cell Effusion. Enthalpies of Vaporization of Indium and Gallium[1]

by G. J. Macur, R. K. Edwards, and P. G. Wahlbeck

Department of Chemistry, Illinois Institute of Technology, Chicago, Illinois 60616 *(Received March 28, 1966)*

In order to determine several vapor pressures at one well-defined temperature, several Knudsen cells were heated simultaneously in a massive molybdenum block which served to provide a uniform temperature environment. With this multiple-cell technique, it was hoped that the precision in a set of vapor pressure measurements determined in a single isothermal experiment would be better than that achieved in individual pressure measurements. The vapor pressures of liquid indium and gallium were determined. The precision of pressure measurements was better than what is usually achieved with the Knudsen method. The standard enthalpies of vaporization of indium and gallium at 298°K were found to be 56.58 ± 0.10 and 64.62 ± 0.22 kcal/g-atom, respectively; these values agree well with the literature values.

I. Introduction

The Knudsen effusion method has been used extensively for the determination of vapor pressures of materials at high temperatures. In many experiments it would be desirable to determine a set of vapor pressures at one fixed temperature. Examples are (1) the evaluation of activities, through vapor pressure measurements at a given temperature, of components of an alloy as a function of composition, *e.g.*, activities for the Cu–Au system by Edwards and Brodsky;[2] (2) the evaluation of nonideality effects of effusion orifices, *e.g.*, the study by Freeman;[3] and (3) the evaluation of effects due to variation of orifice areas, *e.g.*, the nonunit vaporization coefficient. At elevated temperatures there is a considerable error in temperature measurement, and it is very difficult to reproduce temperatures. Therefore, it is most difficult to achieve highly precise agreement in a set of isothermal vapor pressure values which are taken from individual measurements. A higher precision should be achieved when several cells are used simultaneously in an isothermal enclosure. In order to have many Knudsen cell measurements at a well-defined temperature, 14 Knudsen cells were placed in a large molybdenum block. Thus, it was possible to obtain 14 vapor pressure measurements simultaneously at one temperature.

The measurements of vapor pressures of pure liquid gallium and indium reported here were performed in preparation for measurements of the activities of gallium and indium in Ga–In liquid solutions.[1] Standard enthalpies of vaporization of liquid gallium and indium have been calculated from these vapor pressures.

II. Experimental Section

Apparatus. The apparatus as used in this experiment is shown in Figure 1. It consisted of a high-speed vacuum pumping system, an inert gas inlet system, pressure gauges, an electrical furnace with a temperature controller, a temperature-measuring device, and a set of Knudsen cells in a thermostating molybdenum block.

The vacuum pumping system consisted of an oil diffusion pump with forevacuum produced by a mechanical pump. Argon could be admitted through the stopcock at the top of the apparatus. The Philips gauge was used to measure pressures below 1 torr, and

---

[1] Based on a thesis by G. J. Macur, submitted to the Illinois Institute of Technology in partial fulfillment of the requirements for the Ph.D. degree, June 1965.

[2] R. K. Edwards and M. B. Brodsky, *J. Am. Chem. Soc.*, 78, 2983 (1956).

[3] R. D. Freeman, Technical Document No. ASD-TDR-63-754, 1963. He has attempted to establish isothermal conditions for effusion by heating eight Knudsen cells simultaneously in a thermostated block.

cury arc produced strong fluorescence of the $C^1\Sigma \rightarrow X^1\Sigma$ system. This was true whether the filtered light was in the range of 4900 to 6200 A (exciting the $C \leftarrow X$ system) or in the range of 3900 to 5000 A (exciting the $E \leftarrow X$ system). The most intense emission spectrum (see Figure 3) was obtained when the exciting light was in the range of 2400 to 4000 A. This was unexpected since, as noted above, the ScF absorption systems appear to be weak in the ultraviolet, unless the intense 3366-A absorption band is due to ScF.

In the fluorescence spectrum, one observes the expected (0,0), (0,1), and (0,2) transitions of the $C \rightarrow X$ system and those transitions seen in absorption, *i.e.*, (1,0), (2,0), (3,0), and (4,0). Other weaker transitions also appear, perhaps between excited vibrational levels in the two states. The observed frequencies are given in Table V. Notice that $\Delta G_{1/2}$ in the ground $^1\Sigma$ state is 720 cm^{-1} in the matrix as compared to 727.9 cm^{-1} in the gas.[5,7]

Table V: Fluorescence Bands of the ScF Molecule in a Neon Matrix at 4°K

(v',v'')	λ, A	ν, cm^{-1}	$\Delta\nu$, cm^{-1}
	$C^1\Sigma \rightarrow X^1\Sigma$		
(4,0)	5446	18,357	559
(3,0)	5617	17,798	564
(2,0)	5801	17,234	573
(1,0)	6000.5	16,661	586
(0,0)	6219	16,075	719
(0,1)	6510.5	15,356	713
(0,2)	6828.5	14,643	
	Other Weaker Bands		
	5491	18,207	
	5666	17,644	
	5854	17,078	
	5962.5	16,767	
	5977.5	16,725	
	6273.5	15,936	
	6329.5	15,795	

As can be seen from Figure 3 the distribution of intensity among the bands corresponding to the (4,0), (3,0), (2,0), (1,0), and (0,0) transitions is a maximum at (2,0), as in the absorption spectrum. This indicates that the vibrational levels in the upper state are approximately equally populated during emission, and that vibrational relaxation times are long in these levels. This may be modified slightly by the photomultiplier response which begins to drop off rapidly in the region of 6200 A and at longer wavelengths. For this reason the (0,0), (0,1), and (0,2) transitions do not have the expected intensity distribution.

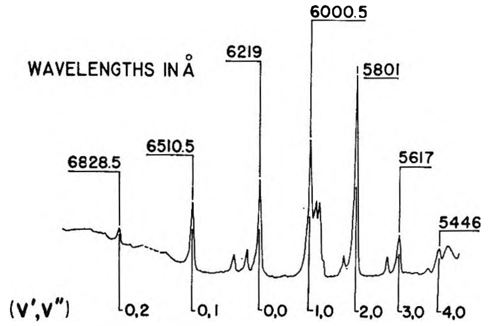

Figure 3. Emission spectrum of ScF in a neon matrix at 4°K (excitation: high-pressure mercury arc in the range of 2400–4000 A).

Spectral changes during excitation of fluorescence were not observed, but it is believed that all of the molecules were emitting from a metastable site. Evidence of this is given by the reproducible small shift, about 25 cm^{-1} to the blue, of the (0,0), (1,0), etc., emission bands relative to the absorption positions. This is in accord with an accelerated changeover of molecules to a metastable site in the neon matrix during the intense irradiation with mercury light. Some of the "other weaker bands" in Table V show differences which indicate that they could be attributed to the (5,1), (4,1), (3,1), (1,1), and (2,2) transitions of the $C \rightarrow X$ system. However, their relative intensities and the missing (2,1) band make this assignment questionable.

The doublet at 5962.5 and 5977.5 A on the short-wavelength side of the (1,0) band in Figure 3 does not always appear that strongly. If irradiation is in the 4000–6000-A range, an intense sharp band at 5950.5 A (16,801 cm^{-1}) appears instead. A smaller band is also observed at 6184.5 A (16,165 cm^{-1}). If this difference of 636 cm^{-1} may be taken as the vibrational frequency in the lower state, it is very close to the value of $\Delta G_{1/2} = 642.9$ cm^{-1} given by Barrow and Gissane[6] for the $^3\Delta_r$ state of ScF. Then this strong emission band may be a (0,0) transition in the triplet–triplet manifold. However, it is unlikely that the upper level is the $^3\Phi_r$ observed in the gas since the matrix shift would be about +1523 cm^{-1} which is rather large.

Infrared Spectra. The vibrational spectrum of the ScF molecule was not detected in the infrared region because it was difficult to prepare a concentrated matrix. (Apparently it absorbs strongly in the visible so that a low concentration suffices for good spectra in that region.) The fluorescence spectrum shows that the ground-state vibrational frequency is 720 cm^{-1} in a neon matrix, but bands near that frequency in the infrared were always attributable to other molecules, probably ScF_2 or ScF_3.

Vaporization of ScF_3 from a tungsten cell at 1600° gave a neon matrix exhibiting five infrared bands at 726 cm^{-1} (medium), 709 (very strong), 661 (weak), 482 (weak), and 446 (?) (very weak). If scandium metal was added to the ScF_3 and the mixture vaporized at 1350°, these same bands were observed with essentially the same relative intensities, but a separate band at 704 cm^{-1} (medium) also appeared on the side of the strong 709-cm^{-1} band. The frequency of this new band and the fact that only very weak ScF bands appeared in the visible region indicate that it cannot be attributed to ScF. It remains unidentified.

Lacking positive mass spectrometric identification of the vaporizing molecules, we can only conjecture that the five bands are absorptions of ScF_2 and ScF_3. If ScF_3 is planar and of D_{3h} symmetry, then one predicts[13] its infrared-active frequencies to be roughly 790 and 370 cm^{-1} (E′) and 280 cm^{-1} (A_2''). If ScF_2 is bent, two stretching frequencies in the region of 600–800 cm^{-1} are expected, but if it is linear, only one will appear. One might then assign the 726-, 482-, and 446-cm^{-1} frequencies to ScF_3, and the 709- and 661-cm^{-1} frequencies to ν_3 and ν_1, respectively, of a slightly bent ScF_2 molecule.

When vaporization took place from the graphite double cell such as to yield good ScF spectra in the visible, many more bands appeared in the infrared, both in the 700-cm^{-1} region and in the 1000–1300-cm^{-1} region. The bands at higher frequencies are presumably due to C–F bands[14] since the temperature of the hot chamber of the double cell is high enough that C_3 bands are observed in the visible spectrum.

Franck–Condon Factors

Because the ScF spectra show such broad Franck–Condon envelopes of well-separated bands, they are ideal for measurements of relative intensities, particularly the $C^1\Sigma \leftarrow X^1\Sigma$ transition. The results of such measurements are given in Table III. The relative intensities of the bands within the progressions shown in Figure 1 are determined principally by the Franck–Condon factors of the two electronic states involved. These factors are, in turn, dependent principally upon the change in the interatomic distance, Δr, during the excitation process and to a lesser extent upon the vibrational anharmonicity in the two states.

The probability of a transition $v' \leftarrow v''$ in absorption is proportional to

$$E_{v'v''}|\Psi_{v'}(r)R_e(r)\psi_{v''}(r)\ dr|^2 \cong E_{v'v''}\bar{R}_e{}^2|\psi_{v'}\psi_{v''}\ dr|^2 \quad (1)$$

where $E_{v'v''}$ is the energy of the transition, $R_e(r)$ is the electronic transition moment for which $\bar{R}_e$ is an average value, and $\psi_{v'}(r)$ and $\psi_{v''}(r)$ are the vibrational wave functions in the upper and lower states, respectively. The approximation of factoring our $\bar{R}_e$ is a usual practice and has been thoroughly discussed elsewhere.[15] The last squared integral in eq 1, containing only the vibrational wave functions, is the Franck–Condon factor $q_{v'v''}$. Then the ratio of the intensity of any band to that of the (0,0) band in a progression of v' values is given to this approximation by $I_{v'0}/I_{00} = E_{v'0}q_{v'0}/E_{00}q_{00}$. The ratio of $q_{v'0}/q_{00}$ is then directly obtained from the relative intensities measured in the matrix spectra. These experimental matrix ratios may be compared with calculated values from gas data, or, what is more meaningful, the Δr_e values derived from these ratios can be compared with those measured in the gas. We will briefly explain our derivation of Δr_e values from the measured Franck–Condon factor ratios.

The method used here to calculate $q_{v'v''}$ values was the subject of two papers by Fraser and Jarmain.[16,17] It utilizes Morse potential functions for the upper and lower electronic states. Their "r_0 shift" procedure[17] was used because of the relatively large changes in anharmonicity, $\omega_e x_e$, in the ScF transitions. Δr_e enters into their equations in the form of $[\exp(-\alpha\Delta r_e)]$, where α is the arithmetic mean of the Morse anharmonicity constants for the upper and lower states. The values of $\omega_e x_e$ are not very well determined from matrix spectra (see Tables I and V), but average values can be derived as about 4.0, 2.5, and 3.5 cm^{-1} for the E, C, and X states. These agree quite well, which is probably fortuitous, with those obtained in the gas by Barrow, *et al.*,[7] 4.1, 2.64, and ~3.3 cm^{-1}, respectively. As mentioned earlier the calculated ratios of Franck–Condon factors are quite sensitive to the value of Δr_e used in the equations, whereas they are much less sensitive to the values of $\omega_e x_e$ employed.

The values of Δr_M necessary to reproduce the measured matrix ratios as given in Table III are compared with the accurate gas values, Δr_G, in Table VI. Discrepancies occur only in the third place and amount to about 7% of Δr_G at most. Variation of $\omega_e x_e$ values by ±1 cm^{-1} from those given above cause variations in Δr_M of about ±0.001 A. Other possible sources of

---

[13] The ScF_3 frequencies were calculated from the stretching force constant of ScF (k = 4.06 × 10^5 dynes/cm) and assuming k_δ/l^2k = 0.094.

[14] See, for example, those for CF_2 given by D. E. Milligan, D. E. Mann, M. E. Jacox, and R. A. Mitsch, *J. Chem. Phys.*, **41**, 1199 (1964).

[15] R. W. Nicholls and A. L. Stewart, "Atomic and Molecular Processes," D. R. Bates, Ed., Academic Press Inc., New York, N. Y., 1962, Chapter 2.

[16] P. A. Fraser and W. R. Jarmain, *Proc. Phys. Soc.* (London), **A66**, 1145 (1953).

[17] W. R. Jarmain and P. A. Fraser, *ibid.*, **A66**, 1153 (1953).

error in the calculation, *i.e.*, uncertainties in ω_e, $E_{v'v''}$, etc., are of no importance. The increasing discrepancy between Δr_M and Δr_G at higher v' may arise from several causes involving both inaccuracies in the theory and the experiments. Inadequacies in the theory are the use of Morse potential functions and the neglect of variations of R_e with r.[18] The measurement of intensities in the matrix spectra may be in error because of our method of choosing a background line. However, it is possible that the difference between Δr_M and Δr_G is real and that the matrix environment affects the change of interatomic distance in the trapped molecule to that extent.

Table VI: Δr_M (Matrix) Compared with Δr_G (Gas) for ScF (Angstrom Units)

(v',v'')	$\Delta r_G - \Delta r_M$
$C^1\Sigma \leftarrow X^1\Sigma$ (observed $\Delta r_G = +0.119$ A)[a]	
(1,0)	$+0.002 \pm 0.002$
(2,0)	-0.006
(3,0)	-0.004
$E^1\Pi \rightarrow X^1\Sigma$ (observed $\Delta r_G = +0.078$ A)[a]	
(1,0)	-0.004
(2,0)	-0.006

[a] These are Δr_0 values obtained from the gas data of Barrow, *et al.*[5,7] The difference between Δr_0 and Δr_e is negligible here.

Discussion

The matrix absorption spectrum of ScF indicates that it has a $^1\Sigma^+$ ground state as compared to a $^3\Delta_r$ ground state for the isoelectronic molecule TiO. In the latter case the lowest state arises from a $\delta\sigma$ configuration, where the σ and δ molecular orbitals have almost the same energy.[3a,4] In ScF the σ orbital is then lower than the δ to a sufficient extent that the σ^2 configuration and $^1\Sigma^+$ ground state are the most stable, as in ZrO.[3a] The $\sigma\delta$ states, $^3\Delta$ and $^1\Delta$, must, however, be very low lying. There is always the possibility that for two electronic levels of nearly the same energy, such as the $^1\Sigma^+$ and $^3\Delta_r$ levels of ScF, matrix perturbations could invert the order of the energy levels in the gas. One can only defend the conclusions drawn from matrix spectra by noting that there is no established case of such an occurrence.[19]

The electronic transitions observed in the matrix are attributed to excitation from the $X^1\Sigma(\sigma^2)$ state to the $B^1\Pi(\sigma\pi^*)$, $C^1\Sigma^+(\pi^3\pi^*)$, and $E^1\Pi(\pi^3\delta)$ levels, in analogy with the singlet states of TiO and ZrO.[3a] [The letters used for these states were suggested by Barrow[7] since in analogy with TiO one also expects a low-lying $A^1\Delta$ $(\sigma\delta)$ level and a $D^1\Phi$ $(\delta\pi^*)$ level, to which the transitions are not allowed from the ground state.] The simple crystal-field model previously discussed[3a,20] must be modified by the inclusion of 4pπ and 4pσ levels of the metal atom as in the theoretical work of Carlson, Nesbet, and Moser[4] and of Carlson, Ludeña, and Moser.[21] This only means that the π^* orbital (see Figure 8 of ref 3a) used in the above configurations could be a 4pπ instead of a 3dπ^* orbital.

An interesting and disturbing feature of the matrix absorption spectrum is the rather large shift (+535 cm^{-1}) of the $E^1\Pi \leftarrow X^1\Sigma$ system of ScF relative to the gas. The spectra of many transition-metal diatomic oxides, including TiO, trapped in neon matrices show shifts in electronic-level spacings, but they are limited to +200 cm^{-1}.[3a,20] However, this same electronic transition in the matrix has not been identified for ZrO or HfO (of course, it would not appear for TiO), so that a more meaningful comparison cannot be made. There is no doubt that the E ← X transition of ScF in the gas is being observed in the matrix; the agreement between observed and calculated ratios of Franck–Condon factors reassures us of that. The upper level of this transition is apparently experiencing a larger matrix effect than other excited levels. Even larger shifts have been observed in the ScO, YO, LaO series[22] where the bands were also found to be broader than those in the E ← X transition, but the theoretical picture for these oxides[21] does not indicate that there is correlation between their transitions and excited states and those of ScF.

There is another interesting "matrix effect" observed in the spectra of ScF. It is the change of the sites for ScF molecules in the lattice to new metastable sites when the matrix is exposed to visible light. This is manifested by the gradual appearance of two or three new bands on the high-frequency side of each of the relatively sharp bands of the C ← X system at intervals of about 13 cm^{-1}. Presumably the same thing is occurring in the E ← X system except that one observes those broader bands to move toward the red and ultimately shift by as much as 70 cm^{-1}. Similar but different effects have been observed in matrices of ScO,

---

[18] P. A. Fraser, *Can. J. Phys.*, **32**, 515 (1954).

[19] C_2 is the only molecule for which there is evidence of trapping in an excited electronic state. [See G. W. Robinson "Methods of Experimental Physics," Vol. 3, "Molecular Physics," D. Williams, Ed., Academic Press Inc., New York, N. Y., 1962, p 233]. However, recent evidence obtained in these laboratories indicates that the C_2 molecule is probably not being observed in that case. This work is about to be submitted for publication.

[20] W. Weltner, Jr., and D. McLeod, Jr., *J. Chem. Phys.*, **42**, 882 (1965).

[21] K. D. Carlson, E. Ludeña, and C. Moser, *ibid.*, **43**, 2408 (1965).

[22] W. Weltner, Jr., D. McLeod, Jr., and P. Kasai, to be published.

YO, and LaO.[22] Unfortunately, in the case of ScF the light was not filtered to allow the excitation of only one electronic transition at a time. One wonders whether all excited states are equally effective in causing the shifts and whether an exceptionally large change of Δr (as in the $C^1\Sigma \leftarrow X^1\Sigma$ transition) might also be influential. Irradiating in the ultraviolet (~2400 to 4000 A) during fluorescence did appear to cause also a shift of the emission of the $C \rightarrow X$ system relative to the absorption by about 20 cm^{-1} to the blue.

The excellent agreement between Δr values for the $C^1\Sigma \leftarrow X^1\Sigma$ and $E^1\Pi \leftarrow X^1\Sigma$ transitions obtained from the relative intensities of bands in the matrix spectra of ScF and those obtained from rotational analysis of the gas spectrum is gratifying (see Table VI). The conversion of relative intensities to Δr values involves the assumption that R_e, the electronic transition moment, is relatively independent of r. This is usually true but there can be large divergencies as discussed, for example, by Halevi.[23] Our calculations indicate that the assumption is valid for ScF to within the accuracy of our observations. That accuracy does not allow anything to be said about the effect of the matrix on the Δr values, except that it cannot be large.

Acknowledgments. The authors thank Professor R. F. Barrow for his helpful correspondence concerning the gas phase spectroscopy and Professor K. D. Carlson for a discussion of his recent theoretical work on the ground state of ScF.

---

[23] P. Halevi, *Proc. Phys. Soc.* (London), **86**, 1051 (1965).

The Double Layer at the Mercury–Formamide Interface

by G. H. Nancollas, D. S. Reid, and C. A. Vincent[1]

Department of Chemistry, State University of New York at Buffalo, Buffalo, New York, and Department of Chemistry, The University, Glasgow, Scotland *(Received May 23, 1966)*

The differential capacitance of the electrical double layer at the interface between the dropping mercury electrode and solutions of potassium chloride (0.05, 0.071, 0.100, and 0.500 *m*), lithium chloride (0.100 *m*), cesium chloride (0.100 *m*), sodium chloride (0.100 *m*), and rubidium chloride (0.100 *m*) in formamide at 25° has been measured. Differential capacitance measurements have also been made on solutions of potassium chloride (0.100 *m*) and cesium chloride (0.100 *m*) in formamide at 5 and 45°. Determinations of the interfacial tension have been carried out using a capillary electrometer. Relative surface excesses of chloride ion and potassium ion have been calculated from the results and evidence is advanced indicating specific adsorption of potassium ions at the dropping mercury electrode–formamide interface. The capacitance–charge curves show a characteristic hump at more cathodic potentials than in aqueous solutions, and the shapes of these curves are discussed in terms of current theory.

Introduction

The measurement of electrical capacitance offers one of the most sensitive methods for studying the structure of the double layer at a metal–solution interface. Most of the work has been done with aqueous systems, and there is now a considerable body of precise capacitance and interfacial tension data for the dropping mercury electrode in aqueous solutions of

---

[1] Visiting Lecturer, University of Illinois, Urbana, Ill.

electrolytes, particularly those of the alkali halides and oxy anions.[2] In the presentation of the theories of electrocapillarity, it is usually assumed that among the inorganic ions, the anions with the possible exception of fluoride ions are capable of superequivalent or specific adsorption while the concentration of the cation at the interface is determined purely by its charge. The possibility of specific adsorption of cations, particularly cesium ions, has been suggested by some workers,[3] but as yet no firm conclusions have been reached.

Another feature of the capacitance–potential curves for the dropping mercury electrode in aqueous solutions which awaits satisfactory explanation is the appearance of the characteristic "hump," usually slightly to the anodic side of the potential of zero charge (pzc). Watts-Tobin[4] and Macdonald and Barlow[5] considered the influence of solvent dipole orientation on the dielectric constant of the inner region of the electrical double layer to be of basic importance in the explanation of this phenomenon. Because of their proximity to the metal surface, and because they may be subjected to very large electrical fields, solvent molecules near the interface behave differently from those in bulk; under certain conditions orientation polarization is almost complete, and hence the dielectric constant in this region may fall to a very low value. It was suggested[4] that at the electrode surface there are two types of oriented water molecules, one with the oxygen toward the metal and the other with the hydrogen atoms directed toward the electrode. In terms of these models, the appearance of the hump in the capacity curve is connected with the changing orientation polarization of the adsorbed water molecules at positive polarization.

Hills and Payne,[6] who measured the surface excess entropy and volume for 0.10 M aqueous solutions of electrolytes, also connected the appearance of the hump with solvent structure at the interface. They considered the two opposing effects which would accompany adsorption of excess solvent molecules into the compact double layer, namely (i) increase in the distortional component of the polarizability with increase in surface density of dipoles, and (ii) increase in the thickness of the compact double layer.

Other workers have postulated that the capacitance hump is due to effects associated with specific adsorption of anions at the mercury–solution interface. Thus, Damaskin, Schwartz, and Frumkin[7] considered polarization of solvent molecules by anions adsorbed into the inner Helmholtz plane, while Bockris, Devanathan, and Muller[8] suggested lateral repulsion between such anions as the main factor.

Study of the capacity hump in aqueous solution is sometimes made difficult since it may be obscured by strong specific adsorption of anions. Recently,[9–12] a similar maximum in the capacity–charge curve has been found for some alkali metal halides in nonaqueous solvents. In formamide, an excellent polar solvent, this occurs at potentials considerably more negative than the potential of zero charge and it is thus less easily masked by anion specific adsorption. In such solvents, quite different ion–solvent interactions are to be expected from those in aqueous solutions.

In the present work, the differential capacity of the dropping mercury electrode has been measured in formamide solutions of lithium, sodium, potassium, rubidium, and cesium chlorides as a function of concentration and temperature. Interfacial tension measurements have also been made using a capillary electrometer.

Experimental Section

Formamide was first saturated with ammonia gas and filtered to remove any precipitated ammonium formate. It was then distilled six times under vacuum at temperatures below 60° to avoid decomposition, and stored under nitrogen. The pure formamide has a melting point of 2.5°, close to the literature value of 2.55°. Analar potassium, rubidium, cesium, and sodium chlorides were all recrystallized three times from conductivity water and dried at 300° just prior to use. Lithium chloride was recrystallized three times from dry ethanol, and the ethanol was removed by gentle heating in a stream of dry nitrogen. The solid was heated to constant weight at 120° and stored under nitrogen. Just before use it was heated again to 240°. All solutions were made up by weight in a drybox filled with nitrogen, and their densities were found by using a pycnometer. Mercury was purified by triple distil-

---

(2) D. C. Grahame, *Chem. Rev.*, **41**, 441 (1947); *J. Electrochem. Soc.*, 98, 343 (1951); 99, 370C (1952); *J. Am. Chem. Soc.*, **74**, 4422 (1952); **76**, 4819 (1954); **79**, 2093 (1957).

(3) B. B. Damaskin, N. V. Nikolaeva-Fedorovich, and A. N. Frumkin, *Dokl. Akad. Nauk SSSR*, **129**, 121 (1958).

(4) R. J. Watts-Tobin, *Phil. Mag.*, **6**, 113 (1961).

(5) J. R. Macdonald and C. A. Barlow, Jr., *J. Chem. Phys.*, **36**, 3062 (1962).

(6) G. J. Hills and R. Payne, *Trans. Faraday Soc.*, **61**, 316 (1965).

(7) B. B. Damaskin, E. Schwartz, and A. N. Frumkin, *Zh. Fiz. Khim.*, **36**, 2419 (1962).

(8) J. O'M. Bockris, M. A. V. Devanathan, and K. Muller, *Proc. Roy. Soc.* (London), **A274**, 55 (1963).

(9) C. A. Vincent, Ph.D. Thesis, Glasgow University, Scotland, 1963.

(10) R. Payne, *J. Chem. Phys.*, **42**, 3371 (1965).

(11) B. B. Damaskin and Yu. M. Povarov, *Dokl. Akad. Nauk SSSR*, **140**, 394 (1961).

(12) S. Minc and M. Brzostowska, *Roczniki Chem.*, **38**, 301 (1964).

lation under reduced pressure after standard chemical treatment, and was stored under nitrogen.

Impedance measurements were made with the self-timing transformer ratio-arm bridge method described in a previous paper.[13] The only modification made was the repositioning of the two 1000-μf blocking capacitors (see Figure 4 in ref 13) so that they were connected between the transformer ratio-arm bridge and the selector switch. Conversion from the measured parallel combination of impedances to the equivalent series combination was made with the aid of a KDF 9 computer (English Electric) using the method described previously.[14]

The cell and general experimental procedure were similar to that outlined in a previous paper,[14] and precautions were taken to prevent moisture from entering the cell at any time. Considerable attention was given to the choice of electrode for use as a reference in these nonaqueous solutions. Although many workers use an aqueous reference electrode necessitating an aqueous–nonaqueous liquid junction, it was felt to be undesirable to introduce an additional uncertainty from this source. The silver–silver chloride electrode has been shown to behave reversibly in formamide solutions,[15] and it was therefore used as the reference electrode dipping directly into the cell solution. The electrodes were prepared by the thermal electrolytic method,[16] washed thoroughly with formamide containing a small quantity of potassium chloride, and allowed to age in the dark for several weeks in a similar solution.

Electrocapillary maximum potentials were determined by method V described by Grahame and his coworkers[17] using a streaming mercury electrode in deaerated cell solutions. The highest attainable potential was taken as that of the electrocapillary maximum.

The capillary electrometer was enclosed in an air thermostat and was similar to that described by Parsons and Devanathan.[18] It incorporated the same reference electrode system as for the capacity measurements, and all solutions were presaturated with nitrogen. The pressurizing system consisted of two large reservoirs containing mercury, one of which was connected to the mercury reservoir of the capillary and to a manometer. The pressure in the system could be sensitively controlled by raising and lowering the reservoir with a micrometer screw. The tip of the capillary was drawn by the method suggested by Conway and Barradas,[19] and the illuminated mercury meniscus, viewed with a travelling microscope, was brought to a position 1.000 mm above the capillary tip each time. A drop of mercury was expelled between each measurement. The heights of the mercury columns were measured with an accuracy of 0.02% on a cathetometer, and the apparatus was calibrated by measuring interfacial tensions in 0.1 *N* potassium chloride aqueous solutions and comparing the results with those of Devanathan and Peries.[20] The results of duplicate experiments in formamide solutions were reproducible to with ± 0.2 erg cm^{-2} except at the most cathodic potentials, where the agreement was ± 0.5 erg cm^{-2}.

Results

The method used for applying back-pressure corrections has been described previously.[14] An approximate surface tension calculated from the drop weight is used to evaluate the equivalent constant rate of flow of mercury which would be obtained with the same mercury head in the absence of back-pressure. This is then used to calculate, by means of an iterative procedure on an electronic computer, the surface tension, the drop weight at any instant in the life of the drop, and the differential capacitance C_0.[14] Differential capacitances at different potentials, *E*, were determined for formamide solutions containing 0.1 *m* lithium, sodium, rubidium, and cesium chlorides, and 0.05, 0.071, 0.1, and 0.5 *m* potassium chloride at 25°. Some 0.1 *m* solutions of potassium chloride and cesium chloride in formamide were also studied at 5 and 45°. Each capacitance value is the averaged result of at least three runs under each set of conditions, the mean deviation being about 0.1%. Interfacial tensions at different potentials were determined for formamide solutions containing 0.05 and 0.10 *m* potassium chloride. In Table I are listed the potentials of the electrocapillary maximum, and Table II includes the potential, interfacial tension, and capacity at the electrocapillary maximum for three of the potassium chloride solutions. In 0.1 *m* solutions of lithium, sodium, rubidium, and cesium chlorides, no significant difference in electrocapillary maximum potential (ecm) was observed from that for potassium chloride at the same concentration and it is clear that the cation has

---

[13] G. H. Nancollas and C. A. Vincent, *J. Sci. Instr.*, **40**, 306 (1963).

[14] G. H. Nancollas and C. A. Vincent, *Electrochim. Acta*, **10**, 97 (1965).

[15] Yu. M. Povorov, Yu. M. Kessler, A. I. Gorbanev, and I. V. Safonova, *Dokl. Akad. Nauk SSSR*, **155**, 1411 (1964).

[16] V. S. K. Nair and G. H. Nancollas, *J. Chem. Soc.*, 4144 (1958).

[17] D. C. Grahame, E. M. Coffin, J. I. Cummings, and M. A. Poth, *J. Am. Chem. Soc.*, **74**, 1207 (1952).

[18] R. Parsons and M. A. V. Devanathan, *Trans. Faraday Soc.*, **49**, 673 (1953).

[19] B. E. Conway and R. G. Barradas, *Electrochim. Acta*, **5**, 319 (1961).

[20] M. A. V. Devanathan and P. Peries, *Trans. Faraday Soc.*, **50**, 1236 (1954).

Table I: Potentials of the Electrocapillary Maximum

Temp, °C	25	25	25	25	45	5
Molality of KCl	0.050	0.071	0.100	0.500	0.100	0.100
E_{ecm}, v[a]	−0.467	−0.465	−0.462	−0.457	−0.442	−0.477

[a] E is the potential of the cell Ag\|AgCl\|KCl in formamide (m)\|Hg.

Table II: Electrocapillary Maximum Data for Potassium Chloride Solutions in Formamide at 25°

Concn, m	E, v	γ, ergs cm^{-2}	C, μf cm^{-2}
0.050	−0.467	382.7	16.69
0.071	−0.465		17.52
0.100	−0.462	381.5	18.36

only a very small effect on the potential of the ecm as is the case in aqueous solution.[21]

The charge on the dropping mercury electrode, q, given by

$$q = \int_{E_{\text{ecm}}}^{E} C_0 \mathrm{d}E$$

was obtained by integration of the capacitance–potential curves. An electronic computer was used to fit the data to a polynomial of any chosen degree, and the closeness of fit was verified by comparing a plot of the polynomial with the experimental points; polynomials of degree six or eight were normally sufficient. The necessary integration constants were taken from the ecm potentials, and the integration was carried out by the computer. Plots of differential capacitance against charge at 25° are shown in Figures 1 and 2; the capacitance–charge curves for potassium and cesium chloride solutions at 5, 25, and 45° are given in Figure 3.

It was found that the maximum cathodic polarization which could be achieved before decomposition of the formamide, and accompanying current flow, depended markedly upon the purity of the solvent. With each successive fractional distillation at reduced pressure and a temperature below 60°, this cathodic region could be extended. In the present work the dropping mercury electrode was studied at charges beyond −20 μcoulombs/cm^2 in contrast to the maximum value of −14 μcoulombs/cm^2 achieved by Payne.[10]

Discussion

It is seen in Figures 1, 2, and 3 that the capacitance curves have a well-defined hump at considerably more cathodic potentials than in aqueous solutions, and similar observations have been made for potassium iodide[10] and fluoride[12] solutions in formamide. In the case of potassium chloride (Figure 2), the specific adsorption of chloride ion does not begin to seriously obscure the hump until quite high concentrations are reached (0.5 m). In aqueous solution this occurs at about 0.1 M. If the maximum in the curve is due to solvent dipole reorientation, this suggests that the formamide molecule has its most stable orientation with the positive pole of the solvent dipole directed away from the mercury surface. This is consistent with the expected most favorable orientation of the formamide molecule in which the oxygen atom is directed toward the mercury surface.

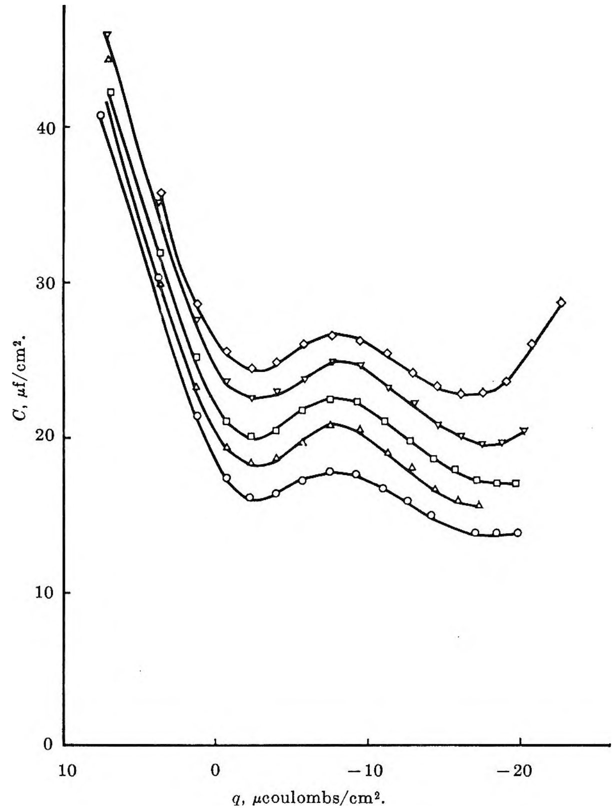

Figure 1. Differential capacitance of the electrical double layer at a mercury electrode in 0.1 m solutions of the alkali metal chlorides in formamide at 25°. For clarity, successive curves are displaced upward by 2 μf/cm^2. ○, LiCl; △, NaCl; □, KCl; ▽, RbCl; ◇, CsCl.

---

(21) D. C. Grahame, *J. Electrochem. Soc.*, 98, 343 (1951).

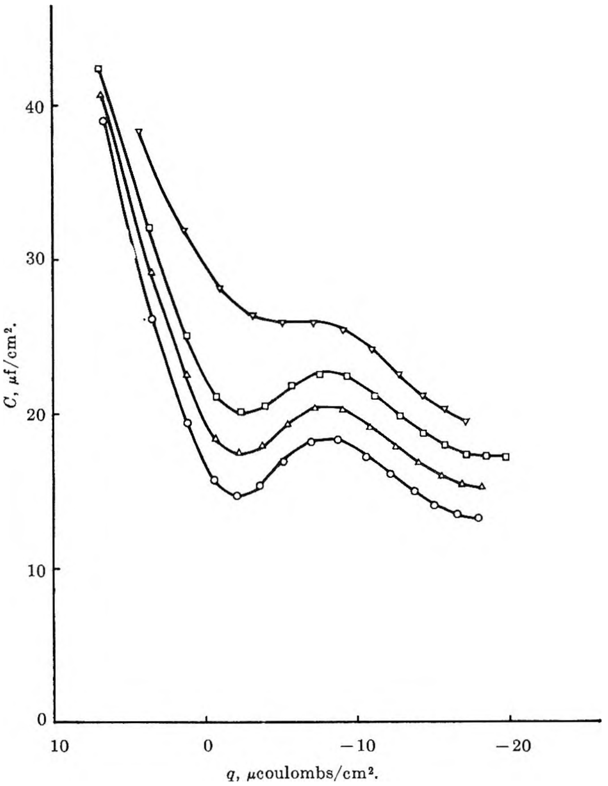

Figure 2. Differential capacitance of the electrical double layer at a mercury electrode in solutions of potassium chloride in formamide at 25°. For clarity successive curves are displaced upwards by 2 μf/cm². ○, 0.050 *m*; △, 0.071 *m*; □, 0.100 *m*; ▽, 0.500 *m*.

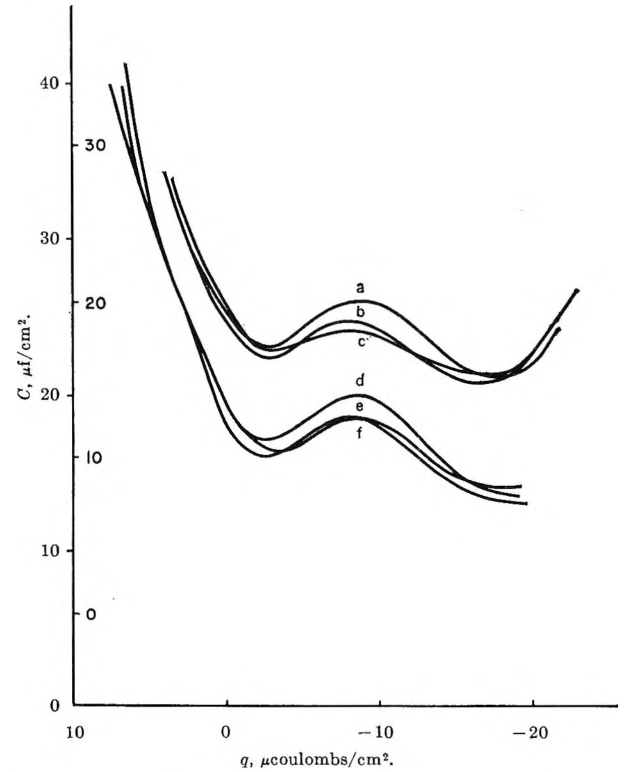

Figure 3. Differential capacitance of the electrical double layer at a mercury electrode in 0.1 *m* solutions of potassium chloride and cesium chloride in formamide as a function of temperature. The left ordinate scale refers to the curves for potassium chloride, that on the right to cesium chloride: a, 0.1 *m* CsCl, 5°; b, 0.1 *m* CsCl, 25°; c, 0.1 *m* CsCl, 45°; d, 0.1 *m* KCl, 5°; e, 0.1 *m* KCl, 25°; f, 0.1 *m* KCl, 45°.

In the far-cathodic region (Figures 1 and 3) there is a very noticeable effect of cation: the capacitance values in formamide fall in the order $K^+ < Na^+ < Li^+ < Rb^+ < Cs^+$. It is interesting that in every case a minimum in the capacity curve at large cathodic polarizations could be observed before the onset of solvent decomposition. The capacitance of cesium chloride and rubidium chloride rises much more rapidly than that of lithium chloride, whereas the rise in capacitance has barely begun for sodium chloride and potassium chloride. This difference is in marked contrast to the results in aqueous solution, and cannot be explained simply on the basis of compressional forces and size of solvated cation. It is of interest to note that a similar behavior has been observed in N-methylformamide solutions.[11]

In formamide solution of potassium iodide, Payne[10] did not take the applied potential to sufficiently negative values to observe the capacitance rise. The expected greater specific adsorption of iodide ions as compared with chloride ions, however, causes masking of the capacitance hump in the former solutions at very much lower electrolyte concentrations (about 0.05 *m* KI as compared with 0.5 *m* KCl).

The effect of temperature on the capacity curves for potassium chloride and cesium chloride is seen in Figure 3. The general lowering of the hump with increasing temperature is similar to that observed in aqueous solutions and has been explained qualitatively by attributing the phenomenon to the orientation of solvent molecules at the interface.[22] A feature of the curves in Figure 3 is that at the higher temperatures the curves intersect twice. At cathodic polarization, the curve at 25° is uniformly lower than at 5°, as would be expected on the basis of the higher specific adsorption of cation (discussed below) at the lower temperature. On the negative side of the hump, however, the 45° curve crosses that at 25°, as is consistent with the temperature dependence of the solvent orientation polarization term of the Watts-Tobin theory. It is very interesting to note that similar temperature-in-

---

[22] D. C. Grahame, *J. Am. Chem. Soc.*, 79, 2093 (1957).

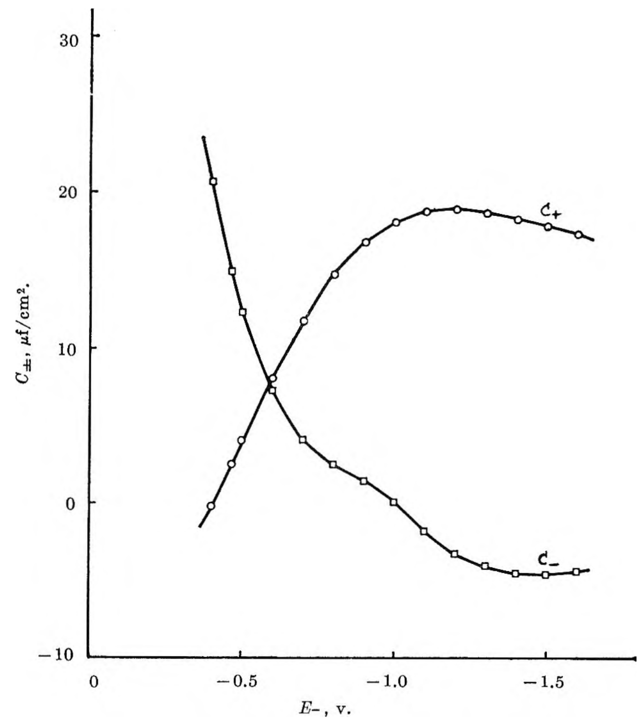

Figure 4. Contribution of anions (C_-) and cations (C_+) to the differential capacitance of the electrical double layer at a mercury electrode in 0.071 *m* potassium chloride in formamide at 25°.

duced double intersection of capacity–charge curves have recently been reported for aqueous 1 *N* solution of perchlorates; the effect in very concentrated solutions (9.3 *N*) was even more marked.[23]

The relative surface excess of anion, Γ_-, and cation, Γ_+, in potassium chloride solution at a concentration of 0.071 *m* was calculated by the method of Grahame and Soderberg.[24] The part of the differential capacitance attributable to the cations, C_+, was obtained by integration of $(\Delta C_0/\Delta \log a_{\pm})_{E_-}$ with respect to E_- using the mean activities given by Povarov, Kessler, and Gorbanev[25] for the evaluation of the mean activity $a_{\pm}$. The integration constant was based on the calculated value of C_+ at the electrocapillary maximum.

$$C_+^{\text{ecm}} = FC_0^{\text{ecm}}\left(\frac{\partial E_-}{RT\partial \ln a}\right)^{\text{ecm}}$$

since it was not possible to assume the absence of specific adsorption of cation at the most negative potential attainable, C_- was obtained from the relationship

$$C_0 = C_+ + C_-$$

and plot of C_+ and C_- against E_- are shown in Figure 4. Γ_+ was evaluated by integration of the C_+ *vs.* E_- curve, the integration constant being obtained from the relationship between the interfacial tension and the chemical potential at the electrocapillary maximum

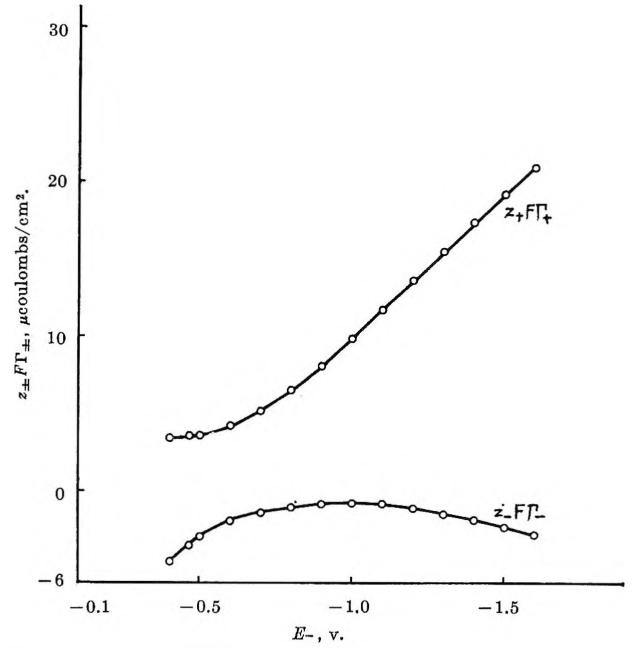

Figure 5. Relative surface excess of anions ($z_-F\Gamma_-$) and cations ($z_+F\Gamma_+$ in the electrical double layer at a mercury electrode in 0.071 *m* potassium chloride in formamide at 25°.

$$\left(\frac{\partial \gamma}{\partial \mu}\right)_{\text{ecm}} = -\Gamma_{\text{salt}} = -\Gamma_+ = -\Gamma_-$$

(for a 1:1 electrolyte)

Γ_- was obtained from the relationship

$$-q = z_+F\Gamma_+ + z_-F\Gamma_-$$

where $z_{\pm}$ is the valence of the ion, with the sign of its charge. The values of the surface excess agreed with those calculated from interfacial tension measurements to within the experimental error. Plots of Γ_+ and Γ_- as a function of E_- are given in Figure 5, and their shapes suggest superequivalent adsorption of the cation, although to a smaller extent than adsorption of the anion under the corresponding anodic conditions. In the case of cesium chloride, the marked rise in capacitance at cathodic potentials may reflect even more extensive superequivalent adsorption of the cation. It is of interest to note that Frumkin[26]

---

[23] V. F. Ivanov, B. B. Damaskin, A. N. Frumkin, A. A. Ivashchenko, and N. I. Feshkova, *Electrokhimiya*, **1**, 279 (1965).

[24] D. C. Grahame and B. A. Soderberg, *J. Chem. Phys.*, **22**, 449 (1954).

[25] Yu. M. Povarov, Yu. M. Kessler, and A. I. Gorbanev, *Izv. Akad. Nauk SSSR, Ser. Khim.*, 1895 (1964).

[26] A. N. Frumkin, B. B. Damaskin, and N. V. Nikolaeva-Fedorovich, *Dokl. Akad. Nauk SSSR*, **115**, 751 (1957); **121**, 129 (1958).

has interpreted the results of electrocapillary and differential capacitance measurements in aqueous cesium halide solutions in terms of similar cationic adsorption.

In an attempt to obtain a more quantitative explanation of the capacitance maximum in formamide, the Watts-Tobin theory for a mercury–water interface has been extended by taking into account the possibility of nonequivalent orientations of the solvent molecule at the mercury interface. The solvent contribution term in the Watts-Tobin theory

$$C_{\text{solvent}} = \frac{N\mu^2}{3d^2kT}\,\text{sech}^2\,\frac{\mu(\varphi - V)}{\sqrt{3}dkT}$$

in which the symbols have the same meaning as in ref 4, was recomputed assuming that the solvent dipole had the possible orientations θ and η with respect to the surface of the mercury. The resulting expression for C_{solvent}

$$C_{\text{solvent}} = \frac{N\mu^2(\sin\theta + \sin\eta)^2}{d^2kT} \times \frac{\exp\{(V - \varphi)\mu(\sin\theta + \sin\eta)/dkT\}}{[1 + \exp\{(V - \varphi)\mu(\sin\theta + \sin\eta)/dkT\}]^2}$$

reduces to the Watts-Tobin expression when $\sin\theta = \sin\eta = 1/\sqrt{3}$. Substitution of this extended C_{solvent} term into the Watts-Tobin expression for water was found to be insufficient to explain the results obtained for formamide. Accordingly, a fourth term of the form $(+N\mu_2^2/d^2kT)(C_1/C_0)^m \exp\{-\mu_2(\varphi + V_2)/dkT\}$ was added to allow for the contribution of superequivalent adsorbed cation to the capacitance. The final capacitance equation

$$C = \frac{K_0}{4\pi d} + \frac{N\mu_1^2}{d^2kT}\left(\frac{C_1}{C_0}\right)^m \exp\left\{\frac{\mu_1(\varphi - V_0)}{dkT}\right\} + \frac{N\mu_2^2}{d^2kT}\left(\frac{C_1}{C_0}\right)^m \exp\left\{\frac{-\mu_2(\varphi + V_2)}{dkT}\right\} + \frac{N\mu^2(\sin\theta + \sin\eta)^2 \exp(V - \eta)\mu(\sin\theta + \sin\eta)/dkT}{d^2kT[1 + \exp\{(V - \varphi)\mu(\sin\theta + \sin\eta)/dkT\}]^2}$$

was found to fit the results quite closely, but a final choice between this theory and that of Hills and Payne[6] cannot be made on the basis of the present data.

Acknowledgments. We thank the Carnegie Trust for the Universities of Scotland for a grant to D. S. Reid.

dihexyl sulfosuccinate),[6] being lowest and fairly constant at the highest detergent concentrations. For potassium laurate, the ratio is between 4 and 6,[2,4,7] but, for dodecylamine hydrochloride, it is between 1.0 and 2.2.[2,4]

If these measurements were made and interpreted correctly, solubilization ratios greater than unity could be due either to wrong mmw values or to the presence of impurities. Considering that one molecule of Orange OT can saturate a micelle, it should cause little surprise that suitable impurities contained in a technical grade detergent, though present only in relatively small amounts, could preempt a large fraction of the solubilizing capacity of the detergent for Orange OT.

In addition to studying the effect of known amounts of added impurities on the solubilizing capacity of pure detergents for Orange OT, it is necessary to establish that the solubilized dye does not change the micellar size.

Experimental Section

Materials. Purifications of Orange OT (1-*o*-tolylazo-2-naphthol) and of the nonionic detergent $C_{12}(EO)_{28}$ have been described.[1] Another nonionic detergent was prepared in the laboratories of General Aniline & Film Corp. by adding an average of 14 EO to 1-dodecanol and stripping out unreacted alcohol plus the lowest adducts, containing up to 5 EO, in a molecular still. The remaining material was freed from any glycols and salts it might have contained by ultrafiltration. The final product, designated $C_{12}(EO)_{16}$, contained 16.1 EO according to the infrared method of determining the EO chain length.[1] Sodium decane sulfonate was prepared from decyl bromide (Humphrey-Wilkinson Inc., taking the middle cut during a fractional distillation) and sodium sulfite. The product was recrystallized three times from water and four times from ethanol; it was twice dissolved in methanol, precipitated with petroleum ether (bp 40-60°), and finally extracted with ethyl ether. A sample which was merely recrystallized and which exhibited a minimum in the surface tension-log concentration curve was used in one experiment. Sodium dodecyl sulfate was prepared by sulfating lauryl alcohol (Givaudan-Delawanna Inc.) with chlorosulfonic acid, neutralizing, precipitating the inorganic salts in hot ethanol, concentrating the filtrate, and cooling and filtering off the crystallized detergent. This was followed by three recrystallizations from a mixture of 50% 2-propanol and 50% ethanol and by washing with acetone. Since this sample had a minimum in the surface tension-log concentration curve, additional solubilization experiments were made with another sample which was further recrystallized from water and from butanol, followed by extraction with ethyl ether. This procedure eliminated the minimum. Behenyl alcohol was prepared by reduction of behenic acid (from the Hormel Institute) with lithium aluminum hydride, followed by treatment with sodium hydroxide in methanol, two recrystallizations from acetone, and a fractional distillation under vacuum. Adol 18 (Archer-Daniels-Midland Co.) was fractionally distilled, and the middle cut was recrystallized from hexane to obtain 1-tetradecanol. Monsanto's 6-phenyldodecane was used as received.

Solubilization Procedure. Excess Orange OT was added either to detergent solutions of the correct concentration or to solutions between three and four times too concentrated, which were later diluted with water or with sodium chloride solutions. Agreement between solubilization data obtained from the side of supersaturation and those obtained by starting with the solid dye indicates that both represent equilibrium values. Impurities, when added, were measured out as solutions in acetone by means of a microburet or were added in bulk form and solubilized by warming the solutions, prior to the dye addition. The highest concentration of acetone tested, 0.6%, did not affect the solubilization limit nor the extinction coefficient of the dye. The highest acetone level actually employed was below 0.4%.

The solutions, protected from light and stored under nitrogen, were agitated on a jar-rolling mill for at least 4 days, followed by at least 1 week of storage at 25.0 ± 0.1 or 29.8 ± 0.2°. The exception was sodium dodecyl sulfate, the solutions of which were agitated for only 2 days and equilibrated at 25° for 3. In the case of all four detergents, halving or quadrupling these times did not alter the amount of dye solubilized. Agitating the solutions on the jar-rolling mill caused agglomeration of suspended dye, including even the finely dispersed dye which had been precipitated by diluting concentrated detergent-dye mixtures. Excess dye was removed by filtration through a tightly packed plug of absorbent cotton,[4] discarding the initial 50 cm^3. Cotton was shown not to adsorb solubilized dye because refiltration of filtered solutions through fresh plugs did not lower the absorbancy. Removal of suspended dye was complete because raising the detergent concentration of filtered samples by adding solid detergent did not increase the absorbancy.

---

(6) J. W. McBain and R. C. Merrill, Jr., *Ind. Eng. Chem.*, **34,** 915 (1942).

(7) J. W. McBain and A. A. Green, *J. Am. Chem. Soc.*, **68,** 1731 (1946).

Concentrations of filtrates were rechecked by their solids contents.

Spectroscopic Measurements. The amount of solubilized dye was determined by measuring the maximum absorbancy around 500 mμ. For dye solubilized in $C_{12}(EO)_{16}$, the absorption maximum was located at 495 mμ, with a weak shoulder at higher wavelengths. For dye solubilized by the two anionic detergents, there were two overlapping absorption maxima in the spectrum, apparently at 499 and 521 mμ, respectively. The former maximum was not much stronger than the latter, and the apparent shift from 495 to 499 mμ is probably due to overlapping by the 521-mμ maximum. The plateau at and above 600 mμ nearly coincided with the base line of the blank and was used as reference intensity (I_0). Every spectrum was taken in duplicate with a Perkin-Elmer 202 ultraviolet–visible spectrophotometer and with a Beckman DK-2 recording spectrophotometer, using quartz cells 0.5, 1.0, 5.0, and 10.0 cm long. Beer's law was obeyed at all absorbancies tested.

The absorbancy $A = \log (I_0/I)$ is the product of the molar extinction coefficient ϵ, molar concentration c_{OOT}, and path length L in centimeters. The molar extinction coefficient of Orange OT was determined by adding very small volumes of its acetone solutions to 2.00% solutions of $C_{12}(EO)_{16}$, 1.50% solutions of sodium dodecyl sulfate, and 2.50 and 3.00% solutions of sodium decane sulfonate. The value of ϵ in $C_{12}(EO)_{16}$ was identical with that in $C_{12}(EO)_{28}$, namely, $(1.740 \pm 0.007) \times 10^4$ l./mole cm.[1] Dye solubilized in the two anionic detergents had a somewhat higher molar extinction coefficient, probably owing to reinforcement of the 499-mμ maximum by the overlapping 521-mμ maximum. Eight absorbancy measurements of Orange OT dissolved in sodium dodecyl sulfate solutions at concentrations between 1.411 and 13.139 mg/l. gave a mean value of 1.994×10^4 l./mole cm for the molar extinction coefficient; the standard deviation of the mean was 0.011×10^4, and the range of values was $\pm 0.040 \times 10^4$. Eight absorbancy measurements of the dye dissolved in sodium decane sulfonate solutions at concentrations between 1.390 and 37.076 mg/l. gave a mean value of 1.987×10^4 l./mole cm for ϵ; the standard deviation of the mean was 0.009×10^4, and the range of values was $\pm 0.065 \times 10^4$. Four dye solutions in each detergent were acidified with gaseous hydrogen chloride, and in three cases each, the dye in acetone was added to acidified detergent solutions; this did not affect the absorbancies. The two ϵ values determined in the two anionic detergents are identical within the accuracy of the measurements, since the difference between the two averages is less than 1 standard deviation. The present ϵ values are in good agreement with those of Kolthoff[2] and Rigg,[4] both measured in aqueous ethanol, but are lower than the ϵ value of Williams, Phillips, and Mysels, measured in acidified sodium dodecyl sulfate solutions,[3] by exactly a factor of 10.

Additional Measurements. Sedimentation constants were determined in a Spinco Model E ultracentrifuge using a synthetic boundary cell, at the temperature of 26.3 ± 0.1° and a speed of 59,780 rpm. Pictures were taken at 16-min intervals. All schlieren patterns contained single, sharp peaks. Densities and viscosities were determined at 26.3 ± 0.1°, the former with a 20-cm³ pycnometer, the latter with a 2-min Cannon–Fenske viscometer, neglecting the kinetic energy correction.

Turbidities were measured in a Brice–Phoenix photometer at 25.0–26.5°, with blue light at 436 mμ and a standard 40 × 40 mm semioctagonal cell. The photometer was calibrated with an opal-glass diffuser. Each solution was made up by weighing the detergent into a volumetric flask rather than by dilution. The solutions were filtered through an ultrafine sintered-glass filter into the cell. The refractive index increment was determined with a Brice–Phoenix differential refractometer at the same temperature and wavelength used in the light-scattering measurements.

Results and Discussion

Effect of Dye Solubilization on Micellar Molecular Weight. In order to ascertain whether solubilized dye changes the mmw, sedimentation velocity measurements were made on three solutions of $C_{12}(EO)_{28}$ without dye, three solutions equilibrated with excess Orange OT and filtered, and one solution half saturated with the dye.

Plots of the logarithm of r, the distance from the axis of rotation, *vs.* time t gave the values for the sedimentation constant s shown below, calculated according to

$$s = \frac{\mathrm{d}r/\mathrm{d}t}{\omega^2 r} = \frac{\mathrm{d}\ln r/\mathrm{d}t}{\omega^2} \qquad (1)$$

where ω is the rotational speed (radians/sec).

Solutions of $C_{12}(EO)_{28}$ with concentrations of 0.498, 0.339, and 0.200% had sedimentation constants of 1.346, 1.394, and 1.516 S, respectively. Solutions containing 0.500, 0.350, and 0.197% $C_{12}(EO)_{28}$ which were saturated with Orange OT had s values of 1.356, 1.445, and 1.487 S, respectively. A solution of 0.409% $C_{12}(EO)_{28}$ which was half saturated with the dye had an s value of 1.452 S.

of the polymer were decomposed by treatment with 2 N NH_4OH, and excess ammonia and acetone were removed by flash evaporation. The chlorophyll–polymer is soluble in water and in mixtures with up to 80% ethanol.

The density of chlorin groups on the polymer chain could be controlled by varying the ratio of polymer anhydride groups to chl/hexanediamine. The samples used in the present work were prepared from an anhydride/chlorin ratio of 100:1. Polymers have been prepared with ratios from 1000:1 to 50:1, but polymers prepared with lower ratios contained too much gel to be useful.

The "chlorophyll–monomer" (chl/m) (II) was prepared by treating chl/hexanediamine with a 100-fold excess of succinic anhydride. The ammonium succinate formed by subsequent treatment of excess anhydride with ammonia was not separated from the chl/m, so that its effect could be compared with that of the succinate groups on the polymer. Chl/p and chl/m solutions differ, therefore, only in the connectivity of the groups to which the chlorin is attached.

Mg chlorin e_6–6-butylamide phytyl methyl ester (chl/butylamine) was prepared by reaction of chlorophyll with n-butylamine.[17]

The Mg-free derivatives of chl/p and chl/m, abbreviated pheo/p and pheo/m, were prepared by treatment of chl/p and chl/m with dilute HCl. Magnesium is slowly lost from the chlorins on storage in a refrigerator (about 10% per week), and many of the samples used for photochemistry contained a small amount of the Mg-free pigment, which appeared not to affect their reactivity unduly. Addition of 10% (v/v) pyridine to the stock solution helped to retain Mg.

Apparatus and Procedure. Absorption spectra were recorded on a Cary 14 spectrophotometer. Polarization of fluorescence was measured on an Aminco-Bowman spectrophotofluorometer. The fluorescence intensities were corrected for an instrumental asymmetry favoring perpendicularly polarized light over parallel polarized light.

Photoreactions were followed on a Perkin-Elmer Model 350 recording spectrophotometer, the sample compartment of which had been adapted to permit simultaneous irradiation and spectral measurement of the sample. With this instrument the transmittance scale can be expanded by a factor of 50, making possible detection of small light-induced changes in absorptivity. Light from a Sylvania Sun-Gun lamp was directed through a red sharp-cutoff filter (Corning 2-63) into one side of the 1-cm square cross-section reaction cell, in a direction perpendicular to the direction of the measuring beam. The light intensity incident on the sample cell was usually 8–9 × 10^4 ergs cm^{-2} sec^{-1}, as measured by a Yellow Springs Instrument Co.–Kettering radiometer. To eliminate scattered actinic light during kinetic runs with phenosafranine, in which spectral changes were followed at 530 nm, Spectrolab interference filters No. 1860 and 1860-1 were placed in the measuring and reference beams.

Although chl/p is fully reactive in aqueous solutions, *e.g.*, in 0.1 M tris(hydroxymethyl)methylamine (Tris)–HCl buffer of pH 7.5, most reactions reported here were conducted in a medium in which chl/m is also soluble, a mixture of equal parts of water, ethanol, and pyridine (1:1:1), pH 9.0; no foreign buffer was included, so that differences in the ionization properties of polymer and monomer might be accentuated. Unless otherwise stated, all reactions were carried out in this solvent, at chl/p and chl/m concentrations of 1.2×10^{-5} M. In sensitized reductions of phenosafranine (D^+) by hydrazobenzene (AH_2), their usual concentrations were 1.0×10^{-5} and 8×10^{-4} M, respectively.

For a sensitized photoreaction, stock solutions of the chlorophyll derivative and the oxidant were mixed with solvent in the reaction tube, which was then sealed with a serum cap and flushed 10 min with Matheson prepurified grade N_2, which had been passed through Oxsorbent and KOH solutions. An aliquot of stock solution of reductant, preserved under N_2, was added by syringe, and the contents flushed 5 min more with N_2.

Results

Spectral Properties. In a given solvent, the spectra of chl/p, chl/m, chl/butylamine, and chl/hexanediamine are almost identical. In the 1:1:1 mixture, the main red and Soret bands of both chl/p and chl/m are at 644 and 417 nm. In water the bands of chl/p are at 642 and 414 nm, and in ethanol the bands of chl/m are at 641 and 415 nm. The band widths and relative intensities in the spectrum of chl/p in water are normal for nonassociated chlorin, and the solution is fluorescent. The extinction coefficients of the red bands of chl/p and chl/m were taken to be the same as that of chl/butylamine, 6.3×10^4 M^{-1} cm^{-1} in acetone, determined by quantitative reaction of n-butylamine with chlorophyll a.

If the fluorescence of a molecule is excited with polarized light and if the molecule is unable to rotate freely during the lifetime of its excited state, the emitted fluorescence may be polarized to some extent. Attachment of the chlorin to the polymer chain somewhat restricts its movement, and it is not surprising that the fluorescence of chl/p retains polarization sodium dodecyl sulfate in water and in 0.03 and 0.10 *M* NaCl solutions.[3] All five published cmc values are in good agreement with their counterparts of Table I. In the case of sodium dodecyl sulfate solutions at the four levels of NaCl, there is a linear relation between the logarithm of the cmc and the logarithm of the concentration of Na^+, as is commonly observed.[5] The sole apparent incongruity is that the cmc of $C_{12}(EO)_{28}$ is half that of $C_{12}(EO)_{16}$, whereas it is well known that the cmc increases with increasing EO content. The incongruity probably results from a difference in the distribution of EO chain lengths, especially since the shortest chain components had been removed from $C_{12}(EO)_{16}$. Crook, *et al.*, have shown that pure, single-species, nonionic surfactants have about twice as large a cmc value as the normal-distribution surfactants of the same EO content and have ascribed the difference to the effect of the species of shortest EO chains in the latter.[10]

Micellar Molecular Weights from Amount of Solubilized Dye. The mmw can readily be calculated from the absorbancy of detergent solutions saturated with dye by making the following two assumptions: (a) the solubilization ratio is one micelle per dye molecule; (b) the concentration of detergent not associated into micelles is constant and equal to the cmc. The results are shown in Tables II–V. According to eq 3, the mmw equals $bL\epsilon$. For $C_{12}(EO)_{28}$, this product, 85,808, is somewhat larger than the mean of Table II because the value of b was calculated only for concentrations below 4 g/l. The high precision of this method of determining mmw is shown by the fact that the standard deviation of the mean amounts to between only 0.3 and 1.8% of the mean. Light-scattering

Table III: Micellar Molecular Weight of $C_{12}(EO)_{16}$ from Absorbancy of Solutions Saturated with Orange OT at 25°

Detergent concn, g of $C_{12}(EO)_{16}$/l.	Absorbancy for 1.00-cm cell	Mmw
7.63	2.055	62,269
5.81[a]	1.558	62,042
4.51	1.210	61,373
4.51[b]	1.212	61,286
3.00	0.789	60,965
2.03	0.485	64,643
1.01	0.219	62,205
	Mean	62,112 ± 463
0.10	0.0000[c]	
0.08[d]	0.0000[c]	
0.05[e]	0.0000[c]	
0.05	0.0000[c]	
4.61[f]	1.213	62,607
4.51[g]	1.198	61,949
4.51[h]	1.163	63,811

[a] Prepared by diluting a 19.50 g/l. solution saturated with dye. [b] Stored 2 months at 25° before filtering. [c] Measured in 10.0-cm cells with instrumental setting of 90–100% transmittance expanded to full scale. [d] Made up by diluting a 1.01 g/l. solution containing excess dye. [e] Made up by diluting a 1.01 g/l. solution saturated with dye. [f] Also contained 2.0 g of acetone/l. [g] Also contained 0.0257 g of behenyl alcohol/l. and 2.1 g of acetone/l. [h] Also contained 0.0153 g of 6-phenyldodecane/l. and 0.7 g of acetone/l.

Table IV: Micellar Molecular Weight of Sodium Decane Sulfonate from Absorbancy of Solutions Saturated with Orange OT at 30°

Detergent concn, g/l.	Absorbancy for 1.0-cm cell	Mmw
	(1) In Water	
20.33	2.774	69,269
14.90	1.222	68,943
14.02	0.964	69,250
14.00[a]	0.959	69,208
13.13	0.713	68,841
12.06[b]	0.396	70,246
	Mean	69,293 ± 204
	Aggregation no.	284
11.16	0.1994	
10.34	0.0476	
10.08[b]	0.0042[c]	
9.810[b]	0.0003[c]	
9.641	0.0006[c]	
6.313[b]	0.0000[c]	
13.00[d]	0.853	54,507
	(2) In 0.10 *M* NaCl	
8.445	0.867	70,600
8.000	0.744	70,406
6.960	0.442	71,763
6.494	0.318	70,607
6.490[a]	0.316	70,818
6.421[b]	0.303	69,311
	Mean	70,584 ± 321
	Aggregation no.	289
4.108	0.0000[c]	

[a] Sample had a minimum in the surface tension–concentration curve. [b] Made up by saturating a detergent solution about 2 or 3 times more concentrated with Orange OT and then diluting. [c] Measured in 10.0-cm cells, with an instrumental setting of 90–100% transmittance expanded to full scale. [d] Also contained 0.084 g of 1-tetradecanol/l.

---

(10) E. H. Crook, D. B. Fordyce, and G. F. Trebbi, *J. Phys. Chem.*, **67**, 1987 (1963).

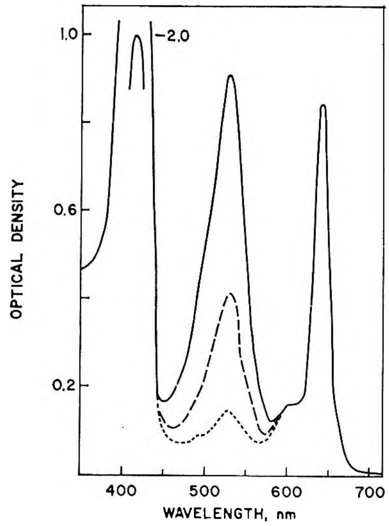

Figure 2. Sensitized photoreduction of phenosafranine by hydrazobenzene: initial concentrations, 1.2×10^{-5} M chl/p or chl/m, 1.25×10^{-5} M phenosafranine, 8×10^{-4} M hydrazobenzene in 1:1:1 water–ethanol–pyridine; initial spectrum (———); photostationary state with chl/m (— — —); photostationary state with chl/p (- - - -). Spectra normalized to Soret band optical density of 2.

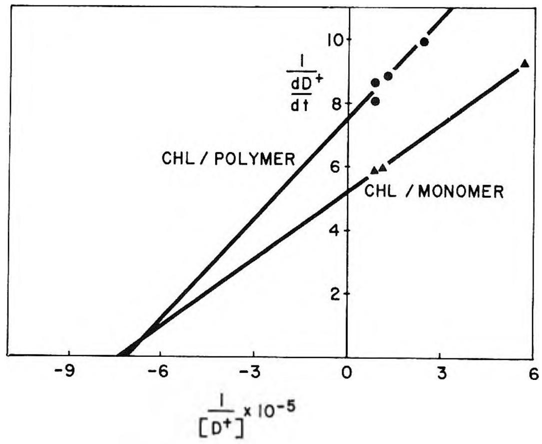

Figure 3. Dependence of initial rate of sensitized reduction on phenosafranine concentration (see eq 2 of text).

states. The dye was not regenerated to any great extent in the dark, although there was often some slow recovery, apparently due to oxidizing impurities or oxygen leakage. Reexposure to light rapidly restored the photostationary state.

Although initial rates were somewhat faster in the monomeric system than in the polymeric, the extent of reduction at the photostationary states represents the most significant difference between the two systems. We have investigated the effects of various alterations in the conditions of the reaction on the initial rate and the photostationary state composition, in an attempt to locate the cause of this difference.

In the absence of phenosafranine, there was no detectable reaction between chl/p or chl/m and hydrazobenzene. In the absence of hydrazobenzene, however, there was a rapid, reversible, small (<1%) decrease in the phenosafranine peak on illumination with red light in the presence of chl/p. The sensitized reduction of phenosafranine is therefore probably initiated by oxidation of the photoexcited chlorin by phenosafranine, as was proposed for the ethyl chlorophyllide sensitized reduction.[18]

Although the initial rate of dye reduction was proportional to light intensity down to one-third of the usual level, the composition of the photostationary state was unchanged. This observation and the absence of a fast dark reaction show that the photostationary state arises from competition between forward and reverse photochemical reactions and not between a forward photochemical reaction and a reverse dark reaction.

With either chl/p or chl/m as sensitizer, the initial rate of dye reduction varied with its concentration according to

$$d[D^+]/dt = (d[D^+]/dt)_\infty k_2[D^+]/(k_1 + k_2[D^+]) \quad (2)$$

in which $(d[D^+]/dt)_\infty$ is the limiting rate at large dye concentration. Values of k_2/k_1, obtained from the $1/[D^+]$ intercept of Figure 3, were about 7.2×10^5 M^{-1} for both chl/p and chl/m. The limiting rates $(d[D^+]/dt)_\infty$ varied somewhat from sample to sample but were always comparable for chl/p and chl/m. The per cent of dye reduced at the photostationary state did not vary with initial dye concentration.

Both the initial rate of reduction and the per cent dye reduced at the photostationary state depend on the concentration of hydrazobenzene (Figure 4). The dependence does not follow an equation like (2) but is better described by (3), with $x = 0.21$, 0.29, and 0.36 for chl/p, chl/m, and chl/butylamine.

$$d[D^+]/dt = -k[AH_2]^x \quad (3)$$

The presence of the polymer only affects the photostationary state when the chlorin is bound to it. Addition of the polymer, decomposed with ammonia but without pigment, to the chl/m-sensitized system did not increase the amount of dye reduced at the photostationary state.

Lowering of the pH by addition of acetic acid considerably decreased the initial rate and the per cent dye reduced at the photostationary state in the chl/p-sensitized system, but left the chl/m-sensitized system comparatively unaltered. With chl/p at pH 6.6 and

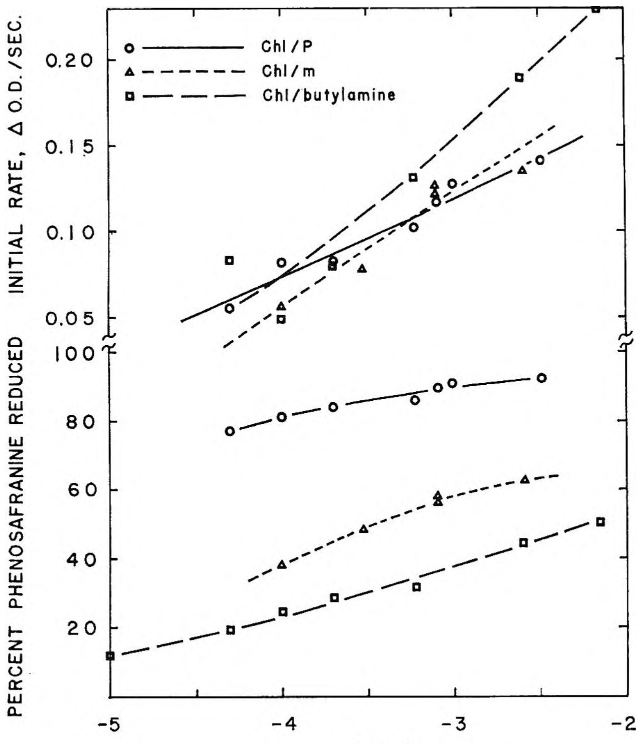

Figure 4. Dependence of initial rate (upper) and photostationary state composition (lower) on initial hydrazobenzene concentration: initial concentrations, 1.1×10^{-5} *M* chl/p or chl/m and 1.0×10^{-5} *M* phenosafranine in 1:1:1 water–ethanol–pyridine, 1.5×10^{-5} *M* chl/butylamine, and 1.2×10^{-5} *M* phenosafranine in 70% ethanol–30% 0.2 *M* Tris–HCl buffer, pH 7.5. Initial rate expressed as rate of optical density change at 530 nm (phenosafranine band).

5.95, the initial rates were 41 and 22% of their usual value at pH 9.0, and the dye was only 56 and 39% reduced at the photostationary state.

Increase of the ionic strength by addition of KCl also decreased the initial rate and the per cent of dye reduced at the photostationary state in the chl/p-sensitized system and had almost no effect in the chl/m-sensitized system (Figure 5). Above 10^{-3} *M* KCl, the polymer began to precipitate, and the initial rates in Figure 5 have been adjusted to correct for loss of pigment from this cause, assuming that the rate is proportional to pigment concentration.

The effect of pH is not clearly separated from that of ionic strength, because the amounts of acetic acid added to lower the pH (1 and 10% of the pyridine) were such as to significantly increase the ionic strength.

A number of runs were made with $FeCl_3$ added to the reaction mixture before illumination. Addition of $FeCl_3$ has two effects: oxidation of an equivalent amount of hydrazobenzene to azobenzene and, thereby, introduction of $FeCl_2$ as a reductant. Points for these runs are also included in Figure 5. Unlike KCl, addition of $FeCl_3$ depresses the initial rate in the chl/m system at lower concentrations than in the chl/p system; the fall of the rate to ~0 may be ascribed to displacement of hydrazobenzene as reductant by $FeCl_2$. However, the composition of the photostationary state is not much altered until the amount of $FeCl_3$ exceeds 10% of that of hydrazobenzene.

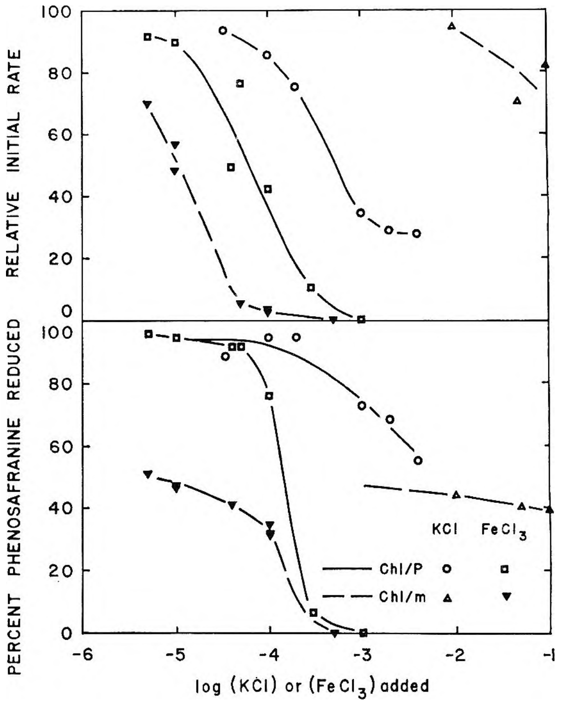

Figure 5. Effects of addition of KCl and $FeCl_3$ on rate and photostationary state of sensitized reduction of phenosafranine by hydrazobenzene: *ca.* 1.0×10^{-5} *M* phenosafranine, 1.2×10^{-5} *M* chl/p or chl/m, and 8×10^{-4} *M* hydrazobenzene. Initial rates expressed as per cent of rate with no added salt ($FeCl_3$ is reduced to $FeCl_2$ by hydrazobenzene before the photoreaction begins).

A few runs were made with hydrazobenzene stock solutions that had become yellow owing to partial oxidation to azobenzene by air. Although the amount of azobenzene in these runs obviously exceeded the amount that would be formed during a sensitized reduction, the initial rates and photostationary states were hardly different from those in the absence of azobenzene.

In order to clarify the nature of the back-reaction leading to the photostationary state, the interaction of chl/m and chl/p with leucophenosafranine (DH) was examined. The photoreduction of a chlorin by leucophenosafranine alone is hard to study, because of extreme sensitivity of the reduced dye to O_2 in

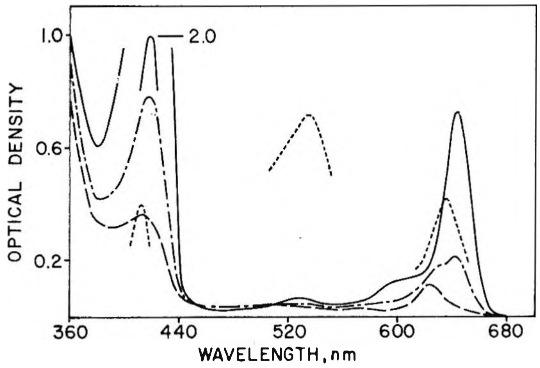

Figure 6. Photoreduction of chl/m by leucophenosafranine (1.25×10^{-5} M) preserved by slight excess of sodium dithionite, in 1:1:1 water–ethanol–pyridine: spectrum before illumination (———); after 5-min illumination (– · – ·), after 10-min illumination (— — —), location of bands after exposure to air overnight (- - - - -).

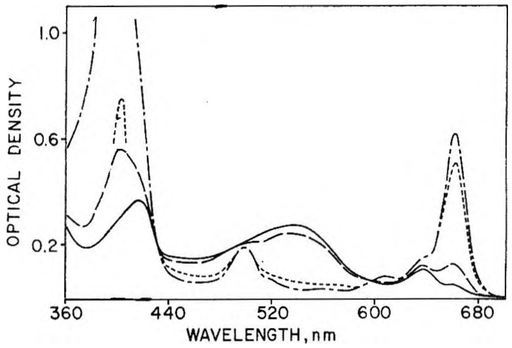

Figure 7. Photoreduction of pheo/m by hydrazobenzene (8×10^{-4} M) in 1:1:1 water–ethanol–pyridine: spectrum before photoreduction (— — —), after 2-min illumination (– – – –), after 10-min illumination (———), after exposure to air for 1 hr (- - - - -).

basic solution and suppression of the reaction by phenosafranine. The reaction can be followed if a small quantity of sodium dithionite is added to keep the dye in its reduced form. Neither chl/p nor chl/m react photochemically with dithionite alone rapidly enough to interfere.

The photoreduction of chl/m by leucophenosafranine/dithionite is shown in Figure 6. The only product which absorbs appreciably in the visible (623 and 412 nm) probably belongs to the class of hypochlorins.[25] The product of its oxidation by air absorbed at 635 nm and was presumably the *meso* derivative of the original Mg chlorin.

The photoreduction of chl/p was very much slower. After 10 min illumination, only 25% of the chl/p had been reduced, even with 2×10^{-4} M leucophenosafranine, and the bands of no reduced product were yet apparent.

If pheo/p is present with chl/p during sensitized reduction of phenosafranine, it is slowly reduced if illumination is continued past the time required to establish the photostationary state. Pheo/m is rapidly reduced by hydrazobenzene alone (Figure 7) to a product similar to those reported from other derivatives of chlorin e_6.[14,15]

Pheo/p sensitized the photoreduction of phenosafranine by hydrazobenzene as rapidly as did chl/p, and the reaction was quantitative; the ensuing reduction of the chlorin was less than 1% as fast. With pheo/m, an initial sensitized reduction of phenosafranine to about half its original concentration was followed by gradual restoration of the phenosafranine and reduction of the chlorin. The net result was reduction of pheo/m by hydrazobenzene, mediated by leucophenosafranine. The reduction of pheo/m continued after the light was turned off, but was probably accelerated by light.

Discussion

Chlorophyll, chemically bound to polymer in the way described, has in aqueous solutions the spectral, fluorescence, and photochemical properties expected of a monomolecularly dispersed pigment. It might therefore be used to study photochemical reactions in systems in which unbound chlorophyll derivatives would aggregate. However, the system has the drawback that the polymer is very susceptible to cross-linking reactions, so that solutions of it generally contain a certain amount of microgel.

The photochemistry of chl/p, chl/m, pheo/p, and pheo/m is very much like that of other chlorin e_6 derivatives and differs from that of chlorophyll most sharply in the ease and manner of photoreduction. The greater resistance of chl/p than of chl/m to photoreduction may have a simple explanation. The reduction of ethyl chlorophyllide a apparently requires the termination step (eq 4).[26] The rate of this step

$$\mathrm{ChlH\cdot} + \mathrm{ChlH\cdot} \longrightarrow \mathrm{ChlH_2} + \mathrm{Chl} \qquad (4)$$

for chl/p would be limited by the rate of diffusion of the polymer and therefore would be very slow compared with the rate for chl/m. However, the slow rate of permanent, two-electron reduction of chl/p and pheo/p would not prevent their acting efficiently as one-electron transfer agents in photosensitized reactions.

The reduction of phenosafranine sensitized by chl/p or chl/m differs from that sensitized by ethyl chloro-

---

[25] G. R. Seely, *J. Am. Chem. Soc.*, **88**, 3417 (1966).

[26] G. R. Seely and A. Folkmanis, *ibid.*, **86**, 2763 (1964).

phyllide[18] in that a photostationary state is attained in the former. The ethyl chlorophyllide sensitized reduction is greatly retarded by a reaction product, probably leucophenosafranine, but there is no evidence for approach to a truly stationary state. On the other hand, there is no indication that the kind of retardation encountered in the chlorophyllide system is operating here, because with chl/p, and $[AH_2] > 8 \times 10^{-4}$ *M*, 90% of the dye is reduced within 1 min, and the rate depends on the ratio $[D^+]/[DH]$ rather than on [DH] alone. Therefore, the photostationary state cannot be just an exaggerated form of the retardation encountered in the chlorophyllide system. To explain the retardation, a metastable complex between hydrazobenzene and oxidized chlorophyllide was postulated; in the present systems, such a complex, if formed at all, must not be long-lived.

The mechanism of the forward reaction (reduction of dye) is probably the same, basically, as that proposed for the ethyl chlorophyllide sensitized reaction, *viz.*

$$\text{Chl} \xrightarrow{\text{light}} \text{Chl}^* \longrightarrow \text{Chl}' \qquad (5)$$

$$\text{Chl}' \xrightarrow{k_1} \text{Chl} \qquad (6)$$

$$\text{Chl}' + \text{D}^+ \xrightarrow{k_2} \text{Chl}^+ + \text{D}\cdot \qquad (7)$$

$$\text{Chl}^+ + \text{AH}_2 \longrightarrow \text{Chl} + \text{AH}\cdot + \text{H}^+ \qquad (8)$$

Chl, Chl*, and Chl′ represent chl/p or chl/m in its ground, singlet-excited, and triplet-excited states. Follow-up reactions convert D· and AH· in part to the final products, DH and A.

The photochemical back-reaction probably begins by reaction of Chl′ with one of the products of the forward reaction, azobenzene or leucophenosafranine. As the presence of azobenzene has little effect on the initial rate of photostationary state, primary reaction with this substance is most unlikely. It is more likely that the initial reaction is with leucophenosafranine, and that the mechanism is analogous to that proposed for the reduction of azobenzene sensitized by ethyl chlorophyllide (eq 9 and 10).[27] As the azobenzene concentration is not rate controlling, reaction 10 must be fast enough to compete favorably with reoxidation of ChlH· by D^+. The follow-up reactions

$$\text{Chl}' + \text{DH} \longrightarrow \text{ChlH}\cdot + \text{D}\cdot \qquad (9)$$

$$\text{ChlH}\cdot + \text{A} \longrightarrow \text{Chl} + \text{AH}\cdot \qquad (10)$$

that dispose of D· and AH· would be the same as in the forward reaction.

One of the questions originally asked was whether the anionic polymer might accelerate the reduction of phenosafranine by concentrating the cationic dye in the vicinity of the photosensitizer. The dependence of initial rate on [KCl] and pH would support an affirmative answer, but the more gradual change in the photostationary state with [KCl] and the identity of the ratios k_2/k_1 (see Figure 3, eq 2, 6, and 7) for chl/p and chl/m do not. It cannot therefore be concluded that concentration of dye about the polymer has any definite effect on the kinetics of the reaction.

The correlation between the dependences of initial rate and photostationary state composition on hydrazobenzene concentration (Figure 4) suggests that the relative rates of step 8 and of reactions competing with it (*e.g.*, eq 11) are an important factor in determining the amount of dye reduced at the photostationary state.

$$\text{Chl}^+ + \text{D}\cdot \longrightarrow \text{Chl} + \text{D}^+ \qquad (11)$$

The apparent fractional-order dependence on $[AH_2]$ suggests that the mechanism of the forward reaction is rather complex, but the data presently available cannot support a more detailed kinetic treatment. The difference between the chl/p and chl/m sensitized reactions appears not to arise from long-range effects of the polymer, but from a difference in the ease of reduction of the pigment, or from ionic or other environmental effects in the immediate vicinity of the pigment.

---

(27) G. R. Seely, *J. Phys. Chem.*, **69**, 2779 (1965).

ions. Both conclusions are based on a comparison of mobilities of the ethanol derivatives with the tetraalkylammonium ions. We have resolved the discrepancy by noting that such comparisons must be made with the correct tetraalkylammonium analog.

Wen and Saito[7] have measured activity coefficients and partial molar volumes of $(EtOH)_4NBr$ and $(EtOH)_4NF$ in aqueous solution at 25° and have found that these thermodynamic properties are more normal in the case of these salts than was found for their tetraalkylammonium analogs. Also, Price[8] has reported that the introduction of hydroxyl groups into the tetraalkylammonium ions reduced the heat of transport significantly, a direction in keeping with less rather than more order in the solution.

Experimental Section

All electrical equipment, cells, salt-cup dispensing device, and general techniques for the conductance measurements were the same as previously described.[9,10] The modification required for the 45°[2b] conductance determination and the method employed for weighing hygroscopic salts[11] have already been reported. The cell constant was determined at 25° and calculated for 45°, the change amounting to less than 0.01%.[2b] The conductance baths were set at 25 ± 0.003° and 45 ± 0.007° with a calibrated platinum resistance thermometer.

The viscosity measurements were carried out using a suspended-level Ubbelohde-type viscometer with a flow time of 500 sec. No kinetic energy correction was found necessary at any temperature. The experimental techniques were the same as those previously described.[3]

Tetraethanolammonium bromide, $(HOC_2H_4)_4NBr$, was prepared by the method described by Wen and Saito[7] with a number of modifications; 0.8 mole of 2-bromoethanol (Fisher Scientific Co.) was refluxed with 1.6 moles of triethanolamine (Fisher Scientific Co.) in 300 ml of methanol for 24 hr. This reaction gives approximately equal amounts of $(EtOH)_4NBr$ and $(EtOH)_3NHBr$, and it is the separation of these two products which presents the greatest difficulty in the synthesis of $(EtOH)_4NBr$. The reaction mixture was titrated with concentrated aqueous hydrobromic acid to pH 3 to convert the remaining free amine to $(EtOH)_3NHBr$. The resulting $(EtOH)_3NHBr$ crystals were removed by filtration and the filtrate was taken to dryness by azeotroping off the last traces of water with ethanol under reduced pressure. The amine hydrobromide is only sparingly soluble in methanol, whereas $(EtOH)_4NBr$ is exceedingly soluble at temperatures as low as −20°. This property permitted further separation of the mixture since only the hydrobromide precipitated on cooling a saturated methanol solution to −20°. The white, nonhygroscopic hydrobromide was detected by its sharp melting point of 187°.

Final purification of $(EtOH)_4NBr$ was effected by dissolving the salt in the minimum volume of methanol and adding four volumes of absolute ethanol. White crystals precipitated on slow cooling with periodic shaking. This recrystallizing procedure was repeated 12 times. Recrystallization from absolute ethanol produced an oil which completely solidified even on slow cooling. Owing to its hygroscopic nature, all recrystallizations and manipulations of $(EtOH)_4NBr$ were carried out in a drybox. The powdered salt was dried under vacuum at 56° for 15 hr. The purified compound melted at approximately 100°, with decomposition. In fact, this salt appeared to undergo decomposition readily at temperatures above 80°, and melting points taken on samples in evacuated sealed tubes gave the same results. Upon standing for 1 month, this salt showed some signs of decomposition, as indicated by the insoluble residue found when an old sample was dissolved in methanol. Our conductance results also confirmed this observation since measurements on month-old samples gave limiting conductances that were somewhat higher than those obtained using freshly prepared salt samples. However, the conductance parameters obtained from freshly recrystallized samples were shown to be independent of further recrystallization.

All attempts to obtain the $(EtOH)_4NBr$ by titration of $(EtOH)_4NOH$ (97.8%, RSA Corp., New York, N. Y.) gave a 90% yield of $(EtOH)_3NHBr$, but we could detect no $(EtOH)_4NBr$.

$(EtOH)_4NI$ was prepared from the purified bromide by ion exchange. When all free amine had been removed from reagent grade anionic exchange resin in the hydroxyl form by repeated washing with water, the resin was converted to the iodide form with KI. One pass through a tenfold excess of resin converted $(EtOH)_4NBr$ to the iodide. The only test performed on the final product to test for complete exchange was to note that the final product was not hygroscopic, whereas the bromide is extremely hygroscopic.

Conductivity grade water[2a] was prepared by passing

---

(7) W. Y. Wen and S. Saito, *J. Phys. Chem.*, **69**, 3569 (1965).

(8) C. D. Price, Technical Report, Armed Services Technical Information Agency, AD 276280 (1961).

(9) J. L. Hawes and R. L. Kay, *J. Phys. Chem.*, **69**, 2420 (1965).

(10) D. F. Evans, C. Zawoyski, and R. L. Kay, *ibid.*, **69**, 3878 (1965).

(11) R. L. Kay, C. Zawoyski, and D. F. Evans, *ibid.*, **69**, 4208 (1965).

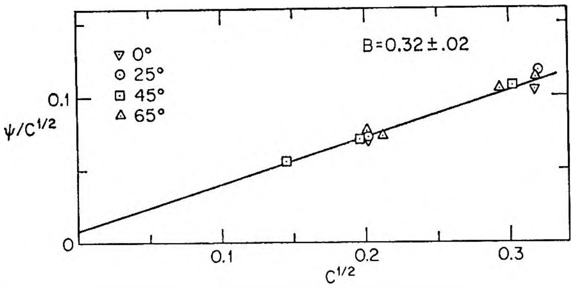

Figure 1. Plots of eq 1 for $(EtOH)_4NBr$ in aqueous solution at various temperatures.

distilled water through a 4-ft mixed-bed ion-exchange column.

Results

The density increments for the volume concentrations and viscosity measurements were obtained by direct measurement on 0.06 M solutions. The θ value in the density equation, $d = d_0 + \theta \bar{m}$, where $\bar{m}$ is the concentration in moles per kilogram of solution, was found to be 0.098 at 25 and 45° for the bromide and was assumed to be constant in the temperature range 0–65° used in the viscosity measurement. The value of θ was assumed to be 0.03 higher for the iodide in keeping with previous experience.[2a]

The viscosity data for $(EtOH)_4NBr$ are given in graphical form in Figure 1 and can be seen to conform to the Jones–Dole equation[12]

$$\psi/C^{1/2} = A + BC^{1/2} \qquad (1)$$

where $\psi = (\eta/\eta_0) - 1$. The intercept $A = 0.008$ is identical with the value calculated from the Falkenhagen equation[13] within the precision of the measurements. It can be seen that $B = 0.32 \pm 0.02$ is independent of temperature within the stated precision. The small amount of spread in the points in Figure 1 can be attributed almost entirely to the temperature dependence or the bromide ion that has been shown to have ionic B values[3] that vary from -0.08 to -0.01 in the temperature range 0–65°, respectively.

The measured equivalent conductances and corresponding concentration in moles per liter are given in Table I along with κ_0, the specific conductances of the solvent. Conductance parameters in Table II were obtained from the Fuoss–Onsager conductance equation[14]

$$\Lambda = \Lambda_0 - SC^{1/2} + EC \log C + (J - B\Lambda_0)C \qquad (2)$$

using a least-square computer analysis.[9] The values 0.8903, 0.5963, 78.38, and 71.51 were used for the viscosity in centipoise and dielectric constant of water at 25[2a] and 45°,[2b] respectively. The limiting ionic conductances, calculated on the basis of $\lambda_0(Br^-)_{25°} = 78.22$ and $\lambda_0(I^-)_{25°} = 76.98$, are $\lambda_0[(EtOH)_4N^+]_{25°} = 27.07$ from the bromide and 26.87 from the iodide. Considering the problems of stability of these salts and the extreme hygroscopic nature of the bromide, this agreement is entirely acceptable. At the higher temperature, a $\lambda_0[(EtOH)_4N^+]_{45°} = 40.0_8$ is obtained from $\lambda_0(Br^-)_{45°} = 110.69$.[2]

Table I: Equivalent Conductances in Aqueous Solution

10^4C	Λ	10^4C	Λ	10^4C	Λ
$(EtOH)_4NBr$, 25°				$(EtOH)_4NBr$, 45°	
$10^7\kappa_0 = 1.6$		$10^7\kappa_0 = 1.9$		$10^7\kappa_0 = 3.2$	
11.991	102.31	10.665	102.47	11.358	146.40
24.631	101.02	23.891	101.03	23.570	144.54
35.153	100.17	37.560	99.97	31.423	143.60
44.402	99.54	49.757	99.18	41.746	142.53
54.642	98.92	62.286	98.46	51.758	141.62
65.980	98.28	73.549	97.89	61.643	140.80
75.307	97.83	84.532	97.38	70.911	140.09
87.613	97.25	98.814	96.77	80.652	139.42
$(EtOH)_4NI$, 25°					
$10^7\kappa_0 = 1.3$		$10^7\kappa_0 = 1.5$			
7.887	101.52	7.415	101.48		
17.570	100.23	17.489	100.20		
26.910	99.30	27.366	99.27		
36.716	98.49	36.063	98.57		
44.803	97.94	44.026	98.01		
53.101	97.39	52.889	97.44		
61.330	96.90	61.858	96.92		
69.680	96.44	71.445	96.41		

The $\mathring{a}$ parameter given in Table II for $(EtOH)_4NBr$ at 25° is in good agreement with the values 1.6, 1.86, and 1.8 reported[2] for Pr_4NBr at 10, 25, and 45°, respectively, and the value at 45° of 2.41 is not too different. On the other hand, the average $\mathring{a}$ value for $(EtOH)_4NI$ of 1.3 reported here is substantially higher than the 0.1, 0.3, and 0.4 obtained for Pr_4NI at 10, 25, and 45°, respectively.[2] In the case of Pr_4NI, the conductance data analyzed for a small amount of association. The same analyses of the data for $(EtOH)_4NI$ detected a small amount of association in the first run but none in the second.

Discussion

In the absence of any change in the interaction with the solvent, replacement of a terminal methyl by a

---

[12] G. Jones and M. Dole, *J. Am. Chem. Soc.*, **51**, 2950 (1929).

[13] H. S. Harned and B. B. Owen, "The Physical Chemistry of Electrolytic Solutions," 3rd ed, Reinhold Publishing Corp., New York, N. Y., 1958, p 240.

[14] R. M. Fuoss and F. Accascina, "Electrolytic Conductance," Interscience Publishers, Inc., New York, N. Y., 1959.

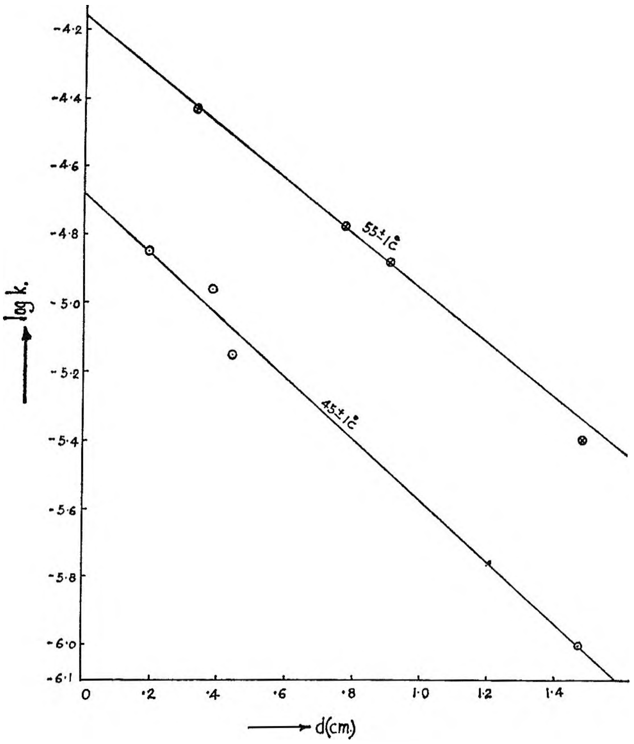

Figure 3. Dependence of rate constant on the length of the air gap.

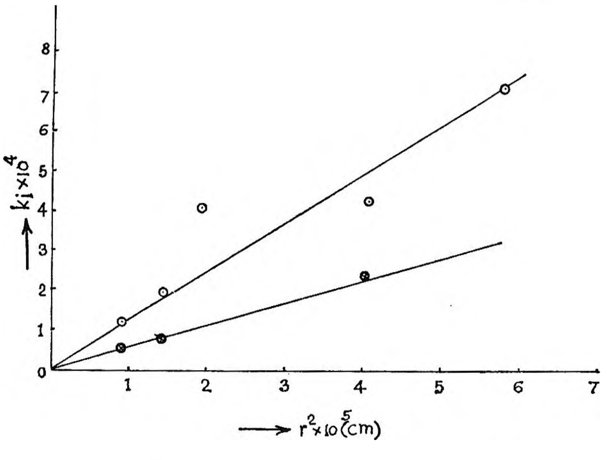

Figure 4. Dependence of reaction rate on particle size: ⊙, reaction between α-naphthol and picric acid; ⊗, reaction between β-naphthol and picric acid.

molarity of picric acid in chloroform layer in absence of naphthol, Z = molarity of naphthol in chloroform, k = solubility depression effect. In the derivation of eq 2 higher powers of $(1 + kZ)$ have not been neglected. Equilibrium constants were calculated with the help of eq 2. These are recorded in Table V.

Determination of Dipole Moment. The dipole moments of naphthols, picric acid, and picrates in dioxane were measured with the help of a dekameter (Type DK 03, Wissenschaftlich-Technische Werkstätten, Weilheim, Germany) at 35° which was maintained by circulating water around the cell from a thermostat. The instrument was calibrated using liquids of known dielectric constants. The refractive index of solutions in dioxane was measured with a Carl Zeiss refractometer. The dipole moments were estimated by the method followed by Richards and Walker.[6] The results are recorded in Table VI.

Results and Discussion

The kinetic data for α-naphthol as well as β-naphthol at various temperatures and for particles of different sizes are best fitted to eq 1. This is supported by Figure 1. k_t is found to depend on temperature as well as on particle size. The values of k_t and p for particles of a definite size at various temperatures are given in Table I. The values of these quantities for particles of different sizes at a fixed temperature are recorded in Table II.

Table I: Influence of Temperature on k_t[a]

Reactants	Temp, °C	k_t, cm²/hr	P, cm⁻¹
α-Naphthol	25 ± 1	3.9×10^{-5}	41.2 ± 2.6
	35 ± 1	1.84×10^{-4}	48.6 ± 2.6
	45 ± 1	5.79×10^{-4}	45.2 ± 2.6
	55 ± 1	1.45×10^{-3}	42.0 ± 2.6
β-Naphthol	35 ± 1	6.74×10^{-5}	74.67 ± 6.5
	45 ± 1	9.97×10^{-5}	64.07 ± 6.5
	55 ± 1	1.87×10^{-4}	55.98 ± 6.5

[a] Particle size, below 150 mesh.

Table II: Influence of Particle Size on k_t[a]

Reactants	Mesh size	k_t, cm²/hr	P, cm⁻¹
α-Naphthol	100	7.0×10^{-4}	19.3 ± 6.1
	120	4.15×10^{-4}	36.5 ± 6.1
	170	3.97×10^{-4}	38.9 ± 6.1
	200	1.87×10^{-4}	45.1 ± 6.1
	240	1.15×10^{-4}	38.2 ± 6.1
β-Naphthol	120	2.23×10^{-4}	73.7 ± 5.4
	200	6.56×10^{-5}	64.2 ± 5.4
	240	5.0×10^{-5}	79.5 ± 5.4

[a] Temperature 45 ± 1°.

---

(6) J. H. Richards and S. Walker, *Trans. Faraday Soc.*, **57**, 406 (1961).

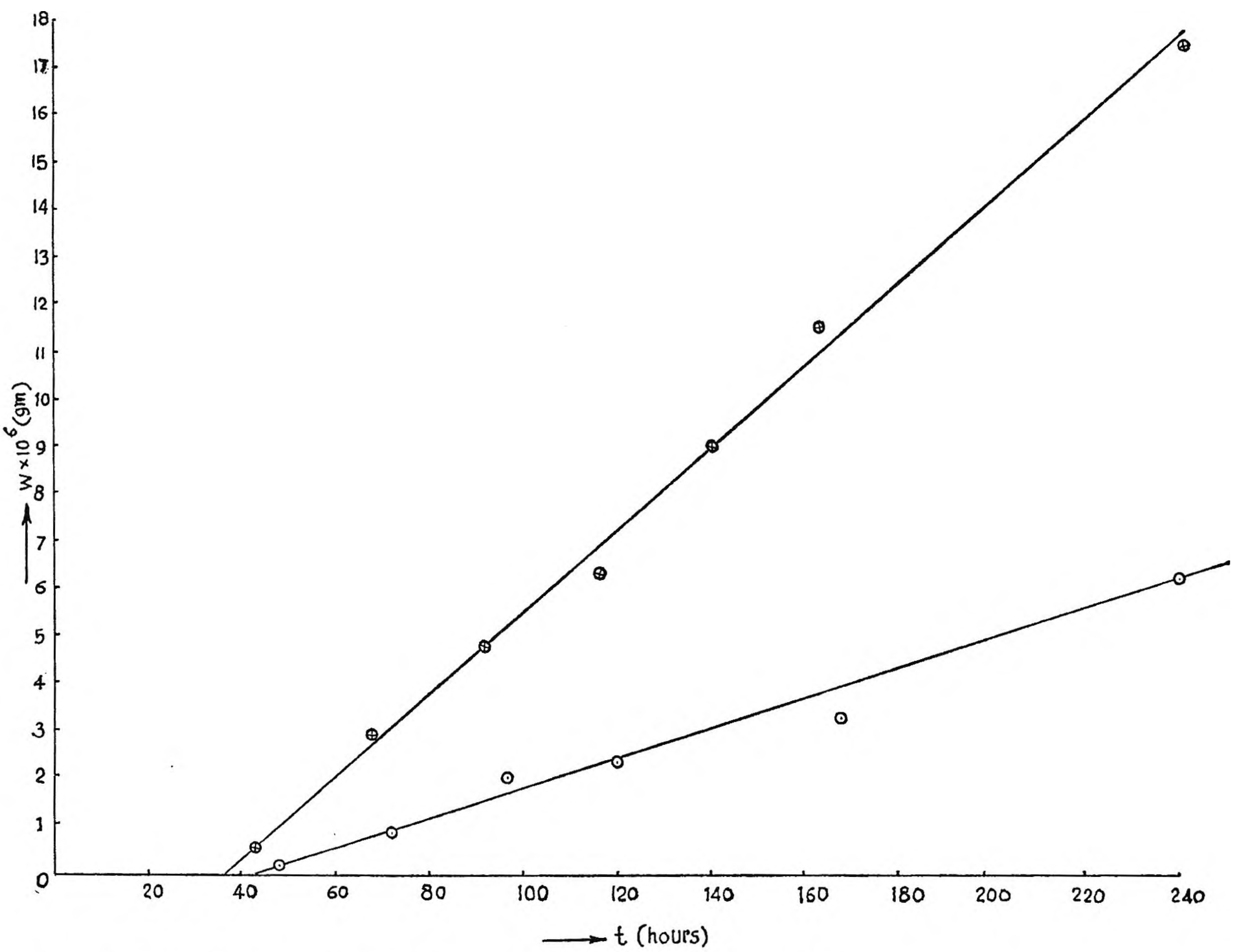

Figure 5. Kinetic data for the reaction between α-naphthol (vapor) and picric acid (solid).

Equation 1 is essentially empirical in nature. The derivation usually given is not correct.[7] However, it can be theoretically justified on the basis of the following arguments.

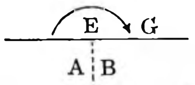

Let us consider two species A and B which are in the solid state. Let EF be the surface of separation. We suppose that molecules of A alone can migrate. We further suppose that migration of A beyond EF takes place by jumps or by surface migration as shown in the illustration above. The interface reaction is practically instantaneous so that any molecule of A striking B at G or H is used up in the chemical reaction. ξ measures the distance of maximum penetration of A molecule in B from plane EF.

Let $f(\xi)$ be the probability of a free jump terminating in the adsorption of molecules of A and subsequent chemical reaction. The probability that no molecular encounter of A and B takes place between ξ and $\xi + d\xi$ is proportional to $d\xi$ and would be equal to $pd\xi$, where p is independent of ξ. At this stage we need not bother about the factor on which p depends. The probability that the encounter occurs between ξ and $\xi + d\xi$ is $(1 - pd\xi)$. The probability that a collision takes place in the distance $(\xi + d\xi)$ is equal to the product of the independent probabilities of adsorption in ξ as well as in $d\xi$. Hence

$$f(\xi + d\xi) = f(\xi)(1 - pd\xi) \tag{3}$$

However, since

$$f(\xi + d\xi) = f(\xi) + \frac{\partial f(\xi)}{\partial \xi}d\xi \tag{4}$$

---

[7] G. Cohn, *Chem. Rev.*, 42, 528 (1948).

Table III: Limiting Ionic Conductances for Aqueous Solutions at 25°[a]

Ion	λ_0^+	Ref	Ion	Ion	Ref
Me_4N^+	44.42	1	Me_3EtN^+	40.86	5, 17
Et_4N^+	32.22	1	Me_3PrN^+	36.64	6
Pr_4N^+	23.22	1	Me_3BuN^+	33.54	17
Bu_4N^+	19.31	1	Me_3-hexyl-N^+	29.52	17
n-Am_4N^+	17.38	16	Me_3-octyl-N^+	26.49	17
			Me_3-decyl-N^+	24.30	17
$Me_3(EtOH)N^+$	38.21	5, 6	Me_3-dodecyl-N^+	22.40	17, 18
$Me_2(EtOH)_2N^+$	33.58	5	Me_3-tetradecyl-N^+	20.96	17
$(EtOH)_4N^+$	27.0	This work			

[a] The cation limiting conductances are based on the following anion limiting conductances:[2] $\lambda_0(Cl^-) = 76.39$, $\lambda_0(Br^-) = 78.22$, $\lambda_0(I^-) = 76.98$, and $\lambda_0(NO_3^-) = 71.57$.

nary ammonium ion below which water structure enforcement drops off rapidly but above which such structure is cooperatively formed with relative ease. Thus, in these ions, the methyl and ethyl groups are poor structure markers, but the propyl group has excellent structure-making properties. Further evidence for this critical size and cooperative aspect can be seen in the ionic conductances for the trimethylalkylammonium ions, as shown in Figure 4. On the basis of number of carbon atoms, they fall on a separate and higher line than do the R_4N^+ ions; that is, they act as ions with fewer carbon atoms. Thus, the three methyl groups are ineffective as structure markers and may well be reflecting some structure-breaking properties. This suggests, therefore, that the logical comparison for the $Me_3(EtOH)N^+$ ion is the Me_3PrN^+ ion and that the correct comparison for the $Me_3(EtOH)_2N^+$ ion is not the Et_4N^+ ion but rather the $Me_2Pr_2N^+$ ion. A calculation shows that the increase in the limiting conductances for $Me_3(EtOH)N^+$ and $(EtOH)_4N^+$ over their correct alkyl analogs is 4.0 ± 0.2% per ethanol group. On this basis, the mobility to be expected for the $Me_2Pr_2N^+$ ion is 31.0 or 8% lower than that for $Me_2(EtOH)_2N^+$. This point is designated by a solid triangle in Figure 4 and, as expected for an ion with water structure enforcement about two side chains, it is between the lines for ions about which there is water enforcement about one side chain and about four side chains.

The obvious conclusion resulting from these data is that an ethanol group does not enforce water structure when substituted in a quaternary ammonium ion. On the other hand, ethanol itself, when added in small amounts to pure water, is known to enforce water structure,[19,20] presumably by being hydrogen bonded into the water cages.[21] However, there is no evidence that the ethanol groups in the $(EtOH)_4N^+$ ion are incorporated into the "flickering clusters"[4] of structured water since a substantial decrease in mobility would result. No such decrease in mobility has been detected here on the basis of any realistic comparison. We conclude that the side chains of the $(EtOH)_4N^+$ ion are not incorporated into the surrounding water structure.

In a previous investigation[1] of the tetraalkylammonium salts in aqueous solution, it was shown that the decrease of the conductance with concentration became greater the larger the anion and cation, contrary to the predictions of theory.[14] The possibility of attributing the effect to ionic association and to changes in solvent structure due to overlap of ionic cospheres has been considered in some detail.[2] The same effect was observed by Skinner and Fuoss[22] in their measurements on i-Am_3BuNBr in aqueous solution, but the effect is particularly evident in the iodides. However, the conductance of $(EtOH)_4NI$ is about 0.5% greater at $C = 0.007\ M$ than that which would be required for the same concentration dependence as Pr_4NI. This is a significant amount considering the agreement in λ_0^+ from the bromide and iodide. It indicates that $(EtOH)_4NI$ acts more like Me_4NI than like Pr_4NI and suggests that the abnormally large decrease in conductance for Pr_4NI and Bu_4NI is due to water structure considerations. Opposed to this conclusion is the fact that sodium tetraphenylboride in aqueous solution has a normal concentration dependence[22] although recent measurements[23] indicate that water structure enforcement around the aryl groups is about the same as that around a butyl group. These results indicate that all

---

(19) F. Franks, *Ann. N. Y. Acad. Sci.*, **125**, 277 (1965).

(20) R. L. Kay and T. Vituccio, to be published.

(21) A. D. Potts and D. W. Davidson, *J. Phys. Chem.*, **69**, 996 (1965).

(22) J. F. Skinner and R. M. Fuoss, *ibid.*, **68**, 1882 (1964).

(23) G. P. Cunningham, D. F. Evans, and R. L. Kay, to be published.

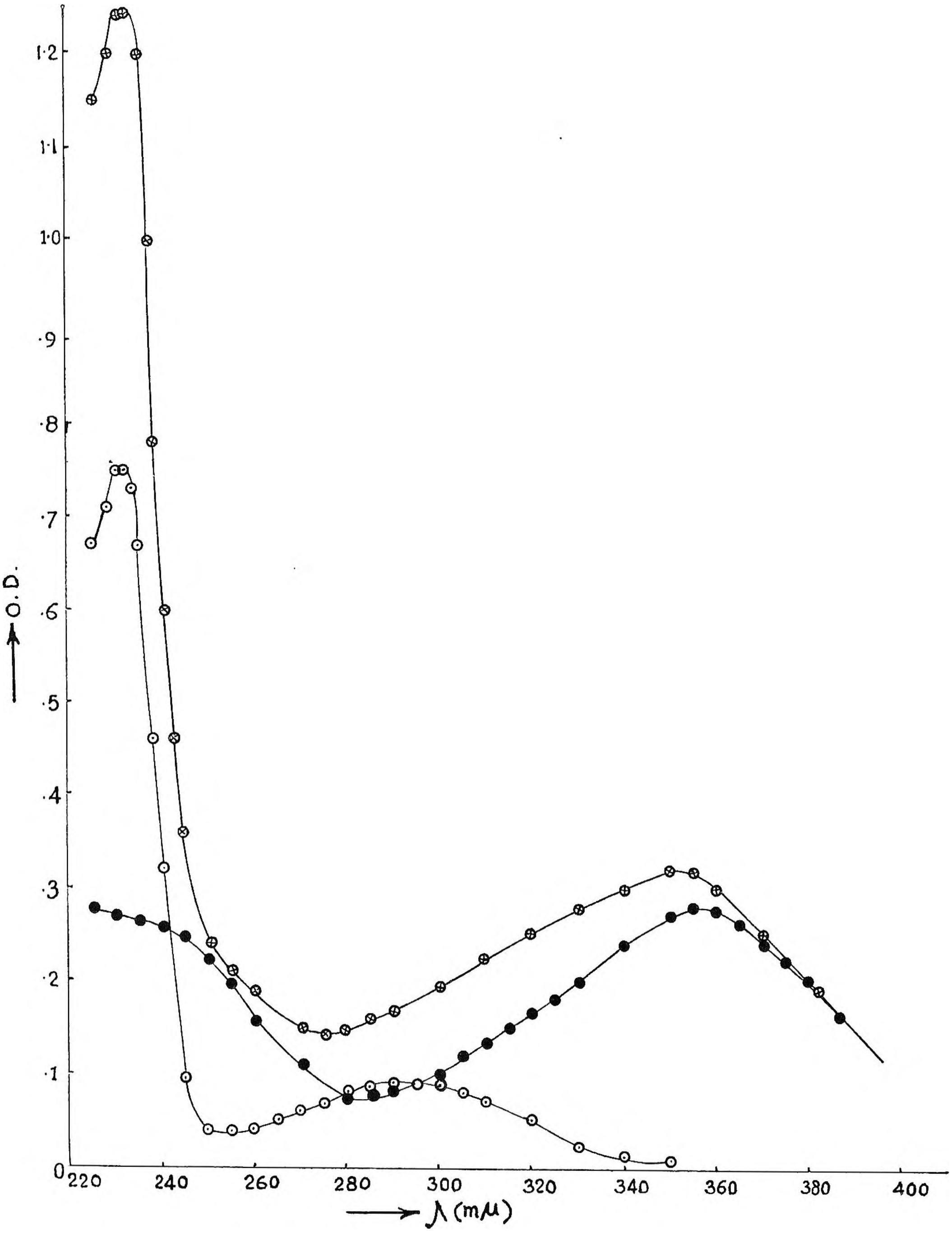

Figure 8. Ultraviolet spectra: ⊙, α-naphthol; ●, picric acid; ⊗, α-naphthol picrate.

we have

$$\frac{df(\xi)}{d\xi} = -pf(\xi) \qquad (5)$$

Since $f(0)$ would be unity, we have on integration of eq 5

$$f(\xi) = e^{-p\xi} \qquad (6)$$

If C_0 is the concentration of the species A at the interface EF, the concentration C of the molecules striking at ξ would be given by

$$C = C_0e^{-p\xi} \qquad (7)$$

Using Fick's law of diffusion, we have

$$\frac{d\xi}{dt} = -AD\frac{\partial c}{\partial x} \qquad (8)$$

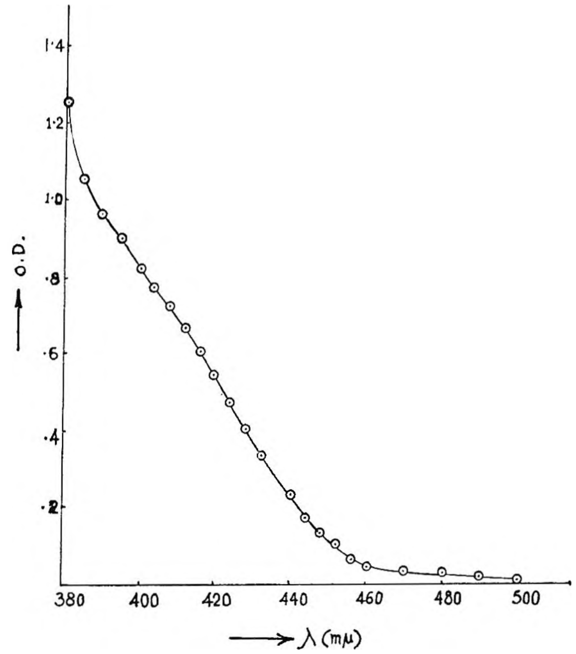

Figure 9. Absorption spectrum of α-naphthol picrate.

where A is the surface area, D is the diffusion coefficient, and $\partial c/\partial x$ is the concentration gradient. Because of the speed of the reaction, very few molecules are actually left within a thin layer of the advancing product zone and therefore the concentration gradient can be taken to be nearly equal to C/ξ, where the value of C is given by eq 7. Therefore we can write

$$\frac{d\xi}{dt} = -AD\frac{C_0e^{-p\xi}}{\xi} \qquad (9)$$

Integration of eq 9 gives

$$\xi^2 = 2ADte^{-p\xi} \qquad (10)$$

which is similar to eq 1 with $k_t = AD$. Since the diffusion coefficient depends on temperature, we have

$$k_t = 4n\pi r^2D_0e^{-E/RT} \qquad (11)$$

where D_0 is a constant and E is the energy of activation involved in diffusion. Surface area A would be given by $n(4\pi r^2)$, where n is the number of particles and r is the radius of particles. For particles of definite size, log k_t would vary directly as the reciprocal of absolute temperature.

When values of log k_t are plotted against the reciprocal of absolute temperature, straight lines are obtained (Figure 2). From (11) it follows that the slope gives the activation energy for diffusion. The energies of activation are given in Table III. The values of heat of sublimation have also been given for the sake of comparison. These were calculated from the known values of heats of fusion[8] and heats of vaporization.[9]

Table III: Energy of Activation for Diffusion

Reactants	Heat of sublimation, kcal	Energy of activation, kcal
α-Naphthol	21.7	19.1
β-Naphthol	19.9	10.1

We shall discuss the following aspects of the reaction mechanism which are worth considering: (1) mechanism of lateral diffusion when bulk quantities of reactants are kept side by side; (2) mechanism of diffusion of the reactant in picric acid grains; (3) mechanism of chemical interaction.

Mechanism of Lateral Diffusion. The lateral diffusion can occur by surface migration, grain-boundary diffusion, or diffusion through vapor phase. Experiments show that diffusion does not occur through the vapor phase. From Table III, it is clear that the energy of activation is less than heat of sublimation. If A_0 is the surface area of picric acid grains, dn/dt, the number of molecules of naphthols per unit time striking these grains from the vapor, would be given by

$$\frac{dn}{dt} = A_0\frac{P}{\sqrt{2\pi MRT}} \qquad (12)$$

where P is the pressure, R is the gas constant, T is the temperature, and M is the molecular weight. If the vapor is assumed to behave ideally, it follows that

$$\frac{dn}{dt} = A_0\frac{P_0e^{-\Delta_SH/RT}}{\sqrt{2\pi MRT}} \qquad (13)$$

where P_0 is a certain constant and Δ_SH is the heat of sublimation. The rate of reaction in the present case is diffusion controlled, and hence, if diffusion occurs through vapor phase, the energy of activation should be equal to the heat of sublimation as $\sqrt{T}$ would not vary much within a small temperature range. Since energy of activation is less than the heat of sublimation, it follows that diffusion *via* vapor phase is not prominent.

The rate of reaction when the reactants are kept adjacent to each other and when the reactants are separated by a distance (air gap) is not the same. In

---

(8) "International Critical Tables," Vol. 5, McGraw-Hill Book Co., Inc., New York, N. Y., 1929, p 134.

(9) O. E. May, J. F. T. Berliner, and D. F. J. Lynch, *J. Am. Chem. Soc*, 49, 1012 (1927).

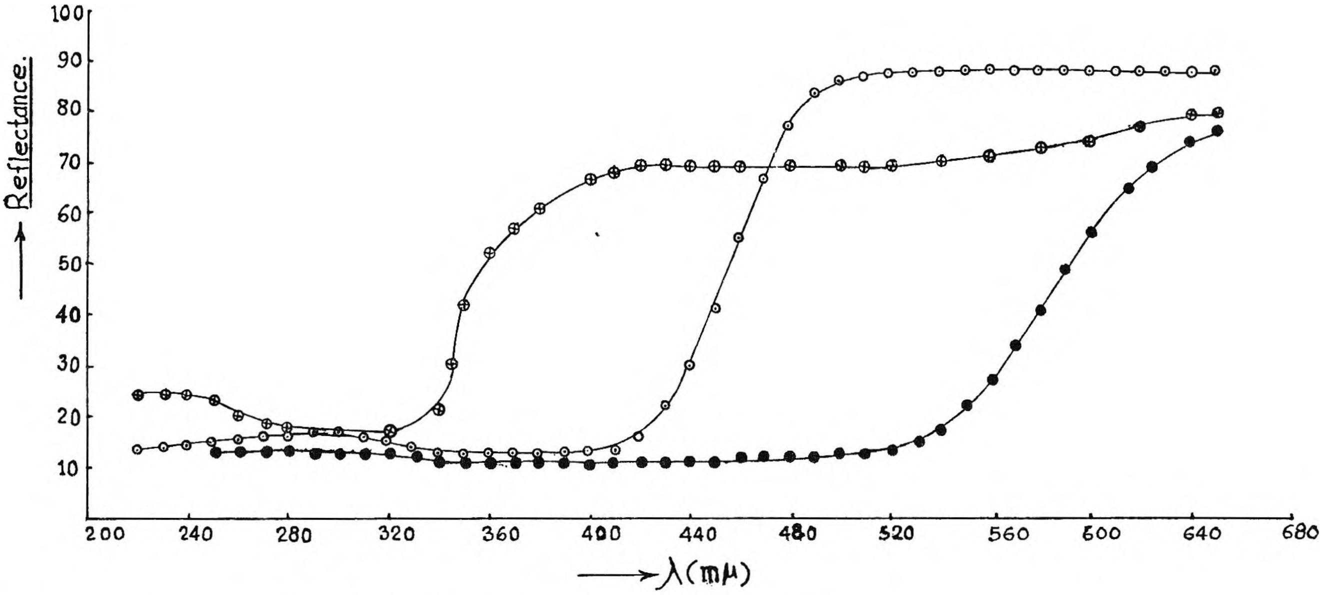

Figure 10. Reflectance spectra: ⊗, α-naphthol; ⊙, picric acid; ●, α-naphthol picrate.

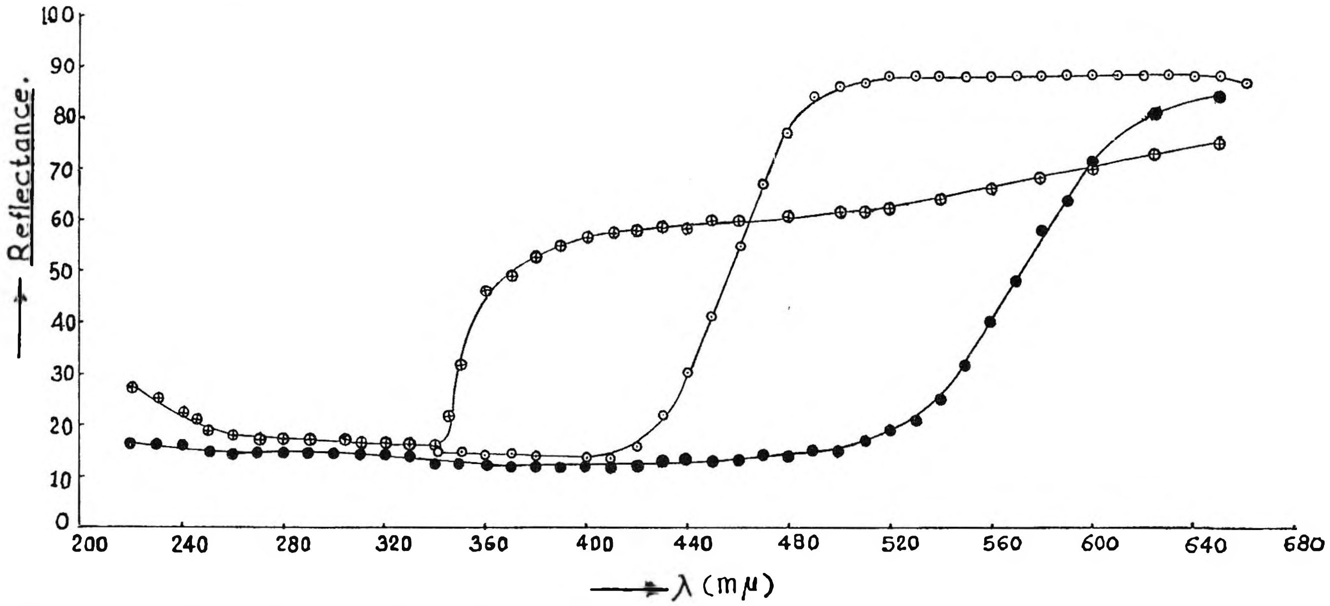

Figure 11. Reflectance spectra: ⊗, β-naphthol; ⊙, picric acid; ●, β-naphthol picrate.

the former case the kinetic data obey eq 1, while in the latter the results are described by the equation

$$\xi^2 = kt \qquad (14)$$

where k is a certain constant. Values of k for different lengths of air gap d are recorded in Table IV.

In Figure 3, log k has been plotted against d, which shows that the following relationship is obeyed

$$k = Ae^{-p'd} \qquad (15)$$

where p' and A are constants. The values of p' are given in the last column of Table IV. It should be noted that eq 15 holds for the case of α-naphthol only. From eq 15 it follows that when $d = 0$, $k = A$ and further when $d = \infty$, $k = 0$. The analysis shows that the vapor phase diffusion is certainly not significant. No reaction occurs when the reactants are separated by a gap in the case of β-naphthol. This further confirms that the vapor phase diffusion is not prominent.

Since the magnitude of the energy of activation is

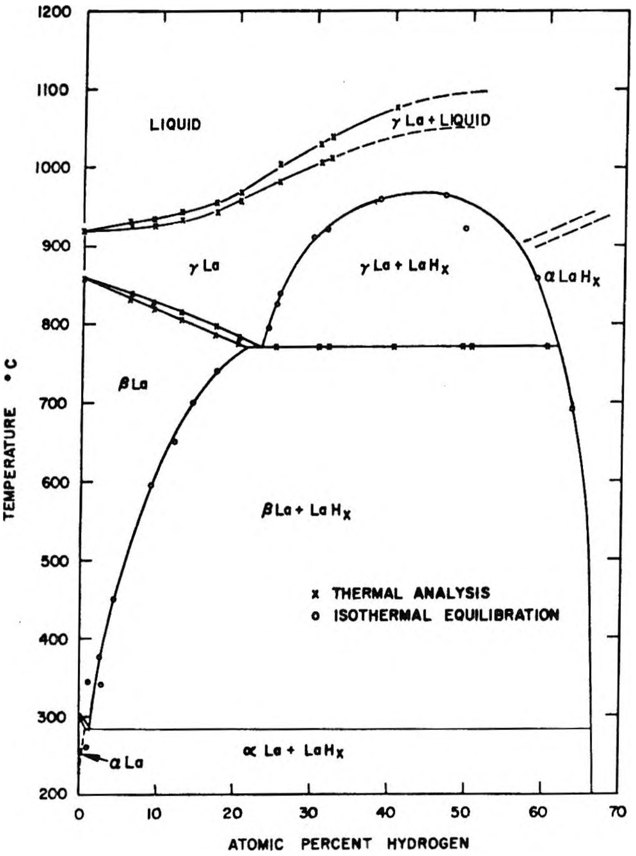

Figure 1. Lanthanum–lanthanum hydride phase diagram.

Table I: Isothermal Equilibration Data

Temp, °C	At. % hydrogen Metal phase	At. % hydrogen Hydride phase	Temp, °C	At. % hydrogen Metal phase	At. % hydrogen Hydride phase
259	1.1		740	17.5	
340	2.9		795	24.2	
345	1.1		826	25.2	
375	2.8		840	25.5	
450	4.6		859		58.7
595	9.3		912	29.8	
652	12.0		922	31.8	49.5
692		63.6	960	39.6	46.3
700	14.5				

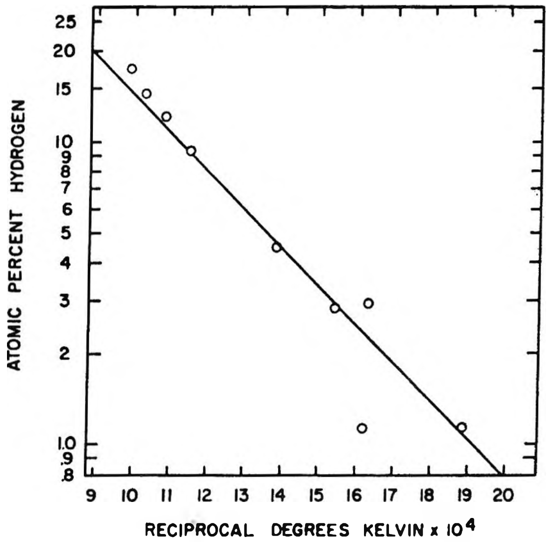

Figure 2. The solubility of lanthanum hydride in lanthanum as a function of temperature.

alloy. The usual heating and cooling rates were 5°/min, and changes in this rate had little effect on the transformation temperatures. The arrests on heating and on cooling always agreed within 4°. The low-temperature hcp to fcc transformation was not observed by thermal analysis in either the pure lanthanum or the lanthanum–hydrogen alloys. This was expected since the enthalpy of this transformation has been reported to be only 67 cal by Berg.[15]

The solubility limits of lanthanum hydride in lanthanum metal were determined by isothermal equilibration and the results are tabulated in Table I.

These solubility limits could not be detected by thermal analysis and could be checked only partially by metallography. The solubility of lanthanum hydride in fcc lanthanum ranged from 2.8 at. % hydrogen at 375° to 21.3 at. % hydrogen at 733°. The solubility of lanthanum hydride in lanthanum metal at 259° was found to be 1.1 at. % hydrogen. This value falls on the extension of the solubility curve for the fcc region but it is not certain whether the metal was in the cubic or hexagonal modification at this temperature. If it was in the hexagonal form, the lanthanum hydride solubility was not appreciably changed by the transformation. A plot of the logarithm of the solubility of lanthanum hydride in fcc lanthanum as a function of reciprocal temperature is shown in Figure 2. An analytical expression was fitted to the data by a least-squares method. This equation was that $\log C = -1260 \pm 30/T + 2.402 \pm 0.507$, where C is the at. % hydrogen. The enthalpy of solution calculated from this equation is $+5.76 \pm 0.17$ kcal.

Above 773° the solubility of lanthanum hydride in bcc lanthanum increased rapidly, and complete solubility occurs at temperatures above 960°. This rapid increase in the solubility of hydrogen in lanthanum metal along with a rapid decrease in the hydrogen concentration of the coexisting lanthanum hydride is

---

(15) J. R. Berg, Ph.D. Thesis, Iowa State University of Science and Technology, Ames, Iowa, 1961.

in agreement with the solubility limits found by Mulford and Holley.[2] This type of relationship has been observed in a number of metal–hydrogen systems.

Lanthanum hydride coexisting with lanthanum metal at room temperature was found by X-ray diffraction to have the fcc fluorite structure reported by Holley, Mulford, and Ellinger.[16] The lattice constant was 5.669 A which is in satisfactory agreement with the value of 5.667 A reported by the above authors. This fcc hydride would not be expected to be able to form a continuous solid solution with the bcc lanthanum metal. Consequently a phase transition in lanthanum hydride has been postulated although no evidence for this transition was found in the thermal analyses. If the phase transition is at a high temperature, it would be very difficult to establish because of the high hydrogen dissociation pressure.

The crystal structure of pure lanthanum and lanthanum–hydrogen alloys at room temperature was investigated with an X-ray diffractometer using bulk samples. The pure lanthanum metal structure was found to be a mixture of fcc lanthanum and hcp lanthanum. The lanthanum–hydrogen alloy also contained both crystal forms of lanthanum but the fcc peaks were slightly stronger than in the pure metal. A sample of this alloy was quenched from a region where all the hydrogen was in solution and reexamined on the X-ray diffractometer. The results showed that both crystal forms of lanthanum were still present but the ratio of fcc lanthanum to hcp lanthanum had greatly increased. A slight increase of the diffraction angles was also found, and this indicated an increase in the lattice parameter of lanthanum apparently due to the retention of some hydrogen in solution.

The effect of hydrogen on the temperature of the hcp to fcc transformation was studied by dilatometer and electrical resistivity measurements. Figure 3 shows the expansion of pure lanthanum and a 3 at. % hydrogen–lanthanum alloy as a function of temperature. The hysteresis in the transformation temperature was found by both the dilatometer and electrical resistivity measurements. The results indicated that a slight excess of hydrogen over the solubility limit in this temperature range lowers the temperature of the hcp to fcc transformation. The transformation temperatures were not changed by variation in the heating and cooling rate. The transformation temperatures shown in Figure 1 are midpoint values of the transformation on heating. The pure lanthanum transformed at 324° and the addition of hydrogen apparently results in an eutectoid reaction of fcc lanthanum to hcp plus lanthanum hydride at 297°.

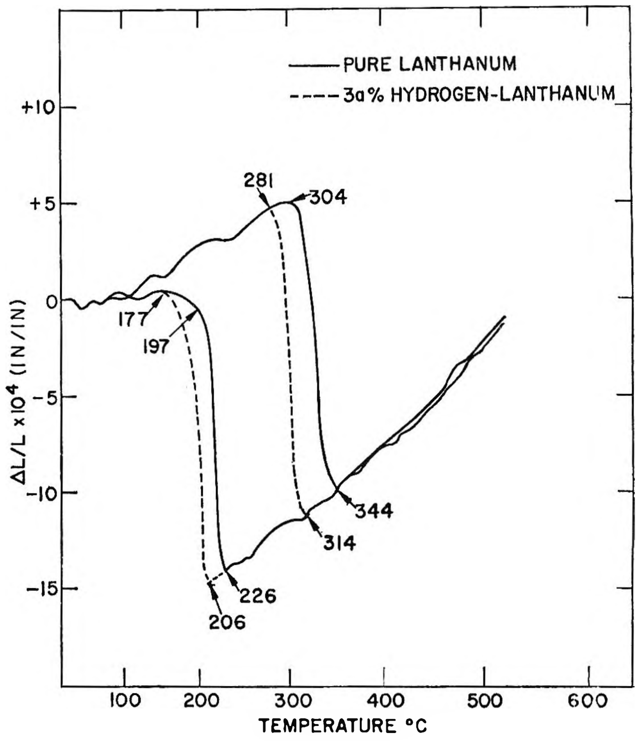

Figure 3. Relative changes in length vs. temperature.

Hydrogen has been found to be extensively soluble in lanthanum at elevated temperatures and to stabilize the bcc phase by raising the melting temperatures and also lowering the transition to fcc lanthanum. The increase in the melting temperature is similar to the effect of hydrogen in the alkaline earth metals. The lowering of the transition to the bcc form is analogous to the effect of hydrogen in zirconium and titanium but differs from the effect of hydrogen in calcium and strontium. The fcc to hexagonal phase transition in lanthanum is lowered slightly by hydrogen but the kinetics and completeness of the transformation are not affected. The interpretation of the influence of hydrogen on the phase transitions in the rare earth metals will probably not be possible until more of these systems have been studied.

Acknowledgments. The authors wish to express their appreciation to Mr. Ardis Johnson for the necessary welding, Mr. John Omohundro and Mr. David Dennison for their experimental assistance during the electrical resistivity and dilatometer measurements, and Mr. Earl Hopkins and Mr. Harlan Baker for their assistance in developing metallography techniques.

---

(16) C. E. Holley, Jr., R. N. R. Mulford, and F. H. Ellinger, *J. Phys. Chem.*, 59, 1226 (1955).

The Vapor Pressure and Enthalpy of Vaporization of Molten Mercuric Chloride to the Critical Point[1]

by J. W. Johnson, W. J. Silva, and D. Cubicciotti

Stanford Research Institute, Menlo Park, California *(Received April 11, 1966)*

The vapor pressure of molten mercuric chloride has been measured by an inverted capillary technique from 573°K and 0.96 atm to 968°K and 111.6 atm. The data are fitted by the linear relation log P(atm) = 4.9929 − 2854.8/T°K from 660 to 968°K with an average deviation of 0.9% for the 25 experimental points. Below 660°K, the experimental points fall below the linear relationship. A critical pressure of 113.7 ± 1.6 atm is predicted by the linear equation at a critical temperature of 972 ± 2°K. The enthalpy of vaporization of molten mercuric chloride has been calculated from 700 to 970°K.

Introduction

An investigation of some of the properties of molten salts above the normal boiling point has been under way for some time in this laboratory. A previous paper[2] reported the critical temperature and coexistence curve of mercuric chloride. This report describes the measurement of the vapor pressure of mercuric chloride from the normal boiling point to the critical point.

Experimental Section

The semimicro boiling point method used in this study was the same as that employed in the determination of the vapor pressure of bismuth chloride.[3] The apparatus has been described in detail elsewhere.[4]

The mercuric chloride was from the same preparation used in the determination of the coexistence curve and critical temperature. The analysis was 73.89% Hg and 26.13% Cl by weight, compared with the theoretical values of 73.88% Hg and 26.12% Cl.

Results and Discussion

The vapor pressure of molten mercuric chloride was determined at 35 points over a temperature range of 573 to 968°K and a pressure range of 0.96 to 111.6 atm. The experimental data are presented in Table I. The temperatures recorded were corrected for gradients between the position of the thermocouple and the liquid surface. These corrections ranged from 2 to 3° depending on the temperature. The listed pressures, up to 17 atm, were corrected by the addition of 0.02 atm for the static head of molten mercuric chloride. Vapor pressures above 17 atm are recorded to the nearest 0.1 atm and the correction was negligible.

Three runs were made using different samples of mercuric chloride as indicated in Table I. It was found that the experimental data could be fitted by the relation

$$\log P(\text{atm}) = 4.9929 - 2854.8/T°\text{K} \qquad (1)$$

from 660 to 968°K with an average deviation of 0.9% for the 25 experimental points. From 660 to 573°K the experimental points tend to fall below the straight line defined by eq 1. In that region the vapor pressure curve is in transition between the high-temperature linear form and the low-temperature Clausius–Clapeyron equation for low pressures, which includes curvature due to a ΔC_p term. Because there is no established theoretical form for the equation in the transition region, a smooth curve was drawn through the data on a large scale plot. Values taken from the curve are compared with the experimental points in the lower part of Table I in the temperature range 570 to 660°K. Values

---

[1] This work was made possible by the support of the Research Division of the U. S. Atomic Energy Commission under Contract No. AT(04-3)-106.

[2] J. W. Johnson, W. J. Silva, and D. Cubicciotti, *J. Phys. Chem.*, 70, 1169 (1966).

[3] J. W. Johnson, W. J. Silva, and D. Cubicciotti, *ibid.*, 69, 3916 (1965).

[4] W. J. Silva, J. W. Johnson, and D. Cubicciotti, *Rev. Sci. Instr.*, 36, 1505 (1965).

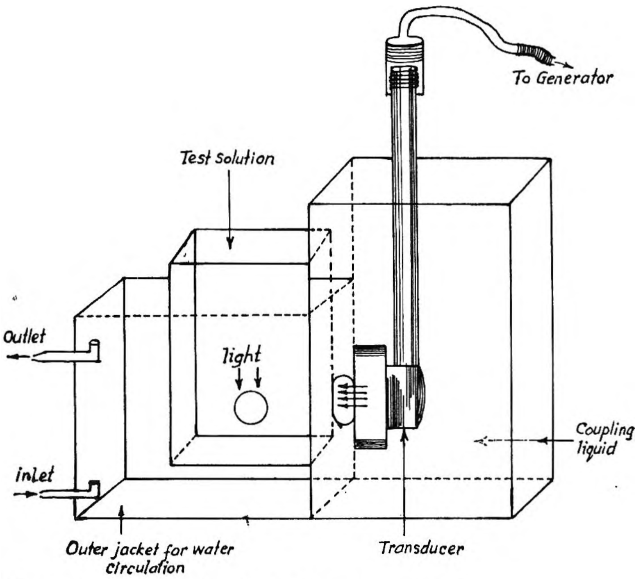

Figure 1. Ultrasonic cell for the measurement of velocity at different temperatures.

2.3 by adding a few drops of alkali. The cell used for the measurement of ultrasonic velocity at different temperatures is shown in Figure 1. The desired temperature of the mixtures was maintained by immersing the flasks in the thermostated bath for about 1 hr. During the exposure the same water from the thermostated bath was circulated in the outer jacket of the cell. Densities of the mixtures were measured by a specific gravity bottle. Adiabatic compressibility was then calculated using the equation

$$\beta = \frac{1}{V^2\rho}$$

where V is the ultrasonic velocity and ρ the density of the medium.

Results and Discussion

From all the curves we find that the variation of ultrasonic velocity is not linear (Figures 2a–c). As the metal ions are gradually added in the solution of catechol, the curve decreases gradually, reaches a minimum value at a certain point, and then increases again. When Zr^{+4} and Cd^{+2} ions are involved, the minima occur at the [M]/([M] + [catechol]) ratio of 0.5, the corresponding molar ratio being 1:1. This indicates the formation of maximum chelate at this point. Had there been no interaction between the respective metal ions and catechol, the variations would have been linear. In the case of a Th^{+4}–catechol system, however, two minima at the ratios corresponding to the molar ratios 1:1 and 1:2 are observed. Thus the variation of ultrasonic velocity gives us information not only regarding the chelate formation, but the positions of minima also indicate the composition at which the maximum chelate formation is taking place.

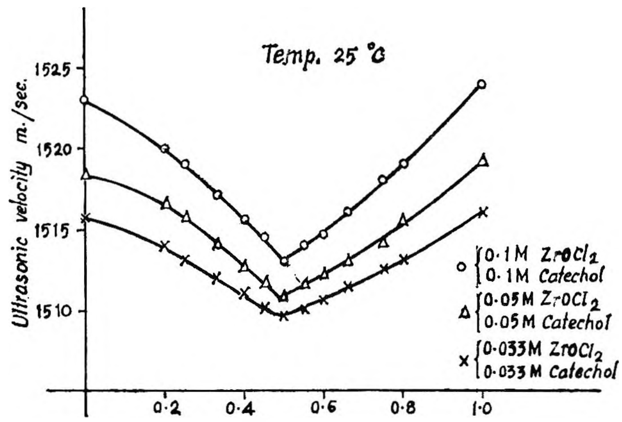

Figure 2a. Ultrasonic velocity variation at 25°.

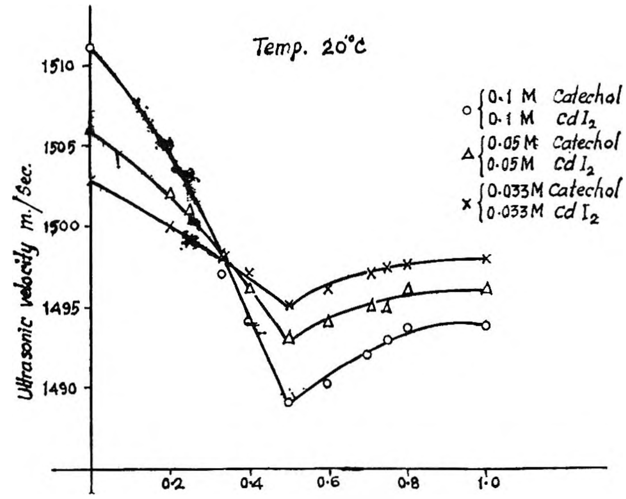

Figure 2b. Ultrasonic velocity variation at 20°.

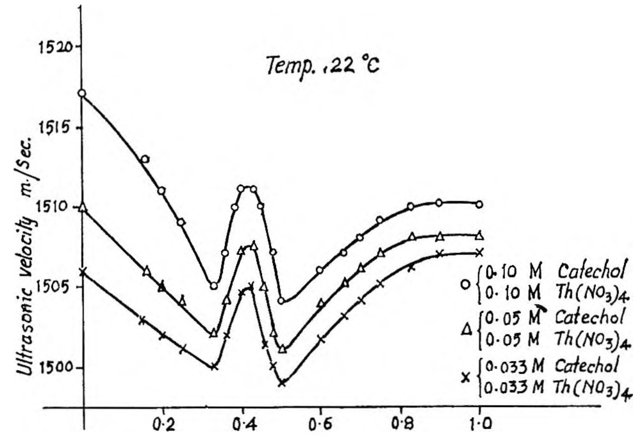

Figure 2c. Ultrasonic velocity variation at 22°.

Table II: Vapor Pressures of $HgCl_2$ from 570 to 660°K (from Smoothed Curve)

T, °K	P, atm	T, °K	P, atm
660	4.64	600	1.67
650	3.99	590	1.37
640	3.40	580	1.11
630	2.88	575.0[a]	1.00
620	2.42	570	0.92
610	2.02		

[a] Boiling point taken from the curve.

higher and melting point lower than those reported in ref 2. The work of Yosim and Mayer[8] shows that Hg_2Cl_2 is soluble in the liquid and lowers the freezing point of $HgCl_2$ and presumably would lower the vapor pressure. Also, since the density of Hg_2Cl_2 is greater, we would expect it to increase the density of $HgCl_2$. These three types of measurement are all in accord in suggesting that there was an impurity of Hg_2Cl_2 in Prideaux's material.

There was no indication of thermal dissociation of $HgCl_2$ at the highest temperature reached in this study. The liquid phase remained transparent and colorless and no mercury deposit was observed in the parts of the apparatus maintained at room temperature. On this basis it is presumed that $HgCl_2$ does not dissociate at the critical temperature.

A comparison of the vapor pressure of $HgCl_2$ with other substances is made in Figure 2. There the log of reduced vapor pressure (vapor pressure divided by value at the critical temperature) is plotted *vs.* reciprocal of reduced temperature. The data for that figure were taken from Din's tables[9] except that H_2O values were from Faxen[10] and $BiCl_3$ from ref 3. The figure indicates that there is a degree of correlation between the relative positions of the vapor pressure curves and the polarity of the molecules of the substance. With increasing polarity, the pressure curve is lower in the figure. The curve for $HgCl_2$ falls intermediate between those for the substances having symmetrical nonpolar molecules (Ar, N_2, C_2H_6) and those having polar molecules (H_2O, $BiCl_3$). In fact, the curves for CO_2 and $HgCl_2$ fall very close together. Since these both have linear, quadrupolar molecules, this rough correlation of molecular structure with similarity of vapor pressure curve is borne out. The fact that NH_3 falls very close to $HgCl_2$ (and CO_2) presumably indicates that its (di-) polarity has the same net effect as the quadrupolarity of $HgCl_2$ and CO_2.

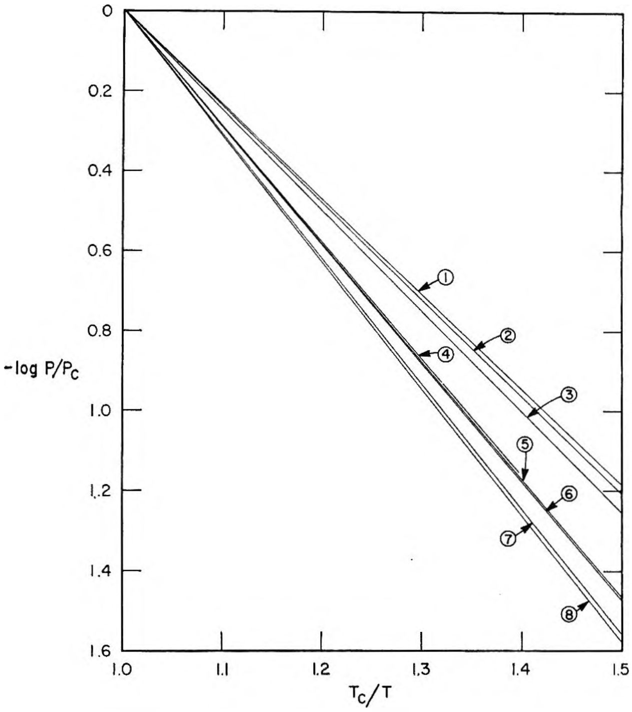

Figure 2. Reduced vapor pressure curves for several substances: 1, Ar; 2, N_2; 3, C_2H_6; 4, CO_2; 5, $HgCl_2$; 6, NH_3; 7, H_2O; 8, $BiCl_3$.

The enthalpy of vaporization of $HgCl_2$ may be calculated from the present data using the Clapeyron relation, which can be written

$$\Delta H_{\text{vap}} = \frac{T(V_g - V_l)(dp/dT)}{41{,}300}$$

where V_g and V_l are the orthobaric volumes of vapor and liquid, respectively, and (dp/dT) is the rate of change of vapor pressure with respect to temperature; the numerical factor converts the value to kilocalories per mole. The orthobaric volumes were calculated from the data of ref 2 and (dp/dT) from eq 1. The results of these calculations are shown in Table III.

Figure 3 shows the variation of the enthalpy of vaporization as a function of temperature. The circles represent the enthalpy of vaporization using the modified Guggenheim relation from ref 2 to calculate $V_g - V_l$ and (dp/dT) from eq 1. The values of the enthalpy of vaporization are reasonable above 750°K, but below this temperature the values are too high. This is probably due to an error in $(V_g - V_l)$ since the modified Guggenheim relation used in ref 2 fits the experimental

---

(8) S. J. Yosim and S. W. Mayer, *J. Phys. Chem.*, **64**, 909 (1960).

(9) F. Din, Ed., "Thermodynamic Functions of Gases," Vol. 1–3, Butterworth and Co. (Publishers) Ltd., London, 1962.

(10) O. H. Faxen, "Thermodynamic Tables in the Metric System for Water and Steam," Nordisk Rotogravyr, Stockholm, Sweden, 1953.

Table III: Vaporization Data for Mercuric Chloride

T, °K	P, atm	dp/dt, atm/deg	ΔV_{vap}, cc/mole	ΔH_{vap}, kcal/mole
700	8.21	0.1102	6856	12.80
725	11.36	0.1420	4642	11.57
750	15.36	0.1795	3254	10.61
775	20.4	0.2231	2393	10.02
800	26.6	0.2732	1763	9.33
825	34.1	0.3292	1326	8.72
850	43.1	0.3922	1004	8.10
860	47.1	0.4187	897.0	7.82
870	51.5	0.4473	804.2	7.58
880	56.1	0.4763	717.9	7.28
890	61.0	0.5063	638.3	6.96
900	66.2	0.5373	565.2	6.62
910	71.7	0.5692	496.9	6.22
920	77.6	0.6028	433.0	5.81
930	83.8	0.6370	372.2	5.34
940	90.3	0.6719	312.7	4.78
950	97.2	0.7081	252.5	4.11
960	104.5	0.7455	187.4	3.25
970	112.2	0.7840	90.84	1.67
972[a]	(113.7)	(0.7917)	(0)	(0)

[a] Critical point.

densities with an average deviation of ±0.008 g/cc. Therefore, the dashed line represents our estimate of the enthalpy of vaporization between 750 and 700°K. It is interesting to note that at 700°K the ideal vapor density and the vapor density calculated from the modified Guggenheim relation of ref 2 are identical, *i.e.*, 0.039 g/cc, while the vapor density corresponding to the enthalpy of vaporization indicated by the dashed line is 0.042 g/cc. With the high sensitivity to the vapor density in this region and the scatter of the experimental vapor densities,[2] it is not surprising that the enthalpy of vaporization cannot be calculated with precision below about 750°K.

Partington[11] has pointed out that there have been many empirical relations evolved between enthalpy of vaporization and temperature. Of these the relatively simple one of Winter modified by Bowden and Jones[12] was applied to the present case, namely

$$\Delta H_{\text{vap}} = l_0\left(\frac{T_c - T}{T_c}\right)^n$$

in which l_0 and n are constants. A log–log plot of the data for $HgCl_2$ is shown in Figure 4. The results fall on a straight line from 2° to about 250° below the critical point, then deviate from the line. The values of the constants derived from the straight line drawn through the data are: $l_0 = 18.50$, $n = 0.394$. These can be compared with values given by Partington for several fluids. For n, his values range from 0.3 to 0.45 and average about 0.39 for nonassociated liquids. Values of l_0 for these same liquids depend on the molecular constitution much more than n and range from about 47 to $SnCl_4$ to about 155 for CO_2. The low value for $HgCl_2$, of course, reflects its relatively higher enthalpies of vaporization (or higher boiling point).

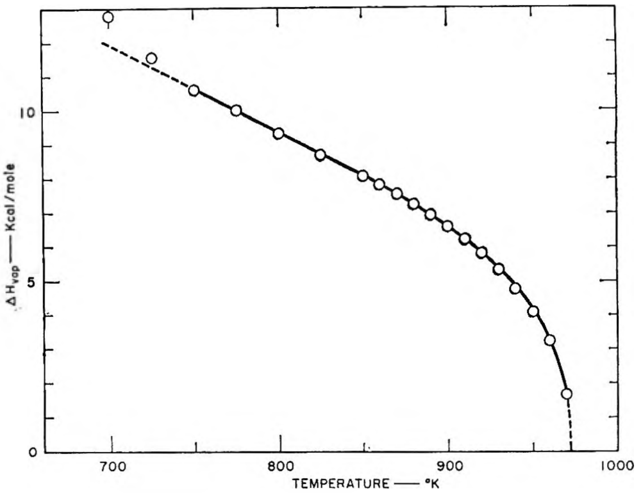

Figure 3. Enthalpy of vaporization of mercuric chloride: O, calculated from eq 3.

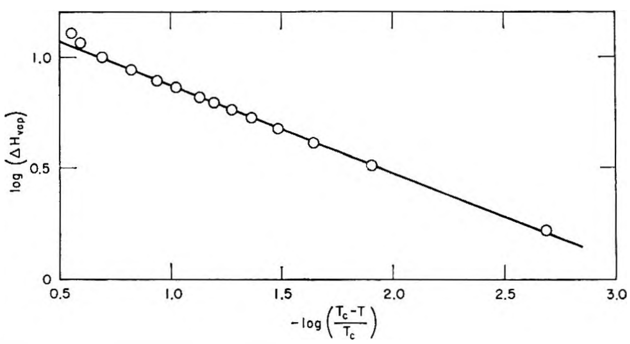

Figure 4. Enthalpy of vaporization *vs.* $(T_c - T)/T_c$ on log–log plot.

---

(11) J. R. Partington, "An Advanced Treatise on Physical Chemistry," Vol. II, Longmans, Green and Co., London, 1951, pp 319–324.

(12) W. J. Jones and S. T. Bowden, *Phil. Mag.*, **37**, 480 (1946).

The Saturation Thermodynamic Functions for Mercuric Chloride from 298°K to the Critical Point[1]

by Daniel Cubicciotti, H. Eding, and J. W. Johnson

Stanford Research Institute, Menlo Park, California 94025

(Received April 29, 1966)

The saturation enthalpy increments above room temperature for $HgCl_2$ in its condensed phases were determined with a drop calorimeter to within 50° of the critical point. These were combined with previously determined enthalpies of vaporization to obtain values for the saturated vapor, and the data were extrapolated to the critical point. Saturation entropies for vapor and condensed phases were calculated from the enthalpies. The internal energy departures of the gas from ideal values were evaluated and compared with similar data for molecular fluids.

Introduction

The present report is a part of our study of the thermodynamic properties of inorganic liquids at elevated temperatures. Recent investigations of bismuth chloride[2-4] are being followed by studies on mercuric chloride. The volume change on vaporization[5] and the vapor pressure[6] of $HgCl_2$ up to its critical point were determined previously in this laboratory, and the enthalpy and entropy of vaporization have been obtained from those results. In the present paper, we have determined the enthalpy increments (above the solid at 298°K) for the condensed phases under saturation conditions, and from them and the enthalpies of vaporization we have obtained values for the saturated vapor. The entropies and free energy functions for both the condensed and gas phases were calculated from the enthalpy increments and their temperature derivatives.

Measured Heat Increments

The same method was used for this work as reported in our $BiCl_3$ study:[4] samples of $HgCl_2$ sealed in evacuated quartz glass ampoules were heated to various temperatures, some within 50° of the critical temperature, and dropped into a modified Parr calorimeter at room temperature. From the heat transferred to the calorimeter, the enthalpy of $HgCl_2$ in the condensed phases, under saturation conditions, was calculated.

The samples heated to the higher temperatures required heavy-walled glass ampoules to withstand the vapor pressure of the $HgCl_2$. As a result, a substantial fraction of the heat evolved came from the glass, and so the accuracy of those determinations was limited. To obtain more accurate data in the lower temperature range, where the vapor pressure was low enough, sealed platinum containers were used. The important details of the samples are listed in Table I.

Table I: Details of Samples Used

Sample no.	Container material	Wt of $HgCl_2$, g	Wt of container, g	Internal vol. of ampoule, cc	Symbol used in Figures 1 and 2
A	Quartz glass	24.0608	6.8617	6.9181	⦶
B	Quartz glass	7.0609	6.4409	2.0891	⊖
C	Quartz glass	5.3083	6.0779	2.2132	⊕
D	Platinum	13.4660	7.7860	...	×

---

[1] This work was made possible by financial support from the Research Division of the U. S. Atomic Energy Commission under Contract No. AT(04-3)-106.

[2] J. W. Johnson and D. Cubicciotti, *J. Phys. Chem.*, **68**, 2235 (1964).

[3] J. W. Johnson, W. J. Silva, and D. Cubicciotti, *ibid.*, **69**, 3916 (1965).

[4] D. Cubicciotti, H. Eding, F. J. Keneshea, and J. W. Johnson, *ibid.*, **70**, 2389 (1966).

[5] J. W. Johnson, W. J. Silva, and D. Cubicciotti, *ibid.*, **70**, 1169 (1966).

[6] J. W. Johnson, W. J. Silva, and D. Cubicciotti, *ibid.*, **70**, 2985 (1966).

The Lone-Pair Model and the Vibrational Force Constants of NF_3[1]

by E. C. Curtis and J. S. Muirhead

Rocketdyne, A Division of North American Aviation, Inc., Canoga Park, California 91304

(Received July 9, 1965)

The repulsion between an atom and a lone pair of electrons, such as may exist on nitrogen atoms, is examined in some detail. The repulsion force constants are estimated using the one-electron theory. A new derivation is shown for the method of introducing forces by the lone pair and subtracting lone-pair motions from the vibrational secular equation. The vibrational force constants for NF_3 are examined with this model in mind. This model suffices to account for the force constants of NF_3, while all other models fail to account for the principle non-Urey–Bradley interaction constant. Implications of this model using the one-electron theory argue for fluorines much less negatively charged than previous estimates.

Introduction

The vibrational force constants have been calculated for ammonia to reproduce with reasonable accuracy the harmonic vibrational frequencies for two different potential functions. Using a hybrid force field, that is, postulating rehybridization with molecular motion, King[2] was able to account for the observed force constants while the simple Urey–Bradley force field was not satisfactory. The only criticism is the value found for the H–H repulsion force constant which seems large. Pariseau, Wu, and Overend[3] accounted for the force constants of NH_3 by including terms for the repulsion between the lone pair and the hydrogen atoms. This model also gave good fit between the observed and computed frequencies. The values they obtained for the force constants agree with our experience although the N–H stretching force constant which they found seems to be unusually large. It is probable that for NH_3 truth lies directly between these two models. It was hoped application of these models to NF_3 might provide similar information.

Wilson and Polo[4] measured the infrared spectrum of NF_3 and found several sets of force constants which exactly reproduce the observed frequencies. The results cannot be unique since there are six parameters in the general harmonic potential function to be determined by only four frequencies. Schatz[5] reconsidered the force constants and included the rotational distortion data to get a further relation between the force constants.

The problem is still interesting since the molecule has several unusual properties. LaPaglia and Duncan[6] considered the observed dipole moment assuming polarized Slater-type orbitals for the bonds and found the lone pair had sp hybridization. The N–F bonds were quite poor in s character from the nitrogen atom and a charge of about 0.4 electron was carried on each fluorine. This is an unusually large charge separation and as shown below would require a large Urey–Bradley repulsion force constant between the fluorine atoms. The hybridization of the bonding orbitals about the nitrogen is also in contradiction to the conclusion of Bent[7] who decided fluorine is an "s-seeking" atom on consideration of the C–F compounds.

The conspicuous fact about the bonding of NF_3 is then the number of contradictions. These can only partially be rationalized by the approximate nature of the theories mentioned. Any new calculation dependent on the hybridization of the bonding should be valuable and so application of the lone-pair model was undertaken. It was also found that a few improve-

---

(1) This study was sponsored by the Propulsion Division of the Air Force Office of Scientific Research of the Office of Aerospace Research under Contract AF49(638)-1135.

(2) W. T. King, *J. Chem. Phys.*, **36**, 165 (1962).

(3) M. Pariseau, E. Wu, and J. Overend, *ibid.*, **39**, 217 (1963).

(4) M. K. Wilson and S. R. Polo, *ibid.*, **20**, 1716 (1952).

(5) P. N. Schatz, *ibid.*, **29**, 481 (1958).

(6) S. R. LaPaglia and A. B. F. Duncan, *ibid.*, **34**, 1003 (1961).

(7) H. A. Bent, *Chem. Rev.*, **61**, 275 (1961).

ments in the original lone-pair model for force constants were needed and these are given below.

The Lone-Pair Model for Vibrational Force Constants

Modification of the Urey–Bradley force field to include terms for repulsion by a lone pair of electrons was reported by the Minnesota group.[3] This involves introducing fictitious internal coordinates for the lone pair and later subtracting them out according to a method used by Shimanouchi.[8] This consists of writing the potential energy for NF_3 as if there were a symmetrically placed atom attached in place of the lone pair. This gives

$$2V = K_R(\Delta R)^2 + \Sigma K_r(\Delta r_i)^2 + \Sigma H_\beta(\Delta\beta_i)^2 + \Sigma H_\alpha(\Delta\alpha_i)^2 + \Sigma[q_\beta F_R'\Delta q_{\beta_i} + F_R(\Delta q_{\beta_i})^2] + \Sigma[q_\alpha F_r'\Delta q_{\alpha_i} + F_r(\Delta q_{\alpha_i})^2] \quad (1)$$

R refers to the lone pair–nitrogen distance, β the angle between the symmetry axis and the fluorine–nitrogen bond, r the N–F distance, and α the F–N–F angle. q_{β_i} gives the distance between the lone pair and the fluorines and q_{α_i}, the distance between the fluorines. The redundant coordinates q_{β_i} and q_{α_i} are eliminated by the method of Shimanouchi.[9] The results of this transformation are shown numerically in Table I for r = 1.37 A and α = 102° 9′.[4] These force constants correspond to eq 4 in ref 3 with internal tension neglected. The problem is reduced to two 3 × 3 matrices by transforming to the symmetry coordinates used in ref 3,[10] which are the same as, *e.g.*, for CF_3H, except that one of the bending coordinates is modified so that it has the same form as in NF_3 and does not involve motion of the lone pair.

Table I: Force Constants for NF_3 in Urey–Bradley Space Including Lone-Pair Coordinates

Force constants	Numerical value of force constants with assumed values of $\bar{N}$, and equivalently F_r, F_r', F_R, and F_R'	
	$\bar{N} = 0$ $F_r = 1.3$, $F_r' = -0.13$ $F_R = -2.3$, $F_R' = 0.4$	$\bar{N} = 17\%$ $F_r = 1.3$, $F_r' =$ $-0.2\sim-0.13$ $F_R = 2.8$, $F_R' = -1.9$
$f_{RR} = K_R + 1.39F_R + 1.61F_R'$	$K_R - 2.55\ (\sim5)$	$K_R + 0.79\ (\sim5)$
$f_{rr} = K_r + 1.21F_r + 0.79F_r' + 0.92F_R + 0.08F_R'$	$K_r\ -0.61$	$K_r\ +3.86$
$f_{\alpha\alpha} = H_\alpha + 0.74F_r - 1.14F_r'$	$H_\alpha\ +1.11$	$H_\alpha\ +1.11$
$f_{\beta\beta} = H_\beta + 0.16F_R - 0.48F_R'$	$H_\beta\ -0.56$	$H_\beta\ +1.36$
$f_{Rr} = 0.65F_R - 0.21F_R'$	−1.58	2.20
$f_{R\beta} = 0.27F_R + 0.96F_R'$	−0.23	−1.08
$f_{r\beta}' = 0.38F_R + 0.11F_R'$	−0.83	0.84
$f_{rr}' = 0.61F_r - 0.39F_r'$	0.84	0.84
$f_{r\alpha}' = 0.67F_r + 0.67F_r'$	0.78	0.78

The lone-pair coordinates may be removed by striking out the rows and columns of the **G** matrix that correspond to lone-pair coordinates. The **F** matrix requires a congruence transformation

$$\mathbf{F} = \mathbf{F}_{22} - \mathbf{F}_{21}\mathbf{F}_{11}^{-1}\mathbf{F}_{12} \quad (2)$$

where $\mathbf{F}_{11}$ is the block of the **F** matrix that corresponds to only lone-pair motions, $\mathbf{F}_{22}$ only to atom motions, and $\mathbf{F}_{12}$ to mixed motions. This transformation was justified by Pariseau, Wu, and Overend, although they noted some misgivings about one step. A proof that shows the nature of the approximation can be based on the partitioning theory described by Lowdin[11] where the Hamiltonian is contracted. If the Hamiltonian is partitioned

$$\mathbf{H} = \begin{bmatrix} \mathbf{H}_{22} & \mathbf{H}_{21} \\ \mathbf{H}_{12} & \mathbf{H}_{11} \end{bmatrix} \quad (3)$$

then the problem can be reduced by solving for the energy levels of $\bar{\mathbf{H}}_{22}$

$$\bar{\mathbf{H}}_{22} = \mathbf{H}_{22} + \mathbf{H}_{21}[\mathbf{E}\mathbf{I}_{11} - \mathbf{H}_{11}]^{-1}\mathbf{H}_{12} \quad (4)$$

In the problem at hand, $\mathbf{H} = \mathbf{T} + \mathbf{V} = \mathbf{G}^{-1} + \mathbf{F}$,[12] where $\mathbf{G}^{-1}$ is the inverse kinetic energy matrix and **F** the force-constant matrix. This gives

$$\bar{\mathbf{H}}_{22} = [\mathbf{G}_{22}^{-1} + \mathbf{F}_{22}] + [\mathbf{G}_{21}^{-1} + \mathbf{F}_{21}][\mathbf{E}\mathbf{I}_{11} - \mathbf{G}_{11}^{-1} - \mathbf{F}_{11}]^{-1}[\mathbf{G}_{12}^{-1} + \mathbf{F}_{12}] \quad (5)$$

$\mathbf{G}_{21}^{-1}$ and $\mathbf{G}_{11}^{-1}$ refer to motions of the lone pair and contain its mass and can be immediately neglected since electronic mass is small relative to **F**, giving

$$\bar{\mathbf{H}}_{22} = [\mathbf{G}_{22}^{-1} + \mathbf{F}_{22}] + \mathbf{F}_{21}[\mathbf{E}\mathbf{I}_{11} - \mathbf{F}_{11}]^{-1}\mathbf{F}_{12} \quad (6)$$

The inverse quantity can be expanded in a power series

$$[\mathbf{E}\mathbf{I}_{11} - \mathbf{F}_{11}]^{-1} = \mathbf{F}_{11}^{-1}\left[\mathbf{I}_{11} + \frac{\mathbf{E}\mathbf{I}_{11}}{\mathbf{F}_{11}} + \left(\frac{\mathbf{E}\mathbf{I}_{11}}{\mathbf{F}_{11}}\right)^2 + \cdots\right] \quad (7)$$

and only the first term need be used since $\mathbf{F}_{11}$ is of the order of the depth of the vibrational well while **E** corresponds to the energy of the first vibrational level, so

---

[8] T. Shimanouchi, *J. Chem. Phys.*, **26**, 594 (1957).

[9] T. Shimanouchi, *ibid.*, **17**, 245 (1949); J. Overend and J. R. Scherer, *ibid.*, **32**, 1289 (1960).

[10] This transformation as published in ref 3 contains a number of typographical errors, but since these quantities are normally found by a computer they need not be corrected here.

[11] P. O. Lowdin, *J. Mol. Spectry.*, **14**, 112 (1964).

[12] See, *e.g.*, E. B. Wilson, Jr., J. C. Decius, and P. C. Cross, "Molecular Vibration," McGraw-Hill Book Co., Inc., New York, N. Y., 1955.

Table II: Thermodynamic Functions for $HgCl_2$ in Standard State Condensed Phases up to 700°K

T, °K	$H°_T - H°_{298}$,[a] kcal/mole	$S°_T$, eu	$-(G°_T - H°_{298})/T$,[a] eu	Vapor press., atm
298	. . .	34.93	34.93	1.63×10^{-7}
320	370	36.12	34.97	1.60×10^{-6}
340	710	37.16	35.07	2.31×10^{-5}
360	1,060	38.15	35.21	5.06×10^{-5}
380	1,415	39.12	35.39	2.12×10^{-4}
400	1,775	40.04	35.60	7.75×10^{-4}
420	2,145	40.94	35.83	2.47×10^{-3}
428	2,295	41.30	35.94	3.81×10^{-3}
428	2,370	41.48	35.94	
440	2,570	41.93	36.09	7.08×10^{-3}
460	2,920	42.70	36.36	1.84×10^{-2}
480	3,280	43.49	36.64	4.42×10^{-2}
500	3,670	44.28	36.93	9.93×10^{-2}
520	4,080	45.07	37.23	0.206
540	4,510	45.88	37.54	0.406
553.7 (s)	4,810	46.44	37.75	0.62
553.7 (l)	9,300	54.55	37.75	
560	9,480	54.86	37.94	0.72
580	10,040	55.85	38.54	1.12
600	10,600	56.80	39.14	1.67
620	11,160	57.72	39.72	2.39
640	11,720	58.62	40.30	3.33
660	12,280	59.48	40.67	4.55
680	12,850	60.32	41.42	6.08
700	13,410	61.13	41.98	7.87

[a] The reference state for these values is the solid in its standard state at 298°K.

and fef represents the free energy function, namely $(G°_T - H°_{298})/T$. Values for fef incr for the condensed phases were calculated from the enthalpy data reported above by the methods of ref 12, while those for the gas were obtained from the data in the "JANAF Tables"[13] (which had been calculated from molecular constant data).

The data given in the following literature references (with temperature range and method in parentheses) were included in the Σ-plot treatment: Prideaux[14] (286 to 309°, boiling point method); Johnson, Silva, and Cubicciotti[6] (300 to 695°, boiling point method); Niwa[15] (45 to 70°, effusion); Ruf and Treadwell[16] (11 to 59°, effusion); Johnson[17] (152 to 302°, spiral gauge); Schmidt and Walter[18] (100 to 180°, transpiration); and Stelzner, Niederschulte, and Wiedemann[19] (60 to 300°, transpiration).

The data of Stock and Zimmermann[20] were not included in the treatment, since their values were so discordant with those of the above authors as to indicate a systematic error in their work. The Σ plot itself is shown in Figure 3. The data fell quite close to a straight line, and more than 90% of the 96 points fell between two straight lines defined by the (Σ', $1/T$) coordinates: (-3.90, 1.6×10^{-3}) and (36.18, 3.6×10^{-3}) for one line and (-3.58, 1.6×10^{-3}) and (35.58, 3.6×10^{-3}) for the other. The thermodynamic parameters for sublimation of $HgCl_2$ and their 90% confidence levels calculated from the data were $\Delta H°_{298} = 19.85 \pm 0.20$ kcal/mole and $\Delta S°_{298} = 35.5 \pm 0.8$ eu.

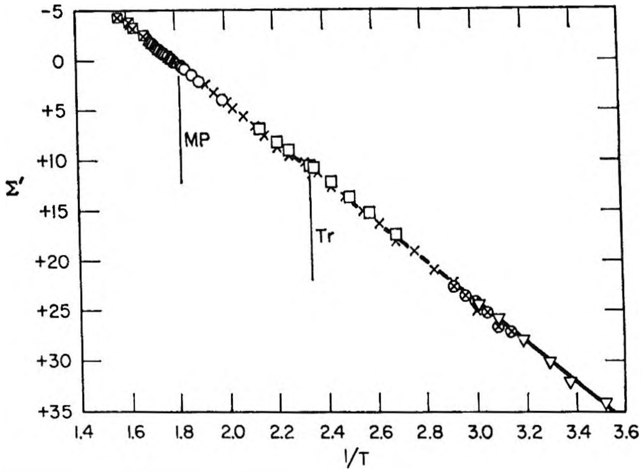

Figure 3. Σ plot for $HgCl_2$ vapor pressure data. Data points were from the following references: ⊠, Johnson, Silva, and Cubicciotti;[6] △, Prideaux;[14] ○, Johnson;[14] ×, Stelzner, Niederschulte, and Wiedemann;[19] □, Schmidt and Walter;[18] ⊗, Niwa;[15] and ▽, Ruf and Treadwell.[16]

The enthalpy increments for the ideal gas, referred to the solid in its standard state at 298°K, were calculated from the enthalpy of sublimation at 298°K and the enthalpy increments for the ideal gas were calculated from molecular constant data and reported in the "JANAF Tables." These are shown as the full curve in the upper part of Figure 2 below 600°K and a dot–dash curve above 600°K. Below 600°K the vapor pressure is low enough so that the enthalpy of the ideal gas is essentially equal to that of the real gas.

---

(12) K. S. Pitzer and L. Brewer, "Thermodynamics," revision of book by G. N. Lewis and M. Randall, McGraw-Hill Book Co., Inc., New York, N. Y., 1961, p 166 ff.

(13) "JANAF Thermochemical Tables," The Dow Chemical Co., Midland, Mich., revised Dec 31, 1965.

(14) E. B. R. Prideaux, *J. Chem. Soc.*, **97**, 2032 (1910).

(15) K. Niwa, *J. Chem. Soc. Japan*, **57**, 1309 (1936).

(16) R. Ruf and W. D. Treadwell, *Helv. Chim. Acta*, **37**, 1941 (1954).

(17) F. M. G. Johnson, *J. Am. Chem. Soc.*, **33**, 777 (1911).

(18) G. C. Schmidt and R. Walter, *Ann. Physik*, **72**, 565 (1923).

(19) K. Stelzner, G. Niederschulte, and E. Wiedemann, *Ber. Deut. Phys. Ges.*, **3**, 159 (1905).

(20) A. Stock and W. Zimmermann, *Monatsh.*, **53–54**, 786 (1929).

Table III: Repulsion Force Constant between an Atom and a Lone Pair of Electrons on a Nitrogen Atom[a]

	Long bond			Short bond			Polarized bond			
Atom	F_R	F_R'/F_R	r	F_R	F_R'/F_R	r	F_R	F_R'	r	$\bar{N}$
H	−2.87	−0.27	1.10	−4.15	−0.28	1.00	2.74	−2.27	1.00	0.1
C	−3.09	−0.20	1.51	−6.86	−0.23	1.30	−0.02	−2.81	1.30	0.2
N	−2.49	−0.19	1.48	−6.33	−0.22	1.27	0.96	−2.29	1.27	0.2
O	−1.84	−0.19	1.47	−8.93	−0.22	1.15	0.63	−2.81	1.15	0.2
F	−1.11	−0.18	1.50	−2.28	−0.20	1.37	3.65	−2.55	1.37	0.2
F*	−2.84	−0.33	1.50	−5.63	−0.34	1.37	7.19	−4.07	1.50	0.4

[a] Where r is the distance between the nitrogen and the atom tabulated. All angles are assumed tetrahedral, including F*, where hybridization of lone pair is assumed to be sp^1. $\bar{N}$ is the excess of an electron on the corresponding atom.

fairly good for NF_3) does not seem justified considering the approximate nature of the one-electron theory. Typical bond lengths were used and Table III gives values for a short and a long bond. The third column gives F_R assuming the bond has been polarized by the amount indicated. The polarization decreases the repulsion by the amount[15]

$$F_R = \langle 4e/q_\beta{}^3\rangle = 92.27\bar{N}\left\langle\frac{1}{q_\beta{}^3}\right\rangle_{\text{av}} \qquad (12)$$

where the right expression gives the polarization in terms of fractional excess of an electron on the atom, $\bar{N}$, in millidynes/angstrom.

This calculation is at best very approximate and rather than subtracting the full correction for lone pair given by eq 8, in molecules of moderate size it would be well to weight it by a "truth" factor.

Calculation of Vibrational Force Constants

The force constants for the internal coordinates (shown in Table II) were adjusted so the vibrational frequencies, calculated by the Wilson FG method,[9,12,16] agreed exactly with the observed frequencies. The observed frequencies were taken as 1032, 647, 905, and 493 cm^{-1} for ν_1 to ν_4, respectively, from Wilson and Polo's measurement[3] of NF_3, and the equilibrium geometry used was $r = 1.37$ A and $\alpha = 102° 9'$ based on microwave and electron-diffraction measurements in agreement with the values chosen by other workers.[4–6] The physical constants were taken from the "Handbook of Physics"[17] and the value used for the mass of nitrogen was that reported for ^{14}N. The **G** matrix was found using a computer program reported earlier,[16] and the transformation from the force constants in eq 1 to the symmetry force constants was done in part by the same program. The pertinent elements are given in Table I.

Since there are four Urey–Bradley force constants and four additional non-Urey–Bradley force constants, criteria in addition to the four observed vibrational frequencies are required. Part of these are from our experience and allow us to set rough limits on the force constants which we will accept as reasonable. First, F_r was assumed to be between 0 and 3 and F_r' was varied between $-0.1F_r$ and $-0.5F_r$ depending on the amount of ionic character assumed. Values were assumed for $\bar{F}_r'$ and $\bar{F}_r$ (which are the same as the fluorine–fluorine repulsions, F_r' and F_r, in eq 1) and also for $\bar{F}_{r\alpha}$ and $\bar{F}_{r\alpha}'$, the stretch–bend interaction force constants. Values were then found for $\bar{K}_r$, $\bar{F}_{rr}$, $\bar{H}_\alpha$, and $\bar{F}_{\alpha\alpha}$, the force constants shown in Table I with the contribution due to F_r and F_r' the fluorine–fluorine repulsions, subtracted. The results are shown in Table IV together with the values found for $\mathfrak{F}_{12}{}^{a_1}$ and $\mathfrak{F}_{12}{}^{e}$, the force constants in symmetry coordinates which are needed below.[18] The locus of solutions is indicated by Table IV, and those solutions with numerical values in accord with our experience are shown in sufficient detail to indicate interdependence of the force constants while the other solutions are shown with no detail. Schatz[5] used the rotational data to find one relation between $\mathfrak{F}_{12}{}^{a_1}$ and $\mathfrak{F}_{12}{}^{e}$ or equivalently between $\bar{F}_{r\alpha}'$ and $\bar{F}_{r\alpha}$. The values that agree with his work are indicated by an asterisk.

Discussion

Several of the sets of force constants shown in Table IV are consistent with the lone-pair model. Our prejudice before starting the calculations had $F_r \approx 1.9$,[15] that is, the repulsion observed between two neon atoms plus the ionic repulsion expected for 20% of an

---

(15) E. C. Curtis, *J. Mol. Spectry.*, **17**, 108 (1965).

(16) E. C. Curtis, *ibid.*, **14**, 279 (1964).

(17) E. U. Condon and H. Odishaw, "Handbook of Physics," McGraw-Hill Book Co., Inc., New York, N. Y., 1958.

(18) The $\mathfrak{F}_{12}{}^{a_1}$ is the same as F_{12} used by Schatz[5] and $\mathfrak{F}_{12}{}^{e}$ corresponds to his F_{34} except the sign is opposite, as is the case with ref 4. This was done to be consistent with ref 2 and 3. We should also note that by $F_{r\alpha}'$ or $f_{r\alpha}'$ we mean a stretch–bend interaction with a bond in common as in ref 3 while ref 2, 4, and 5 designate this by $f_{r\alpha}$ or $F_{r\alpha}$.

Table IV: Computed Force Constants for NF_3[a]

$\bar{F}_r$	$\bar{F}_r'$	$\bar{K}_r$	$\bar{F}_{rr}$	$\bar{F}_{r\alpha}'$	$\bar{F}_{r\alpha}$	$\bar{H}_\alpha$	$\bar{F}_{\alpha\alpha}$	$\mathfrak{F}_{12}^{a_1}$	$\mathfrak{F}_{12}^{e}$
3.3	−1.13	3.05	−0.80	0.	0.	−1.81	0.23	2.91	−1.45
2.3	−0.63	3.44	−0.12	0.	0.	−0.62	0.19	2.24	−1.12
1.9	−0.35	2.78[b]	−0.59	−0.4	−0.4	0.05	0.26	0.88*	−1.04
		3.10	−0.30	−0.3	−0.3	−0.02	0.20	1.18	−1.04
		3.45[c]	0.06	−0.1	−0.1	−0.04	0.17	1.78	−1.04
1.3	−0.13	3.00[b]	−0.21	−0.25	−0.25	0.82	0.34	0.78*	−0.78
		3.26	0.05	−0.2	−0.2	0.72	0.24	0.97	−0.78
		3.70[c]	0.49	0.	0.	0.65	0.17	1.57	−0.78
		2.97	0.20	−0.3	0.	0.77	0.21	0.97*	−0.48
		3.73	0.19	0.	−0.3	0.68	0.19	1.27	−1.08
		3.58	0.71	0.	0.3	0.71	0.15	1.87	−0.48
0.8	−0.08	3.44[b]	0.41	−0.05	−0.05	1.22	0.23	0.81*	−0.48
		3.55	0.51	0.	0.	1.20	0.22	0.96	−0.48
		3.98[c]	0.95	0.2	0.2	1.14	0.14	1.56	−0.48
0.	0.	4.36	0.67	0.47	−0.18	1.92	0.31	0.75*	−0.65

[a] The values marked with an asterisk are those which Schatz[4] finds agree with rotational data. [b] Values of $\bar{F}_{r\alpha}$ and $\bar{F}_{r\alpha}'$ more negative than this have no real solution. [c] Values of $\bar{F}_{r\alpha}$ and $\bar{F}_{r\alpha}'$ more positive than this give the unlikely ratio of $\mathfrak{F}_{12}^{a_1}/\mathfrak{F}_{12}^{e}$.

electron in excess of neutrality residing on each fluorine atom. Requiring values of F_r as near this as possible and moderate values of $\bar{H}_\alpha$ (greater than 0.3, an unusually small value for a bending force constant) gives approximate ranges for the force constants $2.8 < \bar{K}_r < 4.0$, $0.3 < \bar{H}_\alpha < 1.2$, $-0.6 < \bar{F}_{rr} < 1.0$, $0.15 < \bar{F}_{\alpha\alpha} < 0.35$, $-0.5 < \bar{F}_{r\alpha}' < 0.4$, $-0.5 < \bar{F}_{r\alpha} < 0.4$, and $0.8 < F_r < 1.7$, hardly a narrow range of values. Using the rotational information adds further restriction on the range of force constants. These favor the ranges of values $2.8 < \bar{K}_r < 3.4$, $0.3 < \bar{H}_\alpha < 1.0$, $-0.4 < \bar{F}_{rr} < 0.3$, $-0.35 < \bar{F}_{r\alpha}' < 0$, $-0.35 < \bar{F}_{r\alpha} < 0$, $0.21 < \bar{F}_{\alpha\alpha} < 0.35$, and $1 < F_r < 1.7$, and it is to be noted that these limits cannot be realized independently but are correlated as may be seen from Table IV. Both extremes seem unlikely since $F_r = 1.0$ is much lower than expected based on our experience with the noble gases,[15] and, at the other limit, $F_r = 1.7$, the bending force constant, $\bar{H}_\alpha$, assumes an improbably low value. The value $F_r = 1.9$ cannot be realized since it would imply a negative bending force constant.

At this point we may note that these force constants cannot be accounted for in terms of simple rehybridization arguments,[19,20] or equivalently the more elegant orbital following force field which was developed by King[2] for NH_3. The orbital-following field predicts a negative value of moderate size for the bending interaction force constant, King's F_α and our $\bar{F}_{\alpha\alpha}$, and opposite signs on $\bar{F}_{r\alpha}$ and $\bar{F}_{r\alpha}'$ and a small value for $\bar{F}_{rr}$ of indeterminate sign. This work shows a positive value is required for $\bar{F}_{\alpha\alpha}$, small negative values of about the same size for $\bar{F}_{r\alpha}$ and $\bar{F}_{r\alpha}'$, and a small value of indeterminate sign for $\bar{F}_{rr}$. The value required for $\bar{F}_{\alpha\alpha}$ quite convincingly shows that orbital-following arguments do not suffice and the values preferred by $\bar{F}_{r\alpha}$ and $\bar{F}_{r\alpha}'$ give a little additional evidence in the same direction. Comparison of these results with the NF_2 results,[21,22] assuming a Urey–Bradley force field, shows similar interactions, a positive value for $\bar{F}_{rr}$ and a negative value for $\bar{F}_{r\alpha}'$ which may be assumed zero if one can accept a large positive value for $\bar{F}_{rr}$. An orbital-following approach fails here also since orbital-following arguments predict a small positive value for $\bar{F}_{r\alpha}'$ and a small value for $\bar{F}_{rr}$. Going through the transformation to subtract the lone-pair motions for NF_2 would be interesting, but this has not been done since there are seven lone-pair coordinates to be removed, and with only three bits of data one might expect highly indeterminate results.

The force constants in eq 1 cannot be calculated uniquely, of course, but estimates at them should be very informative. If an assumption is made about $\bar{N}$, the degree of polarization of the NF bond, we can then estimate F_r and F_r' using the arguments about atom–

---

(19) J. W. Linnett and P. J. Wheatley, *Trans. Faraday Soc.*, **44**, 556 (1948); **45**, 33, 49 (1949).

(20) N. V. Cohan and C. A. Coulson, *ibid.*, **52**, 1163 (1956).

(21) M. D. Harmony and R. J. Myers, *J. Chem. Phys.*, **37**, 636 (1962).

(22) E. C. Curtis, Rocketdyne Report R-6293, Aug 31, 1965.

Table V: Deduction of Force Constants for Eq 1 from Two Sets of Force Constants That Fit Experiment (Table IV) and Two Assumptions on the Degree of Polarization of the N–F Bond and Hence F_r, F_r', F_R, and F_R'

		$\bar{N} = 0$		$\bar{N} = 17\%$		Force constants found from frequencies and rotational data	
		Soln 1	Soln 2	Soln 1	Soln 2	Soln 1	Soln 2
Force constants required by assumed degree of polarization	F_r	1.3		1.3			
	F_r'	−0.13		−0.2∼−0.13			
	F_R	−2.3		2.8			
	F_R'	0.4		−1.9			
Force constants fit to Table IV	H_β	2.13	1.58	0.77	0.19		
	H_α	0.48	0.56	0.48	0.56		
	K_r	5.8	5.9	1.8	1.9		
Force constants calculated from force constants deduced above	$\bar{F}_{r\alpha}$	0.3	0.3	−0.63	−0.63	−0.25	−0.3
	$\bar{F}_{r\alpha}$	0.3	0.3	−0.63	−0.63	−0.25	0.0
	$\bar{F}_{rr}$	−0.35	−0.31	−0.86	−0.82	−0.21	0.2

atom repulsion discussed above, and using the results of the one-electron quantum mechanics we can estimate values of F_R and F_R'. Assuming further that K_R is large, say $f_{RR} = 5$ (the results are quite insensitive to the exact value), allows substitution into the equations in Table I and calculation of values for H_α, H_β, and K_r. Using these it is possible to compute values for $\bar{F}_{r\alpha}$, $\bar{F}_{r\alpha}'$, and $\bar{F}_{rr}$ which may be compared with the values that were fit to the experimental data.

Using the two solutions called, respectively, 1 and 2 listed in Table IV that agree with the rotational data for $F_r = 1.3$, the force constants for eq 1 were estimated for two arbitrary values of $\bar{N}$. This is shown in Table V. In the four cases shown, the values found for H_α, H_β, and K_r are not too different from each other and we can only remark that their numerical values agree more or less with experience.[23] Solution 1 apparently is quite well fitted by constants that would be deduced from $\bar{N}$ between 0 and 17%, probably about 10%. The exact fit with $\bar{F}_{r\alpha}$, $\bar{F}_{r\alpha}'$, and $\bar{F}_{rr}$ was not sought since it can only be regarded as fortuitous.

The dipole moment can be computed using the one-electron theory and this estimate at the bonding. The dipole moment is given by

$$\mu = 4.8\Sigma_i q_i \langle Z_i \rangle_{av} \qquad (13)$$

where μ is in units of Debyes, q_i is the charge in fractions of an electron, and $\langle Z_i \rangle_{av}$ is the average position of the charges in angstroms along the symmetry axis. Choosing the origin on the symmetry axis in the plane of the fluorines, the position of the lone-pair electron is found from

$$\langle Z_{\text{lone pair}} \rangle = \langle \psi_N^{(2s)} + \lambda \psi_N^{(2p)} | Z | \psi_N^{(2s)} + \lambda \psi_N^{(2p)} \rangle + h \qquad (14)$$

where h is the distance of the nitrogen atom from the origin. Treating the bonding electrons on the nitrogen atom similarly, using the orthogonality relation[24] to find λ, and assuming the bonding electrons on the fluorines are pure p, gives a dipole moment of 1.15 assuming 10% of an electron excess charge on each fluorine atom and that all of this charge comes from the lone pair. The observed dipole moment, 0.234 D.,[25] is found if one assumes an excess charge of 16.6% of an electron on each fluorine. This value is almost the same as was used in two cases in Table V ($\bar{N} = 17\%$) to find the force constants. The difference between 10 and 16.6% is less than several of the approximations inherent in this model and this can be regarded as good agreement.

Conclusion

The lone-pair model for the vibrational force constants for the molecule NF_3 was examined including the procedure for subtracting the lone-pair motions and including the nature of the lone pair–atom and atom–atom repulsions. Assuming that the principal valence force constants should be approximately the same as found in similar cases and that the Urey–Bradley force constants should be approximately the sum of the corresponding noble gas dispersion force and an electrostatic force due to ionic character has allowed placing rather narrow limits on the force constants.[26] In so far as the model is to be believed, the fluorine atoms carry a charge that corresponds to placing approxi-

---

[23] See, for example, the survey by T. Shimanouchi, *Pure Appl. Chem.*, **7**, 131 (1963).

[24] C. A. Coulson, "Valence," Oxford University Press, London, 1952, p 194.

[25] P. Kisliuk, *J. Chem. Phys.*, **22**, 86 (1954).

mately 10% of an electron in excess of neutrality on each fluorine atom. It is gratifying that it was possible to compute the observed dipole moment with a charge distribution so close to the one preferred by the force constant arguments.

The lone-pair model is the only one that has been put forth that correctly accounts for the bend–bend interaction force constant found for NF_3. Certainly other effects, and in particular orbital-following effects, contribute to the potential energy. Using $\bar{H}_\alpha \approx 0.6$ and $\bar{K}_r \approx 3.0$ gives $B = +0.1$ in King's[2] eq 9. This would imply $\bar{F}_{r\alpha} \approx \pm 0.7$ and $\bar{F}_{r\alpha}' \approx \pm 0.7$. These are larger force constants than those preferred by the analysis above, but assuming contributions to the potential energy of up to a half by orbital-following effects permits accounting for the observed force constants, in particular, different values for $\bar{F}_{r\alpha}$ and $\bar{F}_{r\alpha}'$. Attempting to estimate this quantitatively is unrewarding since it corresponds to fitting ten parameters to five pieces of data. We may also note that it seems possible to account for the force constants assuming a bent-bond model.[27]

This work implies that the charge on the fluorine atoms is appreciably less than other estimates. Fitting the dipole moment using one-electron theory requires assuming that a little less than two electrons reside in the lone pair or equivalently assuming the lone pair is richer in s character than required by the orthogonality relation.

Acknowledgment. This research was supported by the Air Force Office of Scientific Research under Contract AF49(638)-1135. We are also grateful for the assistance and cooperation of the Rocketdyne Research Department and to Mrs. Dee Brannon for typing the manuscript.

---

(26) This is much less satisfactory than using a great number of similar molecules or isotopic data. However, it must suffice in this case since the first do not exist and the isotopic shifts for nitrogen are so small as to provide no additional information.

(27) E. C. Curtis, to be published.

NOTES

Estimated Activation Energies for the Four-Center Addition Reaction of H_2, HX, and X_2 to Acetylenes

by Sidney W. Benson and Gilbert R. Haugen

Department of Thermochemistry and Chemical Kinetics, Stanford Research Institute, Menlo Park, California

(Received March 22, 1966)

In this note, we describe the application of an electrostatic model.[1] to predict the activation energy of the four-center addition reactions of acetylenes, $AA^* + -C{\equiv}C- \rightarrow -CA{=}CA^*-$. The transition state is considered an intimate semi ion pair with an equivalent charge separation of $\pm^1/_2$ formal charge. The energy of activation can be equated to the electrostatic energy of interaction of point dipoles.[1]

$$E_{act} = \frac{\epsilon^2}{8}\left\{\frac{r^2_{AA^*}}{\alpha_{AA^*}} + \frac{r^2_{BB^*}}{\alpha_{BB^*}} - \frac{3}{2}\frac{r_{AA^*}r_{BB^*}}{r_e^3}\right\} - \frac{\epsilon^2}{2}\left\{\frac{(\mu^0_{AA^*})^2}{\alpha^0_{AA^*}}\right\} \qquad (1)$$

Table I

Bond ruptured[a]	$r^0_{AA^*}$[b]	α_{AA^*}[c]	Bond formed[d]	r^0_{AB}[b]
$CH{\equiv}CH$	1.21	5.12	C–H	1.07
$CH_3C{\equiv}CH$	1.21	8.02	C–I	2.09
$CH_3C{\equiv}CCH_3$	1.21	10.9	C–Br	1.89
			C–Cl	1.72
			C–F	1.33

[a] The triple bonds in the acetylenes are assumed to be five-electron bonds in the transition state. We have equated this transition-state bond length with the carbon–carbon distance of $^5/_2$ bond order (1.25 A): L. Pauling, "Nature of the Chemical Bond," Cornell University Press, Ithaca, N. Y., 1960. [b] Ground-state bond lengths were obtained from L. E. Sutton, "Table of Interatomic Distances," Special Publication No. 11, The Chemical Society, London, 1958. [c] α_{AA^*} represents the ground-state longitudinal polarizability of the molecule (see ref 1 for details and sources). [d] Transition-state bond lengths = r^0 + 1.0 A.

The distances r_{AA^*}, r_{BB^*}, and r_e are the transition state bond lengths A–A*, B–B*, and the average of the equi-

---

(1) S. W. Benson and G. R. Haugen, *J. Am. Chem. Soc.*, 87, 4036 (1965).

Table II

	Reaction[a] $AA^* + BB^* \rightarrow$ products	E_{AA^*}[b]	E_{BB^*}[b]	E_{int}[b]	E_{gs}[b]	E_{total}^{calcd},[b] 0°K	E_{act}^{calcd},[b,c] 298°K	E_{act}^{obsd},[b] 298°K	$\Delta E°$,[d] 298°K
a-1	$\mathrm{HF + CH{:}CH}$	75.4	12.7	9.64	25.2	53.3	52.1		
	$\mathrm{+\ CH_3C{:}CH}^{e}$		8.09			48.7	47.5		
	$\mathrm{+\ CH_3C{:}CH}^{f}$		8.09			48.7	52.5		
	$\mathrm{+\ CH_3C{:}CCH_3}$		5.95			46.6	45.4		
a-2	$\mathrm{HCl + CH{:}CH}$	37.0	12.7	9.50	2.63	37.6	36.4		-24.0^{1}
	$\mathrm{+\ CH_3C{:}CH}^{e}$		8.09			33.0	31.8		-20.2^{2}
	$\mathrm{+\ CH_3C{:}CH}^{f}$		8.09			33.0	36.8		-20.2^{3}
	$\mathrm{+\ CH_3C{:}CCH_3}$		5.95			30.9	29.7		-17.9^{2}
a-3	$\mathrm{HBr + CH{:}CH}$	32.2	12.7	9.35	1.06	34.5	33.3		-26.2^{3}
	$\mathrm{+\ CH_3C{:}CH}^{e}$		8.09			29.9	28.7		-24.2^{2}
	$\mathrm{+\ CH_3C{:}CH}^{f}$		8.09			29.9	33.7		-24.2^{3}
	$\mathrm{+\ CH_3C{:}CCH_3}$		5.95			27.8	26.6		-20.9^{2}
a-4	$\mathrm{HI + CH{:}CH}$	25.5	12.7	9.44	0.16	28.6	27.4		
	$\mathrm{+\ CH_3C{:}CH}^{e}$		8.09			24.0	22.8		
	$\mathrm{+\ CH_3C{:}CH}^{f}$		8.09			24.0	27.8		
	$\mathrm{+\ CH_3C{:}CCH_3}$		5.95			21.9	20.7		
a-5	$\mathrm{HH + CH{:}CH}$	38.5	12.7	10.0	0.00	41.2	40.0	$\geqq 25 \pm 1^{g}$	-41.1^{1}
	$\mathrm{+\ CH_3C{:}CH}$		8.09			36.6	35.4	$\geqq 35 \pm 3^{h}$	-38.8^{4}
	$\mathrm{+\ CH_3C{:}CCH_3}$		5.95			34.5	33.3		-36.0^{4}
a-6	$\mathrm{F_2 + CH{:}CH}$	81.5	12.7	11.3	0.00	82.9	81.7		
	$\mathrm{+\ CH_3C{:}CH}$		8.09			78.3	77.1		
	$\mathrm{+\ CH_3C{:}CCH_3}$		5.95			76.2	75.0		
a-7	$\mathrm{Cl_2 + CH{:}CH}$	36.0	12.7	9.89	0.00	38.8	37.6		-48.2^{3}
	$\mathrm{+\ CH_3C{:}CH}$		8.09			34.2	33.0		-46.6^{2}
	$\mathrm{+\ CH_3C{:}CCH_3}$		5.95			32.1	30.9		-43.9^{2}
a-8	$\mathrm{Br_2 + CH{:}CH}$	31.0	12.7	9.52	0.00	34.2	33.0		-36.1^{3}
	$\mathrm{+\ CH_3C{:}CH}$		8.09			29.6	28.4		-33.2^{2}
	$\mathrm{+\ CH_3C{:}CCH_3}$		5.95			27.5	26.4		-30.4^{2}
a-9	$\mathrm{I_2 + CH{:}CH}$	22.6	12.7	9.21	0.00	26.1	24.9		
	$\mathrm{+\ CH_3C{:}CH}$		8.09			21.5	20.3		
	$\mathrm{+\ CH_3C{:}CCH_3}$		5.95			19.4	18.2		

[a] r_0, the distance between the dipole centers (in Angstroms) is a-1, 2.20; a-2, 2.39; a-3, 2.47; a-4, 2.55; a-5, 2.07; a-6, 2.32; a-7, 2.66; a-8, 2.80; 1-9, 2.96. (See ref 1 for details.) [b] See ref 1. [c] $E_{thermal}$ is -1.2 kcal/mole for all the reactions tabulated in this table. [d] Standard heat of reaction at 298°K. $\Delta E°$ (298°K) was calculated from the following tables of thermodynamic properties: (1) National Bureau of Standards Circular 500, U. S. Government Printing Office, Washington, D. C., 1950; (2) bond additivity properties, S. W. Benson, "The Foundations of Chemical Kinetics," McGraw-Hill Book Co., New York, N. Y., 1960; (3) group additivity properties, S. W. Benson and J. H. Buss, *J. Chem. Phys.*, **29**, 546 (1958); (4) American Petroleum Institute, Research Project 44 (1953). [e] "Markovnikov" addition; $E_{point\ charge}$ is zero (see ref 1). [f] "Anti-Markovnikov" addition; $E_{point\ charge}$ is $+5.0$ kcal/mole (see ref 1). [g] J. E. Douglas, B. S. Rabinovitch, and F. S. Looney (*J. Chem. Phys.*, **23**, 315 (1955)) noted the absence of H_2 and D_2 in their investigation of the *cis–trans* isomerization of CHD═CHD at 820°K. This implies that the molecular rate is less than or equal to 10% of the observed isomerization rate. This requires a lower limit of 25 kcal/mole for the activation energy of the hydrogenation reaction (the molecular rate was assumed to have the form $10^{13-E/\theta}$). The investigation by K. Kuratani and S. H. Bauer (*J. Am. Chem. Soc.*, **87**, 150 (1965)) of the rate of exchange of C_2H_2 and D_2 (a future publication will describe a possible chain mechanism for this exchange) also places a lower limit of 25 kcal/mole on the hydrogenation reaction. [h] Szwarc (*J. Chem. Phys.*, **17**, 284 (1948)) investigated the pyrolysis of $CH_3CH═CH_2$ at a mean temperature of 1050°K. The unobserved molecular rate cannot be greater than 10% of the observed rate of pyrolysis. A reasonable rate for the molecular dehydrogenation would be $10^{13.0-Em/\theta}$, consequently establishing a lower limit for *Em* of 77 kcal/mole and a lower limit for hydrogenation of 35 kcal/mole.

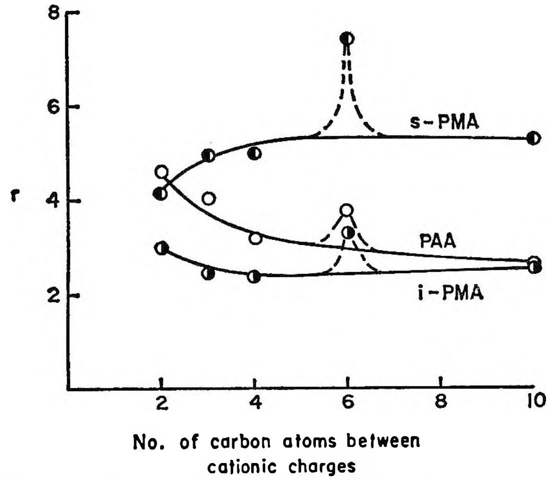

Figure 2. Dependence of the binding ratio r on the spacing of the cationic charges of bolions P2, P3, P4, PX, and P10. Polymeric acid concentration 0.02 N; degree of ionization $\alpha = 0.5$; NaBr concentration 0.02 N).

is being extended. The dependence of the site-binding efficiency on the stereoisomerism of the chain is difficult to interpret. It should be noted, in any case, that the bolion PX, in which the spacing of the pyridinium residues is similar to that to be expected from 1,6-hexamethylenebispyridinium, is bound more tightly to all of the polyanions than expected on the basis of its charge separation. This may be accounted for by the rigidity of the PX structure, which reduces the loss of entropy when the two cationic centers are restrained to lie close to two ionized groups of the polyanions. The extent to which hydrophobic bonding contributes to the binding of PX may be assessed from results obtained with its singly charged analog Q. Under conditions comparable to those illustrated in Figure 2, the binding ratio r for Q is 0.38 with s-PMA and 0.26 with PAA.

It would be expected that an increase in the concentration of added sodium bromide would reduce the extent of binding of the bispyridinium ions. The dependence of the binding ratio r on the total Na^+ concentration (from the neutralization of the polyacid and from the added salt) was found to be of a very simple form, with $r(Na^+)^2$ having a nearly constant value for any given polyacid, degree of neutralization, and bolaform counterion. This generalization is illustrated in Table II on the binding of P2 and PX by the half-ionized polymeric acids. It suggests that the number of countercharges site-bound near the ionized groups of the polyion is independent of whether these charges belong to univalent ions or to bolions. The equilibrium of this process may, therefore, be represented by

$$\mathrm{Bol_f}^{2+} + (\mathrm{Na_b}^+)_2 \rightleftarrows \mathrm{Bol_b}^{2+} + 2\mathrm{Na_f}^+ \qquad (1)$$

Table I: The Dependence of P2 Binding to Half-Neutralized PAA on the Normality of Carboxylate Groups Carried by the Polymer Acid ($C_{P\alpha}$)

C_{NaBr}	$C_{P\alpha}$	r	$r/C_{P\alpha}$
0.02	0.02	8.03	401
0.02	0.01	4.58	458
0.02	0.005	2.27	454
0.04	0.02	3.29	164
0.04	0.01	1.55	155
0.04	0.005	0.80	160
0.06	0.02	1.02	51
0.06	0.01	0.80	80
0.06	0.005	0.40	80

We are representing here the bound sodium ion as $(Na_b^+)_2$ to emphasize that on binding of a bolion two Na^+ ions are released from site binding to the same macromolecule. We should note that in the process represented by eq 1 the charge of the polyion with the site-bound counterions remains unchanged. This conclusion is supported experimentally by the observation that addition of small amounts of bolion salts to partially ionized polycarboxylic acids does not lead to an appreciable drop of pH, as would be expected if bolion binding reduced the polyion charge and increased, in consequence, the acidity of the carboxyl groups. Since the number of Na^+ counterions bound to a polyanion appears to depend little on the concentration of

Table II: Dependence of the Binding of P2 and PX by Half-Ionized 0.02 N Polymeric Acids on the Concentration of Na^+ Counterions

Bolion	Polymer	(Na^+), N	r	$10^4 r(Na^+)^2$	$10^4 r(Na_f^+)^2$
P2	PAA	0.03	4.58	41.2	28.6
		0.05	1.55	38.8	31.4
		0.07	0.80	39.2	33.8
P2	i-PMA	0.03	3.02	27.2	18.9
		0.05	0.88	22.0	17.8
		0.07	0.40	19.6	16.9
P2	s-PMA	0.03	4.15	37.4	25.9
		0.05	1.52	38.0	30.8
		0.07	0.73	35.8	30.8
PX	PAA	0.03	3.85	34.7	24.1
		0.05	1.32	33.0	26.7
		0.07	0.73	35.8	30.8
PX	i-PMA	0.03	3.34	30.1	20.9
		0.05	1.04	26.0	21.1
		0.07	0.53	26.0	22.4
PX	s-PMA	0.03	7.45	67.0	46.6
		0.05	3.03	75.7	61.2
		0.07	1.46	71.5	61.7

$$Q^{\mathrm{El}}(b) = (\tfrac{5}{2} - \Gamma - \tfrac{1}{2}\ln 2) + \ln b + \frac{1}{1-T}\left(\frac{3}{b} + \frac{2}{b^2}\right) + \frac{T}{1-T}\left[Ei(b) - \ln b - \Gamma - \frac{1}{b}e^b - \frac{2}{b^2}e^b + 2\right] + 2\left[Ei(-b) - \ln b - \Gamma + \frac{1}{b}e^{-b} - \frac{1}{b^2}e^{-b}\right]$$

$$Q^{\mathrm{Rel}}(b) = 2\beta + \Gamma - 2 + \frac{1}{b}e^b\left(1 + \frac{1}{b} + \frac{2}{b^2}\right) - Ei(b) + T(b)[2T(b) - 2]^{-1}$$

$$T(b) = \exp(-b)\left[1 + b + \frac{1}{2}b^2\right]$$

$$\beta = 0.4609;\ \Gamma = 0.5772;\ Ei(b) = \int_{-\infty}^{b} t^{-1}e^t\,\mathrm{d}t$$

Qualitatively, our result is in agreement with the conductance formula of Fuoss and Onsager.[1] In particular, the relaxation field strength is nearly equal in both cases. It is given by

$$\delta E = \frac{\mu E}{6(1 + \sqrt{q})} - \frac{1}{12}\mu^2 E\left[\ln \mu + N + e^b \times \left(\frac{1}{b^2} + \frac{1}{b}\right) - Ei(b)\right] + O(\mu^3)$$

Only the function N is different. In our result, N is constant; $N = -0.0010$. Fuoss and Onsager get

$$N = N(b) = 3[1.486 - 4.32\exp(-1.17b)]$$

$N(b)$ depends weakly on b. Our formula for the electrophoretic force differs from that of Fuoss and Onsager by a term $\mu^2 \log \mu$, and there is only qualitative agreement in the μ^2 term. The main difference between the conductance formulas is due to the contribution of the short-range forces. In the case of high b values ($b \gg 1$) we retain only the first term of the asymptotic expansion and get

$$\sigma/\sigma_0 = 1 - K_{\mathrm{A}}c$$

$$K_{\mathrm{A}} = \frac{4\pi La^3}{1000}\frac{e^b}{b}$$

where c is the concentration in moles per liter and K_{A} is the association constant. This formula is in agreement with Bjerrum's theory of ionic association. The asymptotic result of Fuoss and Onsager is

$$K_{\mathrm{A}} = \frac{4\pi La^3}{3000}e^b$$

The difference between the Fuoss–Onsager formula and ours has its origin in the calculation of the contribution of the short-range forces (osmotic term). In our calculation, the terms of order e^b in the electric and short-range forces are equal with opposite sign and only terms of order e^b/b remain. In an earlier paper, it was shown by rigorous statistical considerations that, in the case of thermodynamic equilibrium, the properties of ionic solutions, which have large values of b, are also described by Bjerrums's theory.[4]

Acknowledgment. The authors wish to thank Professors H. Falkenhagen and G. Kelbg for many helpful discussions.

---

[4] W. Ebeling and G. Kelbg, *Z. Physik. Chem.* (Leipzig), in press.

$C_3F_7 + C_2H_5$ and $C_2F_5 + C_2H_5$ Disproportionation/Combination and Cross-Combination Ratios. A Reexamination[1]

by G. O. Pritchard and R. L. Thommarson

Department of Chemistry, University of California,
Santa Barbara, California *(Received March 23, 1966)*

In our experiments on the photolysis of $C_3F_7COC_2H_5$[2] and $C_2F_5COC_2H_5$,[3] the title disproportionation/combination ratios were either very scattered, particularly for $C_2F_5COC_2H_5$,[3] or could be represented by an Arrhenius plot where $E_{\mathrm{disp}} - E_{\mathrm{comb}} \simeq -2$ kcal mole^{-1}. Taking $C_3F_7COC_2H_5$ as an example, the reactions of interest are (C_3F_7 is normal)

$$C_3F_7 + C_2H_5 \longrightarrow C_3F_7H + C_2H_4 \quad (1)$$

$$C_3F_7 + C_2H_5 \longrightarrow C_3F_7C_2H_5 \quad (2)$$

$$C_2H_5 + C_2H_5 \longrightarrow C_2H_6 + C_2H_4 \quad (3)$$

$$C_2H_5 + C_2H_5 \longrightarrow C_4H_{10} \quad (4)$$

$$C_3F_7 + C_2H_5COC_3F_7 \longrightarrow C_3F_7H + C_2H_4COC_3F_7 \quad (5)$$

$$C_2H_5 + C_2H_5COC_3F_7 \longrightarrow C_2H_6 + C_2H_4COC_3F_7 \quad (6)$$

Based on the established value[4] for $k_3/k_4 = 0.14$, the

---

[1] This work was supported by a grant from the National Science Foundation.

[2] G. O. Pritchard and R. L. Thommarson, *J. Phys. Chem.*, **69**, 1001 (1965).

[3] R. L. Thommarson and G. O. Pritchard, *ibid.*, **70**, 2307 (1966).

[4] J. A. Kerr and A. F. Trotman-Dickenson, *Progr. Reaction Kinetics*, 1, 107 (1961).

ethylene formed in reaction 1 was computed, and k_1/k_2 was obtained.[2,3] By performing a series of experiments at constant temperature but varying pressure, an alternative method of obtaining k_1/k_2 (and k_3/k_4) is available,[5] and we may write $R_{C_3F_7H}/R_{C_3F_7C_2H_5} = k_4^{1/2}k_5\cdot$[ketone]$/k_2R^{1/2}{}_{C_4H_{10}} + k_1/k_2$ and $R_{C_2H_6}/R_{C_4H_{10}} = k_6$[ketone]$/k_4^{1/2}R^{1/2}{}_{C_4H_{10}} + k_3/k_4$.

Experimental Details and Results

We have now conducted such experiments, and the data are presented in Figure 1 for $C_3F_7COC_2H_5$. A least-squares treatment of the runs at 92° gives an intercept at zero ketone concentration $= k_1/k_2 = 0.17 \pm 0.01$; the data at 237° yield a value of $k_1/k_2 = 0.23 \pm 0.03$. The previous values[2] of this ratio varied between 0.38 at 80° and 0.16 at 256°, leading to the conclusion that $E_1 - E_2 = -2200$ cal mole^{-1}; the average value was 0.27. The present data negate the reported[2] temperature dependence; the experiments at 92° certainly do not lead to an intercept at ~0.4. It would seem that k_1/k_2 is best represented by ~0.2, independent of temperature. The original data[2] were based on mass spectrometric analysis, while in the present experiments vpc was employed.[3] As an internal check, the ratio $R_{C_2H_6}/R_{C_4H_{10}}$ was obtained; this is arbitrarily extrapolated to $k_3/k_4 = 0.14$ at zero concentration in Figure 1.

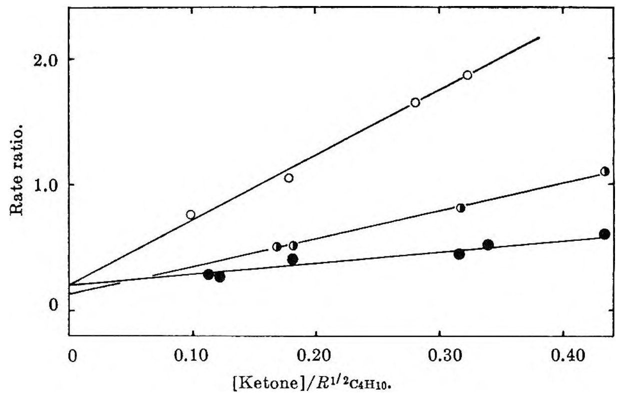

Figure 1. Plots of $R_{C_3F_7H}/R_{C_3F_7C_2H_5}$, ○ at 237°, ● at 92°, and $R_{C_2H_6}/R_{C_4H_{10}}$, ◑ at 92°, both *vs.* [ketone]/$R^{1/2}{}_{C_4H_{10}}$.

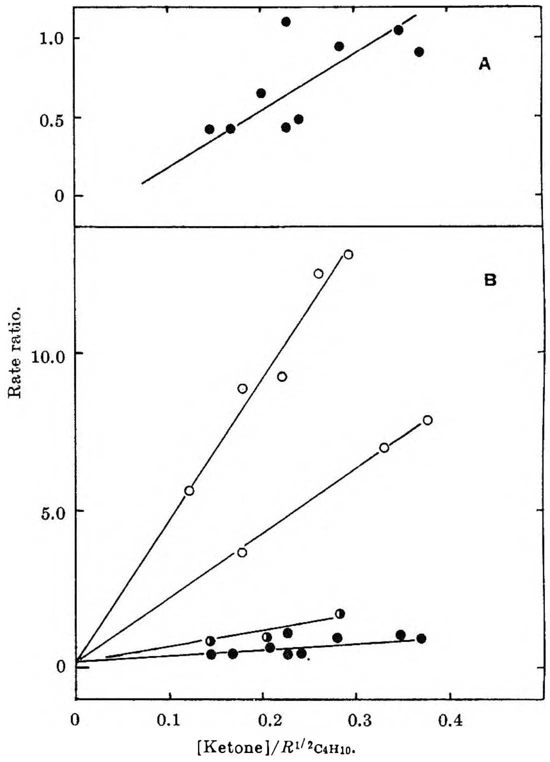

Figure 2. A, plot of $R_{C_2F_5H}/R_{C_2F_5C_2H_5}$ *vs.* [ketone]/$R^{1/2}{}_{C_4H_{10}}$ at 132°; B, the same plot at 265°, ○ (two series), and 132°, ●; also $R_{C_2H_6}/R_{C_4H_{10}}$ at 156°, ◑.

Values of the cross-combination ratio, $k_2/(k_4k_7)^{1/2}$ were found to be 3.15 ± 0.1 at 237°, and 2.56 (range

$$C_3F_7 + C_3F_7 \longrightarrow C_6F_{14} \qquad (7)$$

2.41–2.87) at 92°, which, if significant, leads to $E_2 - {}^1/_2(E_4 + E_7) = 0.53$ kcal mole^{-1}. This is lower than the previous value[2] of 1.9 kcal mole^{-1} based on values of $k_2/(k_4k_7)^{1/2}$ varying from 1.4 at 80° to 4.5 at 256°; the average value was 2.6. A value of 3.2 has also been quoted,[4] based on some rather scattered data.[6]

The data derived from $C_2F_5COC_2H_5$ photolysis (Figure 2) are much less precise. Several series of experiments were carried out at 132°, but the experimental scatter (see Figure 2A) could not be eliminated. Under the chromatographic conditions employed[3] the C_4F_{10}, C_4H_{10}, C_2F_5H, and $C_2F_5C_2H_5$ were eluted from the column in 1.7, 3.2, 5.7, and 9.9 min, respectively; the peaks were distinct and well formed, and mass spectrometric analysis established that each peak represented a pure compound. A least-squares treatment gives k_1'/k_2' (for C_2F_5 and C_2H_5) $= -0.2 \pm 0.3$ (standard deviation). The data are also presented in Figure 2B together with two sets of experiments conducted at 265°. The slopes of the two lines at 265° differ almost exactly by a factor of 2. The experiments leading to the lesser slope were performed first, followed by several series of experiments at 132°, which were rejected. On returning to the original temperature, the line of greater slope was obtained. It may be that some undetected error or change in a calibration factor was involved. The data that we have reported at 132° were then

---

(5) K. O. Kutschke, M. H. J. Wijnen, and E. W. R. Steacie, *J. Am. Chem. Soc.*, **74**, 714 (1952).

(6) G. O. Pritchard, Y. P. Hsia, and G. H. Miller, *ibid.*, **85**, 1568 (1963).

NOTES

Nitrogen Adsorption on Iridium and Rhodium[1]

by V. J. Mimeault and Robert S. Hansen

Institute for Atomic Research and Department of Chemistry, Iowa State University, Ames, Iowa *(Received February 24, 1966)*

According to Bond,[2] nitrogen is not chemisorbed on group VIII-B metals. We have found this to be the case for iridium and rhodium by the absence of a pressure increase on heating a sample filament (Ir or Rh) dosed with nitrogen at 300°K. However, we have found some evidence that nitrogen adsorption does occur on iridium and rhodium if the nitrogen is thermally activated. The source of this thermal energy is the hot tungsten filaments present in conventional ionization gauges. This note is a summary of our findings.

The vacuum system and experimental procedure are described elsewhere.[3] Nitrogen gas was leaked into the vacuum system until the steady-state pressure was 4×10^{-7} torr. On flashing the filament, either iridium or rhodium, the total pressure increase was measured with a Bayard-Alpert ionization gauge containing a thoriated tungsten filament operating at 0.4-ma emission, and the partial pressure increase was measured with a small bakeable mass spectrometer. The residual gases present in the background were less than 0.5% of the total nitrogen pressure. It was observed that under these conditions, no adsorption of nitrogen occurred as indicated by the absence of a pressure increase on flashing after dosing the filament for 15 min at 300°K. At this pressure (4×10^{-7} torr), enough molecules strike the surface to form a monolayer in $\sim$6 sec (if the sticking probability is unity). Since the flash filament technique is capable of detecting 0.02 monolayer, the absence of a pressure increase on flashing implies that the amount of adsorption was negligible.

Nitrogen adsorption can be made to occur on iridium or rhodium if the tungsten filaments in the Nottingham ion gauge[4] are operated at a temperature T_f greater than 2000°K. Since no direct line of sight exists between the tungsten filaments and the iridium or rhodium filament, a particle must make many collisions with the glass walls of the vacuum system in traveling from the tungsten filaments to the sample filament. The amount of nitrogen desorbed is proportional to the dosing interval for fixed T_f, and the proportionality constant increases strongly with T_f (Figure 1). The adsorbing iridium or rhodium filament was held at 300°K during dosing. A plot of the log of the amount of nitrogen desorbed for fixed dosing period (this amount is proportional to the adsorption rate constant) against $1/T_f$ is linear as shown in Figure 2. The slope of this plot corresponds to an activation energy of 58 kcal/mole, which is approximately one-fourth the dissociation energy of molecular nitrogen (226 kcal/mole).

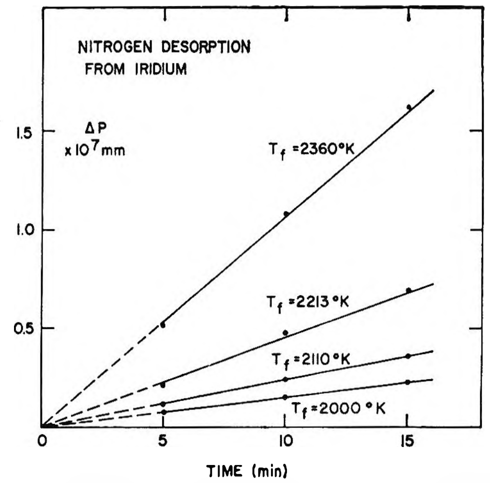

Figure 1. Desorption of nitrogen from iridium as a function of dosing time and temperature of the ion gauge filament.

During the long adsorption time, there was appreciable adsorption of CO from the ambient background impurities. The low-temperature (short time) mass 28 peak in Figure 3 is due to carbon monoxide, as is shown by the coincident peak in the mass 12 fragment. Figure 3 also shows that the high-temperature peak consists of $^{14}N_2$, $^{14}N^{15}N$, and $^{15}N_2$ in substantially statistical ratio although the dosing mixture contained only $^{14}N_2$ and $^{15}N_2$. Hence, substantially complete scrambling of isotopes has occurred in the adsorption–desorption process. This strongly indicates that the nitrogen has been adsorbed as independent atoms mobile on the surface at a temperature below the desorption temperature. The high desorption temperature ($\sim$1000°K) indicates strong binding of the nitrogen to the surface which is also consistent with atomic adsorption.

The adsorption of nitrogen on iridium and rhodium can be explained by a model based on the dissociation

---

[1] Work was performed at the Ames Laboratory of the U. S. Atomic Energy Commission. Contribution No. 1862.

[2] G. C. Bond, "Catalysis by Metals," Academic Press, New York, N. Y., 1962.

[3] V. J. Mimeault and R. S. Hansen, *J. Chem. Phys.*, in press.

[4] W. B. Nottingham, *Natl. Symp. Vacuum Technol. Trans.*, 1, 76 (1954).

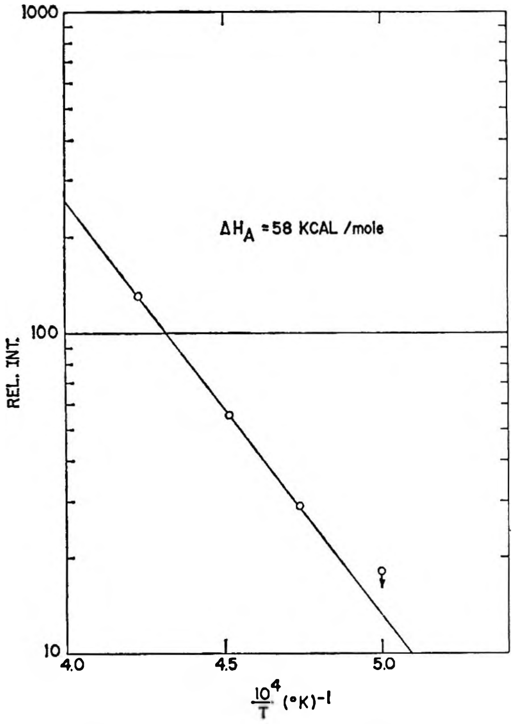

Figure 2. Dependence of the rate of adsorption of activated nitrogen on iridium on the temperature of the activating source.

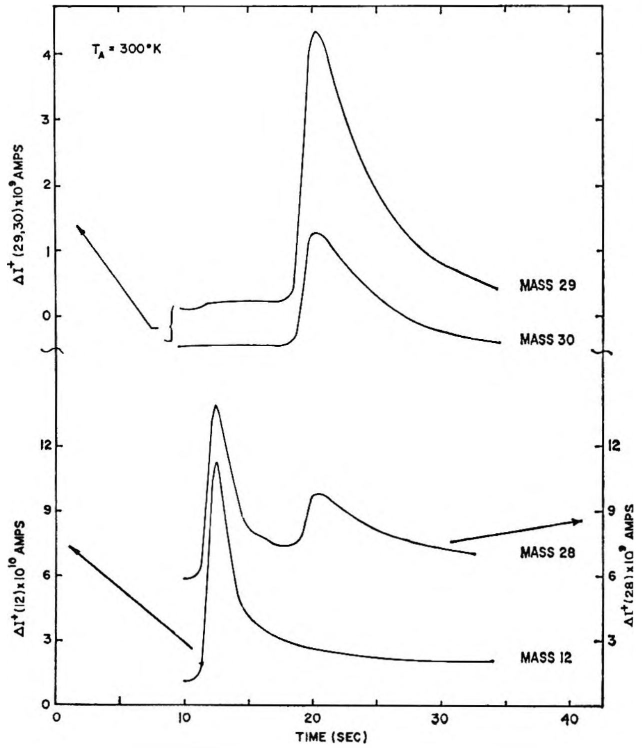

Figure 3. Desorption of nitrogen isotopes from rhodium dosed at 300°K with a mixture of $^{14}N_2$ and $^{15}N_2$. The curves are translated vertically for clarity. The arrows in each case relate the curve to the appropriate scale.

of molecular nitrogen on the hot tungsten filament, with the atomic nitrogen produced largely recombined catalytically on the glass walls so that a steady-state atomic nitrogen concentration is maintained by the balance of thermal dissociation and catalytic recombination. The rate of adsorption on the rhodium or iridium filament is then proportional to the steady-state concentration of atomic nitrogen. Let N_g, N_w, and N_G be the nitrogen atom concentrations (volume or surface as appropriate) in the gas phase and on the tungsten and glass surfaces, respectively, and let N_2(g) be the gas phase concentration of molecular nitrogen. The model is summarized in eq 1–3

$$^1/_2N_2(g) \underset{}{\overset{K}{\rightleftharpoons}} N_w \xrightarrow{k'} N_g \quad \text{(thermal dissociation)} \qquad (1)$$

$$N_g \overset{K'}{\rightleftharpoons} N_G \quad \text{(adsorption)} \qquad (2)$$

$$2N_G \xrightarrow{k''} N_2(g) \quad \text{(catalytic recombination)} \qquad (3)$$

plus the steady-state assumption that N_g is produced by reaction 1 and consumed by reactions 2 and 3 at the same rate.

The rate of production of atomic nitrogen due to the hot filament is

$$\left(\frac{dN_g}{dt}\right)_f = k'N_w = k'KP_{N_2}{}^{1/2} = kP_{N_2}{}^{1/2} = Ae^{-\Delta H_1^{\ddagger}/RT}P_{N_2}{}^{1/2} \qquad (4)$$

where $\Delta H^{\ddagger}$ is the effective activation energy and A is the preexponential term for the over-all reaction 1; presuming the transition state for the second reaction is very nearly desorbed atomic nitrogen, as seems likely, $\Delta H_1{}^{\ddagger}$ = 113 kcal, *i.e.*, half the dissociation energy of nitrogen.

From reactions 2 and 3 we obtain for the rate of recombination of atomic nitrogen on the glass

$$-\left(\frac{dN_g}{dt}\right)_G = k''N_G{}^2 = k''(K'N_g)^2 \qquad (5)$$

For steady state, the production of atomic nitrogen according to eq 4 must be balanced by its consumption according to eq 5, *i.e.*

$$kP_{N_2}{}^{1/2} = k''(K'N_g)^2 \qquad (6)$$

or

$$N_g = \left(\frac{k}{k''}\right)^{1/2}(K')^{-1}P_{N_2}{}^{1/4} \qquad (7)$$

The rate of adsorption is assumed proportional to N_g. Of the rate constants on the right side of eq 7, only k changes as T_f is varied. The effective activation energy for atomic nitrogen adsorption should hence be half

Table II

System	T_c/deg K	$(x_2)_c$	$\tilde{V}^E$/cm³	$\tilde{H}^E$/cal	$T_c\tilde{V}^E/\tilde{H}^E$ deg bar⁻¹	dT_c/dP deg bar⁻¹
Carbon disulfide + acetone	222	0.34	0.5[a]	250[a]	0.011	0.01[b]
Triethylamine + water	292	0.90	−1.30	380	0.024	0.021
n-Perfluoroheptane + 2,2,4-trimethylpentane	296	0.62	4.33	480	0.065	0.065
1-Hydro-*n*-perfluoroheptane + dioxane	308	0.82	1.10	235	0.035	0.028

[a] Extrapolated from room temperature using data from ref 20 and 21. (The α's from Staveley, *et al.*,[20] predict an excess volume independent of temperature, which is surely wrong.) [b] Winnick[21] has observed critical solution phenomena at 271°K and 5000 bars (x_c about 0.3). If T_c is linear in P up to these pressures, these data combined with those of Clusius and Ringer[19] yield dT_c/dP = 0.010 deg bar⁻¹.

while slowly stirring the mixture with a glass-enclosed magnetic bar and while cooling the bath at a rate of 0.1°/min or less. From three to eleven points were determined for each system. Within experimental error all the curves (ΔT_c *vs.* P) were linear.

Results

The derivative dT_c/dP was determined for nine systems. The estimated precision of T_c (at 1 atm) is ±0.05°; the standard deviation σ for dT_c/dP is given in Table I.

Timmermans reported values of T_c and dT_c/dP of 315.6°K and 0.032 deg bar⁻¹, respectively, for methanol + *n*-hexane. Hildebrand's results[16] for *n*-perfluoroheptane + 2,2,4-trimethylpentane are 295.45°K and 0.0653 deg bar⁻¹, while Dunlap and Furrow[6,15] obtained values of 296.57°K and 0.0665 deg bar⁻¹.

There are sufficient data available to compare dT_c/dP with $T_c\tilde{V}^E/\tilde{H}^E$ (eq 3) for four systems: carbon disulfide + acetone,[17-21] triethylamine + water,[3,22-24] *n*-perfluoroheptane + 2,2,4-trimethylpentane,[6,15,25,26] and 1-hydro-*n*-perfluoroheptane + dioxane.[27,28] Table II shows the good agreement for these four systems.

The reasonable agreement (20%) of the fourth system is especially surprising since $\tilde{V}^E$ and $\tilde{H}^E$ clearly do not have the same over-all functional form. The heat of mixing is a sigmoid curve, negative for small values of x_2, positive for larger values; the volume change is positive for all compositions.[28] However, all that is required to obtain eq 3 is that $\tilde{V}^E$ and $\tilde{H}^E$ have the same functional form in the critical region, *i.e.*, for mole fractions in the neighborhood of the critical composition.

Further thermodynamic measurements on these and other systems near the critical solution point are required before the range of validity of the approximate eq 3 can be established.

Acknowledgments. The research program of which this is a part has been supported by the National Science Foundation, the Atomic Energy Commission, and the Petroleum Research Fund of the American Chemical Society. The authors also wish to thank Dr. J. Winnick for supplying his data in advance of publication and for some helpful suggestions.

---

(17) J. Timmermans, *J. Chim. Phys.*, **20**, 493 (1923).

(18) G. C. Schmidt, *Z. Physik. Chem.*, **121**, 221 (1926).

(19) K. Clusius and W. Ringer, *ibid.*, **A187**, 186 (1940).

(20) L. A. K. Staveley, W. I. Tupman, and K. R. Hart, *Trans. Faraday Soc.*, **51**, 340 (1955).

(21) J. Winnick, University of Missouri, personal communication.

(22) J. L. Copp and D. H. Everett, *Discussions Faraday Soc.*, **15**, 174 (1953).

(23) D. E. Tsakalotos, *Z. Physik. Chem.*, **A68**, 34 (1909).

(24) R. V. Mertzlin, *J. Gen. Chem.* (U.S.S.R.), **5**, 161, 886 (1935), quoted in ref 1.

(25) C. Booth and R. L. Scott, unpublished.

(26) A. G. Williamson and R. L. Scott, *J. Phys. Chem.*, **65**, 275 (1961).

(27) J. L. Carson, R. J. Knight, I. D. Watson, and A. G. Williamson, *ibid.*, **69**, 3200 (1965).

(28) R. J. Knight I. R. McKinnon, I. D. Watson, and A. G. Williamson, University of Otago, Dunedin, New Zealand, personal communication.

Relationships between Electrode Potential and Related Functions, and the Hydrogen Content of Alloys of 40% Silver and 60% Palladium

by A. W. Carson and F. A. Lewis

Chemistry Department, The Queen's University of Belfast, Belfast, Northern Ireland *(Received May 31, 1966)*

Some preliminary results have been reported earlier[1] of the values of electrode potential, E, corresponding

---

(1) F. A. Lewis and W. H. Schurter, *Naturwiss.*, **47**, 177 (1960).

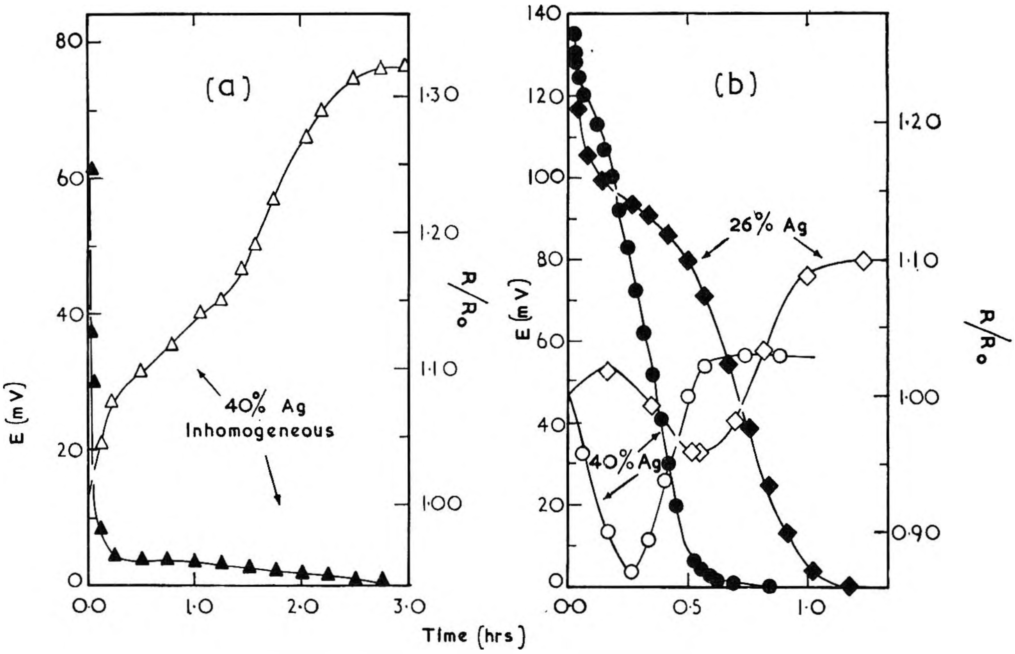

Figure 1. Plots of electrode potential (filled symbols) and relative electrical resistance (open symbols) against time during absorption of hydrogen by wires of 0.0122-cm diameter (coated electrolytically with palladium black) immersed in hydrogen-saturated and stirred 0.02 N HCl at 25°.

to arrests or the maximum values of partial arrests, in plots of changes of E against time obtained during the absorption of hydrogen by both "bright" and "palladized" wire specimens of a series of Pd and Ag alloys. These arrests have been described[1] as "potential plateaux" associated with regions of hydrogen content over which α- and β-phase hydrides coexist.

The purpose of the present note is to report that the 40% Ag alloy has since been found to have been nonhomogeneous. This is shown here to have given rise to apparent plateau potentials unrepresentative of a homogeneous alloy and to related errors in the derivation[2] of pressure-composition relationships from the E against time plots.

Chemical analyses carried out at three independent laboratories each confirmed that the original sample contained only Pd and Ag (except for trace amounts of other metals), that the over-all Ag content was 40 ± 0.5% Ag, and that this content was virtually constant along the whole length of wire samples available. Nevertheless, the specific electrical resistance (25°) was substantially lower ($\sim$23 × 10^{-6} ohm cm^{-1}) than values cited by previous investigators[3,4] ($\sim$40 × 10^{-6} ohm cm^{-1}), and X-ray powder photographs indicated the surface layers to have a substantially higher content of Ag ($\sim$55–58% Ag). These physical measurements suggested the possibility of an inhomogeneity of composition across the diameter of the 0.0122- and 0.0274-cm diameter wires available. This was confirmed by an X-ray fluorescent "microprobe" analysis[5] of a section across the diameter of a 0.0274-cm diameter wire. This not only showed the surface to be relatively poor in palladium, but also revealed, in the interior, well-marked (though rather unsymmetrically distributed) regions which contained >70% Pd.

Changes of E and of relative electrical resistance, R/R_0 (where R_0 is the resistance when free of hydrogen), with time in hydrogen-saturated 0.02 N HCl (chosen to reduce errors resulting from coconduction of the "measuring current" through the electrolyte[6]) of a "palladized" specimen (0.0122-cm diameter) of the inhomogeneous 40% Ag alloy available to Schurter[1] are drawn in Figure 1a and show an apparent potential plateau at $\sim$4 mv, close to the values of 6 mv reported earlier,[1] which had been recorded with a specimen from the 0.0274-cm diameter sample. Figure 1b shows the very different measurements of changes of the same parameters under the same experimental conditions

---

(2) F. A. Lewis, *Platinum Metals Rev.*, **5**, 21 (1961).

(3) B. Svensson, *Ann. Physik*, [5] **14**, 699 (1932).

(4) W. R. G. Kemp, P. G. Klemens, A. K. Sreedhar, and G. K. White, *Proc. Roy. Soc.* (London), **A233**, 480 (1956).

(5) This was carried out by Metals Research Ltd., Cambridge, England.

(6) See, *e.g.*, J. C. Barton and F. A. Lewis, *Talanta*, **10**, 237 (1963).

for a further alloy also with a composition (confirmed by chemical analysis) of 40% Ag–60% Pd. Measurements of lattice parameter and of specific electrical resistance (39.36 × 10^{-6} ohm cm^{-1} at 25°) of this newer alloy were in keeping with those reported for this composition by previous investigators.[3,4,7] Furthermore, the form of the R/R_0 against hydrogen content relationship which may be derived from the E against time plot (assuming the absorption of hydrogen to be governed by transport of hydrogen molecules through solution[8]) is similar in form to relationships obtained earlier by Rosenhall[9] for a 40% Ag alloy. Finally, the form of the initial changes (for times up to ~20 min) of the R/R_0 against time curve for the "original" alloy, in Figure 1a, also seem in keeping with the surface being richer in silver than the interior, since here these changes reflect relationships between hydrogen content and R/R_0 characteristic of homogeneous alloys containing ~50–55% Ag.[9,10]

Nevertheless, however, despite the obvious differences in detailed results between the two specimens, the hydrogen content of the more recently prepared alloy [H/Me (atomic ratio of hydrogen to total number of metal atoms) ~ 0.24] in equilibrium at 25° with hydrogen at 1 atm pressure ($E \approx 0$) was the same, within experimental error, as the value quoted earlier[1] for the inhomogeneous alloy.

In a recent account of a related experimental study, Makrides[11] has reported that he was unable to find evidence to suggest that it was possible for Pd and Ag alloys containing ≥40% Ag to form β-phase hydrides at 25°. However, the plot of E against time for the homogeneous alloy in Figure 1b illustrates a fairly distinct change of slope followed by a shoulder occurring at and after E ~ 120 mv. Indeed, in a further experiment at 0° the E against time curve exhibited a brief minimum, over potentials close to E ~ 120, which could perhaps be associated[11] with "supersaturation" prior to nucleation of a second β-phase. Even if not indicative of the onset of a region of coexistence of α- and β-phase hydrides, the "quasi-arrest" at 25° seems still related in general form to the more pronounced but still rather imperfectly invariant arrest cited[1] as a potential plateau for a 26% Ag alloy, results for which together with a complementary R/R_0 against time measurements also are illustrated in Figure 1b. Pressure–composition isotherms at 25° derived from E against time curves for these alloys have shapes suggestive of isotherms not too far removed in temperature from critical isotherms defined with respect to coexistence of α- and β-phase hydrides.

Acknowledgment. We are indebted to the International Nickel Co. (Mond) Ltd. for the preparation of the alloys and to Johnson Matthey & Co. Ltd., for the award of a research grant to A. W. C.

---

[7] F. Kruger and G. Gehm, *Ann. Physik,* [5] 16, 174 (1933).

[8] See, *e.g.,* J. C. Barton, W. F. N. Leitch, and F. A. Lewis, *Trans. Faraday Soc.,* 59, 1208 (1963).

[9] G. Rosenhall, *Ann. Physik,* [5] 24, 4 (1935).

[10] Results to be published.

[11] A. C. Makrides, *J. Phys. Chem.* 68, 2160 (1964).

The Self-Diffusion Coefficient of Sodium Dodecyl Sulfate Micelles

by J. Clifford and B. A. Pethica

Unilever Research Laboratory, Port Sunlight, Cheshire, England
(Received May 31, 1966)

In a recent paper[1] Mazo derived an expression for the concentration dependence of the self-diffusion coefficient of micelles and compared it with experimental results obtained by Stigter, Williams, and Mysels[2] for sodium dodecyl sulfate micelles. Agreement is good except for solutions containing only surfactant and water with no added salt.

The measurements of Stigter, Williams, and Mysels have been criticized on the grounds that the extensive glass surface of their apparatus catalyzes the hydrolysis of the sulfate to the alcohol.[3] The presence of dodecyl alcohol affects both the critical micelle concentration (cmc) and the properties of the micelles. The over-all effect would be expected to be greatest at low concentrations of dodecyl sulfate and in the absence of added salt.

As data on micellar self-diffusion were required for studies of counterion mobility in these systems,[4] we measured the self-diffusion of sodium dodecyl sulfate in aqueous solution without added salt by a technique not subject to the above objection.

The Anderson and Saddington[5] capillary method was employed. The apparatus and the materials used have been described.[4] Capillaries of 0.1-cm bore and 1.5-cm length were used. Azobenzene was used as a

---

[1] R. M. Mazo, *J. Chem. Phys.,* 43, 2873 (1965).

[2] D. Stigter, R. J. Williams, and K. J. Mysels, *J. Phys. Chem.,* 59, 330 (1955).

[3] K. J. Mysels and L. H. Princen, *ibid.,* 63, 1699 (1959).

[4] J. Clifford and B. A. Pethica, *Trans. Faraday Soc.,* 60, 216 (1964).

[5] J. S. Anderson and K. Saddington, *J. Chem. Soc.,* S381 (1949).

suggested that the effect is associated with differences in the size of the nickel crystallites on the different supports. It is emphasized that such an explanation would require an influence of crystallite size over and above an effect on the extent of metal surface area, since the effect of the latter is accounted for in the determination of specific catalytic activity. Such an effect of crystallite size on specific activity may well exist and may account, in part, for the observed effect of the support. According to this line of reasoning, the higher catalytic activity and greater dispersion of nickel on silica or alumina as compared to silica–alumina indicate that the intrinsic catalytic activity is greater for the smaller crystallites. However, the catalytic data on the effect of nickel concentration indicate just the opposite, since increasing the nickel concentration increases crystallite size and activity correspondingly. Thus, one does not obtain a completely consistent explanation on the basis of crystallite size effects alone. The possibility of an optimum crystallite size for catalytic activity has been considered, but it would be difficult to establish such an effect from the available data.

The results of the present study indicate that the influence of the support on the catalytic properties of nickel is a more complex effect than one of gross differences in the reducibility of the metal or of crystallite size. The true nature of the effect remains to be seen. It is to be noted that the effect is particularly important at low metal concentrations.

---

van der Waals Volumes and Radii of Metals in Covalent Compounds

by A. Bondi

Shell Development Company, Emeryville, California

(Received April 19, 1966)

In an earlier paper,[1] an attempt was made to estimate van der Waals radii of metallic atoms. Additional consistent data could not be obtained from X-ray diffraction patterns of organometallic compounds. Yet, the increasing interest in organometallic compounds makes it desirable to correlate their properties within an existing body of property correlations. Hence, those van der Waals volumes of several compounds have been calculated which yield the correct number of external degrees of freedom ($3c$) per molecule when linked with the known density and heat of vaporization data.[1]

With most metal alkyl compounds, such as dimethyl cadmium, free rotation of the alkyl group around the metal–carbon bond can be assumed, so that, for example, for $CdMe_2$ $3c \approx 7$, etc. The van der Waals volume increments and radii of various metallic elements that are compatible with that requirement are listed in Table I. It is noteworthy that these V_w increments are of the same order as the electronic polarizability $[R]_\infty$ (and as the atomic volume of the element in its metallic state), a well-known result of classical physics for the case of conducting spheres.

Table I: van der Waals Volumes and Radii of Several Metals Derived from Metal Alkyl Data[a]

Compd	$E°$, kcal/mole	Θ_L, °K	$3c$	X	$V_w(X)$, cm³/mole	$r_w(X)$, A	$[R]_\infty$, cm³/mole
$ZnMe_2$	7.78	378	6.2	Zn	8.93	1.39	8.9
$ZnEt_2$	10.10	445	6.9	Zn	8.93		
$CdMe_2$	9.57	443	6.5	Cd	12.46	1.62	12.7
$HgMe_2$	8.91	420	6.4	Hg	13.30	1.70	13.8
$PbMe_4$	9.79	482	6.1	Pb	17.8		17.9

[a] $E°$ is the energy of vaporization at that temperature at which the ratio of molal volume to van der Waals volume $(V/V_w) = 1.70$. Θ_L is the characteristic temperature of liquid $= E°/5cR$, determined experimentally as 1.535 × (temperature (°K) at which $V/V_w = 1.80$). r_w is the van der Waals radius. V_w is the van der Waals volume. $[R]_\infty$ is the molar refractivity. References to the definitions and physical meaning of the first four items are given in ref 1.

The proximity of the V_w *increments* to $[R]_\infty$ is somewhat fortuitous because the increments were calculated for connection with carbon and would have been somewhat (but not very) different had they been calculated for combinations with other elements. The primary result of this investigation is the suggestion that the readily available Lorentz–Lorenz refractivity $[R]_\infty$ of metals[2] can be used as a starting point for the estimation of V_w and of r_w of metals in metal organic compounds.

Should the indicated relation be valid for metal atoms generally, it would mean that the electron density of metal atoms decreases far more steeply with distance outward from the point of maximum electron density[3] than is the case with the atoms of

---

(1) A. Bondi, *J. Phys. Chem.*, **68**, 441 (1964).

(2) S. S. Batsanov, "Refractometry and Crystal Structure," Consultants Bureau, New York, N. Y., 1961.

(3) J. C. Slater, "Quantum Theory of Molecules and Solids," Vol. II, McGraw-Hill Book Co., Inc., New York, N. Y., 1965, p 106 ff.

In this note, the total heat of adsorption has been correlated with coverage taking into consideration the validity of Aston's equation, for lateral interaction, mentioned above. Consequently, this helps to evaluate the heat of adsorption due to the smooth part, that is, the part having the minimum adsorbable energy of the total surface concerned. The heat of adsorption data of Aston, *et al.*,[11] on Ne–, Ar–, and Kr–graphitized carbon black and –zinc crystal systems and Beebe, *et al.*,[14] on the N_2–Graphon system have been used for calculations.

Results and Discussion

The curves given in the respective papers of the aforesaid authors were traced on transparent coordinate papers very carefully to calculate the heat of adsorption. In the case of N_2 adsorption on Graphon,[14] a part of the curve was smoothly drawn on the traced graph and the values of the heat of adsorption were then calculated.

The surface of any solid is not very smooth.[15] For mostly smooth surfaces, *viz.*, graphitized carbon black, Aston, *et al.*,[11a] have shown that the differential energy of lateral interaction (E) is related to the coverage (θ) as $E = (a/b)\theta$, where a and b are van der Waals constants for the gas concerned. According to Aston, *et al.*, the deviation at low coverage is due to surface heterogeneity. It is a common practice to consider the absence of heterogeneity and lateral interaction in cases where the heat of adsorption remains constant with increasing coverage. However, it is not a poor idea, in accordance with Brunauer,[16] to assume that the compensating contributions of the two effects may yield a constant heat of adsorption. Thus the total energy of adsorption (say the heat of adsorption) on any surface at any coverage per mole is that due to the minimum adsorbable energy sites (say the sites at the homogeneous part of the surface) plus the excess due to heterogeneity and lateral interaction at that coverage. In other words, the heat of adsorption is the resultant of these three effects and the nature of its variation with θ depends upon the ways each of them contribute to it.[17] Mathematically

$$E_t = E_h + E_s + E_l \qquad (1)$$

where E stands for energy, and subscripts t, h, s, and l denote total, heterogeneous surface, smooth surface, and lateral interaction parts, respectively. Considering the validity of the equation of Aston, *et al.*

$$E_t - (a/b)\theta = E_h + E_s \qquad (2)$$

Now for a particular adsorbate–adsorbent system E_s is constant, so $(E_h + E_s)$ will vary inversely with θ since the heterogeneity does so. Therefore we have eq 3

$$E_t - (a/b)\theta = (E_h + E_s) = m\theta^{-n} \qquad (3)$$

where m and n are empirical constants.

From eq 2 and 3 we have

$$\log\{E_t - (a/b)\theta\} \text{ or } \log(E_h + E_s) = \log m - n \log \theta \qquad (4)$$

In Figure 1 (curves 1–4), the validity of eq 4 is shown. The deviations indicated by arrowheads are right from the coverages beyond which the equation of Aston, *et al.*, does not hold. This may be due to complications arising from the compressive effect[11a] in the second and higher layers formed. It is seen from the curves that in the case of Ar, eq 4 is valid up to coverage 1, both on graphitized carbon black and zinc crystal, but for Ne

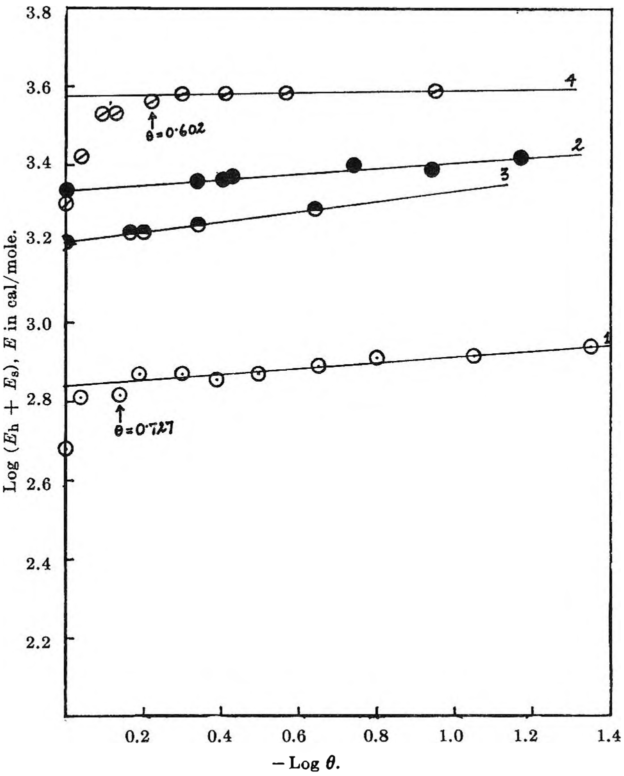

Figure 1. Plot of log (E_h + E_s) *vs.* −log θ: curve 1, Ne–graphitized carbon black system; curve 2, Ar–graphitized carbon black system; curve 3, Ar–Zn crystal system; curve 4, Kr– graphitized carbon black.

---

[15] R. M. Barrer, "Solid/Gas Interface," Proceedings of the Second International Congress of Surface Activity, Academic Press Inc., New York, N. Y., 1957, p 205.

[16] S. Brunauer, "Solid Surface and Gas–Solid Interface," Advances in Chemistry Series, No. 33, American Chemical Society, Washington, D. C., 1961, p 12.

[17] D. Graham, *J. Phys. Chem.*, **57**, 665 (1953).

tally by the usual procedure. The dielectric constants were ϵ_{15° 200.1, ϵ_{25° 182.4, ϵ_{35° 174.3, and ϵ_{45° 167.1 at the temperatures indicated and were those reported by Leader and Gormley.[7] The values of viscosities at the different temperatures were $\eta_{15^\circ} = 0.0199$, $\eta_{25^\circ} = 0.0165$, $\eta_{35^\circ} = 0.0142$, and $\eta_{45^\circ} = 0.0123$ poise.[6,8] The values of the limiting transport numbers, t_+^0, of K^+, at various temperatures, obtained from the plot of the Longsworth function against concentration, are also given in Table I under the concentration heading 0.00 *M*.

Results and Discussion

As can be seen from Table I, the variations in the transport number, t_+, of K ion in N-methylformamide are very much similar to those in formamide[3] and in N-methylacetamide;[4] *i.e.*, t_+ decreases with increase in concentration and increases with increase in temperature. The limiting transport number of potassium ion, *i.e.*, $t_+{}^\circ{}_{(K^+)}$, increases from 0.4945 at 15° to 5290 at 45°. This behavior is opposite to that in aqueous solutions in which $t_+{}^\circ{}_{(K^+)}$ decreases slightly with rise in temperature. Recently, Gill[9] has reported similar behavior of the cationic transport number of KNO_3 in liquid ammonia in which $t_+{}^\circ{}_{(K^+)}$ has been found to decrease with rise in temperature in the range −65 to −45°, although $t_+{}^\circ{}_{(Na^+)}$, $t_+{}^\circ{}_{(Li^+)}$, and $t_+{}^\circ{}_{(NH_4^+)}$ increase with rise in temperature as $t_+{}^\circ{}_{(K^+)}$ (KBr) does in N-methylformamide.

It may be noted that $t_+{}^\circ{}_{(K^+)}$ increases beyond 0.5 with rise in temperature. This is a little unusual although such values of the transport number have been reported in the literature.[10]

Ionic Mobilities

The limiting cationic transport numbers at different temperatures can be used to calculate the ionic mobilities from the available electrolytic conductance data[6] in this solvent and making use of the usual Kohlrausch law of the independent migration of ions. The ionic conductivities at infinite dilution of some ions thus obtained are given in Table II.

Since no ionic conductance data are available in the literature, it is not possible to verify the values given in Table II. However, they seem to be reasonable if they are compared with the corresponding values in formamide and in N-methylacetamide. Since the tetrahedral structure present in water is missing in these solvents, the structure-breaking effect of the larger ions like K^+ is also missing in these solvents and so all the ions behave normally. In view of the lack of sufficient and appropriate electrolytic, and hence the ionic, conductance data in this solvent, it is not possible to make a reasonable estimate of the solvation of ions as was done in NMA.[4] This aspect will be examined later when the required data are available.

Table II: Mobilities of Some Ions in N-Methylformamide at Different Temperatures

	Ionic mobility at			
Ion	15°	25°	35°	45°
Na^+	17.59	21.56	...	...
K^+	18.05	22.13	27.62	32.15
Cs^+	19.90	24.39	...	...
$(C_2H_5)_4N^+$	21.52	26.20	...	...
$Picrate^-$	11.28	13.08	...	...
Cl^-	16.88	19.70	...	...
Br^-	18.46	21.56	25.38	28.60
I^-	19.38	22.76	...	...

Acknowledgment. A grant from the Society of Sigma Xi and RESA Research Fund of the United States of America for the purchase of the solvents (NMA, NMF, and NMP) is very much appreciated.

---

[7] G. R. Leader and J. F. Gormley, *J. Am. Chem. Soc.*, **73**, 5731 (1951).

[8] R. Gopal and S. A. Rizvi, *J. Indian Chem. Soc.*, **43**, 179 (1966).

[9] J. B. Gill, *J. Chem. Soc.*, 5730 (1965).

[10] B. E. Conway, "Electrochemical Data," Elsevier Publishing Co., London, 1952, p 166.

Photooxidation of Perfluoroethyl Iodide and Perfluoro-*n*-propyl Iodide[1a]

by Dana Marsh and Julian Heicklen[1b]

Aerospace Corporation, El Segundo, California

(Received February 15, 1966)

In earlier reports, the oxidation of CF_3[2] and $CFCl_2$[3] radicals was examined. In the former case, the only carbon-containing product was CF_2O, whereas in the latter case only CFClO was found. In the presence of HI, the results were unchanged.

In this work, we extend the oxidation studies to C_2F_5 and n-C_3F_7 radicals in order to determine the products of reaction and the nature of the intermediates. In both cases, the major product is CF_2O.

---

[1] (a) This work was supported by the U. S. Air Force under Contract No. AF 04(695)-669. (b) To whom requests for reprint should be sent.

[2] J. Heicklen, *J. Phys. Chem.*, **70**, 112 (1966).

[3] D. G. Marsh and J. Heicklen, *ibid.*, **69**, 4410 (1965).

metals,[5] although the existence of these species has been deduced by other means.) An ion current due to KOH was also observed, but this species resulted both from the formation of KOH on the amalgam during the loading process and from the reaction of vaporized potassium with residual H_2O in the mass spectrometer. There was no evidence of K_3^+, HgK^+, HgK_2^+, HgK_3^+, or of heavier ion species. At 20 ev, the relative ion intensities (in arbitrary units) of the three species, I_{K^+} (isotope 39), $I_{K_2^+}$ (isotope 78), and I_{Hg^+} (isotope 202) were 400, 0.26, and 40, respectively; the ratios of I_{Hg^+}/I_{K^+} and $I_{K_2^+}/I_{K^+}$ are 0.1 and 6.5×10^{-4}, respectively. The background ion intensities of masses 39 and 78 were nearly at the sensitivity limit of the instrument (0.001), while the background ion intensity of Hg^{202} was 0.0432. (The observed ratio of $I_{K_2^+}/I_{K^-}$ is directly proportional to the ratio P_{K_2}/P_K. From published data[6,7] for potassium at 200°, $P_{K_2}/P_K = 7.7 \times 10^{-4}$.) In contrast, Roeder and Morawietz,[3] to best fit their effusion data, calculated partial pressures for K, Hg, and HgK_3 over a 77.5 at. % potassium amalgam at 200° of 6.00×10^{-3}, 2.60×10^{-3}, and 1.62×10^{-3} torr, respectively; the corresponding ratios of P_{Hg}/P_K and P_{HgK_3}/P_K are 0.43 and 0.27, respectively.

Although HgK_3 was not observed, the question arises as to whether the molecule exists in the vapor but has such a low dissociation energy that it cannot be observed with a mass spectrometer. This question can be qualitatively answered by considering the gaseous K_2 and Hg_2 molecules. Even though the K_2 molecule has a low dissociation energy of 0.51 ev,[8] it was easily observed with the mass spectrometer. If the HgK_3 molecule had a dissociation energy of approximately 0.5 ev and were present in the vapor to the extent proposed by Roeder and Morawietz, it probably would have been detected. The Hg_2 molecule, with a dissociation energy of 0.06 ev,[9] was not observed. The partial pressure expected for Hg_2 under these experimental conditions was calculated to be 1.3×10^{-9} atm. Even though this pressure is very near the limit of detection of the mass spectrometer, it is felt that the Hg_2^+ ion, if present, would have been observed because of the very low background in the region of mass 400. If the dissociation energy of HgK_3 is similarly low, one would not expect to observe HgK_3 even if it were present in the vapor to a considerable extent. However, one might reasonably expect to see one or more of the fragment species K_3^+, HgK^+, or HgK_2^+—none of which was observed. Furthermore, these considerations indicate that the dissociation energy of an Hg–K bond in HgK_3 would lie between 0.5 and 0.06 ev. Roeder and Morawietz,[3] however, calculated an enthalpy of formation for gaseous HgK_3 of 65 kcal/mole, which would correspond to a dissociation energy of 2.8 ev. A dissociation energy of this order of magnitude would certainly render HgK_3 observable with the mass spectrometer unless, of course, its concentration was below the spectrometer's limit of detection.

The results of this experiment, therefore, indicate that the vapor phase over potassium amalgams consists of K, K_2, and Hg. The species HgK_3 apparently does not exist or, at most, is a very minor component of the vapor.

Acknowledgment. Thanks are due to E. Veleckis for the preparation of the amalgam and for discussions concerning the experiment. H. M. Feder and M. Ader are also to be thanked for discussions concerning this note.

---

(5) B. Siegle, *Quart. Rev.* (London), 19, No. 2, 77 (1965).

(6) L. C. Lewis, *Z. Physik*, 69, 805 (1931).

(7) F. D. Rossini, "Selected Values of Chemical Thermodynamic Properties," Series III, National Bureau of Standards, Washington, D. C., 1954.

(8) G. Herzberg, "Spectra of Diatomic Molecules," 2nd ed, D. Van Nostrand Co., Inc., Princeton, N. J., 1950, p 543.

(9) A. G. Gaydon, "Dissociation Energies and Spectra of Diatomic Molecules," 2nd ed, Chapman and Hall, London, 1953, p 226.

Spin Densities in Biphenylaminyl Network and Triphenylimidazolyl Network

by Hisashi Ueda

Department of Chemistry, The University of Texas, Austin, Texas 78712, and Department of Chemistry, Tokyo Institute of Technology, Ohokayama, Meguro, Tokyo, Japan

(Received February 18, 1966)

Spin densities in the biphenylaminium anion,[1] biphenylaminyl radical,[1-4] triphenylimidazoium anion,[1] and triphenylimidazolyl radical[1] have been reported. In those works calculations were made using the va-

Table I: Spin Densities in Biphenylaminyl Radical and Aminium Anion

	Atomic positions				
	ortho	*meta*	*para*	C	N
Radical					
Experimental	0.084	−0.042	0.084	0.046	0.572
SCFMO	0.099	−0.032	0.094	−0.011	0.587
Anion					
Experimental	0.093	0.254	−0.093	−0.078	−0.046
SCFMO	0.172	0.172	−0.087	−0.078	−0.013

tion rapidly dropped to a smaller constant value as the CF_2O approached about 1% of the C_3F_7I. Presumably, the initial reaction is similar to that for C_2F_5 radicals

$$C_3F_7 + O_2 \longrightarrow C_3F_7O_2 \qquad (11)$$

In some manner, the $C_3F_7O_2$ radical must yield primarily CF_2O. How this occurs is not clear at all.

It is of interest to know whether the RO_2 radical has a measurable lifetime. To that end, we did a number of experiments with 5 to 40 mm of HI added. Two series of experiments were done, one with 280 mm of C_2F_5I and 300 mm of O_2, and the other with 100 mm of C_3F_7I and 300 mm of O_2. Hydrogen iodide had no effect at all on CF_3 or $CFCl_2$ oxidation.[2,3] However, with C_2F_5 and C_3F_7, very marked changes occurred in the oxidation. The results, the same for both series, showed no trend with HI pressure, thus indicating that the initially formed perfluoroalkyl radical was completely scavenged by O_2.

The results can be summarized as follows. First, a red deposit was formed. Second, $\Phi(CF_2O)$ was reduced at least 5- to 20-fold. Third, $\Phi(CF_3CFO)$ may have increased to 0.13 to 0.30 for C_2F_5 radicals as based on the 9.05-μ band of CF_3CFO. The analysis is difficult because of the HI absorption in this region. Fourth, the characteristic $\text{C—}\overset{\text{F}}{\text{C}}\text{=O}$ band at 5.31 μ was the most intense band and was formed at the same rate in all experiments with HI. The CF_3CFO can account for only 25 to 50% of the 5.31-μ band in the C_3F_7I series, but perhaps all of it in the C_2F_5I series. At least for the C_3F_7I series, another product probably was formed. There can be no doubt that HI interferes with the oxidation. Consequently, the RO_2 radical must have a lifetime in excess of 10^{-7} sec.

Acknowledgment. The authors wish to thank Mrs. Barbara Peer for assistance with the manuscript.

Heats of Transport of the Rare Gases in a Rubber Membrane[1]

by Mirion Y. Bearman and Richard J. Bearman

Department of Chemistry, University of Kansas,
Lawrence, Kansas *(Received February 21, 1966)*

Revised values for the heats of transport, Q^*, of the rare gases He, Ne, Ar, Kr, and Xe in rubber are presented. In the case of helium, it is shown that, within experimental error, there is no pressure dependence of the heat of transport in the pressure range 25–65 cm. The apparent Q^* varies slightly with temperature difference across the membrane. Nevertheless, departures from linearity in the local phenomenological equations seem to be negligible even though the temperature gradients range up to 900°/in.

Revised Heats of Transport (Q^*)

In an earlier article, Bearman[2] reported the heats of transport (or "transfer"), Q^*, of the rare gases in a rubber membrane. His values were obtained from thermoosmosis experiments where, at steady state

$$\ln (p_H/p_C)_\infty = -(Q^*/R)(1/T_C - 1/T_H) \qquad (1)$$

Here, H and C refer to the hot and cold side, respectively, T is absolute temperature, p is pressure, and R is the gas constant. His measurements were subject to several errors of unknown magnitude arising chiefly from uncertainties in the pressure and temperature.

With the use of strain gauge pressure transducers and several thermocouple probes, we have constructed an improved apparatus, fully described elsewhere,[3,4] in which the errors have been greatly lowered. In Table I, we present revised values for the heats of transport together with a comparison with the earlier results. The error estimates take into account the observed irreproducibility and also errors arising from temperature and pressure measurements. The irreproducibility is caused mostly by leakage, degassing, and adsorption in the system[3] over the long course of the runs, which last days or sometimes weeks. A pure gum rubber membrane 0.0325 to 0.0350 cm in thickness was used for our measurements reported here.

Pressure and Temperature Difference Dependence of Q^*

Some additional measurements were made with helium. In Table II, we show that, within the experimental error, the heat of transport at constant mean temperature and temperature difference is independent of mean gas pressure in the system in the range from 25 to 65 cm. From this, we conclude that the He–He interactions in the membrane play little role

---

[1] This research was supported in its early stages by a grant from the National Science Foundation. We wish to make acknowledgment to the donors of the Petroleum Research Fund, administered by the American Chemical Society, for partial support of this research in its later phases.

[2] R. J. Bearman, *J. Phys. Chem.*, **61**, 708 (1957).

[3] M. Y. Bearman, Dissertation, University of Kansas, 1965. Available from University Microfilms, Ann Arbor, Mich.

[4] M. Y. Bearman and R. J. Bearman, *J. Appl. Polymer Sci.*, **10**, 773 (1966).

Table I

Gas	This work p_{mean}, cm	t_{mean}, °C	Δt, °C	Q^*, cal/mole	Bearman p_{mean}, cm	t_{mean}, °C	Δt, °C	Q^*, cal/mole
He	65–25	31.0	7.9	1375 ± 39	62.5	34.0	4	1130
Ne	65–45	31.4	7.3	1204 ± 37	45	34.5	4	900
Ar	53	30.7	7.7	−58 ± 11	62	34.5	4	−60
Kr	50	30.5	8.2	−275 ± 10	45	34.5	4	−170
Xe	46–26	30.5	8.7	−589 ± 18	40	34.5	4	−320

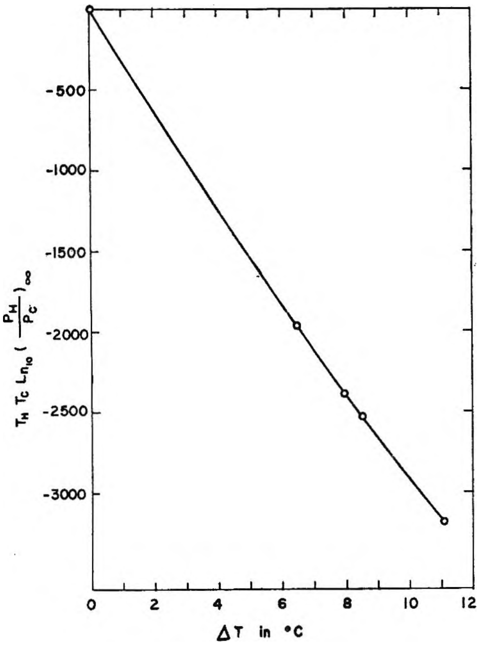

Figure 1.

in determining Q^* at these pressures, and that the gas is effectively at infinite dilution in the membrane.

In Figure 1, we plot, at constant mean temperature, $T_H T_C \log (p_H/p_C)_\infty$ *vs.* ΔT, the temperature difference across the membrane. We see that there is a perceptible departure from linearity in contradiction with eq 1 which predicts that the plot should be a straight line with slope proportional to Q^*. However, eq 1 is not entirely general. It is valid only when Q^* is independent of temperature and mole fraction of gas in the membrane. This can be seen, for example, from eq 13 of ref 2. If we assume that Q^* varies linearly with temperature and that the gas is at infinite dilution in the membrane, then it is not difficult to show that in place of eq 1, we have

$$T_H T_C \ln (p_H/p_C)_\infty = -R^{-1}\left(Q^*\bigg|_{\bar{T}} \Delta T + \frac{\partial Q^*}{\partial T}\bigg|_{\bar{T}} \frac{(\Delta T)^2}{2}\right) \qquad (2)$$

where $\bar{T}$ is the arithmetic mean temperature. In this case, $T_H T_C \ln (p_H/p_C)_\infty$ *vs.* ΔT should be a parabola, which appears to be the shape of the curve in Figure 1. A parabolic least-squares fit of our data gives $Q^* = 1495$ cal/mole and $\partial Q^*/\partial T = -31.4$ cal/mole deg at the mean temperature of 31°. The heat is clearly of the proper magnitude and the temperature coefficient is not unreasonable,[5] so that it appears eq 2 adequately accounts for the experimental results.

If eq 2 does correctly account for the temperature difference data, we may conclude that the usual local linear phenomenological equation for the flux of matter, J_1

$$J_1 = -TL_{11}\frac{\partial \mu_1/T}{\partial z} - \frac{L_{1U}}{T}\frac{\partial T}{\partial z} \qquad (3)$$

in the notation of ref 2, is valid, provided we use values of the phenomenological coefficients, L_{11} and L_{1U}, appropriate to the state at each point of the membrane. The nonlinearity of $T_H T_C \ln (p_H/p_C)_\infty$ in ΔT is then caused solely by the variation of the transport coefficients across the membrane. Our experiments provide a fairly severe test of the linear phenomenological equation since the temperature gradients range up to 900°/in.

Evidently, the values for the heats of transport

Table II

Run	p_{mean}, cm	t_{mean}, °C	Δt, °C	Q^*, cal/mole	Length of run, min
27	64.8	31.2	8.0	1385	4190
40	54.5	31.2	7.6	1383	3255
1	51.8	30.6	8.3	1442	2720
3	51.6	30.9	8.2	1374	4190
30	34.9	30.9	8.0	1365	3420
32	34.9	31.1	7.9	1364	3465
31	25.2	31.0	8.0	1378	3525

---

[5] C. M. Crowe, *Trans. Faraday Soc.*, 53, 692 (1957).

Table I: Definitions of Quantities in Equations of State for Liquid Hydrocarbons[a]

	Q	M_1	M_2
Monomers (*i.e.*, CH_4)	N_Av^*/V	1	$z\epsilon^*$
Aromatic rings		$(s + 3)/3$ for $s = 2$ or 4	
Benzene, biphenyl, etc.	sN_Av^*/V	$(s/2 + 5)/3$ for $s = 4, 6, \ldots$	$qz\epsilon^*$
Oligomer chains			
n-Alkanes (C_nH_{2n+2})	$\dfrac{sN_Av^*_r + 2N_Av^*_e}{V}$	$(s + 5)/3$	$q_rz\epsilon^*_{rr} + q_ez\epsilon^*_{ee} + 2x_{re}w$

[a] N_A = Avogadro's number; v^*_i = volume of a unit (of the model) at the minimum of the 6–12 potential; subscript i = e for end unit; subscript i = r for remaining units; V = molar volume of hydrocarbon at P and T; ϵ^*_{ii} = force constant of the 6–12 potential; $w = \epsilon^*_{re} - (\epsilon^*_{ee} + \epsilon^*_{rr})/2$; z = number of nearest neighbor lattice sites (z = 12 for fcc lattice); $q_rz = s(z - 2)$, $q_ez = 2(z - 1)$; $qz = q_rz + q_ez$ for oligomers, or $qz = s(z - 2) + 2$ for aromatics; $x_{re} = q_rzq_ez/qz$.

1.0110 and 1.2045, respectively. The quantities M_1, M_2, and Q are defined in Table I. The volume-dependent degrees of freedom equal $3M_1$ for the models being considered here. The evaluation of the various molecular parameters in the equations of state have been discussed;[4,6,7] this evaluation requires a set of molar volumes and a computer program for solving nonlinear equations.

From the foregoing description of the models, it is clear that no provision is made for holes or double occupancy in the lattice. Hence, for present purposes, the molecular parameters should be evaluated for conditions of maximum liquid density at atmospheric pressure, *i.e.*, at or near the freezing point temperature. The best available data[8] were used and were smoothed where needed. The values of the molecular parameters obtained are presented in Table II.

Table II: Values of Molecular Parameters for Equations of State

Monomer, for methane using densities at −184.5 and −156.7°	
N_Av^*, ml/mole	35.52
ϵ^*/k, °C	111.9
Aromatics, for benzene and biphenyl using densities at 75°	
N_Av^*, ml/mole of centers	35.095
ϵ^*/k, °C	267.81
n-Alkanes, based on *n*-hexane and heavier alkanes with even number of C atoms using densities at freezing points	
$N_Av^*_r$, ml/mole of centers	26.166
$N_Av^*_e$, ml/mole of centers	19.307
ϵ^*_{rr}/k, °C	136.06
ϵ^*_{ee}/k, °C	23.90
w/k, °C	57.97

Using these values of the molecular parameters and the definitions of Q and M_2 given in Table I, the specific volume and cohesive energy density can be estimated for 0°K. The calculation of specific volume can be symbolized as

$$v_0 = QV/(MW) \qquad (2)$$

where MW is the molecular weight, and the cohesive energy density can be given by

$$\epsilon_0/v_0 = RM_2/(QV) \qquad (3)$$

In the equations for alkanes, the parameter s may have only integer values. However, it is apparently permissible to use steps of one-half in s and thereby include the consecutive members of the homologous series. This previously was found to be true in an equation of state to calculate excess volumes of blends of two alkanes and is used here.

Results calculated for a number of hydrocarbons using eq 2 and 3 are given in Table III and are compared with values obtained by Miller.[1] Values for C_2H_6 and C_3H_8 obtained with eq 2 and 3 are questionable. This arises from the fact that the assumption of free rotation (assumption D) is not valid for models of these two molecules. However, results for the heavier hydrocarbons, which are of main concern here, are satisfactory.

Discussion

Equations of state for three types of hydrocarbon series are briefly discussed and used to estimate volume and energy properties for the hypothetical liquid state at 0°K. The computed results are compared with those of Miller.[1] Excepting methane and benzene, the specific volumes are lower than those of Miller. For alkanes, the differences decrease as molecular weight increases

---

(8) C. S. Matthews and C. O. Hurd, *Trans. Am. Inst. Chem. Engrs.*, **42**, 55 (1946); A. Bellemans and C. Colin-Naar, *J. Polymer Sci.*, **15**, 121 (1955); American Petroleum Institute, Research Project 44, tables.

Table III: Values for Specific Volume and Cohesive Energy Density of Liquid Hydrocarbons at 0°K

	This paper		Miller[1]	
	v_0, ml/g	ϵ_0/v_0, cal/ml	v_0, ml/g	ϵ_0/v_0, cal/ml
C_6H_6	0.899	166.7	0.880	163
CH_4	2.214	75.1	1.88	
C_2H_6			1.40	
C_3H_8	1.172	(83.2)	1.27	
C_4H_{10}	1.114	93.9	1.19	
C_5H_{12}	1.082	97.5	1.15	117
C_6H_{14}	1.055	99.3	1.12	117
C_7H_{16}	1.038	100.3	1.10	117
C_8H_{18}	1.025	100.9	1.08	117
$C_{20}H_{42}$	0.970	102.7	0.976	
Limit	0.933	103.3		

so that for $C_{20}H_{42}$ the difference is less than 1%. This convergence of the values seems to confirm Miller's proposed relation between the van der Waals constants and the volume–energy parameters for the hypothetical liquid state.

Fluorine Bomb Calorimetry. XVII. The Enthalpy of Formation of Tungsten Hexafluoride[1]

by P. A. G. O'Hare and Ward N. Hubbard

Chemical Engineering Division, Argonne National Laboratory, Argonne, Illinois 60439 *(Received April 18, 1966)*

This paper reports a value for $\Delta Hf°(WF_6, g)$ calculated from the energy evolved on combustion of tungsten in fluorine in a bomb calorimeter. Some derived thermodynamic data for $WF_6(l)$ and $WF_6(c)$ are also presented.

Experimental Section

Calorimetric System. The calorimeter, laboratory designation ANL-R2, has been described in detail elsewhere.[2] The combustion bomb, laboratory designation Ni-6, is similar to that used for combustion of molybdenum in fluorine.[3] The energy equivalent of the calorimetric system, $\mathcal{E}$(calor), was measured by combustion of benzoic acid (National Bureau of Standards Sample 39i) in oxygen. A series of nine calibration experiments (some performed before and some after the calorimetric combustions in fluorine) yielded a value for $\mathcal{E}$(calor) of 3523.15 cal deg^{-1}, with a standard deviation of the mean of 0.15 cal deg^{-1} (1 cal $\equiv$ 4.1840 abs. joules).

Materials. High-purity tungsten sheet (0.13 mm thick) and wire (0.15 mm in diameter) were purchased from the Fansteel Metallurgical Corp., North Chicago, Ill. The following impurities (ppm) were detected in the tungsten sheet: Al, 23; Cr, 6; Cu, 1; Fe, 17; Mg, 13; Ni, 20; Si, 35; Ti, 13; Ca, 5; Mo, 25; C, 31; H, 2; O, 37; and N, 2. Because of its small effect on the total evolved heat, the tungsten wire was not analyzed. Fluorine of 99.99% purity was prepared by distillation of a commercial sample in a low-temperature still.[4]

Procedure. The method of sample support was the same as that used for combustion of molybdenum in fluorine.[3] A 1- to 2-g sample of tungsten foil, upon electrical ignition, burned satisfactorily in the bomb which had been charged with fluorine ($\sim$0.1 mole) to 115 psia pressure. In trial experiments, about 0.5% of the sample introduced into the bomb remained as small, easily recoverable beads after combustion. These trial experiments were also used to precondition the bomb. All subsequent operations in which the bomb was open, including introduction of sample, were performed in a helium-atmosphere glove box (H_2O $\sim$ 0.1 ppm). Prior to each run, the assembled bomb was evacuated for 16 hr and then charged with fluorine to 115 psia pressure. When the foregoing precautions were taken, the amount of fluorination of the sample, before ignition, was negligible. Calorimetric measurements were performed in the usual way.[5] The infrared spectrum of the gaseous combustion product, after removal of fluorine, was in good agreement with that published for WF_6.[6] No other products were detected.

Results

The data for eight acceptable calorimetric experiments are presented in Table I. Standard-state corrections were made in the usual way.[7] For the con-

---

[1] (a) This work was performed under the auspices of the U. S. Atomic Energy Commission. (b) For the previous paper in this series, see S. S. Wise, J. L. Margrave, H. M. Feder, and W. N. Hubbard, *J. Phys. Chem.*, **70**, 7 (1966).

[2] E. Greenberg, J. L. Settle, H. M. Feder, and W. N. Hubbard, *ibid.*, **65**, 1168 (1961).

[3] J. L. Settle, H. M. Feder, and W. N. Hubbard, *ibid.*, **65**, 1337 (1961).

[4] L. Stein, E. Rudzitis, and J. L. Settle, "Purification of Fluorine by Distillation," Argonne National Laboratory, ANL-6364, 1961. Available from Office of Technical Services, U. S. Department of Commerce, Washington, D. C.

[5] W. N. Hubbard, C. Katz, and G. Waddington, *J. Phys. Chem.*, **58**, 142 (1954).

[6] T. G. Burke, D. F. Smith, and A. H. Nielsen, *J. Chem. Phys.*, **20**, 447 (1952).

Table I: Results of Tungsten Combustions[a]

Expt no.	m', g	Δt_c, deg	$\Delta E_{\text{ignition}}$, cal	$\Delta E_{\text{contents}}{}^c$, cal	ΔE_{gas}, cal	$\Delta Ec°/M$(sample), cal g^{-1}
1	1.47362 (99.76)[b]	0.93029	0.72	−8.24	−0.03	−2229.3
2	1.79560 (99.49)	1.13665	0.72	−10.09	−0.05	−2235.5
3	2.15351 (99.89)	1.36467	0.72	−12.12	−0.10	−2237.9
4	2.18215 (99.87)	1.37669	0.96	−12.23	−0.09	−2227.9
5	2.29480 (99.76)	1.45105	0.84	−12.90	−0.10	−2233.1
6	2.63995 (99.87)	1.67138	0.48	−14.87	−0.15	−2236.0
7	2.69455 (99.89)	1.70225	0.84	−15.15	−0.17	−2231.1
8	3.24170 (94.95)	2.05048	0.60	−18.29	−0.24	−2234.0

Mean $\Delta Ec°/M$(sample) = −2233.1 cal g^{-1}
Std dev of mean = 1.2 cal g^{-1}
Impurity correction = 1.2 ± 0.2 cal g^{-1}
$\Delta Ec°/M$(W, c) = −2231.9 ± 1.2 cal g^{-1}

[a] Symbols in this table are from ref 7. [b] The figures in parentheses indicate the percentage of tungsten reacted in each experiment. [c] The mass of nickel in the bomb was 78.14 g.

Table II: Derived Data at 25°

	WF_6(g)	WF_6(l)	WF_6(c)
Energy of formation, $\Delta Ef° = \Delta Ec°$, kcal mole^{-1}	−410.3 ± 0.4	−415.9 ± 0.5	−416.4 ± 0.5
Enthalpy of formation, $\Delta Hf°$, kcal mole^{-1}	−411.5 ± 0.4	−417.7 ± 0.5	−418.2 ± 0.6
Entropy of formation, $\Delta Sf°$, cal deg^{-1} mole^{-1}	−71.67	−92.77	−107.58
Gibbs energy of formation, $\Delta Gf°$, kcal mole^{-1}	−390.1 ± 0.4	−390.0 ± 0.5	−386.1 ± 0.7

version of the weight of tungsten to true mass, its density was taken as 19.265 g cc^{-1}.[8] For the calculation of $\Delta E_{\text{contents}}$, heat capacity values for Ni and F_2 were taken from ref 7; in addition, the following data were used: c_p(W, c)[9] = 0.032 cal deg^{-1} g^{-1} and $C_v(WF_6$, g)[9] = 26.46 cal deg^{-1} mole^{-1}. The gas correction, ΔE_{gas}, was estimated by analogy with MoF_6[3] and UF_6.[10] The quantity $\Delta Ec°/M$(sample) is the standard energy of combustion of the tungsten sample in fluorine. The following assumptions were made in calculating the impurity correction: (i) trace metal impurities were initially uncombined and were converted during combustion to their most stable fluorides; (ii) nitrogen and hydrogen impurities were initially present as N_2 and H_2, and finally as N_2 and HF, respectively; and (iii) carbon and oxygen impurities were initially present as WC and WO_2, respectively, and were converted to WF_6, CF_4, and O_2. Appropriate enthalpies of formation were taken from ref 11 and 12, or from work performed at this laboratory. The net impurity correction for the tungsten was 1.2 ± 0.2 cal g^{-1}. In Table I, $\Delta Ec°/M$(W, c) is the standard energy of combustion of tungsten in fluorine according to eq 1.

$$W(c) + 3F_2(g) \longrightarrow WF_6(g) \qquad (1)$$

Derived Data. Thermodynamic data for WF_6(g), WF_6(l), and WF_6(c) are presented in Table II. The atomic weight of tungsten was taken to be 183.85.[13] Barber and Cady[14] have reported values of 6.2 and 0.5

---

(7) W. N. Hubbard in "Experimental Thermochemistry," Vol. II, H. A. Skinner, Ed., Interscience Publishers Ltd., London, 1962, Chapter 6.

(8) H. E. Swanson, R. K. Fuyat, and G. M. Urgrinic, "Standard X-ray Diffraction Powder Patterns," Vol. III, National Bureau of Standards Circular 539, U. S. Government Printing Office, Washington, D. C., 1954.

(9) "JANAF Thermochemical Tables," The Dow Chemical Co., Midland, Mich.

(10) J. L. Settle, H. M. Feder, and W. N. Hubbard, *J. Phys. Chem.*, **67**, 1892 (1963).

(11) F. D. Rossini, D. D. Wagman, W. H. Evans, S. Levine, and I. Jaffe, "Selected Values of Chemical Thermodynamic Properties," National Bureau of Standards Circular 500, U. S. Government Printing Office, Washington, D. C., 1952.

(12) C. E. Wicks and F. E. Block, "Thermodynamic Properties of 65 Elements—Their Oxides, Halides, Carbides, and Nitrides," U. S. Bureau of Mines Bulletin 605, U. S. Government Printing Office, Washington, D. C., 1963.

(13) A. E. Cameron and E. Wichers, *J. Am. Chem. Soc.*, **84**, 4175 (1962).

(14) E. J. Barber and G. H. Cady, *J. Phys. Chem.*, **60**, 505 (1956).

kcal mole^{-1}, respectively, for the enthalpies of vaporization and fusion of tungsten hexafluoride at 25°. These data, in conjunction with the present value for $\Delta Hf°$(WF_6, g), have been used to calculate $\Delta Hf°$(WF_6, l) and $\Delta Hf°$(WF_6, c). Standard entropies, $S°$, at 25°, of W(c), F_2(g), WF_6(g), and WF_6(l) have been taken from ref 9; $S°$(WF_6, c) was estimated to be 45.6 cal deg^{-1} mole^{-1}. The uncertainties given are uncertainty intervals[15] equal to *twice* the combined standard deviations arising from all known sources.

Discussion

Myers and Brady[16] measured the enthalpy of solution of WF_6(g) in aqueous NaOH, and derived a value of -416 ± 4 kcal mole^{-1} for $\Delta Hf°$(WF_6, g). JANAF[9] has revised this value to -421 ± 4 kcal mole^{-1}, but both values are in disagreement with the present measurements. This discrepancy, of unknown origin, parallels that observed[3] previously for MoF_6. The determination reported in this paper is based on *direct* combination of the elements in a well-defined reaction, and is regarded as being more reliable.

Acknowledgments. The authors are grateful to H. M. Feder and M. Ader for helpful discussions. They wish to thank Doris Huff for performance of spectrochemical analyses, and Gerald K. Johnson for preparation of the high-purity fluorine used in this work and for checking calculations.

---

[15] F. D. Rossini, *Chem. Rev.*, **18**, 233 (1936).

[16] O. E. Myers and A. P. Brady, *J. Phys. Chem.*, **64**, 591 (1960).

Interdiffusion and Self-Diffusion in Urea Solutions

by P. C. Carman

National Chemical Research Laboratory,
South African Council for Scientific and Industrial Research,
Pretoria, South Africa (*Received April 25, 1966*)

In a recent paper, Stokes[1] has shown that, by taking dimerization into account in aqueous solutions of urea, the results of Albright and Mills[2] for self-diffusion of urea are consistent with a simple relationship between the mobility of monomeric urea and viscosity. It is shown here that his model can be extended to the correlation between interdiffusion and self-diffusion coefficients.

If subscripts u and w refer to total urea and water, respectively, and D^V represents the interdiffusion coefficient, the relationship advanced first by Darken and by Hartley and Crank,[3-6] in absence of dimerization, is

$$D^V = \frac{\partial \ln a_u}{\partial \ln N_u}(N_w D_u^* + N_u D_w^*) \tag{1}$$

where a_u is activity per mole of urea, N_i is mole fraction of i, and D_i^* is its self-diffusion coefficient. When concentrations, c_i moles/cc, are used, it is convenient to transform this to

$$D^V = \bar{V}_w \frac{\partial \ln a_u}{\partial \ln c_u}(c_w D_u^* + c_u D_w^*) \tag{2}$$

Equations 1 and 2 are derived by assuming each component has an independent diffusive flux determined by the mobility, q_i, *i.e.*

$$J_i = -c_i q_i \nabla \mu_i \tag{3}$$

where μ_i is the molar chemical potential, *i.e.*

$$\nabla \mu_i = RT \nabla \ln a_i \tag{4}$$

and q_i is related to D_i^* by

$$D_i^* = q_i RT \tag{5}$$

When dimerization occurs, however, eq 5 is no longer valid for urea. If α is the fraction of monomeric urea, the concentrations of the two forms are

$$c_1 = \alpha c_u \text{ and } c_2 = {}^1/_2(1 - \alpha)c_u \tag{6}$$

and, if the mobilities of the two forms are q_1 and q_2, Stokes has shown, in effect, that D_u^* is given by

$$D_u^* = RT[\alpha q_1 + (1 - \alpha)q_2] \tag{7}$$

Furthermore, eq 1 and 2 assume a modified form, as can be seen in the following.

The fluxes J_1 and J_2 are given by

$$\left.\begin{aligned} J_1 &= -c_1 q_1 \nabla \mu_1 \\ J_2 &= -c_2 q_2 \nabla \mu_2 \end{aligned}\right\} \tag{8}$$

whence

$$J_u = J_1 + 2J_2 = -(c_1 q_1 \nabla \mu_1 + 2c_2 q_2 \nabla \mu_2)$$

Owing to equilibrium between monomer and dimer

$$\nabla \mu_u = \nabla \mu_1 = {}^1/_2 \nabla \mu_2 \tag{9}$$

---

[1] R. H. Stokes, *J. Phys. Chem.*, **69**, 4012 (1965).

[2] J. G. Albright and R. Mills, *ibid.*, **69**, 3120 (1965).

[3] L. S. Darken, *Trans. Am. Inst. Mining Met. Engrs.*, **175**, 184 (1948).

[4] G. S. Hartley and J. Crank, *Trans. Faraday Soc.*, **45**, 801 (1949).

[5] P. C. Carman and L. S. Stein, *ibid.*, **52**, 619 (1956).

[6] S. Prager, *J. Chem. Phys.*, **21**, 1345 (1953).

Table I

							$D^V \times 10^6$ (calcd)	
$1000c_u$	α^a	$f(\alpha)^b$	$\frac{\partial \ln a_u}{\partial \ln c_u}$	$\frac{1^a}{\eta_r}$	$D_u^* \times 10^5$	$D^V \times 10^5$ (exptl)	With D_w^*	With D_w^*/η_r
0.5	0.969	1.022	0.983	0.981	1.344	1.340	1.340	1.340
1.0	0.941	1.044	0.971	0.960	1.305	1.308	1.303	1.301
2.0	0.891	1.074	0.954	0.916	1.234	1.244	1.238	1.231
3.0	0.848	1.111	0.952	0.870	1.163	1.188	1.192	1.175
4.0	0.812	1.140	0.955	0.822	1.107	1.144	1.160	1.126

[a] From Stokes Table I. [b] Using $q_1/q_2 = 0.7$.

whence

$$J_u = -c_u[\alpha q_1 + 2(1 - \alpha)q_2]\nabla\mu_u \qquad (10)$$

Now, in the derivation of (1) and (2), it is assumed that

$$J_u = -c_u q_u \nabla\mu_u \qquad (3a)$$

and D_u^* is evaluated from

$$D_u^* = q_u RT \qquad (5a)$$

By comparison of (10) and (3a), it follows that a modified form of (1) and (2) is obtained by replacing q_u with the term in square brackets in (10). Further, as D_u^* is now given by (7), it can be introduced by replacing D_u^* with $D_u^* \cdot f(\alpha)$, where

$$f(\alpha) = \frac{\alpha q_1 + 2(1 - \alpha)q_2}{\alpha q_1 + (1 - \alpha)q_2} \qquad (11)$$

i.e., eq 2 modifies to

$$D^V = \bar{V}_w \frac{\partial \ln a_u}{\partial \ln c_u}(c_u D_u^* \cdot f(\alpha) + c_u D_w^*) \qquad (12)$$

In Albright and Mills' paper, experimental values of D_u^* are given, as well as expressions for D^V and $\bar{V}_u$. From the latter, taking $\bar{V}_w$ as 18.04 cc for the whole range of concentrations, c_w can be derived, as $c_w \bar{V}_w = 1 - c_u \bar{V}_u$. Stokes gives values of α, calculated on the assumption that activities of monomer and of dimer equal their respective mole fractions. With regard to the relative mobilities of monomer and dimer, a reasonable choice for q_2/q_1, following considerations advanced by Stokes, is 0.7, but $f(\alpha)$ is not very sensitive to this over the range of concentrations considered and gives almost the same values for ratios between 0.6 and 0.8. The values for $(\partial \ln a_u)/\partial \ln c_u)$ in Table I have been calculated from α, using Stokes theory that monomer and dimer form ideal solutions. They are almost identical with the values calculated from $\ln y_u$, as given by Albright and Mills, and tend to be a little lower than those calculated from the experimental values of γ_u given by Bower and Robinson,[7] but the differences are not large enough to affect the calculation in Table I.

The self-diffusion coefficient of water in urea solutions has not been measured. The value for water itself is about 2.5×10^{-5} cm^2/sec, and, as possible extremes, either this has been used or the value obtained by dividing by the relative viscosity of the solution, η_r, using values given by Stokes.

Values of concentrations below 0.5 mole/l. have not been included as D_u^* and D^V are very close in this range. It can be seen that the experimental values of D^V lie on the whole between the two calculated values, up to the highest concentration of 4 moles/l.

---

[7] V. E. Bower and R. A. Robinson, *J. Phys. Chem.*, **67**, 1524 (1963).

Effect of Inert Gas Pressure and Solubility on Fused Salt Conductance. II. Nitrogen with Sodium Nitrate

by James L. Copeland and Steven Radak

Department of Chemistry, Kansas State University, Manhattan, Kansas 66502

(Received May 2, 1966)

As a continuation of the studies of Copeland and Zybko[1,2] on the manner in which the specific conductance of simple fused salts is affected by "inert" gas pressure and solubility, we wish to report our rather unusual and interesting results for N_2 in high-pressure equilibrium with molten $NaNO_3$.

---

[1] J. L. Copeland and W. C. Zybko, *J. Am. Chem. Soc.*, **86**, 4734 (1964).

[2] J. L. Copeland and W. C. Zybko, *J. Phys. Chem.*, **70**, 181 (1966).

Experimental Section

The general apparatus and method are identical with those reported in ref 2. The cell constant was 384.2 cm^{-1}, as calculated by assigning an interpolated literature value of 1.23_0 ohm^{-1} cm^{-1} to the specific conductance of $NaNO_3$ at 369° and atmospheric pressure.[2,3]

Reagent grade $NaNO_3$ was obtained from the Baker and Adamson Co., as in the prior work.[2] Nitrogen was at least 99.98% pure (Bone Dry grade), and was procured from the National Cylinder Gas Co.

A constant salt temperature of 369° was employed to allow comparison with the He and Ar studies in the same system at the same temperature.[2] The initial N_2 pressure at this salt temperature was 379 atm. After equilibration and the first electrical resistance measurement, increments of N_2 pressure were released at intervals, the system was allowed to equilibrate at each new pressure (with frequent agitation), and equilibrium resistance measurements were made. The "zero" pressure measurement was made with the system being agitated and pumped by a mechanical vacuum pump. The entire experiment was performed over a period of 9 days. The solubilities of N_2 in fused $NaNO_3$ were taken from the work of Copeland and Seibles.[4]

Results

Empirically, the joint effect of increasing N_2 pressure and solubility was to depress linearly the specific conductance, κ, of the $NaNO_3$ at 369° over the range of pressures employed. The data are summarized in Table I. The empirical least-squares relationship resulted as

$$\kappa_{N_2} = (1.231 \pm 0.001) - (7.59 \pm 0.18) \times 10^{-5} P_{N_2} \text{ ohm}^{-1} \text{ cm}^{-1} \quad (1)$$

where P_{N_2} is the saturating pressure of N_2 in atmospheres. The errors are the least-squares probable errors.

Table I: Summary of Specific Conductance of $NaNO_3$ at 369° under N_2 Pressure

Saturating pressure, P_{N_2}, atm	379	309	236	162	69	0
Specific conductance, κ_{N_2}, ohm^{-1} cm^{-1}	1.201	1.208	1.213	1.218	1.226	1.230

The Henry's law constant for N_2 solubility in fused $NaNO_3$ at 369° is[4]

$$K_{N_2} = (19.7 \pm 0.4) \times 10^{-7} \text{ mole of } N_2 \text{ cm}^{-3} \text{ atm}^{-1} \quad (2)$$

where the error is the probable error for a single solubility–pressure point.

Relationships 1 and 2 are to be compared to those for Ar and He in the same system, as summarized below.[2,5]

$$\kappa_{Ar} = (1.228 \pm 0.002) - (1.94 \pm 0.06) \times 10^{-4} P_{Ar} \text{ ohm}^{-1} \text{ cm}^{-1} \quad (3)$$

$$K_{Ar} = (17.2 \pm 1.7) \times 10^{-7} \text{ mole of Ar cm}^{-3} \text{ atm}^{-1} \quad (4)$$

$$\kappa_{He} = (1.230 \pm 0.001) - (9.19 \pm 0.25) \times 10^{-5} P_{He} \text{ ohm}^{-1} \text{ cm}^{-1} \quad (5)$$

$$K_{He} = (22.7 \pm 0.7) \times 10^{-7} \text{ mole of He cm}^{-3} \text{ atm}^{-1} \quad (6)$$

The striking features to be noted are that whereas the solubility of N_2 lies between those of Ar and He (*cf.* eq 2, 4, and 6), the effect of N_2 in diminishing κ is *less* than those of the other two gases (*cf.* slopes of eq 1, 3, and 5).

Discussion

The dilution mechanism, hypothesized earlier to account for the different extents of the depression of κ by the solubilities of different nonreactive gases,[2] may still play a dominant role in the system under study here, but may not be the entire story. With an assumption of ideal dilution effects alone, as a consequence of the effect on κ we would have to conclude that N_2 dilutes the melt to a lesser extent than does either Ar or He, even though the N_2 solubility is intermediate between those of the other two gases. This implies, of course, a smaller partial molal volume for N_2 than for Ar or He in this system. This is not unrealistic in view of the negative enthalpy of solution of −2.73 ± 0.09 kcal mole^{-1} for N_2 in $NaNO_3$ observed by Copeland and Seibles.[4] On the other hand, the large negative standard entropy of solution of −16.6 ± 0.1 eu[4] may imply some subtle ion–molecule interactions which contribute to the effect on κ in an undetermined manner. Detailed determinations of the densities of such gas–salt solutions, for calculations of equivalent conductance, should cast more light on the question of the presence or absence of such influences of solute molecules on the ions.

Acknowledgments. The authors gratefully acknowledge support of this work by the National Science

---

(3) A. Klemm, "Molten Salt Chemistry," M. Blander, Ed., Interscience Publishers, New York, N. Y., 1964, p 566.

(4) J. L. Copeland and L. Seibles, *J. Phys. Chem.*, **70**, 1811 (1966).

(5) J. L. Copeland and W. C. Zybko, *ibid.*, **69**, 3631 (1965).

Foundation, Grant GP-4274. This work will constitute a part of the thesis of S. R. which will be submitted to the Graduate School of Kansas State University in partial fulfillment of the requirements for the degree of Master of Science.

Pulse Radiolysis of Anhydrous Amines

by Larry R. Dalton, James L. Dye,

Department of Chemistry, Michigan State University, East Lansing, Michigan

E. M. Fielden, and Edwin J. Hart

Chemistry Division, Argonne National Laboratory, Argonne, Illinois *(Received May 2, 1966)*

In their original studies, Hart and Boag[1] demonstrated that the hydrated electron absorption band is altered considerably in 12.2 *M* aqueous ammonia and in 12.5 *M* methylamine solutions. In each case the transient absorption peak formed during pulse radiolysis lies beyond 9000 A, the limit of sensitivity of their photographic plates. From the time of these first spectrophotographic observations of the hydrated electron,[1] it has been assumed that solvated electrons produced by the radiolysis of water and other solvents are analogous to those formed when alkali metals are dissolved in liquid ammonia and amines. Comparison of the spectra of metal solutions with those of the transients formed during pulse radiolysis of the same solvent should form a good test of this assumption. Compton and co-workers[2] have shown the spectrum obtained by pulse radiolysis of anhydrous ammonia to be similar to that of metal–ammonia solutions. On the other hand, Anbar and Hart[3] reported an absorption maximum at 9200 A for the transient produced by pulse radiolysis of anhydrous ethylenediamine. They attributed this band to the solvated electron in disagreement with the assignment of Dewald and Dye[4] based upon the spectra of alkali metals in ethylenediamine. The latter investigators found no peak common to the various alkali metals in this region and assigned an absorption maximum at 12,800 A to the solvated electron and loosely bound aggregates of the electron with cations.

This disagreement, and the observation of an anomaly in the hydrated electron absorption spectrum in the region of solvent (water) absorption bands[5] (7500 A), prompted us to reexamine the spectra of the transients produced by pulse radiolysis of anhydrous amines. In the case of the hydrated electron in water, the anomaly had been shown to be an artifact essentially produced by the effect of scattered radiation on the particular photomultiplier used, complicated by effects due to different illumination intensities.

Although an apparent decrease in the radiation-induced absorbance occurs near the ethylenediamine solvent absorption band (10,500 A), by minimizing stray radiation and operating the photomultiplier under constant illumination conditions in a range of proven linearity, the previous results[3] were shown to be incorrect. For each of the amines tested, the absorbance continued to increase up to the cutoff wavelength of the photomultiplier used (11,200 A). The band shape is similar to that attributed to the solvated electron in metal solutions in ethylenediamine,[4] although the comparison suffers from our inability to search far enough into the infrared to locate the absorption maxima in the radiolysis studies.

Experimental Section

Anhydrous ethylenediamine (Matheson Coleman and Bell) was first purified by fractional freezing and distillation as described by Feldman, *et al.*[6] This was followed by two distillations *in vacuo* into a quartz bulb attached to the quartz irradiation cell. The first of these final distillations was from a sodium mirror and the second was from an intermediate vessel containing no metal. In this way, the carry-over of ions by the spray can be avoided. A second sample of ethylenediamine was prepared using a potassium mirror in place of the mirror of sodium. A similar purification procedure was used to prepare the sample of 1,3-propanediamine (Matheson Coleman and Bell). Ethylamine (Eastman Organic Chemicals) and *n*-propylamine (Matheson Coleman and Bell) were purified by two distillations in a nitrogen stream followed by two distillations *in vacuo* as described above.

The absorption spectrum of the solvated electron in these amine solvents was determined by examining the decay of absorbance of the transients produced by a 0.4-μsec pulse of 15-Mev electrons. The pulse intensity was estimated by determining the absorbance (at 7000

---

[1] E. J. Hart and J. W. Boag, *J. Am. Chem. Soc.*, 84, 4090 (1962).

[2] D. M. J. Compton, J. F. Bryant, R. A. Cesena, and B. L. Gehman in "Pulse Radiolysis," M. Ebert, J. P. Keene, A. J. Swallow, and J. H. Baxendale, Ed., Academic Press, London and New York, N. Y., 1965, p 43.

[3] M. Anbar and E. J. Hart, *J. Phys. Chem.*, 69, 1244 (1965).

[4] R. R. Dewald and J. L. Dye, *ibid.*, 68, 121 (1964).

[5] E. M. Fielden and E. J. Hart, unpublished results.

[6] L. H. Feldman, R. R. Dewald, and J. L. Dye, Advances in Chemistry Series, No. 50, American Chemical Society, Washington, D. C., 1965, p 163.

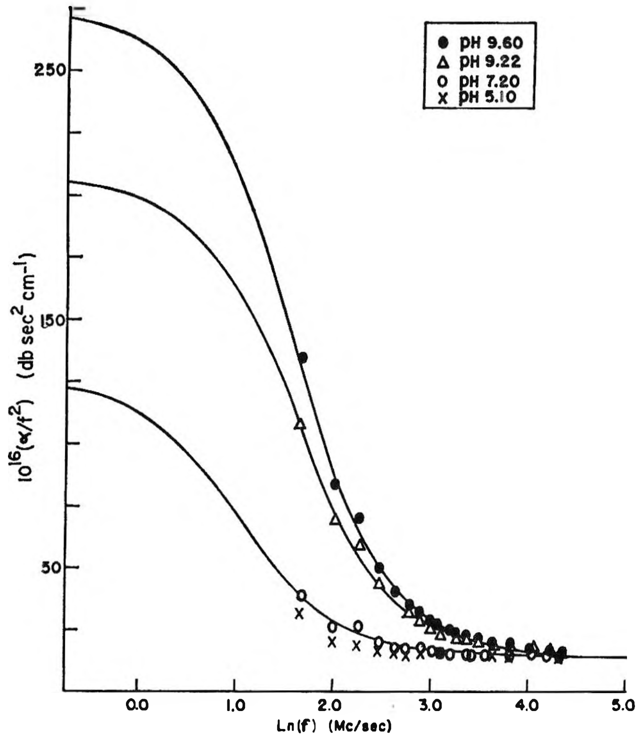

Figure 1. Ultrasonic absorption as a function of frequency in 0.156 *M* (moles of monomer/liter) poly-L-lysine solutions in 0.6 *M* NaCl at 35.8° and various values of the pH. Solid lines are least-square fits to the single relaxation equation. The classical value of α/f^2 is 13.95×10^{-16} db sec^2 cm^{-1}, in good agreement with the value for water interpolated from the data of Herzfeld (see ref 3, p 358).

tion equilibrium. There is no absolute assurance that similar phenomena are not involved in our results; indeed the volume change calculated is rather close to that estimated by Cohn and Edsall[5] for the solvation of a singly ionized group. However, the dependence of C on the pH, much more pronounced than that observed by Burke, Hammes, and Lewis, and in particular the virtually negligible excess absorption at low pH would argue against such an interpretation. The observed variation of C with f_H is consistent with the notion that absorption due to perturbation of the helix-coil equilibrium is being observed.

Our data do not show a significant increase in the relaxation time when f_H is increased as predicted by Schwarz.[6] However, we are restricted to rather low values of f_H by solubility limitations and such behavior cannot be ruled out. When attempts were made to analyze our data in terms of a Davidson-Cole[7] distribution of relaxation times, somewhat surprisingly, values of β close to 1 resulted indicating a satisfactory fit in terms of a single relaxation. In summary, the excess acoustic absorption in polylysine solution may be adequately described by a single process with a relaxation time $3\text{-}6 \times 10^{-8}$ sec and an associated volume change of 6-8 cm^3/mole of monomer. The dependence of the absorption on pH is consistent with the notion that the process is the helix-coil transition.

---

(5) E. J. Cohn and J. T. Edsall, "Proteins, Amino Acids and Peptides as Ions and Dipolar Ions," Reinhold Publishing Corp., New York, N. Y., 1943.

(6) G. Schwarz, *J. Mol. Biol.*, **11**, 64 (1965).

(7) D. W. Davidson and R. H. Cole, *J. Chem. Phys.*, **19**, 1484 (1951).

DEPARTMENT OF CHEMISTRY
UNIVERSITY OF WASHINGTON
SEATTLE, WASHINGTON 98105

R. C. PARKER
K. APPLEGATE
L. J. SLUTSKY

RECEIVED JUNE 16, 1966

Geminate Recombination in Photochemistry: A First-Order Process[1]

Sir: The dependence of G values and quantum yields on solute concentration in radiation chemistry[2,3] and photochemistry[4-6] has been theoretically interpreted by the use of diffusion kinetics. A recent critical review of the pertinent literature in radiation chemistry led the author[7] to induce an alternative model: "excited water," either an electronically excited state or the H_3O-OH radical pair which undergoes geminate recombination by a first-order process, is precursor of intraspur hydrogen in the radiolysis of water.

Woods[8] recently published very important results in the photochemistry of iron(II) in 1 *M* sulfuric acid. The dependence of $\Phi(Fe^{III})$ and $\Phi(As^{III})$ on arsenic acid concentration is identical both with the dependence of intraspur hydrogen G values on solute concentration[7] and with the dependence of geminate recombination on solute concentration deduced by Noyes[5] in that solute concentrations must exceed 0.01 *M* for significant effects. However, Woods[8] concluded that the effect of arsenic acid was not due to inhibition of geminate

---

(1) Research sponsored by the U. S. Atomic Energy Commission under contract with Union Carbide Corp.

(2) A. Samuel and J. L. Magee, *J. Chem. Phys.*, **21**, 1080 (1953).

(3) A. Kuppermann in "The Chemical and Biological Actions of Radiations," Vol. 5, M. Haissinsky, Ed., Academic Press Inc., New York, N. Y., 1961.

(4) J. C. Roy, R. R. Williams, and W. H. Hamill, *J. Am. Chem. Soc.*, **76**, 3274 (1954).

(5) R. M. Noyes, *ibid.*, **77**, 2042 (1955).

(6) L. J. Monchik, *J. Chem. Phys.*, **24**, 381 (1956).

(7) T. J. Sworski, *J. Am. Chem. Soc.*, **86**, 5034 (1964); Advances in Chemistry Series, No. 50, American Chemical Society, Washington, D. C., 1965, p 263.

(8) R. Woods, *J. Phys. Chem.*, **70**, 1446 (1966).

recombination since $\Phi(\text{Fe}^{\text{III}})$ and $\Phi(\text{As}^{\text{III}})$ are not linearly related to the square root of arsenic acid concentration.

The dependence of $\Delta\Phi(\text{Fe}^{\text{III}})$ and $\Phi(\text{As}^{\text{III}})$ on arsenic acid concentration is quantitatively given by

$$1/\Delta\Phi(\text{Fe}^{\text{III}}) = (0.645 \pm 0.068) + 0.297/[\text{As}^{\text{V}}] \quad (\text{I})$$

$$1/\Phi(\text{As}^{\text{III}}) = (1.007 \pm 0.083) + 0.493/[\text{As}^{\text{V}}] \quad (\text{II})$$

with constants and standard deviations determined by the method of least squares. $\Delta\Phi(\text{Fe}^{\text{III}})$ is the increase in $\Phi(\text{Fe}^{\text{III}})$ induced by arsenic acid.

Equations I and II are consistent with a reaction mechanism based on the following assumptions: (1) light absorption yields "excited ferrous ion" which disappears by a first-order process with rate constant of $1/\tau$; (2) arsenic acid reacts only with $\text{Fe}^{\text{II}*}$ with rate constant of k to yield arsenic(IV) which oxidizes iron(II); and (3) the quantum yield for the process which yields iron(III) in the absence of arsenic acid is reduced by a factor equal to the fraction of $\text{Fe}^{\text{II}*}$ which reacts with arsenic acid. This reaction mechanism yields eq I′ and II′

$$1/\Delta\Phi(\text{Fe}^{\text{III}}) = (1 + 1/\tau k[\text{As}^{\text{V}}])/1.777\Phi(\text{Fe}^{\text{II}*}) \quad (\text{I}')$$

$$1/\Delta\Phi(\text{As}^{\text{III}}) = (1 + 1/\tau k[\text{As}^{\text{V}}])/\Phi(\text{Fe}^{\text{II}*}) \quad (\text{II}')$$

Equations I′ and I″ become identical with the equations of Woods[8] with the following substitutions: $\tau k = \epsilon_2 K/\epsilon_1$ and $\Phi(\text{Fe}^{\text{II}*}) = A_2' = (A_2 - A_1)/1.777$. Thus, the two alternative models give the same dependence of $\Phi(\text{Fe}^{\text{III}})$ and $\Phi(\text{As}^{\text{III}})$ on arsenic acid concentration.

Equations I and II yield values for $\Phi(\text{Fe}^{\text{II}*})$ of 0.87 and 0.99, respectively, equal within standard deviations and consistent with $\Phi(\text{Fe}^{\text{II}*}) = 1$. They also yield values of 2.04 and 2.17, respectively, for τk. Assuming reaction of arsenic acid with $\text{Fe}^{\text{II}*}$ is diffusion controlled, τ is 10^{-9} to 10^{-10} sec. There is, therefore, similarity between H_2O^* and $\text{Fe}^{\text{II}*}$. $\text{Fe}^{\text{II}*}$ may be an electronically excited state or may be either the $\text{Fe}^{\text{III}}\text{–e}_{\text{aq}}^-$, $\text{Fe}^{\text{III}}\text{–H}$, or $\text{Fe}^{\text{III}}\text{–H}_3\text{O}$ radical pair which undergoes geminate recombination by a first-order process.

Other recent studies[9-12] in the photochemistry of aqueous solutions indicate that inhibition of geminate recombination is sensibly complete with solute concentrations about 0.01 M. From this apparent contradiction, we may conclude that secondary recombination is inhibited by 0.01 M solute while reaction of solute with $\text{Fe}^{\text{II}*}$ inhibits primary recombination. If this be true, it is of great significance in the radiation chemistry of water since decrease of interspur hydrogen could be attributed to inhibition of secondary recombination while decrease of intraspur hydrogen could be attributed to inhibition of primary recombination.

---

[9] J. Jortner, M. Ottolenghi, and G. Stein, *J. Phys. Chem.*, **68**, 247 (1964).

[10] F. S. Dainton and S. R. Logan, *Proc. Roy. Soc.* (London), **A287**, 281 (1965).

[11] F. S. Dainton and P. Fowles, *ibid.*, **A287**, 312 (1965).

[12] P. L. Airy and F. S. Dainton, *ibid.*, **A292**, 340 (1966).

CHEMISTRY DIVISION T. J. SWORSKI
OAK RIDGE NATIONAL LABORATORY
OAK RIDGE, TENNESSEE 37831

RECEIVED JUNE 28, 1966

Reactivity of Electron-Donor–Acceptor Complexes. III. Hydrogen Exchange between Acetylene and Organic Electron-Donor–Acceptor Complexes

Sir: In previous papers[1,2] we have studied the reactivity of electron-donor–acceptor (EDA) complexes. It was found that the reactivity of such compounds as phthalocyanines and aromatic hydrocarbons increased remarkably when they were brought into contact with sodium, an electron donor, by forming EDA complexes. Accordingly, the exchange reaction of hydrogen between acetylene (or molecular hydrogen) and the complexes takes place at room temperatures, while it does not proceed in the absence of electron donor even at 200°. In this report phenothiazine is employed as an organic electron donor, and the reactivity of the EDA complexes formed with various organic electron acceptors is studied.

Phenothiazine was purified by repeated recrystallization and sublimation. A film was evaporated on the surface of a glass vessel under vacuum, to which various electron acceptors such as 2,3-dicyanoquinone, tetracyanoquinodimethane (TCNQ), pyromellitic dianhydride, 1,3,5-trinitrobenzene, p-chloranil, and 2,3-dicyano-5,6-dichloroquinone were sublimed, which resulted in deep green, red-violet, green-black, gray-green, dark green, and deep green complexes, respectively.

The hydrogen exchange reaction between the complexes and acetylene was studied in the temperature range between 25 and 140° under an acetylene pressure

---

[1] M. Ichikawa, M. Soma, T. Onishi, and K. Tamaru, *J. Phys. Chem.*, **70**, 2069 (1966).

[2] M. Ichikawa, M. Soma, T. Onishi, and K. Tamaru, *J. Catalysis*, accepted for publication.

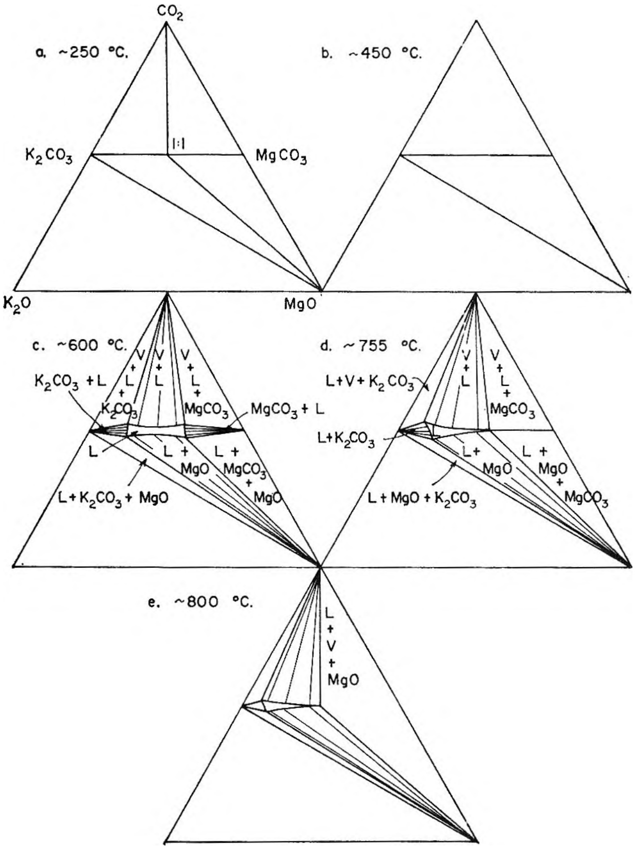

Figure 2. Proposed isothermal–isobaric (15,000 psi) sections for the ternary system K_2O–MgO–CO_2. Solid rather than dotted lines are used to avoid confusion. The diagrams are nevertheless schematic.

quenched to a clear transparent glass. Compositions somewhat removed from the 1:1 ratio formed a brown glass on quenching, and compositions still further removed from the 1:1 ratio formed an intergrowth with crystalline phases on quenching.

The temperature–composition projection of the system in equilibrium with CO_2 at a pressure of 15,000 psi shows a simple eutectic relationship (Figure 1) without solid solution. The eutectic is located at 43 ± 3 mole % $MgCO_3$ and 460°.[4] The decomposition temperature of $MgCO_3$ was placed at 755°, in good agreement with previous work of Harker and Tuttle.[5]

Proposed phase relations in the ternary system, based on Figure 1,[6] are shown in Figure 2 by means of isothermal–isobaric reactions at five different temperatures. Melting in the system probably begins with increasing temperature at an isobaric invariant point involving $MgCO_3$, K_2CO_3, and CO_2 or $MgCO_3$, K_2CO_3, and MgO. In all probability, the two points fall close together in pressure and temperature and it is not improbable that at low pressures they will merge and give rise to an invariant point involving the five phases: $MgCO_3$, MgO, K_2CO_3, liquid, and vapor.

At temperatures above 755°, the system is definitely ternary and the probable phase relations are shown in Figure 2e. At 755°, there is an isobaric invariant point involving $MgCO_3$, MgO, vapor, and liquid (Figure 2d). This represents one point on a univariant pressure–temperature curve for the dissociation of $MgCO_3$ by the reaction $MgCO_3 \rightarrow MgO + \text{vapor}$, and as this temperature falls near the value for the dissociation curve determined by Harker and Tuttle,[5] it is as-assumed that there is very little, if any, solid solution of K_2CO_3 in the $MgCO_3$.

Acknowledgment. This research was performed as part of an investigation of the preparation, properties, and structure of carbonate glasses, under AEC Grant No. AT(30-1)-2887.

---

(4) R. K. Datta and O. F. Tuttle, Progress Report for 1961–1962, "The Preparation, Properties, and Structure of Carbonate Glasses," Contract No. AT(30-1)-2887 (1962).

(5) R. I. Harker and O. F. Tuttle, *Am. J. Sci.*, **253**, 209 (1955).

(6) W. Eitel and W. Skaliks, *Z. Anorg. Allgem. Chem.*, **183**, 263 (1929).

Relative Determinations of Soret Coefficients of Electrolytes. III[1]

by Toshio Ikeda and Hideo Miyoshi

Department of Chemistry, Shizuoka University, Shizuoka, Japan *(Received March 21, 1966)*

The Soret coefficients of a series of symmetric tetraalkylammonium chlorides were determined by using a combined thermocell of the system

$$\underset{T}{\text{Hg–HgCl, LiCl}(m)}, \underset{T + \Delta T}{\text{HgCl–Hg–HgCl}}, \underset{T}{\text{MCl}(m), \text{HgCl–Hg}} \quad (1)$$

where MCl represents a univalent chloride of the same concentration as that of lithium chloride, which was chosen as a reference substance because it shows a very slight Soret effect. Denoting by $(\mathrm{d}E/\mathrm{d}T)_0$ the initial thermoelectric power of the cell system (1),

---

(1) Part II: T. Ikeda and M. Matsumoto, *J. Phys. Chem.*, **69**, 3755 (1965).

Table I: Soret Coefficients of Chlorides in Water at 25° and 0.01 M (the Values in Parentheses Are Adopted as Standards for the Relative Determination of σ)

				$\sigma \times 10^3$ deg^{-1}		
	t_+	B	$(\mathrm{d}E/\mathrm{d}T)_0$, μv/deg	This work	Ref 1	Ref 3
HCl	0.8251[a]	0.958[d]	363.3 ± 2.4	8.95	9.12	9.01
LiCl	0.3289[a]	0.969[d]	...	(−0.01)	−0.19	−0.01
KCl	0.4902[a]	0.956[d]	38.2 ± 0.9	1.58	(1.43)	1.43
Me_4NCl	0.3699[b]	0.941[e]	92.5 ± 3.3	5.17	...	...
Et_4NCl	0.2996[b]	0.943[e]	125.0 ± 3.6	8.61	...	8.38
n-Pr_4NCl	0.2350[b]	0.945[e]	124.6 ± 1.2	10.91	...	...
n-Bu_4NCl	0.2004[b]	0.947[e]	129.5 ± 5.2	13.27	...	...
Me_3BzNCl (Bz = benzyl)	0.216[c]	...	101.0 ± 3.7	...	...	...

[a] B. E. Conway, "Electrochemical Data," Elsevier Publishing Co., Amsterdam, 1952. [b] Calculated from the data on ionic mobilities at 25°, Landolt-Börnstein, "Zahlenwerte und Funktionen aus Physik, Chemie, Astronomie, Geophysik und Technik," II Band, 7 Teil, Elektrische Eigenschaften II, Springer-Verlag, Berlin, 1960. [c] Measured by the present writers. [d] Graphical determination from "Physikalische Chemische Tabellen," Landolt-Börnstein, Erg. Bd. II (1931) and III (1936). [e] Graphical determination from S. Lindenbaum and G. E. Boyd, *J. Phys. Chem.*, **68**, 911 (1964). Values for the concentrations below 0.1 M were estimated by extrapolation.

the Soret coefficient of the unknown MCl can be calculated by the equation[2]

$$\sigma^{\mathrm{MCl}} = \frac{t_{\mathrm{Li}^+}{}^{\mathrm{LiCl}} B^{\mathrm{LiCl}}}{t_{\mathrm{M}^+}{}^{\mathrm{MCl}} B^{\mathrm{MCl}}} \sigma^{\mathrm{LiCl}} - \frac{F(\mathrm{d}E/\mathrm{d}T)_0}{2RTt_{\mathrm{M}^+}{}^{\mathrm{MCl}} B^{\mathrm{MCl}}} - \frac{\bar{\bar{S}}_{\mathrm{Cl}^-}{}^{\mathrm{MCl}} - \bar{\bar{S}}_{\mathrm{Cl}^-}{}^{\mathrm{LiCl}}}{2RTt_{\mathrm{M}^+}{}^{\mathrm{MCl}} B^{\mathrm{MCl}}} \quad (2)$$

where σ's are the Soret coefficients, t's are the ionic transport numbers for ions indicated by the subscripts corresponding to the solution phases indicated by the superscripts, F is the Faraday constant, T is the absolute temperature, and B's are defined by

$$B^{\mathrm{LiCl}} = (1 + \mathrm{d} \ln \gamma_{\pm}{}^{\mathrm{LiCl}}/\mathrm{d} \ln m)_{T,P}$$

$$B^{\mathrm{MCl}} = (1 + \mathrm{d} \ln \gamma_{\pm}{}^{\mathrm{MCl}}/\mathrm{d} \ln m)_{T,P}$$

where $\gamma_{\pm}$'s are the mean activity coefficients on the molality scale in an m molal solution. $\bar{\bar{S}}_{\mathrm{Cl}^-}$'s represent the transported entropies of the chloride ion in the solution phase indicated by the superscripts. In the present work, the third term on the right-hand side of (2) was omitted in the practical calculation because this contribution is negligible in the present experimental condition.[1,2]

Experimental Results

All solutions were prepared by using Kosō Guaranteed reagent grade chemicals (99.8% purity) to a concentration of 0.01 M within 0.3%.

The process of preparing cells, experimental conditions, and measuring methods are nearly the same as those reported in the previous paper,[1,2] except for taking here the lithium chloride thermocell as a reference of the combined thermocell. In the present work, the measurements were begun after allowing the cells to stand at a medium temperature near 25° for more than 2 or 3 weeks, and even for a month in the case of tetra-n-propylammonium chloride, and a satisfactory result could be obtained.

Measurements were repeated on every possible combination of four or five well-conditioned MCl thermocells with four or five well-conditioned reference LiCl thermocells. Some of the typical results are represented in Figure 1. The values of $(\mathrm{d}E/\mathrm{d}T)_0$, the initial thermoelectric power of the combined thermocell, were determined by the method of the least squares, and are listed in Table I. The data are reproducible in most cases within a fluctuation of 1 to 3%.

The Soret coefficient of LiCl, which was used as a reference in the present work, was assigned to be -0.01×10^{-3} deg^{-1}, which was obtained by adjusting Snowdon and Turner's value[3] of -0.02×10^{-3} deg^{-1} at 25.3° and 0.01 M to the 25° value. Using this value and our data on $(\mathrm{d}E/\mathrm{d}T)_0$, the relative value of the Soret coefficients, σ^{MCl}, at 25° and 0.01 M were determined by the aid of (2) taking $\bar{\bar{S}}_{\mathrm{Cl}^-}{}^{\mathrm{MCl}} = \bar{\bar{S}}_{\mathrm{Cl}^-}{}^{\mathrm{LiCl}}$. The results are compared with previous values[2] and with those obtained by the direct method by Snowdon and Turner[3] in Table I. They are found roughly in good agreement with each other. The Soret coefficients

---

(2) T. Ikeda and H. Kimura, *J. Phys. Chem.* **69**, 41 (1965).

(3) P. N. Snowdon and J. C. R. Turner, *Trans. Faraday Soc.*, **56**, 1409 (1960).

Figure 1 was obtained showing peaks of 670, 640, and 600 mμ, clearly very similar to the gas phase spectrum of NO_3.[4] The possibility of this transient being NO_3^{2-} may be discounted as the spectrum is practically unchanged in 6 *M* HNO_3 (Figure 1) and agrees with that obtained by flash photolysis of cerium(IV) in the same medium.[5]

This transient absorption, which decays by a first-order process ($t_{1/2}$ = 40 μsec) is not found in 10^{-2} *M* $NaNO_3$ but is produced in increasing amounts as the concentration of NO_3^- is increased from 0.5 *M* up to the practical limit of 8 *M*. Over this range a considerable amount of energy is deposited in the nitrate, and in order to determine the origin of the NO_3, the absorbance per pulse, *A*, has been treated according to the equation

$$\frac{A}{f_{H_2O}} = A_{H_2O} + \frac{f_{NO_3^-}}{f_{H_2O}}A_{NO_3^-}$$

which has been set up by arbitrarily assuming that NO_3 may originate as a result of energy deposited either in the water or in the nitrate (f_{H_2O} and $f_{NO_3^-}$ are the fractions of energy absorbed in water and nitrate, respectively, and the *A*'s are the respective coefficients). Reference to Figure 2 shows that in fact $A_{H_2O} = 0$; *i.e.*, all of the NO_3 is a transient characteristic of the reactions involved in "direct action." This result clearly makes unnecessary any discussion of excitation effects[6] and energy transfer[7] from solvent (water) to solute (NO_3^-).

However, NO_3 is not the primary species formed by "direct action." This is shown by: (1) under certain conditions the kinetic curves give indications of a rise time, though this could not be clearly resolved; (2) formation of NO_3 can be completely eliminated by the prior addition of NO_2^- and methanol in concentrations not greatly affecting the decay of NO_3.

It may be concluded then that NO_3 has a radical precursor and thus is not formed as a result of the ionization process

$$NO_3^- \longrightarrow NO_3 + e \qquad (1)$$

As alternative primary processes the dissociation reactions

$$NO_3^- \longrightarrow NO_2 + O^- \qquad (2)$$

$$NO_3^- \longrightarrow NO_2^- + O \qquad (3)$$

in which O^- and O are the NO_3 precursors, may be considered. Although the previous finding that $A_{H_2O} = 0$ indicates that OH radicals readily available from the radiolysis of water are ineffective in leading to NO_3 formation and hence are not the precursors of NO_3, additional dif-

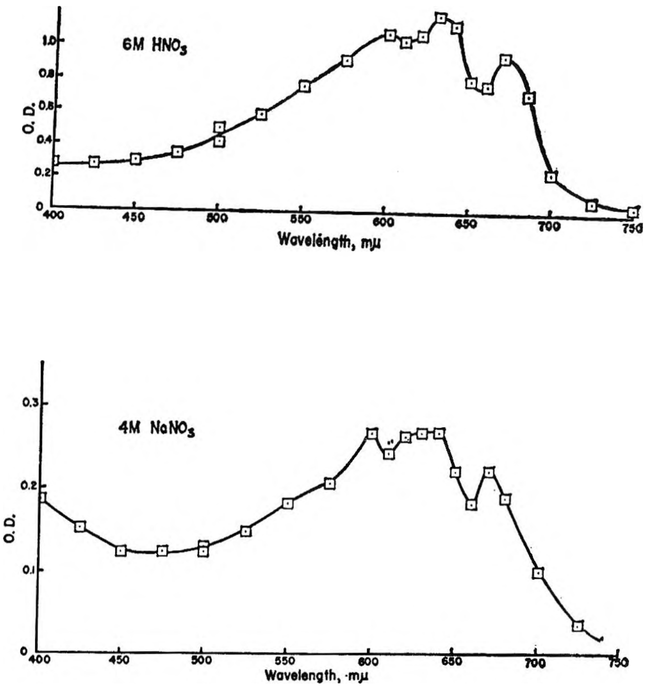

Figure 1. Absorption spectra of transient produced in 4 *M* $NaNO_3$ and 6 *M* HNO_3.

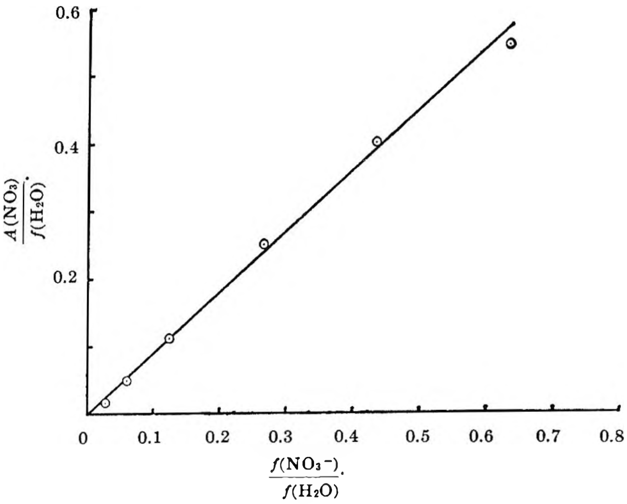

Figure 2. Dependence of NO_3 formation on fractional energy deposition.

---

[4] E. J. Jones and O. R. Wulf, *J. Chem. Phys.*, **5**, 873 (1937); G. Schott and N. Davidson, *J. Am. Chem. Soc.*, **80**, 1841 (1958); D. A. Ramsey, *Proc. Colloq. Spectros. Intern., 10th, Univ. Maryland, 1962*, 583 (1963).

[5] T. W. Martin, A. Henshall, and R. C. Gross, *J. Am. Chem. Soc.*, **85**, 113 (1963).

[6] M. A. Proskurnin and V. A. Sharpatyi, *Russ. J. Phys. Chem.*, **34**, 1009 (1960).

[7] J. Bednar and S. Lukac, *Coll. Czech. Chem. Commun.*, **29**, 341 (1964).

expected to be significant as reported in other studies.[4,5] Since measurements of complex stability are really a measure of the competition of solvent and ligand for ligancy sites, a decrease in the polarity of the solvent, as reflected by a decreased dielectric constant, should favor increased complex stability.

Experimental Section

Reagents. The amines used were reagent grade and were freshly distilled before use except for the di-n-propyl-, diisobutyl-, and tributylamines. These latter were used as obtained. The isopropyl alcohol used was dried over activated synthetic zeolite before use. The silver perchlorate and lithium perchlorate were dried under vacuum and stored over desiccant until used. All additions and transfers of reagents were made in a drybox and solutions were stirred with dry nitrogen during potential measurements.

Procedure. Silver ion activities were determined by a modification of the method of Bodlander[10] and Koch.[11] The reference half-cell consisted of silver-plated platinum electrodes[12] in anhydrous isopropyl alcohol solutions 0.025 M in $AgClO_4$ and 0.5 M in $LiClO_4$. The variable half-cell consisted of a silver-plated platinum electrode in 0.5 M $LiClO_4$ solution in anhydrous isopropyl alcohol containing varying, but always large excess, amounts of amine and varying amounts of $AgClO_4$. For each complex studied, measurements were made on three sets of solutions each having a different amine concentration. In each set there were four solutions in which the amine concentration was kept constant while silver ion concentrations were varied. The two cells were electrolytically connected by an aqueous agar bridge containing KNO_3. The time of contact of the bridges with the alcoholic solutions was kept as small as possible to minimize diffusion effects. KNO_3 solutions in isopropyl alcohol were tried as bridge solutions but were found to be unsatisfactory.[3] In two different sets of measurements the KNO_3 concentration of the bridge solution was varied from 2 to 3 m. No significant change in the cell emf was noted, suggesting that junction potentials were small or at least independent of the concentration of the bridge solution and also of the concentration of the silver ion in the test and reference solutions.

In one set of measurements, the concentration of the $LiClO_4$ background electrolyte was varied to determine the effects of ionic strength on instability constant, K_i (Table I). pK_i values increased in a somewhat regular way with decreasing electrolyte concentration, but no simple relationship between K_i and concentration or ionic strength could be observed.

Table I: Effect of Background Electrolyte Concentration on pK_i Values for n-Butylamine–Silver(I) Complex

Concn of $LiClO_4$, M	0.8	0.5	0.2	0.0
pK_i	9.1	9.2	9.4	10.4

Measurements were made using an L and N student potentiometer and extended range galvanometer. Two pairs of essentially identical electrodes were compared for each emf determination in each solution to eliminate spurious electrode effects.

Coordination numbers and instability constants were calculated from observed potentials by the method of Jonassen, *et al.*,[2] except that concentrations were used rather than activities in the absence of reliable data for activity coefficients. The relationship derived by these investigators is given by

$$\mathrm{p}K_i = \frac{E}{0.0591} - \log \mathrm{Ag_R}^+ - n(\log L_T - n\mathrm{Ag_T}^+) + \log \mathrm{Ag_T}^+ \quad (1)$$

where pK_i is the negative log of the instability constant, $\mathrm{Ag_R}^+$ is the silver ion concentration in the reference half-cell, E is the observed potential, n is the coordination number of the silver ion, L_T is the total added ligand concentration, and $\mathrm{Ag_T}^+$ is the total silver ion concentration in the variable half-cell. A plot of $-E/0.05916$ *vs.* $-n(\log L_T - n\mathrm{Ag_T}^+) + \log n\mathrm{Ag_T}^+$ should give a straight line with a slope of 1.0 for $n = 2$ if the silver ion shows its normal coordination number and if the system is reversible.

Results

Average values of the slopes obtained on the basis of eq 1 are shown in Table II. Values represent the average of three sets of experiments. For each run, silver ion concentrations varied from 0.0007 to 0.02 M. All results are the average of values for two independent pairs of electrodes.

As can be seen, the slopes do not vary appreciably from 1 except perhaps for the diisobutyl, tri-n-propyl, and tri-n-butylamine complexes. It is possible that in these complexes the silver ion may have a coordination number other than 2. One might predict, on the basis of steric effects, that the coordination number of the silver ion might be decreased for these amines and the lower value for the diisobutyl complex would be

---

[10] G. Bodlander as cited in S. Glasstone, "Textbook of Physical Chemistry," 2nd ed, D. Van Nostrand Co., Inc., New York, N. Y., 1946, pp 972–974.

[11] F. K. V. Koch, *J. Chem. Soc.*, 2053 (1930).

[12] A. S. Brown, *J. Am. Chem. Soc.*, **56**, 646 (1934).

Table II: Slope of Plot of $-E/0.0591$ *vs.* $-n$ Log $(L_T - n\text{Ag}_T{}^+)$ + Log $(\text{Ag}_T{}^+)$ for Different Amine Complexes[a]

	Run A		Run B		Run C	
Amine	Amine concn, *M*	Slope	Amine concn, *M*	*M*	Amine concn, *M*	Slope
n-Propyl	1.94	1.0 ± 0.1	2.43	0.98 ± 0.1	2.92	0.96 ± 0.1
n-Butyl (0.2 *M* LiClO_4)	1.62	1.0 ± 0.1	2.02	0.98 ± 0.1	2.42	0.99 ± 0.1
n-Butyl	1.62	1.0 ± 0.1	2.02	1.0 ± 0.1	2.42	0.99 ± 0.1
n-Butyl (0.8 *M* LiClO_4)	1.62	0.95 ± 0.3	2.02	1.0 ± 0.1	2.42	1.0 ± 0.1
Isobutyl	1.60	1.0 ± 0.1	2.00	0.98 ± 0.2	2.40	0.97 ± 0.1
t-Butyl	1.52	1.0 ± 0.1	1.90	1.0 ± 0.1	2.28	0.97 ± 0.2
Di-*n*-propyl	1.17	0.89 ± 0.6	1.46	0.91 ± 0.3	1.75	0.92 ± 0.3
Di-*n*-butyl	1.78	0.98 ± 0.1	2.02	0.99 ± 0.3	2.26	0.96 ± 0.3
Diisobutyl	1.73	0.92 ± 0.3	1.96	0.86 ± 0.5	2.19	0.76 ± 0.3
Triethyl	1.58	1.08 ± 0.1	1.87	0.98 ± 0.3	2.16	0.96 ± 0.2
Tri-*n*-propyl	1.59	1.48 ± 0.4	1.80	1.46 ± 0.3	...	...
Tri-*n*-butyl	...	...	1.85	1.22 ± 0.5	...	...

[a] Background electrolyte is 0.5 *M* LiClO_4, except as noted.

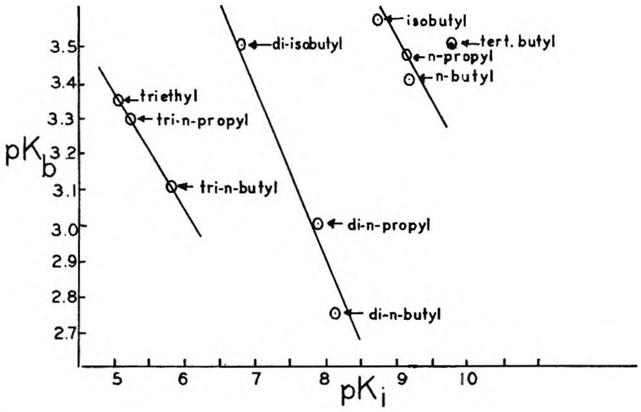

Figure 1.

consistent with this. It does not seem reasonable, however, to postulate an increase in coordination number of the silver ion with the tri-*n*-butyl- and tri-*n*-propylamines in concentration ranges where less hindered amines show no such increase. It is thus concluded that the deviations noted for these three complexes represent failure of the equations to represent adequately the system rather than any real change in the coordination number of the silver ion.

The independence of the slope upon the concentration of the background electrolyte, observed for the *n*-butylamine complex suggests that the background electrolyte does not compete successfully with the amine for ligancy sites of the silver ion, and also that the ligancy of the silver ion is not significantly affected by the electrolyte concentration.

Various workers have reported a general relationship between $\text{p}K_\text{i}$ and $\text{p}K_\text{B}$, the negative log of the base ionization constant of the amine.[5,13,14] Experimental values of $\text{p}K_\text{i}$ obtained in this investigation, plotted against $\text{p}K_\text{B}$ values for the various amines in water, are shown in Figure 1. $\text{p}K_\text{B}$[15,16] values in water were used in the absence of such data in isopropyl alcohol and on the assumption that the relative values for the various amines would not be greatly changed in going from water to isopropyl alcohol.

The amines fall clearly into three groups, primary, secondary, and tertiary. In each of these groups a reasonably linear proportionality exists between $\text{p}K_\text{i}$ and $\text{p}K_\text{B}$. The silver complexes formed from primary amines are about one to two orders of magnitude more stable than those with secondary amines, which are in turn two to three orders of magnitude more stable than complexes with tertiary amines. This is the order found by Brown[17] for the basic strength of ethyl-, diethyl-, and triethylamines with the highly hindered reference acid, tri-*t*-butylboron rather than the order when HCl is used as the reference acid. This suggests that for the silver–amine complexes, steric effects are more significant than inductive effects in determining changes in stability with substitution. This does not

---

(13) R. J. Bruehlman and F. H. Verhoek, *J. Am. Chem. Soc.*, **70**, 1401 (1948).

(14) J. Bjerrum, *Chem. Rev.*, **46**, 381 (1950).

(15) H. K. Hall, Jr., *J. Am. Chem. Soc.*, **79**, 5441 (1957).

(16) N. A. Lange, Ed., "Handbook of Chemistry," 9th ed, Handbook Publishers, Inc., Sandusky, Ohio, 1956.

(17) A. R. Day, "Electronic Mechanisms of Organic Reactions," American Book Co., New York, N. Y., 1950, pp 220–221.

appear to be unique to the isopropyl alcohol solvent system since the same order is observed in water and acetone as shown in Table III.

Table III: pK_i of Silver–Amine Complexes in Different Solvents

Solvent system	Dielectric constant	pK_i of silver–amine complex n-Butyl	 Isobutyl	 Di-n-butyl	 Diisobutyl	 Tri-n-butyl
Isopropyl alcohol, 0.5 M $LiClO_4$	18.3	9.17	8.75	8.13	6.84	5.70
Acetone, 0.5 M $LiClO_4$	20.7	10.29	9.68	10.05	8.83	...
Water	78.54	7.48	7.24	4.10	...	3.82

Jonassen[4] and others have suggested that the pK_i of amine complexes should increase as the dielectric constant of the solvent decreases and in the case of ethylamine in the solvents water, ethanol, and isopropyl alcohol such a correlation appears to exist, perhaps because of the very similar nature of the solvents. That this is not the only factor involved can be seen by comparing the values of pK_i in isopropyl alcohol, acetone, and water as shown in Table III. Although it is often difficult to compare results of different investigations, the comparison shown in Table III would suggest that specific solvent effects must play a significant factor in complex stabilities although dielectric constant effects almost certainly are of importance. Further studies involving different solvent systems may be useful in determining the relative importance of these factors.

Conclusions

Complexes of silver with amines fall into three groups, those with primary, secondary, and tertiary amines. Within these groups, the stability of the complexes correlates with the base strength of the amine. It does not, however, correspond to the order of the base strength of the amines in going from primary to secondary to tertiary, suggesting that steric hindrance is a significant factor. The relative stabilities of the amine complexes do not appear to change with changes in solvent although the solvent does affect the absolute values of instability constants. The dielectric constant may have a significant bearing on solvent changes on stability of complexes but specific solvent effects are also significant and may, in the case of solvents of quite different nature, be more important than the effects of dielectric constant.

Acknowledgments. This work was financed in part by an Academic Year Extension of the Research Participation Program at Oklahoma State University sponsored by the National Science Foundation. The assistance and suggestions of Dr. Paul Arthur of Oklahoma State University are gratefully acknowledged.

Kinetics of the Gas Phase Pyrolysis of Tetranitromethane[1]

by J. M. Sullivan and A. E. Axworthy

Rocketdyne, A Division of North American Aviation, Canoga Park, California *(Received May 10, 1966)*

Reported herein are the results of our study of the pyrolysis of tetranitromethane (TNM).

Experimental Section

The 90.6-ml monel electrically heated, stirred flow reactor was identical with that described by Sullivan and Houser.[2] TNM vapor of 99% purity was mixed with helium and passed through the reactor at 1 atm total pressure and a TNM initial partial pressure of 1.09 mm (runs 1–23). The storage tank was repressurized with helium prior to run 24 giving an initial TNM partial pressure of 0.48 mm in the final eight experiments. The reactor was by-passed to permit analysis of the unreacted TNM. A sample of the gas stream from the reactor (or the by-pass) was periodically analyzed for TNM by introducing it into the helium carrier gas stream of a gas chromatograph by means of an unlubricated Beckman gas sampling valve. The reduction in TNM concentration with residence time in the reactor was followed chromatographically using a 3-ft column of 5% S.E.-30 silicone oil on Celite, 60–100 mesh, at room temperature and a thermal conductivity detector. The flow rates through the reactor were measured with a soap bubble flow meter connected to the exit stream. The measured flow rates and reactor volume were corrected to reactor temperature.

Mass spectrometric analysis of the decomposition products showed the presence of the species NO_2, NO, N_2O, and CO_2. The presence of NO_2 and CO_2

---

(1) This work was supported by the U. S. Air Force and the Advanced Research Projects Agency under Contract No. AF04(611)-9380 and ARPA Order No. 24.

(2) J. M. Sullivan and T. J. Houser, *Chem. Ind.* (London), 1057 (1965).

was further substantiated by infrared spectrometry. However, attempts to establish a mass balance for these species proved unsuccessful.

Results

The results obtained for the thermal decomposition of TNM over the temperature range 170–223° are presented in Table I. The rate equation for a simple order, single-reactant reaction in a stirred flow reactor is

$$k_n = (P^0 - P)/(P^n\tau) \qquad (1)$$

where P^0 and P are the partial pressures, respectively, of the reactant in the gas streams entering and leaving the reactor, τ is the *average* residence time in the reactor, and n is the order of the reaction.[3,4] It is of interest to note that for a first-order reaction in a stirred flow reactor a plot of $1/P$ *vs.* τ will yield a straight line, whereas such a plot will be linear only for a second-order reaction in a plug flow or static reactor.

Table I: Experimental Kinetic Data for the Pyrolysis of Gaseous Tetranitromethane

Run no.	Temp, °C	τ, sec	Fraction reacted, α	k_1, sec^{-1}	k_1^A, sec^{-1}
17	170.0	99.2	0.171	0.00208	0.00222
18		169.5	0.249	0.00196	
19		172.9	0.307	0.00256	
20		174.0	0.283	0.00227	
21	181.2	123.5	0.452	0.00668	0.00680
22		126.1	0.455	0.00662	
23		128.0	0.479	0.00719	
1	186.9	14.3	0.154	0.0127	0.0130
2		27.0	0.265	0.0134	
3		41.5	0.355	0.0133	
4		43.7	0.340	0.0118	
5		54.7	0.416	0.0130	
6		63.0	0.468	0.0140	
10	192.2	13.4	0.229	0.0221	0.0232
11		16.9	0.274	0.0224	
12		23.4	0.310	0.0192	
13		24.3	0.376	0.0248	
14		36.8	0.477	0.0248	
27	198.0	9.69	0.266	0.0375	0.0382
28		9.78	0.276	0.0390	
15	206.7	13.7	0.541	0.0856	0.0856
16		14.1	0.546	0.0855	
7	213.0	5.98	0.474	0.151	0.144
8		6.70	0.475	0.135	
9		7.07	0.510	0.147	
24	215.0	4.74	0.414	0.149	0.150
25		4.89	0.442	0.162	
26		5.02	0.410	0.144	
29	223.2	2.43	0.438	0.320	0.328
30		2.50	0.455	0.334	
31		2.71	0.417	0.264	

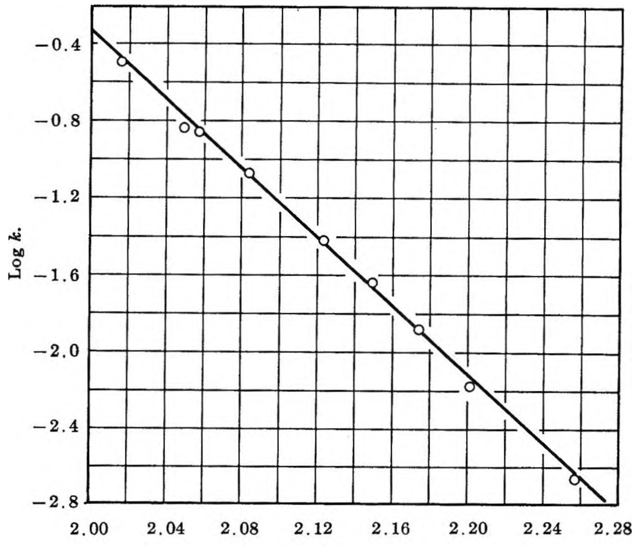

Figure 1. Arrhenius plot for the gas phase pyrolysis of tetranitromethane.

The first-order nature of the decomposition of TNM is illustrated in Table I, particularly with the data obtained at 186.9°. It can be shown from eq 1 that a plot of $\alpha/(1 - \alpha)$ *vs.* τ, where α is the fraction reacted, should be linear for a first-order reaction. The rate constant, k_1, from each experiment is listed in Table I. The best first-order rate constant, k_1^A, at each temperature, obtained from the slope of the best line from an $\alpha/(1 - \alpha)$ *vs.* τ plot, is given in the last column of Table I. The Arrhenius plot (Figure 1) of these rate constants yields the rate expression

$$k_1 = 10^{17.53} \exp(-40{,}875/RT) \text{ sec}^{-1} \qquad (2)$$

The uncertainty in activation energy is about 1.2 kcal/mole.

The possibility of a heterogeneous contribution to the rates obtained in this study has not been completely eliminated. It appears, however, from the high pre-exponential factor and the magnitude of the activation energy, that the reaction is homogeneous.

Discussion

We believe that the kinetic parameters obtained indicate that the rate-determining step is the rupture of a single C–N bond

$$(NO_2)_3C\text{–}NO_2 \longrightarrow (NO_2)_3C\cdot + NO_2 \qquad (3)$$

---

[3] W. C. Herndon, *J. Chem. Educ.*, **41**, 425 (1964).

[4] A. A. Frost and R. G. Pearson, "Kinetics and Mechanism," John Wiley and Sons, Inc., New York, N. Y., 1956, p 185.

This is in agreement with Benson[5,6] who has suggested that for bond rupture within a molecule a "high" preexponential factor of 10^{15} to 10^{18} sec^{-1} is to be expected. Reaction 3 is then followed by further bond rupture or, more likely, by an isomerization process in which an oxygen atom is transferred to the unsaturated carbon atom.

Since the reverse of reaction 3 should have nearly a zero activation energy, the measured activation energy for the pyrolysis of TNM is approximately equal to the dissociation energy of the first C–N bond in TNM if reaction 3 is rate determining. Reaction 3 will be rate determining if the radical formed reacts much more rapidly by another path than by recombination with NO_2. The only other apparent mechanism which could give first-order kinetics independent of the buildup of product NO_2 would be one in which reaction 3 was rapidly reversible and the rate-determining step involved the reaction

$$NO_2 + (NO_2)_3C\cdot \longrightarrow \text{products} \qquad (4)$$

In this case, the measured activation energy would be equal to the dissociation energy of the C–N bond plus the activation energy of reaction 4.

Marshall, Borgardt, and Noble[7] have reported kinetic parameters for the condensed-phase pyrolysis of hexanitroethane (HNE). In the case of solid HNE, the preexponential factor was $10^{18.6}$ and the activation energy 38.9 kcal/mole. Within experimental error, this activation energy is the same as that for gaseous TNM.

It was postulated for solid HNE that the rate-determining step is the simultaneous cleavage of two C–N bonds to give a diradical intermediate.[7] This was based partly on the high preexponential factor of $10^{18.6}$ which was attributed to the unfreezing in the activated complex of the carbon–nitro system (however, the uncertainty in this preexponential factor is a factor of 10^3 to 10^4 since the stated average deviation in the activation energy is 10%). Our results with TNM (one carbon atom) indicate that unfreezing of the carbon–nitro system is not required to obtain a high preexponential factor. The mounting evidence that bond rupture yielding two polyatomic radicals is associated with a "high" Arrhenius factor,[5,6] supported by unpublished work from this laboratory, makes it apparent that the kinetic results reported for solid HNE[7] fit equally well a simpler mechanism in which the rate-determining step is the rupture of the initial C–N bond.

---

[5] S. W. Benson, *Ind. Eng. Chem.*, **56**, 18 (1964).

[6] S. W. Benson and W. B. DeMore, *Ann. Rev. Phys. Chem.*, **16**, 426 (1965).

[7] H. P. Marshall, F. G. Borgardt, and P. Noble, Jr., *J. Phys. Chem.*, **69**, 25 (1965).

The Dissociation of Tetra-*n*-hexylammonium Iodide in Dichloromethane

by R. A. Matheson

Chemistry Department, Victoria University of Wellington, Wellington, New Zealand *(Received July 15, 1966)*

A recent spectrophotometric investigation[1] led to the conclusion that solutions of tetra-*n*-hexylammonium iodide in dichloromethane contain ion pairs $(n\text{-hexyl})_4N^+I^-$ as well as free ions. Assuming the activity coefficients of both free ions and ion pairs to be unity, an equation[2] was derived which related the optical density of a solution of this salt to its concentration. As this equation contained three unknown parameters [the dissociation constant of the ion pair (K_D) and the extinction coefficients of free iodide ions (ϵ_F) and ion pairs (ϵ_p)], it was asserted that measurement of the optical densities of three solutions having different concentrations (C_i) suffices for the evaluation of K_D. A value of 10^{-3} M for this quantity was obtained from the optical densities of solutions of concentrations 3.86×10^{-3}, 9.64×10^{-4}, and 4.82×10^{-5} M.

In order to test this assertion, we have examined the consistency of these optical densities with a variety of values K_D and activity coefficient assumptions identical with those used in the original work.[1] For the values of K_D shown in Table I, extinction coefficients ϵ_F and ϵ_p can be found such that the optical densities calculated from K_D, ϵ_p, ϵ_F, and C_i agree with the experimental optical densities of the three solutions in question. The maximum discrepancy between calculated and experimental optical densities was 1%, which is less than the maximum uncertainty consistent with the manufacturer's specifications for the instrument used in the measurements. Since none of the extinction coefficients is physically unreasonable, it may be concluded that the measurements reported by Blandamer, Gough, and Symons[1] are not sufficient for the evaluation of K_D, and that their estimate of this quantity is uncertain by several powers of ten.

---

[1] M. J. Blandamer, T. E. Gough, and M. C. R. Symons, *Trans. Faraday Soc.*, **62**, 286 (1966).

[2] See eq 3 in ref 1.

Table I

K_D, M	$\epsilon_P \times 10^{-4}$, $cm^{-1} M^{-1}$	$\epsilon_F \times 10^{-4}$, $cm^{-1} M^{-1}$
10^{-1}	3.800	1.479
10^{-2}	1.857	1.472
10^{-3}	1.616	1.453
10^{-4}	1.568	1.425
10^{-5}	1.550	1.320
10^{-6}	1.546	1.000

Because of the low dielectric constant of dichloromethane (9.08 at 20°),[3] activity coefficients of ions in this solvent may be expected to deviate significantly from unity at quite low ionic strengths. For this reason we modified the foregoing analysis by calculating the mean activity coefficient of the free ions from the equation

$$-\log \gamma = \frac{A\sqrt{I}}{1 + Bd\sqrt{I}}$$

with $A = 13.29\ M^{-1/2}$, $B = 0.9746 \times 10^8\ M^{-1/2}\ cm^{-1}$, and d = distance of closest approach of free ions. Assuming d = 10 A, values of K_D between 10^{-2} and 10^{-6} M were found to be consistent with the experimental results. Further, the range of acceptable values of K_D did not depend greatly on the choice of d. Thus the conclusions of the last paragraph remain valid.

Blandamer, Gough, and Symons[1] remarked on the large difference between their result for the dissociation constant of tetra-*n*-hexylammonium iodide in dichloromethane (10^{-3} M) and the figure (7.21×10^{-6} M) obtained for tri(ethyl)methylammonium iodide from conductance measurements in the same solvent. Our analysis of the experimental data for tetra-*n*-hexylammonium iodide shows that the difference may be due to the large uncertainty in the result for this salt rather than to "the difficulties involved in comparing dissociation constants derived from analysis of absorption spectra and conductivity data."

---

(3) "Handbook of Chemistry and Physics," 45th ed, Chemical Rubber Co., Cleveland, Ohio, 1964, p E31.

COMMUNICATIONS TO THE EDITOR

An Activation Energy for the Transport of Carbon Dioxide through a Monolayer of Hexadecanol at the Air–Water Interface

Sir: The influence of monolayers, at the air–water interface, on the loss of CO_2 from its aqueous solution is being studied in these laboratories. This communication deals with the effect of temperature on the permeability of a hexadecanol monolayer to CO_2.[1]

The initial concentration of the $^{14}CO_2$ solution was determined by the method of Harlan.[2] The hexadecanol, supplied by Applied Science Laboratories Inc., State College, Pa., was 99.8+% pure. The monolayers were spread from a 1 mg/ml ethereal solution and the spreading pressures obtained are shown in Table I. Since all pressures are above 15 dynes cm^{-1}, all monolayers investigated were in the "solid" state. The radiotracer technique described by Hawke[3,4] was used to measure the amount of gas appearing above the surface. The apparatus used was similar to that described by Hawke and Crawshaw.[5]

The recorder traces obtained were analyzed by the

Table I: Transmission Coefficients and Equilibrium Spreading Pressures for a Monolayer of Hexadecanol at Various Temperatures

Temperature, °C	0.1	5.1	10.0	15.0
Spreading pressure (Π_e) dynes cm^{-1}	17.4	23.2	29.2	33.6
Transmission coefficient (T_s), $\times 10^4$ cm sec^{-1}	3.7	5.9	7.0	13.6

---

(1) I. White, M.Sc. Thesis, University of Sydney, 1966.

(2) J. W. Harlan, *Atom Light*, **19**, 8 (1961).

(3) J. G. Hawke, Australian Atomic Energy Symposium, 1958, p 634.

(4) J. G. Hawke, Ph.D. Thesis, University of Sydney, 1959.

(5) J. G. Hawke and S. J. Crawshaw, to be published.

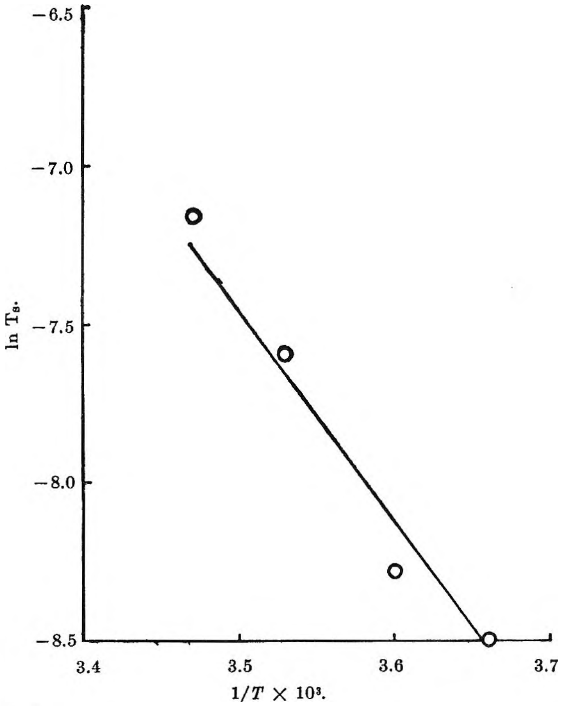

Figure 1.

method described by Hawke and Parts,[6] allowing a transmission coefficient to be assigned to the monolayer. Transmission coefficients were calculated for the monolayer at the temperatures of 0.1, 5.1, 10.0, and 15.0° and these are shown in Table I.

Barnes and La Mer,[7] by considering that the monolayer acts as an energy barrier to gas transport, have applied the transition state theory of Eyring to the permeability (or transmission coefficient) of a monolayer by

$$T_s = c' \exp[S^{\ddagger}/R - \Pi_s NoA^{\ddagger}/RT - E^{\ddagger}/RT] \qquad (1)$$

where T_s is the monolayer's transmission coefficient, c' is a constant, $S^{\ddagger}$ and $E^{\ddagger}$ are the entropy and energy of activation, and $NoA^{\ddagger}$ is the increase in area per mole of activated state caused by the formation of "holes" in the monolayer "lattice."

For measurements made at constant surface pressure, eq 1 becomes

$$T_s = c'' \exp[\Delta S^{\ddagger}/R - \Pi_s NoA^{\ddagger}/RT - E^*/RT] \qquad (2)$$

where E^* is the experimental activation energy and c'' is a constant.

By plotting ln T_s against $1/T$ (Figure 1), values for $c'' \exp \Delta S^{\ddagger}/R$ and $(\Pi_s NoA^{\ddagger} + E^*)$ were obtained for CO_2 transport through hexadecanol monolayers. These values were, respectively, 10^7 cm sec^{-1} and 12 ± 2 kcal mole^{-1}. In order to obtain an approximate value of the activation energy, E^*, a mean value of Π_s (27.6 dynes cm^{-1}) was assumed and a value for $A^{\ddagger}$ (25 A^2) was calculated from the CO_2 transport results of Hawke.[4] These approximations give E^* a value of 11 ± 2 kcal mole^{-1} which is in good agreement with the activation energy for water transport through hexadecanol monolayers found by Barnes and La Mer.[7] Thus, the activation energy for gaseous transport through monolayers appears to be the energy required to form a hole in the two-dimensional monolayer "lattice" as predicted by the energy barrier theory.[7]

The value of the activation energy found here is in marked contrast to that of 2.0 kcal mole^{-1} found by Blank[8] for the absorption of CO_2 into alkaline buffered solutions through a hexadecanol monolayer. This may be due to the presence of water molecules in the monolayer.

Further studies are being carried out on the effect of chain length and the composition of the polar head group on the permeability of monolayers to CO_2. A detailed account will be published elsewhere.[9]

Acknowledgment. We wish to thank the U. S. Public Health Service for financial assistance under the terms of Grant WP00877-01.

---

(6) J. G. Hawke and A. G. Parts, *J. Colloid. Sci.*, 19, 448 (1964).

(7) G. T. Barnes and V. K. La Mer in "Retardation of Evaporation by Monolayers," V. K. La Mer, Ed., Academic Press, New York, N. Y., 1962.

(8) M. Blank, ref 7, p 75.

(9) J. G. Hawke and I. White, to be published.

PHYSICAL CHEMISTRY LABORATORIES
DEPARTMENT OF PHARMACY
UNIVERSITY OF SYDNEY
SYDNEY, AUSTRALIA
J. G. HAWKE
I. WHITE

RECEIVED JULY 18, 1966

Comments on the Effects of the Nonbonded Electrons on Barriers to Internal Rotation

Sir: Over the past several years, there has been considerable interest in barriers to internal rotation. Perhaps most of this interest stems from the lack of any adequate theory describing the origin of such barriers. One very recent theory worked out by Parr and co-workers using the integral Hellmann-Feynman theorem[1] has had considerable success.[2] These workers describe a very simple, semiempirical electrostatic model for calculating barrier heights in molecules.

---

(1) H. Kim and R. G. Parr, *J. Chem. Phys.*, 41, 2892 (1964).

(2) J. Lowe and R. G. Parr, *ibid.*, 44, 3001 (1966).

Table I: $V_{3(\mathrm{M-H})}$ Contribution to Barrier Heights in CH_3MH_3, CH_3MH_2, and CH_3MH Molecules

Molecule	$V_{3(\mathrm{M-H})}$[j]	∠C–M–H	Molecule	$V_{3(\mathrm{M-H})}$	∠C–M–H	Molecule	$V_{3(\mathrm{M-H})}$	∠C–M–H
CH_3CH_3[a]	338	109° 37′	CH_3SiH_3[d]	194	108° 15′	GH_3GeH_3[g]	145	109° 35′
CH_3NH_2[b]	343	112° 3′	CH_3PH_2[e]	430	97° 30′	CH_3AsH_2[h]	~340	(~94°)
CH_3OH[c]	375	108° 52′	CH_3SH[f]	444	96° 30′	CH_3SeH[i]	350	95° 15′

[a] W. Lafferty and E. Plyler, *J. Chem. Phys.*, **37**, 2688 (1962). [b] D. R. Lide, Jr., *ibid.*, **27**, 343 (1957). [c] P. Venkateswarlu and W. Gordy, *ibid.*, **23**, 1200 (1955). [d] Kilb and L. Pierce, *ibid.*, **27**, 108 (1957). [e] See ref 4. [f] T. Kojima, *J. Phys. Soc. Japan*, **15**, 1284 (1960). [g] V. Laurie, *J. Chem. Phys.*, **30**, 1210 (1959). [h] A. B. Harvey and M. K. Wilson, *ibid.*, **44**, 3535 (1966). [i] A. B. Harvey and M. K. Wilson, *ibid.*, **45**, 678 (1966); C. Thomas and E. B. Wilson, Jr., private communication. [j] Barrier in cm^{-1}.

Their model is based on the experimental data now available for several types of molecules and on more elaborate calculations on ethane.[3]

The conclusion reached by these workers was that barriers in molecules like ethane may be regarded as arising primarily from nuclear–nuclear repulsion modified by electron density near the hydrogen nucleus. It is stated[2] that s–p hybrids on one end of the molecule, *e.g.*, on the oxygen atom in CH_3OH, do not contribute to the threefold electron density and hence do not affect the barrier. The threefold component apparently arises from the 1s orbitals of the hydrogen atoms and the overlap of the 1s orbital with the s–p hybrid. If this is so, then nonbonded electrons should not significantly contribute to the magnitude of the barrier in molecules such as CH_3MH_n, where M is a group IV ($n = 3$), V ($n = 2$), or VI ($n = 1$) atom which uses only s–p hybrids. Reported here are some conclusions which support this theory.

It is possible to estimate the nonbonded electron contribution to the barriers in some of these molecules in the following way. If the total barrier height in a CH_3MH_2 molecule is assumed to be a sum of two M–H barriers, then it is possible to compute an individual barrier height contribution for each M–H group, $V_{3(\mathrm{M-H})}$, by the relation

$$V_{3(\mathrm{M-H})} = \frac{-V_{3(\mathrm{CH_3MH_2})}}{2 \cos 3x/2}$$

where $V_{3(\mathrm{CH_3MH_2})}$ is the *total* barrier height in the molecule and x is the projected H–M–H angle. This was first carried out for CH_3PH_2 by Kojima, *et al.*[4] In Table I are listed the $V_{3(\mathrm{M-H})}$ contributions in CH_3MH_2 and CH_3MH_3 molecules. In the latter, $V_{3(\mathrm{M-H})}$ was taken to be $V_{3(\mathrm{CH_3MH_3})}/3$ since ∠H–M–H is almost tetrahedral in every case. These $V_{3(\mathrm{M-H})}$ may now be compared with the total barrier heights in the CH_3MH compounds. Note that when M is in the same periodic series and ∠C–M–H angles are alike, the $V_{3(\mathrm{M-H})}$ are remarkably similar. Since the molecules of the same periodic series have different numbers of nonbonded electrons, it can be concluded that nonbonded electrons contribute little to the barrier heights. This idea is consistent with Parr's model and was recognized some years ago by Pauling,[5] who made the comparison in the first row of Table I.

Based on the barriers known for CH_3GeH_3 and CH_3SnH_3, Lowe and Parr[2] conclude that the heavy M atom will have considerably more d and f orbital participation. These orbitals will contribute a threefold component to the electron density and hence the nonbonded electrons will affect the barrier height. However, no significant nonbonded contribution is found from the information available for CH_3AsH_2 and CH_3SeH (see Table I), although it is admitted that the uncertainty in the barrier of CH_3AsH_2 is large and the structure has not yet been determined. The agreement here may therefore be somewhat fortuitous.

---

(3) R. E. Wyatt and R. G. Parr, *J. Chem. Phys.*, **44**, 1529 (1966).

(4) T. Kojima, E. L. Breig, and C. C. Lin, *ibid.*, **35**, 2139 (1961).

(5) L. Pauling, *Proc. Natl. Acad. Sci. U. S.*, **44**, 211 (1958).

(6) Address correspondence to U. S. Naval Research Laboratory, Washington, D. C.

DEPARTMENT OF CHEMISTRY
TUFTS UNIVERSITY
MEDFORD, MASSACHUSETTS
ALBERT B. HARVEY[6]

RECEIVED JULY 21, 1966

A 2:1 Pyrene–PMDA Molecular Complex

Sir: Molecular complexes of aromatic hydrocarbons with pyromellitic dianhydride (PMDA) have been extensively studied recently.[1–4] The stoichiometry of these complexes has been reported to be 1:1 except for *o*-xylene which forms a 2:1 complex, and perylene

---

(1) J. C. A. Boeyens and F. H. Herbstein, *J. Phys. Chem.*, **69**, 2153 (1965).

(2) J. C. A. Boeyens and F. H. Herbstein, *ibid.*, **69**, 2160 (1965).

(3) Y. Nakayama, Y. Ichikawa, and T. Matsuo, *Bull. Chem. Soc. Japan*, **38**, 1674 (1965).

(4) T. Matsuo, *ibid.*, **38**, 2110 (1965).

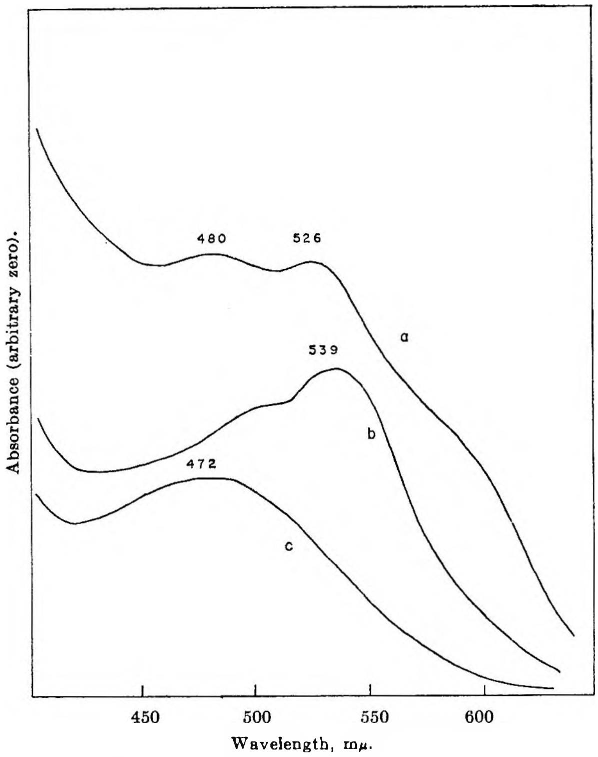

Figure 1. Charge-transfer spectra of (a) 2:1 complex of pyrene with PMDA; (b) 1:1 complex; (c) complex in solution of acetic anhydride.

for which there is evidence[1] for a 2:1 complex in addition to the 1:1 complex actually isolated. We wish to report the isolation of a 2:1 complex of pyrene with PMDA in addition to the previously known 1:1 complex. There seem to be only rare references in the literature on the isolation of hydrocarbon complexes of the same donor and acceptor but of differing stoichiometry, and apparently in no case have their spectra been compared.

PMDA complexes of 1:1 stoichiometry have been found in general to crystallize in parallel stacks with the donor and acceptor molecules alternating within the stacks. From the similarities of the charge-transfer spectra of the two complexes of pyrene, shown in Figure 1, it would seem reasonable to assume that the main structural characteristics of the 1:1 complex are retained in the 2:1 complex. A structure where stacks of the 1:1 complex alternate with stacks of pure pyrene, with the pyrene–pyrene distance comparable to the same distance in the complex stack rather than that in pyrene itself, would account for the similarities in the charge-transfer spectra as well as the observed stoichiometry. An arrangement of alternating stacks of different composition has been found for the 1:1 complex between hexabromobenzene and 1,2,4,5-tetrabromobenzene.[5] A slight interpenetration of the different stacks would serve to maintain the pyrene–pyrene separation as well as to allow for a rather close approach, especially if the molecular planes were tilted to the stack axis, between the molecules in the pyrene stack and the acceptor molecules in the complex stack. Cross-stack charge transfer could then account for the long-wavelength shoulder in the spectrum of the 2:1 complex. The slight blue shift of the absorption band of the 2:1 complex with respect to the 1:1 complex would also be accounted for by the above model. The conditions under which the 2:1 complex is precipitated and the ease with which it is decomposed into the 1:1 complex, and the fact that the spectra of even the most concentrated solutions show no evidence of species other than the 1:1 complex, tend to support the hypothesis of a weak lattice complex between the 1:1 complex and pyrene as opposed to a true 2:1 complex.

We were able to precipitate the 2:1 complex only from highly concentrated (6.1 g of pyrene and 1.4 g of PMDA in 60 ml of nearly boiling solvent) solutions in acetic anhydride. For best results, the initial concentrations should be adjusted until the hot solvent evaporating from the tip of a stirring rod leaves a purplish film, rather than an orange or a red one. Further prerequisites are cooling without agitation, and rapid filtration and drying before room temperature is reached. Even under the most favorable condition, some contamination from the 1:1 complex is to be expected and manual separation under a microscope is suggested for final purification. Vacuum sublimation yields a residue of the 1:1 complex and a sublimate of pyrene. *Anal.* Calcd: C, 81.03; H, 3.56. Found: C, 80.92; H, 3.58 (based upon a 2:1 ratio of pyrene to PMDA). The spectra were recorded on a Cary 14 spectrophotometer on Nujol mulls of the complexes held beween glass plates, most of the scattering being compensated by neutral density screens.

---

(5) G. Gafner and F. H. Herbstein, *J. Chem. Soc.*, 5290 (1964).

(6) National Science Foundation Undergraduate Research Participation Program Fellow for summer, 1965.

DEPARTMENT OF CHEMISTRY
UNIVERSITY OF CONNECTICUT
STORRS, CONNECTICUT 06268

IVOR ILMET
LAWRENCE KOPP[6]

RECEIVED AUGUST 11, 1966

Electron Spin Resonance of Thioketyls. A Large Metal Ion Splitting

Sir: We wish to report the preparation and first electron spin resonance study of thioketyls. It is well

Table I: Ketyl Esr Data[a]

Ketone	Color	g Value[b]	Splitting constants[c]
Xanthene-9-one	Blue	2.00355	3.80 (4-H), 0.94 (2-H), 0.95 (Na),[8] <0.2 (K)[8]
Xanthene-9-thione[d]	Reddish brown	2.00571	3.35 (4-H), 0.77 (2-H), 0.32 (2-H), 4.0 (Na), 0.77 (K)
Thioxanthene-9-one	Blue	2.00348	3.5 (4-H),[e] line width = 17.3[e]
Thioxanthene-9-thione[d]	Reddish brown	2.00577	2.99 (4-H), 0.91 (2-H), 0.79 (2-H), 3.78 (Na)
p-$CH_3OC_6H_4COC_6H_4OCH_3$-p[f]	Blue	2.00359	Complex spectrum Line width = 26 (Na)
p-$CH_3OC_6H_4CSC_6H_4OCH_3$-p	Red	2.00617	3.7 ± 0.3 (4-H), 0.75 ± 0.1 (4-H), 0.28 (6-H), 3.7 ± 0.2 (Na) Line width = 15.5 (K)
p-$(CH_3)_2NC_6H_4COC_6H_4N(CH_3)_2$-$p$	Blue	2.00361	Complex spectrum Line width = 28 (K)
p-$(CH_3)_2NC_6H_4CSC_6H_4N(CH_3)_2$-$p$	Reddish brown	2.00575	Complex spectrum Line width = 32 (Na), 27 (K)

[a] Sodium or potassium ketyls in tetrahydrofuran. [b] ±0.00005. [c] Splitting constants in gauss; total line width in gauss calculated from first maximum to last minimum of the first derivative spectrum. [d] Synthesized by treating the ketone with P_2S_5 in benzene; xanthene-9-thione, mp 154–156°; thioxanthene-9-thione, mp 164–168° (ref 4). [e] E. T. Kaiser and D. H. Eargle, Jr., *J. Am. Chem. Soc.*, **85**, 1821 (1963), potassium ketyl in 1,2-dimethoxyethane. [f] Synthesized by treating p,p'-dihydroxybenzophenone with methyl iodide in basic ethanol, mp 141–144° (K. Auwers, *Ber.*, **36**, 3893 (1903)).

known that aryl ketones react with alkali metals to form colored solutions containing stable anion radicals known as ketyls. Solutions of ketyls give well-resolved esr spectra.[1] Certain ketyls in some solvents may be in equilibrium with diamagnetic dimers, the pinacolates.[2] Paramagnetic dimers are also present in some cases.[3] Electronic and esr spectra have provided evidence for ion pairs.[1,2]

No detailed studies of thioketone reactions with alkali metals have been made.[4] We have found that thioketones react with alkali metals to produce colored solutions which contain free radicals stable for at least several weeks. Table I lists the observed colors and esr data obtained from thioketones and their oxygen analogs.[5]

The hyperfine spectra obtained from the substituted thiobenzophenones are very complex due to the large number of interacting nuclei in the anion radical. Simplified spectra are obtained from xanthene-9-thione (Figure 1) and thioxanthene-9-thione. The hyperfine splitting is due to four approximately equivalent hydrogens, two pairs of hydrogens and one metal ion. Splitting constants obtained for the oxygen analogs are similar although somewhat larger for the same hydrogens. These observations are in good agreement with the thioketyl structure for the anion radicals, *e.g.*

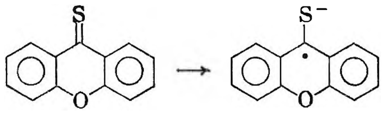

The higher g values found for the thioketyls as compared to the oxygen analogs are also in accord with this structure since an increase in g value is usually observed for free radicals containing atoms of higher atomic number.[6,7] The smaller hydrogen hyperfine

---

(1) F. C. Adam and S. I. Weissman, *J. Am. Chem. Soc.*, **80**, 1518 (1958); P. B. Ayscough and R. Wilson, *Proc. Chem. Soc.*, 229 (1962); N. Hirota, *J. Chem. Phys.*, **37**, 1884 (1962).

(2) H. E. Bent and A. J. Harrison, *J. Am. Chem. Soc.*, **66**, 969 (1944), and references therein; H. V. Carter, B. J. McClelleand, and E. Warhurst, *Trans. Faraday Soc.*, **56**, 455 (1960); J. F. Garst, D. Walmsley, C. Hewitt, W. R. Richards, and E. R. Zabolotny, *J. Am. Chem. Soc.*, **86**, 412 (1964).

(3) N. Hirota and S. I. Weissman, *ibid.*, **82**, 4424 (1960); N. Hirota and S. I. Weissman, *Mol. Phys.*, **5**, 537 (1962); N. Hirota and S. I. Weissman, *J. Am. Chem. Soc.*, **86**, 2538 (1964).

(4) E. Campaigne, *Chem. Rev.*, **39**, 1 (1946). A red solution attributed to the thioketyl has been observed in the reaction of $p,p,$-dimethoxythiobenzophenone with potassium (A. Schonberg, *Ber.*, **58**, 1793 (1925); E. Bergmann, M. Magat, and D. Wagenberg, *ibid.*, **63**, 2576 (1930), see footnote p 2579). A similar product of xanthene-9-thione was found to be weakly paramagnetic (E. Muller and W. Wiesemann, *Ann.*, **537**, 86 (1939)).

(5) A Varian 4502 epr spectrometer with 12-in. magnet and Fieldial regulation was used for the esr measurements. g Values were calculated from the resonance equation. The magnetic field was monitored with a proton probe utilizing a Magnion G502 gaussmeter and a Hewlett-Packard 5245L frequency counter. The klystron frequency was measured by means of a Hewlett-Packard 540B transfer oscillator and 5253B frequency converter.

Samples were prepared using standard high-vacuum techniques. Since thioketones are readily oxygenated to ketones,[4] it was thought advisable to compare all results obtained from thioketones with those found for their oxygen analogs. Chemicals not mentioned in footnotes, Table I, are commercially available.

(6) M. S. Blois, Jr., H. W. Brown, and J. E. Maling in M. S. Blois, "Free Radicals in Biological Systems," Academic Press, New York, N. Y., 1961, p 117; B. G. Segal, M. Kaplan, and G. K. Fraenkel, *J. Chem. Phys.*, **43**, 4191 (1965).

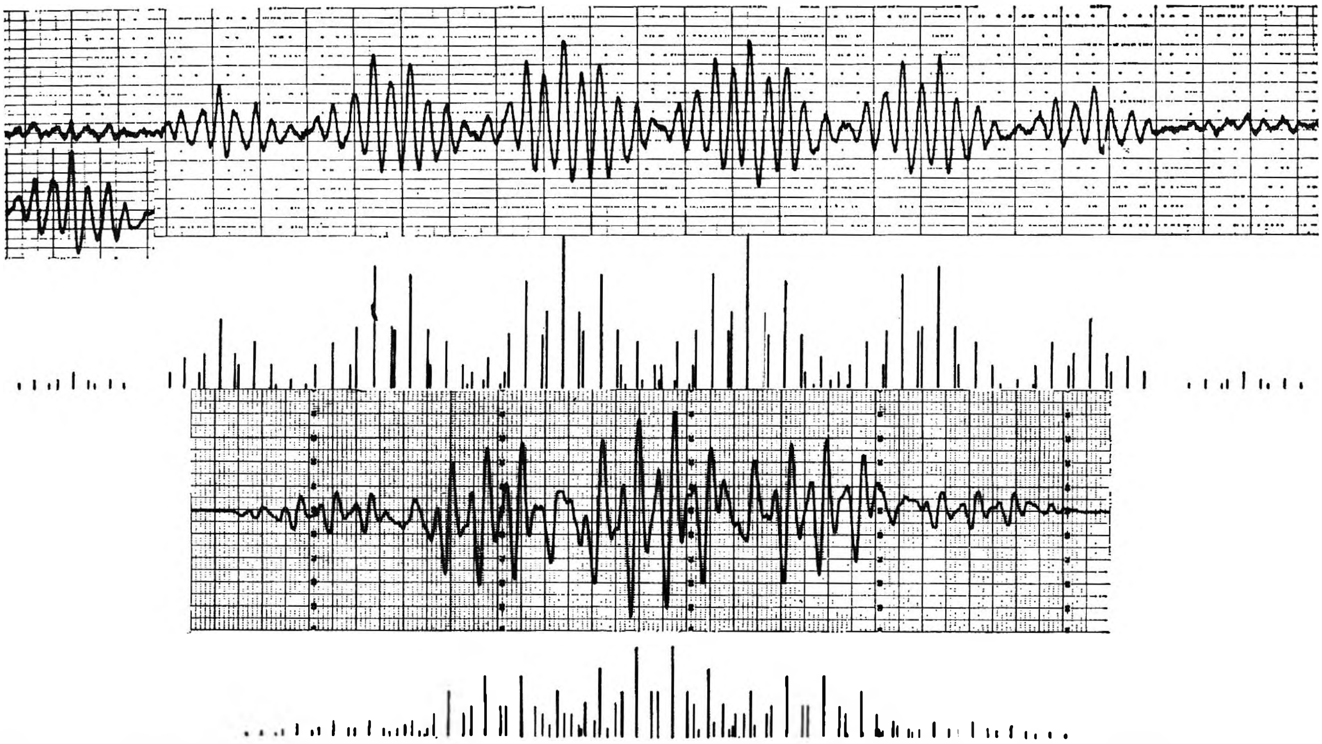

Figure 1. Electron spin resonance spectra of sodium (top) and potassium (bottom) xanthene-9-thione ketyl. The splitting constants given in Table I produce the synthetic line spectrum. The spacing between the largest peaks of the top spectrum due to sodium splitting is 5 gauss.

splitting in thioketyls reflects a decrease in spin density at carbons bearing hydrogens and presumably an increase in spin density on the thiocarbonyl function.

The most remarkable feature of the esr spectrum of thioketyls is the large metal ion splitting. Whereas in the case of xanthone ketyl, sodium splitting is 0.95 gauss and potassium splitting probably ~0.1 gauss,[8] the sodium splitting for xanthone thioketyl is 4.0 gauss and potassium 0.77 gauss. A large metal ion splitting is also undoubtedly part of the spectrum of the other thioketyls since a much larger total line width is observed for sodium than for potassium (Table I). The larger metal ion splitting in the thioketyls may be attributed to a higher spin density on the thiocarbonyl function and/or more efficient spin transfer from sulfur to metal ion. These effects may involve sulfur *d*-orbital participation. Molecular orbital calculations are in progress. Peliminary results have been obtained for other thioketones, *e.g.*, thiobenzophenone and thiofluorenone.[8a]

DEPARTMENT OF CHEMISTRY
THE UNIVERSITY OF GEORGIA
ATHENS, GEORGIA

EDWARD G. JANZEN
COIT M. DUBOSE, JR.[9]

RECEIVED AUGUST 15, 1966

---

[7] Free radicals with the unpaired electron entirely localized on sulfur have *g* value of 2.027: J. J. Windle, A. K. Wiersema, and A. L. Tappel, *J. Chem. Phys.*, **41**, 1996 (1964).

[8] N. Hirota and S. I. Weissman, *J. Am. Chem. Soc.*, **86**, 2537 (1964).

[8a] NOTE ADDED IN PROOF. The coupling constants for the cesium ketyl of thioxanthene-9-thione in tetrahydrofuran are ~3 (4-H ≅ Cs), 0.86 (2-H), and 0.50 (2-H) gauss.

[9] National Aeronautics and Space Administration Traineeship, 1965–1966.

Intramolecular Energy Transfer in γ-Irradiated Alkylbenzenes

Sir: Voevodskii,[1,2] using epr and Bagdasaryan,[3] using iodine scavenger techniques, have shown that in phenyl substituted saturated hydrocarbons besides intermolecular energy transfer, intramolecular energy transfer also takes place. Recently, Jones, *et al.*,[4]

---

[1] Yu. N. Molin, I. I. Chkeidze, N. Ya. Buben, and V. V. Voevodskii, *Kinetika i Kataliz*, **2**, 192 (1961).

[2] Yu. N. Molin, I. I. Chkeidze, A. A. Petrov, N. Ya. Buben, and V. V. Voevodskii, *Dokl. Akad. Nauk SSSR*, **131**, 125 (1960).

[3] Kh. S. Bagdasaryan, N. S. Izrailevich, and V. A. Krongauz, *ibid.*, **141**, 887 (1961).

[4] K. H. Jones, W. van Dusen, Jr., and L. M. Theard, *Radiation Res.*, **23**, 128 (1964).

studied hydrogen formation in a series of *n*-alkylbenzenes in an effort to determine the effect of side-chain length on intramolecular energy transfer. They conclude from their experimental results that the extent of alkyl group protection is unaffected by the size of the alkyl side chain. In this communication, we wish to present further information on this subject because our experimental results are not in agreement with the statement of Jones, *et al.*[4] We investigated the hydrogen formation of *n*-alkylbenzenes and several equimolar mixtures of alkane and benzene. Addition of iodine up to 0.5% had no effect on $G(H_2)$. It is reasonable to assume that the unscavengable hydrogen in alkylbenzenes is produced *via*

$$C_6H_5C_nH_{2n+1} \longrightarrow C_6H_5C_nH_{2n}\cdot + H\cdot_{kin} \quad (1a)$$

$$C_6H_5C_nH_{2n+1} + H\cdot_{kin} \begin{array}{l} \longrightarrow C_6H_5C_nH_{2n}\cdot \\ \longrightarrow C_6H_4C_nH_{2n+1}\cdot \end{array}\Bigg\} + H_2 \quad (1b)$$

$$C_6H_5C_nH_{2n+1}{}^{\ddagger} \longrightarrow C_6H_5C_nH_{2n-1} + H_2 \quad (2)$$

$$C_6H_5C_nH_{2n+1}{}^{\ddagger} + C_6H_5C_nH_{2n+1} \longrightarrow C_{12+2n}H_{10+4n} + H_2 \quad (3)$$

Table I[a]

n-Alkylbenzene (or alkane–benzene mixture)	$G(H_2)$		$g_{alkyl}(H_2)$	
	Jones, *et al.*	This work	Jones, *et al.*	This work
Toluene	0.12	...	0.49	...
Ethylbenzene	0.16	0.18	0.45	0.51
Propylbenzene	0.20	0.23	0.46	0.55
Butylbenzene	0.25	0.27	0.51	0.56
Amylbenzene	0.25	0.34	0.46	0.64
Amylbenzene + 0.5% I_2	...	0.35	...	...
Hexylbenzene	0.29	0.40	0.50	0.70
(Hexane–benzene)	...	(0.53)	...	(0.94)
(Hexane–benzene + 0.5% I_2)	...	(0.53)	...	...
Heptylbenzene	0.31	0.42	0.50	0.69
Octylbenzene	0.33	0.48	0.51	0.75
Nonylbenzene	...	0.59	...	0.89
Nonylbenzene + 0.5% I_2	...	0.58	...	...
(Nonane–benzene)	...	0.78	...	(1.19)
(Nonane–benzene + 0.5% I_2)	...	(0.83)	...	...
Dodecylbenzene	...	0.67	...	0.94
Tridecylbenzene	...	0.75	...	1.03
Tridecylbenzene + 0.5% I_2	...	0.73	...	...
(Tridecane–benzene)	...	0.93	...	(1.28)
(Tridecane–benzene + 0.5% I_2)	...	0.94	...	...
Heptadecylbenzene	...	0.95	...	1.23
(Heptadecane–benzene)	...	(1.21)	...	(1.56)

[a] Compounds were synthesized using known methods and purified by preparative gas chromatography. Samples (1 ml) were outgassed by freeze–pump–thaw cycles and sealed at 10^{-4} torr. H_2 determination was by gas chromatography (see E. J. Weber and H. Heusinger, *Radiochim. Acta*, **4**, 92 (1965)); accuracy better than ±5%; irradiation temperature 35 ± 5°; total dose 6.85×10^{20} ev/g; dose rate 0.95×10^{19} ev/g hr.

The reactive species (‡) may be an ion or an excited state. Reaction 3 is assumed to contribute the bulk of hydrogen since *n*-alkylbenzenes show a sharp drop of $G(H_2)$ in the solid phase.[5,6] Table I shows the experimental values of $G(H_2)$. Furthermore, it contains $g_{alkyl}(H_2)$ values calculated from the equation

$$G_{alkylbenzene}(H_2) = e_{phenyl}g_{phenyl}(H_2) + e_{alkyl}g_{alkyl}(H_2)$$

(For $g_{phenyl}(H_2)$ the value of 0.038 was used; g_{alkyl} (H_2) refers to the hydrogen produced per 100 ev absorbed in the alkyl part; e_{phenyl} and e_{alkyl} are the electron fractions of the phenyl and alkyl part, respectively.

The observed differences in $G(H_2)$ between the *n*-alkylbenzenes and the equimolar mixtures of alkane and benzene should be due to intramolecular energy transfer, because no scavengable hydrogen could be detected in both systems.

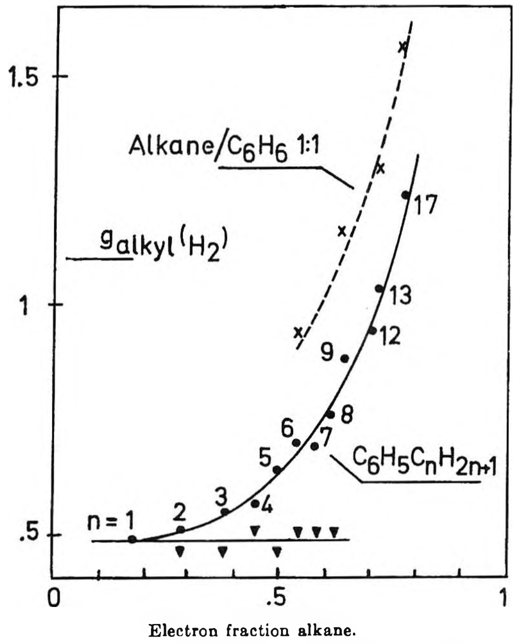

Figure 1. $g_{alkyl}(H_2)$ as a function of side-chain length: ●, this work (*n*-alkylbenzenes); +, this work (1:1 alkane–benzene mixtures); ▼, Jones, *et al.*[4]

---

(5) D. Verdin, *J. Phys. Chem.*, **67**, 1263 (1963).

(6) G. K. Wassiljew and I. I. Chkeidze, *Kinetika i Kataliz*, **5**, 802 (1964).

Contrary to the results of Jones, *et al.*,[4] we find (see Figure 1) that the extent of alkyl group protection by the phenyl group is affected by the length of the alkyl side chain. The protection decreases with increasing distance of the primarily affected portion of the $-CH_2-$ chain from the phenyl group. Additional evidence for this statement follows from the hydrogen production of various phenyl-*n*-nonanes (Table II). The protection is a maximum when the phenyl group is in the center of the alkane chain, in agreement with earlier results on cross linking of 1- and 6-naphthyldodecane by Alexander and Charlesby.[7] We feel that the experimental discrepancies may be due to impurities (possibly branched alkylbenzenes) in the commercially available compounds used by Jones, *et al.* In order to evaluate in more detail the mechanism of hydrogen formation and the nature of the protection in *n*-alkylbenzenes, we are carrying out epr studies and work on deuterated compounds.

Table II

Phenylalkane	$G(H_2)$	$g_{\text{alkyl}}(H_2)$
1-Phenylnonane	0.59	0.89
3-Phenylnonane	0.50	0.75
5-Phenylnonane	0.42	0.62

---

(7) P. Alexander and A. Charlesby, *Nature*, **173**, 578 (1954).

INSTITUT FÜR RADIOCHEMIE DER TECHNISCHEN HOCHSCHULE MÜNCHEN
MÜNCHEN, GERMANY

A. ZEMAN
H. HEUSINGER

RECEIVED AUGUST 15, 1966

A Method for Predicting the Effect of Solvation on Hydrogen-Bonding Association Equilibria

Sir: A perplexing problem that frequently arises in hydrogen-bonding studies is the prediction of variations occurring in the thermodynamic parameters for association reactions as the medium is changed. In previous investigations of the hydration of polar solutes we have noted that the solubility of water in various solvents is a good index to relative solvation ability.[1] However, reliable methods for calculating solvent effects are not presently available. This communication describes a simple technique for predicting the effects of solvation on the thermodynamic parameters characteristic of hydrogen-bonding reactions.

Suppose that an association reaction $A + B = AB$ occurs in a series of solvents, including the vapor phase. For any two of the solvents, the association constants may be written $K_{AB}{}^{I} = c_{AB}{}^{I}/c_{A}{}^{I}c_{B}{}^{I}$ and $K_{AB}{}^{II} = c_{AB}{}^{II}/c_{A}{}^{II}c_{B}{}^{II}$, where the superscripts refer to solvents I and II and the species concentrations, c_A, c_B, and c_{AB}, are expressed in units of moles per liter. It is assumed that solute concentrations are sufficiently small so that each species individually obeys Henry's law (in condensed phases) or the ideal gas law (in the vapor phase). The distribution constants $K_{D,A} = c_{A}{}^{II}/c_{A}{}^{I}$, $K_{D,B} = c_{B}{}^{II}/c_{B}{}^{I}$, and $K_{D,AB} = c_{AB}{}^{II}/c_{AB}{}^{I}$ are defined in terms of the same concentrations. The association and distribution constants are related by the equality

$$K_{AB}{}^{II}/K_{AB}{}^{I} = K_{D,AB}/K_{D,A}K_{D,B} \qquad (1)$$

By making one simple assumption, it is possible to correlate variations in the equilibrium constant and enthalpy of the association reaction occurring in different media. Assume that

$$\underset{I\rightarrow II}{\Delta F^\circ_{AB}} = \alpha(\underset{I\rightarrow II}{\Delta F^\circ_{A}} + \underset{I\rightarrow II}{\Delta F^\circ_{B}}) \qquad (2)$$

where $\underset{I\rightarrow II}{\Delta F^\circ_{AB}}$ represents the change in standard free energy of the complex upon transfer from phase I to phase II (using standard states of 1 mole/l. in each phase), $\underset{I\rightarrow II}{\Delta F^\circ_{A}}$ and $\underset{I\rightarrow II}{\Delta F^\circ_{B}}$ are the corresponding free energy changes for transfer of A and B, respectively, and α is a parameter, presumably less than unity and not strongly dependent on either temperature or choice of solvents. α is related to the fraction of the free energy of solvation of the monomers that is retained by the molecular pair after the complex is formed. In general, the complex will not solvate so extensively as the two separated monomers, since the reactive parts of the monomers are brought closely together in forming the complex, thus "squeezing out" some solvent molecules. The bulkier and more complicated the monomers, the more nearly should α approach unity. Furthermore, if a cyclic complex forms, α should be smaller than if only linear aggregates are present, because a larger percentage of the total molecular surface is involved in cyclic as opposed to chain complexes.

If eq 2 is valid, with α nearly constant and temperature independent for a range of solvents, several interesting conclusions can be drawn.

(1) The relation which is shown in eq. 3

---

(1) J. R. Johnson, Ph.D. Dissertation, The University of Oklahoma, 1966; D. D. Mueller, Ph.D. Dissertation, The University of Oklahoma, 1966.

$$K_{D,AB} = (K_{D,A}K_{D,B})^{\alpha} \quad (3)$$

follows immediately from eq 2 since the standard free energy changes are logarithmically related to equilibrium concentrations of the reacting species. Therefore, eq 1 reduces to

$$K_{AB}^{II}/K_{AB}^{I} = (K_{D,A}K_{D,B})^{\alpha-1} \quad (4)$$

(2) Upon differentiating eq 2 with respect to temperature, one obtains

$$\underset{I\rightarrow II}{\Delta H^{\circ}_{AB}} = \alpha(\underset{I\rightarrow II}{\Delta H^{\circ}_{A}} + \underset{I\rightarrow II}{\Delta H^{\circ}_{B}}) \quad (5)$$

Similarly, differentiation of (4) yields

$$\Delta H^{\circ}_{II} - \Delta H^{\circ}_{I} = (\alpha - 1)(\underset{I\rightarrow II}{\Delta H^{\circ}_{A}} + \underset{I\rightarrow II}{\Delta H^{\circ}_{B}}) \quad (6)$$

where ΔH°_{I} and ΔH°_{II} are the standard enthalpy changes for the association reaction in solvents I and II, respectively. Related equalities can be derived for the standard entropy changes.

In order to test and apply these relations, it is convenient to examine eq 4. This relation predicts that a plot of log K_{AB} *vs.* log $(K_{D,A}K_{D,B})$ for a series of solvents will be linear with slope equal to $\alpha - 1$. For convenience, the distribution constants are calculated with reference to the particular solvent for which K_{AB} is largest. By definition, $K_{D,A}$ and $K_{D,B}$ are equal to unity for the reference solvent; the product, $K_{D,A} \cdot K_{D,B}$, is expected to be greater than unity for each of the other solvents. A plot of this type is shown in Figure 1 for the reaction: water (A) + pyridine (B) = pyridine monohydrate (AB), which has been studied in detail in this laboratory.[2] The points corresponding to the various solvents lie nearly on a single straight line having a slope of 0.29; hence, $\alpha = 1.00 - 0.29 = 0.71$. The linearity of the plot indicates that a single value of α suffices to correlate the effects of solvents having a wide range of properties. As the solvent is varied from cyclohexane to 1,2-dichloroethane, the product $K_{D,A}K_{D,B}$ increases by a factor greater than 300.

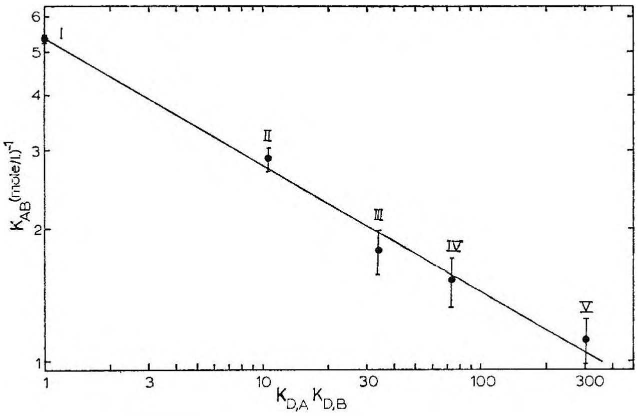

Figure 1. Correlation of association and distribution constants for the reaction: water + pyridine = water–pyridine at 25°: I, cyclohexane; II, carbon tetrachloride; III, toluene; IV, benzene; V, 1,2-dichloroethane. Indicated uncertainties in K_{AB} are standard errors.

Acknowledgment. This work was supported by the United States Department of the Interior, Office of Saline Water.

---

[2] J. R. Johnson, P. J. Kilpatrick, S. D. Christian, and H. E. Affsprung, in preparation.

DEPARTMENT OF CHEMISTRY
THE UNIVERSITY OF OKLAHOMA
NORMAN, OKLAHOMA 73069

SHERRIL D. CHRISTIAN
JAMES R. JOHNSON
HAROLD E. AFFSPRUNG
PAUL J. KILPATRICK

RECEIVED AUGUST 18, 1966

Chemiluminescent Gas-Phase Reactions Involving Electronically Excited Oxygen Molecules. Trimethylaluminum and Diborane near 3 mtorr[1]

Sir: It is known[2] that some 10% $O_2(a^1\Delta)$ and 0.1% $O_2(b^1\Sigma)$ are present together with O atoms in the products of a microwave discharge through O_2. Chemiluminescent reactions involving these excited molecules have been observed at ~1 torr.[3] Because of the presence[2,4] of these O_2 species in the upper atmosphere, it is of interest to establish whether they can produce a detectable chemiluminescence at pressures in the millitorr range encountered in that medium. We wish to report such reactions involving (1) trimethylaluminum (TMA) and (2) B_2H_6. The former does not require the participation of O atoms, and the latter does.

The products of a 2450-MHz discharge at 0.8 torr in an 1.1-cm i.d. Vycor tube through (1) 95% Ar–5% O_2 and (2) 100% O_2 were expanded, 40 cm downstream from the discharge, through a sonic orifice into a 15-cm i.d., 130 cm long Pyrex pipe where they were mixed with TMA, B_2H_6, or NO.[5] A Teflon baffle plate located

---

[1] This work was supported by the NASA Langley Research Center under Contract NAS1-5035.

[2] L. W. Bader and E. A. Ogryzlo, *Discussion Faraday Soc.*, **37**, 46 (1964); R. E. March, S. G. Furnival, and H. I. Schiff, *Photochem. Photobiol.*, **4**, 971 (1965).

[3] S. J. Arnold, N. Finlayson, and E. A. Ogryzlo, *J. Chem. Phys.*, **44**, 2529 (1966).

[4] H. P. Gush and H. L. Buijs, *Can. J. Phys.*, **42**, 1037 (1964).

immediately downstream from the orifice prevented flow and cooling effects of the expansion from influencing the observations. Light intensities were measured with a 1P28 phototube which viewed the Pyrex pipe directly and could be moved along its length. The wavelength region detected was about 3000 to 6500 A. In some experiments an HgO mirror was deposited in the discharge arm which removed O atoms but not $O_2(a^1\Delta, b^1\Sigma)$.[2] Typical results are shown in Table I for the reaction conditions given in its footnotes.

Table I: Observed Intensities[a,b]

	Discharge type			
Reagent	Ar + O_2	Ar + O_2 with O_2 added[c]	O_2	O_2 with HgO mirror
TMA	0.4	1	20	3-30[d]
B_2H_6	9	80	300	<0.01[e]
NO	6	6	6	<0.01[e]

[a] Intensities are expressed in arbitrary units (aiu) proportional to phototube current and were measured 10 cm downstream from the baffle plate. [b] Initial concentrations in molecule per cubic centimeter were $[Ar] + [O_2]$ or $[O_2] = 8 \times 10^{13}$; [TMA], $[B_2H_6]$, or $[NO] \approx 1 \times 10^{13}$; $P = 3$ mtorr; $T \approx 300°K$; average gas velocity is 1 m sec^{-1}. [c] Additional O_2 introduced directly into reaction tube at 1.7×10^{14} molecules cc^{-1}; $P = 8$ mtorr. Addition of the same amount of Ar instead of O_2 had no effect on the intensities of column 2. [d] Value varied within this range depending upon the "history" of the mirror. [e] No detectable intensity.

The NO data indicate that [O] from both discharges was approximately the same (since $I \propto [O][NO]$)[5,6] and that no detectable amount of O atoms was present once the HgO mirror was deposited. Column 5 shows that TMA produces a relatively intense chemiluminescence with excited O_2. Addition of water vapor between the discharge and the sonic orifice in concentrations exceeding $[O_2]$ did not influence I, indicating the active species to be $O_2(a^1\Delta)$, which contrary to $O_2(b^1\Sigma)$ is not deexcited by H_2O.[2] This I is at least some 10^4 times that obtained with ground-state $(X^3\Sigma)$ O_2 (no luminescence could be detected when the discharge was off). The results of column 2 are probably representative of those obtained with O atoms without $O_2(a^1\Delta, b^1\Sigma)$, since no luminescence could be observed using the Ar–O_2 discharge with the HgO mirror. Column 3 indicates a slight enhancement of initial I of the Ar–O–O_2–TMA system upon O_2 addition; this increase was accompanied by a faster decrease in I, which had the value 0.3 aiu at the downstream end of the reaction tube for the flow conditions of both columns 2 and 3. Chemiluminescence has been observed upon release of TMA in the upper atmosphere.[7] The present results suggest that this glow, at least in part, can be caused by $O_2(a^1\Delta)$ molecules.

B_2H_6 needed O atoms for the chemiluminescent reactions to be initiated since no emission was observed in the presence of the HgO mirror. Addition of increasing amounts of $O_2(X^3\Sigma)$ strongly and continuously enhanced the initial I without causing a noticeable decrease downstream. Comparison of columns 3 and 4 of Table I shows that the excited O_2 molecules are more efficient than ground-state O_2 in producing this enhancement. Based upon $[O_2(a^1\Delta)]/[O_2(X^3\Sigma)] \approx 0.1$, $O_2(a^1\Delta)$ can be shown[5] to be about a factor of 10 more efficient (assuming the contribution of $O_2(b^1\Sigma)$ to be negligible). Crude spectral measurements indicated the BO-α bands $(A^2\Pi - X^2\Sigma)$ to be the dominant emission. A plausible mechanism for $BO(A^2\Pi)$ formation is that $O + B_2H_6$ produces BH_2 either *via*[8] BH_3 followed by H-atom stripping or directly—in accord with recent findings on diborane dissociation;[9] BH_2 can then react with both O and $O_2(X^3\Sigma)$ to produce BO in the sufficiently exothermic reactions, $BH_2 + O \rightarrow BO + H_2$ and $BH_2 + O_2 \rightarrow BO + H_2O$ for which $\Delta H = -4.7$ and -4.6 ev, respectively. It is thus likely that, in the reaction with BH_2, $O_2(a^1\Delta)$ is a more efficient $BO(A^2\Pi)$ producer than $O_2(X^3\Sigma)$. Similar schemes involving BH_3 or $BH(X^1\Sigma)$ as the direct light emitter precursors are less likely since they involve either endothermic or spin-forbidden reactions. In view of their high relative intensity, it would be interesting to extend the study of the B_2H_6 reactions to the upper atmosphere.

---

(5) For details, see A. Fontijn, H. S. Pergament, P. H. Vree, and G. D. Bleich, "Studies Supporting An Upper-Atmospheric Chemical Release Program," AeroChem TP-137, 1966.

(6) G. Doherty and N. Jonathan, *Discussions Faraday Soc.*, **37**, 73 (1964).

(7) N. W. Rosenberg, D. Golomb, and E. F. Allen, *J. Geophys. Res.*, **68**, 5895 (1963); **69**, 145 (1964).

(8) F. P. Fehlner and R. L. Strong, *J. Phys. Chem.*, **64**, 1522 (1960).

(9) T. P. Fehlner, *J. Am. Chem. Soc.*, **87**, 4200 (1965).

AEROCHEM RESEARCH LABORATORIES, INC.
SUBSIDIARY OF RITTER PFAUDLER
CORPORATION
PRINCETON, NEW JERSEY 08540

ARTHUR FONTIJN
PIETER H. VREE

RECEIVED AUGUST 25, 1966